UNIVERSITY OF CALIFORNIA
RIVERSIDE

Developing Modular Syntheses of Diverse Nitrogen Heterocycle-Based Compounds for Metal Complexes, Catalysis, and Therapeutics

A Dissertation submitted in partial satisfaction
of the requirements for the degree of

Doctor of Philosophy

in

Chemistry

by

Michael David Elliott Sterling

March 2019

Dissertation Committee:
Dr. Catharine H. Larsen, Chairperson
Dr. Christopher Switzer
Dr. Chia-en Chang

The Dissertation of Michael David Elliott Sterling is approved:

Committee Chairperson

University of California, Riverside

DEDICATION

To all the people in my life who, without their support, guidance, and love, I would not be where I am today. This section and the following are dedicated to you.

First, to my advisor Catharine: thank you for seeing the potential in me, even when I didn't see it myself. I entered this journey feeling thoroughly unconvinced I could handle it, but your unwavering support and guidance is the reason I am here today. I know it hasn't been an easy five years by any means, but I wouldn't rather have taken this trip with anyone but you. I will look back on my time at UCR with pride, as I was fortunate to work for such an amazing chemist, person, and friend.

To the members of the Larsen Lab: Zack – I honestly didn't think I was going to be able to get through this last year without you in the group. Thankfully, your example (both as a chemist and a leader) prepared me better than I could have ever imagined. Keegan – you always knew exactly what to say when I felt things were going off the rails. Your level head, your twisted humor, and your constant availability as a sounding board kept my sanity in the craziest moments. Bobby – I have never seen someone take to research chemistry as quickly and elegantly as you. You have poise, work ethic, and chemical knowledge far beyond your years and I am truly excited to see where your professional life takes you. Jay – just as everyone takes their own path in life, there is no "standard" way to experience graduate school. Whatever you decide to pursue, know this: you deserve to reach your full potential. Don't sell yourself short into thinking that you *can't* do something, because I promise you that you *can*. To all of you – stay in touch. We share a bond going through this process that is unlike any other relationship, so please reach out – even if only just to catch up on life.

To Hector: you could have been included in the Larsen Lab, but just like everything you have achieved in the last few years, you deserve special recognition. You are, without a doubt, one of the brightest, kindest, best people I have had the pleasure of knowing in life. Even though our relationship began where I was the mentor and you were the student, that dynamic quickly shifted. We became equals – your advanced knowledge in chemistry and passion for learning allowed us to discuss as peers. At this point, sometimes it feels like *I* am the one looking up to *you*: the enthusiasm you have for this subject is infectious and it drives me to be a better chemist. You are destined for greatness, and I am beyond lucky to have experienced your nascency as a scientist.

To the family I have made in Riverside: Shane & Stephen, you welcomed me with an open door and open arms. I truly love both of you and am endlessly thankful for your friendship. Dorie, Gary, and Hallie: you didn't just welcome me into your lives – you embraced me. The love that you have all given me has assuaged the stress in my work life, and for that I cannot express enough gratitude.

To my Mom and Lillie: this section is short, not because there isn't anything to say, but because there aren't words to encapsulate how important you both are to me. We wouldn't have made it without each of us, and I love you both to my heart's capacity.

Finally, to Ryan: I wouldn't be the man I am today without you. You have brought out the best version of myself, believed in me when I didn't believe in myself, and let me know that I deserve to be excellent. I love you.

ACKNOWLEDGEMENTS

The text and results discussed in the following chapters of this dissertation are, in part or in full, a reprint of the material as they appear in the following publications:

Chapter 2:

Laguna, E. M.; Olsen, P. M.; Sterling, M. D.; Eichler, J. F.; Rheingold, A. L.; Larsen, C. H. *Inorg. Chem.* **2014**, *53* (23), 12231. DOI: 10.1021/ic501965m

Chapter 3:

Sterling, M. D.; Bishop, L. E.; Nelson, K. G.; Rheingold, A. L.; Larsen, C. H. *Dalton Trans.* Submitted.

I acknowledge the National Science Foundation (CHE-1352665) and the UCR MARCU Star Program for partial support of this research.

ABSTRACT OF THE DISSERTATION

Developing Modular Syntheses of Diverse Nitrogen Heterocycle-Based Compounds for Metal Complexes, Catalysis, and Therapeutics

by

Michael David Elliott Sterling

Doctor of Philosophy, Graduate Program in Chemistry
University of California, Riverside, March 2019
Dr. Catharine H. Larsen, Chairperson

The Larsen group develops new methods to synthesize nitrogen-containing molecules, focusing on accessing hindered and aromatic amines using green catalyst systems to convert inexpensive starting materials directly to high-value products. Amines and heteroaromatic compounds permeate the list of top-grossing pharmaceuticals. Developing novel methodologies for the formation of these drug-like molecules streamlines the discovery of treatments for cancer, HIV, malaria, and other maladies, while decreasing environmental impact. In addition to purely organic therapeutics, metal-based treatments to effectively treat ailments, and there continues to be special interest in their ligands, the organic molecules which enable metallic drug delivery. To this end, we have developed solvent- and chromatography-free, catalytic methods that provide a wide range of 2-(2'-pyridyl)quinolines, 2-(2'-pyridyl)triazoles, and 2-(2'-pyridyl)pyrazoles, heteroaromatic ligands that also offer their own intrinsic bioactivity.

Our modular methods provide these heteroaromatic compounds with a variety of substituents simply by selecting the appropriate starting materials. Due to the facile construction of an electronically-diverse library, a series of each type of 2-(2'-pyridyl)quinoline (PyQuin), 2-(2'-pyridyl)triazole (PyTri), and 2-(2'-pyridyl)pyrazole (PyPyr) ligands were complexed to different transition metals, including gold, copper, palladium, and platinum. The effect of the ligands' substituents on the metal complex were tracked by proton NMR spectroscopy and X-ray crystal structure analysis. Ready access to mixed LX-type PyPyr ligands resulted in the discovery of a thoroughly unique 5-coordinate, square-based pyramidal copper(II) complex. Catalytic activity was observed with both palladium(II) and gold(III) complexes of the PyTri ligands. In culmination, PyTri-gold(III) complexes were found to be essential for formation of an unprecedented 1,4-dihydroquinoline product from the hydroamination reaction of aniline and phenylacetylene.

Table of Contents

List of Schemes

List of Tables

List of Figures

Chapter One: Nitrogen Containing Small Molecules and Heterocycles

1.1 Introduction:

Due to humans' inherent desire for healthier and lengthier lives, the drive to create small molecules which have high activities against both preventable diseases as well as incurable (but treatable) diseases is likely never going to fade.[1] In this vast library of small molecules which have been deemed valuable, the number which contain heteroatoms, more specifically nitrogen atoms, is staggering. Amine containing compounds are currently found at the forefront for treating cancers,[2] HIV,[3] diabetes,[4] depression,[5] and countless other maladies. Within each of these treatments, efforts are constantly being made to increase production, lower cost, and diversify the structure of these targets in hopes of finding more active variants of current targets.[6]

1.2 Heterocycles

While it cannot be denied that amine-containing molecules have high inherent value as potential drug targets, small molecules that contain heterocycles, primarily amine heterocycles i.e. pyridine, pyrrolidine, quinoline, are especially sought-after.[7] Their value is derived from both their history as potent therapeutics against treatable diseases such as malaria[8] and tuberculosis,[9] but also for how difficult they can be to incorporate into a structure. Nitrogen-containing aromatic heterocycles (for example, quinoline) are incredibly stable

once formed.[10] According to the Hückel definition of aromaticity, the delocalization of the electrons in the ring stabilize the overall structure which reduces the possibility of subsequent chemical transformations or degradation.[11] For these reasons, any method that allows for the construction of small molecules which contain amine heterocycles can offer high value when designing novel chemical therapeutics.[12]

1.3 Small Molecules and their Role in Therapeutics

When discussing the nature of novel chemical compounds, a descriptor that is frequently used is “small molecule.” The importance we place on these “small molecules” lies in their ability to engage in biological processes.[13] On a fundamental level, it is these interactions which are responsible for many ailments occurring in the human body, and unless a drug target can actively participate, its value is moot.

Within their ability to affect biological processes, the small molecule can behave in many different modes to achieve an “activity” that is desired: in some circumstances, a drug target is responsible for interrupting these interactions, while in other situations a small molecule is meant to accentuate the process.[14] For this reason, the ability to simply design a small molecule which will behave exactly how it is meant to is unlikely. This difficulty stems from the many ways a small molecule can interact with proteins, the variable shape typical protein interfaces can take, bioavailability, and countless other considerations.[15,16]

Inside a protein, there is (on average) 750-1500 Å^2 of surface area and obtaining an X-ray structure that actually shows a small molecule bound to an enzyme active site can be quite problematic. Thoroughly discussed in their comprehensive review of X-ray diffraction studies of enzymes, Steitz & Blow highlight the many limitations of obtaining an X-ray structure of a small molecule-protein complex.[17] The crux of these difficulties is that the structures of enzymes and enzyme-substrate complexes can change based on many parameters, including concentration, homogeneity, and the possibility for conformational changes. This means that an observed crystal may not actually be representative of how the protein-small molecule adduct actually exists in solution. Since small molecules are not required to cover the entire surface of a binding site, the drug target often binds to a very small portion of the protein in order to facilitate the activation/deactivation which leads to the desired activity.[18] To have this happen, in most basic terms, the small molecule must fit in this pocket. The size of a small molecule is generally restricted by molecular weight, which has been determined (through both experimental observation and computational methods) to be between 160-500 AMU with a polar surface area less than 140 Å^2.[19,20] While these restrictions are fairly clear, there are also a series of guidelines that have been constructed in order to assist in determining if a molecule can be even considered “biologically active.”

1.4 Lipinski's Rule of Five

As more therapeutic-focused research has been conducted, the guidelines for what makes a target drug viable have become more well-defined. While molecular weight is still a necessary attribute of a small molecule to consider, other qualities of drug-like compounds have been studied to see their effects on drug viability.[21] A rule of thumb has been constructed through much experimentation in order to determine the "drug likeness" of a compound in regard to pharmacological activity. These qualities are based off the fact that drugs are introduced into the human body, an incredibly complex environment in which many different factors need to be considered. These rules, or *Lipinski's Rule of Five*, were initially articulated in 1997 by Christopher Lipinski based on his observation that many orally administered drugs are both small and lipophilic in character.[22]

The rules state that a drug candidate, if it were to have the greatest chance of reaching the pharmaceutical market, should not violate more that one of the following criteria, should it be an orally administered drug: (**1**) there cannot be more than 5 hydrogen-bond donors present in the molecule; (**2**) there cannot be more than 10 hydrogen-bond acceptors present in the molecule; (**3**) the compounds should not have a molecular weight greater than 500 Daltons; and (**4**) the compound should not have an octanol-water partition coefficient (log *P*) greater than 5.[23] While there are many exceptions to these rules, the general logic behind each point is sound. With too many hydrogen-bond donors (N-H or

O-H bonds) or hydrogen-bond acceptors (N or O atoms), the drug is likely going to exhibit poor absorption. Solubility in water is crucial (as the body is an aqueous environment) and this is directly impacted by the lack or abundance of hydrogen-bond donors and acceptors. Aqueous solubility is also impacted by molecular weight, and the general upper limit, according to Lipinski, is 500 Daltons. The final rule (**4**) is intended to mimic a drug's ability to enter a cell (i.e. pass through a cell wall), which hinges on the drug's lipophilicity.

In summary, a drug must be polar enough to be soluble in the body when administered orally, but lipophilic enough to enter the cell or interact with the largely non-polar protein active sites. For these reasons, it is beneficial to construct a general backbone of a viable molecule and derivatize it, as small, systematic changes are unlikely to violate one of Lipinski's Rules of 5.[24] Because of our (current) inability to fashion a perfect drug target, modification of a core structure and the ability to create a library of potential compounds via high-throughput syntheses is often the best route.

1.5 Examples of Nitrogen Heterocycle-Containing Small Molecule Therapeutics

While there exists a wide range of natural products and drug therapeutics that contain nitrogen as heteroatoms, in recent years nitrogen-based heterocycles have become of high-importance in anticancer drug design. Between 2010 and 2015, almost three-quarters of the heterocyclic anticancer

agents approved by the FDA were nitrogen heterocycles (with indoles being the most valuable).[25] They have shown to have many pathways toward the inhibition of cancer, whether through the prevention of cell signaling, tumor vascularization, or the ability to directly induce cell death.[26] Some compounds which have shown high activity against a variety of maladies are shown in **Figure 1.1** with the heterocycle highlighted in red.

Omeprazole, sold under the brand name Prilosec in its racemic form, is used to treat general gastroesophageal reflux disease, peptic ulcer disease, and upper gastrointestinal bleeding.[27] At the core is an imidazole ring, with the N-H being instrumental in its activity; omeprazole undergoes a chiral shift in acidic environment which results in the formation of a disulfide bridge with a cysteine group in H^+/K^+ ATPase, inhibiting the parietal cells to produce gastric acid.[28]

Quinine, arguably the most well-known quinoline-containing molecule, is added to tonic water for its unique flavor and has historically been a treatment for malaria.[29] While it was successfully synthesized by Woodward in 1944 in a lengthy synthesis, isolation from the Cinchona tree remains the only economically practical source of quinine.[30] The quinoline core has recently been shown to have high potency against not just malaria but tuberculosis and babesiosis.[31]

Fludarabine is highly effective in the treatment of chronic lymphocytic leukemia as well as in combination therapies with mitoxantrone, dexamethasone, and rituximab for treating non-Hodgkin's lymphoma.[32] A purine analogue, it

inhibits DNA synthesis by interfering with both ribonucleotide reductase and DNA polymerase. As it is phosphorylated, Fludarabine is ionized at physiologic pH and is effectively “trapped” in the blood, giving it a high level of specificity for cancerous (and healthy) blood cells.[33]

Fluconazole is a triazole-based antifungal treatment which has shown success in treating a high number of fungal infections.[34] It behaves similarly to imidazole-class antifungals by inhibiting the fungal cytochrome P450 enzyme 14α-demethylase.[35] This inhibition prevents the conversion of lanosterol to ergosterol, an essential compound found in fungi. Even if the specific heterocycle present in the antifungal medication varies, a heterocyclic moiety’s presence is crucial in order to show effectiveness.[36]

While there has been much development in the synthesis and modification of heterocycles (some novel methods will be discussed in the following chapters) as therapeutics, there are other applications for these compounds other than their use as drug-like molecules. Also, heterocycles have been shown to be extremely useful and valuable ligands for metal centers.

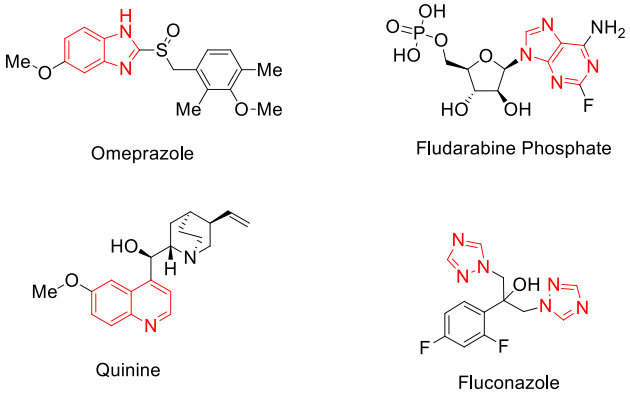

Figure 1.1 Prominent therapeutics which feature aromatic heterocycles

1.6 Heterocycles as Ligands for Metal Complexes

While the construction of linked heteroaromatic rings in order to bind to a metal center may seem distant from the world of therapeutics and drug-like molecules, there are many examples of heteroaromatic metal complexes found in living systems.[37] Hemoglobin, the iron-containing oxygen transport protein in red blood cells, consists of four globular proteins each tightly associated to a *heme* group.[38] The four heteroaromatic rings (porphyrin) bound to the iron (II) center are essential for the stabilization of the oxidized iron species (used to catalyze many chemical transformations in the body) in addition to ensuring solubility in the physiological environment.

In a similar way, synthesizing heteroaromatic systems which can bind to a metal center can dramatically affect the resulting complex's reactivity, solubility, and selectivity. For the work described herein, the novel ligands investigated all mimic the binding of 2,2´-bipyridine or "bpy." Bipyridine ligands show great affinity for metal centers, they do not change the oxidation state as both chelates are L-type (will be discussed in later chapters), and the geometry of the resulting complex tends to be favorable.[39] Bpy complexes have been made with a variety of metals, and even simple changes on the ligand backbone can change the properties of the complex. For this reason, design of novel ligands can open the door to fascinating reactivity, some which has been never been reported until now.

1.7 References

1) Rafi, M. A.; Alavi, A. *BioImpacts* **2017**, *7* (3), 135–137.

2) Feling, R. H.; Buchanan, G. O.; Mincer, T. J.; Kauffman, C. A.; Jensen, P. R.; Fenical, W. *Angew. Chem. Int. Ed.* **2003**, *42*, 355.

3) Huffman, M. A.; Yasuda, N.; DeCamp, A. E.; Grabowski, E. J. J. *J. Org. Chem*. **1995**, *60*, 1590.

4) Ahrén, B. *Expert Opin. Emerg. Drugs.* **2008**, *13*, 593.

5) Oshiro, Y.; Sato, S.; Kurahashi, N.; Tanaka, T.; Kikuchi, T.; Tottori, K.; Uwahodo, Y.; Nishi, T. *J. Med. Chem.* **1998***, 41*, 658.

6) Groot, C. A. U.; Löwenberg, B. *Nature Reviews Clinical Oncology.* **2018**, *15* (7), 405.

7) El Sayed, M.T. *Adv. Mod. Oncol. Res.* **2015**, *1*, 20.

8) Ahrén, B. *Expert Opin. Emerg. Drugs* **2008**, *13*, 593.

9) Sharma, S.; Sharma, P. K.; Kumar, N.; Dudhe, R. *Biomedicine & Pharmacotherapy* **2011**, *65* (4), 244.

10) Steel, P. J. *Coordination Chemistry Reviews.* **1990**, *106*, 227.

11) Huang, Y.-Z.; Yang, S.-Y.; Li, X.-Y. *Journal of Organometallic Chemistry* **2004**, *689* (6), 1050.

12) Vitaku, E.; Smith, D. T.; Njardarson, J. T. *J. Med. Chem*. **2014**, *57* (24), 10257.

13) Arkin, M. R.; Wells, J. A. *Nat. Rev. Drug Discov.* **2004**, *3*, 301.

14) Bogan, A. A.; Thorn, K. S. *J. Mol. Biol.* **1998***, 280*, 1.

15) Sundberg, E. J.; Mariuzza, R. A. *Structure Fold. Des.* **2000**, *8*, R137.

16) DeLano, W. L.; Ultsch, M. H.; de Vos, A. M.; Wells, J. A.; *Science* **2000**, *287*, 1279.

17) Blow, D. M.; Steitz, T. A. *Annu. Rev. Biochem.* **1970** *39*, 63.

18) Clackson, T.; Wells, J. A. *Science* **1995**, *267*, 383.

19) Ghose, A. K.; Viswanadhan, V. N.; Wendoloski, J. J. *J. Comb. Chem*. **1999**, *1*, 55.

20) Veber, D. F.; Johnson, S. R.; Cheng, H. Y.; Smith, B. R.; Ward, K. W.; Kopple, K. D. *J. Med Chem.* **2002**, *45,* 2615.

21) Lipinski, C. A. *J. Pharmacol. Toxicol. Methods* **2000**, *44*, 235.

22) Lipinski, C. A.; Lombardo, F.; Dominy, B. W.; Feeney, P. J. *Adv. Drug. Deliv. Rev.* **1997**, *46,* 3.

23) Lipinski, C. A. *Drug Discovery Today* **2004**, *1*, 337.

24) Oprea, T. I.; Davis, A. M.; Teague, S. J.; Leeson, P. D. *J. Chem. Inf. Comput. Sci.* **2001**, *41* (5), 1308.

25) Komeilizadeth, H. *Iran J Pharm Res.* **2006**, *4*, 229.

26) Haque, I.U. *J Chem Soc Pak*. **2010**, *2*, 245.

27) Langtry, H.D. & Wilde, M.I. *Drugs.* **1998** *56*, 447.

28) Asghar, W.; Pittman, E.; Jamali, F. *DARU J. Pharm. Sci*. **2015**, *23*.

29) Renslo, A. R. *ACS Med. Chem. Lett.* **2013**, *4* (12), 1126.

30) R. B. Woodward, W. E. Doering. *J. Am. Chem. Soc*. **1944**, *66*, 849.

31) Wittner M, Rowin K.S, Tanowitz H.B. *Ann. Intern. Med*. **1982**, *96*, 60.

32) Romano, M. F.; Lamberti, A.; Turco, M. C.; Venuta, S*. Leukemia & Lymphoma*. **2000**, *36*, 255.

33) Rai, K. R.; Peterson, B. L.; Appelbaum, F. R.; Kolitz, J.; Elias, L.; Shepherd, L.; Hines, J.; Threatte, G. A.; Larson, R. A.; Cheson, B. D. *N Engl. J Med.* **2000**, *343* (24), 1750.

34) Peyton, L.R., Gallagher, S. Hashemzadeh, M. *Drugs of Today*. **2015**, *51*, 705.

35) Herreros, J. M. C.; Matía, *Clin. Microbiol. Infect.* **2006**, *12*, 53.

36) Owens, J.N, Skelley, J.W., Kyle, J.A. *US Pharm*. **2010**, *35* (8), 44.

37) Haas, K. L.; Franz, K. J. *Chem Rev.* **2009**, *109* (10), 4921.

38) Hardison, R. C. *Proc Natl Acad Sci*. **1996**, *93* (12), 5675.

39) Ferguson, J.; Hawkins, C. J.; Kane-Maguire, L. A. P.; Lip, H. *Inorg. Chem.* **1969**, *8 (*4), 771.

Chapter Two: Modular Syntheses of Highly Substituted Quinolines and the Development of 4-phenyl-2-(2´-pyridyl)quinolines (PyQuins)

2.1 Introduction:

Developing pathways which allow for the facile construction of complex compounds is inherently valuable; when these compounds also possess unique bioactive utility in addition to being structurally interesting, the value increases significantly. One such family of compounds, being both complex in structure and chemically/therapeutically valuable, are quinolines. Quinolines are known therapies for a broad range of ailments, ranging from malaria[1] to cancer.[2] As discussed in the introduction, the notable quinoline-containing compound Quinine has been utilized as a malaria treatment for almost 400 years.[3] Similarly, the synthetic pathways towards the quinoline moiety also has historical precedent, albeit with low degrees of substitution and derivatization of the quinoline core allowed.

2.2 Precedential Methods for the Synthesis of Quinolines:

There are several well-known methods for synthesizing quinolines, and while each are able to construct the bicyclic heteroaromatic core, each have their advantages and drawbacks when it comes to functionalizing and modifying the core moiety. One of the oldest methods for building quinolines is the Skraup reaction.[4] The Skraup synthesis of quinoline (**Scheme 2.1**) combines aniline with

sulfuric acid, glycerol, and nitrobenzene. The sulfuric acid converts glycerol to the active reagent acrolein which undergoes attack by the aniline and subsequent ring closure and oxidation. While elegant in its atom economy and direct access of a quinoline core, the opportunity for modifying the quinoline core is quite low. As the glycerol is converted to acrolein which is eventually condensed upon, there cannot be any change in the electrophile.

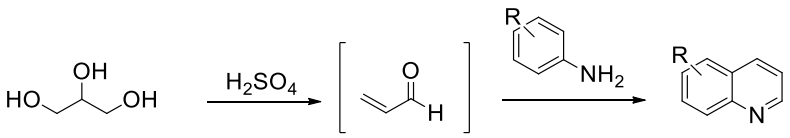

Scheme 2.1 Skraup synthesis of quinoline

The only freedom for modifying the product comes from using a substituted aniline which will carry through to the product. This means that, through the Skraup method, the only allowed carbons for substitution are on carbons 5-8 (as two substituents *ortho* to the amino group would prevent cyclization). In addition to this, aniline is generally considered a fairly poor nucleophile, so installing electron-withdrawing groups (EWG) as substituents could limit or even prevent the reaction from occurring. [5]

Advancing from the Skraup synthesis one year later, the Doebner-Miller reaction differs mainly in the electrophile **(Scheme 2.2)**. Under acidic conditions, α,β-unsaturated carbonyl compounds (mostly α,β-unsaturated aldehydes) are combined to give quinoline.[6] The carbonyl compound is protonated, activating

the β-position for nucleophilic attack by aniline, followed by ring closure and oxidation/rearomatization to form the heterocyclic system.

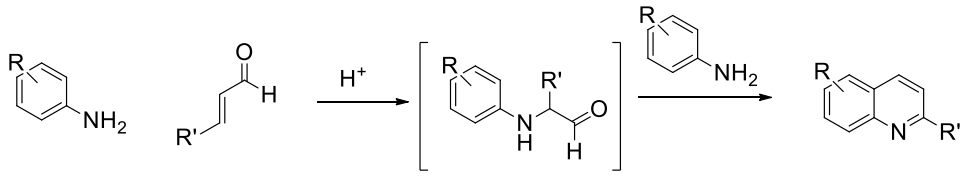

Scheme 2.2 Doebner-Miller process gives substituted quinolines

As there is no need for an analogous initial conversion of starting materials (e.g. glycerol to acrolein), the degrees of substitution on the final product can be much higher. An open *ortho* position is required on the aniline ring (as expected), but the α,β-unsaturated carbonyl can be substituted on all 3 carbons. It should be noted, however, that the best results are when EDG such as esters are installed on the carbonyl. This is not surprising, as the intermediate would undergo cyclization more easily with higher electron density.[7] While the ease of substitution may seem attractive, without including electron-donating groups (EDG) on the aniline nucleophile and EWG on the carbonyl electrophile, yields tend to be quite low. In addition, there is some debate on the mechanism this transformation takes.[8] Carbon isotope experiments have suggested two equivalents of aniline participate in the process, with two sets of nucleophilic attack/imine formation. This leads to scrambling of isotopes in the product. While this would be unnoticed in an achiral system, should there be any desire for

stereospecificity in the product (stemming from a chiral starting material), the fragmentation/two pathways could be problematic. Additionally, the more difficult to access the starting material, the less ideal; α,β-unsaturated carbonyls are commercially available, however substituted species (which would impart substitution on the quinoline product) would require synthesis, likely through an aldol condensation.

Both the Skraup and Doebner-Miller methods for synthesizing quinoline require at least one *ortho* position open on the aniline to allow for closing of the ring. In the Friedländer synthesis **(Scheme 2.3)**, published one year after the Doebner-Miller method, the position *ortho* to the amino group is pre-functionalized with an aldehyde. These 2-aminobenzaldehyde starting materials are reacted with ketones to yield quinolines in significantly higher yields than both the Skraup and Doebner-Miller reactions.[9] The increase in yield is due to the relative rates of reaction steps: each involves an early attack of the aniline nucleophile onto the carbonyl electrophile (either directly or at the β -position).

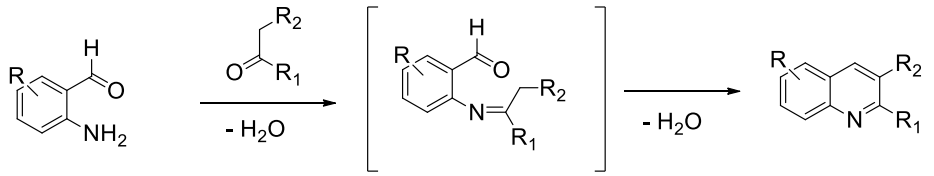

Scheme 2.3 Friedländer synthesis offers highly substituted quinolines

Condensations, even with a sub-optimal nucleophile/electrophile pair like aniline and a ketone, can easily be facilitated by Lewis or Brønsted acids.[10] The rate-limiting step is the eventual ring-closure and oxidation/rearomatization; in the Friedländer method, the aldehyde at the *ortho* position acts as a second electrophile, which is attacked intramolecularly by the Schiff base-side of the molecule (this closes the ring, which is oxidized to the quinoline).[11] A clear disadvantage to this route to quinolines is the necessity for a bifunctional starting material. Amino-benzaldehydes can be formed through the facile reduction of a nitro-benzaldehyde, however the resulting products are quite unstable due to the fact that they can self-condense.[12] For this reason, the Friedländer method generally only permits substitution at the 2 and 3 positions on the quinoline, the carbons stemming from the ketone.

The Combes method for synthesizing quinolines circumvents the bifunctional aniline issue that the Friedländer reaction has while also promoting the ring closure through inclusion of a second electrophile.[13] Shown in **Scheme 2.4**, aniline is condensed upon a β-ketone to form an imine intermediate. This imine can tautomerize to the most stable enamine (depending on substitution of the ketone) and function as a nucleophile again to attack the other ketone intramolecularly.

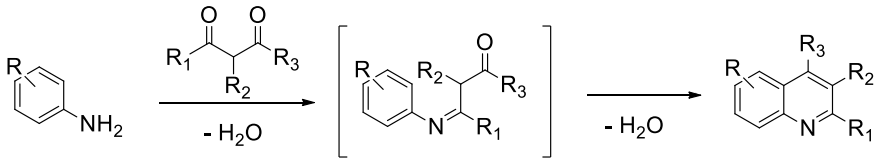

Scheme 2.4 Combes synthesis offers most substituted quinolines

While this method seems to sidestep problematic qualities of the aforementioned reactions, selectivity is an issue in the Combes method. There have been efforts to determine selectivity based on substituents, confirming that without directing groups on the ketone/aniline, the electrophiles can be too similar in reactivity to ensure one over the other.[14] It should be noted, however, that this method is one of the few that allows for substitution at every position on the resulting quinoline ring. As is the norm, positions 5-8 come from the aniline starting material, but since the β-ketone can be substituted on both ketones as well as the methylene separating them, each position is accessible. As described, however, the chance of an isomeric mixture based on initial nucleophilic attack and preferential tautomerization is quite high, thus making the Combes method less than ideal.

Each of these historic methods for accessing quinolines were published one year after the other from 1880-1883. Almost a century later, the Povarov reaction was published as a method to form quinolines from preformed imines using a Lewis acid catalyst.[15] As shown in **Scheme 2.5**, condensation of aniline onto an aldehyde yields the Schiff base via a condensation reaction. This imine

would normally be too unreactive to undergo nucleophilic attack by an alkene, but the use of a Lewis acids like boron trifluoride (BF_3) or metal triflates activate the imine sufficiently.[16,17] In addition to activating the imine, an activated alkene is required to function as a nucleophile. Often, this is achieved through the use of enol ethers or enamines.[18]

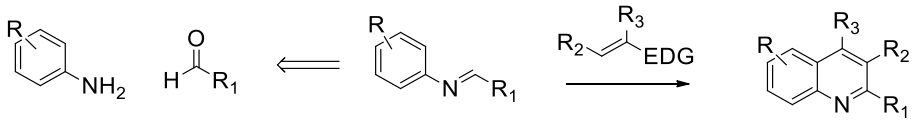

Scheme 2.5 Povarov reaction most direct and recent route to substituted quinolines

Both enol ethers and enamines will yield electrophilic intermediates (either oxonium or iminium, respectively) following nucleophilic attack of the alkene, which facilitates ring closure. Unlike previously discussed methods, these intermediates are charged, which strongly encourage the ring closing step. Oxidation and rearomatization of the bicyclic system yields quinoline, which has been shown with many types of substrates to proceed in high yield.[19] This method boasts the ability to add a nucleophile to preformed imine, however both the requirement of using an aldehyde as well as necessitating an activated alkene means the type of groups that can be installed on the quinoline core are limited. Nevertheless, this method is considerably more robust than the aforementioned historical methods, which leads to the work done in the Larsen lab regarding the modular, green synthesis of substituted quinolines.

2.3 Green Synthesis of 2,4-substituted Quinolines via 3-Component Coupling

Within the Larsen group, there has been a continuous effort to develop and optimize methodologies that access structurally and chemically interesting products in as "green" of a fashion as possible. If there is the opportunity to eliminate unnecessary waste, whether it be solvent, excess catalyst, excess equivalents of reagents, or simply fewer steps, it would benefit all involved to take those measures. In 2012, the three-component coupling of an amine, an aldehyde, and alkyne catalyzed by copper (II) triflate to yield trisubstituted propargylamines was reported.[20] This method was able to incorporate cyclic, acyclic, and the unprecedented electron-deficient sulfonamines **(Scheme 2.6)**.

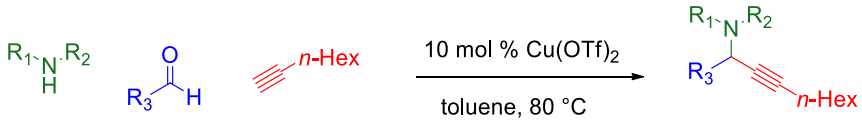

Scheme 2.6 Three-component coupling of amine, aldehyde, and alkyne gives propargylamine products in a single step

When *p*-anisidine and benzaldehyde were used under identical conditions as the respective amine and aldehyde source, it was observed that an appreciable amount of quinoline product was formed in addition to the expected propargylamine product **(Scheme 2.7)**.[21]

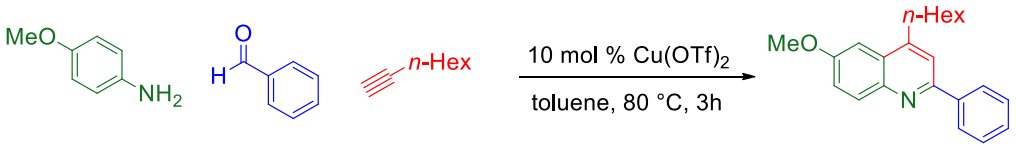

Scheme 2.7 Three-component with aniline and aryl-aldehyde gives quinoline products

It was found, in the efforts to optimize and develop a "greener" process, that removal of solvent and reducing the catalyst loading from 10% to 5% copper (II) triflate gave access to 2,4-substituted quinolines in moderate to high yields **(Scheme 2.8)**.[21]

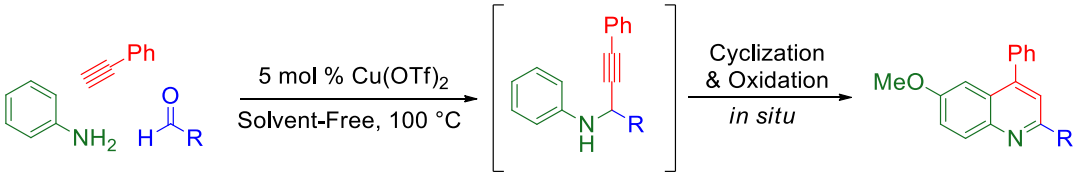

Scheme 2.8 Propargylamine intermediate is formed followed by cyclization to give quinoline

When this method is compared to the discussed historical methods for forming quinolines, the modular quality that comes from using a three-component reaction is what is so valuable. Aside from the substituents on the aniline, a plethora of commercially-available alkynes and aldehydes can be selected to impart whatever functionality desired to the quinoline product. In addition to tolerating both electron-rich and electron-deficient starting materials, this method also boasts the ability to incorporate heteroaromatic substrates, which ultimately is the basis for the work described herein.

2.4 Synthesis of 4-phenyl-2-(2´-pyridyl)quinolines (PyQuins)

With the success of being to incorporate both alkyl and aryl substituents in a single-step quinoline synthesis, an effort was made to develop quinoline products that could function other than being potentially bioactive. As mentioned in the introduction, heteroaromatic molecules which have multiple atoms that can associate with an electrophilic metal center can be classified as multidentate ligands (e.g. two nitrogen chelates = **bi**dentate). Easily, the most ubiquitous bidentate heteroaromatic ligand is 2,2´-bipyridine (bpy). Its appeal in using as a metal chelate lies in its facile synthesis, a bite-angle that will incorporate both large and small atomic radii (this will be elaborated on further in later chapters), and the fact that both chelating atoms are L-type, meaning that they will not affect the oxidation state of the metal center.[22]

The synthesis of 2-(2´-pyridyl)quinoline can be achieved using a variety of methodologies (**Figure 2.1).**

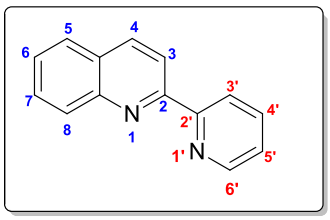

Figure 2.1 Structure and numbering of 2-(2'-Pyridyl)quinoline

The first reported synthesis of 2-(2´-pyridyl)quinoline was accomplished using a modified Friedländer reaction (**Scheme 2.9)**.[23] Similar to the Friedländer

synthesis of quinolines, the bifunctional starting material 2-aminobenzaldehyde is combined with 2-acetylpyridine and base.

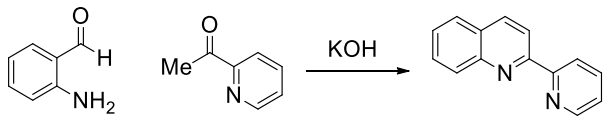

Scheme 2.9 Smirnoff synthesis with bifunctional starting materials gives 2-(2'-pyridyl)quinolines in a single step

The obvious downside to this approach is the necessity of highly modified starting materials which is both synthetically taxing and expensive. An example of this is the multi-step synthesis of a substituted 2-(2´-pyridyl)quinoline by the Recca group in 2010 (**Scheme 2.10).**[24] Pre-functionalizing the α-aminoacetophenone followed by Smirnoff chemistry gives a 33% yield over a 70 hours of reaction time, three recrystallizations, and one purification using column chromatography.

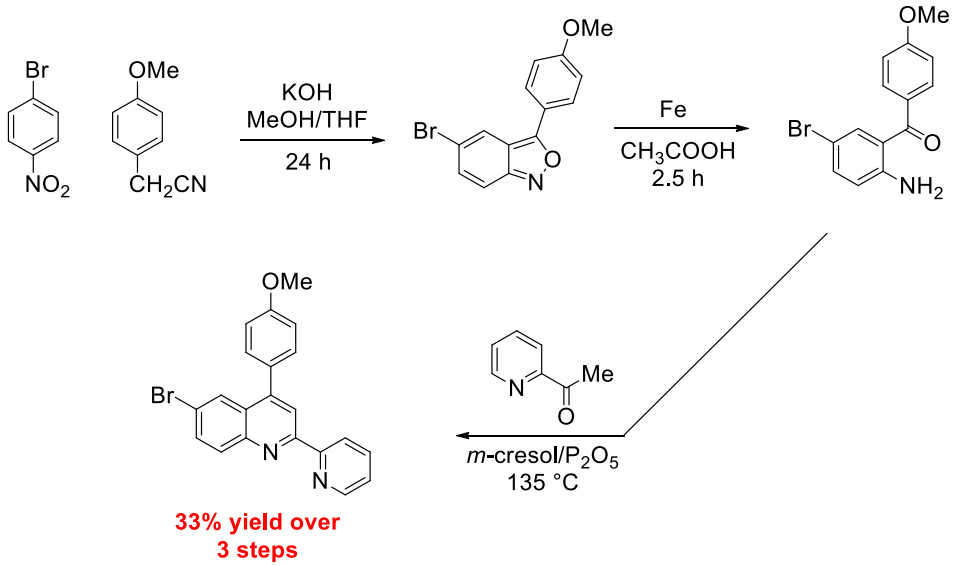

Scheme 2.10 Precedent for substituted 2-(2'-pyridyl)quinolines gives low yield and requires multiple steps

The other common approach for accessing 2-(2´-pyridyl)quinolines is via cross-coupling reactions, which directly connects the pyridine group at the 2-position of a pre-formed quinoline ring (**Scheme 2.11)**.[25] Although this method generally results in high yields, there is the requirement of using a metal catalyst and coupling partner, which in the shown example is a stannylpyridine.

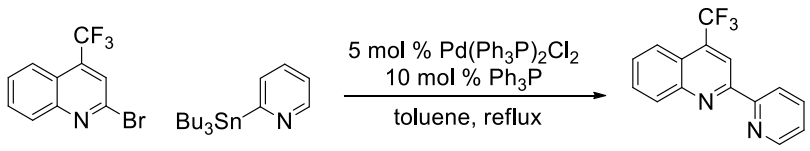

Scheme 2.11 Direct synthesis of 2-(2'-pyridyl)quinoline performed by Stille cross-coupling

The alkyl-tin byproduct is undesirable due to its toxicity and practically ensures the resulting compound would be disqualified from any therapeutic applications. Furthermore, if the quinoyl- half of the molecule contains any halogen substituents, there would be competition at that position as well as the desired 2-position of the quinoline.

Using 2,2´-bipyridine as the model system, forming a quinoline using the method developed by the Larsen group would entail replacing benzaldehyde with the heteroaromatic analogue, 2-pyridinecarboxaldehyde. However, incorporating heteroaromatic substrates into existing methodologies is often not as simple as switching starting materials. When nitrogen heterocycles are present, there is the possibility of the reagent functioning as a base, nucleophile, or ligand. This was illustrated when the copper (II) triflate catalyzed three-component coupling of aniline, 2-pyridinecarboxaldehyde, and phenylacetylene (a reaction which had been able to incorporate many types of aldehyde and amine substrates) gave very poor yields **(Table 2.1)**.

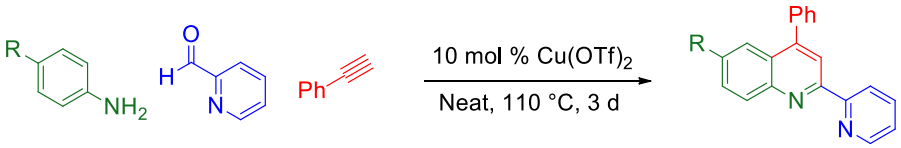

Aniline	Isolated Yield (%)
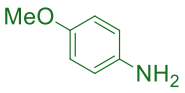	15
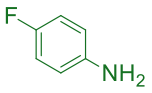	3

[a] General conditions: 0.5 mmol scale; aniline 1.0 equiv.; alkyne and aldehyde 1.2 equiv.

Table 2.1 Low isolated yields of 2-(2'-pyridyl)quinolines using copper (II) triflate catalyst[a]

Using a copper (II) catalyst had shown great effectiveness in past methodologies, however in this case, the combination of an electrophilic metal and a product which will function as a metal chelate is problematic. Copper (II) complexes with both 2,2´-bipyridine (bpy) and pyridylquinoline (PQ) ligands have been well studied, so it is not surprising that our 4-phenyl-2-(2´-pyridyl)quinoline (PyQuin) ligands would form a metal complex with the catalyst.[26] As the initial proparylamine product (formed from the condensation and subsequent nucleophilic attack by the metal acetylide) converts to the pyridylquinoline, it binds to the copper (II) triflate thus inhibiting any further reactivity.

For this reason, a catalyst that could facilitate the condensation and cyclization to form the 4-phenyl-2-(2´-pyridyl)quinoline (PyQuin) compounds but would also not cause product binding inhibition was necessary. Lewis acids were screened and while some did not cause as severe of a decrease yield, it was determined that

Brønsted-Lowry would be preferable. The use of Brønsted-Lowry acids to promote quinoline formation is well precedented; all the discussed methods for quinoline synthesis have been shown to be catalyzed with both Lewis and Brønsted-Lowry acids. When determining the most effect acid catalyst, GC chromatography was used to observe disappearance of alkyne, as initial imine formation requires no catalyst and will happen at ambient conditions. The activation of the imine/alkyne to cyclize and form the quinoline was found to be catalyzed best with Triflic Acid (TfOH) in a 10 mol % catalyst loading. Using this organic acid, a library of substituted 4-phenyl-2-(2´-pyridyl)quinolines was synthesized (**Table 2.2)**.

These novel compounds were isolated in moderately low yields (>50%), however the facile nature of this reaction makes up for the low conversion to product. Requiring no solvent, inert atmosphere, or additives, the three inexpensive and commercially available starting materials are converted to a product which generally requires much more/complicated synthetic steps. In addition to this, the isolation is a simple plug filtration through basic alumina with ether, concentration of the solution, and rinsing the collected solids with cold hexanes. This method gives spectroscopically clean product for every PyQuin listed in **Table 2.2**. If these PyQuins were to be tested for bioactivity, they were recrystallized from a hexanes/ether solution before being submitted (this will be discussed in a later chapter).

Table 2.2 Isolated yields of one-step synthesis of 2-(2'-pyridyl)quinolines (PyQuins)[a]

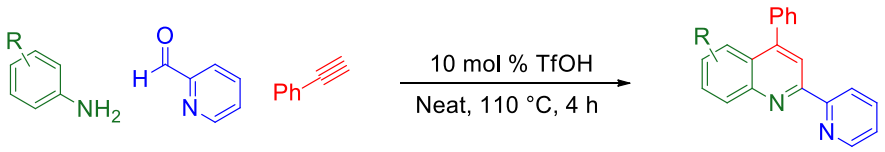

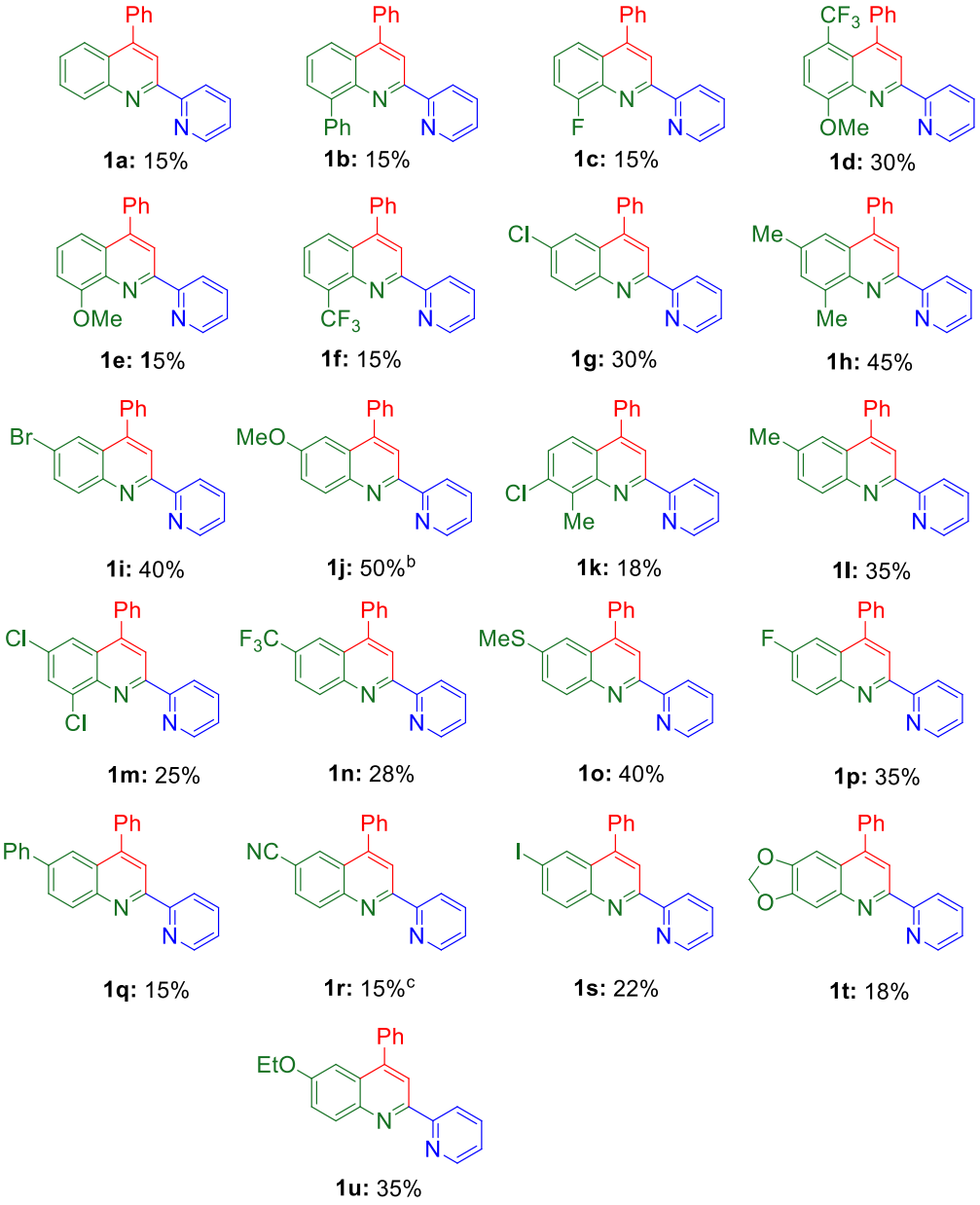

[a]General conditions: 2 mmol scale; aniline, 1.0 equiv.; alkyne and aldehyde, 1.2 equiv.
[b]Yield 42% when run at 10 mmol scale
[c]No reaction to product when using triflic acid; used boron trifluoride diethyerate catalyst

2.5 Alternative Syntheses of PyQuins

Triflic Acid has been shown to facilitate the reaction of many anilines, pyridine carboxaldehyde, and phenylacetylene, however certain aniline substrates are unable to participate in this process. In a similar fashion to the issues that arise with using a metal triflate as the catalyst when synthesizing ligand-type molecules, using a strong Brønsted-Lowry acid as the catalyst when using an acid-sensitive substrate requires investigation of other options. Nitriles are readily hydrolyzed to carboxylic acids in the presence of strong acid and water, so 4-aminobenzonitrile would be unviable under the triflic acid-catalyzed PyQuin synthesis methodology. With both Brønsted-Lowry acids and metal-based Lewis acids being problematic, a non-metal lewis acid is required. The Lewis acid boron trifluoride diethyl etherate ($BF_3 \cdot OEt$) can catalyze the cyclization to the 4-CN-PyQuin without hydrolyzing the nitrile in moderately low yields **(Scheme 2.12)**.

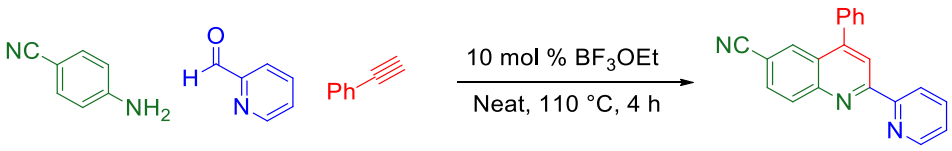

Scheme 2.12 Alternative method for PyQuin Synthesis uses $BF_3 \cdot OEt$ Catalyst

It is important to note that the nitrile in the product is a great synthetic handle for more potential chemistry: it could now be hydrolyzed to the acid without affecting

the PyQuin formation or reduction of the nitrile to the amine would allow for another condensation/cyclization to build larger molecular structures.

In an effort to streamline syntheses of interesting compounds, many groups are developing methods that solid resins as opposed to liquid or soluble catalysts. Acidic resins have shown success in aiding cyclization/heterocycle formation with other systems, so using an acidic resin to catalyze the synthesis of PyQuins could be a reasonable alternative to the acutely hazardous triflic acid.[27] Nafion, a sulfonated tetrafluoroethylene-based fluoropolymer developed by Du Pont in 1976, has been shown to catalyze many acid-catalyzed chemical transformations.[28] The combination of Nafion's high catalytic activity, its ease of separation from the crude mixture, and the potential of recycling of catalyst makes it a very attractive alternative to conventional catalysts.[29]

Initially it was believed that solvent would be necessary using Nafion as the large pellets would have difficulty functioning in a neat reaction. With acetonitrile (MeCN) as solvent, it was observed that no cyclization occurred and only imine was isolated from the reaction mixture. Under identical reaction conditions with Nafion replacing the triflic acid as catalyst and no addition of solvent, conversion of starting materials to PyQuin product was comparable. Additionally, Nafion can be recovered, washed with organic solvent, and recycled as a catalyst. This was done by soaking the Nafion pellets in a methanol/dichloromethane mixture (1:1) for 1 hour then letting them dry overnight. It was noted that while the pellets are opalescent white when taken

from a new bottle, after catalyzing the PyQuin synthesis they turned dark black in color. This color did not dissipate or dilute at all when washed and dried, so it was suspected that they would be unable to be recycled for another reaction; however, this was not the case (**Table 2.3**). The now black Nafion pellets were used over 5 reactions to catalyze the same PyQuin synthesis. It was observed that until the 4th use the catalytic activity remains unchanged. After three rounds of catalysis the activity drops off very steeply, with the 5th attempt being virtually unreactive (imine isolated, no quinoline observed). While it would be ideal if the Nafion could retain its activity over more reactions, the fact that it can be easily isolated, cleaned off, and used again is a great alternative to traditional catalysts.

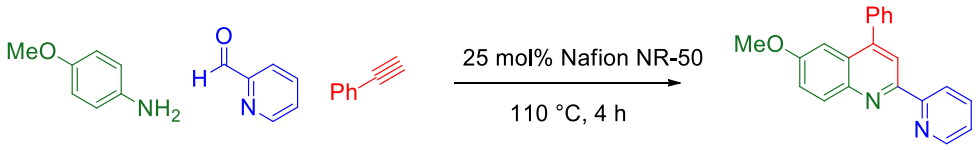

Nafion Trial	Solvent	Isolated Yield (%)
1	MeCN	45
2	Neat	43
3	Neat	45
4	Neat	13
5	Neat	0

[a] General conditions: 0.5 mmol scale; aniline 1.0 equiv.; alkyne and aldehyde 1.2 equiv.

Table 2.3 Recycling of Nafion NR-50 catalyst for synthesis of MeO-PyQuin[a]

Regardless of the method used to synthesize these PyQuins, one of the biggest draws is the modularity of the synthesis: because the aniline starting material is both cheap and available with many different substituents, the PyQuins themselves can have a range of substituents. A series of PyQuins with a range of groups from electron-donating to electron-withdrawing was compared using ^{1}H NMR (**Figure 2.2**).

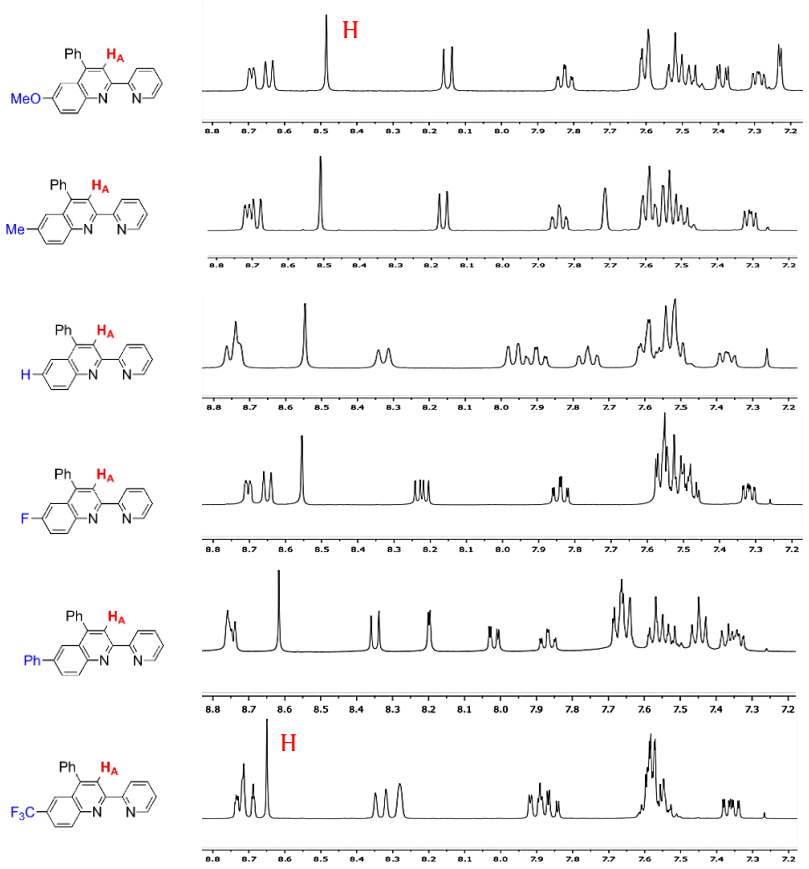

Figure 2.2 ^{1}H NMR comparison of electronically different substituted PyQuins

The effect of the group at the 6-position is evident: as the group changes from the electron-donating **MeO**- to the electron-withdrawing **CF_3-**, the

resonances shift downfield. The explicitly drawn proton **H_A** illustrates this trend well, both because of its singlet multiplicity but also with it being affected solely by the electronics, not sterics of the system. The success of altering the substituents on the aniline and having it change the PyQuin as a whole is reassuring, as conclusions can be drawn from whatever application the PyQuins are used in based on their electron richness or deficiency.

Exploring the different methods that these novel 4-phenyl-2-(2´-pyridyl)quinoline (PyQuin) compounds can be synthesized has brought insight into the reaction itself. Due to the fact that under metal-free conditions product is still formed in good yields and can be isolated, the mechanism of how the quinoline forms needed to be reproached. Initially, the copper (II) triflate catalyst formed a copper acetylide with the alkyne as the amine and aldehyde condensed. This acetylide nucleophile attacks the formed imine and, with the use of the nitrogen's lone pair of electrons, cyclization occurs and liberates the metal-alkyne coordination. With no metal to form an acetylide, this cannot be the pathway to the formation of PyQuin from imine. It is believed that the mechanism is like that of the Povarov reaction: imine forms from the condensation of amine and aryl-substituted aldehyde then the alkyne approaches the aza-diene and cyclizes in a concerted fashion (**Scheme 2.13**). The cyclized product requires oxidation to rearomatize and form the heteroaromatic quinoline which is facilitated by the air it is run under.

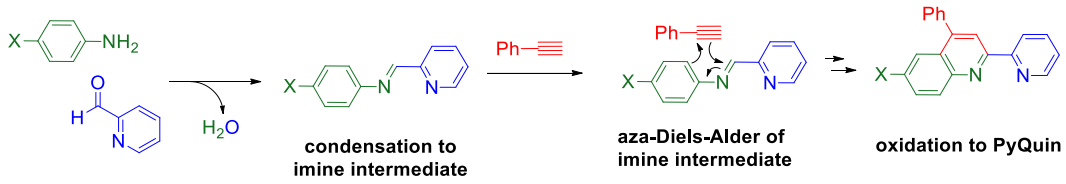

Scheme 2.13 Proposed mechanism for the formation of PyQuins involves aza-Diels-Alder due to metal-free conditions

2.6 Eli Lilly Open Innovation Drug Discovery: Bioactivity of PyQuins

The PyQuin compounds are not only structurally interesting, but they possess motifs that are present in many successful therapeutics. Often quinolines and their derivatives are quite active against malaria but, as mentioned earlier, there are recent reports that they have applications in other medicinal applications. To assess the therapeutic value of the different synthesized PyQuins, the Eli Lilly Open Innovation Drug Discovery program was utilized. In the interest of discovering new therapeutics for lower-cost options in low-income communities and countries, the OIDD program was developed as an accessible source for high-throughput drug bioactivity screening. Not all research groups have access to biological testing methods, so Eli Lilly provides a means for testing which, should a valuable drug target be identified, benefits both parties involved as Eli Lilly is given the first option to purchase the rights to the drug.

Upon contacting Eli Lilly for access to the OIDD program, the first step is to submit compounds for an *in silico* evaluation. When compounds are submitted

for an *in silico* screening, the OIDD platform creates a molecular descriptor profile and similarity profile of the compound structure. This essentially assess whether the compound is “drug-like” enough (see Lipinski’s Rule of Five in the Introduction) and whether the compound is novel enough. Based on a database of structures for countless therapeutics, this *in silico* screening is quite adept at selecting compounds that will be both viable candidates as well being unique from current drugs. Once screened, feedback is given to the submitter of the compound on whether or not further screening is desired. The ultimate goal of this evaluation is to maximize the chance of success for both parties, however there are some significant limitations. First, there are very strict rules on what will and will not even be considered for testing. More specifically, any compound with a metal (i.e. a metal complex) instantly fails the *in silico* screening. While this is reasonable, as many metals are quite cytotoxic, it completely shuts down the opportunity for finding metal-based therapeutics. Cisplatin, a platinum-based chemotherapy drug, wouldn’t pass this step even through it is arguably the most significant metal-based therapy on the market. Another issue that comes with the *in silico* assessment is that, should a group submit a set of compounds and synthesize more after testing has completed on the first set, the second set will almost undoubtedly fail. This is due to the “novelty” of the drug candidate being a one-time opportunity. For this reason, a full library must be submitted together since further functionalization on the compounds will likely not pass the similarity profile generated on the first compounds.

Once a compound or set of compounds pass the *in silico* evaluation, they advance to the biological evaluation process. Eli Lilly sends the submitter vials which are to be filled with 5 mg of each successful compound and shipped back. Once in Eli Lilly's hands, the compounds undergo an *in vitro* screening. This screening consists of consecutive tests which assesses not only if the submitted compound has activity, but also the potency of the drug candidate. First, primary screening assays (either phenotypic or target-based approaches) determine what, if any, maladies the compound has activity for treating. These activities can be assessed through the compound's ability to inhibit or activate biological processes depending on the disease in question. This is incredibly powerful, as one 5 mg sample can be tested for activity against significantly more diseases than would be done normally due to the high-throughput automated system Eli Lilly uses. Once the primary screening assays are completed, compounds which show good activity are then tested for their potency. If a compound is bioactive but only at high concentrations, then they are significantly less desirable than one which performs the same function at low concentrations. Due to the body's requirement of metabolizing the drug, the lowest concentration that still causes the desired effect is ideal. Once the functioning concentrations (IC_{50}, EC_{50}, etc.) of the submitted compounds are determined, they are compared to current therapeutics for their viability. Should they be competitive, secondary assays are performed to confirm the results of the primary assay. The final step of this process is advanced evaluation including *in vivo* testing, more concentration

studies, and direct collaboration with Eli Lilly. Unless a compound is deemed highly valuable, it will likely not reach this stage, however there is always the possibility; given that this program is free of charge for the group submitting the compounds, participating in the Open Innovation Drug Discovery program has very few downsides.

For the first step, the library of 4-phenyl-2-(2´-pyridyl)quinolines (**Table 2.2**) was submitted to the *in silico* screening. In total, 19 PyQuins were submitted and, of those 19, six were progressed to the biological assay stage (**Table 2.4**).

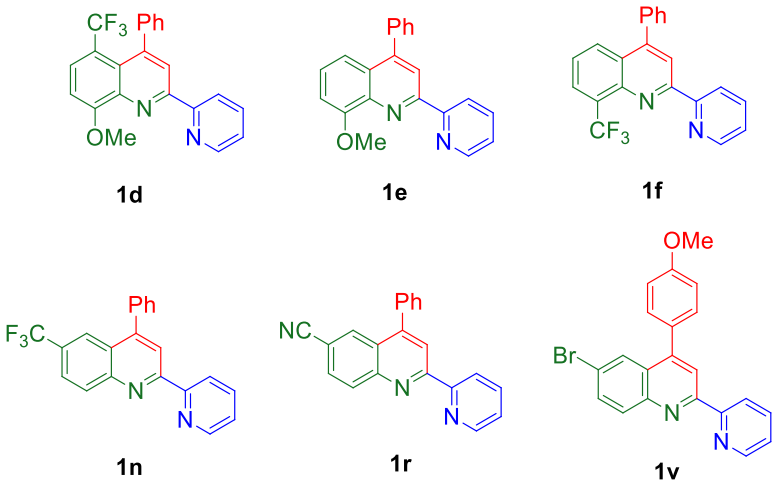

Table 2.4 PyQuins which passed the Eli Lilly OIDD's *in silico* evaluation

One compound, the 6-bromo-4-(4-methoxyphenyl)-2-2´-pyridyl)quinoline (**Xf**) was actually a PyQuin that had yet to be synthesized, as it uses 4-ethynylanisole as the alkyne instead of the usual phenylacetylene. This illustrates the benefit of an

in silico primary screening, as compounds which pass can be synthesized as opposed to the inverse order, saving time and money. Another benefit is that from the *in silico* evaluation alone a preliminary structure-activity relationship (SAR) can be constructed. Based on the PyQuins that passed, it is clear that having polar substituents (like MeO- and CF_3- groups) at the 6- and 8-position makes the PyQuin more drug-like.

With these results, Eli Lilly requested the six PyQuins for further testing. Per the instructions received with the shipping materials, each compound was to be re-synthesized and recrystallized to ensure purity. After isolating and purifying the six compounds, they were submitted back to Eli Lilly and underwent the primary assays. In the case of the PyQuins, eleven primary assays were selected by Eli Lilly based on the molecular descriptor profile generated in the *in silico* screening; these assays determine activity for maladies for which novel therapeutics are still being developed:[30] N′-Nicotinamide Methyltransferase (NNMT) inhibition, Interleukin 17A Proton Pump inhibition, KCNQ2-3 agonist, Tau protein inhibition, Na_v antagonist, Malaria, CD73 inhibition, Glucagon-like Peptide-1 secretion (Sec) and positive allosteric modulation (PAM), G-protein coupled receptor 120 (GPR120) agonist, and Tuberculosis.

After the six PyQuins were screened for activity in the aforementioned assays, it was found that five of the six had significant therapeutic activity (**Table 2.5**).

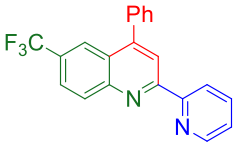

ID: 2351658014
IL-17 PP: 16.07% @ 100 uM
Malaria: 21.91% inhib @ 12.5 uM

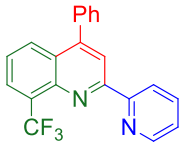

ID: 2351658015
Malaria: 33.81% inhib @ 12.5 uM

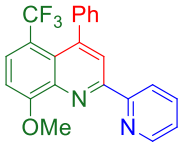

ID:2351658016
Tau: 93.36% inhib @ 40 uM
Tuberculosis: 57.2% inhib @ 20 uM
GLP1-Sec: 57.04% stim @ 20 uM
mSTC-1 GLP1-Sec EC50: 25.92 uM
GLP-1R PAM: 14.81% stim @ 20 uM

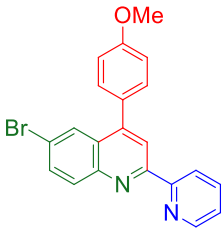

ID: 2351658019
KCNQ2-3 Agonist: 9.557% stim @ 10 uM

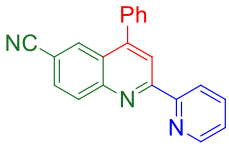

ID: 2351658020
CD73: 7.895@ inhib @ 50 uM
GLP- 1R PAM: 29.97% stim @ 20 uM
GLP-1R PAM EC50: >29.83 uM

Table 2.5 Results of the Bioactivity Evaluation for the submitted PyQuins

It is impressive that five of the six submitted PyQuins showed activity against at least one disease, as it validates the effectiveness of the *in silico* screening to detect bioactive compounds. Due to the small sample size, it is difficult to construct an SAR for these compounds and their therapeutic activity, although as mentioned earlier the presence of polar substituents definitely contributes to their drug-likeness. While much of the data collected showed that the PyQuins had activity below the threshold required for further testing, the 6-CN-PyQuin and 5-CF_3-8-MeO-PyQuin both showed activity that advanced them to the second level of testing. The 6-CN-PyQuin gave enough stimulation for the glucagon-like peptide-1 positive allosteric modulator at 20 uM that a potency assay was run to see the required concentration to achieve the necessary $EC_{50,}$ or half the

maximal response. While the EC_{50} was higher than allowed for further testing, the fact that the PyQuin made it to the second round is encouraging, as the general motif clearly has therapeutic value. Similarly, the 5-CF_3-8-MeO-PyQuin was advanced to the concentration round for the glucagon-like peptide-1 secretion stimulation, however was also rejected once the necessary concentration was found to be nonideal.

Glucagon-like peptide-1 (GLP1) is produced by the proglucagon gene in ileal L-cells in response to nutrient intake in the small intestine. It is responsible for many biological functions, including reducing hepatic glucose output by inhibiting glucagon release, promoting satiety in the central nervous system, and stimulating glucose-dependent insulin secretion. All of these functions are related to the mode of which type 2 diabetes affects the body, as secretion of GLP1 has been shown to be decreased in patients with this disease.[31] A current approach for the treatment of type 2 diabetes is increasing GLP1 levels, so any therapeutic that can either stimulate GLP1 secretion or inhibit GLP-1's positive allosteric modulator has high value. Interestingly, the two PyQuins with the highest therapeutic activity both were involved in the potential treatment of type 2 diabetes. Despite not being active enough for further testing, the value for being able to form a library of differently substituted heteroaromatic compounds has been clearly demonstrated. With many methods available to form potentially bioactive PyQuins and a good understanding of the mechanism by which this takes place, the next step was to utilize these unique structures. As discussed

previously, the functional backbone of a PyQuin molecule is quite similar to that of 2,2´-bipyridine, a ubiquitous ligand used in metal complexes. With literature precedent and a library of novel ligands, the exploration of gold (III) complexes with 4-phenyl-2-(2´-pyridyl)quinolines was commenced.

2.7 References:

1) (a) Kaur, K.; Jain, M.; Reddy, R.; Jain, R. *Eur. J. Med. Chem*. **2010**, *45*, 3245; (b) Jain, M.; Vangapandu, S.; Sachdeva, S.; Singh, S.; Singh, P. P.; Jena, G. B.; Tikoo, K.; Ramarao, P.; Kaul, C. L.; Jain, R. *J. Med. Chem*. **2004**, *47*, 285; (c) Raynes, K. *Int. J. Parasitology* **1999**, *29*, 367; (d) Raynes, K.; Foley, M.; Tilley, L.; Deady, L. W. *Biochemical Pharmacology* **1996**, *52*, 551.

2) (a) Borthwick, A. D. *Chem. Rev.* **2012**, *112*, 3641; (b) Wang, Y.; Ai, J.; Wang, Y.; Chen, Y.; Wang, L.; Liu, G.; Geng, M.; Zhang, A. *J. Med. Chem.* **2011**, *54*, 2127.

3) Staines, H. M., Krishna, S., Eds.; *Milestones in Drug Therapy*; Springer: Basel, **2012**.

4) Skraup, Z. H. *Ber. Dtsch. Chem. Ges.* **1880**, *13*, 2086.

5) Manske, R. H. *Chem. Rev.* **1942**, *30* (1), 113–144.

6) Doebner, O.; Von Miller, W. *Ber. Dtsch. Chem. Ges.* **1881**, *14*, 2812.

7) Reddy, P. V. N.; Banerjee, B.; Cushman, M. *Org. Lett.* **2010**, *12* (13), 3112.

8) Denmark, S. E.; Venkatraman, S. *J. Org. Chem.* **2006**, *71* (4), 1668.

9) Friedländer, F. *Ber. Dtsch. Chem. Ges*. **1882**, *15*, 2572.

10) Corey, E. J.; Tramontano, A. *J. Am. Chem. Soc.* **1981**, *103* (18), 5599.

11) Marco-Contelles, J.; Pérez-Mayoral, E.; Samadi, A.; Carreiras, M. do C.; Soriano, E. *Rev.* **2009**, *109* (6), 2652.

12) Smith, L. I.; Opie, J. W. *Org. Synth.* **1948**, *28*, 11.

13) Combes, A. *Bull. Soc. Chim. Fr.* **1883**, *49*, 89.

14) Sloop, J. C. *J. Phys. Org. Chem.* **2009**, *22* (2), 110.

15) Povarov, L. S.; Mikhailov, B. M. *Izv. Akad. Nauk SSR, Ser. Khim*. **1963**, 953.

16) Truong, P. M.; Mandler, M. D.; Zavalij, P. Y.; Doyle, M. P. *Org. Lett.* **2013**, *15* (13), 3278.

17) Kobayashi, S.; Ishitani, H.; Nagayama, S. *Synthesis,* **1995,** 1195.

18) Katritzky, A.R.; Rachwal, B.; Rachwal, S. *J. Org. Chem.* **1995**, *60*, 3993.

19) (a) Powell, D.A.; Batey, R.A. *Org. Lett*. **2002**, *4*, 2913. (b) Batey, R. A.; Powell, D. A. *J. Chem. Soc., Chem. Comm*. **2001,** 2362. (c) P.; Lough, A. J. *J. Chem. Soc., Chem. Comm.* **1999,** 651. (d) Xia, C. F.; Heng, L. S.; Ma, D.W.; *Tet. Lett.* **2002**, *43*, 9405.

20) Meyet, C. E.; Pierce, C. J.; Larsen, C. H*. Org. Lett*. **2012**, *14*, 964.

21) Meyet, C. E.; Larsen, C. H. *J. Org. Chem.* **2014**, *79*, 9835.

22) Kaes, C.; Katz, A.; Hosseini, M. W. *Chem. Rev.* **2000**, *100* (10), 3553.

23) Smirnoff, A. P. *Helv. Chim. Acta* **1921**, *4,* 802.

24) Mamo, A.; Aureliano, A.; Recca, A. *Molecules* **2010**, *15*, 1324; (b) Mamo, A.; Nicoletti, S.; Tat, N. C. *Molecules* **2002**, *7*, 618; (c) Campagna, S.; Mamo, A.; Stille, J. K. J. C. S. *Dalton* **1991**, 2545.

25) (a) Dick, G. R.; Woerlv, E. M.; Burke, M. D. *Angew. Chem. Int. Ed.* **2012**, *51*, 2667; (b) Michel, B. W.; Steffens, L. D.; Sigman, M. S. *J. Am. Chem. Soc*. **2011**, *133*, 8317; (c) Verniest, G.; Wang, X.; De Kimpe, N.; Padwa, A. *J. Org. Chem.* **2010**, *75*, 424; (d) Jones, N. A.; Antoon, J. W.; Bowie, A. L.; Borak, J. B.; Stevens, E. P. J. *Heterocyclic Chem.* **2007**, *44*, 363; (e) Kimber, M.; Anderberg, P. I.; Harding, M. M. *Tetrahedron* **2000**, *56*, 3575.

26) Muthuramalingam, S.; Khamrang, T.; Velusamy, M.; Mayilmurugan, R. *Dalton Trans.* **2017**, *46* (46), 16065.

27) Xu, L.; Yuan, S.; Li, Z. *J. Heterocyclic Chem.* **2010,** *47*, 446*.*

28) (a) Olah, G. A.; Mathew, T.; Prakash, G. K. S. *Chem. Commun*. **2001**, 1696; (b) Prakash, G. K. S.; Mathew, S. K.; Krishnaraj, S.; Marinez, E. R.; Olah, G. A. *Appl. Catal., A: General* **1999**, *181*, 283; (c) Hachoumy, M.; Mathew, T.; Tongo, E. C.; Vankar, Y. D.; Prakash, G. K. S.; Olah, G. A. *Synlett* ***1*999**, 363; (d) Yamato, T.; Hideshima, C.; Prakash, G. K. S.; Olah, G. A. *J. Org. Chem.* **1991**, *56*, 3192; (e) Olah, G. A.; Iyer, P. S.; Prakash, G. K. S. *Synthesis* **1986**, 513.

29) Stanescu, M. A.; Varma, R. S. *Tet. Lett.* **2002**, *43* (41), 7307.

30) (a) Neelakantan, H.; Wang, H.-Y.; Vance, V.; Hommel, J. D.; McHardy, S. F.; Watowich, S. J *J. Med. Chem.* **2017**, *60* (12), 5015. (b) Luchetti, M. M.; Benfaremo, D.; Gabrielli, A. *Curr. Pharm. Biotech.* **2018**, *18* (12), 989. (c) Manville, R. W.; Abbott, G. W. *Mol. Pharmacol.* **2018**, *94* (4), 1155. (d) Berrocal, M.; Corbacho, I.; Vázquez-Hernández, M.; Ávila, J.; Sepúlveda, M. R.; Mata, A. M. *BBA – Molecular Basis of Disease* **2015**, *1852* (7), 1465. (e) Joca, H. C.; Vieira, D. C. O.; Vasconcelos, A. P.; Araújo, D. A. M.; Cruz, J. S *Eur. J. Pharmacol.* **2015**, *756*, 22. (f) Deitsch, K. W.; Chitnis, C. E. *PNAS* **2012**, *109* (26), 10130. (g) Dumontet, C.; Peyrottes, S.; Rabeson, C.; Cros-Perrial, E.; Géant, P. Y.; Chaloin, L.; Jordheim, L. P. *Eur. J. Med. Chem.* **2018**, *157*, 1051–1055. (h) Goldenberg, R. *Curr. Med. Res. Opin.* **2014**, *30* (3), 431. (i) (1) Zhang, O. & G. H.; Yu, Y.-Y.; Chen, C.; Kong, F*. Drug Des. Dev. Ther.* **2014**, 2423. (j) Liu, Z.; Dong, Z.; Qiu, P.; Wang, Q.; Yan, J.; Lu, Y.; Wasu, P.; Hong, K.; She, Z. *Steroids* **2018**, *140*, 32.

31) Lee, S.; Lee, D. Y. *Ann. Pediatr. Endocrinol. Metab.* **2017**, *22* (1), 15.

2.8 Supporting Information:

General analytical information

^{1}H and ^{13}C NMR spectra were measured on a Varian Inova 500 (500 MHz) spectrometer using acetone-d_6 or $CDCl_3$ as solvents and tetramethylsilane as an internal standard. The following abbreviations are used singularly or in combination to indicate the multiplicity of signals: s - singlet, d - doublet, t - triplet, q - quartet, qn - quintet, sx - sextet, sp - septet, m - multiplet and br - broad. NMR spectra were acquired at 300 K. Gas chromatography (GC) was carried out on an Agilent Technologies 6850 Network GC System, and dodecane was used as the internal standard. ATR-IR spectra were taken on a Bruker:ALPHA FTIR Spectrometer. Attenuated total reflection infrared (ATR-IR) was used and the spectra was analyzed using the OPUS software with selected absorption maxima reported in wavenumbers (cm^{-1}). Mass spectrometric data was collected on a HP 5989A GC/MS quadrupole instrument. Exact masses were recorded on a Waters GCT Premier TOF instrument using direct injection of samples in methanol/acetonitrile into the electrospray source.

General Procedure for 4-phenyl-2-(2'-pyridyl)quinolines (PyQuins)

For synthesizing R-PyQuin, the corresponding substituted R-aniline (1 equiv.), 2-pyridinecarboxaldehyde (1.2 equiv), phenylacetylene (1.2 equiv.), and trifluoromethanesulfonic acid (10 mol %) are stirred together at 110˚C for 4h; the reaction turns jet black upon addition of acid catalyst. After 4 hours, the reaction

is cooled and, if let sit at room temperature, will solidify. Minimal methylene chloride is to be added when reaction is no longer hot but also not completely cool to solubilize the crude reaction mixture. The crude mixture in dichloromethane is loaded onto a basic alumina plug in a sintered glass funnel and eluted with diethyl ether. The collected filtrate is deep orange in color and is concentrated to give a dark colored solid. Cold hexanes is used to rinse the solid which removes the color impurity as well as excess phenylacetylene, yielding spectroscopically clean product without the need for column chromatography.

4-phenyl-2-(2'-pyridyl)quinoline (1a)

Aniline (91 µL, 1 mmol), 2-pyridinecarboxaldehyde (114 µL, 1.2 mmol), phenylacetylene (132 µL, 1.2 mmol), trifluoromethanesulfonic acid (9 µL, 10 mol%) were stirred at 110˚C for 4h to afford the title compound as a light beige/white solid in 15% yield (0.029 g, 0.1 mmol) after flushing through a basic aluminum oxide plug with 100% diethyl ether, removing solvent *in vacuo*, and rinsing solid with cold hexanes. ^{1}H NMR (300 MHz, $CDCl_3$, 25˚C) δ 8.74 (t, J = 5.1 Hz, 2H), 8.55 (s, 1H), 8.33 (d, J = 8.4 Hz, 1H), 8.01-7.85 (m, 2H), 7.76 (t, J = 7.1 Hz, 1H), 7.65-7.45 (m, 6H), 7.37 (dd, J = 7.3, 5.7 Hz, 1H). ^{13}C NMR (75 MHz, CDCl3, 25˚C) δ 156.04, 155.48, 149.83, 149.28, 148.24, 138.38, 137.21, 130.05, 129.80, 128.63, 128.55, 127.08, 126.92, 125.99, 124.33, 122.27, 119.48.

4,8-diphenyl-2-(2'-pyridyl)quinoline (1b)

2-aminobiphenyl (169 mg, 1 mmol), 2-pyridinecarboxaldehyde (114 µL, 1.2 mmol), phenylacetylene (132 µL, 1.2 mmol), trifluoromethanesulfonic acid (9 µL, 10 mol%) were stirred at 110˚C for 4h to afford the title compound as a light beige solid in 15% yield (0.157 g, 0.44 mmol) after flushing through a basic aluminum oxide plug with 100% diethyl ether, removing solvent *in vacuo*, and rinsing solid with cold hexanes. IR (crystal) 3055, 1587, 1488, 769, 692 cm^{-1}. HRMS (ESI) *m/z* calcd for $[M+H]^+$ $C_{26}H_{19}N_2$ requires 359.1543, found 359.1559. ^1H NMR (400 MHz, $CDCl_3$, 25˚C) δ 8.73-8.67 (m, 1H), 8.65 (s, 1H), 8.52 (d, J = 8.0 Hz, 1H), 7.98 (dd, J = 8.4, 1.2 Hz, 1H), 7.95-7.87 (m, 2H), 7.84-7.76 (m, 2H), 7.68-7.47 (m, 9H), 7.34-7.28 (m, 1H). ^{13}C NMR (100 MHz, CDCl3, 25˚C) δ 156.57, 154.78, 149.60, 148.98, 145.90, 141.28, 140.06, 138.88, 136.97, 131.33, 130.30, 129.83, 128.56, 128.35, 127.76, 127.37, 127.23, 126.62, 125.63, 124.02, 122.16, 118.90.

8-fluoro-4-phenyl-2-(2'-pyridyl)quinoline (1c)

2-fluoroaniline (387 µL, 4 mmol), 2-pyridinecarboxaldehyde (457 µL, 4.8 mmol), phenylacetylene (521 µL, 4.8 mmol), trifluoromethanesulfonic acid (35 µL, 10 mol%) were stirred at 110˚C for 4h to afford the title compound as a light beige solid in 15% yield (0.079 g, 0.26 mmol) after flushing through a basic aluminum oxide plug with 100% diethyl ether, removing solvent *in vacuo*, and rinsing solid with cold hexanes. IR (crystal) 3058, 1588, 1488, 1403, 1245, 1071, 756, 702

cm^{-1}. HRMS (ESI) *m/z* calcd for [M+H]+ $C_{20}H_{14}N_2F$ requires 300.1057, found 300.1063. ^1H NMR (400 MHz, $CDCl_3$, 25˚C) δ 8.77 (dd, J = 8.0, 0.9 Hz, 1H), 8.73-8.68 (m, 1H), 8.61 (s, 1H), 7.93-7.84 (m, 1H), 7.75-7.69 (m, 1H), 7.60-7.48 (m, 5H), 7.44-7.34 (m, 3H). ^{19}F NMR (376 MHz, $CDCl_3$) δ -124.71 – -124.82 (m). ^{13}C NMR (100 MHz, $CDCl_3$, 25˚C) δ 159.93, 157.38, 156.03, 155.78, 149.34, 149.21, 138.21, 137.15, 129.71, 128.65, 126.40, 126.32, 124.45, 122.31, 121.66, 120.20, 113.65, 113.46.

8-methoxy-4-phenyl-2-(2'-pyridyl)-5-(trifluoromethyl)quinoline (1d)

2-methoxy-5-(trifluoromethyl)aniline (382 mg, 2 mmol), 2-pyridinecarboxaldehyde (228 µL, 2.4 mmol), phenylacetylene (264 µL, 2.4 mmol), trifluoromethanesulfonic acid (18 µL, 10 mol%) were stirred at 110˚C for 4h to afford the title compound as a light beige solid in 30% yield (0.174 g, 0.46 mmol) after flushing through a basic aluminum oxide plug with 100% diethyl ether, removing solvent *in vacuo*, and rinsing solid with cold hexanes. IR (crystal) 3050, 2965, 1588, 1553, 1457, 1319, 1230, 1119, 700 cm^{-1}. HRMS (ESI) *m/z* calcd for $[M+H]^+$ $C_{22}H_{16}N_2OF_3$ requires 381.1209, found 381.1197. ^1H NMR (400 MHz, $CDCl_3$, 25˚C) δ 8.70 (d, J = 7.9 Hz, 1H), 8.65 (dd, J= 2.8, 2.0 Hz, 1H), 8.50 (s, 1H), 7.89 (d, J = 8.5 Hz, 1H), 7.82 (td, J = 7.7, 1.8 Hz, 1H), 7.39 (s, 5H), 7.29 (ddd, J = 7.5, 4.8, 1.1 Hz, 1H), 7.01 (d, J = 8.4 Hz, 1H), 4.12 (s, 3H). ^{19}F NMR (376 MHz, $CDCl_3$, 25˚C) δ -52.78 (s). ^{13}C NMR (100 MHz, $CDCl_3$, 25˚C) δ

158.73, 155.46, 153.92, 149.21, 149.06, 141.34, 136.99, 129.42, 129.03, 128.96, 127.99, 127.82, 127.32, 125.28, 125.00, 124.33, 122.56, 122.20, 105.67, 56.51.

8-methoxy-4-phenyl-2-(2'-pyridyl)quinoline (1e)

o-anisidine (1.1 mL, 10 mmol), 2-pyridinecarboxaldehyde (1.3 mL, 12 mmol), phenylacetylene (1.3 mL, 12 mmol), trifluoromethanesulfonic acid (89 µL, 10 mol%) were stirred at 110˚C for 4h to afford the title compound as a light beige solid in 15% yield (0.061 g, 0.20 mmol) after flushing through a basic aluminum oxide plug with 100% diethyl ether, removing solvent *in vacuo*, and rinsing solid with cold hexanes. IR (crystal) 3067, 3017, 1588, 1452, 1402, 1260, 1094, 739, 697 cm^{-1}. HRMS (ESI) *m/z* calcd for $[M+H]^+$ $C_{21}H_{17}N_2O$ requires 313.1336, found 313.1342. ^1H NMR (400 MHz, $CDCl_3$, 25˚C) δ 8.75 (d, J = 8.0 Hz, 1H), 8.71-8.67 (m, 1H), 8.55 (s, 1H), 7.86 (td, J = 7.7, 1.7 Hz, 1H), 7.58 (dd, J = 8.0, 1.4 Hz, 2H), 7.54-7.43 (m, 4H), 7.40 (t, J = 8.1 Hz, 1H), 7.32 (dd, J = 6.6, 5.2 Hz, 1H), 7.08 (d, J = 7.6 Hz, 1H), 4.13 (s, 3H). ^{13}C NMR (100 MHz, $CDCl_3$, 25˚C) δ 156.48, 155.90, 154.55, 149.40, 149.13, 140.51, 138.76, 137.02, 129.75, 128.49, 128.34, 128.06, 126.91, 124.06, 122.30, 119.94, 117.84, 107.93, 56.39.

4-phenyl-2-(2'-pyridyl)-8-(trifluoromethyl)quinoline (1f)

2-(trifluoromethyl)aniline (251 µL, 2 mmol), 2-pyridinecarboxaldehyde (228 µL, 2.4 mmol), phenylacetylene (264 µL, 2.4 mmol), trifluoromethanesulfonic acid (18 µL, 10 mol%) were stirred at 110˚C for 4h to afford the title compound as a light

beige solid in 15% yield (0.133 g, 0.38 mmol) after flushing through a basic aluminum oxide plug with 100% diethyl ether, removing solvent *in vacuo*, and recrystallizing from diethyl ether. IR (crystal) 3062, 1588, 1560, 1306, 1121, 768, 698 cm^{-1}. HRMS (ESI) *m/z* calcd for $[M+H]^+$ $C_{21}H_{14}N_2F_3$ requires 351.1104, found 351.1122. ^1H NMR (400 MHz, $CDCl_3$, 25˚C) δ 8.84 (d, *J* = 8.0 Hz, 1H), 8.73 – 8.69 (m, 1H), 8.68 (s, 1H), 8.12 (dd, *J* = 13.9, 7.8 Hz, 2H), 7.91 (td, *J* = 7.7, 1.7 Hz, 1H), 7.61 – 7.46 (m, 6H), 7.37 (ddd, *J* = 7.4, 4.8, 1.0 Hz, 1H). ^{19}F NMR (376 MHz, $CDCl_3$) δ -60.23 (s). ^{13}C NMR (100 MHz, $CDCl_3$, 25˚C) δ 155.90, 155.85, 149.68, 149.13, 144.98, 138.03, 137.27, 130.42, 129.79, 128.74, 128.10, 128.04, 127.38, 125.89, 125.27, 124.62, 123.16, 122.56, 119.75.

6-chloro-4-phenyl-2-(2'-pyridyl)quinoline (1g)

4-chloroaniline (255 mg, 2 mmol), 2-pyridinecarboxaldehyde (228 µL, 2.4 mmol), phenylacetylene (264 µL, 2.4 mmol), trifluoromethanesulfonic acid (18 µL, 10 mol%) were stirred at 110˚C for 4h to afford the title compound as a white solid in 30% yield (0.190 g, 0.60 mmol) after flushing through a basic aluminum oxide plug with 100% diethyl ether, removing solvent *in vacuo*, and rinsing solid with cold hexanes. IR (crystal) 3059, 1587, 1485, 699 cm^{-1}. HRMS (ESI) *m/z* calcd for $[M+H]^+$ $C_{20}H_{14}N_2Cl$ requires 317.0840, found 317.0849. ^1H NMR (400 MHz, $CDCl_3$, 25˚C) δ 8.70 (d, *J* = 3.9 Hz, 1H), 8.65 (d, *J* = 7.9 Hz, 1H), 8.55 (s, 1H), 8.15 (d, *J* = 8.9 Hz, 1H), 7.91 (s, 1H), 7.84 (t, *J* = 6.9 Hz, 1H), 7.69 – 7.60 (m, 1H), 7.61 – 7.39 (m, 5H), 7.39 – 7.28 (m, 1H). ^{13}C NMR (100 MHz, $CDCl_3$, 25˚C)

δ 155.97, 155.87, 149.25, 148.50, 146.93, 137.79, 136.98, 132.76, 131.86, 130.37, 129.61, 128.76, 128.66, 127.51, 124.70, 124.26, 121.86, 120.04.

6,8-dimethyl-4-phenyl-2-(2'-pyridyl)quinoline (1h)

2,4-dimethylaniline (247 µL, 2 mmol), 2-pyridinecarboxaldehyde (228 µL, 2.4 mmol), phenylacetylene (264 µL, 2.4 mmol), trifluoromethanesulfonic acid (18 µL, 10 mol%) were stirred at 110˚C for 4h to afford the title compound as a white solid in 45% yield (0.261 g, 0.84 mmol) after flushing through a basic aluminum oxide plug with 100% diethyl ether, removing solvent *in vacuo*, and rinsing solid with cold hexanes. IR (crystal) 3059, 2910, 1588, 1557, 858, 793, 701 cm^{-1}. HRMS (ESI) *m/z* calcd for $[M+H]^+$ $C_{22}H_{19}N_2$ requires 311.1543, found 311.1557. ^1H NMR (400 MHz, $CDCl_3$, 25˚C) δ 8.89 – 8.80 (m, 1H), 8.79 – 8.71 (m, 1H), 8.62 (s, 1H), 7.84 (td, *J* = 7.8, 1.7 Hz, 1H), 7.70 – 7.60 (m, 3H),7.60 – 7.47 (m, 3H), 7.45 (s, 1H), 7.34 – 7.26 (m, 1H), 3.00 (s, 3H), 2.45 (s, 3H). ^{13}C NMR (100 MHz, $CDCl_3$, 25˚C) δ 156.81, 153.11, 148.90, 148.55, 145.97, 139.10, 137.52, 136.65, 136.25, 131.80, 129.71, 128.35, 128.01, 126.69, 123.65, 122.51, 121.60, 118.82, 21.87, 18.31.

6-bromo-4-phenyl-2-(2'-pyridyl)quinoline (1i)

4-bromoaniline (344 mg, 2 mmol), 2-pyridinecarboxaldehyde (228 µL, 2.4 mmol), phenylacetylene (264 µL, 2.4 mmol), trifluoromethanesulfonic acid (18 µL, 10

mol%) were stirred at 110˚C for 4h to afford the title compound as a white solid in 40% yield (0.180 g, 0.50 mmol) after flushing through a basic aluminum oxide plug with 100% diethyl ether, removing solvent *in vacuo*, and rinsing solid with cold hexanes. IR (crystal) 3053, 1586, 1483, 1360, 780, 704 cm^{-1}. HRMS (ESI) *m/z* calcd for $[M+H]^+$ $C_{20}H_{14}N_2Br$ requires 361.0335, found 361.0353. ^1H NMR (400 MHz, $CDCl_3$, 25˚C) δ 8.71 (d, *J* = 4.0 Hz, 1H), 8.66 (d, *J* = 8.0 Hz, 1H), 8.55 (s, 1H), 8.10 (d, *J* = 8.9 Hz, 2H), 7.87 (td, *J* = 7.8, 1.7 Hz, 1H), 7.79 (dd, *J* = 8.9, 2.2 Hz, 1H), 7.60 – 7.47 (m, 5H), 7.39 – 7.31 (m, 1H). ^{13}C NMR (100 MHz, $CDCl_3$, 25˚C) δ 156.03, 149.32, 148.50, 147.18, 137.80, 137.06, 132.99, 132.01, 129.66, 128.81, 128.72, 128.06, 124.34, 121.94, 121.10, 120.09.

6-methoxy-4-phenyl-2-(2'-pyridyl)quinoline (1j)

p-anisidine (246 mg, 2 mmol), 2-pyridinecarboxaldehyde (228 µL, 2.4 mmol), phenylacetylene (264 µL, 2.4 mmol), trifluoromethanesulfonic acid (18 µL, 10 mol%) were stirred at 110˚C for 4h to afford the title compound as a colorless solid in 50% yield (0.265 g, 0.85 mmol) after flushing through a basic aluminum oxide plug with 100% diethyl ether, removing solvent *in vacuo*, and rinsing solid with cold hexanes. IR (crystal) 3055, 2935, 1622, 1587, 1477, 1223, 1032, 714 cm^{-1}. HRMS (ESI) *m/z* calcd for $[M+H]^+$ $C_{21}H_{17}N_2O$ requires 313.1336, found 313.1337. ^1H NMR (400 MHz, $CDCl_3$, 25˚C) δ 8.69 (d, J = 4.7 Hz, 1H), 8.64 (d, J = 8.0 Hz, 1H), 8.48 (s, 1H), 8.15 (d, J = 9.2 Hz, 1H), 7.82 (td, J = 7.7, 1.7 Hz, 1H), 7.60 (d, J = 6.9 Hz, 2H), 7.49 (dt, J = 22.2, 7.1 Hz, 3H), 7.39 (dd, J = 9.2, 2.8

Hz, 1H), 7.29 (dd, J = 6.9, 5.3 Hz, 1H), 7.23 (d, J = 2.7 Hz, 1H), 3.77 (s, 3H). ^{13}C NMR (100 MHz, $CDCl_3$, 25˚C) δ 158.20, 156.56, 153.47, 149.13, 147.84, 144.61, 138.75, 136.87, 131.75, 129.50, 128.61, 128.28, 127.77, 123.71, 121.85, 121.51, 119.60, 103.78, 55.46.

*Reaction also successful when scaled to 10 mmol scale, yield drops to 42%.

7-chloro-8-methyl-4-phenyl-2-(2'-pyridyl)quinoline (1k)

3-chloro-2-methylaniline (478 µL, 4 mmol), 2-pyridinecarboxaldehyde (457 µL, 4.8 mmol), phenylacetylene (527 µL, 4.8 mmol), trifluoromethanesulfonic acid (35 µL, 10 mol%) were stirred at 110˚C for 4h to afford the title compound as a colorless solid in 18% yield (0.265 g, 0.85 mmol) after flushing through a basic aluminum oxide plug with 100% diethyl ether, removing solvent *in vacuo*, and rinsing solid with cold hexanes. IR (crystal) 3058, 2923, 1592, 1574, 1440, 761, 699 cm^{-1}. HRMS (ESI) *m/z* calcd for $[M+H]^+$ $C_{21}H_{16}N_2Cl$ requires 331.0997, found 331.1003. ^{1}H NMR (400 MHz, $CDCl_3$, 25˚C) δ 8.75 (d, *J* = 8.0 Hz, 1H), 8.72 – 8.67 (m, 1H), 8.54 (s, 1H), 7.85 (td, *J* = 7.7, 1.8 Hz, 1H), 7.70 (d, *J* = 9.0 Hz, 1H), 7.56 – 7.45 (m, 5H), 7.42 (d, *J* = 9.0 Hz, 1H), 7.32 (ddd, *J* = 7.4, 4.8, 1.0 Hz, 1H), 3.03 (s, 3H). ^{13}C NMR (100 MHz, $CDCl_3$, 25˚C) δ 156.36, 154.90, 149.63,149.10, 147.84, 138.42, 136.90, 135.40, 134.94, 129.74, 128.57, 128.44, 127.88, 125.33, 124.22, 124.18, 121.94, 118.79, 14.96.

6-methyl-4-phenyl-2-(2'-pyridyl)quinoline (1l)

p-toluidine (429 mg, 4 mmol), 2-pyridinecarboxaldehyde (457 µL, 4.8 mmol), phenylacetylene (527 µL, 4.8 mmol), trifluoromethanesulfonic acid (35 µL, 10 mol%) were stirred at 110˚C for 4h to afford the title compound as a white solid in 35% yield (0.328 g, 1.12 mmol) after flushing through a basic aluminum oxide plug with 100% diethyl ether, removing solvent *in vacuo*, and rinsing solid with cold hexanes. IR (crystal) 3047, 2920, 1587, 1490, 765, 699 cm^{-1}. HRMS (ESI) *m/z* calcd for $[M+H]^+$ $C_{21}H_{17}N_2$ requires 297.1386, found 297.1400. ^1H NMR (400 MHz, $CDCl_3$, 25˚C) δ 8.75 – 8.65 (m, 2H), 8.51 (s, 1H), 8.17 (d, J = 8.6 Hz, 1H), 7.84 (ddd, J = 9.6, 1.7, 0.8 Hz, 1H), 7.71 (s, 1H), 7.63 – 7.45 (m, 6H), 7.34 – 7.27 (m, 1H), 2.47 (s, 3H). ^{13}C NMR (100 MHz, $CDCl_3$, 25˚C) δ 156.51, 154.79, 149.15, 148.54, 147.11, 138.64, 136.89, 136.84, 131.70, 129.98, 129.69, 128.50, 128.23, 126.75, 124.60, 123.89, 121.74, 119.35, 21.92.

6,8-dichloro-4-phenyl-2-(2’pyridyl)quinoline (1m)

2,4-dichloroaniline (324 mg, 2 mmol), 2-pyridinecarboxaldehyde (228 µL, 2.4 mmol), phenylacetylene (264 µL, 2.4 mmol), trifluoromethanesulfonic acid (18 µL, 10 mol%) were stirred at 110˚C for 4h to afford the title compound as a white solid in 25% yield (0.177 g, 0.50 mmol) after flushing through a basic aluminum oxide plug with 100% diethyl ether, removing solvent *in vacuo*, and rinsing solid with cold hexanes. IR (crystal) 3058, 1587, 1477, 1359, 1154, 782, 699 cm^{-1}. HRMS (ESI) *m/z* calcd for $[M+H]^+$ $C_{20}H_{13}N_2Cl_2$ requires 351.0451, found

351.0455. ^{1}H NMR (400 MHz, $CDCl_3$, 25˚C) δ 8.82 (d, *J* = 8.0 Hz, 1H), 8.70 (ddd, *J* = 4.7, 1.6, 0.8 Hz, 1H), 8.63 (s, 1H), 7.90 (td, *J* = 7.7, 1.8 Hz, 1H), 7.83 (dd, *J* = 5.5, 2.2 Hz, 2H), 7.60 – 7.47 (m, 5H), 7.37 (ddd, *J* = 7.5, 4.8, 1.2 Hz, 1H). ^{13}C NMR (100 MHz, $CDCl_3$, 25˚C) δ 156.03, 155.66, 149.22, 143.33, 137.57, 137.19, 135.67, 131.92, 130.24, 129.66, 128.90, 128.86, 128.51, 124.64, 124.01, 122.43, 120.76.

4-phenyl-2-(2'-pyridyl)-6-(trifluoromethyl)quinoline (1n)

4-(trifluoromethyl)aniline (252 µL, 2 mmol), 2-pyridinecarboxaldehyde (228 µL, 2.4 mmol), phenylacetylene (264 µL, 2.4 mmol), trifluoromethanesulfonic acid (18 µL, 10 mol%) were stirred at 110˚C for 4h to afford the title compound as a colorless solid in 28% yield (0.137 g, 0.39 mmol) after flushing through a basic aluminum oxide plug with 100% diethyl ether, removing solvent *in vacuo*, rinsing solid with cold hexanes followed by recrystallization in 100% diethyl ether. IR (crystal) 3062, 1459, 1308, 1106, 706 cm-1. HRMS (ESI) *m/z* calcd for $[M+H]^+$ $C_{21}H_{14}N_2F_3$ requires 351.1104, found 351.1116. ^{1}H NMR (400 MHz, $CDCl_3$, 25˚C) δ 8.75 – 8.66 (m, 2H), 8.64 (s, 1H), 8.33 (d, J = 8.8 Hz, 1H), 8.27 (s, 1H), 7.94 – 7.80 (m, 2H), 7.68 – 7.44 (m, 5H), 7.35 (ddd, J = 7.5, 4.7, 1.2 Hz, 1H). 19F NMR (376 MHz, CDCl3, 25˚C) δ -62.54 (s). ^{13}C NMR (100 MHz, $CDCl_3$, 25˚C) δ 157.54, 155.66, 150.19, 149.56, 149.29, 137.50, 137.01, 131.44, 129.65, 128.88, 125.90, 125.09, 124.56, 123.91, 123.87, 122.09, 120.37.

6-(methylthio)-4-phenyl-2-(2'-pyridyl)quinoline (1o)

4-(methylthio)aniline (249 µL, 2 mmol), 2-pyridinecarboxaldehyde (228 µL, 2.4 mmol), phenylacetylene (264 µL, 2.4 mmol), trifluoromethanesulfonic acid (18 µL, 10 mol%) were stirred at 110˚C for 4h to afford the title compound as a white solid in 40% yield (0.236 g, 0.72 mmol) after flushing through a basic aluminum oxide plug with 100% diethyl ether, removing solvent *in vacuo*, and rinsing solid with cold hexanes. IR (crystal) 3057, 3003, 1584, 1484, 703 cm^{-1}. HRMS (ESI) *m/z* calcd for $[M+H]^+$ $C_{21}H_{17}N_2S$ requires 329.1107, found 329.1123. ^1H NMR (400 MHz, $CDCl_3$, 25˚C) δ 8.72 – 8.69 (m, 1H), 8.66 (dd, *J* = 8.0, 0.6 Hz, 1H), 8.50 (s, 1H), 8.13 (d, *J* = 8.9 Hz, 1H), 7.86 (td, *J* = 7.6, 1.2 Hz, 1H), 7.70 (d, *J* = 2.0 Hz, 1H), 7.64 – 7.46 (m, 6H), 7.33 (dd, *J* = 7.4, 4.8 Hz, 1H), 2.47 (s, 3H). ^{13}C NMR (100 MHz, $CDCl_3$, 25˚C) δ 156.40, 154.92, 149.27, 147.99, 146.83, 138.34, 137.86, 137.02, 130.53, 129.67, 128.85, 128.67, 128.50, 127.25, 124.04, 121.80, 121.00, 119.93, 15.76.

6-fluoro-4-phenyl-2-(2'-pyridyl)quinoline (1p)

4-fluoroaniline (190 µL, 2 mmol), 2-pyridinecarboxaldehyde (228 µL, 2.4 mmol), phenylacetylene (264 µL, 2.4 mmol), trifluoromethanesulfonic acid (18 µL, 10 mol%) were stirred at 110˚C for 4h to afford the title compound as a white solid in 35% yield (0.212 g, 0.71 mmol) after flushing through a basic aluminum oxide plug with 100% diethyl ether, removing solvent *in vacuo*, and rinsing solid with cold hexanes. IR (crystal) 3060, 1491, 1194, 794, 700 cm^{-1}. HRMS (ESI) *m/z*

calcd for $[M+H]^+$ $C_{20}H_{14}N_2F$ requires 301.1136, found 301.1148. ^1H NMR (400 MHz, $CDCl_3$, 25˚C) δ 8.77 – 8.68 (m, 1H), 8.65 (d, *J* = 8.0 Hz, 1H), 8.55 (s, 1H), 8.22 (dd, *J* = 9.2, 5.6 Hz, 1H), 7.84 (td, *J* = 7.7, 1.8 Hz, 1H), 7.63 – 7.43 (m, 7H), 7.32 (ddd, *J* = 7.4, 4.8, 1.1 Hz, 1H). ^{19}F NMR (376 MHz, $CDCl_3$, 25˚C) δ -112.52 – -112.69 (m). ^{13}C NMR (100 MHz, $CDCl_3$, 25˚C) δ 160.92 (d, *J* = 247.9 Hz), 156.12, 155.14, 149.21, 148.75 (d, *J* = 5.2 Hz), 145.64, 137.99, 136.96, 132.70 (d, *J* = 9.0 Hz), 129.52, 128.72, 128.60, 127.61 (d, *J* = 9.5 Hz), 124.12, 121.72, 119.82, 119.62 (d, *J* = 26.1 Hz), 109.28 (d, *J* = 23.2 Hz).

4,6-diphenyl-2-(2'-pyridyl)quinoline (1q)

4-aminobiphenyl (338 mg, 2 mmol), 2-pyridinecarboxaldehyde (228 µL, 2.4 mmol), phenylacetylene (264 µL, 2.4 mmol), trifluoromethanesulfonic acid (18 µL, 10 mol%) were stirred at 110˚C for 4h to afford the title compound as a light beige/white solid in 15% yield (0.245 g, 0.68 mmol) after flushing through a basic aluminum oxide plug with 100% diethyl ether, removing solvent *in vacuo*, and rinsing solid with cold hexanes. IR (crystal) 3054, 1588, 1486, 763, 695 cm^{-1}. HRMS (ESI) *m/z* calcd for $[M+H]^+$ $C_{26}H_{19}N_2$ requires 359.1543, found 359.1545. ^1H NMR (400 MHz, $CDCl_3$, 25˚C) δ 8.81 – 8.69 (m, 2H), 8.62 (s, 1H), 8.35 (d, *J* = 8.7 Hz, 1H), 8.20 (d, *J* = 1.9 Hz, 1H), 8.02 (dd, *J* = 8.7, 2.0 Hz, 1H), 7.87 (ddd, *J* = 7.6, 5.6, 1.7 Hz, 1H), 7.73 – 7.61 (m, 4H), 7.61 – 7.48 (m, 3H), 7.45 (t, *J* = 7.6 Hz, 2H), 7.40 – 7.30 (m, 2H). ^{13}C NMR (100 MHz, $CDCl_3$, 25˚C) δ 156.31, 155.53, 149.34, 149.17, 147.96, 140.59, 139.48, 138.41, 136.90, 130.73, 129.72,

129.19, 128.92, 128.62, 128.41, 127.65, 127.45, 126.93, 124.04, 123.54, 121.86, 119.72.

6-cyano-4-phenyl-2-(2'-pyridyl)quinoline (1r)

4-aminobenzonitrile (473 mg, 4 mmol), 2-pyridinecarboxaldehyde (457 µL, 4.8 mmol), phenylacetylene (527 µL, 4.8 mmol), boron trifluoride diethyl etherate (49 µL, 10 mol%) were stirred at 110˚C for 4h to afford the title compound as clear crystals in 15% yield (0.057 g, 0.19 mmol) after flushing through a basic aluminum oxide plug with 100% diethyl ether, removing solvent *in vacuo*, and rinsing solid with cold hexanes. IR (crystal) 3050, 2227, 1586, 1547, 1364, 801, 763, 702 cm^{-1}. HRMS (ESI) *m/z* calcd for $[M+H]^+$ $C_{21}H_{14}N_3$ requires 308.1182, found 308.1181. ^1H NMR (400 MHz, $CDCl_3$, 25˚C) δ 8.72 (d, *J* = 4.6 Hz, 1H), 8.69 (d, *J* = 8.1 Hz, 1H), 8.65 (s, 1H), 8.31 (s, 1H), 8.27 (d, *J* = 8.7 Hz, 1H), 7.89 (t, *J* = 7.7 Hz, 1H), 7.84 (d, *J* = 8.7 Hz, 1H), 7.60 – 7.51 (m, 5H), 7.42 – 7.35 (m, 1H). ^{13}C NMR (100 MHz, $CDCl_3$, 25˚C) δ 158.27, 155.37, 149.85, 149.55, 149.43, 137.14, 136.99, 132.52, 131.64, 130.09, 129.63, 129.16, 129.00, 126.38, 124.87, 122.26, 120.68, 119.00, 110.22.

6-iodo-4-phenyl-2-(2'-pyridyl)quinoline (1s)

4-iodoaniline (110 mg, 0.5 mmol), 2-pyridinecarboxaldehyde (57 µL, 0.6 mmol), phenylacetylene (264 µL, 2.4 mmol), trifluoromethanesulfonic acid (4 µL, 10 mol%) were stirred at 110˚C for 4h to afford the title compound as a white solid in

22% yield (0.060 g, 0.10 mmol) after flushing through a basic aluminum oxide plug with 100% diethyl ether, removing solvent *in vacuo*, and rinsing solid with cold hexanes. IR (crystal) 3030, 1566, 1480, 1360, 770, 702 cm^{-1}. HRMS (ESI) *m/z* calcd for $[M+H]^+$ $C_{20}H_{14}N_2I$ requires 409.0201, found 409.0208. ^1H NMR (400 MHz, $CDCl_3$, 25˚C) δ 8.69 (d, *J* = 4.0 Hz, 1H), 8.66 (d, *J* = 8.0 Hz, 1H), 8.51 (s, 1H), 8.28 (d, *J* = 8.9 Hz, 2H), 7.95 (td, *J* = 7.8, 1.7 Hz, 1H), 7.87 (dd, *J* = 8.9, 2.2 Hz, 1H), 7.54 – 7.50 (m, 5H), 7.36 – 7.33 (m, 1H).

6,7-(methylenedioxy)-4-phenyl-2-(2'-pyridyl)quinoline (1t)

3,4-(methylenedioxy)aniline (69 mg, 0.5 mmol), 2-pyridinecarboxaldehyde (57 µL, 0.6 mmol), phenylacetylene (264 µL, 2.4 mmol), trifluoromethanesulfonic acid (4 µL, 10 mol%) were stirred at 110˚C for 4h to afford the title compound as a white solid in 18% yield (0.067 g, 0.10 mmol) after flushing through a basic aluminum oxide plug with 100% diethyl ether, removing solvent *in vacuo*, and rinsing solid with cold hexanes. IR (crystal) 3055, 1540, 1477, 1368, 777, 708 cm^{-1}. HRMS (ESI) *m/z* calcd for $[M+H]^+$ $C_{21}H_{14}N_2O_2$ requires 137.1447, found 137.1445. ^1H NMR (400 MHz, $CDCl_3$, 25˚C) δ 8.68 (d, *J* = 4.0 Hz, 1H), 8.60 (d, *J* = 8.0 Hz, 1H), 7.85 (m, 2H), 7.51-7.31 (m, 6H), 7.35 (m, *J*, 1H), 7.17 (s, 1H), 6.08 (s, 1H), 5.95 (s, 1H).

6-ethoxy-4-phenyl-2-(2'-pyridyl)quinoline (1u)

p-phenetidine (137 mg, 1 mmol), 2-pyridinecarboxaldehyde (228 µL, 2.4 mmol), phenylacetylene (264 µL, 2.4 mmol), trifluoromethanesulfonic acid (18 µL, 10 mol%) were stirred at 110˚C for 4h to afford the title compound as a colorless solid in 35% yield (0.117 g, 0.85 mmol) after flushing through a basic aluminum oxide plug with 100% diethyl ether, removing solvent *in vacuo*, and rinsing solid with cold hexanes. IR (crystal) 3052, 2938, 1630, 1580, 1478, 1233, 1026, 712 cm^{-1}. HRMS (ESI) *m/z* calcd for $[M+H]^+$ $C_{22}H_{18}N_2O$ requires 326.1388, found 326.1391. ^1H NMR (400 MHz, $CDCl_3$, 25˚C) δ 8.68 (d, J = 4.7 Hz, 1H), 8.63 (d, J = 8.0 Hz, 1H), 8.44 (s, 1H), 8.14 (d, J = 9.2 Hz, 1H), 7.84 (td, J = 7.7, 1.7 Hz, 1H), 7.57 (d, J = 6.9 Hz, 2H), 7.45 (dt, J = 22.2, 7.1 Hz, 3H), 7.37 (dd, J = 9.2, 2.8 Hz, 1H), 7.31 (dd, J = 6.9, 5.3 Hz, 1H), 7.20 (d, J = 2.7 Hz, 1H), 4.01 (q, J= 2.7 Hz, 2H), 1.40 (t, J = 2.7 Hz, 3H).

4-p-methoxyphenyl-6-bromo-2-(2'-pyridyl)quinoline (1v)

4-bromoaniline (86 mg, 0.5 mmol), 2-pyridinecarboxaldehyde (57 µL, 0.6 mmol), 4-ethynylanisole (78 µL, 0.6 mmol), trifluoromethanesulfonic acid (4 µL, 10 mol%) were stirred at 110˚C for 4h to afford the title compound as a white solid in 20% yield (0.040 g, 0.10 mmol) after flushing through a basic aluminum oxide plug with 100% diethyl ether, removing solvent *in vacuo*, and rinsing solid with cold hexanes. ^1H NMR (300 MHz, $CDCl_3$, 25˚C) δ 8.71 (d, *J* = 4.0 Hz, 1H), 8.65 (d, *J* = 8.0 Hz, 1H), 8.51 (s, 1H), 8.12 (d, *J* = 2.1 Hz, 1H), 8.08 (d, *J* = 9.0 Hz,

1H), 7.86 (td, *J* = 7.8, 1.7 Hz, 1H), 7.78 (dd, *J* = 9.0, 2.2 Hz, 1H), 7.54 – 7.47 (m, 2H), 7.35 (ddd, *J* = 7.4, 4.8, 1.0 Hz, 1H), 7.11 – 7.03 (m, 2H), 3.90 (s, 3H). ^{13}C NMR (100 MHz, $CDCl_3$, 25˚C) δ 160.11, 156.12, 156.04, 149.31, 148.25, 147.27, 137.05, 132.89, 132.01, 130.95, 130.08, 128.25, 128.14, 124.29, 121.94, 120.96, 119.96, 114.30, 55.52.

Adapted procedure with Nafion NR-50 catalyst for the synthesis of 4-phenyl-2-(2'-pyridyl)quinolines (PyQuins)

In an effort for a greener process, the synthesis of R-PyQuins can also be achieved by stirring substituted R-aniline (1 equiv.), 2-pyridinecarboxaldehyde (1.2 equiv), phenylacetylene (1.2 equiv.), and Nafion NR-50 pellets (25 mol %, ~5 pellets) together at 110˚C for 4h; as with the triflic acid catalyst, the reaction turns jet black upon heating with Nafion pellets. An identical workup as stated earlier is effective at isolating the PyQuin from the crude mixture, however removal of Nafion pellets is required through the use of forceps. These pellets can be soaked in dichloromethane, dried, and used again; the effectiveness of the Nafion catalyst decreases after 4 uses.

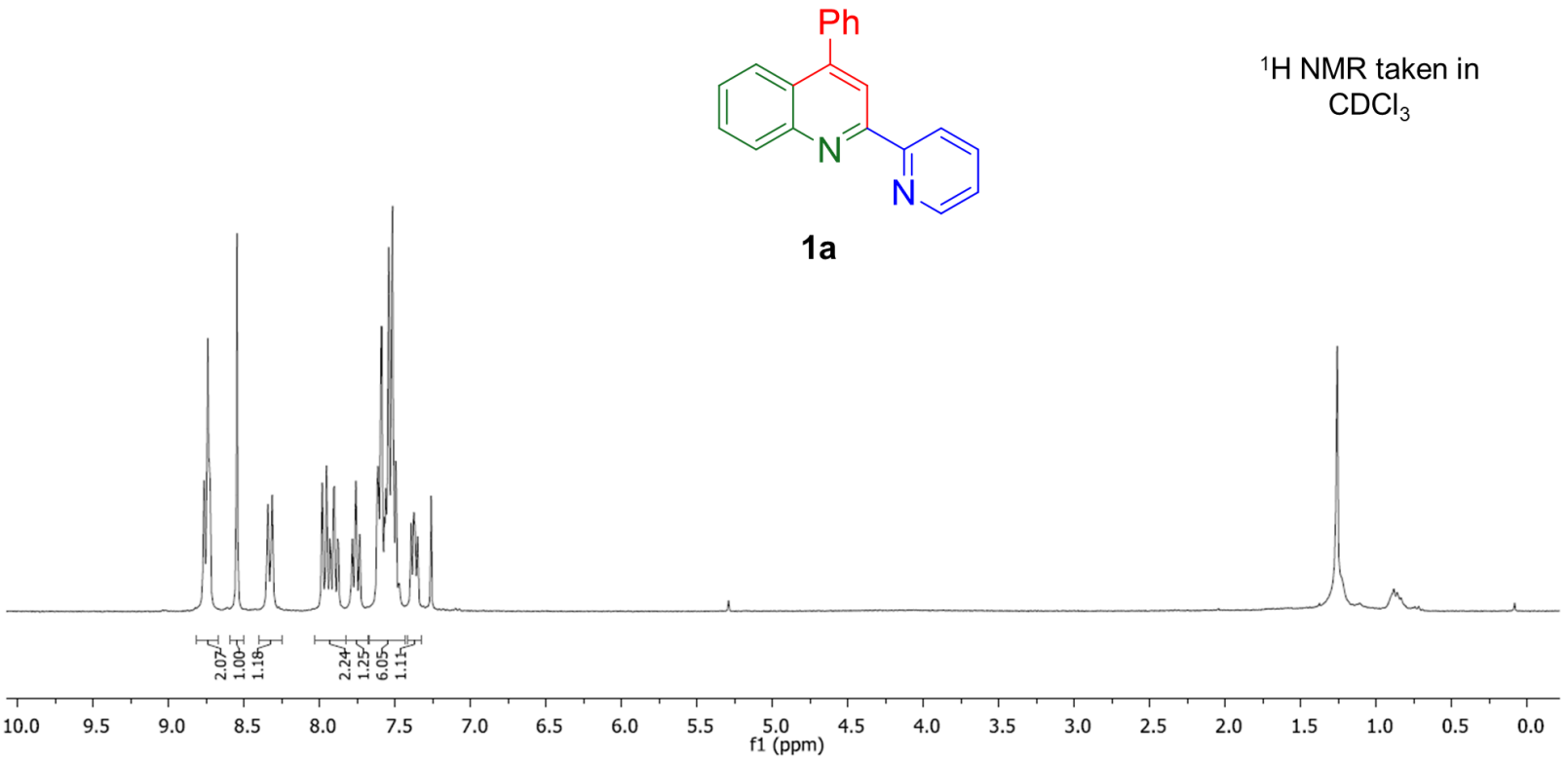
Ph
N
N
1a
^{1}H NMR taken in
$CDCl_3$
2.07
1.00
1.18
2.24
1.25
6.05
1.11
10.0
9.5
9.0
8.5
8.0
7.5
7.0
6.5
6.0
5.5
5.0
4.5
4.0
3.5
3.0
2.5
2.0
1.5
1.0
0.5
0.0
f1 (ppm)

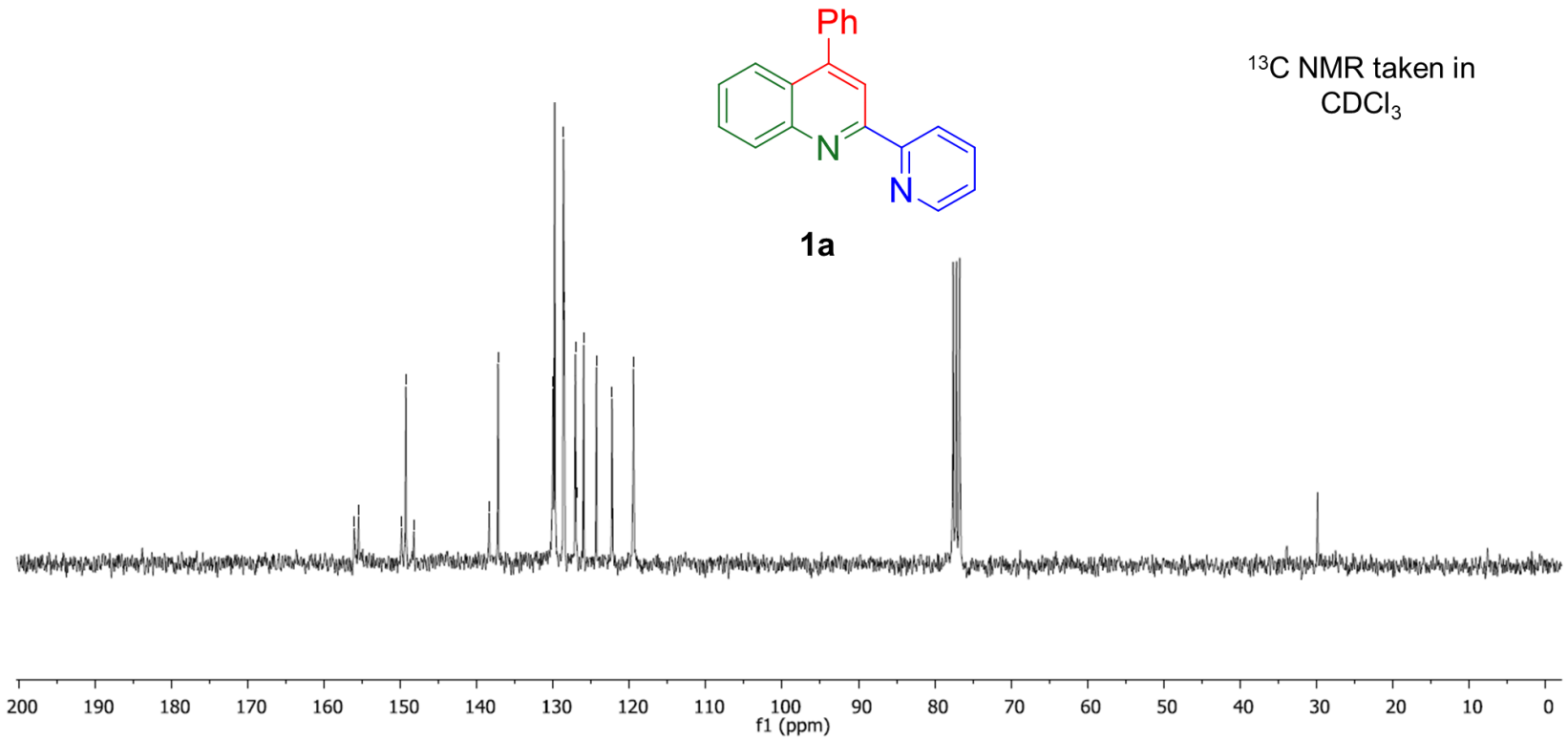
Ph
N
N
1a
^{13}C NMR taken in
$CDCl_3$
200
190
180
170
160
150
140
130
120
110
100
90
80
70
60
50
40
30
20
10
0
f1 (ppm)

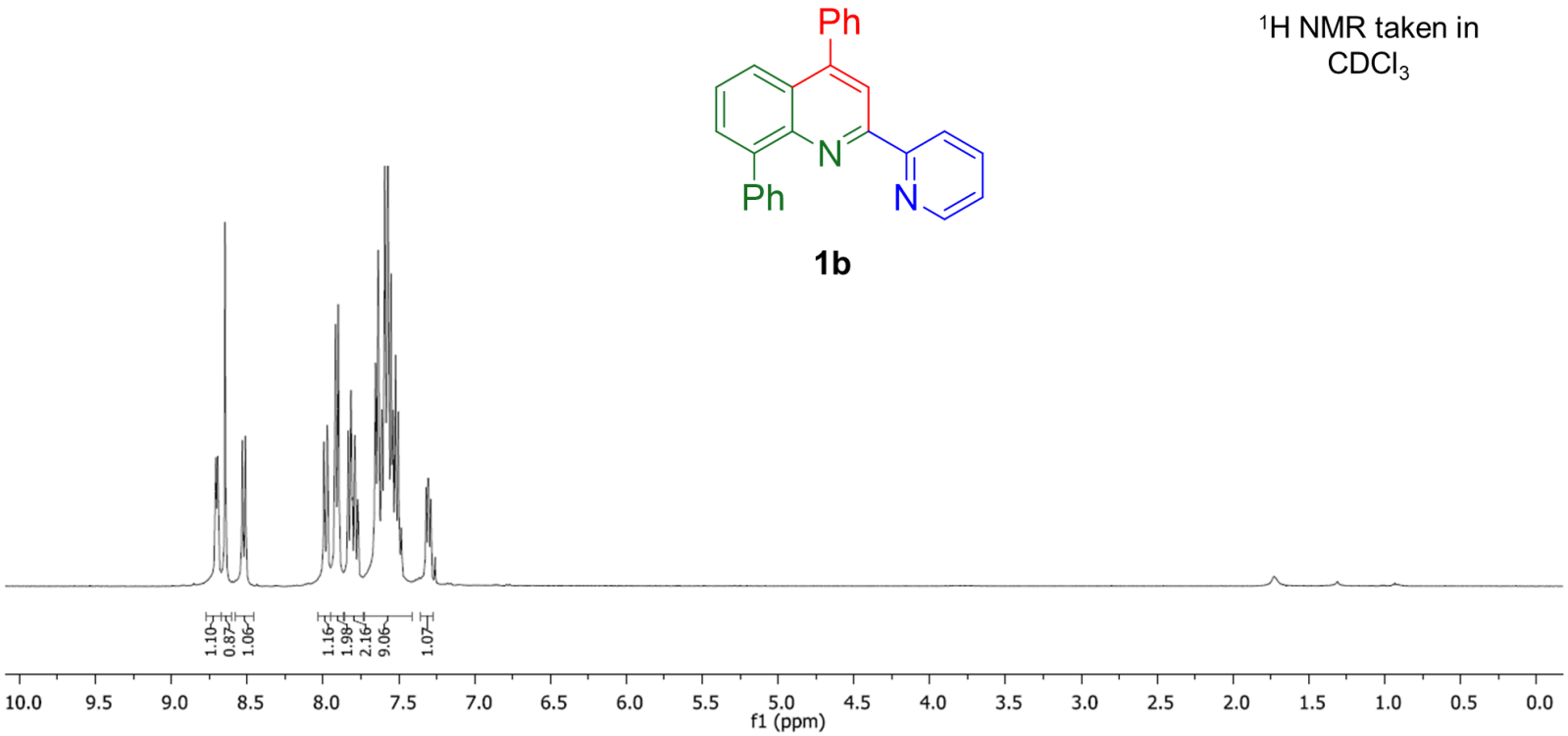

1b

^{1}H NMR taken in $CDCl_3$

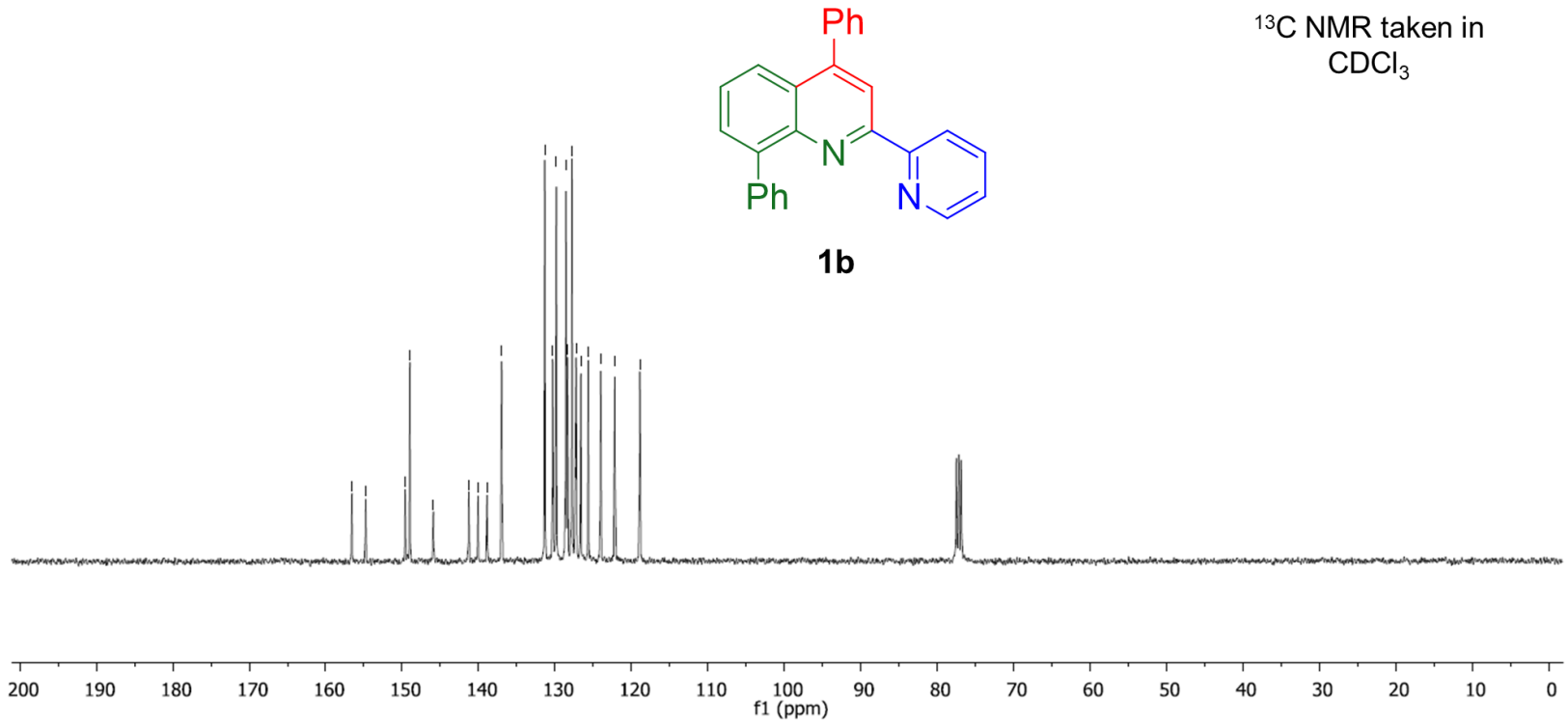

1b

^{13}C NMR taken in $CDCl_3$

^{1}H NMR taken in $CDCl_3$

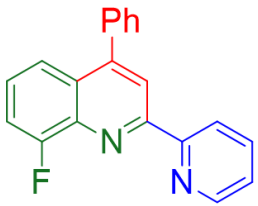

1c

^{13}C NMR taken in $CDCl_3$

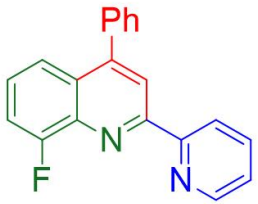

1c

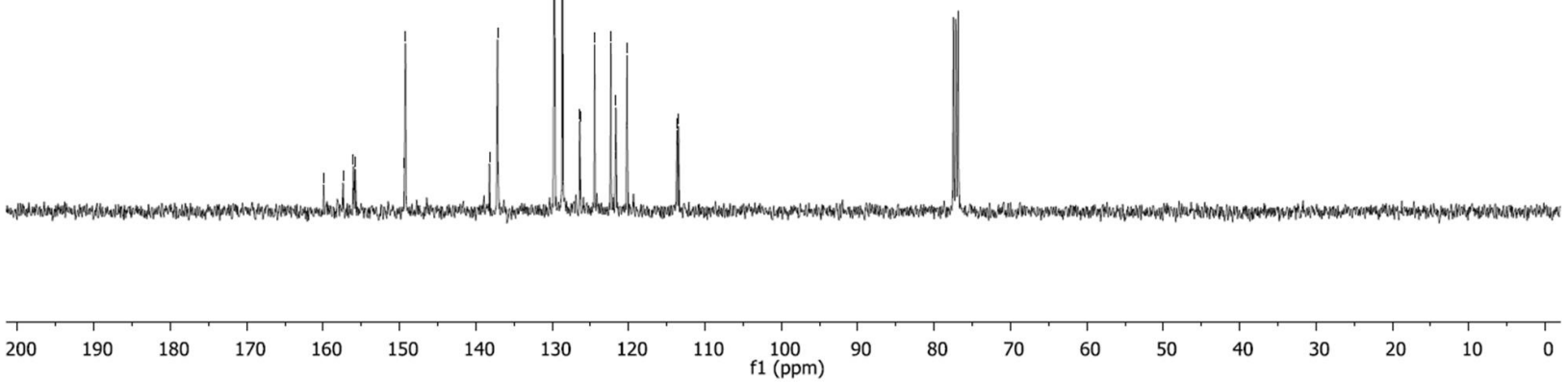

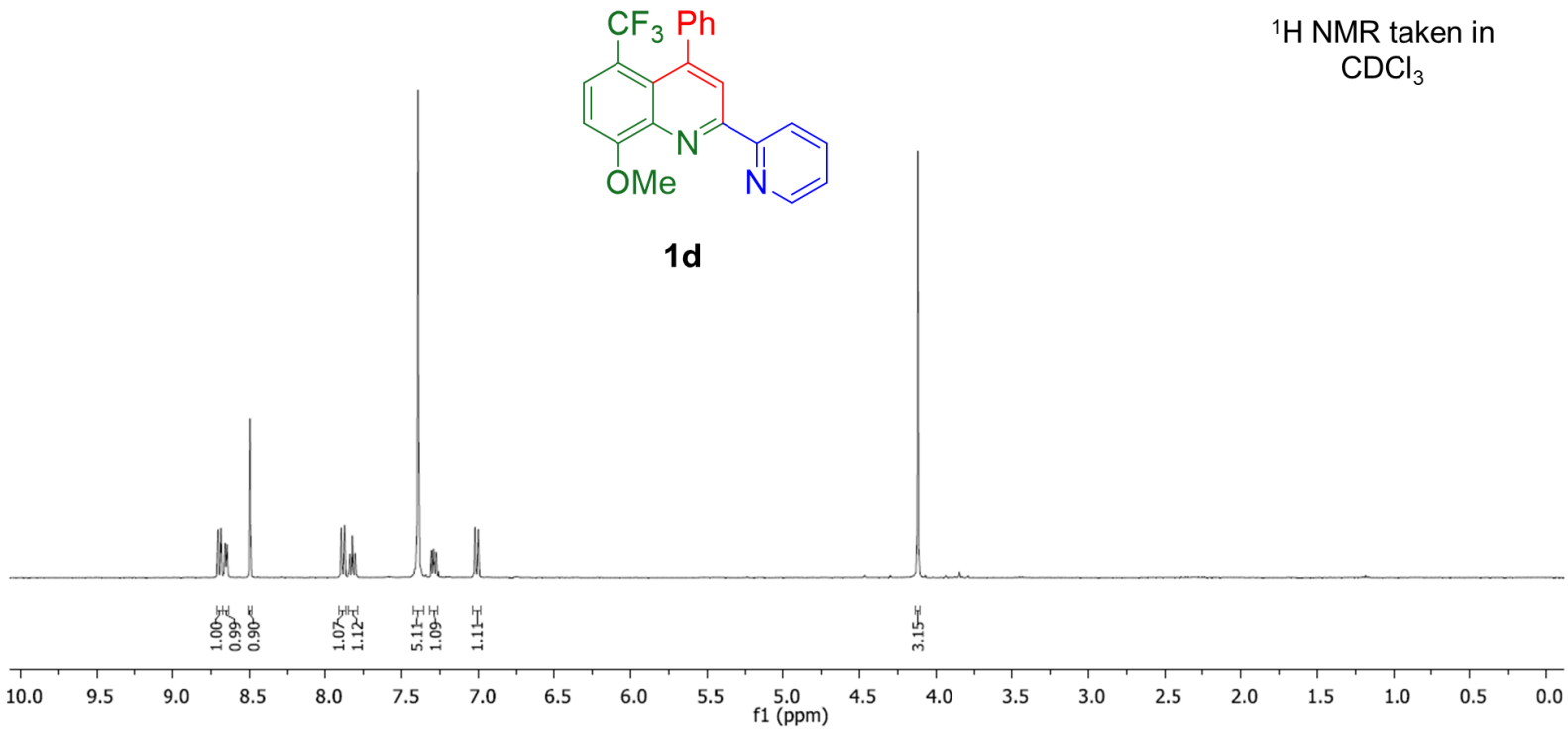
CF3
Ph
N
OMe
N
1d
1H NMR taken in
CDCl3
1.00
0.99
0.90
1.07
1.12
5.11
1.09
1.11
3.15
10.0
9.5
9.0
8.5
8.0
7.5
7.0
6.5
6.0
5.5
5.0
4.5
4.0
3.5
3.0
2.5
2.0
1.5
1.0
0.5
0.0
f1 (ppm)

1d

^{13}C NMR taken in $CDCl_3$

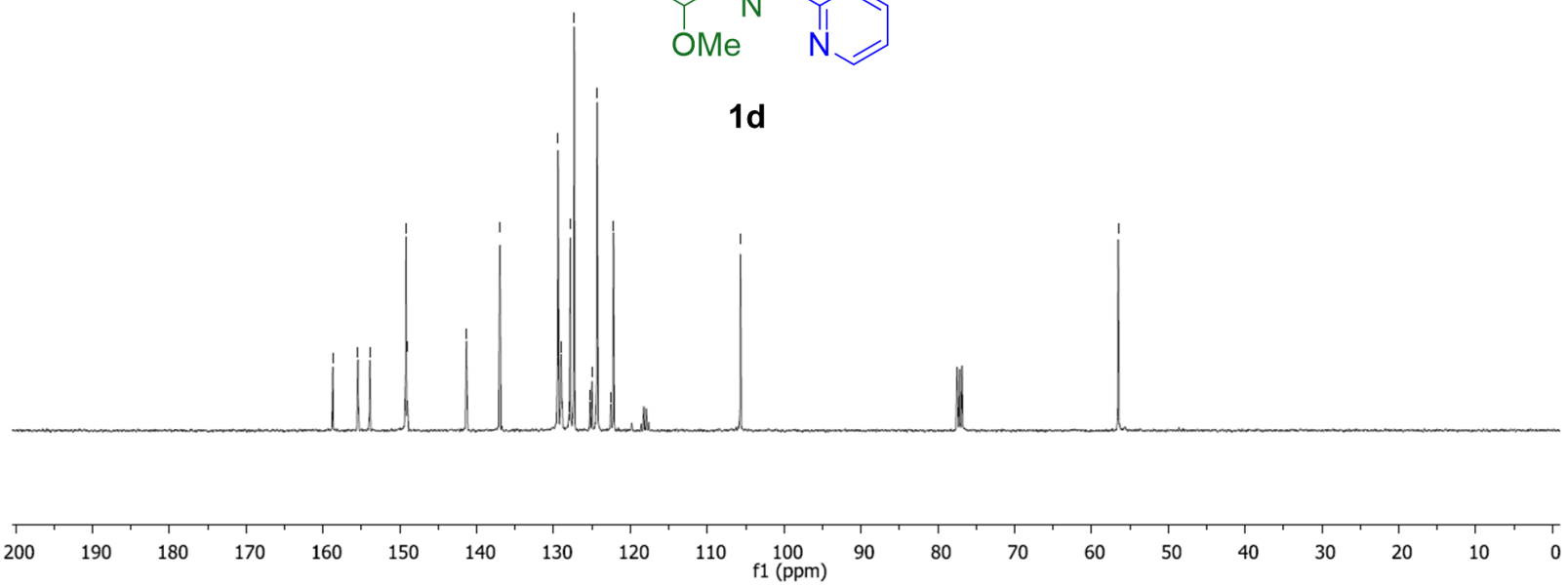

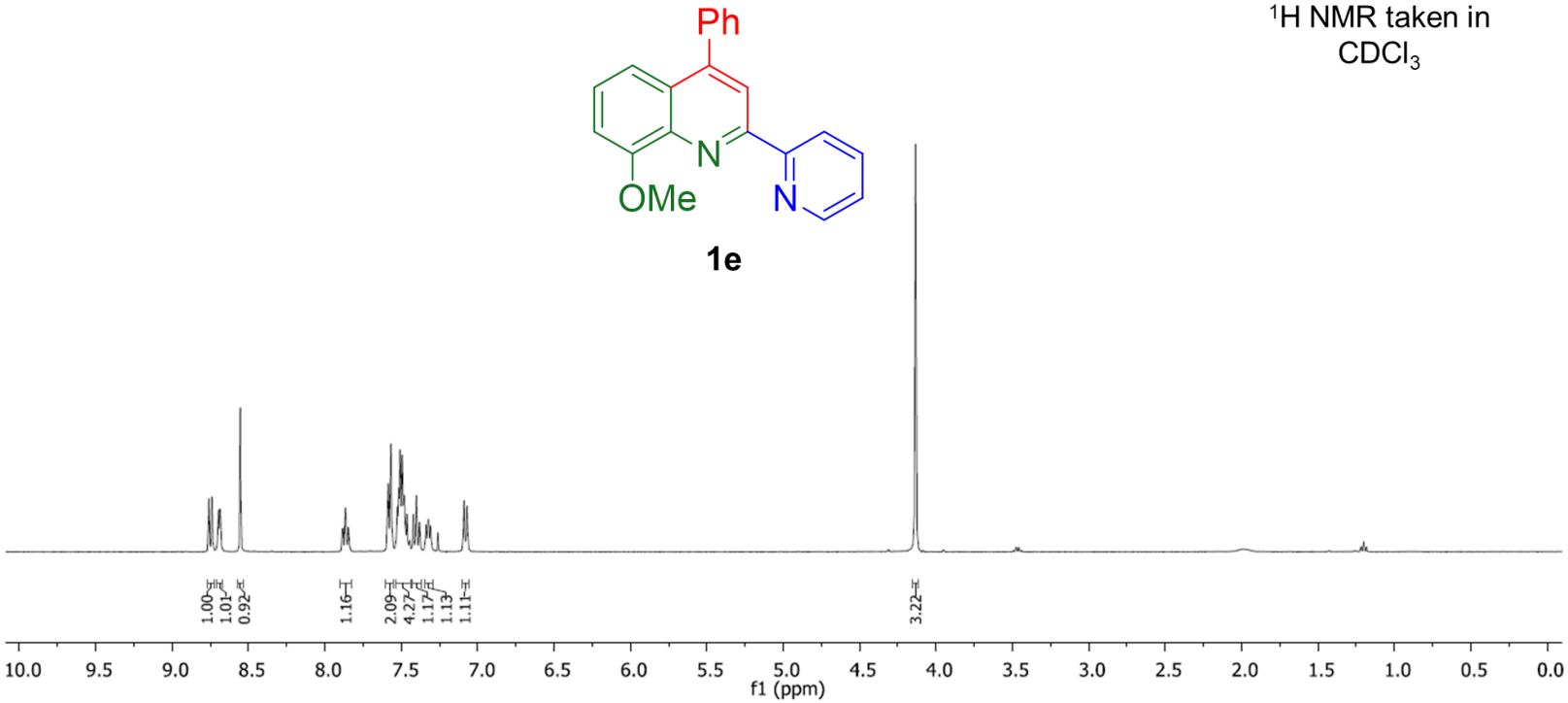
Ph
N
OMe
N
1e
1H NMR taken in
CDCl3
1.00
1.01
0.92
1.16
2.09
4.27
1.17
1.13
1.11
3.22
10.0
9.5
9.0
8.5
8.0
7.5
7.0
6.5
6.0
5.5
5.0
4.5
4.0
3.5
3.0
2.5
2.0
1.5
1.0
0.5
0.0
f1 (ppm)

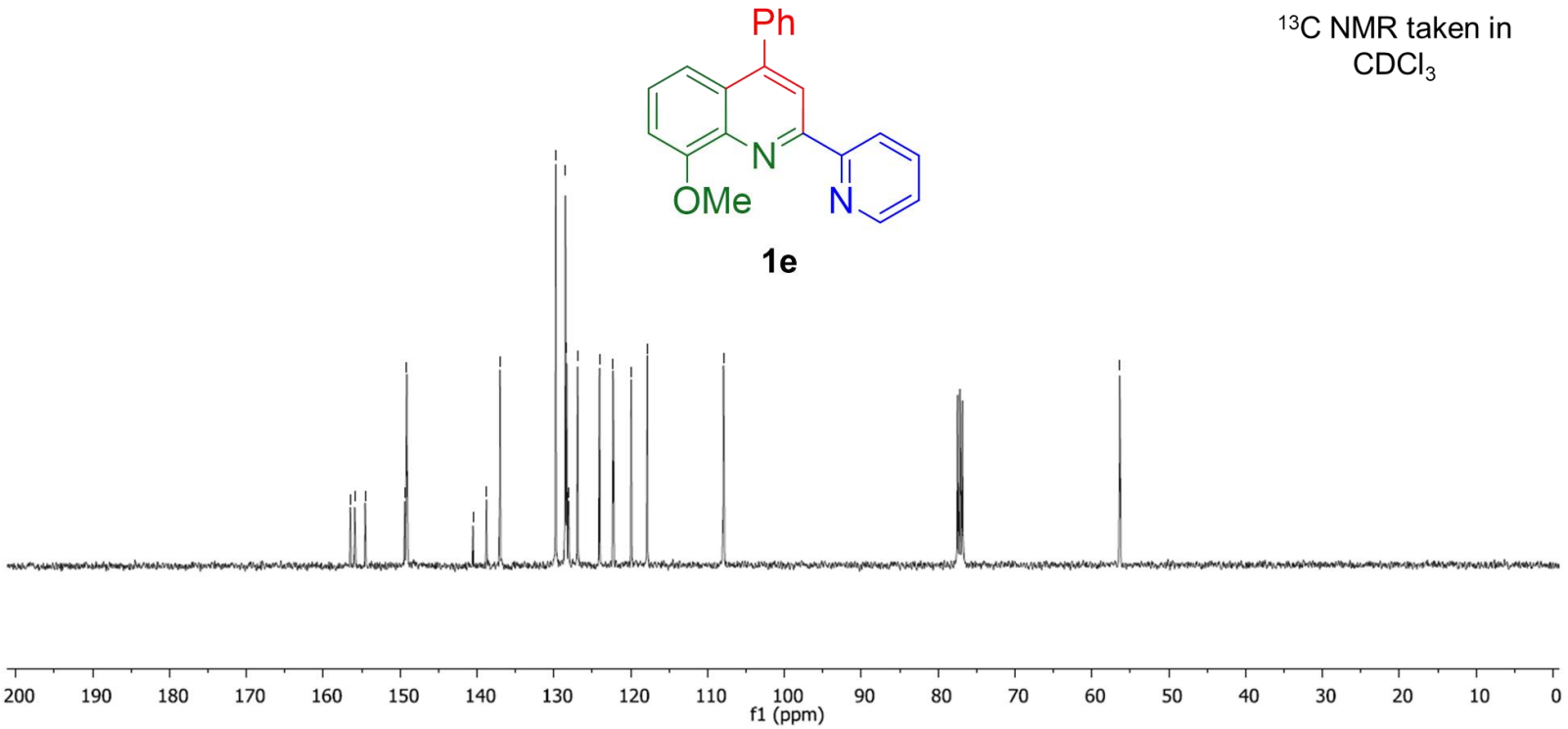
Ph
N
OMe
N
1e
^{13}C NMR taken in
$CDCl_3$
200 190 180 170 160 150 140 130 120 110 100 90 80 70 60 50 40 30 20 10 0
f1 (ppm)

^{1}H NMR taken in $CDCl_3$

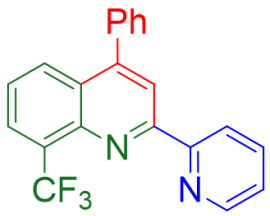

1f

^{13}C NMR taken in $CDCl_3$

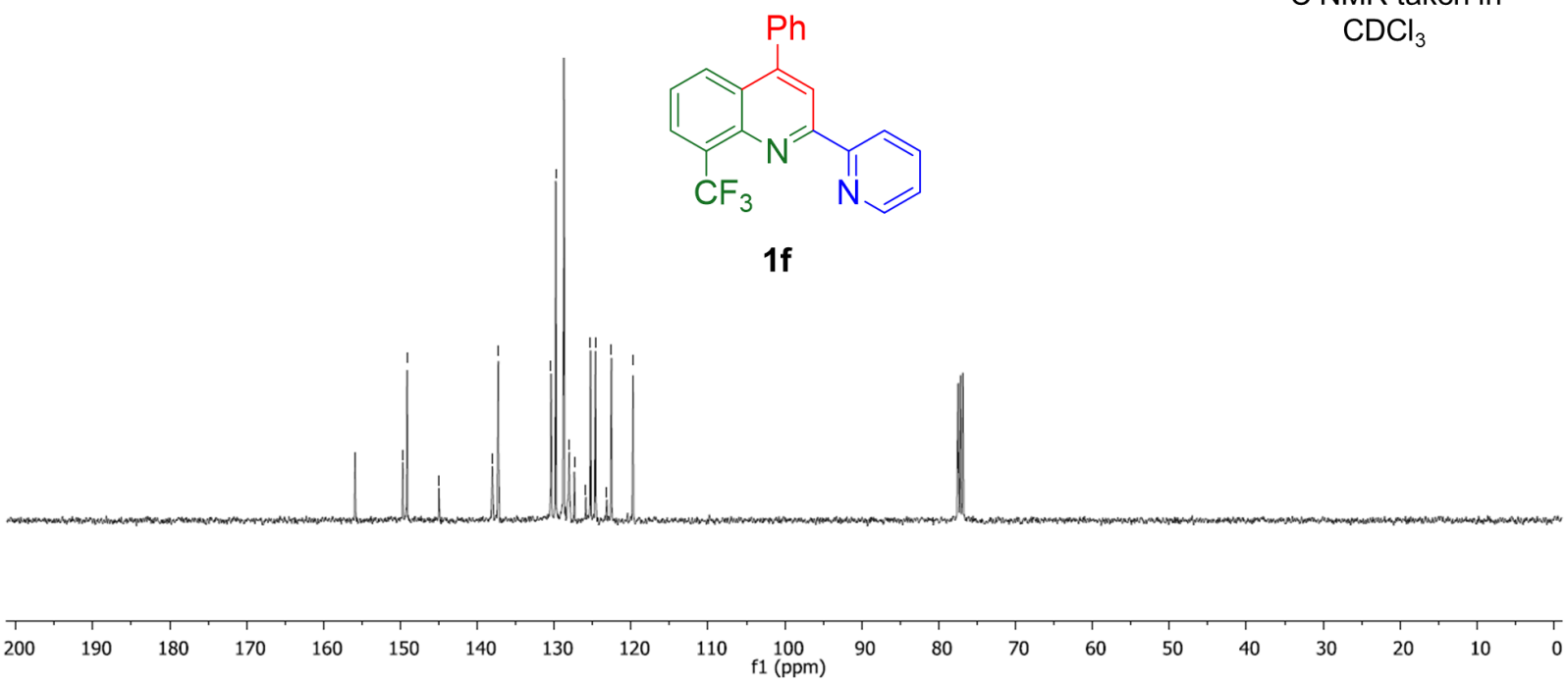

1f

^{1}H NMR taken in $CDCl_3$

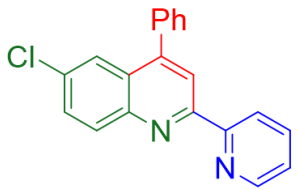

1g

^{13}C NMR taken in $CDCl_3$

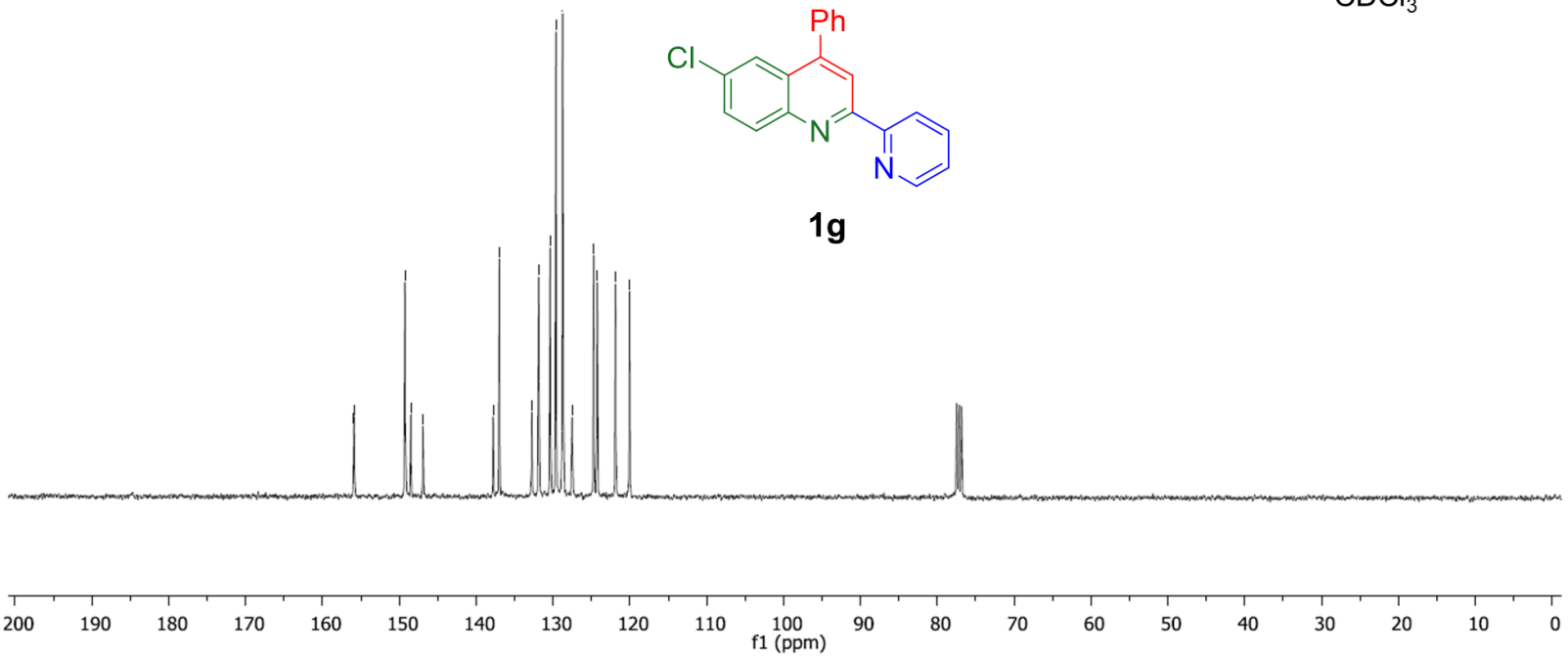

1g

^{1}H NMR taken in $CDCl_3$

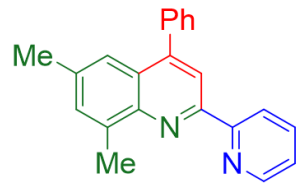

1h

^{13}C NMR taken in $CDCl_3$

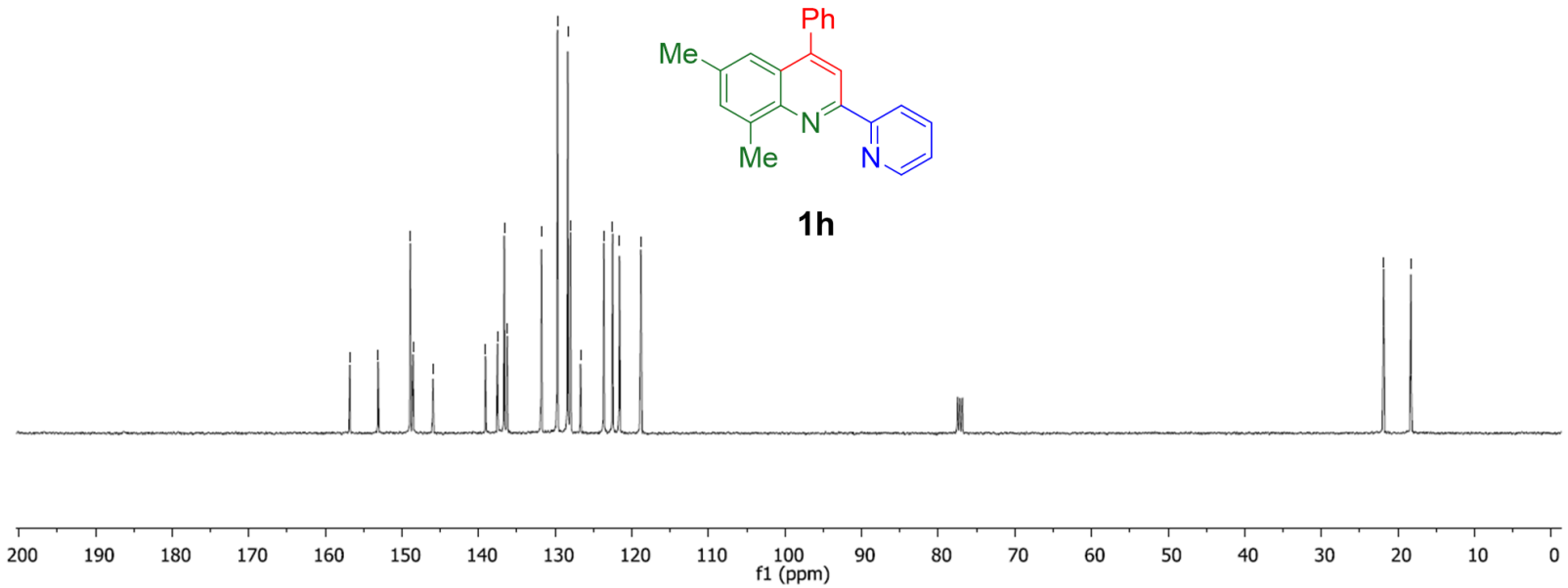

1h

^{1}H NMR taken in $CDCl_3$

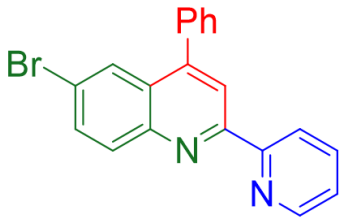

1i

^{13}C NMR taken in $CDCl_3$

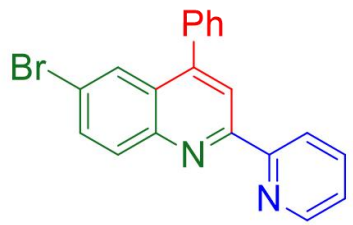

1i

^{1}H NMR taken in $CDCl_3$

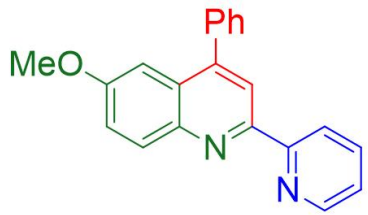

1j

^{13}C NMR taken in $CDCl_3$

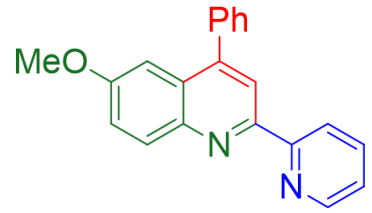

1j

^{1}H NMR taken in $CDCl_3$

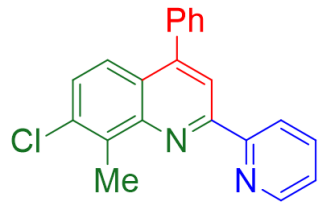

1k

^{13}C NMR taken in $CDCl_3$

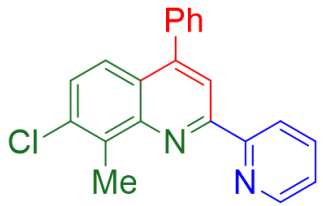

1k

^{1}H NMR taken in $CDCl_3$

1l

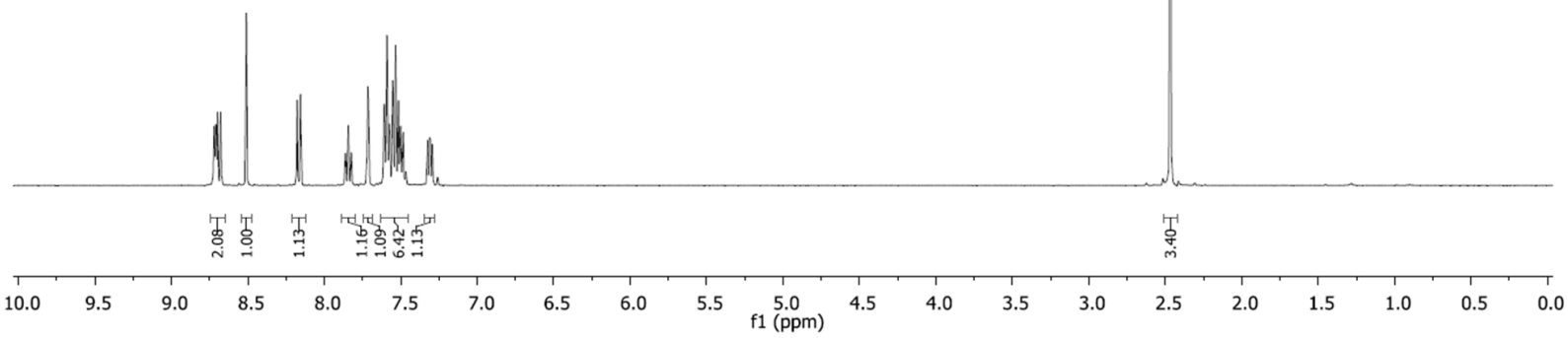

^{13}C NMR taken in $CDCl_3$

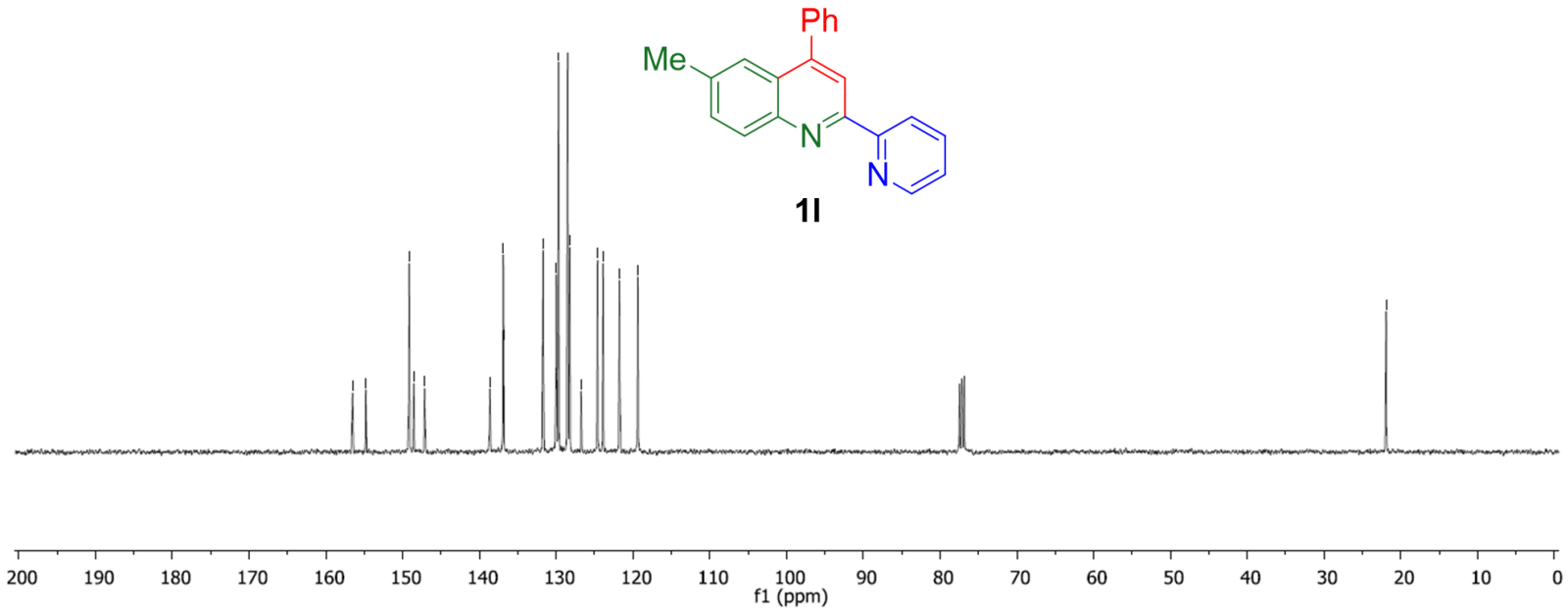

1l

^{1}H NMR taken in $CDCl_3$

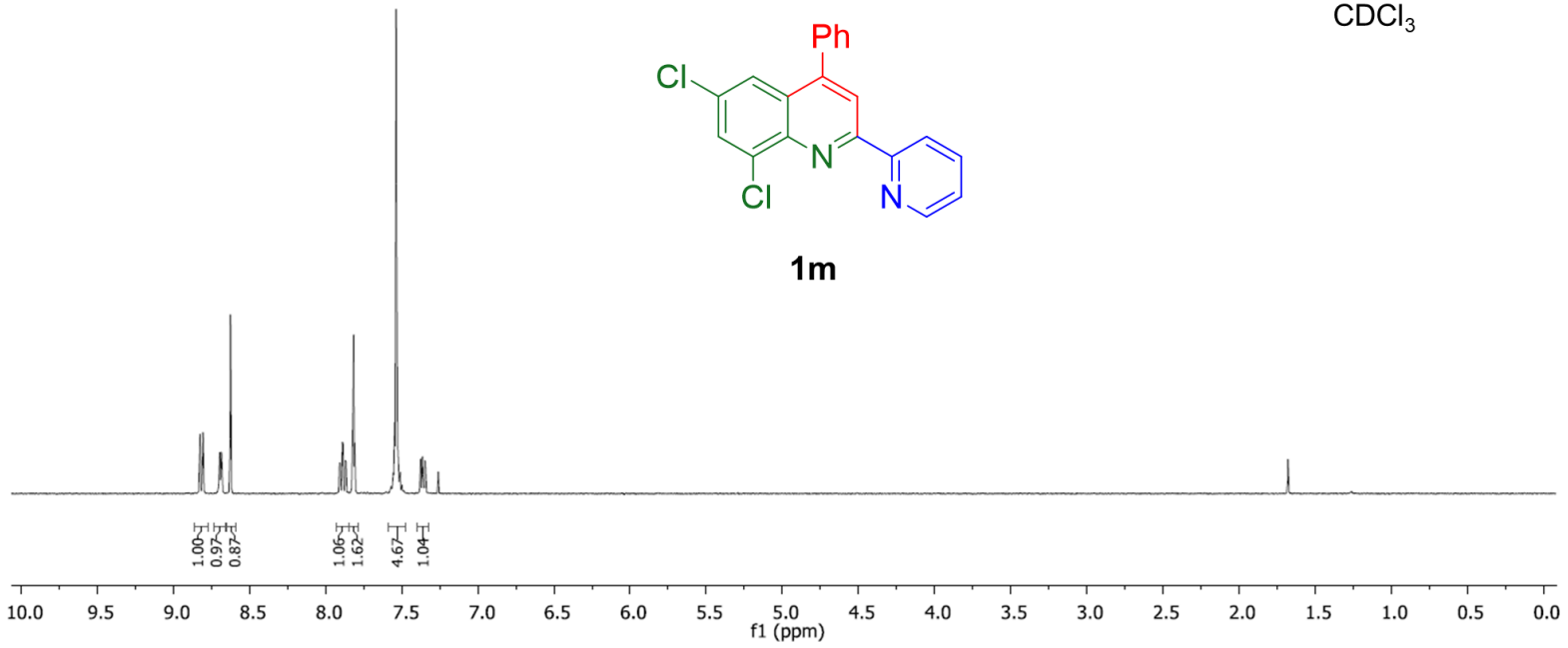

1m

^{13}C NMR taken in $CDCl_3$

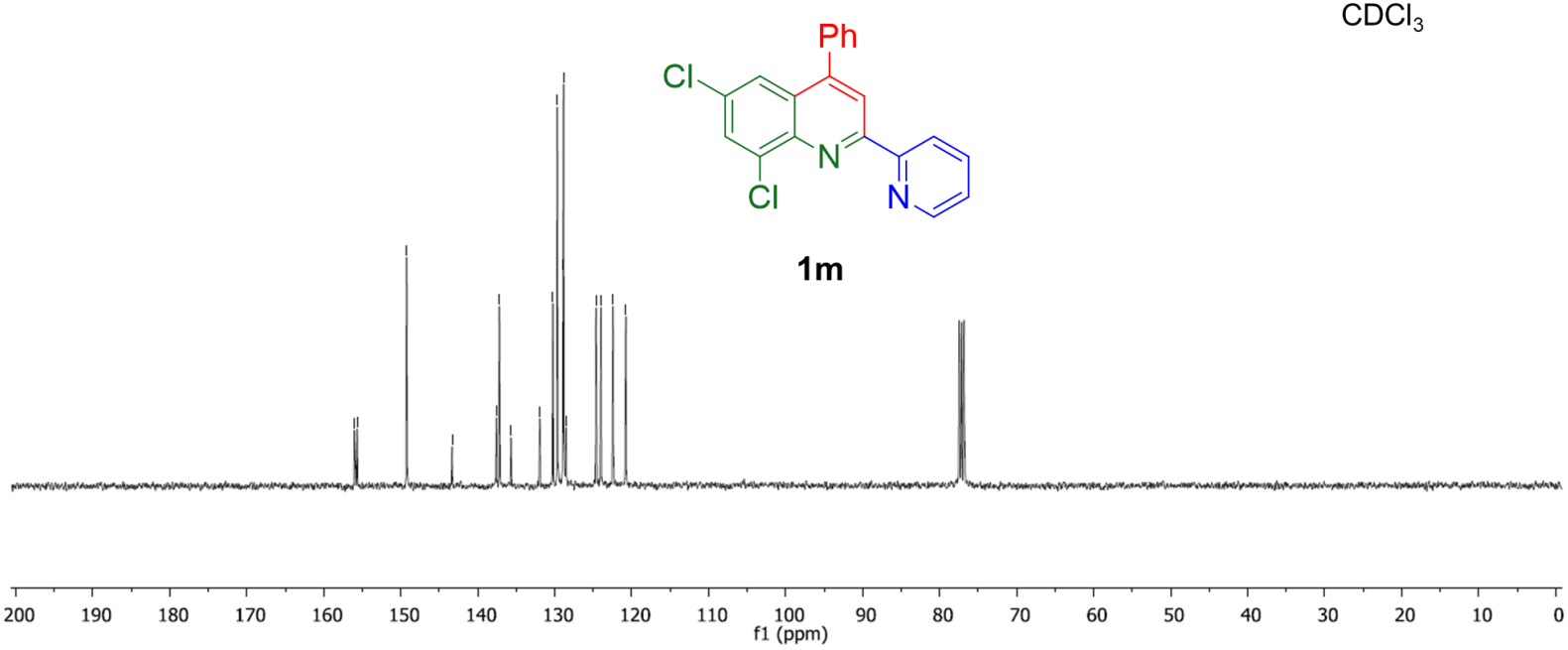

1m

^{1}H NMR taken in $CDCl_3$

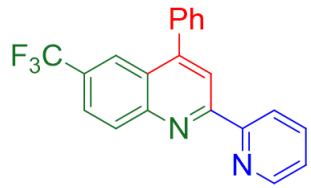

1n

^{13}C NMR taken in $CDCl_3$

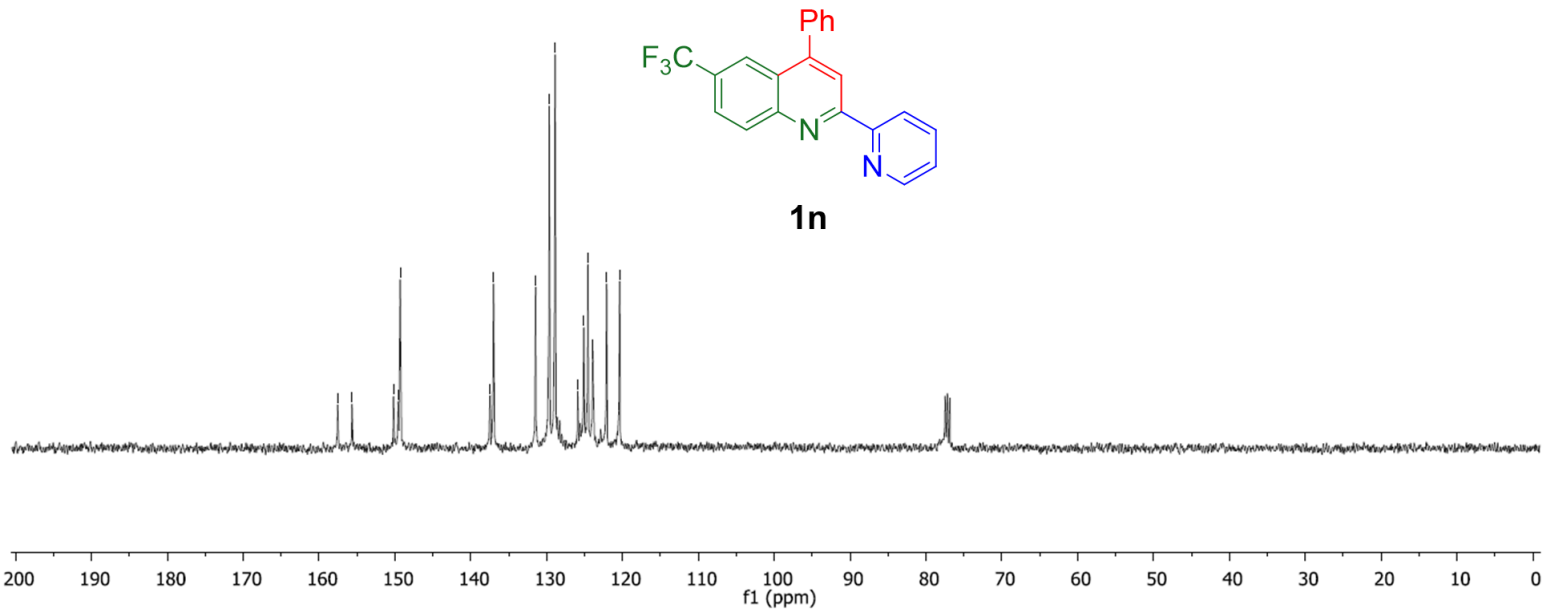

1n

^{1}H NMR taken in $CDCl_3$

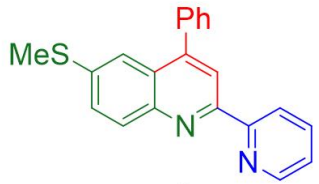

1o

^{13}C NMR taken in $CDCl_3$

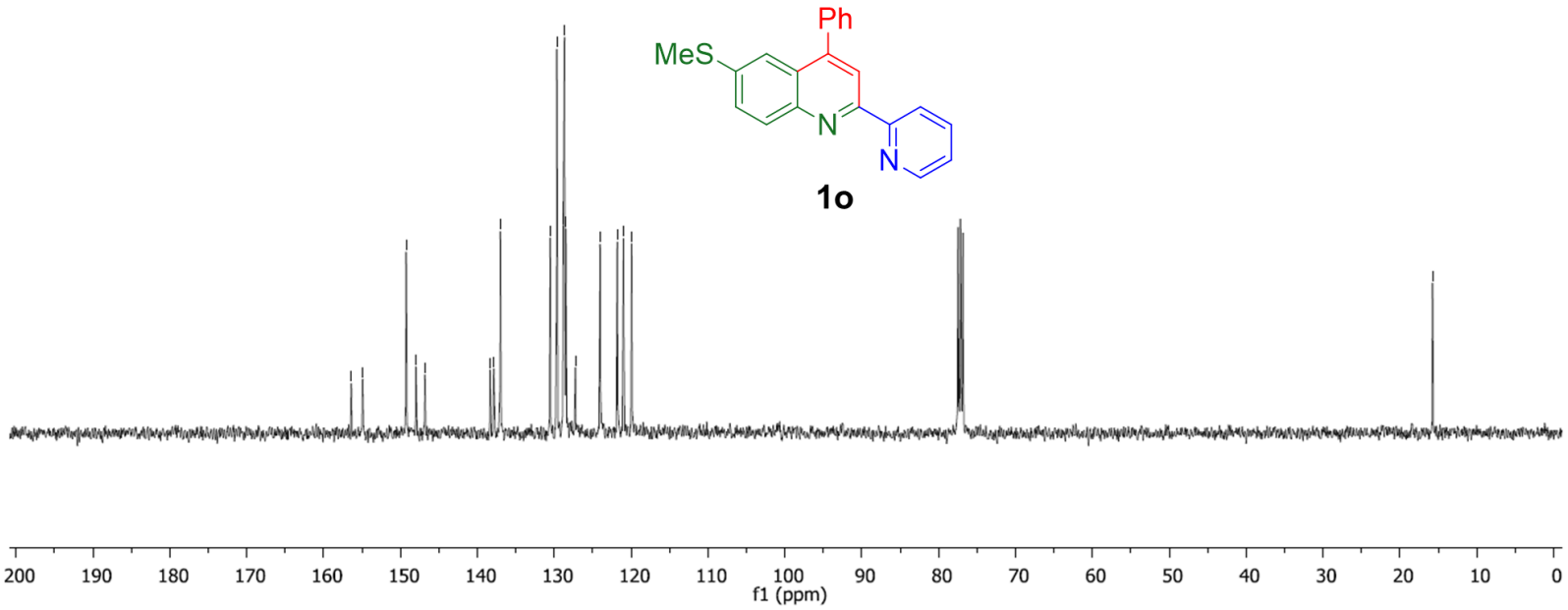

1o

^{1}H NMR taken in $CDCl_3$

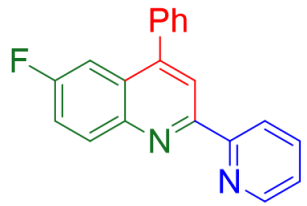

1p

^{13}C NMR taken in $CDCl_3$

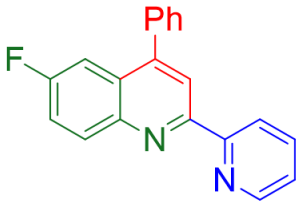

1p

^{1}H NMR taken in $CDCl_3$

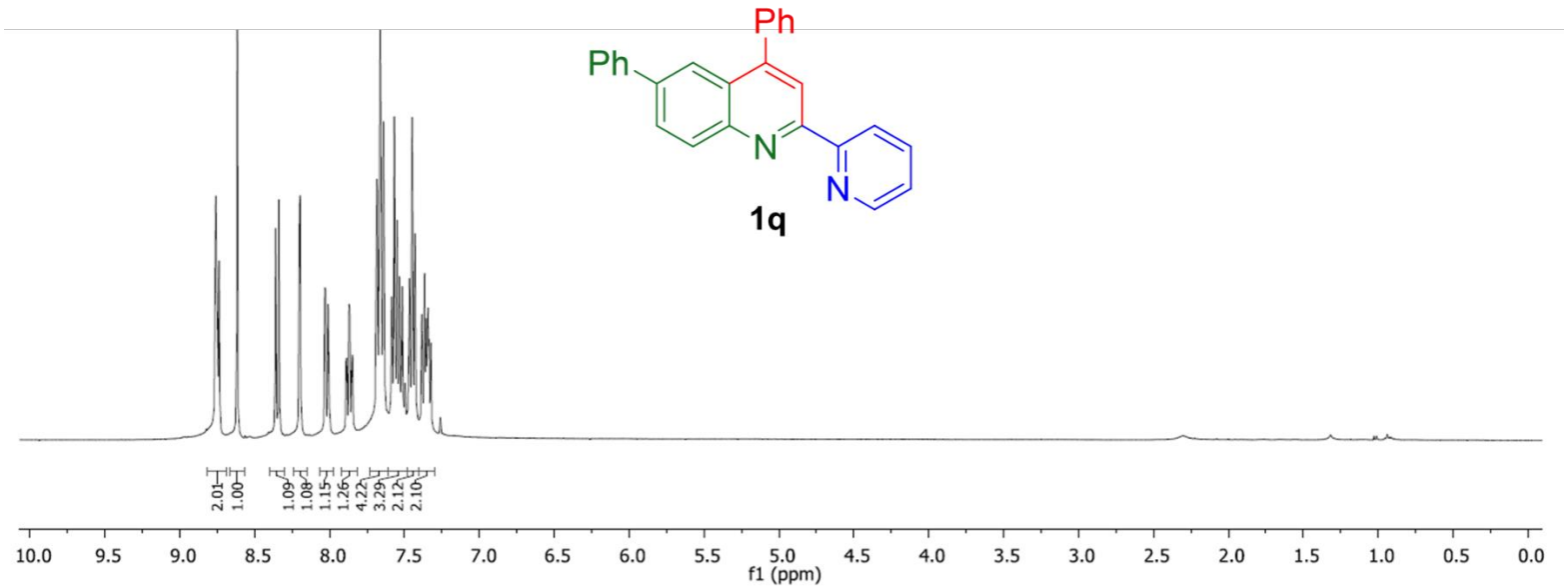

^{13}C NMR taken in $CDCl_3$

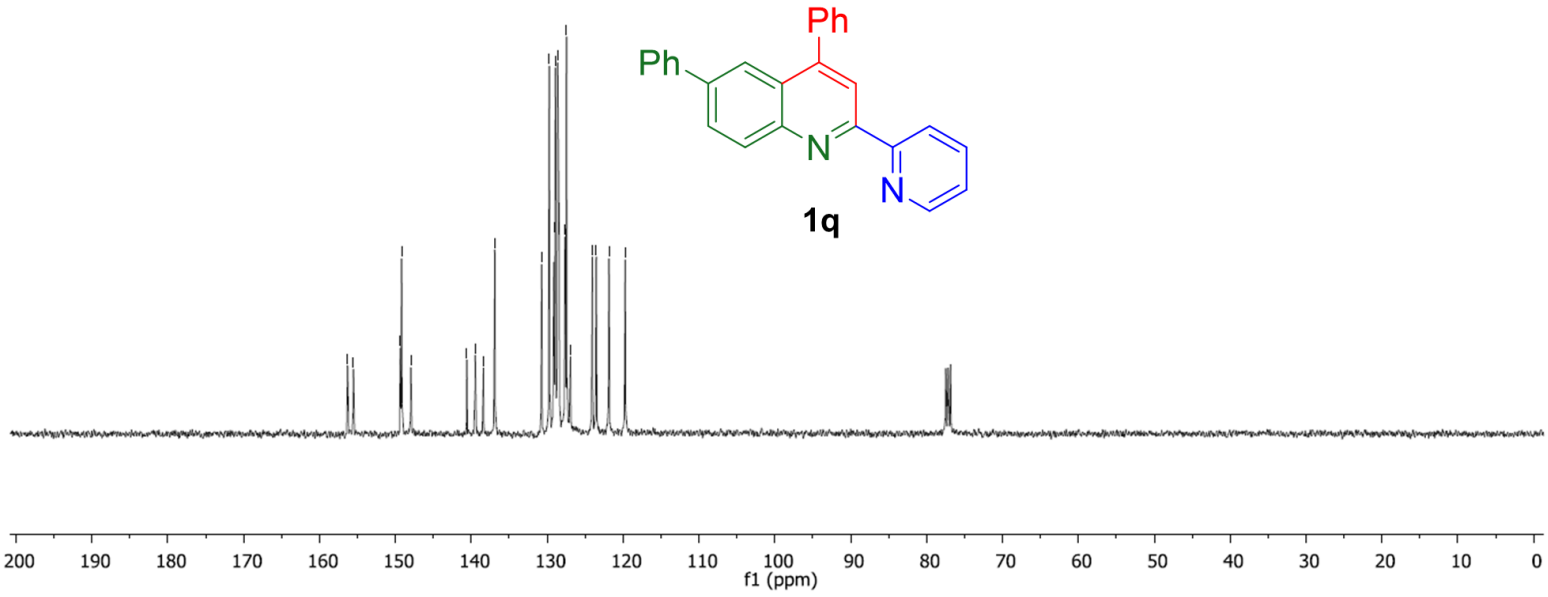

^{1}H NMR taken in $CDCl_3$

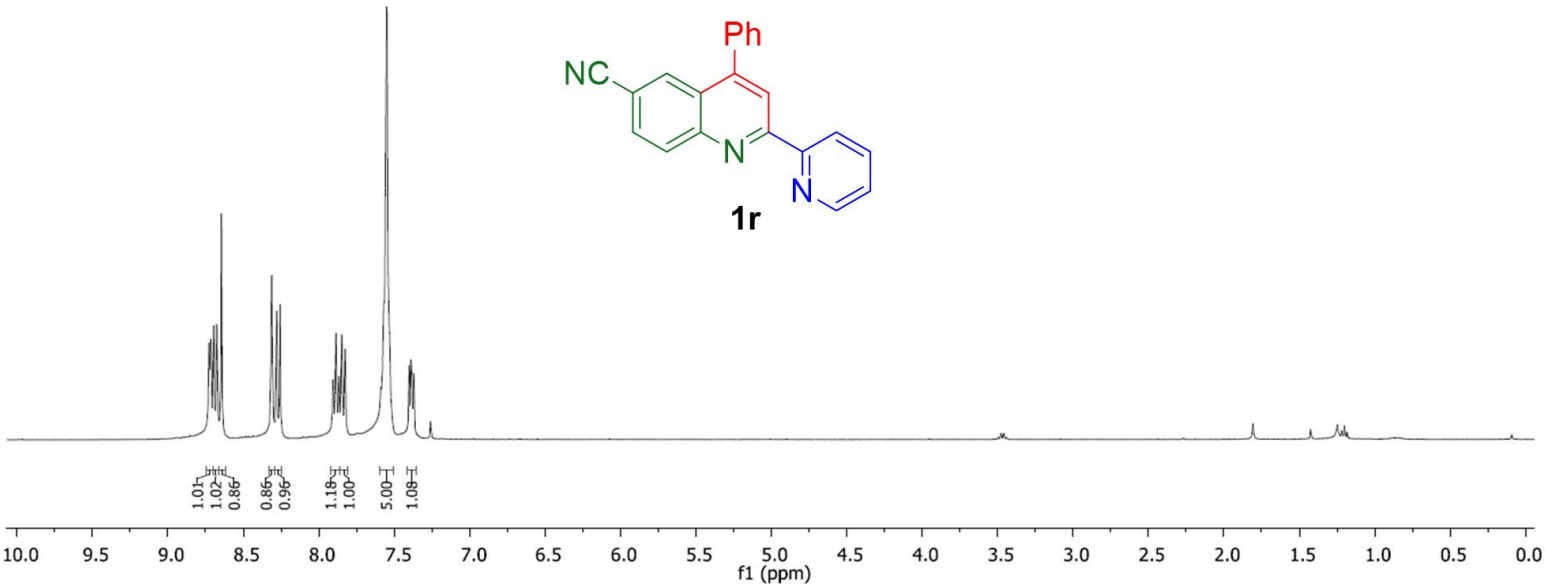

^{13}C NMR taken in $CDCl_3$

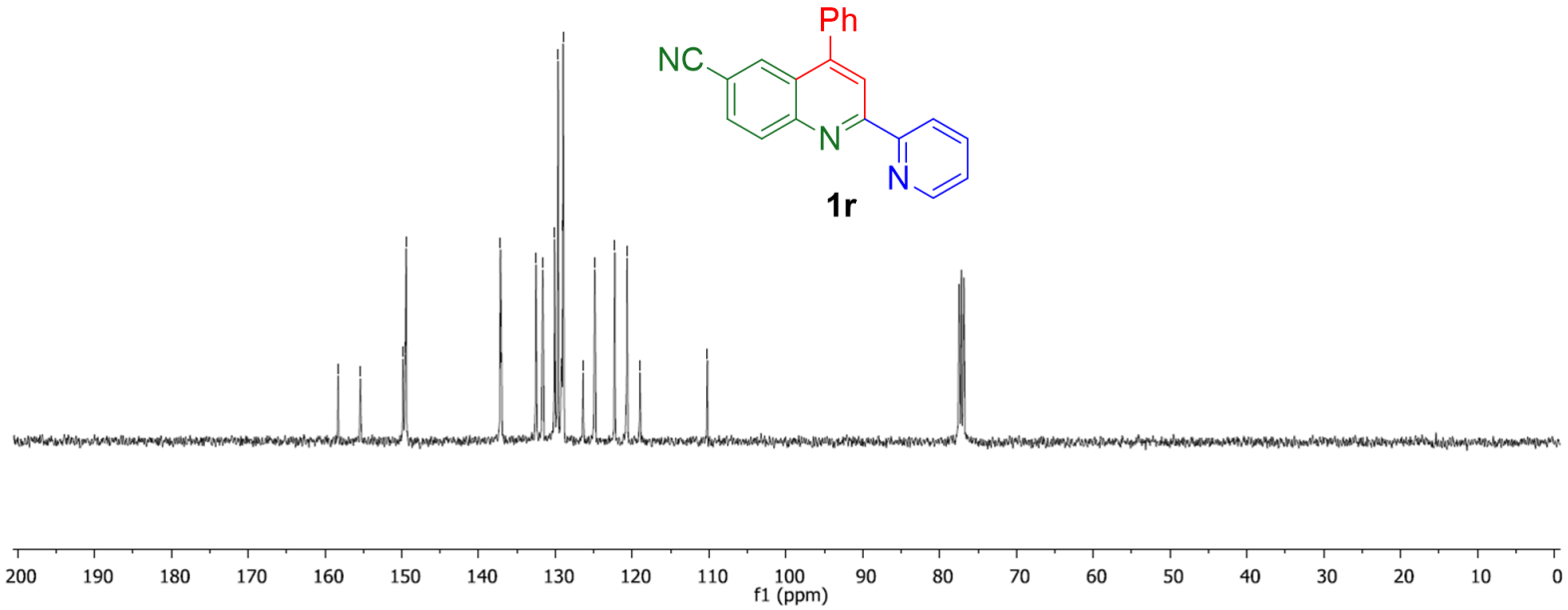

^{1}H NMR taken in $CDCl_3$

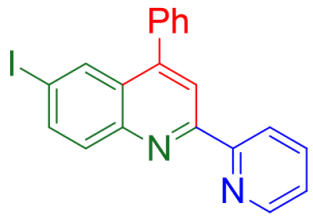

1s

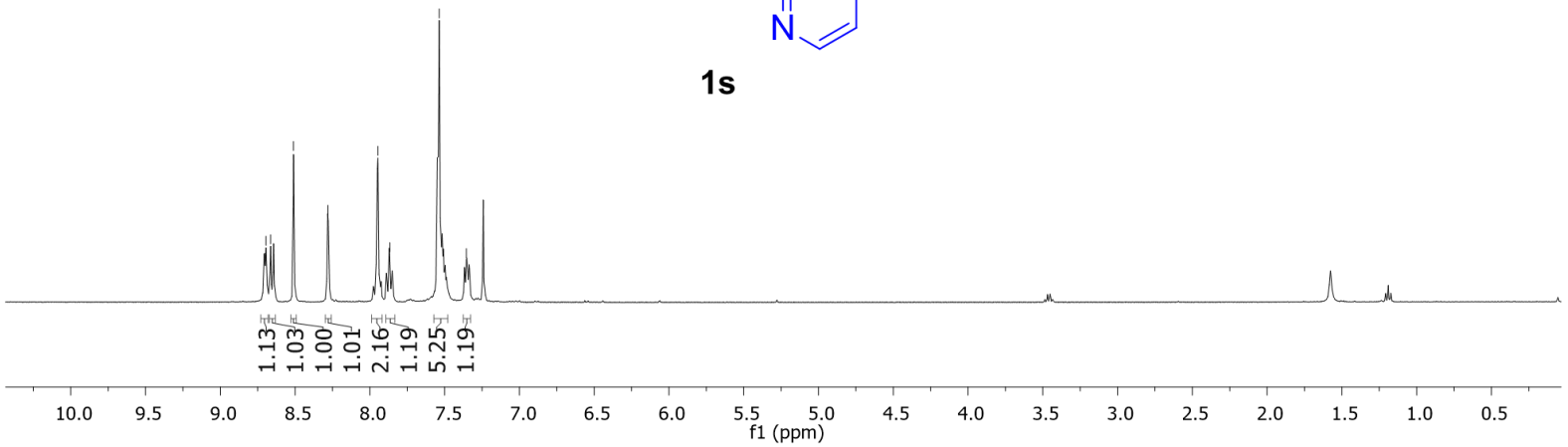

^{1}H NMR taken in $CDCl_3$

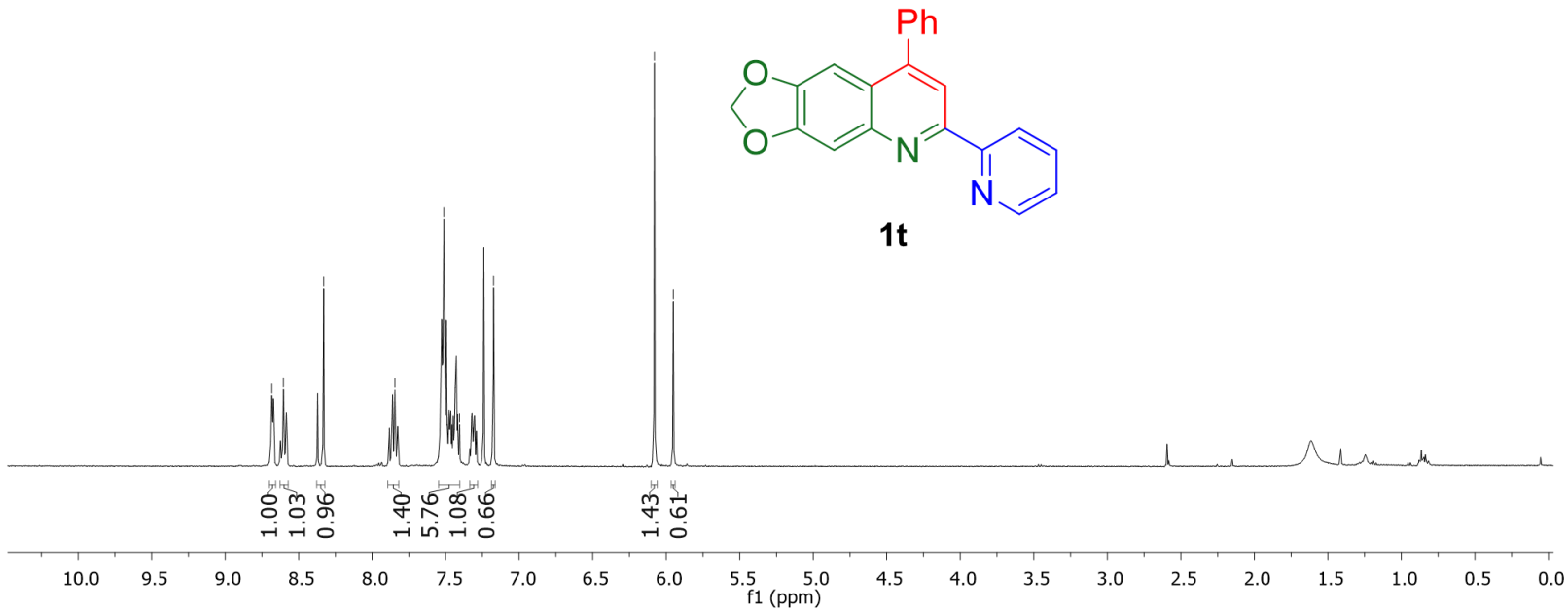

1t

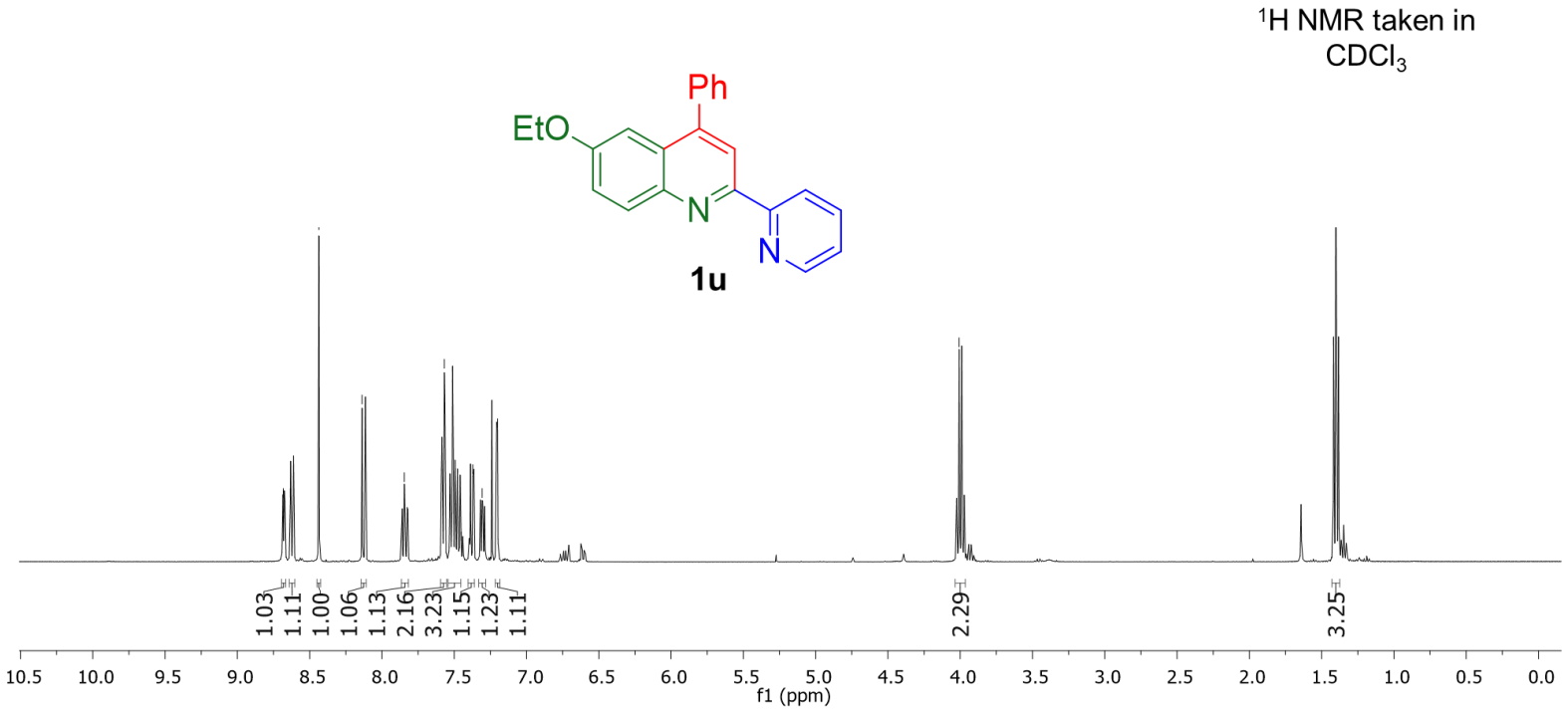
^{1}H NMR taken in
$CDCl_3$
Ph
EtO
N
N
1u
1.03
1.11
1.00
1.06
1.13
2.16
3.23
1.15
1.23
1.11
2.29
3.25
10.5
10.0
9.5
9.0
8.5
8.0
7.5
7.0
6.5
6.0
5.5
5.0
4.5
4.0
3.5
3.0
2.5
2.0
1.5
1.0
0.5
0.0
f1 (ppm)

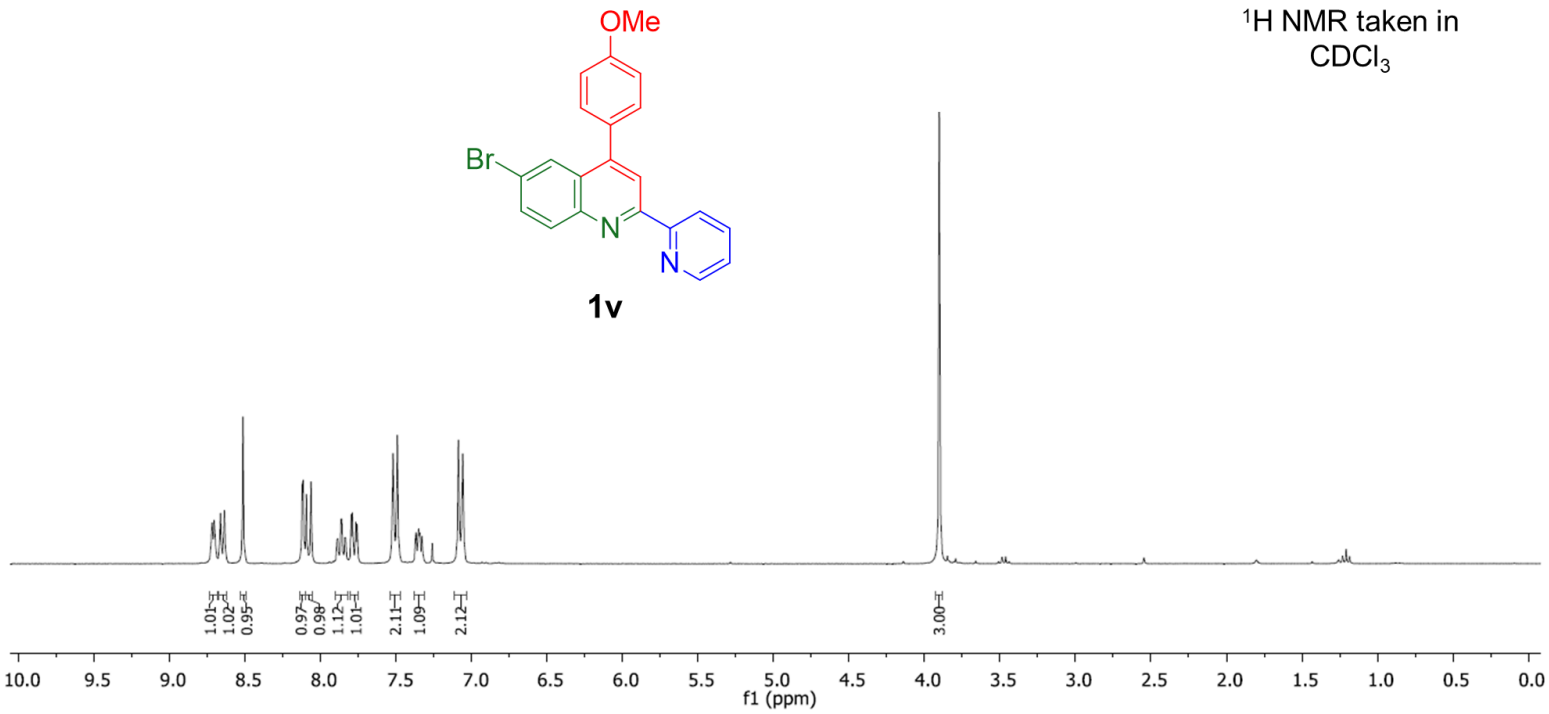
OMe
Br
N
N
1v
^{1}H NMR taken in
$CDCl_3$
1.01
1.02
0.95
0.97
0.98
1.12
1.01
2.11
1.09
2.12
3.00
10.0 9.5 9.0 8.5 8.0 7.5 7.0 6.5 6.0 5.5 5.0 4.5 4.0 3.5 3.0 2.5 2.0 1.5 1.0 0.5 0.0
f1 (ppm)

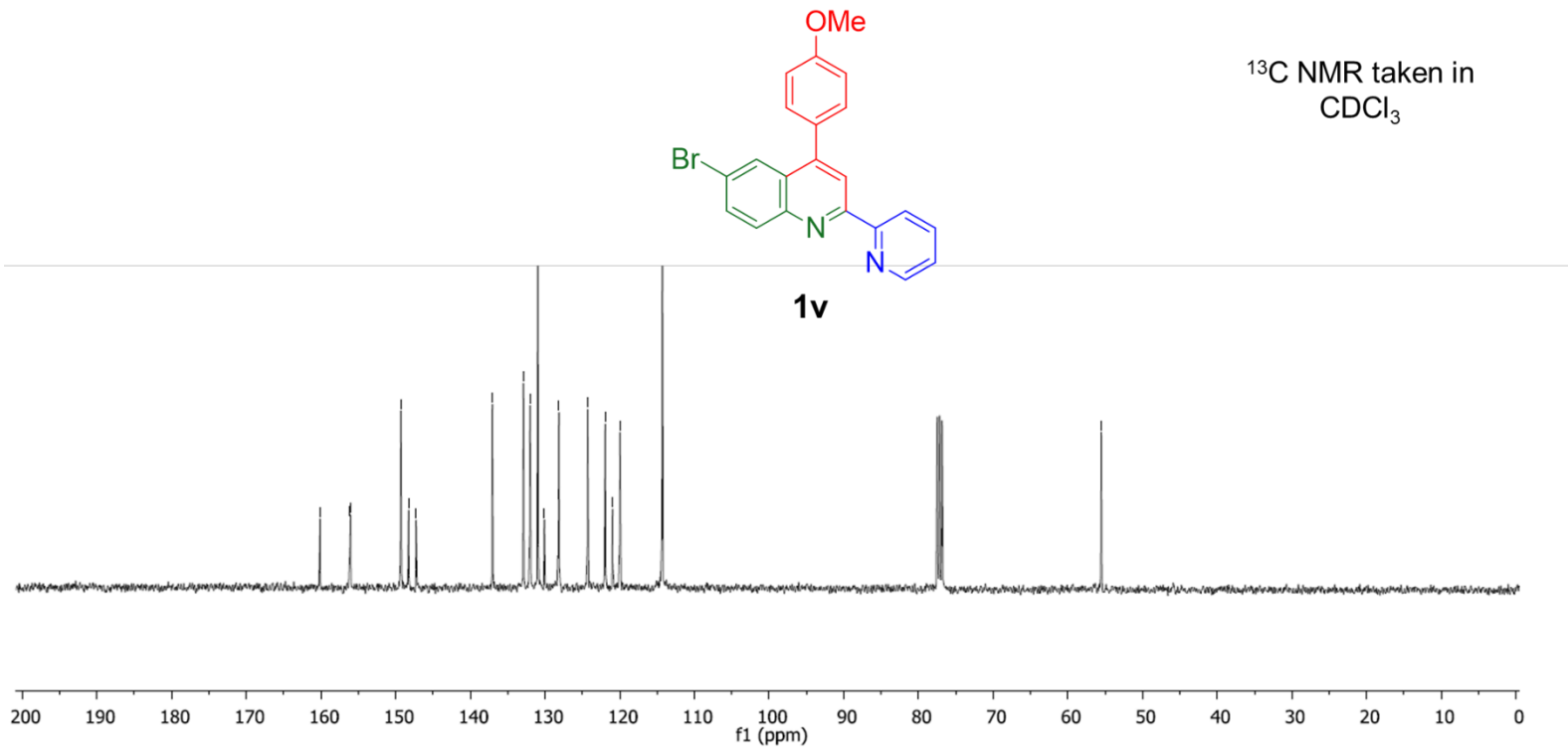
OMe
Br
N
N
1v
^{13}C NMR taken in
$CDCl_3$
200
190
180
170
160
150
140
130
120
110
100
90
80
70
60
50
40
30
20
10
0
f1 (ppm)

Neurodegeneration and Pain – C3AR1

Biological background

- The complement system is a key part of the immune system that enhances the ability of antibodies and phagocytic cells to clear microbes and damaged cells, promotes inflammation, and attacks the pathogen plasma membrane.
- The complement system has been identified as a component of disease risk and response in Alzheimer's disease (AD) through genetics, pathological studies, post mortem gene expression analysis and systems biology, supported by studies of model organisms (mouse).
- Systems biology analysis identified C3AR1 (complement component 3a receptor 1) as a regulatory hub in an innate immunity network, which is upregulated in the AD brain.
- C3AR1 is at the terminal part of the complement system, where it regulates chemotaxis and signaling. **Targeting C3AR1 should ameliorate inflammation while avoiding critical impairment of important complement processes: phagocytosis and clearance (C3b) and the membrane attack complex (C5b/MAC), which could both carry risk.**

Zhang et al., (2013)"Integrated systems approach identifies genetic nodes and networks in late-onset Alzheimer's disease". Cell; 153(3):707-720.
Lian et al.'(2016) "Astrocyte-Microglia Cross Talk through Complement Activation Modulates Amyloid Pathology in Mouse Models of Alzheimer's Disease". Journal of Neuroscience, 36 (2) 577-589.

Flow Scheme & Assay Measures

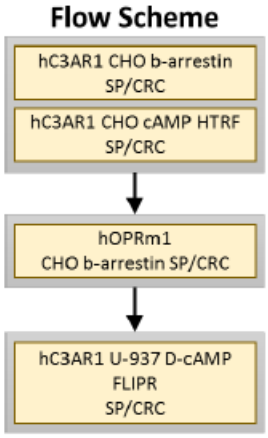

C3AR1 Assay Measures

Primary Assays
hC3AR1 CHO Beta-arrestin Inhibition SP (% Inhibition)
hC3AR1 CHO Beta-arrestin Inhibition CRC (IC50)
hC3AR1 CHO cAMP HTRF Inhibition SP (% Inhibition)
hC3AR1 CHO cAMP HTRF Inhibition CRC (IC50)

Secondary Assays
hOPRm1 CHO Beta-arrestin Antagonist SP (% Inhibition)
hOPRm1 CHO Beta-arrestin Antagonist CRC (IC50)

Confirmatory Assays
hC3AR1 U-937 D-cAMP induced FLIPR SP (% Inhibition)
hC3AR1 U-937 D-cAMP induced FLIPR CRC (IC50)

SP = Single Point
CRC = Concentration Response Curve

Oncology – CD73

CD73 (Cluster of Differentiation 73, or 5'-nucleotiase) is an enzyme in human encoded by *NT5E* gene. It is an extracellular enzyme that catalyzes a rate-limiting step in the conversion of ATP to adenosine. It serves as an immune suppressant that impairs antitumor immune responses and enhances tumor immune escape via activation of adenosine receptors. CD73 generates immunosuppressive adenosine within hypoxic tumor microenvironment which leads to abnormality in immune cell infiltration, tumor progression, metastasis and poor disease outcomes. CD73 knock-out mice are significantly protected against the development of tumor and metastasis. Therefore, therapies targeting CD73 through adenosinegergic pathway may lead to novel cancer immune therapy.

Compounds of interest that inhibit CD73 activity will be further characterized for their effects on the target in a cellular assay system.

- Young A, Mittal D, Stagg J, Smyth MJ. (2014). Targeting cancer-derived adenosine: new therapeutic approaches. Cancer Discov. Aug;4(8):879-88.
- Allard B, Pommey S, Smyth MJ, Stagg J. (2013). Targeting CD73 enhances the antitumor activity of anti-PD-1 and anti-CTLA-4 mAbs. Clin Cancer Res. Oct 15;19(20):5626-35.

Flow Scheme & Assay Measures

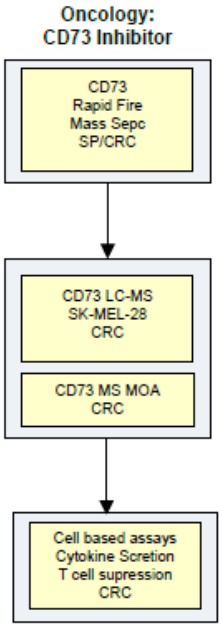

CD73 Inhibitor

Primary Assays
CD73 RapidFire Mas Spec assays SP (% Inhibition)*
CD73 RapidFire Mas Spec assays CRC (IC_{50})*

Secondary assays
Adenosine CD73 AMP LC-MS, SK-MEL-28 cells, SP/CRC (% Inhibition/IC_{50})
Adenosine CD73 CMP LC-MS, SK-MEL-28 cells, SP/CRC (% Inhibition/IC_{50})
CD73 MS MOA CRC (IC_{50})

SP= Single Point
CRC= Concentration Response Curve

Endocrine/Cardiovascular – GLP-1 Secretion

Glucagon-like peptide 1 (GLP-1) is derived from transcription of the proglucagon gene followed by post-translational modifications of proglucagon to the following biologically active peptides: GLP-1 (7-37) and GLP-1 (7-36) NH2. GLP-1 secretion by ileal L cells is dependent on the presence of nutrients in the lumen of the small intestine. GLP-1 is a potent anti-hyperglycemic hormone inducing glucose-dependent insulin secretion and suppressing glucagon secretion. The glucose dependency of this mechanism is particularly important because GLP-1 does not stimulate insulin secretion and cause hypoglycemia when plasma glucose concentrations are in the normal fasting range.

The GLP-1 secretion, diabetes phenotypic module identifies compounds that stimulate secretion of glucagon-like peptide one (GLP-1) in mouse and human cell lines derived from gastrointestinal tract tissue. GLP-1 secretion is measured using a Lilly proprietary ELISA assay that was specifically designed to detect the appropriate forms of GLP-1 secreted from these cells. If active in the cell-based GLP-1 assay, molecules will be further tested for selectivity in assays that measure activation of GPCRs known to stimulate GLP-1 secretion. Compounds of interest act to stimulate GLP-1 secretion through novel, unknown mechanisms.

- Glucagon-Like Peptide 1-Based Therapies for Type 2 Diabetes: A Focus on Exenatide (2011) Kathleen Dungan and John B. Buse; *Clinical Diabetes*: 29 (1).
- Glucagon-Like Peptide 1 Secretion by the L-Cell (2006) Gareth E. Kim and Patricia L. Brubaker; *Diabetes*: 55 (supplement 2)

Flow Scheme & Assay Measures

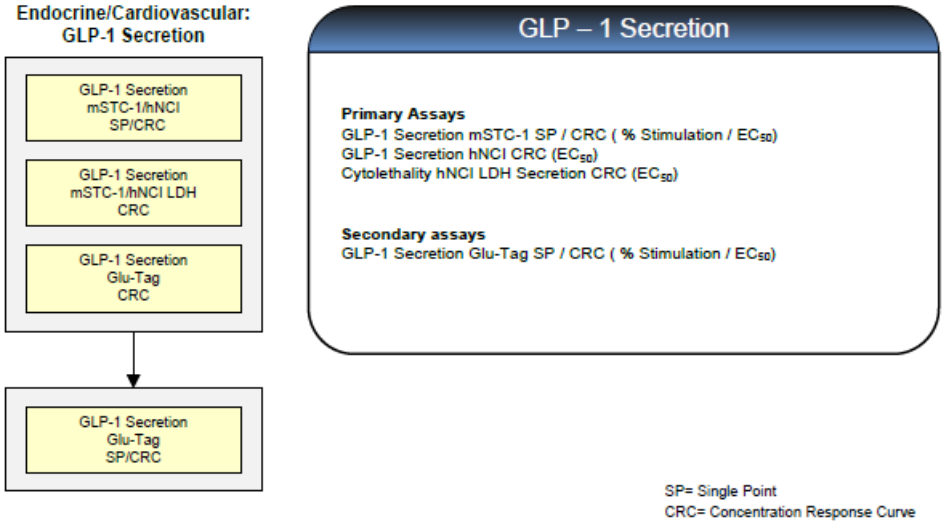

Endocrine/Cardiovascular – GLP-1R PAM

The glucagon-like peptide-1 receptor (GLP-1R) is a member of the peptide hormone binding class B family of G-protein coupled receptors. The best characterized function of the GLP-1R is in pancreatic β cells where its activation increases cAMP production thereby enhancing glucose-dependent insulin secretion. The therapeutic success of injectable GLP-1R peptide agonists for the treatment of type 2 diabetes mellitus (T2DM) has inspired efforts to identify non-peptide activators of the GLP-1R that would offer the advantage of being orally bioavailable.

We seek to identify small molecule positive allosteric modulators (PAMs) of the GLP-1R for the treatment of T2DM. We desire compounds that are orally bioavailable with a suitable solubility.

- Willard et al, (2012) "Small molecule allosteric modulation of the glucagon-like peptide-1 receptor enhances the insulinotropic effect of oxyntomodulin." *Mol Pharmacol*, 82:1066-73.
- Wootten et al, (2012) "Allosteric modulation of endogenous metabolites as an avenue for drug discovery." *Mol Pharmacol*, 82:281-90.

Flow Scheme & Assay Measures

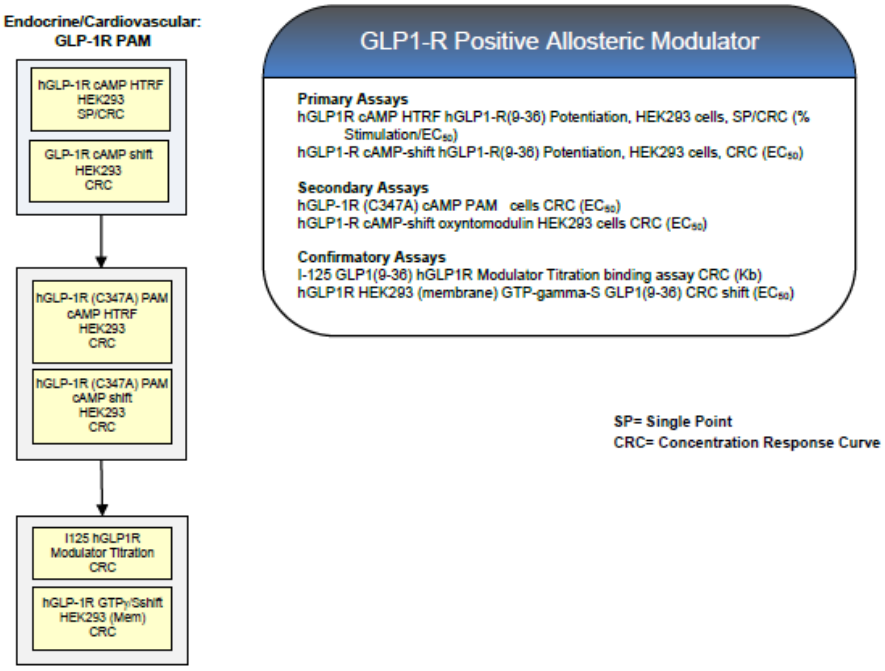

Endocrine/Cardiovascular – FFAR4 (GPR120) Agonist

FFAR4 (GPR120) is a receptor for long-chain fatty acids including Omega-3 fatty acids. GPR120 is expressed in tissues relevant to metabolic disease and diabetes, including the pancreas, adipose tissue, gastrointestinal tract, and the pituitary gland. Activation of GPR120 plays a pivotal role in the regulation of body weight and glucose homeostasis. In humans a loss of function mutation in GPR120 (R270H mutation) is associated with increased body mass index and fasting glucose levels. Moreover, GPR120 knockout mice are obese and insulin resistant/glucose intolerant. Recently, small molecule GPR120 agonists have demonstrated glucose lowering by an improvement in insulin sensitivity and reduction in inflammation in obese. These data support activation of GPR120 would provide therapeutic benefit in the treatment of diabetes.

Identification of GPR120 agonists with selectivity against other free fatty acid receptors will allow us to further evaluate the role of GPR120 in the regulation of metabolism and glucose homeostasis.

- Ichimura A, et al., (2012) "Dysfunction of lipid sensor GPR120 leads to obesity in both mouse and human." *Nature* 483:350-354.
- Bonnefond A, et al., (2015) "Contribution of the low-frequency, loss-of-function p.R270H mutation in FFAR4 (GPR120) to increased fasting plasma glucose levels." *J Med Genetics* doi: 10.1136/jmedgenet-2015-103065
- Oh da Y, et al., (2014) "A GPR120-selective agonist improves insulin resistance and chronic inflammation in obese mice." *Nat Med* 20(8): 942-947.

Flow Scheme & Assay Measures

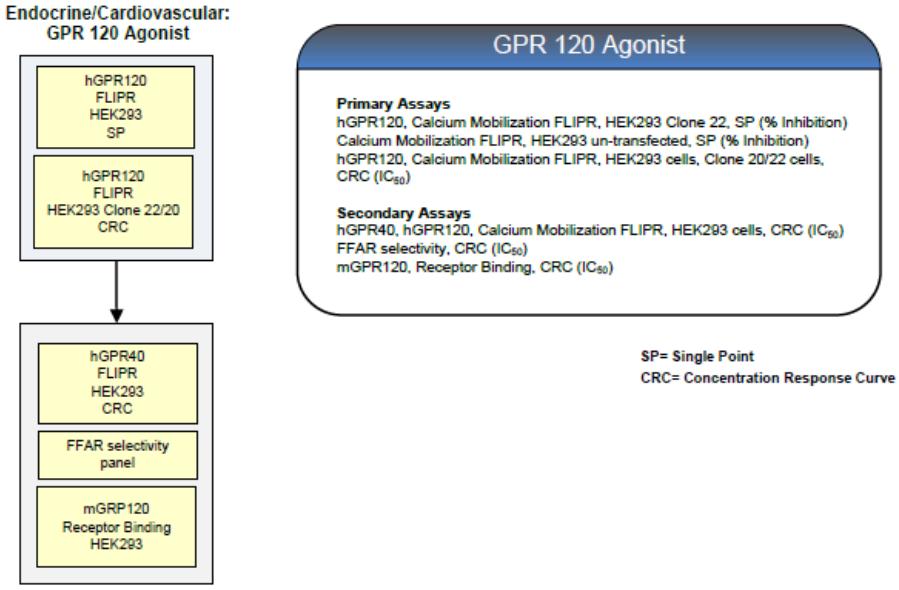

Oncology – NNMT Inhibitor

Metabolic changes driven by activation of oncogenes, inactivation of tumor suppressors, and pro-tumorigenic mutations are considered a hallmark of cancer. One cancer-associated metabolic enzyme, **N**icotinamide **N**-**M**ethyl**T**ransferase (NNMT), catalyses the transfer of methyl groups from the methyl donor S-adenosyl-L-methionine (SAM) to nicotinamide, generating S-Adenosylhomocysteine (SAH) and methylnicotinamide (MNAM). Previous reports have connected the increased expression levels of NNMT in cancer cells with chemotherapy and radiation resistance as well as increased tumor aggressiveness.

Furthermore, downregulation or silencing of NNMT has been shown to increase the sensitivity of carcinoma cells to radiation therapy and decrease tumorigenicity, providing key support for the role of NNMT in promoting treatment resistance and tumorigenesis in cancer cells. Thus, compounds able to modulate the activity of NNMT in the setting of oncology may have therapeutic utility.

- Ulanovskaya OA, Zuhl AM, Cravatt BF. (2013) NNMT promotes epigenetic remodeling in cancer by creating a metabolic methylation sink. Nature chemical biology. 9(5):300-6.
- Sauve AA. (2008) NAD+ and vitamin B3: from metabolism to therapies. J Pharmacol Exp Ther.324(3):883-93.
- van Haren, M.J., Sastre Toraño, J., Sartini, D., Emanuelli, M., Parsons, R.B., *Martin, N.I. (2016). A rapid and efficient assay for the characterization of substrates and inhibitors of nicotinamide N-methyltransferase. Biochemistry, 55(37):5307-15.

Flow Scheme & Assay Measures

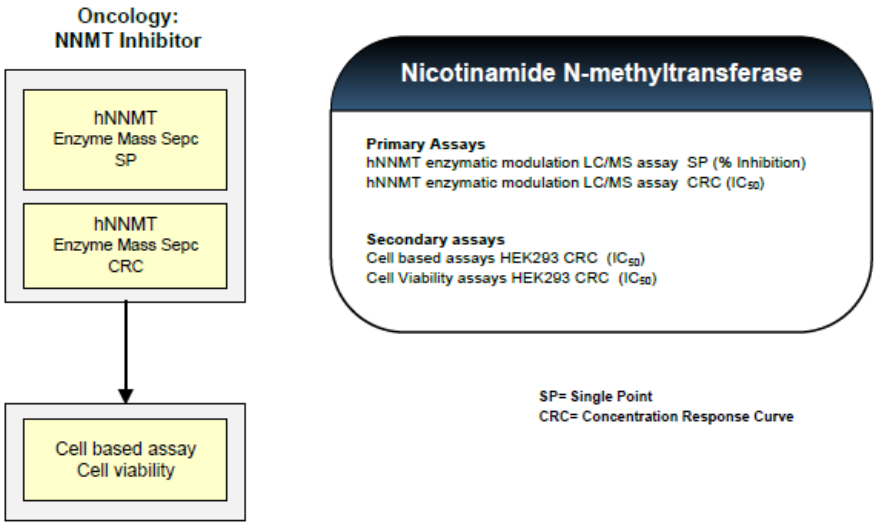

Autoimmune – IL-17 Protein Protein Interaction

Current literature suggests that IL-17A has three main roles: 1) host defense against extracellular bacteria and fungi, 2) neutrophil homeostasis, and 3) chronic pathogenic inflammation. IL-17A exists as a homodimer (A/A) or as a heterodimer (A/F) with IL-17F. IL-17A is expressed by a subset of T cells, called Th17 cells, at inflammatory sites. Most cell types can respond to the local production of IL-17A because of the near ubiquitous expression of IL-17A receptors, IL-17RA and IL-17RC. IL-17A stimulates the release of cytokines and chemokines designed to recruit and activate both neutrophils and memory T cells to the site of injury or inflammation and maintain a proinflammatory state. IL-17A-producing "pathogenic" T cells contribute to the pathogenesis of autoimmune diseases, including psoriasis, psoriatic arthritis, rheumatoid arthritis and anklyosing spondylitis. Neutralizing antibodies to IL-17A have demonstrated profound clinical efficacy in patients with plaque psoriasis.

- Gaffen, S. L., R. Jain, et al. (2014). "The IL-23-IL-17 immune axis: from mechanisms to therapeutic testing." *Nat Rev Immunol* 14(9): 585-600.
- Gaffen, S. L. (2009). "Structure and signalling in the IL-17 receptor family." *Nat Rev Immunol* 9(8): 556-567.

Flow Scheme & Assay Measures

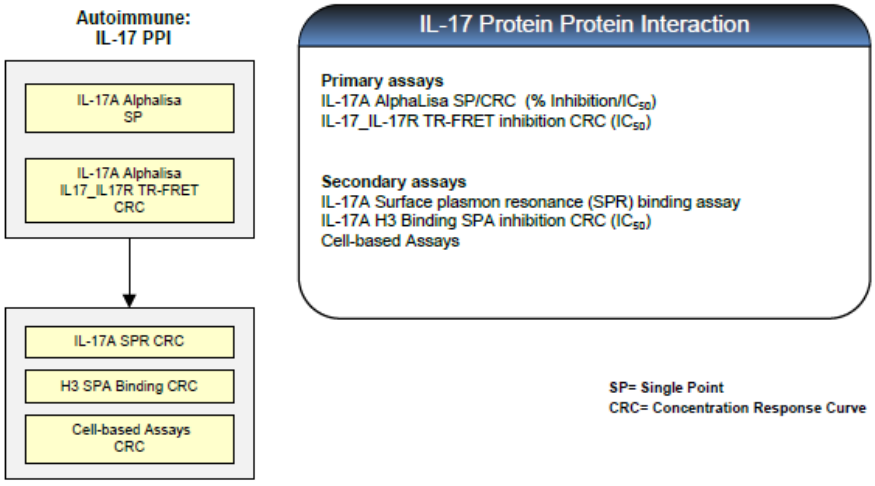

Neurodegeneration and Pain – KCNQ2/3 Agonist

KCNQ2/3 (also known as Kv7.2/7.3) is a heteromeric voltage-gated potassium channel. Together with other members of the Kv7 subfamily of voltage-gated potassium channels, KCNQ2/3 underlies the neuronal M current [1] that modulates excitability in many neurons of the central and peripheral nervous system. KCNQ2/3 is exclusively expressed in the nervous system, and it is the predominant subtype in pain sensing neurons in the dorsal root ganglion (DRG) and spinal cord. Agonists of KCNQ2/3 hyperpolarize sensory neurons [2], reduce excitability and show efficacy in rodent models of persistent pain [3]. Flupirtine, an agonist of KCNQ channels other than KCNQ1, is used for the short term treatment of neuropathic and musculoskeletal pain[4, 5]. A more selective KCNQ2/3 agonist is expected to have better tolerability than Flupirtine.

1. Wang HS, Pan Z, Shi W, et al. KCNQ2 and KCNQ3 potassium channel subunits: molecular correlates of the M-channel. *Science*. 1998;282:1890-1893.
2. Du X, Hao H, Gigout S, et al. Control of somatic membrane potential in nociceptive neurons and its implications for peripheral nociceptive transmission. *Pain*. 2014;155:2306-2322.
3. Rose K, Ooi L, Dalle C, Robertson B, Wood IC, Gamper N. Transcriptional repression of the M channel subunit Kv7.2 in chronic nerve injury. *Pain*. 2011;152:742-754.
4. Friedel HA, Fitton A. Flupirtine. A review of its pharmacological properties, and therapeutic efficacy in pain states. *Drugs*. 1993;45:548-569.
5. Devulder J. Flupirtine in pain management: pharmacological properties and clinical use. *CNS Drugs*. 2010;24:867-881.

Flow Scheme & Assay Measures

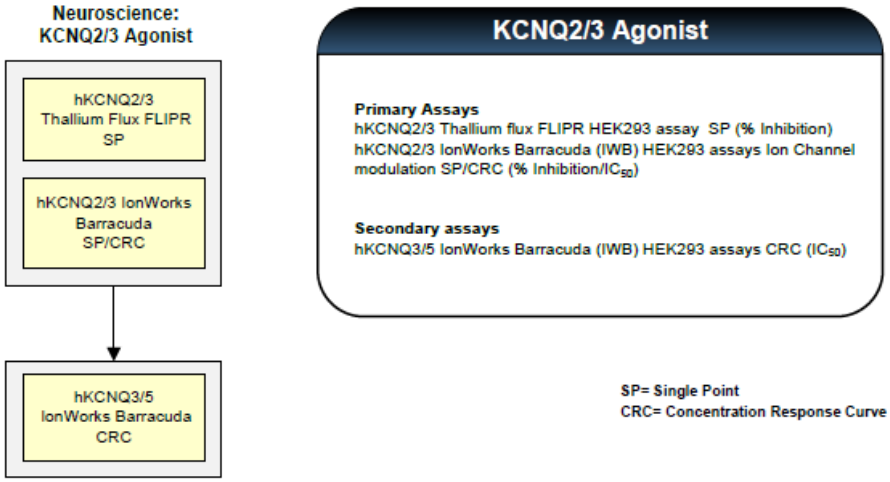

Medicines for Malaria Venture

Malaria Screening Module Description

Medicines for Malaria Venture [MMV] and Lilly are partnering to find compounds that can play an important role in the fight to eradicate malaria. MMV, headquartered in Geneva, Switzerland, is a leading product development partnership (PDF) in the field of antimalarial drug research and development.

The malaria screening module is designed to test compounds in **primary assays** that target activity against liver stages of the parasitic strain of *Plasmodium berghei* (Pb), in particular, against the sporozite infection and the viability of liver schizonts of liver cells. To evaluate parasitic growth, activity in the asexual blood stages of the parasite *Plasmodium falciparum* (DD2 strain) will be tested as well as non-specific cytotoxicity screen.

The ***secondary assay*** will confirm activity in a concentration response curve (CRC) format. Compounds are assessed in pure, stage V gametocytes of *Plasmodium falciparium* (Pf, strain NF54, Saponin-lysis Sexual Stage Assay (SaLSSA). The goal is to identify compounds with gametocytocidal activity which may be suitable candidates for potential transmission blocking ability.

Malaria Research Module Flow Scheme & Assay Measures

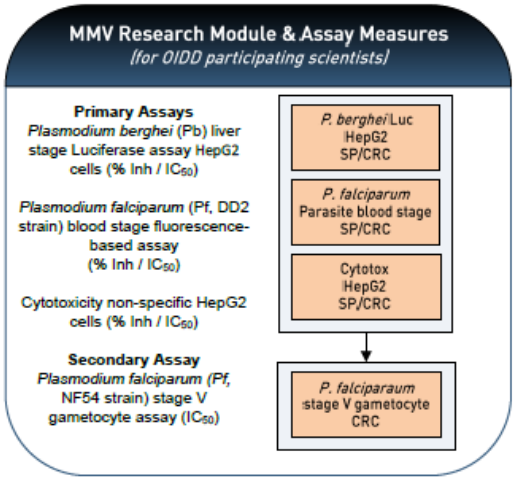

Neuroscience – Nav1.7 Antagonist

Nav1.7 is encoded by the SCN9A gene and is one of nine currently described voltage-gated sodium ion channels. All sodium channels in this family are involved in action potential generation, propagation, and/or neurotransmitter release in excitable tissues. Nav1.7 is expressed primarily in the peripheral nervous system and sympathetic ganglia. Interest in Nav1.7 as a potential therapeutic target for pain comes from several converging lines of evidence. First, many nonselective sodium channels inhibitors are used clinically as anesthetics and analgesics, however their efficacy is typically limited by their lack of selectivity over the other sodium channel anti-targets. In addition, human populations that do not express functional Nav1.7 channels display a phenotype marked by a complete insensitivity to pain, with lack of smell or anosmia as their only noted deficit. Finally, patients with activating or gain of function mutations in Nav1.7 display varying degrees of chronic and intermittent pain.

Collectively, the efficacy of nonselective sodium channel inhibitors combined with the wealth of genetic information (both gain and loss of function) strongly suggests that selective Nav1.7 inhibitors may provide a novel therapeutic approach to chronic pain of different etiologies without significant safety/tolerability side-effects. As such, identification of compounds/chemical scaffolds with high potency and selectivity for blocking Nav1.7 channels is a high priority for Lilly Research Labs.

- Dib-Hajj SD, Yang Y, Black JA, Waxman SG. (2013) "The Na[V]1.7 sodium channel: from molecule to man". *Nat Rev Neurosci.* 14(1): 49-62.
- Goldberg YP, MacFarlane J, MacDonald ML, Thompson J, Dube MP, Mattice M, Fraser R, Young C, Hossain S, Pape T, Payne B, Radomski C, Donaldson G, Ives E, Cox J, Younghusband HB, Green R, Duff A, Boltshauser E, Grinspan GA, Dimon JH, Sibley BG, Andria G, Toscano E, Kerdraon J, Bowsher D, Pimstone SN, Samuels ME, Sherrington R, Hayden MR. (2007) "Loss-of-function mutations in the Nav1.7 gene underlie congenital indifference to pain in multiple human populations". *Clin Genet.* 71(4): 311-319.
- Yang Y, Wang Y, Li S, Xu Z, Li H, Ma L, Fan J, Bu D, Liu B, Fan Z, Wu G, Jin J, Ding B, Zhu X, Shen Y. (2004) "Mutations in SCN9A, encoding a sodium channel alpha subunit, in patients with primary erythermalgia". *J Med Genet.* 41(3): 171-174.

Flow Scheme & Assay Measures

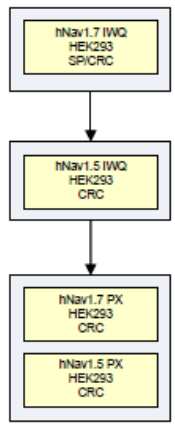

Nav1.7 Antagonist

Primary Assays
hNav1.7 IWQ ephys platform antagonist HEK293 cells SP (% Inhibition)
hNav1.7 IWQ ephys platform antagonist HEK293 cells CRC (IC_{50})

Secondary Assays
hNav1.5 IWQ ephys platform HEK293 cells CRC (IC_{50})

Confirmatory Assays
hNav1.7 PatchXpress ephys antagonist HEK293 cells CRC (IC_{50})
hNav1.5 PatchXpress ephys antagonist HEK293 cells CRC (IC_{50})

SP= Single Point
CRC= Concentration Response Curve

OPEN INNOVATION DRUG DISCOVERY | Lilly | IDRI | The Lilly TB Drug Discovery Initiative

Tuberculosis Screening Module Description

The tuberculosis screening module is designed to test compounds for their ability to prevent growth of a virulent strain of *Mycobacterium tuberculosis* (H37Rv) in liquid medium.

In the **primary assay** compounds are tested for their ability to prevent growth of a genetically-modified, fluorescent reporter strain of *M. tuberculosis* at a single concentration.

The **secondary assay** is determination of the minimum inhibitory concentration (MIC) required to completely inhibit proliferation of *M. tuberculosis* in liquid medium. Compounds of interest have activity against *M. tuberculosis*, with no (or lower) activity against mammalian cells. Concurrently, compounds are assayed in a counter-screen for inhibition of HeLa cells proliferation using CellTiter-Glo® Luminescent Cell Viability Assay. This monitors cell growth by quantitation of ATP levels which correlate with the number of metabolically active cells. Data is reported as reduction of the luminescent signal.

The confirmatory assays form part of a collaborative work agreement with the Lilly TBDDI. These include the following assays:

- measurement of cytotoxicity against VERO cells
- determination if compounds are bactericidal or bacteriostatic
- determination of the kinetics of cidal activity over time (% bacteria killed over a time course of 7 days)
- determination of the resistance frequency i.e. the rate at which spontaneous resistant mutants occur in the population
- activity against non-replicating bacteria (measurement of kill kinetics against bacteria under starvation or hypoxia)
- spectrum of activity against other bacterial species (MIC_{90}s against closely related *mycobacteria*, Gram-positive and Gram-negative bacterial species) and minimum bactericidal concentration (minimum concentration required to kill bacteria over a period of 7-14 days).

TB Research Module Flow Scheme & Assay Measures

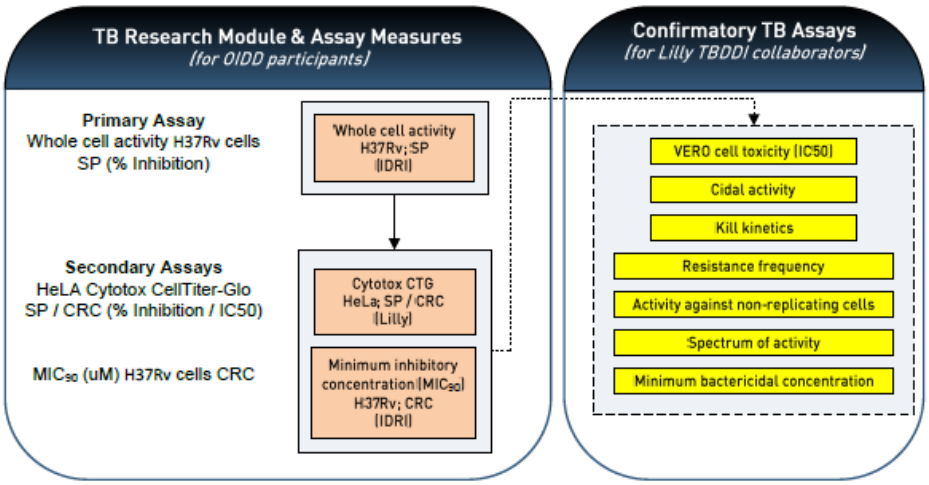

Neurodegeneration and Pain – Protein Translation Inhibition for Alzheimer's disease

Biological background

Alzheimer's disease (AD) is characterized pathologically by the extracellular accumulation of amyloid plaques and intracellular formation of neurofibrillary tangles (NFTs); the former is composed of Aβ protein and the latter is composed of tau protein. Current therapeutic strategies for AD are attempting to target these disease-associated proteins by preventing their accumulation and/or removing them once deposited. Regulating or inhibiting the expression of such proteins, at a protein translation level, may also have therapeutic benefit.

1. Citron M. Alzheimer's disease: strategies for disease modification. Nat Rev Drug Discov. 2010 May;9(5):387-98.
2. Farr SA, Erickson MA, Niehoff ML, Banks WA, Morley JE. Central and peripheral administration of antisense oligonucleotide targeting amyloid-β protein precursor improves learning and memory and reduces neuroinflammatory cytokines in Tg2576 (AβPPswe) mice. J Alzheimers Dis. 2014;40(4):1005-16.
3. DeVos SL, Miller RL, Schoch KM, Holmes BB, Kebodeaux CS, Wegener AJ, Chen G, Shen T, Tran H, Nichols B, Zanardi TA, Kordasiewicz HB, Swayze EE, Bennett CF, Diamond MI, Miller TM. Tau reduction prevents neuronal loss and reverses pathological tau deposition and seeding in mice with tauopathy. Sci Transl Med. 2017 Jan 25;9(374).

Flow Scheme & Assay Measures

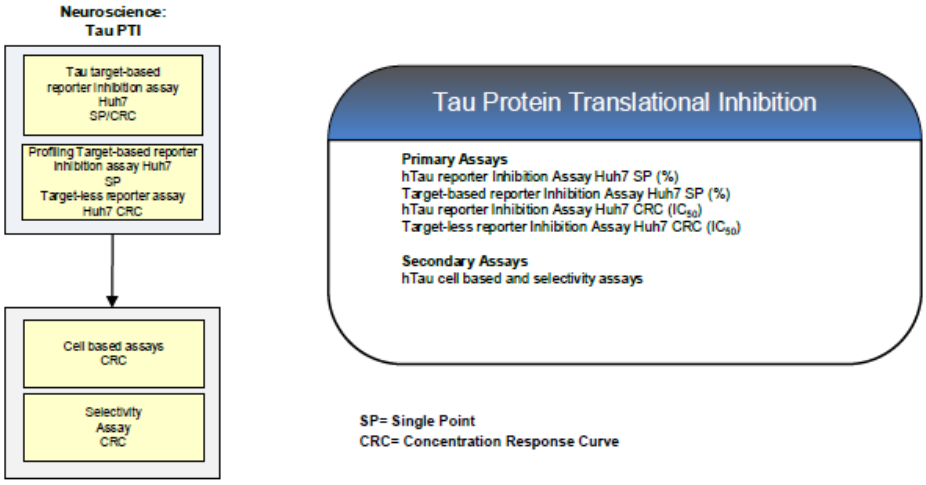

SP= Single Point
CRC= Concentration Response Curve

Chapter 3: Synthesis of Novel Gold (III) Complexes with PyQuin Ligands

3.1 Introduction

The rich history of gold and its impact on mankind is undeniable: the high positive normal potential reduces reactivity and allows it to be found in large deposits (i.e. nuggets), causing onrushes of miners seeking fortune;[1] its high luster, malleability, and resistance toward oxidation and dulling meant it was an ideal material for crafting and ancient art;[2] the innate preciousness of gold gave foundation for cultural myths, one example being the avarice of king Midas.[3] While it is irrefutable that gold is one of the most tightly associated elements with the human race, the chemical history of the element has left much to be desired.

The basis for many of the applications of gold, whether it be in dental medicine, treatment of arthritis, or anticancer therapeutics, have relied on the assumption that gold is more-or-less inert.[4] Gold crowns are ideal because they can mold around dental cavities and be unperturbed by acidic food and drink or oxidation; arthritic gold treatments, most popularly sodium aurothiomalate injections, are successful due to the gold's immunosuppressive and anti-rheumatic effects and the solubilizing ability of the thiomalate backbone;[5] Anti-cancer therapeutics that use gold almost always incorporate metallic, not ionic gold. Metallic gold has shown to have beneficial properties when treating certain cancers (this will be discussed further in later chapters), however gold in any ionic form is considered toxic.[6]

In terms of chemical applications, namely as a catalyst, gold has often been overlooked, which is interesting given all of the elements surrounding it on the periodic table have rich histories of catalysis. This is likely due to two major reasons: first, because gold has been observed to be incredibly stable in environments where other elements would normally react, it may have been considered too inert to participate in any chemistry. Elemental gold is notoriously insoluble in any "normal" conditions, which is a large contributor to its high value: extracting gold from rock is typically done through the MacArthur-Forrest process in which ore is crushed into a powder, combined with a solution of a metal cyanide, and slacked lime ($Ca(OH)_2$) to limit generation of hydrogen cyanide, an toxic gas byproduct.[7] Due to gold's alleged inability to dissolve in anything other than cyanides or aqua regia, developing methods for its use as a catalyst seemed completely futile.

The other major reason for gold's absence in common catalytic methods is the high value associated with gold, which makes it appear unaffordable. Anything with the tag "gold" is generally higher-end, whether it be the purity grade of a chemical or a credit card. This reasoning, however, is erroneous as there are *many* industrial processes which use highly expensive metals as catalysts, one of which being the Monsanto Acetic Acid Process.[8] This process, which produces acetic acid through the catalytic carbonylation of methanol, is a rhodium complex-catalyzed transformation. This process, which was developed in 1960 by BASF and improved by the Monsanto Company in 1966, has largely

been supplanted by the Cativa process, developed in 2000.[9] Albeit similar, as both processes are methods for carbonylating methanol, the Cativa process differs in that it is catalyzed by an iridium complex. Both rhodium and iridium are incredibly expensive in their chloride salt forms which are necessary to synthesize the active metal complexes. Gram-for-gram, the analogous gold chloride salts are actually the *least* expensive when compared to iridium and rhodium, however the history of successful catalysis with the latter two metals appears to outweigh their upfront cost.

While historically gold has been overlooked for other metals in terms of viability as a catalyst, recent advances in gold chemistry have proven its worth. When organic molecules (ligands) are attached to an ionic gold center, these gold complexes are significantly more functional as catalysts. The solubilizing effect of the ligands in addition to them preserving the gold in an active ionic form (rather than its inert metallic form) allow for exploration of gold catalysis. Gold complexes have shown prowess in catalyzing a wide variety of chemical transformations, many on par with the respective traditional catalysts.[10] When one looks at the gold complexes that have been investigated for their use as functional catalysts, the overwhelming majority of these complexes utilize gold in its +1-oxidation state.

Apart from elemental gold (0), gold has two major oxidation states: gold (I) has 10 *d*-shell electrons and forms 2-coordinate, linear, 14 electron complexes; gold (III) has 8 *d*-shell electrons and are almost always 4-coordinate, square

planar, diamagnetic 16 electron complexes. As stated earlier, these ionic gold species are purportedly toxic, however there has been much success in developing gold (III) chloride complexes that combat cancer, specifically cisplatin-resistant cell lines.[11] In addition to potential therapeutic applications, gold (III) has characteristics that would, in theory, make it a much more desirable catalyst than gold (I): first, the higher oxidation state means the gold center is significantly more electrophilic than a gold (I) analogue. If there is any coordination to the metal by the reaction substrate, a tighter association could lead to heightened selectivity, yield, etc. Secondly, since gold (I) complexes are strictly linear and two-coordinate, there is a limitation in how many ligands can actually associate to the metal. Gold (III) complexes can incorporate multiple ligands that can dissociate from the metal center, thus creating the opportunity for an oxidative addition – transmetalation – reductive elimination style of catalysis. Being four-coordinate, gold (III) complexes are much more analogous to Pt (II), Pd (II)/(IV), and other catalytically successful complexes. Finally, gold (III) complexes, in comparison gold (I) complexes, are *vastly* under-investigated. Strictly from a novel research perspective, there are many ligand families that have yet to be complexed to a gold center and, in turn, have never been used as catalysts for basic chemical transformations. This is not to say that gold (III) complexes are completely unexplored: many metal complexes of various bidentate nitrogen ligands employing a gold (III) center have been synthesized.

3.2 Gold (III) Complexes as Catalysts

In a +3 oxidation state, gold conforms to a square planar, four coordinate geometry with either halides or other X-type ligands used to stabilize the metal center. The simplest neutral gold (III) halide complex, gold trichloride or $AuCl_3$, has been shown to be a potent catalyst for cyclization reactions. In 2006 Dyker et al. (**Scheme 3.1**) used auric chloride to facilitate the cyclization of substrates constructed from Ugi four-component reactions (later in this document, the affinity gold (III) has for cyclizing compounds that contain alkyne and amine moieties will be fully discussed).[12]

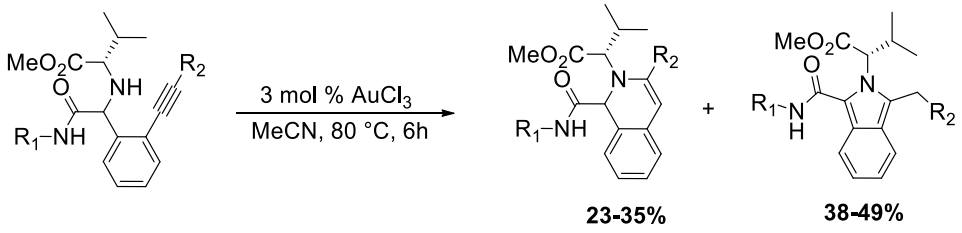

Scheme 3.1 Ugi cyclization catalyzed by the gold salt $AuCl_3$

While gold trichloride is functional as a catalyst in this process, it has been observed that sometime the neutral gold (III) species is not reactive enough and a salt is required. The acidic salt of $AuCl_3$, $H[AuCl_4]$ or "auric acid", is significantly more reactive than $AuCl_3$. While $AuCl_3$ can be weighed out and handled on a benchtop, auric acid readily decomposes upon exposure to air and requires weighing and storage in inert atmosphere. While more taxing to worth with,

H[$AuCl_4$] has been shown to catalyze very useful chemical transformations, namely the hydrochlorination of alkynes (**Scheme 3.2**).[13]

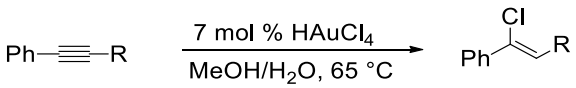

Scheme 3.2 Hydrochlorination of alkynes performed with auric acid catalyst

It is generally agreed upon that an anionic metal species and some positively charged species to form an ionic salt pair is a more ideal way to introduce a metal rather than a neutral one. If the pair is too reactive, such is the case with auric acid, the benefit of a more reactive compound can be overshadowed by its practical difficulty. For this reason, the gold (III) salt sodium tetrachloroaurate ($NaAuCl_4$) has supplanted auric acid as a way to introduce gold (III) as a catalyst or as a precursor to forming a gold (III) complex. The catalytic potential of $NaAuCl_4$ has been explored thoroughly, finding great success in the hydroamination of alkynes, both internal and external (**Scheme 3.3**).[14]

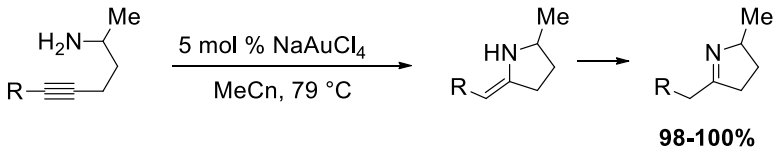

Scheme 3.3 Sodium tetrachloroaurate-catalyzed intramolecular hydroamination

Gold (I) complexes, many being a combination of one phosphine ligand and one x-type ligand, have been used thoroughly to catalyze reactions, both racemic and stereoselective.[15] These complexes are quite stable and can employ many different phosphines and halides/triflates/etc., however sometimes the overall neutral gold (I) species was not able to catalyze the desired process. Using a silver salt (e.g. $AgBF_4$, AgOTf, $AgPF_6$ etc.), the coordinated halide could be abstracted from the gold center, leaving an exposed cationic gold complex.[16] Gold (I) has had a rich history of catalysis, both as salts and in synthesized complexes, however examples of gold (III) complexes are few and far between. For this reason, an exploration into the construction of gold (III) complexes using our group's ability to modularly synthesize heteroaromatic, bidentate nitrogen ligands in single step was commenced.

3.3 Gold (III) Complexes with Bidentate Ligands Precedent

One ligand class, 2-(2′-pyridyl)quinoline ligands, have resulted in some unprecedented results when complexed to gold. As stated earlier, gold (III) are *almost* always observed to have a four-coordinate, square planar geometry. In 1978, a 2-(2′-pyridyl)quinoline gold (III) dichloride complex was synthesized using sodium tetrachloroaurate and it was found to have a 5-coordinate, pseudo square-based pyramidal geometry with 3 chlorines bound to the gold center (**Figure 3.1**).[12] This unconventional geometry has been seen in other situations with other ligands, and it is attributed to the steric crowding of the gold-chloride

bond and protons on the ligand, forcing the halide out of the bidentate ligand plane.[13] As shown in **(Figure 3.1)**, a chlorine ligand on the gold center and a proton from the ligand (shown in red) become very close in proximity which, if the geometry were to stay in the preferred square planar, would result in the two atoms trying to occupy the same space.

Figure 3.1 Series of ligands which force five-coordinate geometry due to steric crowding

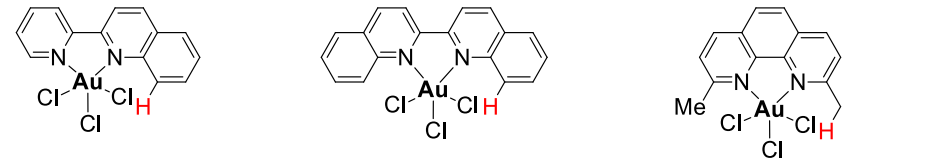

Pyridyl Quinoline (pq) **Biquinoline (biq)** **2,9-dimethylphenanthroline (dmp)**

By contorting into a 5-coordinate geometry where the chlorines and one of the nitrogen atoms on the ligand form a plane, the remaining nitrogen forms a long-distance electrostatic interaction with the gold, pulling it out of the plane. This relieves the steric interference and results in the unconventional pseudo square-based pyramidal geometry observed across all these complexes. Even though there have been efforts to determine the cause of the novel structure of these gold complexes, there had not been an investigation into the effect of systematic changes to the ligand. In other words, comparing three classes of ligands may give insight into why the geometry is distorted, but comparing the same ligand with different substitution patterns would allow for drawing conclusions about the nature of the complex as a whole.

3.4 Synthesis of R-PyQuin($AuCl_3$) and R-PyQuin($AuCl_2$)$^+$ Complexes

As discussed in an earlier chapter, there are multiple routes for synthesizing 2-(2′-pyridyl)quinolines: a Friëdlander cyclization of o-aminobenzaldehyde and 2-acetylpyridine forms 2-(2′-pyridyl)quinoline;[19] another synthesis could be through Stille cross-coupling with a 2-bromoquinoline and a stannylpyridine.[20] Because o-aminobenzaldehydes for the Friedlander cyclization and substituted 2-bromoquinolines for cross-coupling cost hundreds of dollars per gram, these starting materials are generally synthesized as opposed to purchased.[21] The method developed in the Larsen group allows for the synthesis of 2-(2′-pyridyl)quinoline ligands in a single step through the three-component reaction of an aniline, phenylacetylene, and 2-pyridinecarboxaldehyde; additionally, the low-cost of these commercially available starting materials and their substituted variants allow for building a library of PyQuins ranging from electron-rich to electron-poor **(Table 3.1)**.

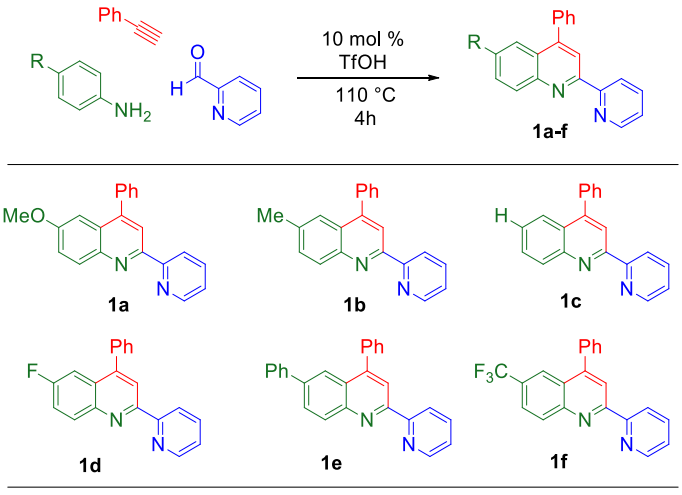

Table 3.1 One-Step Synthesis of PyQuin Ligands with Electron-Rich to Electron-Poor Substituents

These novel compounds were then used to form gold (III) chloride complexes in a fashion similar to O'Connor and Sinn's report in 1978. Their reported synthesis, however, did yield a discrete gold (III) complex with our PyQuin ligand (**Scheme 3.4)**. As discussed earlier, there is precedent that sodium tetrachloroaurate ($NaAuCl_4$), although more pleasant to work with than auric acid, is sometimes not a labile enough gold (III) source.

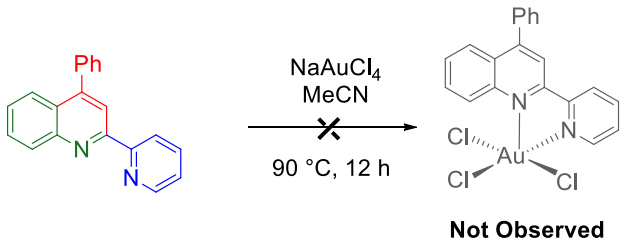

Scheme 3.4 Literature precedent unsuccessful for PyQuin ligands

Since this was suspected to be the problem, an equivalent of silver tetrafluoroborate ($AgBF_4$) was added in addition to the gold salt. Upon dissolution, four species form in the solution: Na^+, Ag^+, $[AuCl_4]^-$, and BF_4^-. The silver abstracts a chloride from the gold center, generating $AuCl_3$ *in situ* and precipitating out of solution as AgCl. While $NaAuCl_4$ was not electrophilic enough to complex with the PyQuin ligand, the generated $AuCl_3$ is: from this reaction, four discrete gold (III) complexes were isolated and characterized (**Scheme 3.5**). As desired, this series ranged from electron-rich to electron-poor PyQuin ligands

which allowed for further investigation into the electronic nature of these gold (III) complexes.

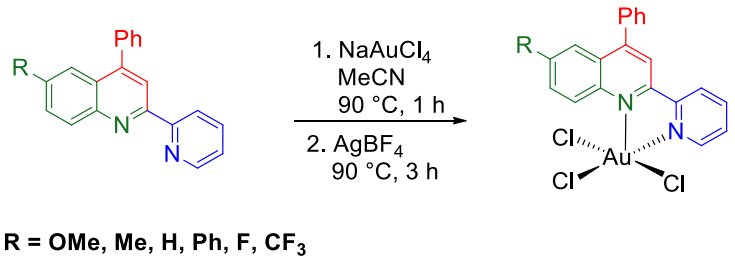

Scheme 3.5 Synthesis of Diverse R-PyQuin($AuCl_3$) complexes

Using silver tetrafluoroborate to abstract one chlorine atom to form net-neutral R-PyQuin($AuCl_3$) complexes has shown to be a robust method that works for structurally different PyQuin ligands. While neutral complexes are inherently more stable than charged species, the other side of the coin is that they are less reactive. This is fine if the goal was to make a stable gold (III) complex (which was successful), however it is also desirable to synthesize novel catalysts. For this reason, a method for cationic gold (III) complexes was also developed. This was shown to be successful in two ways, one being direct and the other step-wise. As described earlier, an equivalent of silver tetrafluoroborate is added alongside the sodium tetrachloroaurate in order to abstract one chloride atom and produce $AuCl_3$ in situ. A cationic gold (III) dichloride complex can be formed simply by increasing the stoichiometry of $AgBF_4$ to 2 equivalents instead of 1 (**Scheme 3.6**). In addition to the direct method, a solution of previously isolated PyQuin($AuCl_3$) in acetonitrile can be heated with an equivalent of $AgBF_4$. This

results in a large amount of white precipitate formation (AgCl), indicating a second chloride has been abstracted and the cationic complex has formed.

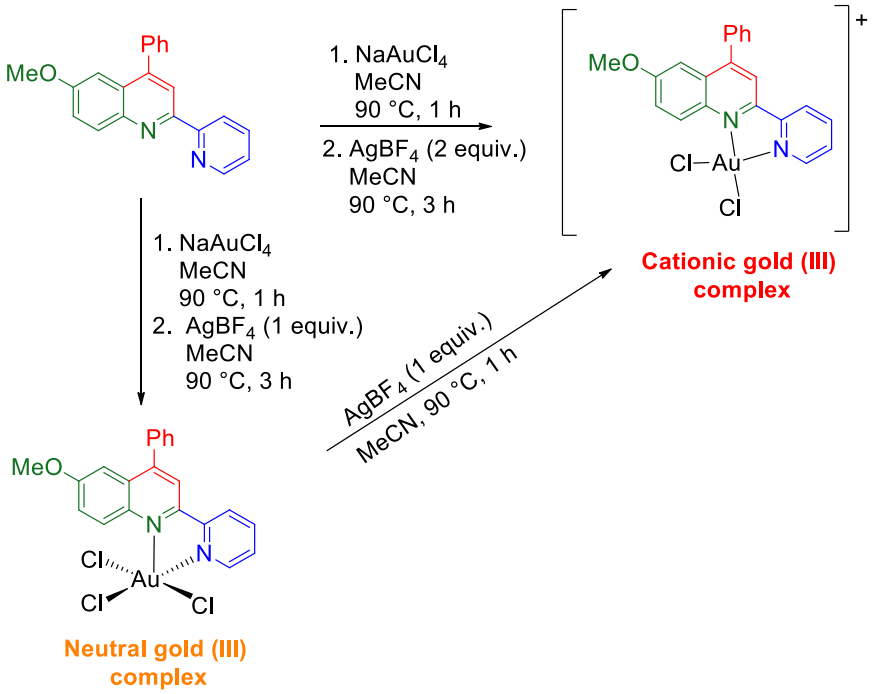

Scheme 3.6 Syntheses of Cationic MeO-PyQuin$(AuCl_2)^+$

While it is important to determine the difference between the synthesized complexes using common characterization methods such as NMR (which will be discussed shortly), metal complexes often display interesting qualitative properties and the PyQuin gold (III) complexes are no different. On the periodic table, gold is surrounded by metals that are, frankly, quite dull in color; relativistic effects of electrons slowing down around the gold nucleus give gold its vibrant yellow color.[22] It also happens to be the case that gold (I) and gold (III)

complexes differ significantly in color: gold (I) complexes tend to be very pale yellow; gold (III) complexes are often orange and in the case of cationic species, deep ruby red. This differentiation is seen with other metals (e.g. copper (I) is intensely green whereas copper (II) is clearly blue) and can be a very useful way to determine complexation rather than weak association of two non-coordinated species.

This is seen explicitly with the neutral gold (III) PyQuin complexes. Sodium tetrachloroaurate is a yellow powdery solid and dissolves readily in acetonitrile. All PyQuin ligands are white/colorless solids and are also soluble in acetonitrile. Upon mixing at elevated temperature for an hour, if the solution is cooled down and concentrated, the resulting solid is a yellow powder. ^{1}H NMR of this solid matches the spectrum of the PyQuin ligand but slightly shifted downfield, indicating it is now more deshielded/electron deficient. The addition of silver tetrafluoroborate to the reaction mixture causes two things to occur: first, the solution goes from yellow to orange almost instantly and second, precipitation of AgCl. This color change is consistent across all PyQuin ligands that are complexed to gold. A similar transformation occurs going from neutral complex to cationic: the solution goes from orange to ruby red over an hour, with the resulting solid being tiny garnet crystals. This color change, whether from yellow to orange or from orange to red is crucial to observe, as the solids obtained after complexation have dramatically altered ^{1}H NMR spectra from their starting materials.

3.5 NMR Characterization and Comparison of Complexes

As discussed in the previous chapter, the effect of the substituent on the PyQuin has a dramatic effect on its ^{1}H NMR. Electron donating substituents such as MeO- or Me- shift the whole spectrum upfield whereas the F-substituted PyQuin has all resonances shifted downfield. It would be expected, then, for the analogous complexes of this series to show a similar trend. As shown in **Figure 3.2**, the effect of the substituent at the 6-position on the PyQuin ligand has an effect on the chemical shift for the complexes as well, however it is significantly less than the unbound PyQuins.

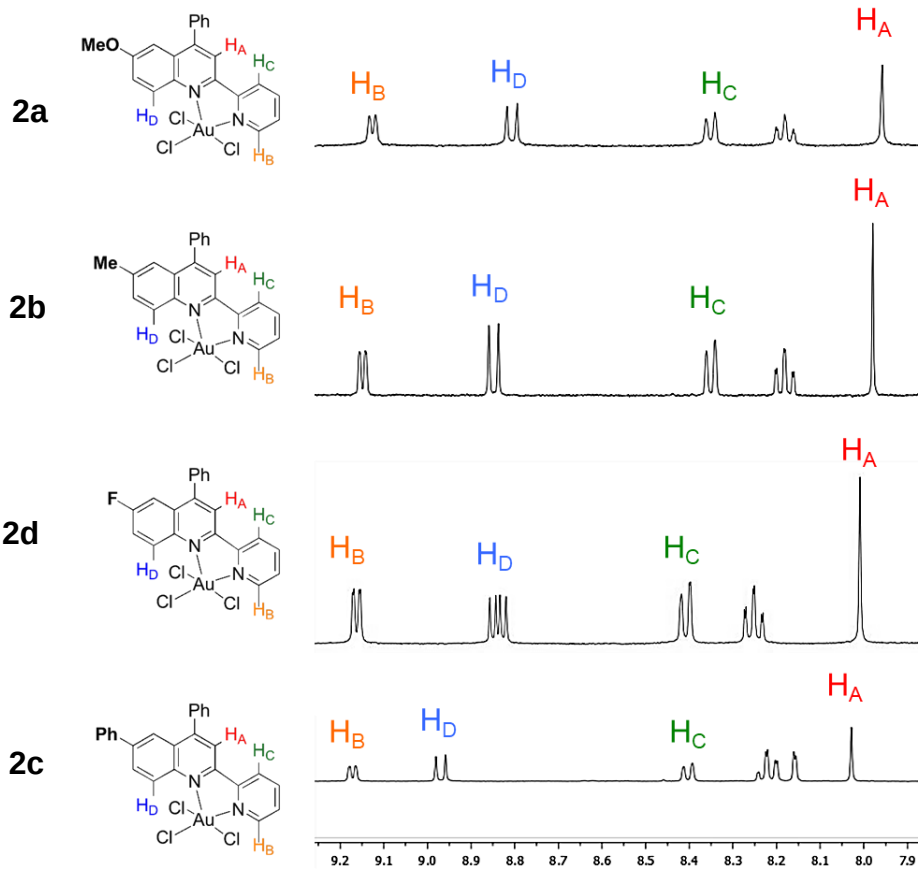

Figure 3.2 ^{1}H NMR comparison of different substituted PyQuin($AuCl_3$) complexes

What stands out in this series is that, when comparing chemical shifts, the phenyl substituent appears to be more electron-withdrawing than a fluorine. While somewhat surprising, it makes sense, as extending conjugation by another phenyl ring would delocalize the electrons significantly, even more than a traditionally strong electron withdrawing substituent like fluorine. While the PyQuin gold (III) complexes don't appear to change much depending on the substituent, the change between bound and unbound PyQuin ligand is quite dramatic, and it gives insight into both how the complex affects the ligand but also how the ligand exists without any chelation. As shown in **Figure 3.3**, there is a dramatic change in the chemical shift as well as order in the resonances for the MeO-PyQuin and MeO-PyQuin($AuCl_3$).

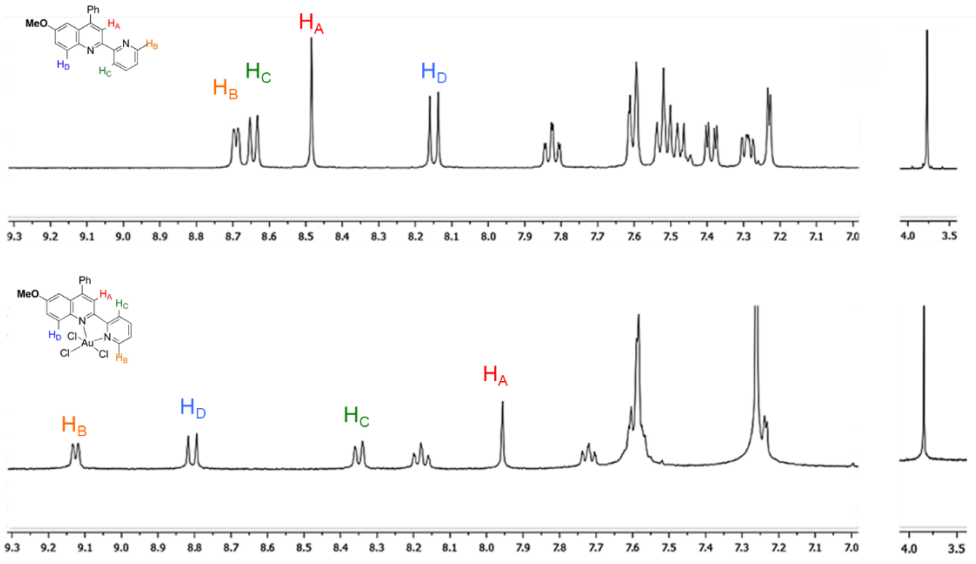

Figure 3.3 ^{1}H NMR comparison of MeO-PyQuin ligand and MeO-PyQuin($AuCl_3$)

The first thing to note is the lack of change in the methoxy-group's protons: even upon binding, the ether does not shift up or downfield. This is normal, as the oxygen heteroatom limits the effect changes to the rest of the compound has on the methyl ether group's chemical shift (and vice-versa). Next, based on the explicitly drawn protons, the order changes. This is due to the "flipping" of the pyridine section of the PyQuin molecule upon binding to the gold center. In order to minimize dipole, it is ideal for the PyQuin nitrogen atoms pointing away from each other. When the PyQuin binds to the gold, the pyridyl group must rotate and use the nitrogen lone pairs to bind, which moves them from pointing at H_A. This results in H_A no longer being deshielded by the pyridine nitrogen, causing an upfield shift upon binding. Conversely, H_D shifts dramatically downfield upon binding due to the proximity of the chlorine ligand which deshields it. These changes are consistent across all PyQuins when they bind to gold since the pyridine must flip regardless of the PyQuin's substituents.

3.6 X-Ray Crystallographic Confirmation of Complexes

As it had been observed previously, the geometry of the R-PyQuin($AuCl_3$) complexes are similar to those of 2,(2´-pyridyl)quinoline, biquinoline, and 2,9-dimethylphenantholine gold (III) complexes. The proton at the 8-position on the PyQuin ring would interfere with a chlorine bound to the gold if a traditional square-planar geometry were to form; because of this, a pseudo square-based pyramidal, five-coordinate species forms under these conditions. This is

confirmed by x-ray crystallographic data, obtained by Dr. Arnold Rheingold at the University of California San Diego. One such crystal structure, the MeO-PyQuin($AuCl_3$), is shown in **Figure 3.4**.

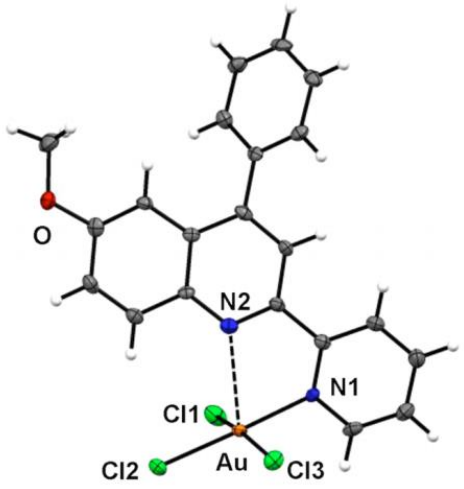

Figure 3.4 X-ray crystal structure of MeO-PyQuin($AuCl_3$)

It is clear by the x-ray data that the geometry of this complex is strongly influenced by both the proton at the 8-position as well as the nature of the nitrogen chelates. The bond lengths of nitrogen in the pyridine (**N1**) and the nitrogen in the pyridine (**N2**) are 2.039 Å and 2.633 Å, respectively. While the association of **N2** and the **Au** center is within the Van der Waals radii, the bond length is significantly longer than that of **N1** and **Au**. When comparing the four complexes (**Figure 3.5)** which formed x-ray quality crystals (R= **MeO, Me, Ph, and F**), the outlier is clearly the Ph-PyQuin($AuCl_3$). If the metric used is the **N2-Au** length, they are fairly equal across the board excluding the phenyl-substituted PyQuin complex.

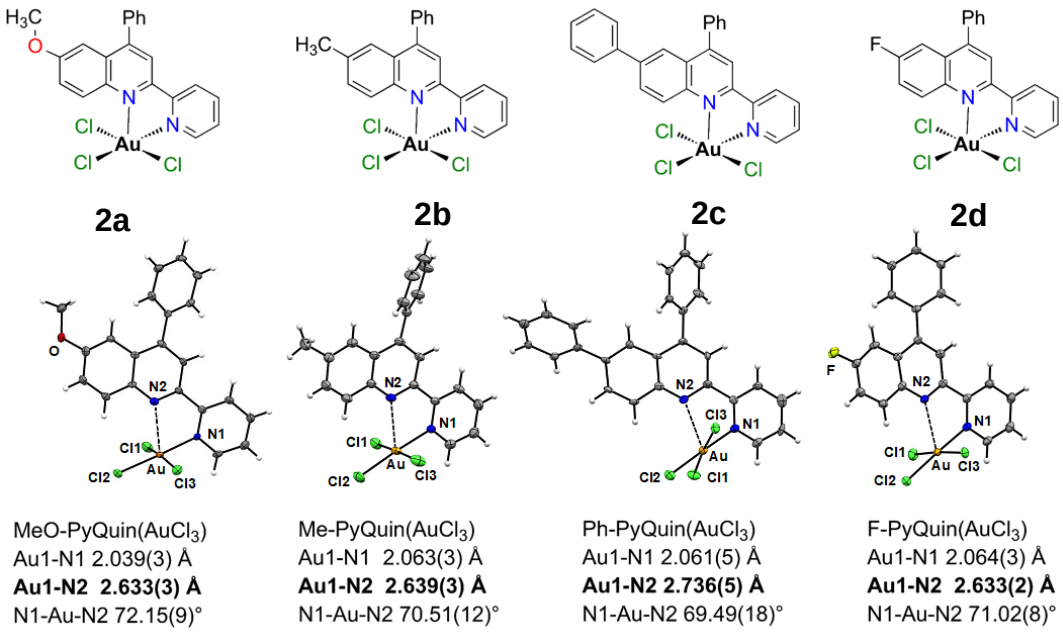

Figure 3.5 Comparison of X-ray crystal structures for PyQuin($AuCl_3$) complex series

This ~0.1 Å increase in bond length is attributed to the withdrawing nature of the aromatic ring, as the extended conjugation of the quinoline ring weakens the chelation ability of the heterocycle. For this to be verifiable, however, another characterization method should show the same trend, that phenyl ring is truly more withdrawing to the overall system than a fluorine.

The geometry of the neutral PyQuin gold (III) chloride complexes matches that of the precedent: due to the unfavorable steric hinderance of the ligand backbone proton, the complex conforms to a more stable five-coordinate square-based pyramidal geometry. A cationic, four-coordinate analogous gold (III) complex had, at the time, no literature precedent, and so the x-ray crystallographic data was especially valuable for these species. As shown in

Figure 3.6, the crystal structure of the cationic complex verifies the proposed structure: a four-coordinate complex with one PyQuin ligand, one gold (III) center, and two x-type chlorine ligands (**2e**) (thus rendering the overall complex cationic).

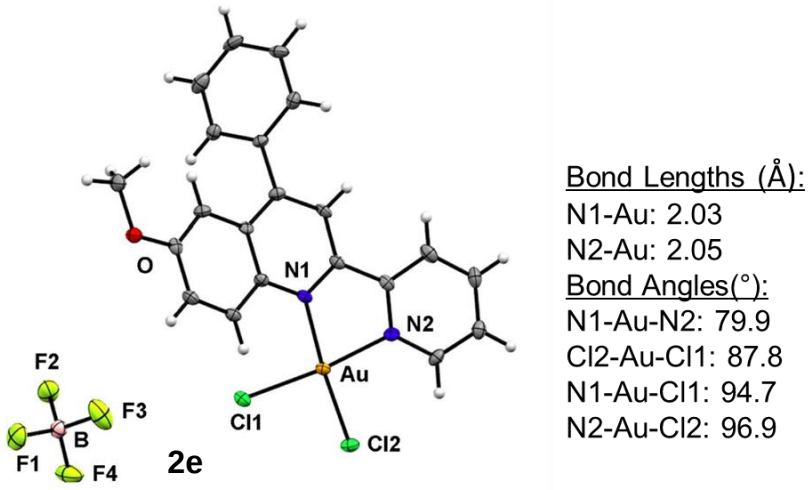

Figure 3.6 X-ray crystal structure of cationic MeO-PyQuin$(AuCl_2)^+$ BF_4^- complex

To stabilize the cationic complex, a non-coordinating anionic species must be present and, in the case of this crystal structure, it is the tetrafluoroborate anion. It is important to note that a cationic crystal forms with whichever anion is the most stable, not necessarily the anion that is most abundant (this will be important point in a future chapter). Additionally, the bond angles indicate a bite angle (that is quite similar to 2,2´-bipyridine, which verifies the similarity of these two ligands.[23] It is evident by the bond lengths that, unlike the neutral PyQuin gold (III) complex, the nitrogen-gold bonds are much more similar in the cationic complex, indicating that they are both true bonds and not long distance

electrostatic interactions. However, the bond angles show the distortion from the ideal square planar geometry. This can be seen more clearly if the crystal structure is rotated for an on-side view, as shown in **Figure 3.7**.

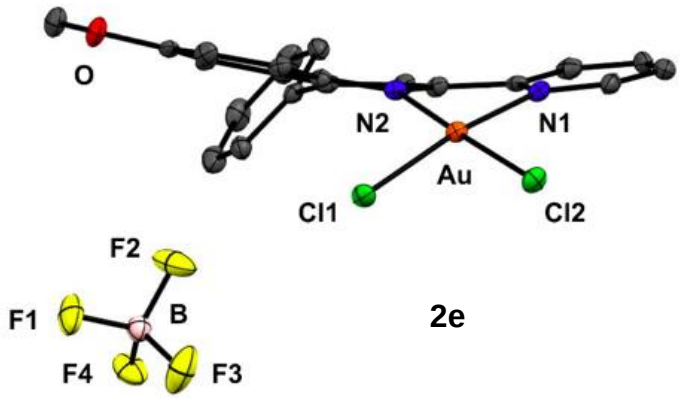

Figure 3.7 Crystal structure shows distorted geometry for MeO-PyQuin$(AuCl_2)^+$ BF_4^-

The plane formed by the gold, chloride, and nitrogen atoms is actually twisted perpendicular from the rest of the molecule. This illustrates that even abstracting a second chloride and forcing a four-coordinate species does not alleviate the steric issue which causes the five-coordinate neutral complex in the first place. The isolation and characterization of these complexes' crystals is actually incredibly important. While there is precedent for gold (III) forming pseudo square-based pyramidal complexes with sterically challenging ligands, other novel ligands (which will be discussed in future chapters) have no history of being complexed with gold, or other metals for that matter. With the structure of these complexes confirmed, both cationic and neutral, an analysis of their

solution-phase behavior and reactivity in the presence of other molecules was commenced.

3.7 References:

1) Serapian, S. A.; Bearpark, M. J.; Bresme, F. *Nanoscale* **2013**, *5* (14), 6445.

2) Iordanidis, A.; Garcia-Guinea, J.; Strati, A.; Gkimourtzina, A. *Analytical Letters* **2013**, *46* (6), 936.

3) Hashmi, A. S. K. *Chem. Rev*. **2007**, *107*, 3180.

4) (a) Shaw, C. F., III. *Uses Inorg. Chem. Med*. **1999**, *26*. (b) Demann, E. T. K.; Stein, P. S.; Haubenrich, J. E. *J. Long-Term Effects Med. Implants* **2005**, *15*, 687. (c) Messori, L.; Gabbiani, C. *Met. Comp. Cancer Chemother*. **2005**, 355. (d) Kostova, I. *Anti-Cancer Agents Med. Chem.* **2006**, *6*, 19.

5) Davis, P. *Can. Fam. Phys.* **1988**, *34*, 445.

6) Messori, L.; Abbate, F.; Marcon, G.; Orioli, P.; Fontani, M.; Mini, E.; Mazzei, T.; Carotti, S.; O'Connell, T.; Zanello, P. *J. Med. Chem.* **2000**, *43* (19), 3541.

7) MacArthus, J.S.; Ellis, C.J. *US-555,463,* **1896**.

8) Cheung, H.; Tanke, R. S.; Torrence, G. P. "Acetic Acid." *Ullmann's Encyclopedia of Industrial Chemistry*, **2000**.

9) Jones, J. H. *Platinum Metals Rev*. **2000** *44* (3),105.

10) (a) Höffmann-Rö der, A.; Krause, N. *Org. Biomol. Chem*. **2005**, *23*, 387. (b) Li, Z.; Brouwer, C.; He, C. *Chem. Rev*. **2008**, *108*, 3239. (c) Arcadi, A. *Chem. Rev.* **2008**, *108*, 3266. (d) Gorin, D. J.; Sherry, B. D.; Toste, F. D. *Chem. Rev*. **2008**, *108*, 3351.

11) (a) Cinellu, M. A.; Maiore, L.; Manassero, M.; Casini, A.; Arca, M.; Fiebig, H.-H.; Kuelter, G.; Michelucci, E.; Pieraccini, G.; Gabbiani, C.; Messori, L. *ACS Med. Chem. Lett.* **2010**, *1,* 336. (b) Casini, A.; Diawara, M. C.; Scopelliti, R.; Zakeeruddin, S. M.; Gratzel, M.; Dyson, P. J. *Dalton Trans*. **2010**, *39*, 2239. (c) Wein, A. N.; Stockhausen, A. T.; Hardcastle, K. I.; Saadein, M. R.; Peng, S. B.; Wang, D.; Shin, D. M.; Chen, Z. G.; Eichler, J. F. *J. Inorg. Biochem*. **2011**, *105*, 663. (d) Che, C.-M.; Sun, R. W.-Y. *Chem. Commun*. **2011**, *47*, 9554. (e) Sanghvi, C. D.; Olsen, P. M.; Elix, C.; Peng, S. B.; Wang, D.; Chen, Z. G.; Shin, D. M.; Hardcastle, K. I.; MacBeth, C. E.; Eichler, J. F. *J. Inorg. Biochem*. **2013**, *128*, 68.

12) Kadzimirsz, D.; Hildebrandt, D.; Merz, K.; Dyker, G. *Chem. Commun*. **2006**, 661.

13) Norman, R. O. C.; Parr, W. J. E.; Thomas, C. B. *J. Chem. Soc. Perkin Trans*. *1* **1976**, 1983.

14) (a) Fukuda, Y.; Utimoto, K.; Nozaki, H. *Heterocycles* **1987**, *25*, 297. (b) Fukuda, Y.; Utimoto, K. *Synthesis* **1991**, 975.

15) Teles, J. H.; Brode, S.; Chabanas, M. *Angew. Chem*. **1998**, *110*, 1475.

16) Dube, P.; Toste, F. D. *J. Am. Chem. Soc*. **2006**, *128*, 12062.

17) O'Connor, C. J.; Sinn, E. *Inorg. Chem*. **1978**, *17*, 2067.

18) (a) Charlton, R. J.; Harris, C. M.; Patil, H.; Stephenson, N. C. *Inorg. Nucl. Chem*. *Lett.* **1960**, *2*, 409. (b) Robinson, W. T.; Sinn, E. *J. Chem. Soc., Dalton Trans*. **1975**, *726*. (c) Hudson, Z. D.; Sanghvi, C. D.; Rhine, M. A.; Ng, J. J.; Bunge, S. D.; Hardcastle, K. I.; Saadein, M. R.; MacBeth, C. E.; Eichler, J. F. *Dalton Trans.* **2009**, 7473.

19) (a) Harris, C. M.; Kokot, S.; Patil, H. R. H.; Sinn, E.; Wong, H. *Aust. J. Chem*. **1972**, *25*, 1631. (b) Campagna, S.; Mamo, A.; Stille, J. K. *J. Chem. Soc., Trans.* **1991**, 2545. (c) Smirnoff, A. P. *Helv. Chim. Acta* **1921**, *4*, 802.

20) Michel, B. W.; Steffens, L. D.; Sigman, M. S. *J. Am. Chem. Soc*. **2011**, *133*, 8317.

21) (a) Sadiq, M. F.; Zaghal, M. H. *Polyhedron* **1997**, *16*, 1483. (b) Dahal, U. P.; Joswig-Jones, C.; Jones, J. P. *J. Med. Chem*. **2012**, *55*, 280. (c) Tsoupras, A. B.; Papakyriakou, A.; Demopoulos, C. A.; Philippopoulos, A. I. *J. Inorg. Biochem*. **2013**, *120*, 63.

22) Lein, M.; Rudolph, M.; Hashmi, S. K.; Schwerdtfeger, P. *Organometallics* **2010**, *29* (10), 2206.

23) Sasi, D.; Ramkumar, V.; Murthy, N. N. *ACS Omega* **2017**, *2* (6), 2474.

3.8 Supporting Information

General analytical information

^{1}H and ^{13}C NMR spectra were measured on a Varian Inova 500 (500 MHz) spectrometer using acetone-d_6 or $CDCl_3$ as solvents and tetramethylsilane as an internal standard. The following abbreviations are used singularly or in combination to indicate the multiplicity of signals: s - singlet, d - doublet, t - triplet, q - quartet, qn - quintet, sx - sextet, sp - septet, m - multiplet and br - broad. NMR spectra were acquired at 300 K. Gas chromatography (GC) was carried out on an Agilent Technologies 6850 Network GC System, and dodecane was used as the internal standard. ATR-IR spectra were taken on a Bruker:ALPHA FTIR Spectrometer. Attenuated total reflection infrared (ATR-IR) was used and the spectra was analyzed using the OPUS software with selected absorption maxima reported in wavenumbers (cm^{-1}). Mass spectrometric data was collected on a HP 5989A GC/MS quadrupole instrument. Exact masses were recorded on a Waters GCT Premier TOF instrument using direct injection of samples in methanol/acetonitrile into the electrospray source.

General Procedure for Synthesis of Neutral Gold(III) PyQuin Complexes

A 2-(2'-pyridyl)quinoline ligand (1 equiv.) is added to a dry 100-mL round-bottom flask charged with a dry magnetic stir bar. Anhydrous acetonitrile (10 mL per ~0.3 mmol PyQuin) is added to dissolve the ligand. Sodium tetrachloroaurate(III) dihydrate (1 equiv.) is added and rinsed down with anhydrous acetonitrile (10 mL

per ~0.3 mmol Au salt) are added, and the mixture is heated to reflux (vented to ambient atmosphere) in a 90 °C oil bath. After 2 hours, a solution of silver tetrafluoroborate in anhydrous acetonitrile (10 mL per ~0.3 mmol AgBF4) is added. After refluxing overnight, the cooled reaction is gravity filtered through Celite. Additional filtrations through Celite with acetonitrile may be necessary to remove the silver solids completely. X-ray quality crystals form overnight from the acetonitrile solution.

(MeO-PyQuin)$AuCl_3$ (2a)

Prepared according to general procedure: 6-Methoxy-4-phenyl-2-(2'-pyridyl)quinoline (105 mg, 0.34 mmol), sodium tetrachloroaurate(III) dihydrate (135 mg, 0.34 mmol), and silver tetrafluoroborate (66 mg, 0.34 mmol) afford the title complex as red-orange crystals in 60% yield (0.125 g, 0.20 mmol). Anal. Calcd. for $C_{21}H_{16}N_2OAuCl_3$: C, 40.97; H, 2.62. Found: C, 41.20; H, 2.62. IR (crystal) 3047, 2836, 1601, 1486, 1225, 776, 710 cm^{-1}. HRMS (ESI) *m/z* calcd for $[M+H]^+$ $C_{21}H_{17}N_2OCl_3Au$ requires 615.0066, found 615.0084. ^1H NMR (400 MHz, $CDCl_3$, 25°C) δ 9.13 (d, *J* = 5.9 Hz, 1H), 8.81 (d, *J* = 9.2 Hz, 1H), 8.35 (d, *J* = 8.1 Hz, 1H), 8.21 – 8.15 (m, 1H), 7.96 (s, 1H), 7.74 – 7.70 (m, 1H), 7.67 – 7.50 (m, 6H), 7.24 (d, *J* = 2.7 Hz, 1H), 3.85 (s, 3H).

(Me-PyQuin)$AuCl_3$ (2b)

Prepared according to general procedure: 6-Methyl-4-phenyl-2-(2'-pyridyl)quinoline (202 mg, 0.68 mmol), sodium tetrachloroaurate(III) dihydrate (271 mg, 0.68 mmol), and silver tetrafluoroborate (132 mg, 0.68 mmol) afford the title complex as red-orange crystals in 72% yield (0.294 g, 0.49 mmol). Anal. Calcd. for $C_{21}H_{16}N_2AuCl_3$: C, 42.06%; H, 2.69%. Found: C, 41.90%; H, 2.66%. IR (crystal) 3040, 1571, 1488, 762, 700 cm^{-1}. HRMS (ESI) *m/z* calcd for $[M+H]^+$ $C_{21}H_{17}N_2Cl_3Au$ requires 599.0117, found 599.0129. ^1H NMR (400 MHz, $CDCl_3$, 25°C) δ 9.15 (d, *J* = 5.6 Hz, 1H), 8.85 (d, *J* = 8.7 Hz, 1H), 8.35 (d, *J* = 7.9 Hz, 1H), 8.21 – 8.15 (m, 1H), 7.98 (s, 1H), 7.80 (dd, *J* = 8.7, 1.8 Hz, 1H), 7.74 (t, *J* = 6.6 Hz, 2H), 7.65 – 7.51 (m, 5H), 2.54 (s, 3H).

(Ph-PyQuin)$AuCl_3$ (2c)

Prepared according to general procedure: 4,6-Diphenyl-2-(2'-pyridyl)quinoline (240 mg, 0.67 mmol), sodium tetrachloroaurate(III) dihydrate (267 mg, 0.67 mmol), and silver tetrafluoroborate (130 mg, 0.67 mmol) afford the title complex as orange crystals in 43% yield (189 g, 0.29 mmol). Anal. Calcd. for $C_{26}H_{18}N_2AuCl_3$: C, 47.19; H, 2.74. Found: C, 47.04; H, 2.74. IR (crystal) 3046, 1482, 1433, 842, 760, 694 cm^{-1}. HRMS (ESI) *m/z* calcd for $[M+H]^+$ $C_{26}H_{19}N_2Cl_3Au$ requires 661.0274, found 661.0295. ^1H NMR (400 MHz, $CDCl_3$, 25°C) δ 9.17 (d, *J* = 5.6 Hz, 1H), 8.97 (d, *J* = 8.8 Hz, 1H), 8.40 (d, *J* = 7.9 Hz,

1H), 8.26 – 8.18 (m, 2H), 8.16 (d, *J* = 1.9 Hz, 1H), 8.03 (s, 1H), 7.80 – 7.74 (m, 1H), 7.71 – 7.54 (m, 6H), 7.49 (dd, *J* = 14.7, 7.6 Hz, 2H), 7.45 – 7.37 (m, 2H).

(F-PyQuin)$AuCl_3$ (2d)

Prepared according to general procedure: 4,6-Diphenyl-2-(2'-pyridyl)quinoline (240 mg, 0.67 mmol), sodium tetrachloroaurate(III) dihydrate (267 mg, 0.67 mmol), and silver tetrafluoroborate (130 mg, 0.67 mmol) afford the title complex as orange crystals in 43% yield (189 g, 0.29 mmol). Anal. Calcd. for $C_{26}H_{18}N_2AuCl_3$: C, 47.19; H, 2.74. Found: C, 47.04; H, 2.74. IR (crystal) 3046, 1482, 1433, 842, 760, 694 cm^{-1}. HRMS (ESI) *m/z* calcd for $[M+H]^+$ $C_{26}H_{19}N_2Cl_3Au$ requires 661.0274, found 661.0295. ^1H NMR (400 MHz, $CDCl_3$, 25°C) δ 9.17 (d, *J* = 5.6 Hz, 1H), 8.97 (d, *J* = 8.8 Hz, 1H), 8.40 (d, *J* = 7.9 Hz, 1H), 8.26 – 8.18 (m, 2H), 8.16 (d, *J* = 1.9 Hz, 1H), 8.03 (s, 1H), 7.80 – 7.74 (m, 1H), 7.71 – 7.54 (m, 6H), 7.49 (dd, *J* = 14.7, 7.6 Hz, 2H), 7.45 – 7.37 (m, 2H).

Synthesis of Cationic Gold(III) MeO-PyQuin Complex (2e)

[(MeO-PyQuin)$AuCl_2$]BF_4 (**2e**) To a dry 100-mL round-bottom flask charged with a dry magnetic stir bar, MeO-PyQuin (105 mg, 0.34 mmol) and sodium tetrachloroaurate(III) dihydrate (135 mg, 0.34 mmol) are dissolved in acetonitrile (10 mL) and heated to reflux at 90 °C. After 2 hours, a solution of silver tetrafluoroborate (66 mg, 0.34 mmol) in anhydrous acetonitrile (10 mL) is added, and the mixture is refluxed overnight at 90 °C. The second equivalent of silver

tetrafluoroborate (66 mg, 0.34 mmol) is added as a solution in anhydrous acetonitrile (10 mL), and the mixture is refluxed at 90 °C for an additional 4 hours. The cooled reaction mixture is filtered through Celite, and thenfiltrate is reduced *in vacuo*. The solid is recrystallized in toluene overnight at room temperature to afford the title complex as red-black crystals in 27% yield (0.054 g, 0.093 mmol). Anal. Calcd. for $C_{21}H_{16}N_2OAuCl_2BF_4$: C, 35.14; H, 2.41. Found: C, 35.87; H, 2.35. IR (crystal) 3087, 2840, 1600, 1489, 1250, 1234, 1048, 1032, 778, 699 cm^{-1}. HRMS (ESI) *m/z* calcd for $[M]^+$ $C_{21}H_{17}N_2OAuCl_2$ requires 579.0305, found 579.0325. ^1H NMR (400 MHz, DMSO-D_6, 25°C) δn8.77 (d, *J* = 4.5 Hz, 1H), 8.69 (d, *J* = 8.0 Hz, 1H), 8.46 (s, 1H), 8.19 (d, *J* = 9.2 Hz, 1H), 8.17 – 8.12 (m, 1H), 7.73 – 7.52 (m, 7H), 7.25 (d, *J* = 2.7 Hz, 1H), 3.81 (s, 3H).

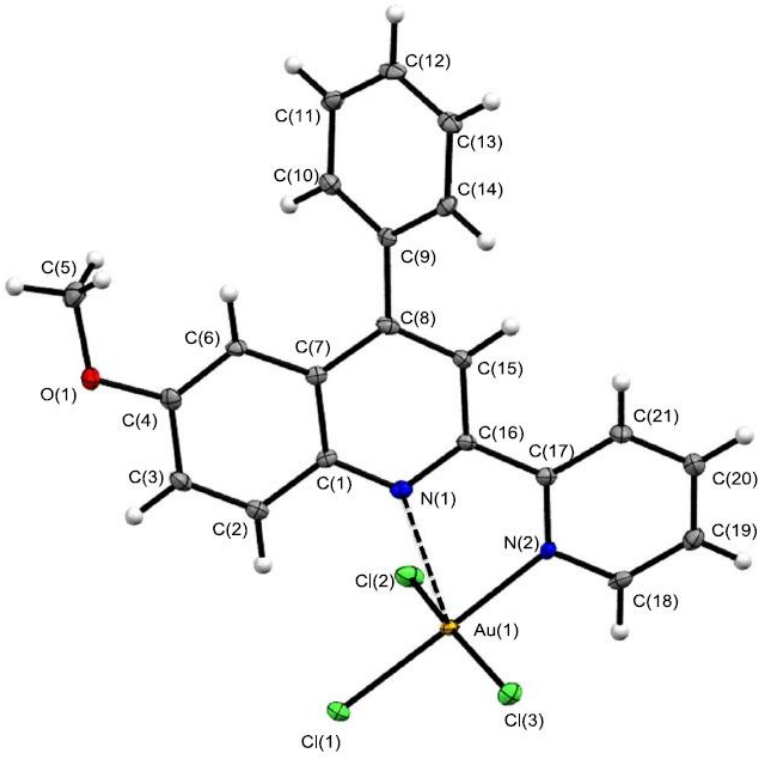

Table 1. Crystal data and structure refinement for larsen01. (6-methoxy-PyQuin)$AuCl_3$•CH_3CN (**2a**)

Identification code	larsen01	
Empirical formula	C23 H19 Au Cl3 N3 O	
Formula weight	656.73	
Temperature	100(2) K	
Wavelength	0.71073 Å	
Crystal system	Monoclinic	
Space group	P2(1)/n	
Unit cell dimensions	a = 7.2272(4) Å	a= 90°
	b = 12.8348(7) Å	b= 94.064(2)°
	c = 24.2847(13) Å	g = 90°
Volume	2247.0(2) $Å^3$	
Z	4	

Density (calculated)	1.941 g/cm^3
Absorption coefficient	6.925 mm^{-1}
F(000)	1264
Crystal size	0.28 x 0.24 x 0.22 mm^3
Theta range for data collection	2.89 to 26.46°
Index ranges	-9<=h<=9, -15<=k<=15, -29<=l<=30
Reflections collected	13480
Independent reflections	4584 [R(int) = 0.0332]
Completeness to theta = 25.00°	99.7 %
Absorption correction	Multi-scan
Max. and min. transmission	0.3111 and 0.2473
Refinement method	Full-matrix least-squares on F^2
Data / restraints / parameters	4584 / 0 / 282
Goodness-of-fit on F^2 GOF on F^2	1.084
Final R indices [I>2sigma(I)]	R1 = 0.0234, wR2 = 0.0584
R indices (all data)	R1 = 0.0262, wR2 = 0.0598
Final R1 [$I > 2(I)$]^a x 0.22 mm^3 wR2 [$I > 2(I)$]^a	0.28 x 0.24

^{a} R1 $= \Sigma||F_o| - |F_c||/\Sigma|F_o|$, wR2 $= \{\Sigma[w(F_{o^2} - F_{c^2})^2]/\Sigma[wF_{o^4}]\}^{1/2}$.

Largest diff. peak and hole	1.195 and -1.094 e Å^{-3}

Table 2. Atomic coordinates (x 10^4) and equivalent isotropic displacement parameters ($Å^2$x 10^3)for larsen01. U(eq) is defined as one third of the trace of the orthogonalized U^{ij} tensor.

	x	y	z	U(eq)
Au(1)	1242(1)	6073(1)	661(1)	9(1)
Cl(1)	3724(1)	4995(1)	808(1)	15(1)
Cl(2)	281(1)	5738(1)	1521(1)	18(1)
Cl(3)	1705(1)	6172(1)	-261(1)	14(1)
O(1)	8652(3)	9071(2)	2305(1)	15(1)
N(1)	2384(4)	7915(2)	1022(1)	11(1)
N(2)	-883(4)	7102(2)	509(1)	9(1)
N(3)	7120(5)	11265(3)	861(1)	23(1)
C(1)	3900(4)	8260(2)	1337(1)	9(1)
C(2)	5362(4)	7545(3)	1466(1)	12(1)
C(3)	6900(5)	7850(3)	1782(1)	14(1)
C(4)	7050(5)	8881(2)	1986(1)	12(1)
C(5)	8839(5)	10074(3)	2568(2)	19(1)
C(6)	5675(4)	9594(3)	1868(1)	11(1)
C(7)	4046(4)	9301(3)	1546(1)	9(1)
C(8)	2519(5)	9982(3)	1417(1)	11(1)
C(9)	2431(4)	11075(2)	1622(1)	10(1)
C(10)	2844(5)	11316(3)	2177(1)	13(1)
C(11)	2654(4)	12332(3)	2368(1)	14(1)
C(12)	2036(4)	13104(3)	2007(1)	16(1)
C(13)	1614(4)	12884(3)	1452(1)	14(1)
C(14)	1814(4)	11863(3)	1263(1)	12(1)
C(15)	1008(4)	9602(3)	1105(1)	10(1)
C(16)	989(4)	8562(3)	911(1)	10(1)
C(17)	-704(4)	8144(3)	600(1)	10(1)
C(18)	-2459(4)	6703(3)	258(1)	13(1)
C(19)	-3907(5)	7327(3)	72(1)	14(1)
C(20)	-3743(5)	8395(3)	142(1)	16(1)

C(21)	-2146(5)	8799(3)	410(2)	16(1)
C(22)	6947(5)	11951(3)	1146(1)	17(1)
C(23)	6730(5)	12829(3)	1516	

Table 3. Bond lengths [Å] and angles [°] for larsen01.

Au(1)-N(2)	**2.039(3)**
Au(1)-Cl(1)	**2.2745(8)**
Au(1)-Cl(2)	**2.2886(8)**
Au(1)-Cl(3)	**2.2910(8)**
Au(1)-N(1)	**2.633(3)**
O(1)-C(4)	1.368(4)
O(1)-C(5)	1.440(4)
N(1)-C(16)	1.320(4)
N(1)-C(1)	1.365(4)
N(2)-C(18)	1.354(4)
N(2)-C(17)	1.360(4)
N(3)-C(22)	1.132(5)
C(1)-C(2)	1.418(5)
C(1)-C(7)	1.431(4)
C(2)-C(3)	1.363(5)
C(3)-C(4)	1.415(5)
C(4)-C(6)	1.366(5)
C(6)-C(7)	1.417(4)
C(7)-C(8)	1.425(5)
C(8)-C(15)	1.374(5)
C(8)-C(9)	1.491(4)
C(9)-C(10)	1.394(5)
C(9)-C(14)	1.389(5)
C(10)-C(11)	1.395(5)
C(11)-C(12)	1.377(5)
C(12)-C(13)	1.389(5)
C(13)-C(14)	1.399(5)
C(15)-C(16)	1.415(5)

C(16)-C(17)	1.491(4)
C(17)-C(21)	1.392(5)
C(18)-C(19)	1.368(5)
C(19)-C(20)	1.386(5)
C(20)-C(21)	1.384(5)
C(22)-C(23)	1.456(5)

N(2)-Au(1)-Cl(1)	**176.67(8)**
N(2)-Au(1)-Cl(2)	**90.73(7)**
Cl(1)-Au(1)-Cl(2)	**91.64(3)**
N(2)-Au(1)-Cl(3)	**87.06(7)**
Cl(1)-Au(1)-Cl(3)	**91.10(3)**
Cl(2)-Au(1)-Cl(3)	**167.78(3)**
N(2)-Au(1)-N(1)	**72.15(9)**
Cl(1)-Au(1)-N(1)	**105.58(6)**
Cl(2)-Au(1)-N(1)	**88.45(6)**
Cl(3)-Au(1)-N(1)	**102.27(6)**
C(4)-O(1)-C(5)	117.4(3)
C(16)-N(1)-C(1)	118.8(3)
C(16)-N(1)-Au(1)	106.2(2)
C(1)-N(1)-Au(1)	134.3(2)
C(18)-N(2)-C(17)	120.8(3)
C(18)-N(2)-Au(1)	115.8(2)
C(17)-N(2)-Au(1)	123.1(2)
N(1)-C(1)-C(2)	118.0(3)
N(1)-C(1)-C(7)	122.6(3)
C(2)-C(1)-C(7)	119.4(3)
C(3)-C(2)-C(1)	120.3(3)
C(2)-C(3)-C(4)	120.3(3)
C(6)-C(4)-O(1)	125.0(3)
C(6)-C(4)-C(3)	121.1(3)
O(1)-C(4)-C(3)	113.9(3)
C(4)-C(6)-C(7)	120.2(3)
C(6)-C(7)-C(8)	124.0(3)

C(6)-C(7)-C(1)	118.7(3)
C(8)-C(7)-C(1)	117.3(3)
C(15)-C(8)-C(7)	118.4(3)
C(15)-C(8)-C(9)	117.9(3)
C(7)-C(8)-C(9)	123.7(3)
C(10)-C(9)-C(14)	118.9(3)
C(10)-C(9)-C(8)	121.3(3)
C(14)-C(9)-C(8)	119.7(3)
C(9)-C(10)-C(11)	120.7(3)
C(12)-C(11)-C(10)	119.7(3)
C(11)-C(12)-C(13)	120.7(3)
C(12)-C(13)-C(14)	119.2(3)
C(9)-C(14)-C(13)	120.8(3)
C(8)-C(15)-C(16)	120.5(3)
N(1)-C(16)-C(15)	122.4(3)
N(1)-C(16)-C(17)	117.7(3)
C(15)-C(16)-C(17)	119.8(3)
N(2)-C(17)-C(21)	118.7(3)
N(2)-C(17)-C(16)	120.1(3)
C(21)-C(17)-C(16)	121.2(3)
N(2)-C(18)-C(19)	121.7(3)
C(18)-C(19)-C(20)	118.8(3)
C(21)-C(20)-C(19)	119.3(3)
C(20)-C(21)-C(17)	120.6(3)
N(3)-C(22)-C(23)	179.6(4)

Table 4. Anisotropic displacement parameters ($Å^2 x\ 10^3$) for larsen01. The anisotropic displacement factor exponent takes the form: $-2p^2[\ h^2\ a^{*2}U^{11} + ... + 2\ h\ k\ a^*\ b^*\ U^{12}]$

	U^{11}	U^{22}	U^{33}	U^{23}	U^{13}	U^{12}
Au(1)	12(1)	7(1)	9(1)	-1(1)	0(1)	0(1)
Cl(1)	16(1)	11(1)	18(1)	-2(1)	-2(1)	4(1)

Cl(2)	28(1)	16(1)	11(1)	2(1)	5(1)	7(1)
Cl(3)	15(1)	17(1)	11(1)	0(1)	3(1)	-1(1)
O(1)	10(1)	15(1)	20(1)	-2(1)	-3(1)	1(1)
N(1)	12(1)	11(1)	11(1)	-1(1)	3(1)	0(1)
N(2)	11(1)	10(1)	7(1)	-1(1)	-2(1)	1(1)
N(3)	22(2)	18(2)	30(2)	3(2)	-1(2)	5(1)
C(1)	10(2)	8(2)	9(2)	0(1)	2(1)	-2(1)
C(2)	13(2)	11(2)	13(2)	-1(1)	3(1)	2(1)
C(3)	15(2)	13(2)	13(2)	1(1)	2(1)	6(2)
C(4)	9(2)	15(2)	12(2)	1(1)	4(1)	1(1)
C(5)	14(2)	21(2)	22(2)	-6(2)	-2(1)	-3(2)
C(6)	13(2)	7(2)	12(2)	0(1)	1(1)	0(1)
C(7)	11(2)	8(2)	8(2)	1(1)	3(1)	-2(1)
C(8)	15(2)	8(2)	10(2)	2(1)	3(1)	2(1)
C(9)	6(2)	9(2)	15(2)	-1(1)	2(1)	-2(1)
C(10)	12(2)	13(2)	14(2)	1(1)	1(1)	2(1)
C(11)	12(2)	16(2)	14(2)	-5(1)	2(1)	-1(1)
C(12)	12(2)	8(2)	27(2)	-6(1)	4(1)	-3(1)
C(13)	12(2)	10(2)	21(2)	2(1)	2(1)	-1(1)
C(14)	10(2)	13(2)	12(2)	-1(1)	1(1)	-3(1)
C(15)	10(2)	9(2)	12(2)	-1(1)	1(1)	2(1)
C(16)	12(2)	8(2)	9(2)	-1(1)	2(1)	1(1)
C(17)	14(2)	9(2)	8(2)	1(1)	2(1)	1(1)
C(18)	14(2)	13(2)	12(2)	-5(1)	3(1)	-3(1)
C(19)	12(2)	18(2)	13(2)	-3(1)	-1(1)	-3(2)
C(20)	15(2)	17(2)	16(2)	-2(1)	-2(1)	4(2)
C(21)	17(2)	10(2	20(2)	-	-3(2)	2(1)

		)		3(1)		
C(22)	14(2)	18(2)	18(2)	5(2)	-1(1)	-1(2)
		)				
C(23)	18(2)	27(2)	31(2)	-7(2)	9(	

Table 5. Hydrogen coordinates (x 10^4) and isotropic displacement parameters ($Å^2$ x 10^3) for larsen01.

	x	y	z	U(eq)
H(16)	5269	6851	1332	14
H(15)	7877	7368	1866	16
H(1)	8891	10618	2286	29
H(2)	9982	10089	2811	29
H(3)	7772	10198	2787	29
H(14)	5811	10287	2002	13
H(8)	3258	10782	2427	15
H(7)	2950	12491	2746	17
H(6)	1897	13795	2138	19
H(5)	1194	13420	1204	17
H(4)	1523	11708	884	14
H(13)	-31	10040	1019	12
H(12)	-2562	5970	209	15
H(11)	-5004	7033	-102	17
H(10)	-4716	8846	8	19
H(9)	-2033	9530	464	19
H(19)	7503	12718	1859	37
H(18)	5427	12887	1599	37
H(17)	7116	13471	1338	37

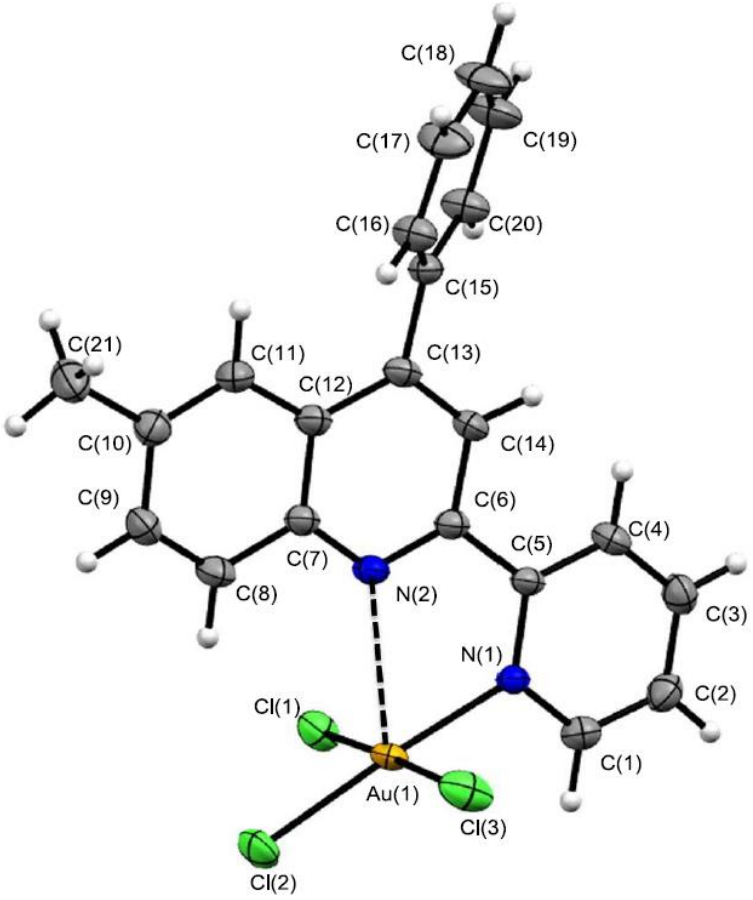
C(18)
C(17)
C(19)
C(16)
C(20)
C(15)
C(21)
C(11)
C(13)
C(12)
C(10)
C(14)
C(9)
C(6)
C(4)
C(5)
C(7)
N(2)
C(8)
C(3)
N(1)
C(2)
Cl(1)
C(1)
Au(1)
Cl(3)
Cl(2)

Table 1. Crystal data and structure refinement for larsen02. (6-methyl-PyQuin)$AuCl_3$ (**2b**)

Identification code	larsen02
Empirical formula	C21 H16 Au Cl3 N2
Formula weight	599.68
Temperature	245(2) K
Wavelength	0.71073 Å
Crystal system	Triclinic
Space group	P-1
Unit cell dimensions	a = 8.5146(4) Å a= 102.905(2)° b = 11.2882(6) Å b= 101.006(2)° c = 11.2979(6) Å g = 104
Volume	990.01(9)
Z	2
Density (calculated)	2.012 g/cm^3
Absorption coefficient	7.843 mm^{-1}
F(000)	572
Crystal size	0.25 x 0.20 x 0.15 mm^3
Theta range for data collection	2.56 to 26.45°
Index ranges	-10<=h<=9, -14<=k<=13, -14<=l<=14
Reflections collected	19138
Independent reflections	4051 [R(int) = 0.0599]
Completeness to theta = 25.00°	99.2 %
Absorption correction	Multi-scan
Refinement method	Full-matrix least-squares on F^2
Data / restraints / parameters	4051 / 0 / 246
Goodness-of-fit on F^2	1.107
Final R indices [I>2sigma(I)]	R1 = 0.0226, wR2 = 0.0514
R indices (all data)	R1 = 0.0281, wR2 = 0.0663
Extinction coefficient	0.0003(3)
Largest diff. peak and hole	0.875 and -1.582 e $Å^{-3}$

Table 2. Atomic coordinates (x 10^4) and equivalent isotropic displacement parameters ($Å^2$x 10^3)for larsen02. U(eq) is defined as one third of the trace of the orthogonalized U^{ij} tensor.

	x	y	z	U(eq)
Au(1)	6649(1)	5291(1)	1887(1)	22(1)
Cl(1)	7091(2)	3601(1)	2566(1)	32(1)
Cl(2)	8744(2)	5290(1)	922(1)	36(1)
Cl(3)	6068(2)	6866(1)	1091(1)	41(1)
N(1)	4642(4)	5217(3)	2671(3)	19(1)
N(2)	7685(4)	6853(3)	4190(3)	24(1)
C(1)	3169(5)	4389(4)	1935(4)	26(1)
C(2)	1730(5)	4169(4)	2337(5)	30(1)
C(3)	1795(6)	4818(4)	3526(5)	30(1)
C(4)	3303(5)	5693(4)	4278(4)	26(1)
C(5)	4741(5)	5898(4)	3854(4)	21(1)
C(6)	6378(5)	6841(4)	4637(4)	22(1)
C(7)	9190(5)	7697(4)	4874(4)	23(1)
C(8)	10572(5)	7683(4)	4367(4)	29(1)
C(9)	12120(6)	8510(4)	4999(5)	31(1)
C(10)	12382(5)	9381(4)	6180(4)	29(1)
C(11)	11060(5)	9394(4)	6693(4)	27(1)
C(12)	9424(5)	8582(4)	6060(4)	23(1)
C(13)	7981(5)	8562(4)	6526(4)	23(1)
C(14)	6470(5)	7685(4)	5798(4)	24(1)
C(15)	8004(5)	9427(4)	7737(4)	24(1)
C(16)	8761(6)	10743(4)	8061(4)	31(1)
C(17)	8622(7)	11516(5)	9152(5)	44(1)
C(18)	7803(7)	11007(5)	9938(5)	47(2)
C(19)	7082(7)	9721(5)	9631(5)	42(1)
C(20)	7172(6)	8938(4)	8546(4)	31(1)
C(21)	14118(6)	10274(5)	6844(5)	44(1)

Table 3. Bond lengths [Å] and angles [°] for larsen02.

Au(1)-N(1)	**2.063(3)**
Au(1)-Cl(2)	**2.2608(12)**
Au(1)-Cl(3)	**2.2790(12)**
Au(1)-Cl(1)	**2.2948(12)**
Au(1)-N(2)	**2.639(3)**
N(1)-C(1)	1.346(5)
N(1)-C(5)	1.360(5)
N(2)-C(6)	1.305(6)
N(2)-C(7)	1.355(5)
C(1)-C(2)	1.372(7)
C(2)-C(3)	1.362(6)
C(3)-C(4)	1.388(6)
C(4)-C(5)	1.385(6)
C(5)-C(6)	1.494(6)
C(6)-C(14)	1.414(6)
C(7)-C(8)	1.406(6)
C(7)-C(12)	1.426(6)
C(8)-C(9)	1.361(6)
C(9)-C(10)	1.411(6)
C(10)-C(11)	1.362(6)
C(10)-C(21)	1.505(6)
C(11)-C(12)	1.409(6)
C(12)-C(13)	1.423(6)
C(13)-C(14)	1.383(6)
C(13)-C(15)	1.486(6)
C(15)-C(20)	1.386(6)
C(15)-C(16)	1.397(6)
C(16)-C(17)	1.386(7)
C(17)-C(18)	1.368(8)
C(18)-C(19)	1.363(8)
C(19)-C(20)	1.369(6)

N(1)-Au(1)-Cl(2)	**176.64(9)**

N(1)-Au(1)-Cl(3)	**89.17(10)**
Cl(2)-Au(1)-Cl(3)	**90.60(5)**
N(1)-Au(1)-Cl(1)	**90.33(10)**
Cl(2)-Au(1)-Cl(1)	**89.66(4)**
Cl(3)-Au(1)-Cl(1)	**175.90(4)**
N(1)-Au(1)-N(2)	**70.51(12)**
Cl(2)-Au(1)-N(2)	**112.85(8)**
Cl(3)-Au(1)-N(2)	**90.89(9)**
Cl(1)-Au(1)-N(2)	**92.77(9)**
C(1)-N(1)-C(5)	120.3(4)
C(1)-N(1)-Au(1)	115.0(3)
C(5)-N(1)-Au(1)	124.7(3)
C(6)-N(2)-C(7)	118.6(4)
C(6)-N(2)-Au(1)	108.2(3)
C(7)-N(2)-Au(1)	132.8(3)
N(1)-C(1)-C(2)	122.5(4)
C(3)-C(2)-C(1)	118.7(4)
C(2)-C(3)-C(4)	119.0(4)
C(5)-C(4)-C(3)	121.4(4)
N(1)-C(5)-C(4)	118.1(4)
N(1)-C(5)-C(6)	119.2(4)
C(4)-C(5)-C(6)	122.6(4)
N(2)-C(6)-C(14)	122.5(4)
N(2)-C(6)-C(5)	117.0(4)
C(14)-C(6)-C(5)	120.5(4)
N(2)-C(7)-C(8)	117.1(4)
N(2)-C(7)-C(12)	123.4(4)
C(8)-C(7)-C(12)	119.5(4)
C(9)-C(8)-C(7)	120.3(4)
C(8)-C(9)-C(10)	121.1(4)
C(11)-C(10)-C(9)	119.3(4)
C(11)-C(10)-C(21)	121.6(4)
C(9)-C(10)-C(21)	119.1(4)
C(10)-C(11)-C(12)	121.8(4)

C(11)-C(12)-C(13)	124.8(4)
C(11)-C(12)-C(7)	118.0(4)
C(13)-C(12)-C(7)	117.2(4)
C(14)-C(13)-C(12)	117.5(4)
C(14)-C(13)-C(15)	118.5(4)
C(12)-C(13)-C(15)	124.0(4)
C(13)-C(14)-C(6)	120.8(4)
C(20)-C(15)-C(16)	118.2(4)
C(20)-C(15)-C(13)	119.8(4)
C(16)-C(15)-C(13)	122.0(4)
C(17)-C(16)-C(15)	119.5(5)
C(18)-C(17)-C(16)	121.1(5)
C(19)-C(18)-C(17)	119.4(5)
C(18)-C(19)-C(20)	120.6(5)
C(19)-C(20)-C(15)	121.2(4)

Table 4. Anisotropic displacement parameters ($Å^2 x\ 10^3$) for larsen02. The anisotropic displacement factor exponent takes the form: $-2p^2[\ h^2\ a^{*2}U^{11} + ... + 2\ h\ k\ a^*\ b^*\ U^{12}]$

	U^{11}	U^{22}	U^{33}	U^{23}	U^{13}	U^{12}
Au(1)	27(1)	24(1)	15(1)	3(1)	9(1)	8(1)
Cl(1)	41(1)	32(1)	33(1)	14(1)	19(1)	18(1)
Cl(2)	36(1)	49(1)	32(1)	16(1)	21(1)	17(1)
Cl(3)	68(1)	34(1)	34(1)	15(1)	23(1)	27(1)
N(1)	23(2)	21(2)	15(2)	5(1)	5(1)	9(1)
N(2)	29(2)	27(2)	17(2)	4(2)	7(2)	10(2)
C(1)	30(2)	26(2)	21(2)	5(2)	5(2)	7(2)
C(2)	25(2)	29(2)	29(3)	4(2)	0(2)	6(2)
C(3)	25(2)	34(3)	33(3)	11(2)	12(2)	10(2)
C(4)	31(2)	27(2)	22(2)	4(2)	12(2)	11(2)
C(5)	28(2)	23(2)	15(2)	5(2)	7(2)	13(2)
C(6)	27(2)	22(2)	17(2)	4(2)	6(2)	10(2)

C(7)	27(2)	24(2)	18(2)	6(2)	6(2)	10(2)
C(8)	33(2)	29(2)	23(2)	1(2)	10(2)	11(2)
C(9)	27(2)	36(3)	30(3)	7(2)	13(2)	11(2)
C(10)	29(2)	27(2)	29(3)	5(2)	6(2)	10(2)
C(11)	28(2)	30(2)	21(2)	2(2)	5(2)	9(2)
C(12)	29(2)	24(2)	18(2)	6(2)	7(2)	10(2)
C(13)	32(2)	24(2)	17(2)	6(2)	9(2)	12(2)
C(14)	27(2)	28(2)	19(2)	4(2)	10(2)	11(2)
C(15)	26(2)	26(2)	18(2)	3(2)	5(2)	10(2)
C(16)	36(2)	27(2)	26(3)	5(2)	12(2)	6(2)
C(17)	53(3)	27(3)	37(3)	-7(2)	12(3)	3(2)
C(18)	61(4)	43(3)	28(3)	-9(2)	20(3)	9(3)
C(19)	56(3)	44(3)	26(3)	5(2)	22(2)	14(3)
C(20)	43(3)	27(2)	24(3)	5(2)	14(2)	8(2)
C(21)	30(2)	45(3)	45(3)	-6(3)	9(2)	9(2)

Table 5. Hydrogen coordinates (x 10^4) and isotropic displacement parameters ($Å^2$ x 10^3) for larsen02.

	x	y	z	U(eq)
H(1)	3124	3945	1113	32
H(2)	720	3581	1804	36
H(3)	833	4675	3832	36
H(16)	3348	6156	5093	31
H(15)	10426	7100	3587	34
H(14)	13029	8500	4642	37
H(10)	11244	9960	7490	33
H(4)	5493	7650	6078	29
H(9)	9359	11103	7543	37
H(8)	9098	12404	9355	52
H(7)	7738	11540	10684	57
H(6)	6518	9368	10169	50
H(5)	6661	8054	8346	38
H(12)	14126	11144	6896	66

H(11)	14906	10061	6380	66
H(13)	14443	10191	7686	66

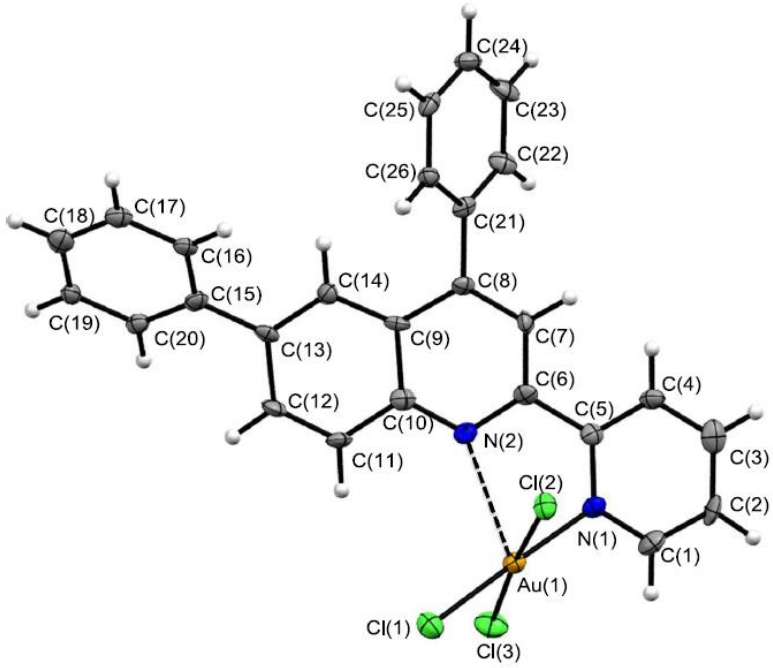

Table 1. Crystal data and structure refinement for larsen04. (6-phenyl-PyQuin)$AuCl_3$ (**2c**)

Identification code	larsen04
Empirical formula	C26 H18 Au Cl3 N2
Molecular formula	C26 H18 Au Cl3 N2
Formula weight	661.74
Temperature	100(2) K
Wavelength	0.71073 Å
Crystal system	Monoclinic
Space group	P2(1)/c

Unit cell dimensions	a = 9.2431(16) Å	a= 90°.
	b = 17.093(3) Å	b= 99.481(5)°.
	c = 14.727(3) Å	g = 90°.
Volume	2294.9(7) $Å^3$	
Z	4	
Density (calculated)	1.915 Mg/m^3	
Absorption coefficient	6.777 mm^{-1}	
F(000)	1272	
Crystal size	0.18 x 0.07 x 0.07 mm^3	
Crystal color, habit	gold / block	
Theta range for data collection	1.84 to 26.43°.	
Index ranges	-11<=h<=11, -21<=k<=21, -18<=l<=18	
Reflections collected	22596	
Independent reflections	4722 [R(int) = 0.0900]	
Completeness to theta = 25.00°	100.0 %	
Absorption correction	None	
Max. and min. transmission	0.6484 and 0.3751	
Refinement method	Full-matrix least-squares on F^2	
Data / restraints / parameters	4722 / 0 / 289	
Goodness-of-fit on F^2	1.004	
Final R indices [I>2sigma(I)]	R1 = 0.0379, wR2 = 0.0610	
R indices (all data)	R1 = 0.0720, wR2 = 0.0693	
Largest diff. peak and hole	1.263 and -1.159 $e.Å^{-3}$	

Table 2. Atomic coordinates (x 10^4) and equivalent isotropic displacement parameters ($Å^2$x 10^3) for larsen04. U(eq) is defined as one third of the trace of the orthogonalized U^{ij} tensor.

	x	y	z	U(eq)
Au(1)	5485(1)	685(1)	2644(1)	18(1)
Cl(1)	6028(2)	-153(1)	3850(1)	27(1)
Cl(2)	6902(2)	1624(1)	3462(1)	22(1)
Cl(3)	4213(2)	-272(1)	1763(1)	30(1)
N(1)	5092(5)	1456(3)	1555(4)	19(1)
N(2)	3142(5)	1624(3)	2801(3)	18(1)
C(1)	5728(7)	1315(4)	825(4)	25(2)
C(2)	5749(7)	1844(4)	133(4)	24(2)
C(3)	5055(7)	2555(4)	184(5)	26(2)
C(4)	4328(7)	2692(4)	922(4)	20(2)
C(5)	4337(6)	2141(4)	1612(4)	18(2)
C(6)	3526(6)	2272(4)	2388(4)	17(2)
C(7)	3138(6)	3020(4)	2642(4)	16(1)
C(8)	2289(6)	3122(3)	3312(4)	15(1)
C(9)	1817(6)	2451(3)	3761(4)	13(1)
C(10)	2339(6)	1705(4)	3481(4)	18(2)
C(11)	1948(6)	1018(4)	3920(4)	19(2)
C(12)	1095(6)	1065(4)	4593(4)	20(2)
C(13)	534(6)	1784(3)	4867(4)	14(1)
C(14)	891(6)	2449(4)	4433(4)	17(2)
C(15)	-387(6)	1809(4)	5588(4)	19(2)
C(16)	-213(6)	2415(3)	6240(4)	17(2)
C(17)	-1059(7)	2433(4)	6939(5)	22(2)
C(18)	-2083(7)	1847(4)	7009(5)	25(2)
C(19)	-2268(6)	1253(4)	6362(4)	18(2)
C(20)	-1435(6)	1233(4)	5667(4)	18(2)
C(21)	1839(6)	3929(4)	3553(4)	16(2)
C(22)	1180(7)	4420(3)	2850(5)	22(2)
C(23)	743(7)	5167(4)	3050(5)	27(2)

C(24)	955(7)	5423(4)	3941(5)	26(2)
C(25)	1610(6)	4944(4)	4654(5)	21(2)
C(26)	2062(6)	4204(3)	4449(4)	17(1)

Table 3. Bond lengths [Å] and angles [°] for larsen04.

Table 4. Anisotropic displacement parameters ($Å^2 x\ 10^3$) for larsen04. The anisotropic displacement factor exponent takes the form: $-2p^2[\ h^2\ a^{*2}U^{11} + ... + 2\ h\ k\ a^*\ b^*\ U^{12}\ ]$

	U^{11}	U^{22}	U^{33}	U^{23}	U^{13}	U^{12}
Au(1)	18(1)	18(1)	19(1)	0(1)	4(1)	2(1)
Cl(1)	31(1)	24(1)	26(1)	4(1)	4(1)	-1(1)
Cl(2)	24(1)	24(1)	20(1)	0(1)	4(1)	-4(1)
Cl(3)	34(1)	23(1)	32(1)	-6(1)	-2(1)	-2(1)
N(1)	12(3)	22(3)	21(3)	0(3)	1(2)	3(2)
N(2)	17(3)	18(3)	18(3)	-5(2)	3(2)	-2(2)
C(1)	25(4)	29(4)	22(4)	-7(3)	7(3)	3(3)
C(2)	23(4)	38(5)	11(4)	-1(3)	9(3)	-2(3)
C(3)	19(4)	36(4)	22(4)	1(3)	-2(3)	-10(3)
C(4)	21(4)	18(4)	20(4)	0(3)	2(3)	6(3)
C(5)	15(3)	16(4)	22(4)	-4(3)	2(3)	-4(3)
C(6)	13(3)	20(4)	15(3)	2(3)	-3(3)	5(3)
C(7)	18(3)	15(3)	18(4)	2(3)	7(3)	-5(3)
C(8)	7(3)	14(4)	22(4)	0(3)	-1(3)	1(3)
C(9)	14(3)	8(3)	15(3)	-2(3)	-4(3)	3(3)
C(10)	14(3)	17(4)	22(4)	-3(3)	0(3)	-2(3)
C(11)	16(3)	12(3)	30(4)	-4(3)	4(3)	5(3)
C(12)	21(4)	8(3)	30(4)	1(3)	3(3)	0(3)
C(13)	12(3)	11(3)	17(3)	2(3)	-5(3)	2(3)
C(14)	17(3)	19(4)	16(4)	2(3)	3(3)	2(3)
C(15)	16(3)	21(4)	21(4)	2(3)	4(3)	7(3)
C(16)	16(3)	13(3)	22(4)	0(3)	1(3)	4(3)
C(17)	18(4)	18(4)	29(4)	-2(3)	1(3)	2(3)

C(18)	23(4)	27(4)	24(4)	6(3)	2(3)	7(3)
C(19)	14(3)	15(4)	25(4)	3(3)	5(3)	0(3)
C(20)	18(3)	18(4)	17(4)	0(3)	2(3)	4(3)
C(21)	6(3)	17(3)	24(4)	-7(3)	1(3)	-3(3)
C(22)	20(3)	16(4)	28(4)	-3(3)	-2(3)	-4(3)
C(23)	23(4)	13(4)	43(5)	4(3)	0(3)	-4(3)
C(24)	23(4)	16(4)	40(5)	-2(3)	10(3)	4(3)
C(25)	18(3)	24(4)	23(4)	-8(3)	10(3)	-6(3)
C(26)	15(3)	16(4)	20(3)	2(3)	3(3)	1(3)

Table 5. Hydrogen coordinates (x 10^4) and isotropic displacement parameters ($Å^2$x 10^3) for larsen04.

	x	y	z	U(eq)
H(1A)	6190	823	783	30
H(2A)	6230	1726	-373	28
H(3A)	5075	2943	-276	31
H(4A)	3817	3171	954	24
H(7A)	3466	3464	2346	20
H(11A)	2280	522	3747	23
H(12A)	868	597	4888	24
H(14A)	494	2933	4592	21
H(16A)	487	2815	6203	21
H(17A)	-936	2849	7373	26
H(18A)	-2647	1855	7493	30
H(19A)	-2974	855	6397	22
H(20A)	-1576	819	5231	21
H(22A)	1031	4242	2231	26
H(23A)	296	5501	2568	32
H(24A)	651	5935	4075	31
H(25A)	1745	5123	5273	25
H(26A)	2534	3879	4932	21

Table 6. Torsion angles [°] for larsen04.

Cl(1)-Au(1)-N(1)-C(1)	60(4)

Cl(2)-Au(1)-N(1)-C(1)	108.1(4)
Cl(3)-Au(1)-N(1)-C(1)	-67.6(4)
N(2)-Au(1)-N(1)-C(1)	-165.2(5)
Cl(1)-Au(1)-N(1)-C(5)	-113(3)
Cl(2)-Au(1)-N(1)-C(5)	-64.7(4)
Cl(3)-Au(1)-N(1)-C(5)	119.6(4)
N(2)-Au(1)-N(1)-C(5)	22.0(4)
N(1)-Au(1)-N(2)-C(6)	-30.5(4)
Cl(1)-Au(1)-N(2)-C(6)	147.6(3)
Cl(2)-Au(1)-N(2)-C(6)	59.3(3)
Cl(3)-Au(1)-N(2)-C(6)	-118.2(3)
N(1)-Au(1)-N(2)-C(10)	-173.3(5)
Cl(1)-Au(1)-N(2)-C(10)	4.7(5)
Cl(2)-Au(1)-N(2)-C(10)	-83.6(5)
Cl(3)-Au(1)-N(2)-C(10)	98.9(5)
C(5)-N(1)-C(1)-C(2)	4.0(9)
Au(1)-N(1)-C(1)-C(2)	-168.9(5)
N(1)-C(1)-C(2)-C(3)	-1.2(10)
C(1)-C(2)-C(3)-C(4)	-2.0(9)
C(2)-C(3)-C(4)-C(5)	2.2(9)
C(1)-N(1)-C(5)-C(4)	-3.6(8)
Au(1)-N(1)-C(5)-C(4)	169.0(4)
C(1)-N(1)-C(5)-C(6)	175.1(5)
Au(1)-N(1)-C(5)-C(6)	-12.3(7)
C(3)-C(4)-C(5)-N(1)	0.5(9)
C(3)-C(4)-C(5)-C(6)	-178.1(5)
C(10)-N(2)-C(6)-C(7)	0.6(8)
Au(1)-N(2)-C(6)-C(7)	-148.6(5)
C(10)-N(2)-C(6)-C(5)	-176.7(5)
Au(1)-N(2)-C(6)-C(5)	34.1(5)
N(1)-C(5)-C(6)-N(2)	-23.1(8)
C(4)-C(5)-C(6)-N(2)	155.6(5)
N(1)-C(5)-C(6)-C(7)	159.6(5)
C(4)-C(5)-C(6)-C(7)	-21.7(8)

N(2)-C(6)-C(7)-C(8)	-2.4(9)
C(5)-C(6)-C(7)-C(8)	174.7(5)
C(6)-C(7)-C(8)-C(9)	0.8(8)
C(6)-C(7)-C(8)-C(21)	-177.9(5)
C(7)-C(8)-C(9)-C(14)	-177.0(6)
C(21)-C(8)-C(9)-C(14)	1.7(9)
C(7)-C(8)-C(9)-C(10)	2.2(8)
C(21)-C(8)-C(9)-C(10)	-179.1(5)
C(6)-N(2)-C(10)-C(11)	-179.4(5)
Au(1)-N(2)-C(10)-C(11)	-41.8(8)
C(6)-N(2)-C(10)-C(9)	2.8(8)
Au(1)-N(2)-C(10)-C(9)	140.4(5)
C(14)-C(9)-C(10)-N(2)	175.1(5)
C(8)-C(9)-C(10)-N(2)	-4.2(8)
C(14)-C(9)-C(10)-C(11)	-2.6(8)
C(8)-C(9)-C(10)-C(11)	178.1(5)
N(2)-C(10)-C(11)-C(12)	-177.9(5)
C(9)-C(10)-C(11)-C(12)	0.0(9)
C(10)-C(11)-C(12)-C(13)	1.6(9)
C(11)-C(12)-C(13)-C(14)	-0.5(9)
C(11)-C(12)-C(13)-C(15)	179.6(6)
C(12)-C(13)-C(14)-C(9)	-2.3(9)
C(15)-C(13)-C(14)-C(9)	177.6(5)
C(8)-C(9)-C(14)-C(13)	-176.9(5)
C(10)-C(9)-C(14)-C(13)	3.9(9)
C(14)-C(13)-C(15)-C(20)	141.6(6)
C(12)-C(13)-C(15)-C(20)	-38.4(8)
C(14)-C(13)-C(15)-C(16)	-39.6(8)
C(12)-C(13)-C(15)-C(16)	140.3(6)
C(20)-C(15)-C(16)-C(17)	0.3(8)
C(13)-C(15)-C(16)-C(17)	-178.5(5)
C(15)-C(16)-C(17)-C(18)	0.5(9)
C(16)-C(17)-C(18)-C(19)	-1.1(9)
C(17)-C(18)-C(19)-C(20)	1.0(9)

C(18)-C(19)-C(20)-C(15)	-0.3(9)
C(16)-C(15)-C(20)-C(19)	-0.4(9)
C(13)-C(15)-C(20)-C(19)	178.4(5)
C(7)-C(8)-C(21)-C(26)	-127.9(7)
C(9)-C(8)-C(21)-C(26)	53.4(8)
C(7)-C(8)-C(21)-C(22)	51.7(8)
C(9)-C(8)-C(21)-C(22)	-127.0(6)
C(26)-C(21)-C(22)-C(23)	-0.8(9)
C(8)-C(21)-C(22)-C(23)	179.6(6)
C(21)-C(22)-C(23)-C(24)	-0.1(10)
C(22)-C(23)-C(24)-C(25)	0.2(10)
C(23)-C(24)-C(25)-C(26)	0.7(10)
C(24)-C(25)-C(26)-C(21)	-1.7(9)
C(22)-C(21)-C(26)-C(25)	1.7(9)
C(8)-C(21)-C(26)-C(25)	-178.7(5)

Symmetry transformations used to generate equivalent atoms:

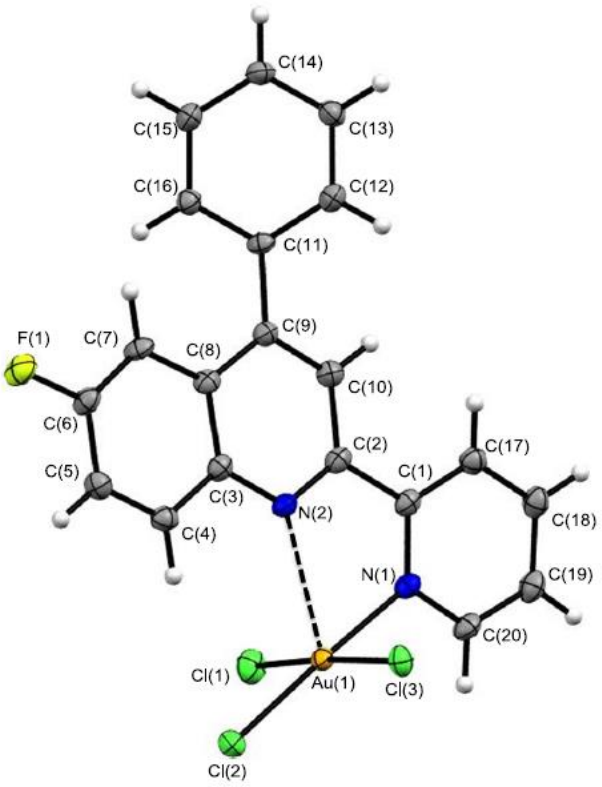

Table 1. Crystal data and structure refinement for larsen04. (6-fluorol-PyQuin)$AuCl_3$ (**2c**)

Identification code	larsen04	
Empirical formula	C26 H18 Au Cl3 N2 F	
Molecular formula	C26 H18 Au Cl3 N2 F	
Formula weight	661.74	
Temperature	100(2) K	
Wavelength	0.71073 Å	
Crystal system	Monoclinic	
Space group	P2(1)/c	
Unit cell dimensions	a = 9.2431(16) Å	a= 90°.
	b = 17.093(3) Å	b= 99.481(5)°.
	c = 14.727(3) Å	g = 90°.
Volume	2294.9(7) $Å^3$	

Z	4
Density (calculated)	1.915 Mg/m^3
Absorption coefficient	6.777 mm^{-1}
F(000)	1272
Crystal size	0.18 x 0.07 x 0.07 mm^3
Crystal color, habit	gold / block
Theta range for data collection	1.84 to 26.43°.
Index ranges	-11<=h<=11, -21<=k<=21, -18<=l<=18
Reflections collected	22596
Independent reflections	4722 [R(int) = 0.0900]
Completeness to theta = 25.00°	100.0 %
Absorption correction	None
Max. and min. transmission	0.6484 and 0.3751
Refinement method	Full-matrix least-squares on F^2
Data / restraints / parameters	4722 / 0 / 289
Goodness-of-fit on F^2	1.004
Final R indices [I>2sigma(I)]	R1 = 0.0379, wR2 = 0.0610
R indices (all data)	R1 = 0.0720, wR2 = 0.0693
Largest diff. peak and hole	1.263 and -1.159 $e.Å^{-3}$

Table 2. Atomic coordinates (x 10^4) and equivalent isotropic displacement parameters ($Å^2$x 10^3) for larsen04. U(eq) is defined as one third of the trace of the orthogonalized U^{ij} tensor.

	x	y	z	U(eq)
Au(1)	5485(1)	685(1)	2644(1)	18(1)
Cl(1)	6028(2)	-153(1)	3850(1)	27(1)
Cl(2)	6902(2)	1624(1)	3462(1)	22(1)
Cl(3)	4213(2)	-272(1)	1763(1)	30(1)
F(1)	824(1)	6467(1)	7082(1)	30(1)
N(1)	5092(5)	1456(3)	1555(4)	19(1)
N(2)	3142(5)	1624(3)	2801(3)	18(1)
C(1)	5728(7)	1315(4)	825(4)	25(2)
C(2)	5749(7)	1844(4)	133(4)	24(2)
C(3)	5055(7)	2555(4)	184(5)	26(2)
C(4)	4328(7)	2692(4)	922(4)	20(2)
C(5)	4337(6)	2141(4)	1612(4)	18(2)
C(6)	3526(6)	2272(4)	2388(4)	17(2)
C(7)	3138(6)	3020(4)	2642(4)	16(1)
C(8)	2289(6)	3122(3)	3312(4)	15(1)
C(9)	1817(6)	2451(3)	3761(4)	13(1)
C(10)	2339(6)	1705(4)	3481(4)	18(2)
C(11)	1948(6)	1018(4)	3920(4)	19(2)
C(12)	1095(6)	1065(4)	4593(4)	20(2)
C(13)	534(6)	1784(3)	4867(4)	14(1)
C(14)	891(6)	2449(4)	4433(4)	17(2)
C(15)	-387(6)	1809(4)	5588(4)	19(2)
C(16)	-213(6)	2415(3)	6240(4)	17(2)
C(17)	-1059(7)	2433(4)	6939(5)	22(2)
C(18)	-2083(7)	1847(4)	7009(5)	25(2)
C(19)	-2268(6)	1253(4)	6362(4)	18(2)
C(20)	-1435(6)	1233(4)	5667(4)	18(2)
C(21)	1839(6)	3929(4)	3553(4)	16(2)
C(22)	1180(7)	4420(3)	2850(5)	22(2)

C(23)	743(7)	5167(4)	3050(5)	27(2)
C(24)	955(7)	5423(4)	3941(5)	26(2)
C(25)	1610(6)	4944(4)	4654(5)	21(2)
C(26)	2062(6)	4204(3)	4449(4)	17(1)

Table 3. Bond lengths [Å] and angles [°] for larsen04.

C(24)-C(23)-C(22)	119.9(6)	C(26)-C(25)-C(24)	119.0(6)
C(24)-C(23)-H(23A)	120.1	C(26)-C(25)-H(25A)	120.5
C(22)-C(23)-H(23A)	120.1	C(24)-C(25)-H(25A)	120.5
C(23)-C(24)-C(25)	120.8(6)	C(25)-C(26)-C(21)	121.1(6)
C(23)-C(24)-H(24A)	119.6	C(25)-C(26)-H(26A)	119.5
C(25)-C(24)-H(24A)	119.6	C(21)-C(26)-H(26A)	119.5

Symmetry transformations used to generate equivalent atoms:

Table 4. Anisotropic displacement parameters ($Å^2 x\ 10^3$) for larsen04. The anisotropic displacement factor exponent takes the form: $-2p^2[\ h^2\ a^{*2}U^{11} + ... + 2\ h\ k\ a^*\ b^*\ U^{12}\ ]$

	U^{11}	U^{22}	U^{33}	U^{23}	U^{13}	U^{12}
Au(1)	18(1)	18(1)	19(1)	0(1)	4(1)	2(1)
Cl(1)	31(1)	24(1)	26(1)	4(1)	4(1)	-1(1)
Cl(2)	24(1)	24(1)	20(1)	0(1)	4(1)	-4(1)
Cl(3)	34(1)	23(1)	32(1)	-6(1)	-2(1)	-2(1)
N(1)	12(3)	22(3)	21(3)	0(3)	1(2)	3(2)
N(2)	17(3)	18(3)	18(3)	-5(2)	3(2)	-2(2)
C(1)	25(4)	29(4)	22(4)	-7(3)	7(3)	3(3)
C(2)	23(4)	38(5)	11(4)	-1(3)	9(3)	-2(3)
C(3)	19(4)	36(4)	22(4)	1(3)	-2(3)	-10(3)
C(4)	21(4)	18(4)	20(4)	0(3)	2(3)	6(3)
C(5)	15(3)	16(4)	22(4)	-4(3)	2(3)	-4(3)
C(6)	13(3)	20(4)	15(3)	2(3)	-3(3)	5(3)

C(7)	18(3)	15(3)	18(4)	2(3)	7(3)	-5(3)
C(8)	7(3)	14(4)	22(4)	0(3)	-1(3)	1(3)
C(9)	14(3)	8(3)	15(3)	-2(3)	-4(3)	3(3)
C(10)	14(3)	17(4)	22(4)	-3(3)	0(3)	-2(3)
C(11)	16(3)	12(3)	30(4)	-4(3)	4(3)	5(3)
C(12)	21(4)	8(3)	30(4)	1(3)	3(3)	0(3)
C(13)	12(3)	11(3)	17(3)	2(3)	-5(3)	2(3)
C(14)	17(3)	19(4)	16(4)	2(3)	3(3)	2(3)
C(15)	16(3)	21(4)	21(4)	2(3)	4(3)	7(3)
C(16)	16(3)	13(3)	22(4)	0(3)	1(3)	4(3)
C(17)	18(4)	18(4)	29(4)	-2(3)	1(3)	2(3)
C(18)	23(4)	27(4)	24(4)	6(3)	2(3)	7(3)
C(19)	14(3)	15(4)	25(4)	3(3)	5(3)	0(3)
C(20)	18(3)	18(4)	17(4)	0(3)	2(3)	4(3)
C(21)	6(3)	17(3)	24(4)	-7(3)	1(3)	-3(3)
C(22)	20(3)	16(4)	28(4)	-3(3)	-2(3)	-4(3)
C(23)	23(4)	13(4)	43(5)	4(3)	0(3)	-4(3)
C(24)	23(4)	16(4)	40(5)	-2(3)	10(3)	4(3)
C(25)	18(3)	24(4)	23(4)	-8(3)	10(3)	-6(3)

C(26)	15(3)	16(4)	20(3)	2(3)	3(3)	1(3)

Table 5. Hydrogen coordinates (x 10^4) and isotropic displacement parameters ($Å^2$x 10^3) for larsen04.

	x	y	z	U(eq)
H(1A)	6190	823	783	30
H(2A)	6230	1726	-373	28
H(3A)	5075	2943	-276	31
H(4A)	3817	3171	954	24
H(7A)	3466	3464	2346	20
H(11A)	2280	522	3747	23
H(12A)	868	597	4888	24
H(14A)	494	2933	4592	21
H(16A)	487	2815	6203	21
H(17A)	-936	2849	7373	26
H(18A)	-2647	1855	7493	30
H(19A)	-2974	855	6397	22
H(20A)	-1576	819	5231	21
H(22A)	1031	4242	2231	26
H(23A)	296	5501	2568	32
H(24A)	651	5935	4075	31
H(25A)	1745	5123	5273	25
H(26A)	2534	3879	4932	21

Table 6. Torsion angles [°] for larsen04.

Cl(1)-Au(1)-N(1)-C(1)	60(4)
Cl(2)-Au(1)-N(1)-C(1)	108.1(4)
Cl(3)-Au(1)-N(1)-C(1)	-67.6(4)
N(2)-Au(1)-N(1)-C(1)	-165.2(5)
Cl(1)-Au(1)-N(1)-C(5)	-113(3)
Cl(2)-Au(1)-N(1)-C(5)	-64.7(4)
Cl(3)-Au(1)-N(1)-C(5)	119.6(4)
N(2)-Au(1)-N(1)-C(5)	22.0(4)
N(1)-Au(1)-N(2)-C(6)	-30.5(4)
Cl(1)-Au(1)-N(2)-C(6)	147.6(3)
Cl(2)-Au(1)-N(2)-C(6)	59.3(3)
Cl(3)-Au(1)-N(2)-C(6)	-118.2(3)
N(1)-Au(1)-N(2)-C(10)	-173.3(5)
Cl(1)-Au(1)-N(2)-C(10)	4.7(5)
Cl(2)-Au(1)-N(2)-C(10)	-83.6(5)
Cl(3)-Au(1)-N(2)-C(10)	98.9(5)
C(5)-N(1)-C(1)-C(2)	4.0(9)
Au(1)-N(1)-C(1)-C(2)	-168.9(5)
N(1)-C(1)-C(2)-C(3)	-1.2(10)
C(1)-C(2)-C(3)-C(4)	-2.0(9)
C(2)-C(3)-C(4)-C(5)	2.2(9)
C(1)-N(1)-C(5)-C(4)	-3.6(8)
Au(1)-N(1)-C(5)-C(4)	169.0(4)
C(1)-N(1)-C(5)-C(6)	175.1(5)
Au(1)-N(1)-C(5)-C(6)	-12.3(7)
C(3)-C(4)-C(5)-N(1)	0.5(9)
C(3)-C(4)-C(5)-C(6)	-178.1(5)
C(10)-N(2)-C(6)-C(7)	0.6(8)
Au(1)-N(2)-C(6)-C(7)	-148.6(5)
C(10)-N(2)-C(6)-C(5)	-176.7(5)
Au(1)-N(2)-C(6)-C(5)	34.1(5)

N(1)-C(5)-C(6)-N(2)	-23.1(8)
C(4)-C(5)-C(6)-N(2)	155.6(5)
N(1)-C(5)-C(6)-C(7)	159.6(5)
C(4)-C(5)-C(6)-C(7)	-21.7(8)
N(2)-C(6)-C(7)-C(8)	-2.4(9)
C(5)-C(6)-C(7)-C(8)	174.7(5)
C(6)-C(7)-C(8)-C(9)	0.8(8)
C(6)-C(7)-C(8)-C(21)	-177.9(5)
C(7)-C(8)-C(9)-C(14)	-177.0(6)
C(21)-C(8)-C(9)-C(14)	1.7(9)
C(7)-C(8)-C(9)-C(10)	2.2(8)
C(21)-C(8)-C(9)-C(10)	-179.1(5)
C(6)-N(2)-C(10)-C(11)	-179.4(5)
Au(1)-N(2)-C(10)-C(11)	-41.8(8)
C(6)-N(2)-C(10)-C(9)	2.8(8)
Au(1)-N(2)-C(10)-C(9)	140.4(5)
C(14)-C(9)-C(10)-N(2)	175.1(5)
C(8)-C(9)-C(10)-N(2)	-4.2(8)
C(14)-C(9)-C(10)-C(11)	-2.6(8)
C(8)-C(9)-C(10)-C(11)	178.1(5)
N(2)-C(10)-C(11)-C(12)	-177.9(5)
C(9)-C(10)-C(11)-C(12)	0.0(9)
C(10)-C(11)-C(12)-C(13)	1.6(9)
C(11)-C(12)-C(13)-C(14)	-0.5(9)
C(11)-C(12)-C(13)-C(15)	179.6(6)
C(12)-C(13)-C(14)-C(9)	-2.3(9)
C(15)-C(13)-C(14)-C(9)	177.6(5)
C(8)-C(9)-C(14)-C(13)	-176.9(5)
C(10)-C(9)-C(14)-C(13)	3.9(9)
C(14)-C(13)-C(15)-C(20)	141.6(6)
C(12)-C(13)-C(15)-C(20)	-38.4(8)
C(14)-C(13)-C(15)-C(16)	-39.6(8)
C(12)-C(13)-C(15)-C(16)	140.3(6)
C(20)-C(15)-C(16)-C(17)	0.3(8)

C(13)-C(15)-C(16)-C(17)	-178.5(5)
C(15)-C(16)-C(17)-C(18)	0.5(9)
C(16)-C(17)-C(18)-C(19)	-1.1(9)
C(17)-C(18)-C(19)-C(20)	1.0(9)
C(18)-C(19)-C(20)-C(15)	-0.3(9)
C(16)-C(15)-C(20)-C(19)	-0.4(9)
C(13)-C(15)-C(20)-C(19)	178.4(5)
C(7)-C(8)-C(21)-C(26)	-127.9(7)
C(9)-C(8)-C(21)-C(26)	53.4(8)
C(7)-C(8)-C(21)-C(22)	51.7(8)
C(9)-C(8)-C(21)-C(22)	-127.0(6)
C(26)-C(21)-C(22)-C(23)	-0.8(9)
C(8)-C(21)-C(22)-C(23)	179.6(6)
C(21)-C(22)-C(23)-C(24)	-0.1(10)
C(22)-C(23)-C(24)-C(25)	0.2(10)
C(23)-C(24)-C(25)-C(26)	0.7(10)
C(24)-C(25)-C(26)-C(21)	-1.7(9)
C(22)-C(21)-C(26)-C(25)	1.7(9)
C(8)-C(21)-C(26)-C(25)	-178.7(5)

Symmetry transformations used to generate equivalent atoms:

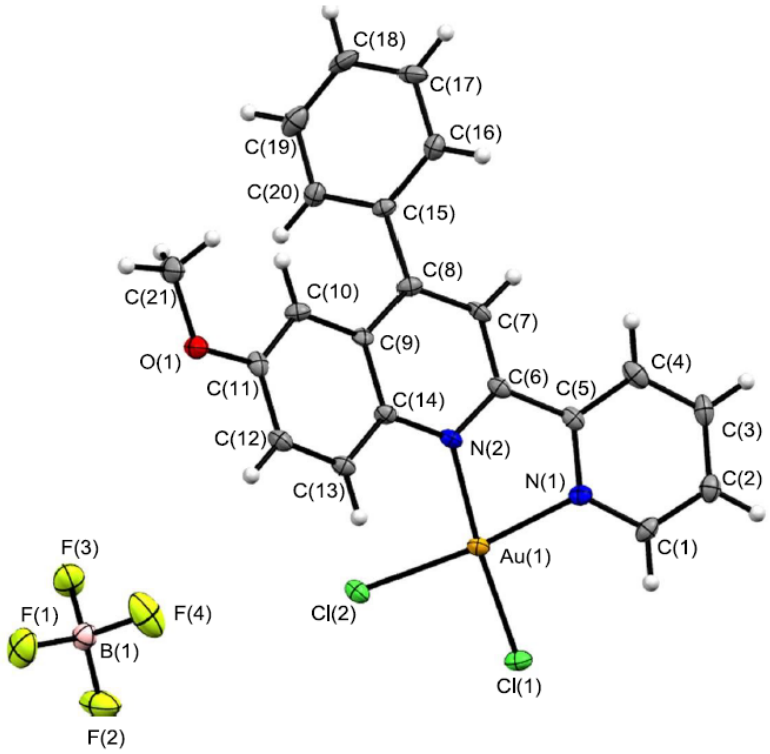

Table 1. Crystal data and structure refinement for larsen06. [(6-methoxy-PyQuin)$AuCl_2$]BF_4•CH_2Cl_2 (**3a**) Identification code larsen06

Empirical formula	C20 H13 Au Cl3 F N2
Formula weight	603.64
Temperature	100(2) K
Wavelength	0.71073 Å
Crystal system	Monoclinic
Space group	C 2/c
Unit cell dimensions	a = 19.3904(8) Å .
	b = 13.6914(6) Å
	c = 15.9497(5) Å
Volume	3781.7(3) $Å^3$
Z	8
Density (calculated)	2.120 Mg/m^3
Absorption coefficient	8.221 mm^{-1}
F(000)	2288

Crystal size	0.240 x 0.200 x 0.120 mm^3
Theta range for data collection	1.896 to 28.336°.
Index ranges	-25<=h<=25, -17<=k<=18, -21<=l<=16
Reflections collected	17528
Independent reflections	4710 [R(int) = 0.0347]
Completeness to theta = 25.000°	99.9 %
Absorption correction	Multi-scan
Refinement method	Full-matrix least-squares on F^2
Data / restraints / parameters	4710 / 0 / 244
Goodness-of-fit on F^2	1.037
Final R indices [I>2sigma(I)]	R1 = 0.0221, wR2 = 0.0519
R indices (all data)	R1 = 0.0261, wR2 = 0.0538
Extinction coefficient	n/a
Largest diff. peak and hole	1.630 and -1.198 e.$Å^{-3}$

Table 2. Atomic coordinates (x 10^4) and equivalent isotropic displacement parameters ($Å^2$x 10^3) for larsen06. U(eq) is defined as one third of the trace of the orthogonalized U^{ij} tensor.

	x	y	z	U(eq)
Au(1)	786(1)	1308(1)	5572(1)	17(1)
Cl(1)	-455(1)	1451(1)	4424(1)	27(1)
Cl(2)	361(1)	1172(1)	6677(1)	22(1)
Cl(3)	2026(1)	1022(1)	6705(1)	22(1)
F(1)	824(1)	6467(1)	7082(1)	30(1)
N(1)	1168(2)	1373(2)	4557(2)	19(1)
N(2)	1145(2)	3127(2)	5406(2)	19(1)
C(1)	1430(2)	2201(2)	4321(2)	18(1)
C(2)	1360(2)	3154(2)	4732(2)	18(1)
C(3)	1073(2)	3986(2)	5793(2)	18(1)
C(4)	852(2)	3926(2)	6531(2)	21(1)
C(5)	768(2)	4754(2)	6949(2)	21(1)
C(6)	908(2)	5657(2)	6646(2)	21(1)

C(7)	1141(2)	5763(2)	5959(2)	20(1)
C(8)	1213(2)	4919(2)	5496(2)	18(1)
C(9)	1442(2)	4927(2)	4758(2)	18(1)
C(10)	1511(2)	4045(2)	4390(2)	19(1)
C(11)	1630(2)	5843(2)	4398(2)	18(1)
C(12)	2282(2)	5855(2)	4239(2)	20(1)
C(13)	2477(2)	6682(2)	3888(2)	21(1)
C(14)	2010(2)	7501(2)	3667(2)	21(1)
C(15)	1355(2)	7494(2)	3810(2)	22(1)
C(16)	1160(2)	6673(2)	4169(2)	19(1)
C(17)	1744(2)	2130(2)	3695(2)	21(1)
C(18)	1774(2)	1242(2)	3295(2)	23(1)
C(19)	1479(2)	419(2)	3524(2)	24(1)
C(20)	1183(2)	509(2)	4163(2)	22(1)

Table 3. Bond lengths [Å] and angles [°] for larsen06.

Au(1)-N(1)	2.064(3)
Au(1)-Cl(2)	2.2647(7)
Au(1)-Cl(1)	2.2834(8)
Au(1)-Cl(3)	2.3011(8)
Au(1)-N(2)	2.633(2)
F(1)-C(6)	1.358(3)
N(1)-C(20)	1.346(4)
N(1)-C(1)	1.363(4)
N(2)-C(2)	1.316(4)
N(2)-C(3)	1.365(4)
C(1)-C(17)	1.388(4)
C(1)-C(2)	1.493(4)
C(2)-C(10)	1.420(4)
C(3)-C(4)	1.423(4)
C(3)-C(8)	1.430(4)
C(4)-C(5)	1.362(4)
C(5)-C(6)	1.398(4)

C(6)-C(7)	1.367(4)
C(7)-C(8)	1.412(4)
C(8)-C(9)	1.432(4)
C(9)-C(10)	1.375(4)
C(9)-C(11)	1.493(4)
C(11)-C(12)	1.397(4)
C(11)-C(16)	1.398(4)
C(12)-C(13)	1.389(4)
C(13)-C(14)	1.383(4)
C(14)-C(15)	1.389(4)
C(15)-C(16)	1.389(4)
C(17)-C(18)	1.385(4)
C(18)-C(19)	1.386(4)
C(19)-C(20)	1.382(4)

N(1)-Au(1)-Cl(2)	177.76(7)
N(1)-A(1)-Cl(1)	89.30(8)
Cl(2)-Au(1)-Cl(1)	90.62(3)
N(1)-Au(1)-Cl(3)	90.28(8)
Cl(2)-Au(1)-Cl(3)	89.60(3)
Cl(1)-Au(1)-Cl(3)	175.11(3)
N(1)-Au(1)-N(2)	71.02(8)
Cl(2)-Au(1)-N(2)	111.22(5)
Cl(1)-Au(1)-N(2)	93.95(6)
Cl(3)-Au(1)-N(2)	90.52(6)
C(20)-N(1)-C(1)	120.9(3)
C(20)-N(1)-Au(1)	114.8(2)
C(1)-N(1)-Au(1)	124.26(19)
C(2)-N(2)-C(3)	118.8(2)
C(2)-N(2)-Au(1)	107.71(18)
C(3)-N(2)-Au(1)	133.11(19)
N(1)-C(1)-C(17)	118.6(3)
N(1)-C(1)-C(2)	119.1(3)

C(17)-C(1)-C(2)	122.3(3)
N(2)-C(2)-C(10)	122.3(3)
N(2)-C(2)-C(1)	117.3(3)
C(10)-C(2)-C(1)	120.4(3)
N(2)-C(3)-C(4)	117.1(3)
N(2)-C(3)-C(8)	123.0(2)
C(4)-C(3)-C(8)	119.9(3)
C(5)-C(4)-C(3)	120.2(3)
C(4)-C(5)-C(6)	118.8(3)
F(1)-C(6)-C(7)	118.9(3)
F(1)-C(6)-C(5)	117.2(2)
C(7)-C(6)-C(5)	123.9(3)
C(6)-C(7)-C(8)	118.5(3)
C(7)-C(8)-C(3)	118.6(2)
C(7)-C(8)-C(9)	124.3(3)
C(3)-C(8)-C(9)	117.0(3)
C(10)-C(9)-C(8)	118.1(3)
C(10)-C(9)-C(11)	119.1(2)
C(8)-C(9)-C(11)	122.9(3)
C(9)-C(10)-C(2)	120.9(3)

C(12)-C(11)-C(16)	118.7(3)
C(12)-C(11)-C(9)	118.5(3)
C(16)-C(11)-C(9)	122.7(3)
C(13)-C(12)-C(11)	120.9(3)
C(14)-C(13)-C(12)	119.9(3)
C(13)-C(14)-C(15)	119.7(3)
C(16)-C(15)-C(14)	120.8(3)
C(15)-C(16)-C(11)	119.9(3)
C(18)-C(17)-C(1)	121.0(3)
C(17)-C(18)-C(19)	119.0(3)
C(20)-C(19)-C(18)	118.6(3)
N(1)-C(20)-C(19)	121.8(3)

Table 4. Anisotropic displacement parameters ($Å^2 x\ 10^3$) for larsen06. The anisotropic displacement factor exponent takes the form: $-2p^2[\ h^2\ a^{*2}U^{11} + ... + 2\ h\ k\ a^*\ b^*\ U^{12}\ ]$

	U^{11}	U^{22}	U^{33}	U^{23}	U^{13}	U^{12}
Au(1)	16(1)	13(1)	21(1)	-1(1)	8(1)	0(1)
Cl(1)	17(1)	31(1)	28(1)	0(1)	5(1)	2(1)
Cl(2)	21(1)	22(1)	27(1)	0(1)	14(1)	-1(1)
Cl(3)	17(1)	26(1)	21(1)	-1(1)	8(1)	3(1)
F(1)	48(1)	20(1)	26(1)	-4(1)	21(1)	2(1)
N(1)	20(1)	15(1)	18(1)	-2(1)	6(1)	-1(1)
N(2)	21(1)	14(1)	21(1)	0(1)	9(1)	0(1)
C(1)	15(2)	17(1)	18(1)	0(1)	3(1)	1(1)
C(2)	17(2)	16(1)	19(1)	-1(1)	4(1)	1(1)
C(3)	16(2)	18(1)	17(1)	0(1)	4(1)	1(1)
C(4)	19(2)	21(1)	22(1)	2(1)	8(1)	-1(1)
C(5)	22(2)	23(2)	19(1)	0(1)	9(1)	0(1)
C(6)	26(2)	17(1)	20(1)	-2(1)	10(1)	2(1)
C(7)	26(2)	12(1)	20(1)	-2(1)	8(1)	-3(1)
C(8)	16(2)	17(1)	18(1)	-2(1)	5(1)	-2(1)
C(9)	18(2)	16(1)	19(1)	1(1)	7(1)	0(1)

C(10)	19(2)	19(1)	18(1)	0(1)	7(1)	-1(1)
C(11)	21(2)	13(1)	17(1)	-2(1)	7(1)	-3(1)
C(12)	20(2)	18(1)	19(1)	-1(1)	7(1)	2(1)
C(13)	19(2)	24(2)	23(1)	2(1)	11(1)	-1(1)
C(14)	24(2)	18(1)	23(1)	4(1)	11(1)	-1(1)
C(15)	23(2)	17(1)	25(1)	0(1)	11(1)	3(1)
C(16)	17(2)	19(1)	21(1)	0(1)	7(1)	0(1)
C(17)	21(2)	21(2)	21(1)	2(1)	9(1)	1(1)
C(18)	26(2)	24(2)	20(1)	-2(1)	11(1)	3(1)
C(19)	26(2)	21(2)	23(1)	-6(1)	9(1)	1(1)
C(20)	23(2)	15(1)	24(1)	-3(1)	8(1)	-2(1)

Table 5. Hydrogen coordinates (x 10^4) and isotropic displacement parameters ($Å^2$x 10^3) for larsen06.

	x	y	z	U(eq)
H(9)	764	3306	6733	25
H(8)	616	4719	7438	26
H(7)	1252	6391	5797	24
H(1)	1662	4032	3900	23
H(6)	2597	5289	4373	23
H(5)	2930	6686	3800	26
H(4)	2137	8065	3418	26
H(3)	1036	8058	3660	26
H(2)	707	6674	4258	23
H(10)	1942	2699	3538	26
H(11)	1994	1199	2871	28
H(12)	1479	-195	3246	28
H(13)	985	-54	4329	26

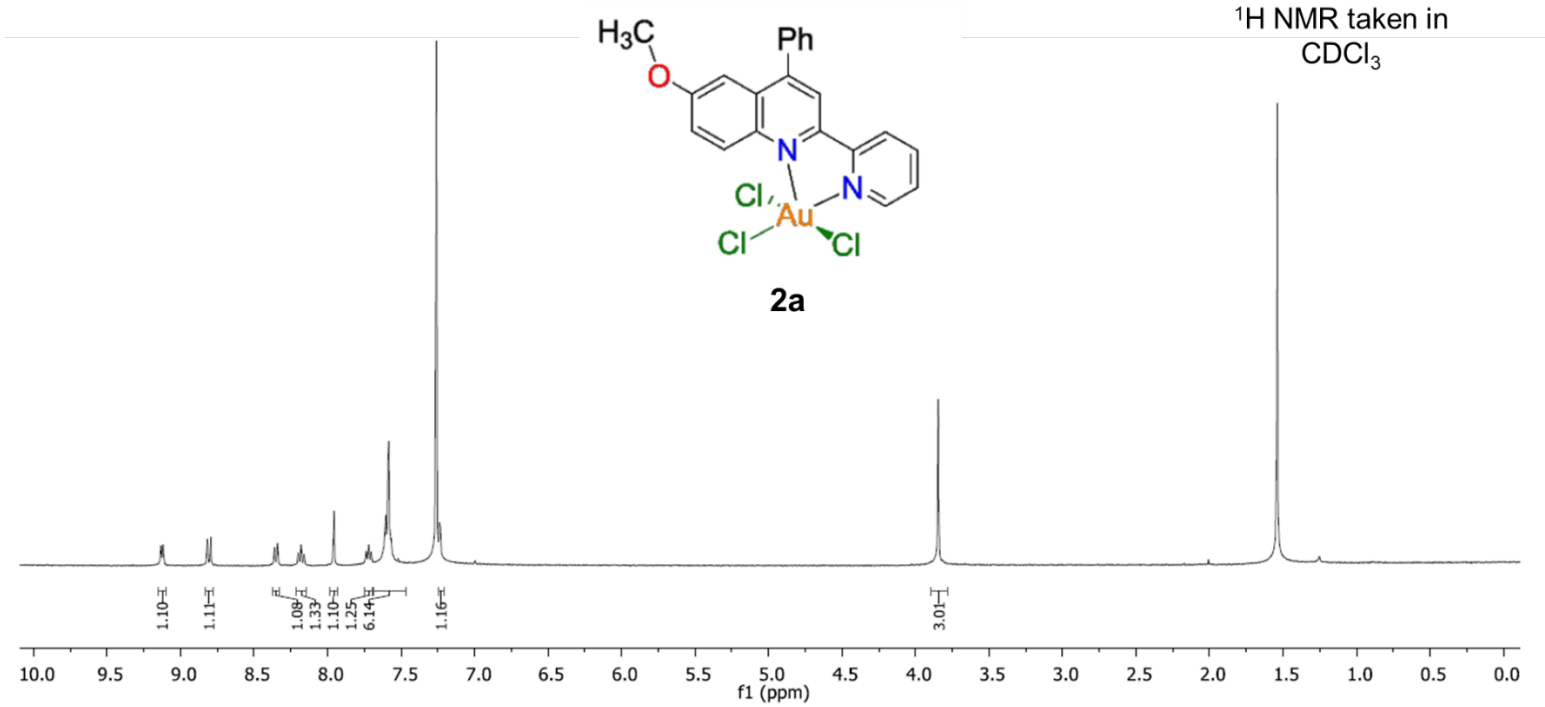
^{1}H NMR taken in
$CDCl_3$
H_3C
O
Ph
N
N
Cl
Au
Cl
Cl
2a
1.10
1.11
1.08
1.33
1.10
1.25
6.14
1.16
3.01
10.0 9.5 9.0 8.5 8.0 7.5 7.0 6.5 6.0 5.5 5.0 4.5 4.0 3.5 3.0 2.5 2.0 1.5 1.0 0.5 0.0
f1 (ppm)

^{1}H NMR taken in $CDCl_3$

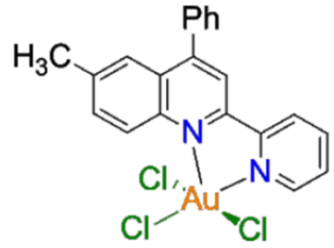

2b

^{1}H NMR taken in $CDCl_3$

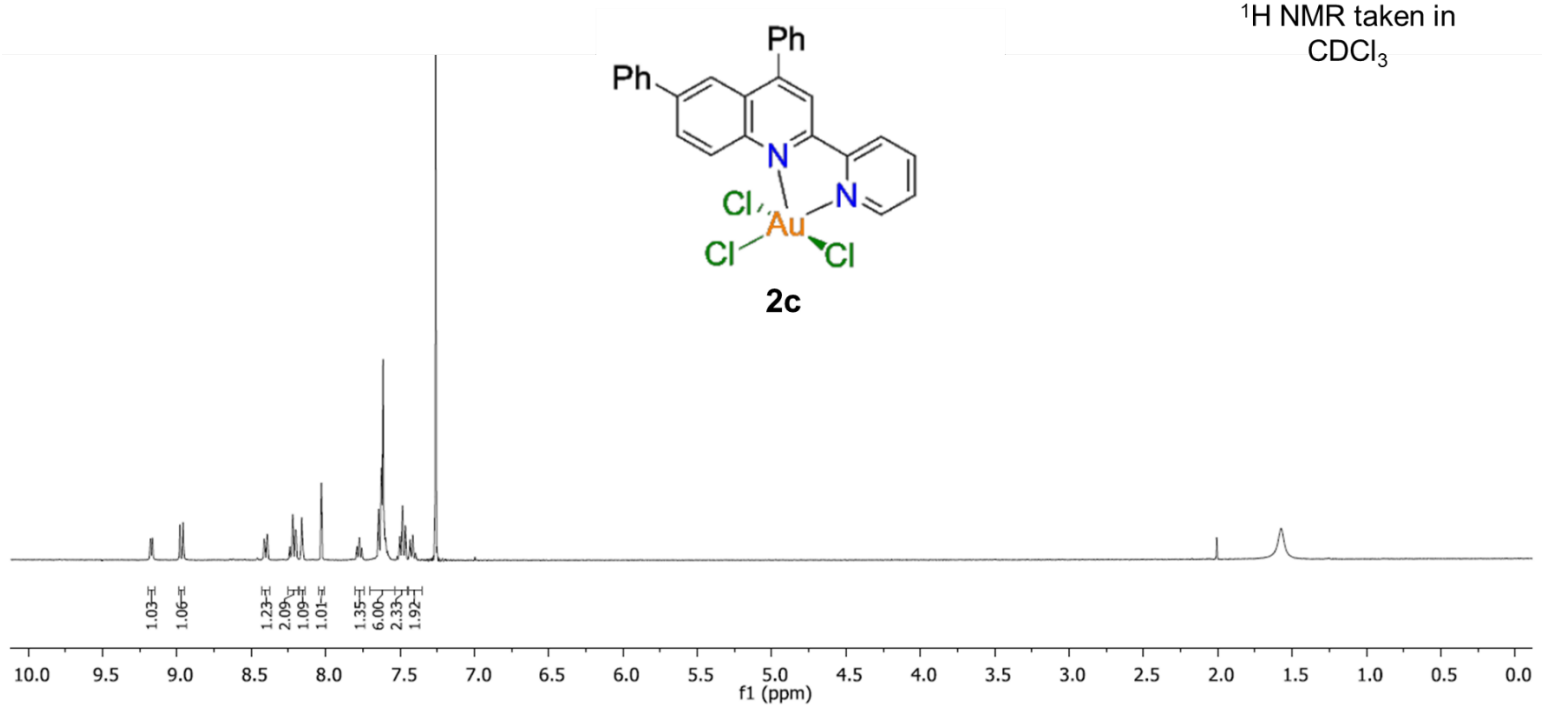

2c

^{1}H NMR taken in $CDCl_3$

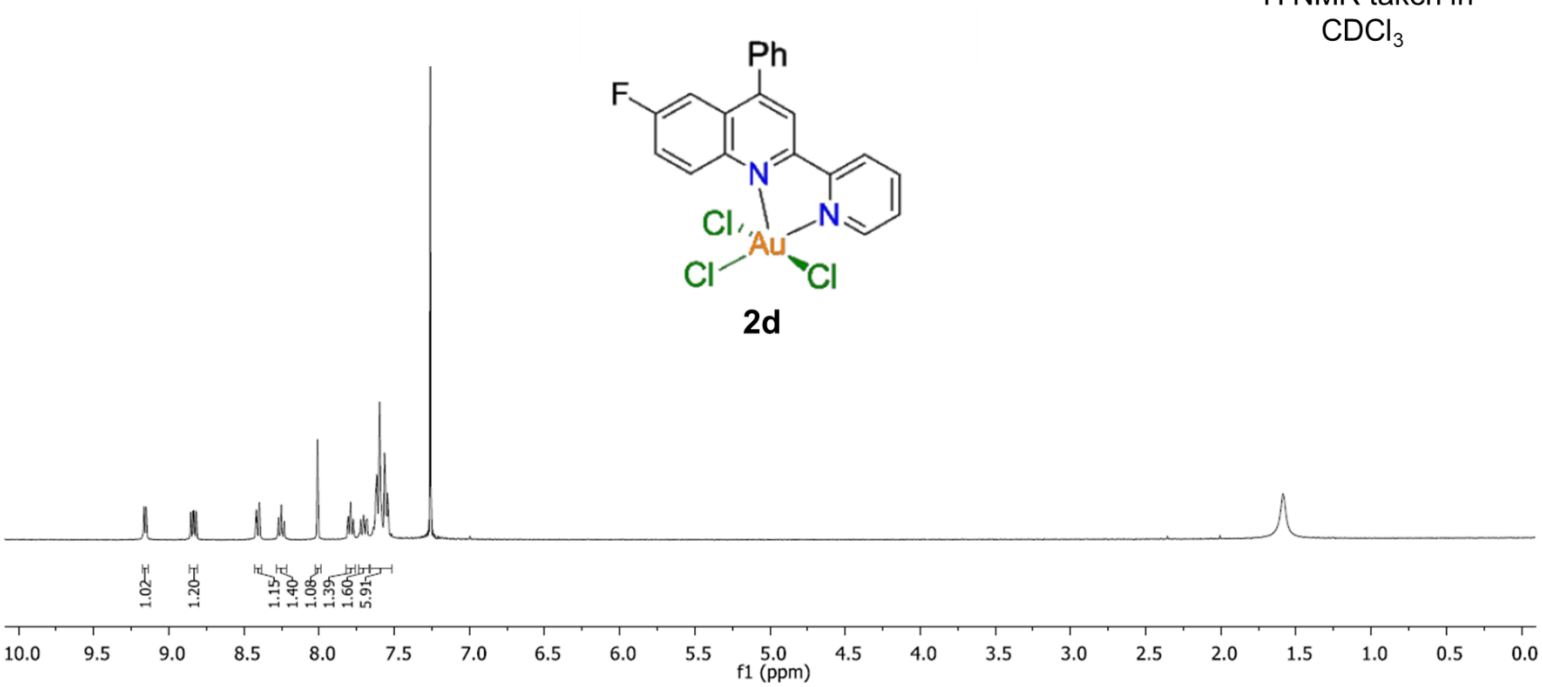

2d

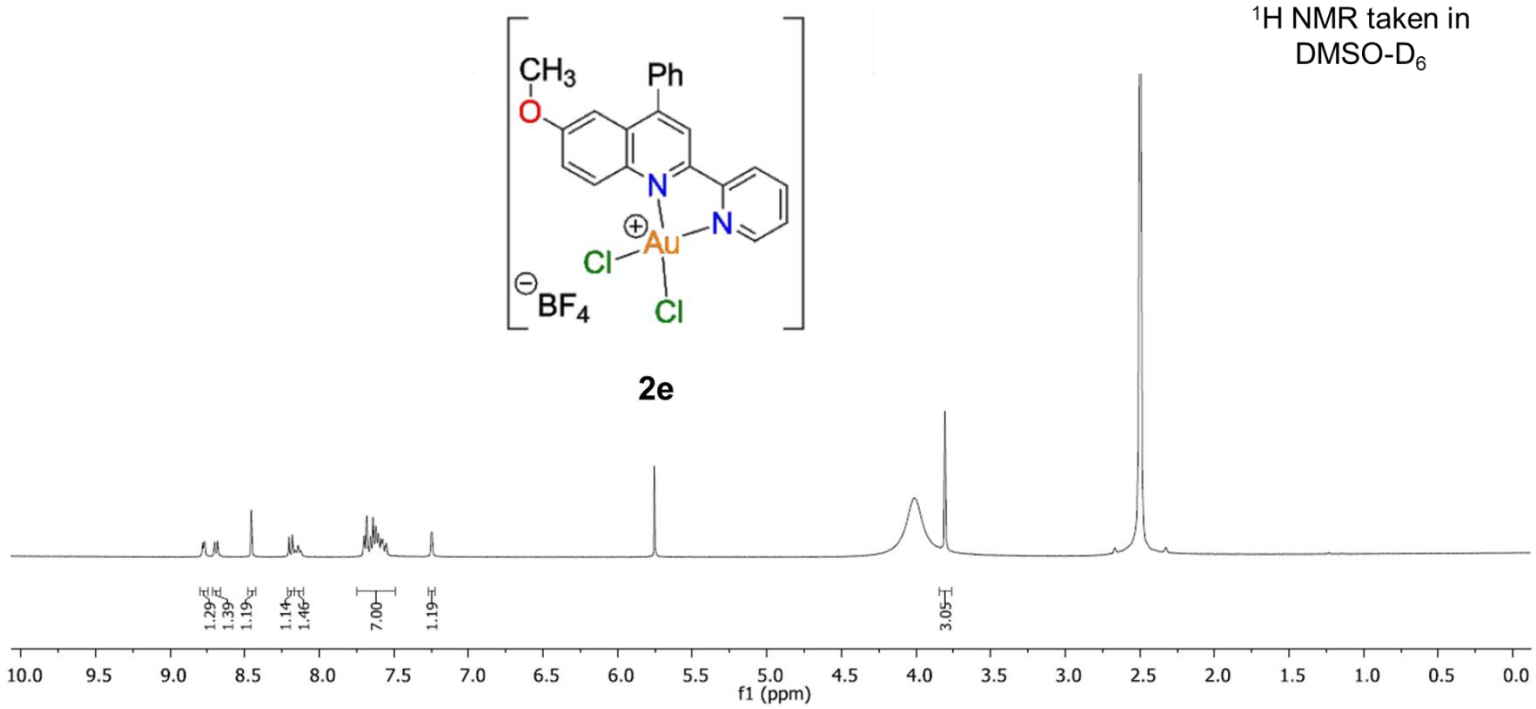
^{1}H NMR taken in
DMSO-D$_6$
CH$_3$
O
Ph
N
N
Au
Cl
Cl
BF$_4$
1.29
1.39
1.19
1.14
1.46
7.00
1.19
3.05
10.0 9.5 9.0 8.5 8.0 7.5 7.0 6.5 6.0 5.5 5.0 4.5 4.0 3.5 3.0 2.5 2.0 1.5 1.0 0.5 0.0
f1 (ppm)

2e

Chapter Four: Investigation of the Solution-Phase Behavior for PyQuin Gold (III) Complexes and Observance of Gold Nanoparticles

4.1 Introduction:

In recent years, gold (III) chemistry has emerged as a subject of growing interest: in 2008, *Chemical Reviews* dedicated an entire issue to the rise of coinage-metal catalysis, specifically gold chemistry.[1,2] In it, they described the the first asymmetric gold-catalyzed reaction, which employed a chiral ferrocenylphosphine-Au(I) complex. This complex catalyzed the aldol reaction of isocyanoacetates with aldehydes to yield substituted oxazolines.[3] During the groups' screening of catalysts, it was observed that while other coinage metal could facilitate the desired transformation, the copper and silver catalysts were significantly less selective. The ability of linear, monodentate gold (I) phosphine complexes to induce high levels of enantioselectivity is actually quite prolific.[4] While there has been much research involving gold (I) complexes with various types of carbon, phosphorous, and halide ligands, gold (III) complexes cannot boast the same history. In fact, it was twenty years after the first chiral Au(I) catalyst that a catalytic asymmetric hydrogenation with a gold (III) complex was reported by Debono, Iglesias, and Sanchez (**Scheme 4.1**).[5]

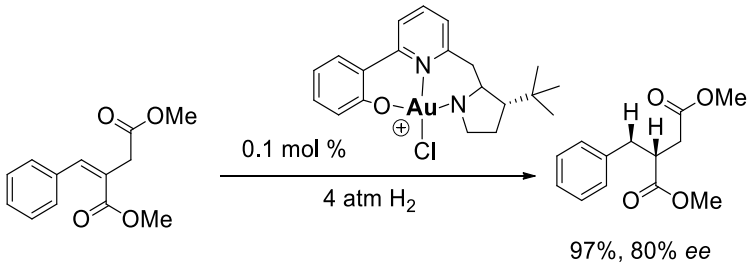

Scheme 4.1. First example of catalytic asymmetric hydrogenation with a gold (III) complex

Employing phenolate, pyridyl, pyrrolidine, and chloride ligands, their cationic gold (III) complex compared favorably with the analogous palladium (II) complex. These complexes were quite successful in both hydrogenation and hydrosilylation reactions, however cross-couplings were exclusively catalyzed by the palladium analogue. This observation is not that surprising, as there has been no published evidence that a gold (III) center can undergo oxidative addition/reductive elimination in the way palladium (II) complexes can. Regardless, the evidence put forth by the Sanchez group strongly supports the impetus for developing gold (III) catalysts.

Another of the few examples of asymmetric gold (III) catalysis was published as recently as 2009.[6] In an effort to develop methods for gold-catalyzed hydroxy- and alkoxycyclization of 1,6-enynes, Genêt and Michelet observed that phosphine ligands, while excellent for Au(I) catalysis, are problematic with Au(III) as their phosphine ligands are chlorinated then oxidized to phosphine-oxide while Au(III) is reduced to Au(I) (**Scheme 4.**2)[6]

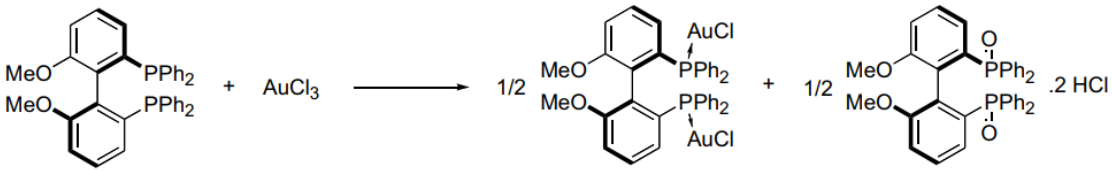

Scheme 4.2. Phosphine-based ligands on gold (III) results in reduction to gold (I) and oxidation of phosphine to phosphine oxides

This observed disproportionation is very significant, as phosphine ligands are some of the most ubiquitous in all of metal-based catalysis. The fact that phosphine ligands on a gold (III) center are unviable illustrates both the fascinating reactivity as well as the inherent challenge gold (III) chemistry poses.

Perhaps the reason that there are so few reports of asymmetric gold (III) catalysis is that the parameters that dictate the reactivity of achiral gold (III) complexes are also not understood. It has been shown by many groups that gold (III) is excellent at forming a wide range of heterocycles,[7] and key reports from 2008 demonstrate that the ligands and counter anions can actually supersede the importance of oxidation state of the metal center in determining reaction pathway (**Figure 4.1**)

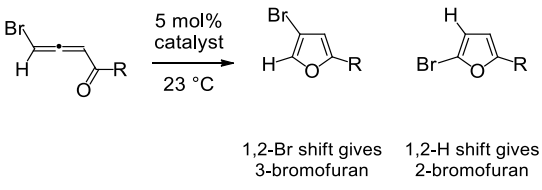

entry	catalyst	R	solvent	ratio **3 : 4**
1	$Au(PPh_3)BF_4$	CH_3	toluene	>98 : 2
2	$Au(PPh_3)SbF_6$	CH_3	toluene	100 : 0
3	$Au(PPh_3)OTf$	CH_3	toluene	0 : 100
4	AuCl	CH_3	toluene	80 : 20
5	$Au(PPh_3)Cl$	C_8H_{17}	toluene	16 : 84
6	$AuCl_3$	C_8H_{17}	toluene	95 : 5
7	$AuCl_3$	C_8H_{17}	THF	5 : 95

Figure 4.1 Ligand, counterion, and solvent change product distribution with either Au(I) or Au(III)

The importance that both ligand and oxidation state can play on a reaction is not specific to gold catalysis, however it is surprising, then, that there has been little work in developing gold (III) complexes with different types of ligands in a more systematic manner.

In 2008, the first bisoxazoline-Au(III) complex, [(*R*,*R*)-Bnbox $AuCl_2$]SbF_6, was formed from potassium tetrachloroaurate ($KAuCl_4$) and silver hexafluoroantimonate ($AgSbF_6$). $AgSbF_6$, like the previously discussed silver tetrafluoroborate ($AgBF_4$), is used to abstract halogens via salt metathesis. Upon precipitating silver chloride, it leaves in solution the non-coordinating hexafloroantimonate (SbF_6^-)counter anion. In terms of Hard Soft Acid Base, hexafluoroantimonate is a significantly softer counter anion than tetrafluoroboate, which is why it pairs so well with gold cationic complexes which are also quite soft. **Figure 4.2** shows the x-ray crystal structure of this complex, which exhibits the expected square-planar geometry. This cationic complex was further characterized by ^1H and ^{13}C NMR in deuterated methylene chloride.[9]

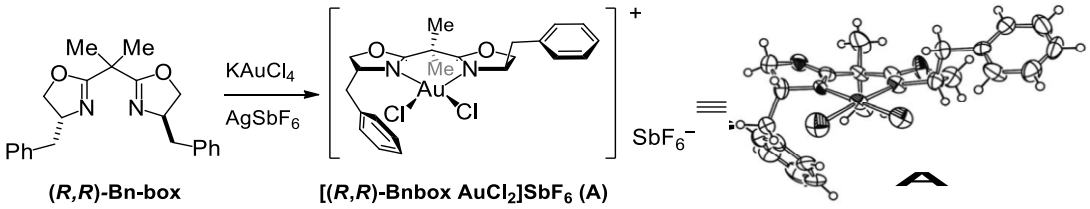

Figure 4.2 Synthesis of one of the two first Au(III) complexes of any chiral bisoxazoline ligand

It is important to note that the fact that this bisoxazoline-Au(III) complex is soluble in solvents that should not displace labile ligands (in this case, displacing one of the chloride ligands) bodes well for the development of enantioselective Au(III) catalysis. Methylene chloride, unlike other common organic solvents like DMSO and acetonitrile, has no ability to coordinate to the metal center and thus has no potential for ligand displacement/exchange.

In terms of comparing analogous gold (I) and gold (III) complexes, not salts, there is very little precedent. In 2008, the Akita group observed the effectiveness of different gold species on cycloisomerization of an allenyl-alkynyl acetate (**Figure 4.3**).

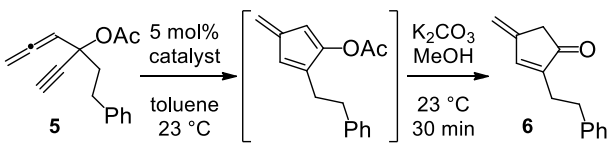

entry	catalyst	time	yield (%)
1	AuCl	48 h	36
2	$AuCl_3$	1 h	49
3	$KAuCl_4$	1 h	52
4	[(*R*,*R*)-Bn-box $AuCl_2$]SbF_6	10 min	60

Figure 4.3 Superior activity of Au(III) over Au(I) increased further with nitrogen-based ligands

Comparing gold (I) chloride (AuCl), gold (III) chloride ($AuCl_3$), the gold (III) salt potassium tetrachloroaurate ($KAuCl_4$), and a synthesized bisoxazoline gold (III) complex, it was found that the chiral Au(III) complex used provides superior catalysis compared to other gold sources. Between the gold (I) gold (III) chlorides, it was apparent that gold (III) outperformed gold (I) both in terms of conversion to product and reaction time. $AuCl_3$ and $KAuCl_4$ provide 49% or 52%

yield, respectively, of the enone product in 1 hour as opposed to the 48-hour reaction time required to obtain 36% yield with gold (I) chloride (AuCl).[9] The salt $KAuCl_4$ outperformed the gold trichloride slightly, however it is clear that the gold (III) complex employing the bisoxazoline ligand was the superior catalyst, giving comparable yield in 10-min versus a 60-min reaction time. This example highlights the reactivity that ligand-supported gold (III) can provide, and also demonstrates how little is known about gold catalysis in general.

4.2 Ligand Exchange Experiments with Metal Complexes

As discussed in the introduction of this chapter, metal catalysts can function in many ways when they catalyze reactions: they can be Lewis acids which activate specific parts of a molecule without forming permanent bonds; they can form metallocycles with the substrates and facilitate the key bond formations with stereospecificity; and they can utilize their multiple coordination sites and oxidation states to break, transfer, and make new bonds with high catalytic turnover. When exploring a new type of catalyst, in this case gold (III) based complexes, their solution-phase behavior needs to be investigated to determine how they will interact with other molecules. Often, this is done through ligand-exchange experiments, where a metal complex dissolved in a solvent has different types of new ligands introduced and observed if and how they displace the original ligands.

An example of this process is when, in 1989, the van Koten group synthesized a pair of palladium complexes (**Scheme 4.3**).

Scheme 4.3 Ligand exchange precedent with palladium square planar complexes

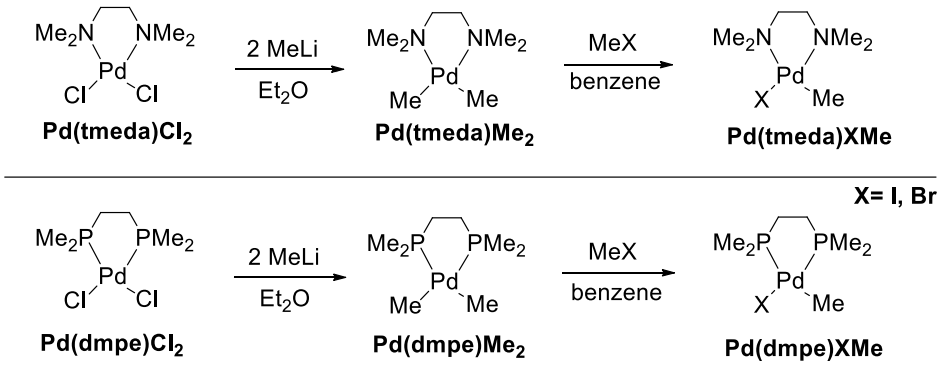

These complexes were four-coordinate, palladium (II) complexes with two methyl ligands and one of two bidentate ligands which they synthesized prior to complexation. The bidentate ligands, either *N,N,N´,N´*-tetramethylethanediamine (tmeda) or 1,2-bis(dimethylphosphino)ethane (dmpe), both interact with the electrophilic palladium center in similar ways. Due to either the phosphorus or nitrogen heteroatom present in the dmpe or tmeda, respectively, the lone pair of electrons is attracted electrostatically to the electropositive metal. This interaction results in two-electron coordination which, due to the neutral state of the heteroatom, does not affect the oxidation state of the metal; these types of ligands are referred to as L-type, and they form dative covalent bonds. On the other hand, the methyl ligands on these palladium complexes function differently than the dmpe or tmeda ligand. They are installed on the palladium center though the addition of methyllithium to a precomplex of either Pd(tmeda)Cl_2 or Pd(dmpe)Cl_2, yielding Pd(tmeda)Me_2 or Pd(dmpe)Me_2. The alkyl group is added via a charged carbon reagent (the salt, Li^+ Me^-) and uses its one labile electron to

form a bond to the metal with the palladium donating the other. This results in a net change of +1 to the oxidation state of the metal, and these ligands are referred to as X-type.

This distinction is important to make, as in ligand exchange experiments there is ideally no change in the oxidation state of the metal and whatever type of ligand is introduced (X vs L) should only displace a ligand of the same type. In the example of the palladium complexes from the van Koten group, the ligand exchange experiments involved taking the dimethyl palladium complex and, in a solution of benzene, adding a methylhalide. This would introduce a new X^- to the solution to compete with one of the Me^- ligands on the palladium and, should it be a favorable process, it would displace the methyl group and form a new Pd(L)MeX complex. To reiterate, this results in no net change of the overall charge of the complex, it just swaps out one of the ligands. They were able to determine though low temperature NMR studies that this exchange goes through an octahedral, six-coordinate intermediate which, upon the release of ethane, reforms the isolated four-coordinate square planar palladium (II) complex.

These experiments gave insight into the nature of these novel palladium complexes: it was determined that a palladium halide complex could be converted through conventional means to a more active dimethyl palladium complex; the methyl ligands could be displaced with the introduction of other X^-, in this case Br^- or I^-, species, indicating that the palladium halide complex is more stable; and through NMR experiments, it was determined that the ligand

exchange is not a concerted substitution but rather goes through a change in geometry to an octahedral Pd (IV) intermediate, which alludes that an oxidative addition on this complex would go through a similar path. With the same impetus, a ligand-exchange experiment using the novel PyQuin gold (III) chloride complexes was undertaken.

4.3 Ligand Exchange Experiments with PyQuin Gold (III) Complexes – UV-Vis

There is a long history of using metals or metal-containing complexes for therapeutic purposes, however it is still significantly less explored that purely organic treatments.[13] The reason for this is likely the fact that uptake of a metal species would counteract the potential activity of the ligand attached to it, however there is also evidence to the contrary that the metal itself is what provides anticancer activity.[14] Cisplatin is a potent chemotherapy treatment due to its strong affinity of DNA binding which occurs through the displacement of its chlorine ligands and binding to guanine residues (**Figure 4.4**).[15]

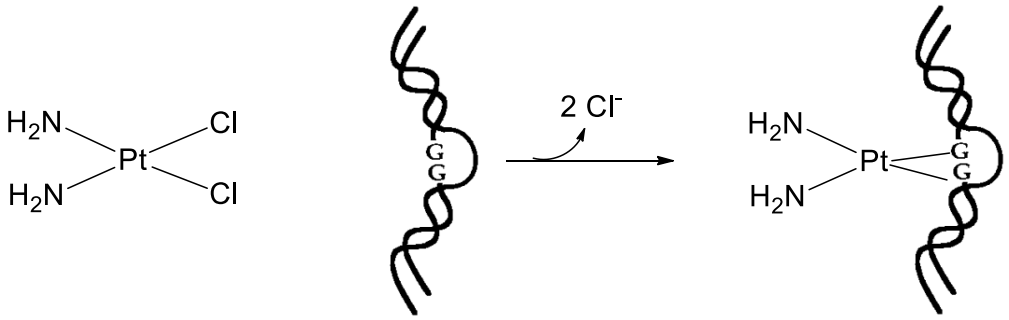

Figure 4.4 Cisplatin's general mode of action

This displacement, or “ligand exchange,” is a key factor in many metal-based therapies, and it mimics the oxidative-addition/reductive-elimination process when complexes are used in catalytic applications. The feature that a complex must possess, whether for therapeutic uses or catalysis, is that its ligands/coordination sites must have some amount of fluidity. If the complex has four fully occupied coordination sites and the ligands are unable to be displaced, the complex will almost certainly be inert. For this reason, ligand exchange experiments are vital to determine if and how a newly synthesized complex will function. Just as important as the experiment itself is the ability to determine if ligand exchange has occurred on a metal center.

There are many different methods of characterization that are used to determine if ligand exchange has occurred on a substrate. It is not an uncommon practice to synthesize a cationic complex, which will fundamentally require a non-coordinating anionic species, and desire to change the anion. This can be done for a multitude of reasons (solubility, stability in air/solution, etc), and the practice is as easy as dissolving the complex in an organic solvent and introducing the desired anion in a high concentration. This way, the most abundant anion has the ability to beat out a potentially more preferable anion (common anions to do this with are BF_4, PF_6, SbF_6, and halides). To determine if anion exchange was successful, however, a crystal structure is generally required, as the overall electronic effect of one anion to another is difficult to see by common spectroscopic methods. Fortunately, performing ligand exchange with metal-

coordinating ligands, such as the chlorides and PyQuin ligand on the gold (III) center in our PyQuin($AuCl_3$) complexes, is significantly easier to determine. Changes to ligands directly bound to the metal center affect the electronic environment of the complex as a whole, and for this reason, UV-Vis spectroscopy can be used to visualize this change.

UV-Vis spectroscopy is a common method to determine the presence and effect of ligand exchange in metal complexes, especially those with heteroaromatic ligands.[16] This is desirable, as the ligand itself will have a very characteristic UV-Vis spectrum which can then be compared to the complex with which it is bound as well as the complex post-ligand exchange. For the PyQuin($AuCl_3$) complexes that were to be investigated, the first hurdle was to find a solvent system that would keep the complex dissolved in solution and not precipitate out. Initially, acetonitrile was used as that was the solvent used in the synthesis of the complex and appeared to have no trouble keeping the complex solubilized. However, when the solutions of MeO-PyQuin($AuCl_3$) in MeCN were observed by UV-Vis, the data was incredibly inconsistent. This could have been due to a variety of issues: first, acetonitrile is known to be a moderately strong ligand (similar to ^{-}OH in the spectrochemical series), so there could be an on-off solvent binding; additionally, gold (III) is known to form gold hydroxide species in the presence of water, so any trace water would result in the rendering of insoluble gold hydroxides. After many attempts of at least getting consistent initial

spectra, it was decided that perhaps a different solvent mixture would give better data.

For this reason, initial solutions of MeCN were diluted with dimethyl sulfoxide (DMSO) until they reached a concentration of 0.03 mM, which was found to be appropriate with the UV-Vis absorption window (these solutions did not lose color or result in any precipitation). Initially, absorption maxima at 340-360 nm seemed indicative of ligand-to-metal charge transfer (LMCT) for the gold complexes, but the spectral data proved inconsistent. UV-vis experiments in anhydrous acetonitrile showed almost no visible LMCT band—suggesting that the old batches of acetonitrile likely contained water. When the same experiments are carried out solely in anhydrous dimethylsulfoxide (DMSO), the LMCT band is weaker but could at least consistently be observed.

As their LMCT absorbances are most distinctive, the UV-vis spectra of the MeO-PyQuin ligand (1a) and its $AuCl_3$ complex (2a) are compared in **Figure 4.5** with alternating solvent systems. The results in 100% dry DMSO contrast with the original protocol in which the final ratio of MeCN to DMSO is 200:1 (labeled DMSO + MeCN in **Figure 2** to indicate the manner in which the samples are prepared but referred to as MeCN below). **Spectrum A** is comparing the absorption spectra of 1a in DMSO (black) and 2a in DMSO (orange) shows the LCMT band of MeO-PyQuin gold complex 2a (orange) between 375 and 400 nm**.** **Spectrum B** shows the absorption spectra of 2a in DMSO (orange) versus 2a in MeCN (purple), and the key LMCT band does not appear to exist in MeCN

(purple). The spectra of ligand 1a in MeCN (blue) and complex 2a in MeCN (purple) lead to the same conclusion (**Spectrum C**). **Spectrum D** indicates that the absorption spectra of ligand 1a is slightly red-shifted moving from MeCN (blue) to DMSO (black).

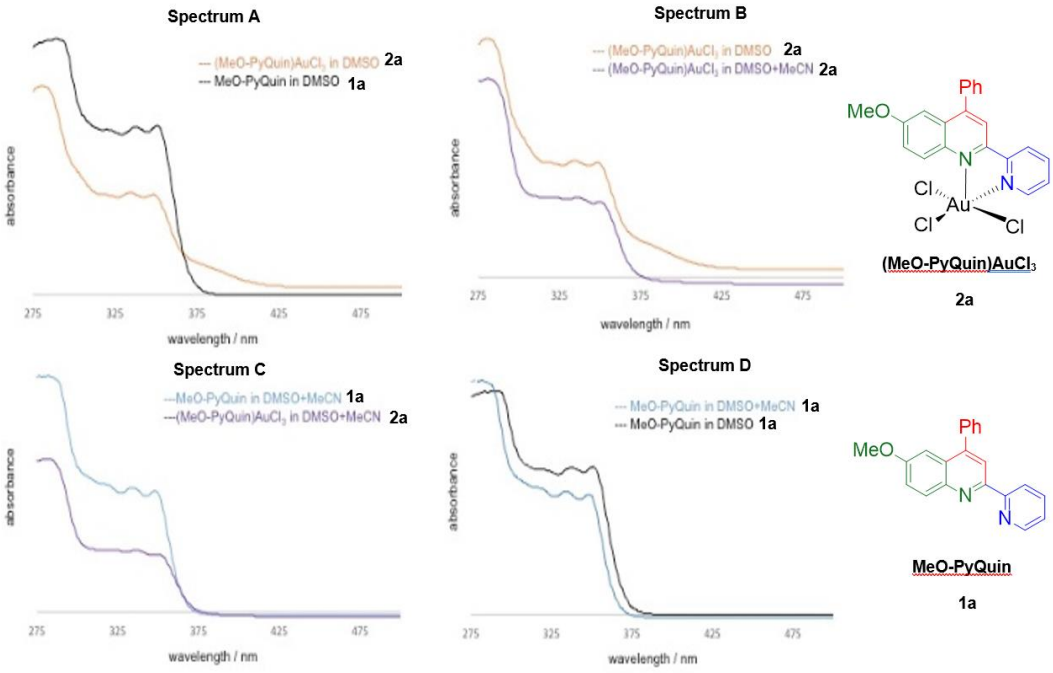

Figure 4.5 UV-Vis Spectra for MeO-PyQuin($AuCl_3$) and MeO-PyQuin in both neat DMSO and DMSO/Acetonitrile show small differences

Due to the unexpectedly small change between ligand and complex, it was proposed that upon dissolution the gold (III) center was slowly dissociating from its ligands and forming colloidal gold species. These gold nanoparticles (AuNPs) are known to form in reducing environments and while it was unlikely, it was necessary to rule out. To detect any unexpected gold nanoparticle

formation, these UV-vis spectra are acquired in windows from 240 nm to 700 nm. As no absorbances are recorded above 450 nm, the formation of gold nanoparticles, generally detected by peaks around 500 nm, are not indicated.[17] A big difference that was noticed between the MeCN/DMSO solutions and pure DMSO solutions was their clarities. The UV samples in dry MeCN slowly turned opaque as they sat, while the DMSO solutions stayed crystal clear. It was determined that a consistently clear solution cannot be achieved in MeCN, but warming the complex in DMSO does solvate gold complex 2a. Additionally, it was found that the complex was fully soluble in chloroform ($CHCl_3$). Unfortunately, when UV-Vis was taken of the PyQuin($AuCl_3$) complex in $CHCl_3$, no LMCT band was observed. It was eventually decided that using UV-Vis spectroscopy was, for this system, going to be too inconsistent and unpredictable, however, one method of characterization had proven very successful for the PyQuins and their corresponding gold (III) complexes: ^{1}H NMR.

4.4 Observing Solution-phase Behavior of PyQuin Gold (III) Complexes by ^{1}H NMR

Proton NMR was instrumental in determining much about the gold (III) PyQuin complexes: significant shifting downfield indicated binding of the ligand to the metal center; the downfield shift of resonances corresponding to the protons on the pyridine ring indicated that it flips upon binding and, when not bound, it points away from the quinoline ring; and the chlorine ligand significantly

deshields the proton at the 8-position on the quinoline ring, which reinforces the reasoning behind the complex's pseudo square-based pyramidal, five-coordinate geometry. Additionally, it was observed that substituent changes to the ligand backbone impacts the ^{1}H NMR of the complex greatly, so changes of the ligands on the metal center could have the same effect. Before immediately jumping into ligand exchange with ^{1}H NMR, however, all the possible gold and ligand species needed to first be characterized. Each of the ligands had been isolated and fully characterized, however when the complexes were proposed it was questioned if the complex was truly discrete, if it was a salt pair, or if it was just protonated ligand. It was observed that prior to adding $AgBF_4$, the ligand and gold *do* have an association with each other and the ligand exhibits a slightly shifted ^{1}H NMR spectrum, though not very significant. This loose "pre-complex" is easily distinguished from complex, as it looks much more like ligand than it does complex (**Figure 4.6**).

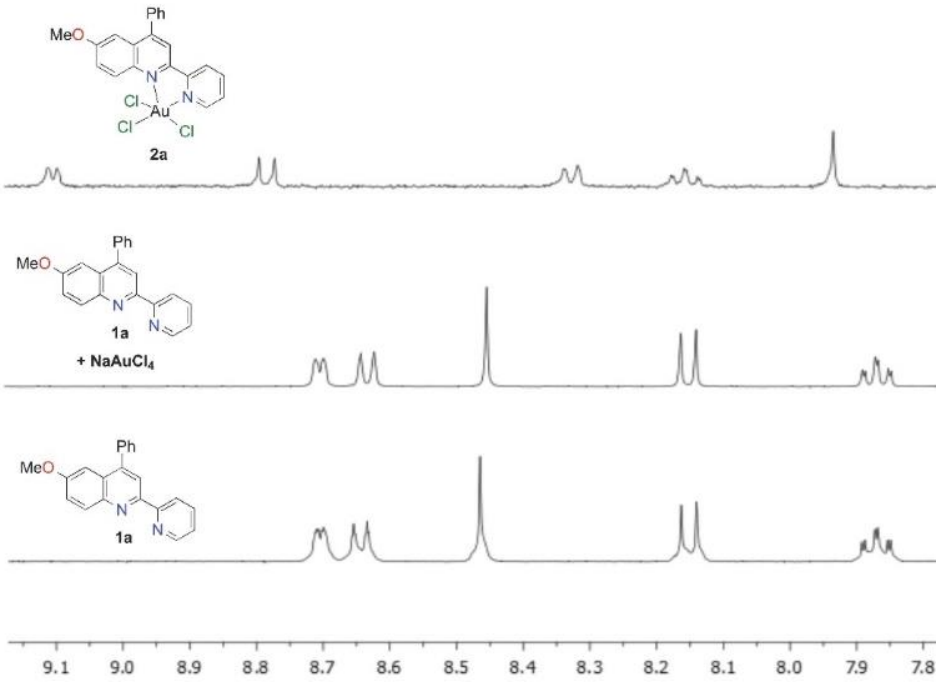

Figure 4.6 ^{1}H NMR comparison of MeO-PyQuin($AuCl_3$) complex, solution of MeO-PyQuin ligand and gold salt, and pure MeO-PyQuin ligand

Protonated ligand, on the other hand, has very similar chemical shifts to the discrete PyQuin($AuCl_3$) complex. As shown in **Figure 4.7**, if one were to be simply looking for downfield shifting of resonances, it would be easy to mistake protonated MeO-PyQuin^{+} for MeO-PyQuin($AuCl_3$) when comparing to MeO-PyQuin.

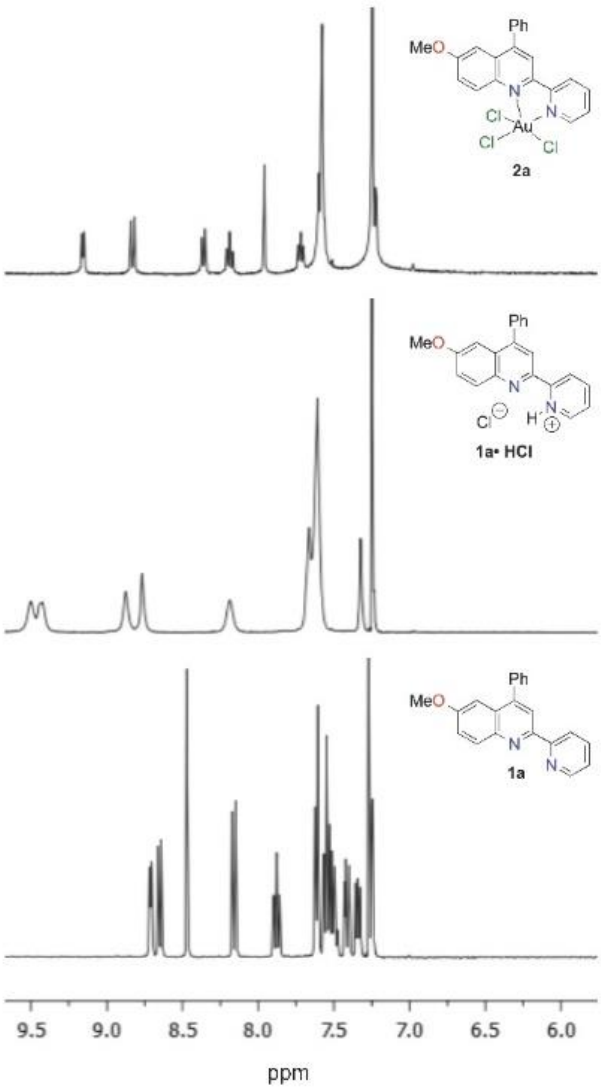

Figure 4.7 ^{1}H NMR comparison of MeO-PyQuin($AuCl_3$) complex, protonated MeO-PyQuin ligand, and pure MeO-PyQuin ligand

The “pyridine flip” occurs as expected with complexation, however this is due to the hydrogen bonding between the quinoline and protonated pyridine. This is an important feature, as other ligands (which will be discussed in later chapters) with N-H’s are seen to adopt the same resting geometry. Regardless, the difference between complex and protonated ligand is clearly seen when

compared, as the chemical shifts differ and the resolution of the peaks in the neutral gold (III) complex is much higher than that of protonated PyQuin. With the complexes and other gold and ligand species fully characterized, a ligand-exchange experiment monitored by ^{1}H NMR was begun.

4.5 Ligand Exchange Experiments with PyQuin Gold (III) Complexes using ^{1}H NMR

With the plan to use ^{1}H NMR as a detection method for ligand exchange on PyQuin gold (III) complexes set, the nucleophiles with which to do ligand exchange needed to be chosen. It was postulated that the chlorine ligands on the gold center would be the most labile and susceptible to displacement, so another x-type ligand needed to be introduced. Initially one might think a halide exchange (e.g. bromine displacing chlorine) would be the most logical choice, however this lead to difficult characterization. During the UV-Vis experiments, a Me-PyQuin($AuBr_3$) complex was synthesized from Me-PyQuin, $NaAuBr_4$, and $AgBF_4$ in order to see if the gold (III) bromide complexes would be easier to solubilize or give more consistent data. It was observed that they behaved very similarly to the chloro-complexes but by ^{1}H NMR had very different chemical shifts (**Figure 4.8**).

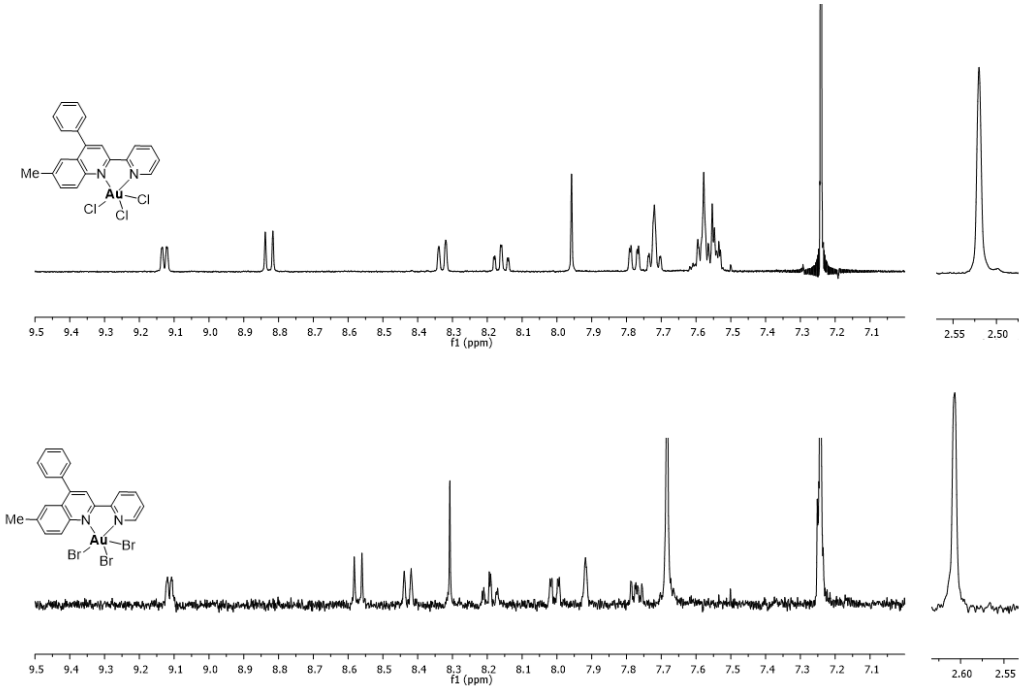

Figure 4.8 ^{1}H NMR comparison of Me-PyQuin($AuCl_3$) and Me-PyQuin($AuBr_3$)

As suggested by the ^{1}H NMR of the Me-PyQuin($AuBr_3$) complex, the major issue with the bromo-complexes are their lack of solubility in common organic solvents and primarily in $CDCl_3$. It was decided that using organic molecules as nucleophiles like amines and alcohols would not only give insight into how the complex would act as a catalyst, but the NMR of the nucleophile itself could be observed for change as well as the complex. With this in mind, a series amine and alcoholic nucleophiles were selected, including 1°, 2°, and 3°, cyclic, acyclic, and aryl variants and are shown in **Figure 4.8**. Using the difference in chemical shift between the initial PyQuin($AuCl_3$) complex and the complex formed post-exchange, PyQuin($AuCl_2X$) where X is the nucleophile

introduced, a Stern-Volmer plot would be constructed using this data which would give the binding constant K_b as the slope of the linear regression.

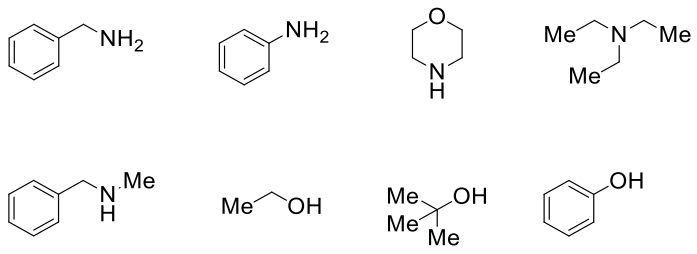

Figure 4.8 Nucleophile series for PyQuin($AuCl_3$) ligand exchange

The combination of PyQuin gold complex and nucleophile had to be chosen with care, as the goal was to have spectra that could clearly indicate if binding occurred. F-PyQuin($AuCl_3$) was the last of the PyQuin gold (III) complexes to be synthesized (as it required recrystallization in toluene rather than acetonitrile) and would offer a great handle by ^{19}F NMR, so this complex was picked for the first round of ligand exchange. The first nucleophile selected was benzylamine for a number of reasons: first, the fact that it is a primary amine suggested it would be more powerful nucleophile than something like aniline without having any steric hinderance around the heteroatom; secondly, the methylene resonance would be very diagnostic by ^1H NMR, as there is nothing else in the sp^3 region other than the substituent on the PyQuin, which would be identifiable based on integration and previous spectra; finally, benzylamine has two labile protons, so if an ammonium intermediate forms after binding, HCl

could leave as a byproduct and the amine would still have one N-H leaving it as X-type. The process of the first experiment was to dissolve F-PyQuin($AuCl_3$) in $CDCl_3$ at a specific concentration (in this case, 10 mM) and a stock solution of benzylamine in $CDCl_3$ was made so it could be added incrementally. An initial ^1H NMR of the yellow solution of F-PyQuin($AuCl_3$) in $CDCl_3$ was taken to ensure purity and to have as a starting point. To this solution, 1 mol % (0.1 mM) of benzylamine was added just to see if it could be detected by the NMR. Surprisingly over the span of 1 minute, the solution went from clear yellow to opaque yellow to clear and colorless. An NMR spectrum was obtained and a dramatic change was seen (**Figure 4.9**). This was shocking, as a 1:99% solution of benzylamine:complex would mean that only 1 out of 100 molecules of F-PyQuin($AuCl_3$) could have had ligand exchange occur, but clearly that was not the case (**X2)**. As more benzylamine was added, the spectrum only changed in terms of benzylamine concentration; the dramatic shift occurred only upon introduction of benzylamine and regardless of how much excess nucleophile was added, those peaks were constant (**X2-X4)**.

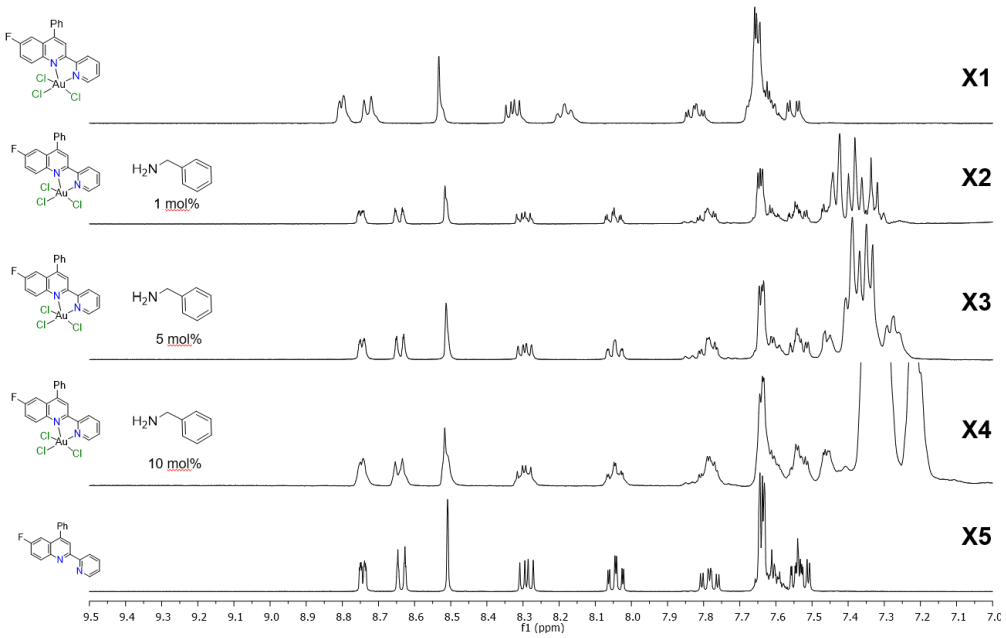

Figure 4.9 ^{1}H NMR spectra used to illustrate dissociation of F-PyQuin from the gold complex F-PyQuin($AuCl_3$) upon addition of benzylamine

The NMR spectra were stacked and, when compared with the unbound ligand (**X5**), the result was clear: even just the introduction of 1 mol % benzylamine caused the PyQuin ligand to dissociate from the gold center, resulting in a spectrum of what appeared to be free ligand and benzylamine (**X4**). This experiment was replicated for other complexes (MeO, Ph, CF_3) and other amine nucleophiles (aniline, triethylamine, pyridine) and the result was the same each time: when in solution, the introduction of any amine nucleophile results in the dissociation of PyQuin ligand and gold (III) center, which by ^{1}H NMR appears as free ligand + nucleophile. Interestingly, all alcoholic nucleophiles tested were completely unreactive towards the PyQuin($AuCl_3$) complex.

While it seemed as though there was little success in performing ligand exchange on the PyQuin gold (III) complexes, there was still a question that needed to be answered: what was happening to the gold? When running UV-Vis experiments with the complexes, there was no indication of gold nanoparticles, however by NMR it is clear that the complex disassembles to its pieces. If the gold center was loosely coordinated to the ligand, it would be distinguishable by ^{1}H NMR as that pre-complex had been isolated and characterized previously. If the amine nucleophile was binding, generating HCl and protonating the ligand which results in dissociation, that also would be detectable by NMR. It was postulated that perhaps that colloidal gold *was* forming, but in such small aggregates that it was not detectable by UV-Vis. As there is a scarcity of research being done on gold (III) complexes themselves, it is not surprising that it is difficult to find precedent for gold nanoparticle formation from gold complexes as opposed to salts/Au(0); there is, however, some precedent when it comes to amines as stabilizing agents for the synthesis of gold nanoparticles.[18] It is described that amines act both as reducing agents as well as stabilizers after AuNP formation, and that the aggregation can be accelerated with heating.[19]

With this in mind, a solution of Me-PyQuin($AuCl_3$) in $CDCl_3$ was made and to it, benzylamine was added (**Figure 4.10**).

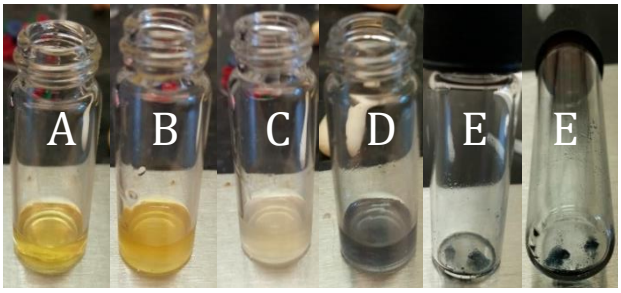

Figure 4.10 Qualitative observations show clear yellow solution of complex converting to clear solution of unbound ligand; heating results in AuNPs

As was the case with the other complexes, the solution went from vibrant yellow (**A**) to opaque yellow (**B**) to clear and colorless (**C**). Heating this solution, however, resulted in the solution changing from clear to blueish-purple (**D**) with small amounts of solid forming at the bottom of the vial. These solids (**E**) were isolated, washed, and characterized by ^{1}H NMR and UV-Vis. By ^{1}H NMR, the solids were virtually NMR silent (small amounts of Me-PyQuin impurity were seen with the intensity raised 10x) (**Figure 4.12**).

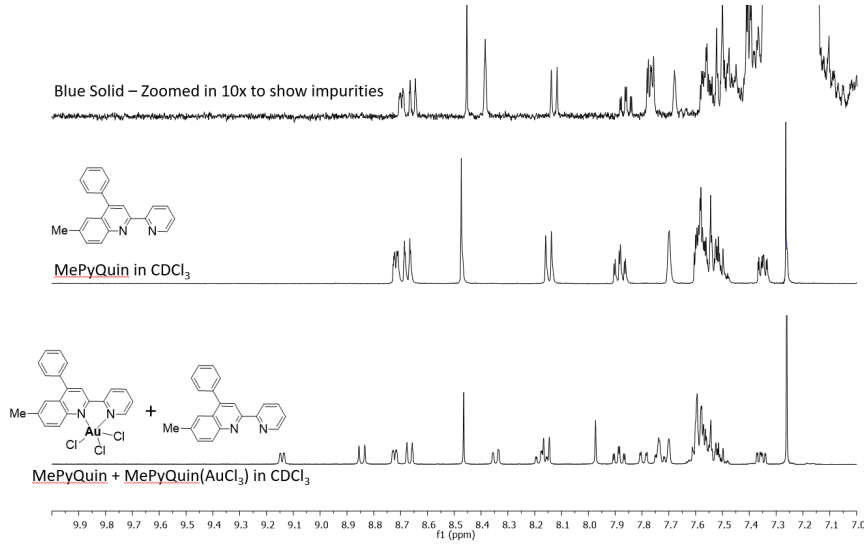

Figure 4.11 ^{1}H NMR shows gold nanoparticles formed from heating solution are virtually NMR silent with small amounts of ligand impurity

By UV-Vis, however, the solids in solution displayed a large absorbance from 500-800 nm, which is characteristic of the presence of gold nanoparticles (**Figure 4.13**).

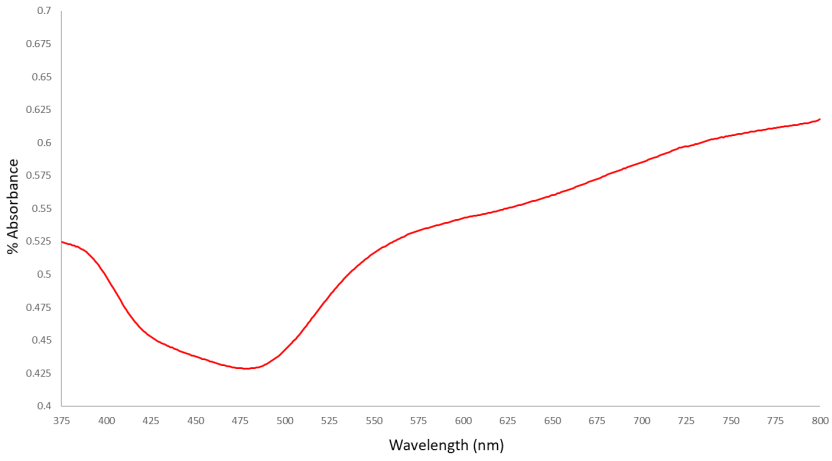

Figure 4.12 UV-Vis of sample in **Figure 4.12** shows large absorbance >500nm, indicating colloidal gold species indeed formed

This was key in supporting the idea that the amine nucleophiles do not participate in ligand exchange with the PyQuin($AuCl_3$) complexes; rather, they assist in the reduction of the gold (III) metal center to gold (0) and facilitate the formation of gold nanoparticles. Amine-assisted gold nanoparticle formation is catalytic, not stoichiometric, which is why such small amounts of benzylamine can fully disassemble the PyQuin gold (III) complex.

Based on the multiple attempts to observe ligand-exchange on the neutral PyQuin($AuCl_3$) complexes, it was determined that while it was a great foray into gold (III) complexes, it is not going to be the most representative substrate for potential catalysis. The five-coordinate, pseudo square-based pyramidal geometry is uncharacteristic of other gold (III) complexes. With other bidentate 2,2´-bipyridine type ligands and two halides, the corresponding gold (III) complex should be a stable, cationic, square-planar complex. Since the Larsen group is significantly more interested in the development of potential catalysts rather than exploring the geometric anomaly of hindered pyridylqunioline-type ligands, an effort was made to utilize other bidentate, heteroaromatic ligands which could be bound to metals in a more traditional way. Fortunately, the development of another similar ligand set was already underway.

4.6 References

1) a) Lipshutz, B. H.; Yamamoto, Y. *Chem. Rev*. **2008**, *108*, 2793. b) Arcadi, A. *Chem. Rev.* **2008**, *108*, 3266. c) Patil, N. T.; Yamamoto, Y. *Chem. Rev.* **2008**, *108*, 3395. d) Li, Z.; Brouwer, C.; He, C. *Chem. Rev.* **2008**, *108*, 3239. e) Gorin, D. J.; Sherry, B. D.; Toste, F. D. *Chem. Rev.* **2008**, *108*, 3351.

2) a) Abu Sohel, S. M.; Liu, R.-S. *Chem. Soc. Rev*. 2009, **38**, 2269. b) Fürstner, A. *Chem. Soc. Rev*. **2009**, *38*, 3208. c) Hashmi, A. S. K.; Rudolph, M. *Chem. Soc. Rev.* **2008**, *37*, 1766. d) Hashmi, A. S. K. *Chem. Rev.* **2007**, *107*, 3180. e) Fürstner, A.; Davies, P. W *Angew. Chem. Int. Ed*. **2007**, *46*, 3410. f) Hashmi, A. S. K.; Hutchings, G. J. *Angew. Chem. Int. Ed.* **2006**, *45*, 7896. g) Höffmann-Röder, A.; Krause, N. *Org. Biomol. Chem.* **2005**, *23*, 387.

3) Ito, Y.; Sawamura, M.; Hayashi, T. *J. Am. Chem. Soc*. **1986**, *108*, 6405.

4) Pradal, A.; Toullec, P. Y.; Michelet, V. *Synthesis* **2011**, *10*, 1501.

5) Debono, N.; Iglesias, M.; Sanchez, F. *Adv. Synth. Catal.* **2007**, *16*, 2470.

6) Toullec, Y.; Genêt, J.; Michelet, V. *J. Organomet. Chem.* **2009**, *694*, 538.

7) a) Das, A.; Abu Sohel, S. M.; Liu, R.-S. *Org. Biomol. Chem*. **2010**, *8*, 960. b) Shen, H. C. *Tetrahedron* **2008**, *64*, 3885. c) Morita, N.; Krause, N. *Angew. Chem. Int. Ed.* **2006**, *45*, 1897. d) Zhang, L. M. *J. Am. Chem. Soc*. **2005**, *127*, 16804. e) Suhre, M. H.; Reif, M.; Kirsch, S. F. *Org. Lett*. **2005**, *7*, 3925.

8) a) Dudnik, A. S.; Sromek, A. W.; Rubina, M.; Kim, J. T.; Kel'i, A. V.; Gevorgyan, V. *J. Am. Chem. Soc*. **2008**, *130*, 1440. b) Xia, Y.; Dudnik, A. S.; Gevorgyan,V.; Li, Y. *J. Am. Chem. Soc*. **2008**, *130*, 6940.

9) Kato, K.; Kobayashia, T.; Fujinamia, T.; Motodatea, S.; Kusakabea, T.; Mochidab, T.; Akita, H. *Synlett* **2008**, *7,* 1081.

10) Old, D. W.; Wolfe, J. P.; Buchwald, S. L. *J. Am. Chem. Soc*. **1998**, *120*, 9722.

11) Lam, F. L.; Kwong, F. Y.; Chan, A. S. C. Ma, S., Ed.; *Springer Berlin Heidelberg*: Berlin, Heidelberg, **2011**; pp 29–65.

12) De Graaf, W.; Boersma, J.; Smeets, W. J. J.; Spek, A. L.; Van Koten, G. *Organometallics* **1989**, *8* (12), 2907.

13) Desoize, B. *Anticancer Research*, **2004**.*24* (3),1529.

14) Messori, L.; Merlino, *Dalton Trans.* **2014**, *43*(16) 6128.

15) Jamieson, E. R.; Lippard, S. J. *Chem. Rev.* **1999**, *99* (9), 2467.

16) Hart, K. F.; Joe, N. S.; Miller, R. M.; Nash, H. P.; Blake, D. J.; Morris, A. M. *Bioinorg. Chem. Appl.* **2018**, 1.

17)(a) Newman, J. D. S.; Blanchard, G. J. *Langmuir* **2006**, *22*, 5882. (b) Stanglmair, C.; Scheeler, S. P.; Pacholski, C. *Eur. J. Inorg. Chem*. **2014**, 3633.

18) Bhargava, S. K.; Booth, J. M.; Agrawal, S.; Coloe, P.; Kar, G. *Langmuir* **2005**, *21*, 5949.

19) (a) Aslam, M.; Fu, L.; Su, M.; Vijayamohanan, K.; Dravid, V. P. *J. Mater. Chem*. **2004**, *14*, 1795. (b) Leff, D. V.; Brandt, L.; Heath, J. R. *Langmuir* **1996**, *12*, 4723. (c) Subramaniam, C.; Tom, R. T.; Pradeep, T. *J. Nanopart. Res*. **2005**, *7*, 209.

4.7 Supporting Information

General Procedure for UV-Vis Studies on PyQuin($AuCl_3$) Complexes

Solutions of (MeO-PyQuin)$AuCl_3$ or MeO-PyQuin ligand (0.03 mM) are prepared in anhydrous DMSO. 15 µL of (MeO-PyQuin)$AuCl_3$ or MeO-PyQuin solution is diluted to a final volume of 3 ml with anhydrous DMSO. The solution is shaken and left to equilibrate for 10 minutes prior to acquisition. The same procedure is used for the control experiments involving acetonitrile except that the dilution to a final volume of 3 mL is carried out with anhydrous CH_3CN. A UV-Visible spectrum is acquired from 240-700 nm in case of unexpected gold nanoparticle formation above 450 nm. This was seen upon heating solution and isolating blue solids.

General Procedure for ^{1}H NMR Experiments

A solution of (MeO-PyQuin)$AuCl_3$ (0.03 mM) in deuterated chloroform, dimethylsulfoxide, or acetonitrile is prepared. ^{1}H NMR spectra are displayed in the Supporting Information. To MeO-PyQuin (156 mg, 0.5 mmol) in 0.7 mL $CDCl_3$, HCl (0.06 mL, 0.5 mmol) is added to give the spectrum of MeO-PyQuin•HCl displayed in **Figure 4.7**. For **Figure 4.6**, a solution of (MeO-PyQuin)$AuCl_3$ or MeO-PyQuin (0.03 mM) in $CDCl_3$ is prepared and a ^{1}H NMR spectrum is acquired. For ligand exchange experiments, a solution of (F-PyQuin)$AuCl_3$ (0.03 mM) in dimethylsulfoxide-D_6 is prepared and 10 mol% of a nucleophile (also diluted in DMSO-D_6) is added and NMR is taken

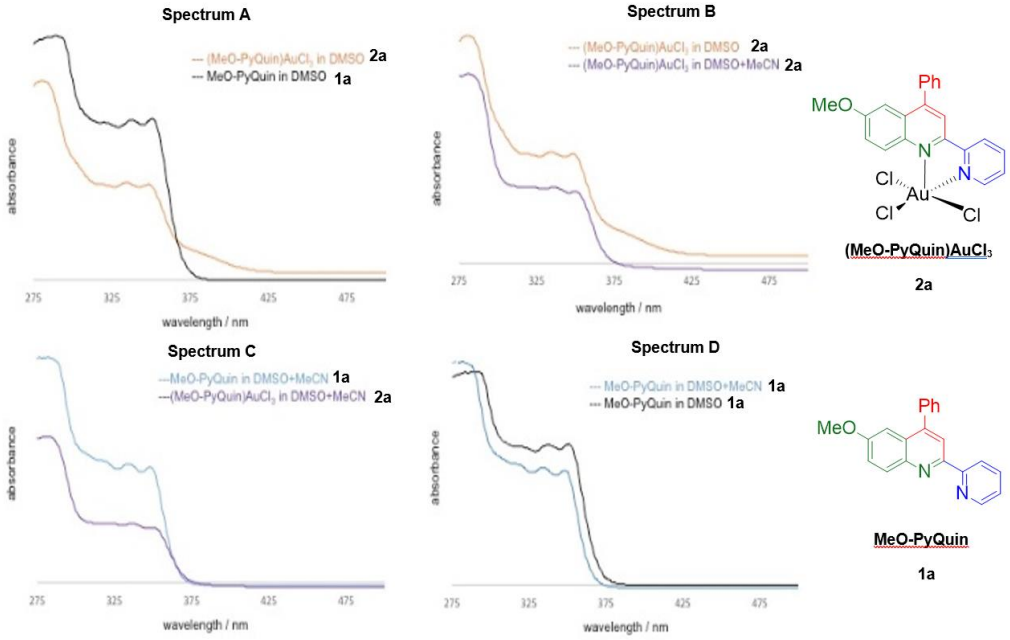

Normalized absorption spectra of MeO-PyQuin (1a, black) in DMSO (0.03 mM) and (MeO-PyQuin)$AuCl_3$ (2a, orange) in DMSO (0.03 mM). (b) Normalized absorption spectra of (MeO-PyQuin)$AuCl_3$ (1b, orange) in DMSO (0.03 mM) and (MeO-PyQuin)$AuCl_3$ (2b, purple) in DMSO/MeCN (0.03 mM). (c) Normalized absorption spectra of MeO-PyQuin (1c, blue) in DMSO/MeCN (0.03 mM) and (MeO-PyQuin)$AuCl_3$ (2c, purple) in DMSO/MeCN (0.03 mM). (d) Normalized absorption spectra of MeO-PyQuin (1d, black) in DMSO (0.03 mM) and MeO-PyQuin (2d, blue) in DMSO/MeCN (0.03 mM).

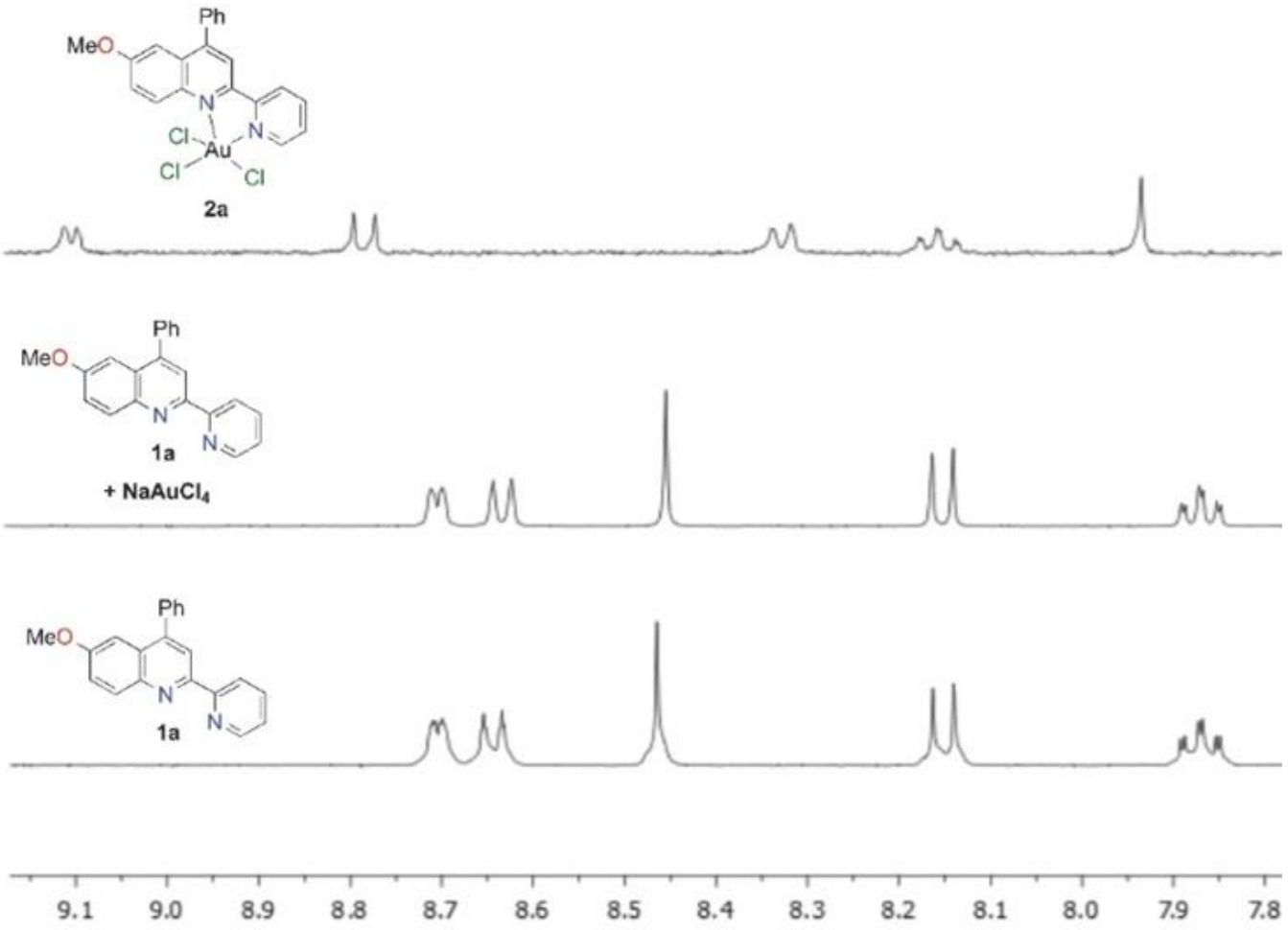

Comparison of MeO-PyQuin($AuCl_3$), MeO-PyQuin and $NaAuCl_4$ solution, and MeO-PyQuin (all taken in DMSO-D_6):

^{1}H NMR comparison of MeO-PyQuin($AuCl_3$), protonated MeO-PyQuin, and MeO-PyQuin in DMSO-D_6

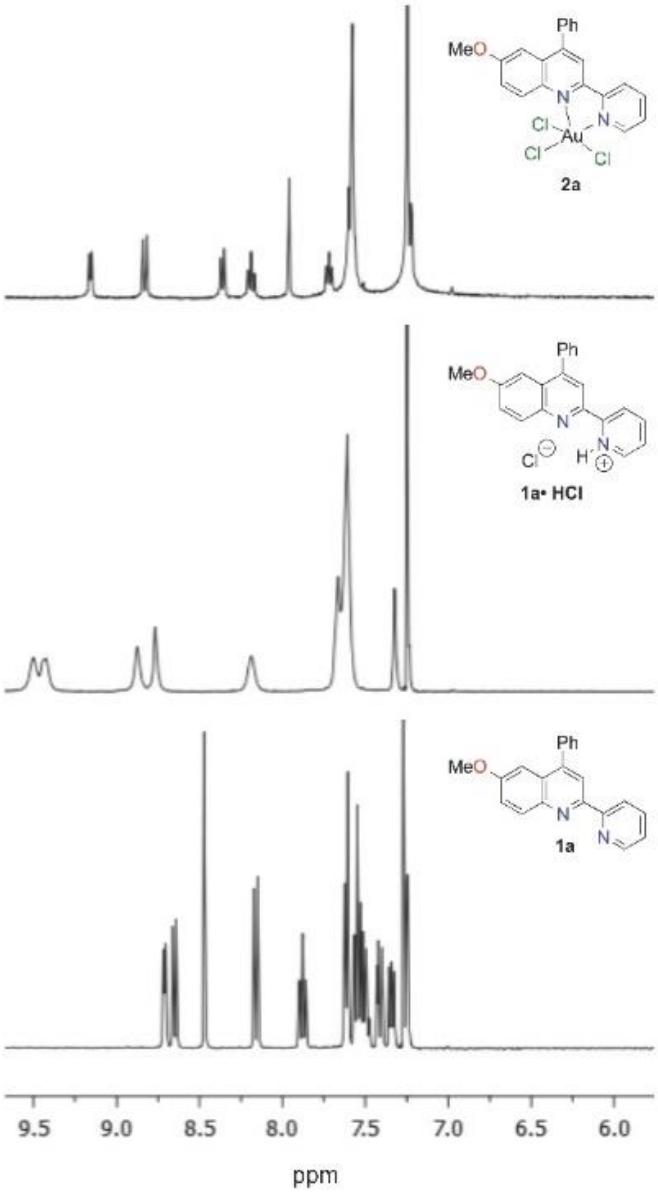

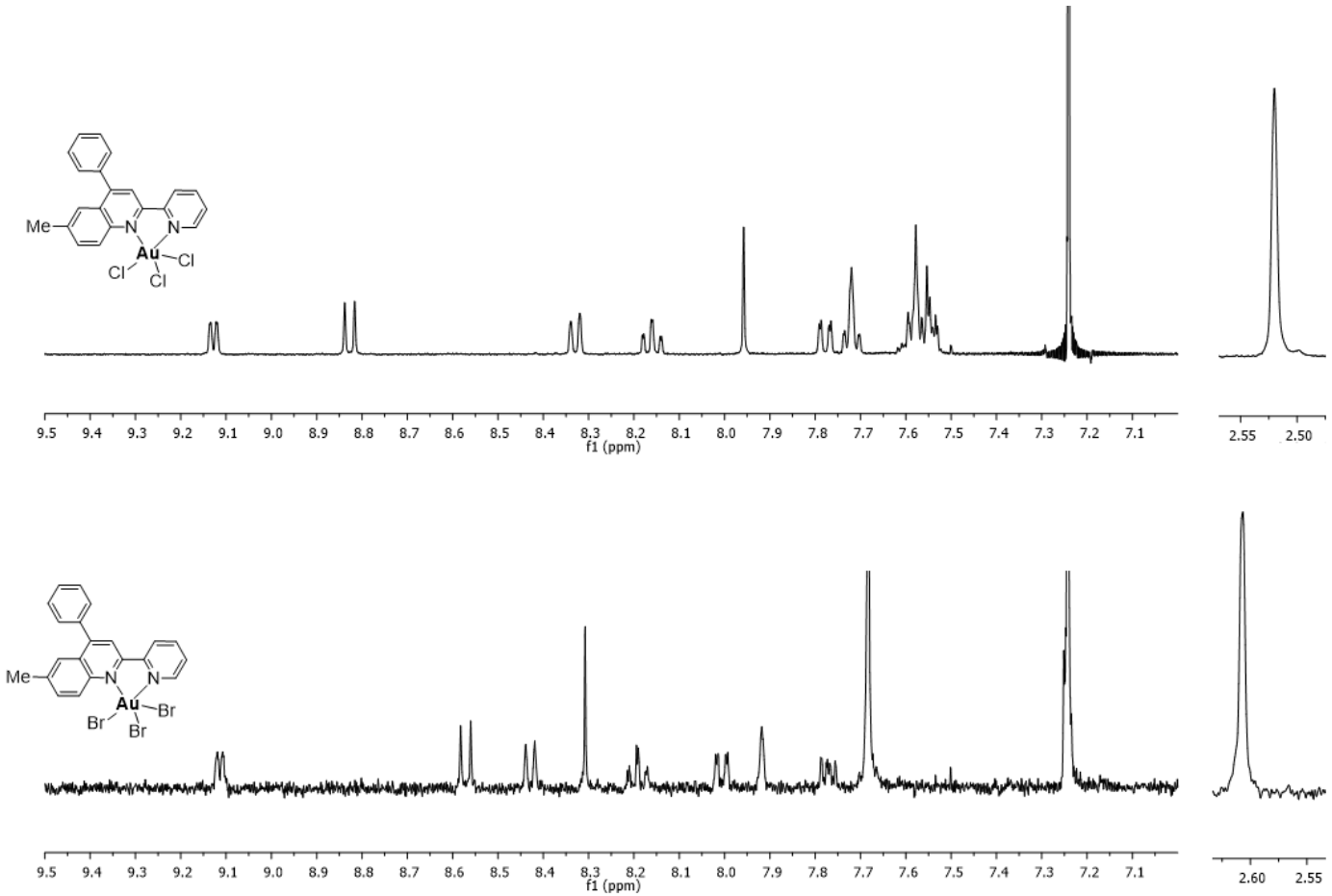

^{1}H NMR Comparison of MeO-PyQuin($AuCl_3$) and MeO-PyQuin($AuBr_3$) taken in DMSO-D_6

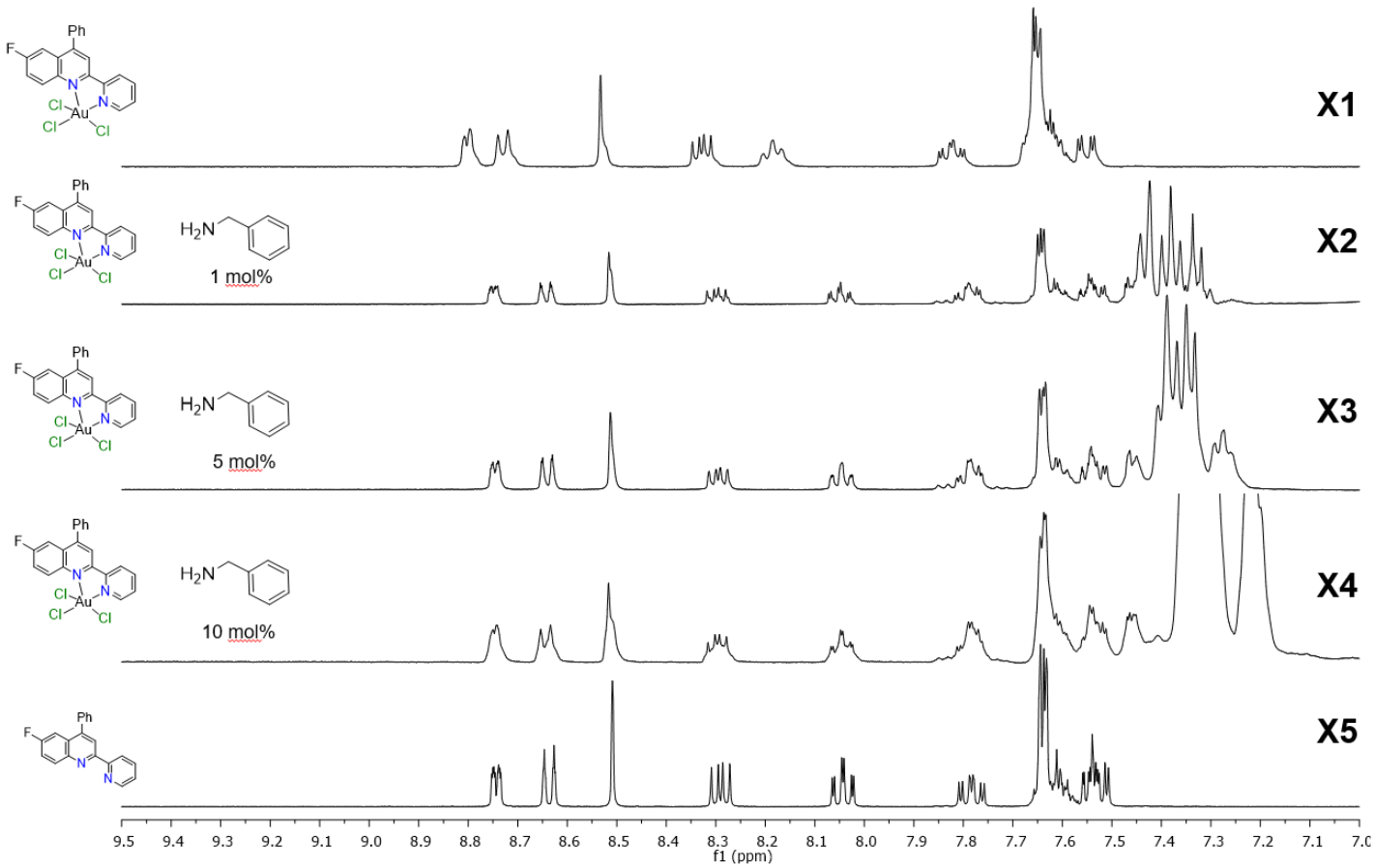

Ligand exchange study of F-PyQuin($AuCl_3$) with benzylamine in DMSO-D_6

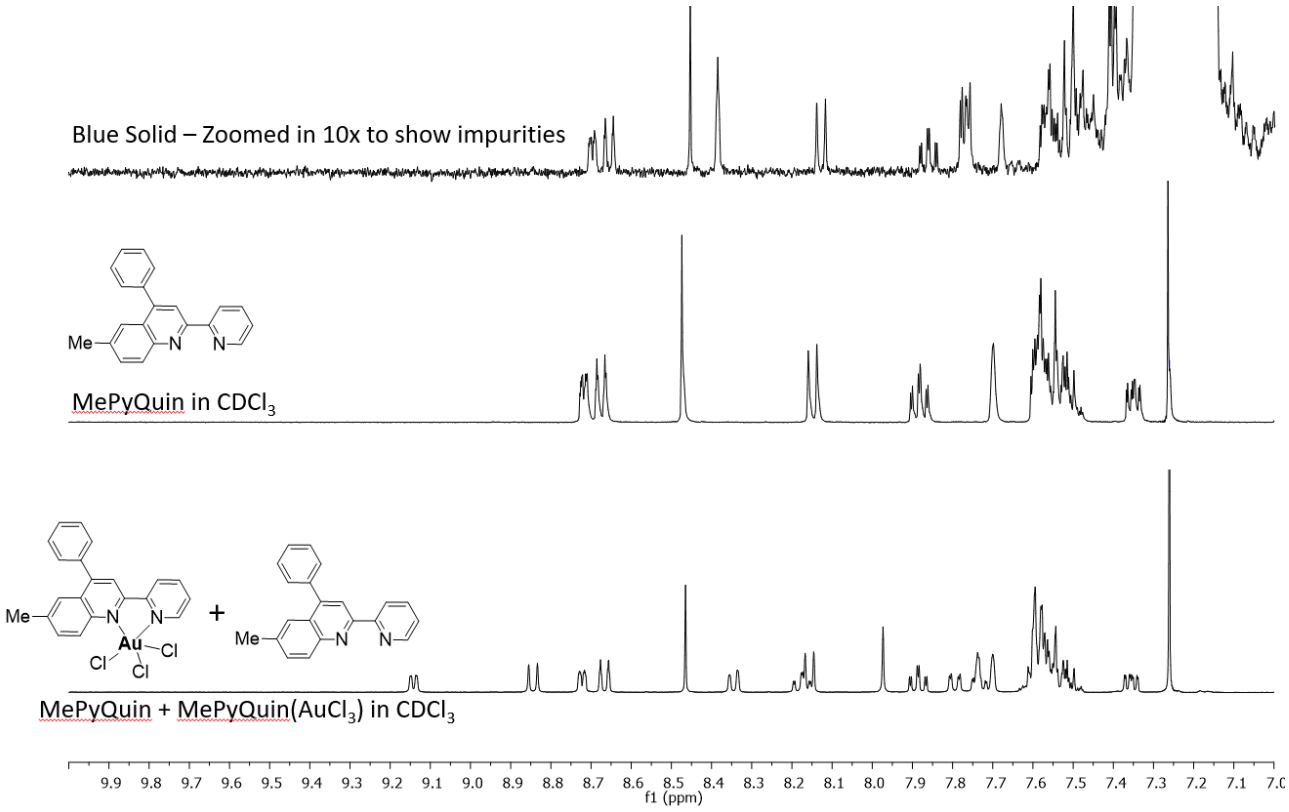

^{1}H NMR of isolated blue solids from heated ligand exchange show only small amounts of ligand impurity

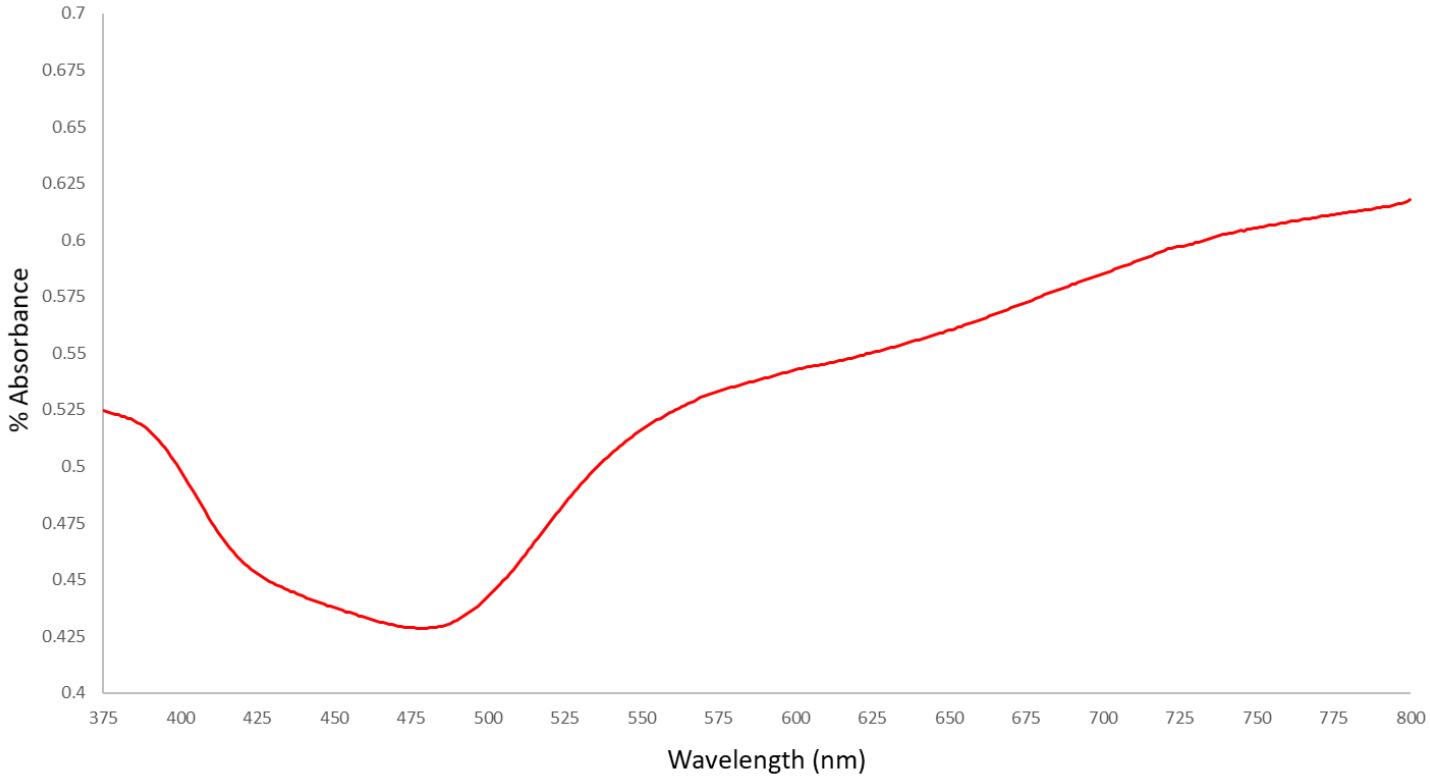

UV-Vis spectrum of isolated blue solid shows large absorbance above 500 nm, indicative of AuNPs

Chapter Five: Pyridyl Triazole Gold (III) Complexes and 1,4-Dihydroquinolines

5.1 Introduction

The creation of other heterocycle-based ligands is best pursued through examining seminal research in which novel heterocycles are formed. Sometimes, this work can be found within the same group, which was the case in this situation. There has been a constant effort in the Larsen group to develop methods for accessing small, nitrogen-containing molecules with either tri- or tetra-substituted carbons at the α-position. One route to a series of interesting α-tetrasubstituted amines was through condensation of an amine onto cyclohexanone followed by alkynylation using triisopropylsilyl (TIPS) acetylene. This yielded a silyl-protected propargylamine which, using the copper-catalyzed azide-alkyne cycloaddition (CuAAC) or “click” reaction, offered 1,2,3-triazoles which were fully substituted at the alpha position after just a two-step reaction sequence. (**Scheme 5.1**). While most often a benzyl-azide was used in the click reaction, the reaction also tolerated aryl-azides, which offer products that possess many similarities to the aryl-substituted quinolines previously discussed.

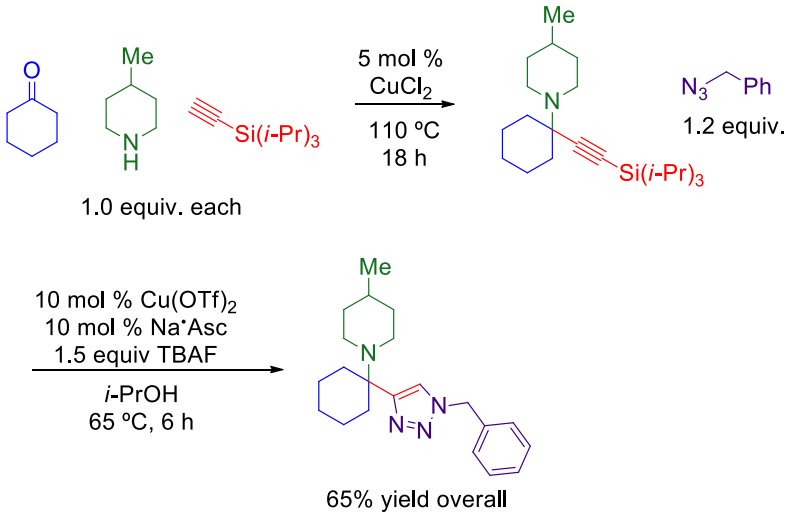

Scheme 5.1 High yield for 2-step synthesis of alpha-tetrasubstituted triazoles

As seen with the PyQuin ligands, the modification of an aryl-quinoline to a pyridylquinoline can be achieved simply through changing one starting material. The 1,2,3-disubstituted triazoles derived from click reactions can be simply derivatized by the modification of the azide (stemming from an aniline starting material) or alkyne. In an analogous fashion to the PyQuins, using 2-ethynylpyridine as the alkyne source allows for the synthesis of pyridyl triazoles that can be tuned both electronically and sterically through the aniline (**Scheme 5.2**).

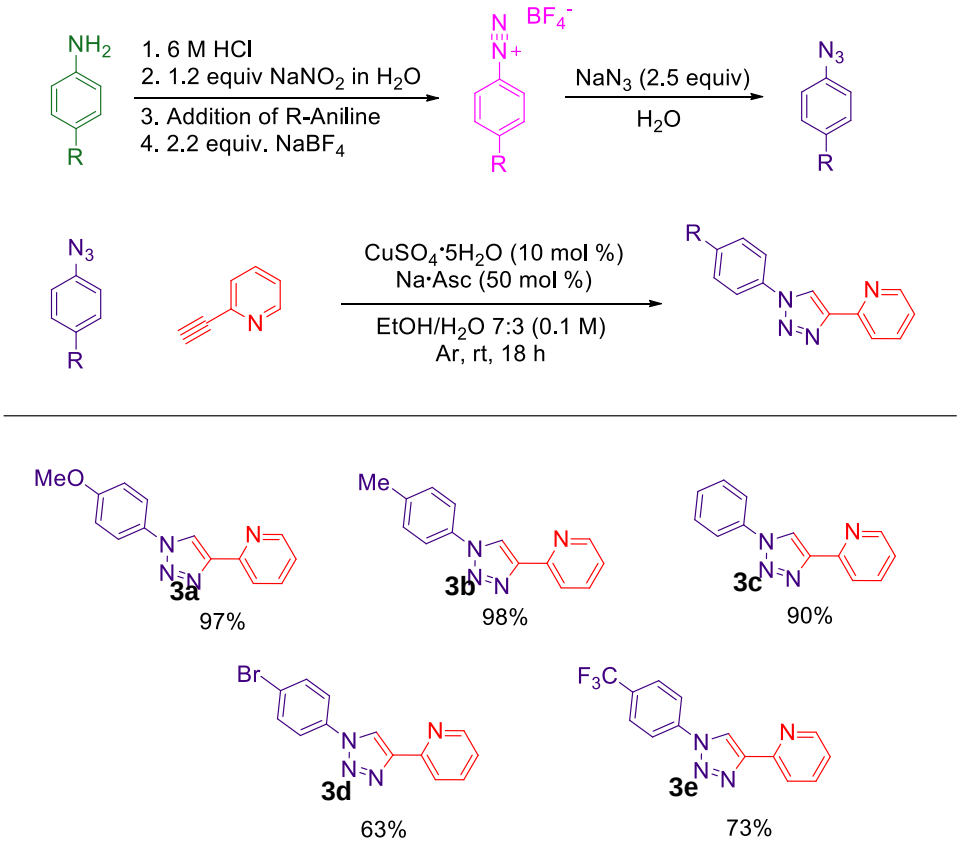

Scheme 5.2 High yield for 2-step synthesis of alpha-tetrasubstituted triazoles

The development of these 2-pyridyl triazoles (PyTri) offered both a ligand with which to make metal complexes but also as another library of potentially bioactive compounds. Pyridyl triazoles have been synthesized with varied substituents and it has been determined that they are potent nicotinamide phosphoribosyltransferase (NMPRTase) inhibitors as well as inhibitors of the tautomerase activity of human macrophage migration inhibitory factor.[1,2] The inhibition of NAD synthesis has been proposed to be a viable way to combat cancerous cell growth, as cells with high usage of this pyridine nucleotide are

often tumoral cells.[3] As discussed in previous chapters, the behavior a bioactive ligand can differ in many ways when it is bound to a metal center, whether it be increased, decreased, rendered inert, or go through a completely different mode of action.

In a manner similar to the synthesis of the PyQuin ligands, the modularity of the PyTri synthesis allows for tuning of the electronic nature of the final product. For the PyQuins, ^{1}H NMR was found to be very useful in determining the effect of the aniline substituent on the eventual ligand, and this was found to be no different for the PyTris. Using the proton on the triazole backbone (explicitly shown in **Figure 5.1**), the donating and withdrawing effects of the substituent derived from the aniline can be observed through chemical shift. The compound for which this resonance is most upfield is the MeO-PyTri and increases in chemical shift ppm going to Me-PyTri, to H-PyTri, to Br-PyTri, with the most downfield being CF_3-PyTri. It is important to note that the triazole proton is the

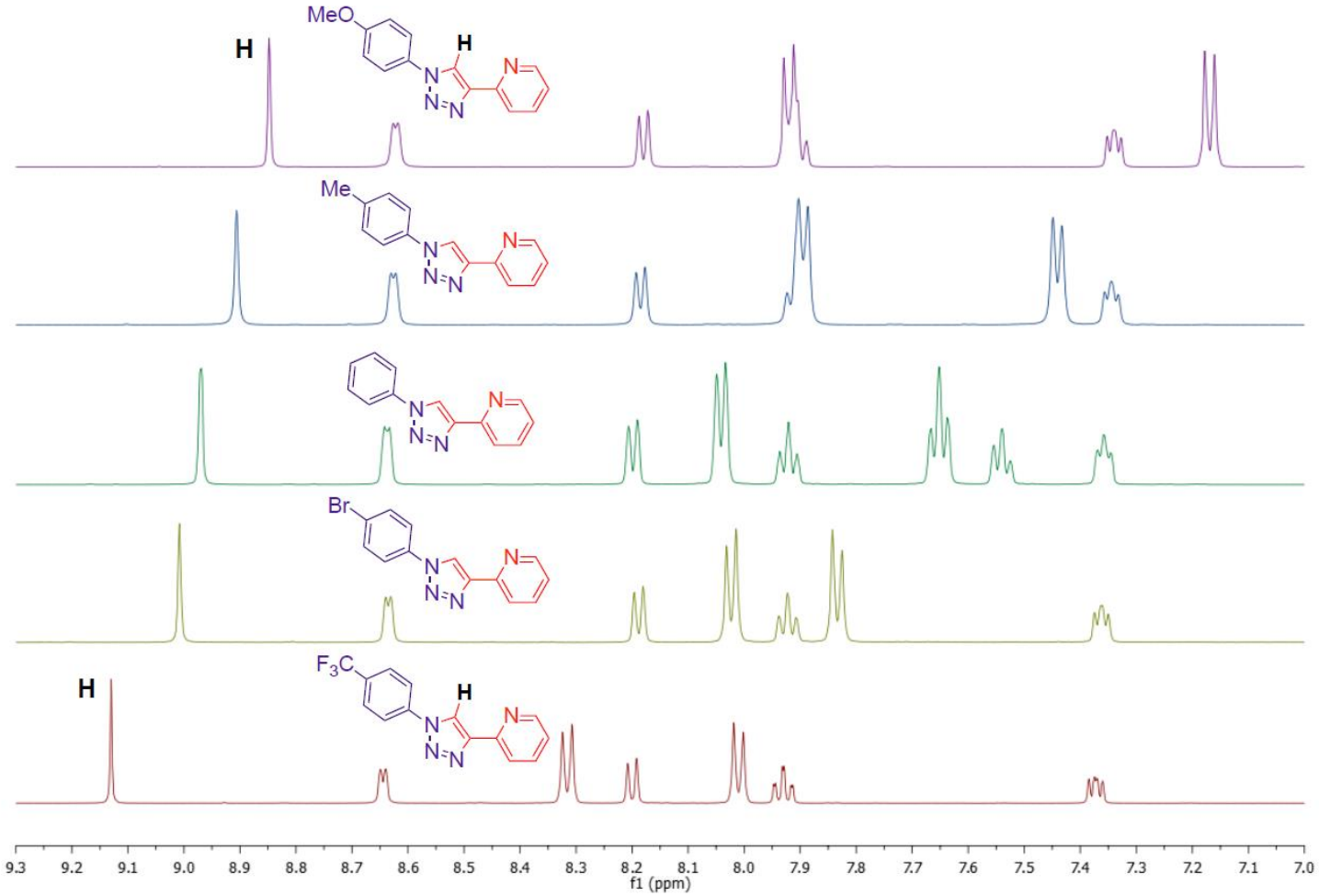

Figure 5.1 ^{1}H NMR comparison of differently substituted R-PyTri ligands

most downfield resonance across all spectra, which is due to it being withdrawn both by the heterocycle it is a part of as well as the proximal pyridine deshielding it. As with the PyQuins, it proposed that the pyridine and triazole face away from each other in order to minimize dipole; because of this, the binding of this ligand to a metal center should be even more apparent than the PyQuins, as the triazole proton singlet could dramatically shift upon the pyridine “flipping” over to chelate.

5.2 Pyridyl Triazole Complexes – Precedence, Platinum & Palladium

As thoroughly discussed in the preceding chapters, there is much support in the development of metal complexes which possess biological activity. With the resistance limitations of current therapeutics like cisplatin, many metal complexes have been identified to combat cancers with equivalent or higher potential in modes of action that differ from current treatments.[4-8] This is a key quality, as the resistance that certain cancers innately have against cisplatin can be circumvented using other treatment options.

This chapter will focus on the utilization of 2-pyridyl triazoles (PyTris) as ligands to form metal complexes of two types: ML and ML_2, where M represents a metal center and L represents a PyTri ligand. In tandem work with Dr. Zachary L. Palchak from the Larsen group, there was an effort to synthesize metal complexes with a variety of metal centers and determine if they had catalytic activity for organic transformations. Due to the fact that designing and synthesizing heterocyclic ligands continues to be at the cutting edge of modern

coordination chemistry for both metallo-pharmaceuticals[9-18] and catalysis, the modularity of our ligand synthesis is highly desirable.[19-26] The CuAAC reaction using terminal alkynes and azides has become a favored methodology in the synthesis of functional ligands due to reasonable reaction conditions, toleration of many substrates, and high yields despite its complex structure.[27-29] The fact that 1,4-triazoles have the ability to bind to metals though either N (being L-type) or C (x-type) atoms have resulted tremendous amounts of research into their utilization as ligands to form mono-, bis-, tris-, and polydentate ligand scaffolds on metal complexes.[30-40]

There is a wide variety of metals that have been used in forming metal complexes with PyTri ligands, including copper (II),[41] silver (I),[42-43] ruthenium (II),[44] rhenium (I),[45] palladium (II),[46-48]platinum (II),[49-50] and iridium.[51] Although there has been much work making PyTri metal complexes, there had yet to be a systematic approach in order to study analogous by electronically diverse complexes through derivatizing the PyTri ligand. With this charge, four series of complexes were synthesized using palladium and platinum metal centers and, using the library of PyTri ligands, the effect of the ligand substituent was investigated.

Platinum (II), much like gold (III) and palladium (II), adopts a four-coordinate, square planar geometry. For this reason, it was expected that using platinum dichloride ($PtCl_2$) as the metal source would result in a R-PyTri($PtCl_2$) complex. However, the result was a mixture of both R-PyTri($PtCl_2$) and (R-

PyTri)$_2$Pt(Bf$_4$)$_2$. This indicated that the bis-PyTri complex was more favorable under these conditions and, upon increasing the stoichiometry of the ligand, the bis complex could be isolated cleanly (**Scheme 5.3**). A crystal structure verified that two PyTri ligands were bound to the dicationic metal center and ^{1}H NMR illustrated the effect the PyTri substituent had on the complex (EDG caused upfield shifting of resonances, EWG resulted in downfield shifted spectrum).

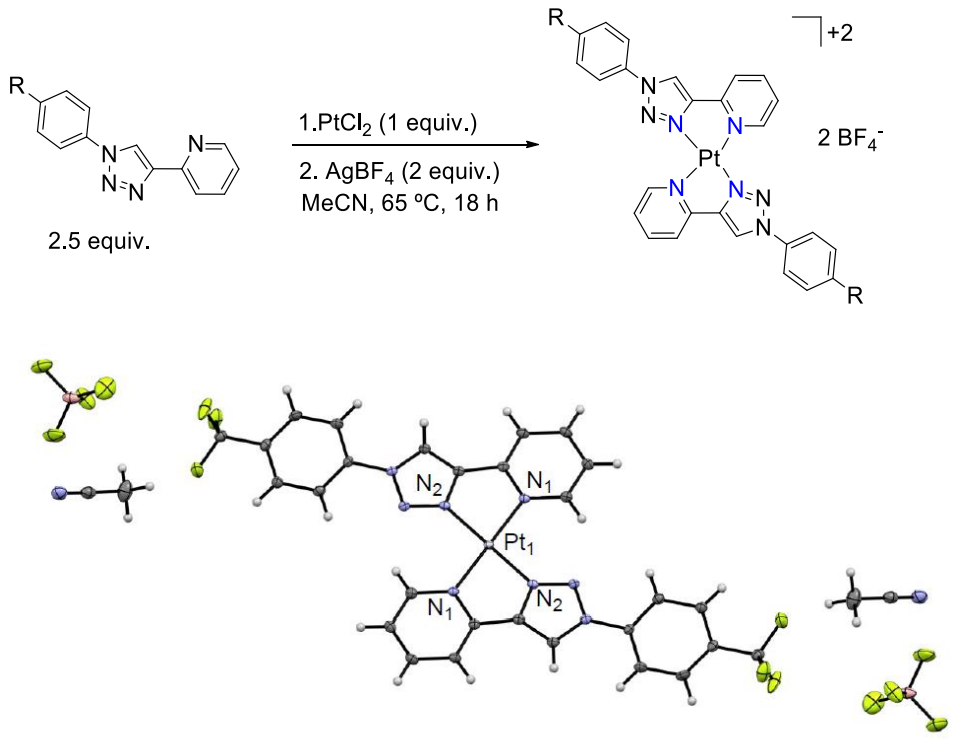

Scheme 5.3 Bis-PyTri platinum (II) complexes synthesized and X-ray crystal structure confirms a 2 ligand to 1 metal ratio

For a mono R-PyTri(PtCl$_2$) complex to be formed cleanly, the platinum (II) source PtCl$_2$DMSO$_2$ had to be used instead of PtCl$_2$. This could initially seem

odd, since the only one PyTri ligand is needed for the mono complex and $PtCl_2$ has open coordination sites, however this actually tracks well with the gold (III) complexes. When synthesizing the PyQuin($AuCl_3$) complexes, $AuCl_3$ fared far poorer than $NaAuCl_4$ in forming the neutral complex, so its possible the displacement of weakly coordinated ligands upon dissolution actually facilitates the complexation. The series of mono complexes was synthesized, verified by an x-ray diffraction crystal structure, and like the bis complexes, the substituent was found to affect the ^1H NMR spectrum in the same manner as previously observed (**Scheme 5.4**).

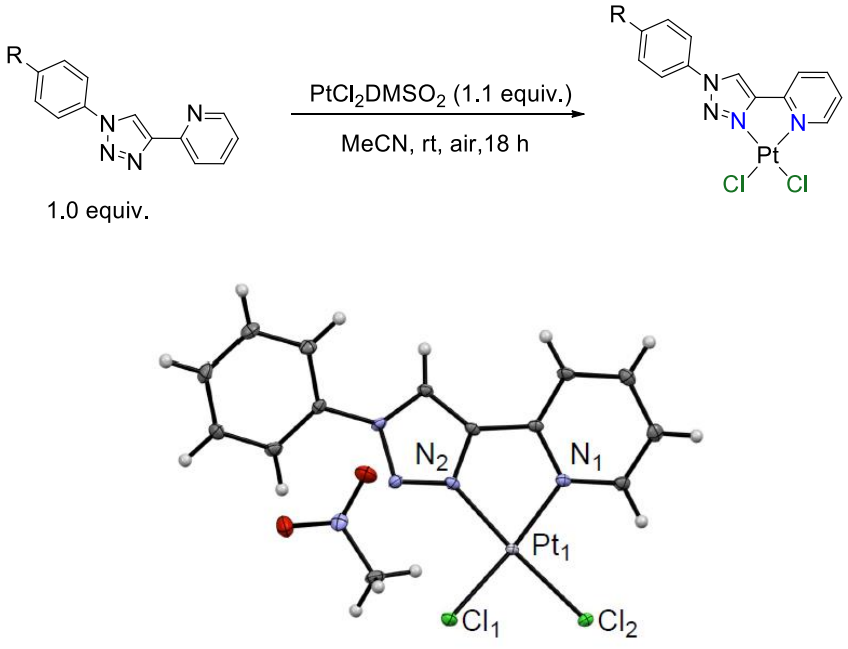

Scheme 5.4 Mono-PyTri platinum (II) complexes synthesized, and X-ray crystal structure confirms a 1 ligand to 1 metal ratio

While platinum (II) complexes have shown to be effective catalysts for many different types of chemical transformations[52] as well as therapeutic uses,[53]

easily the most notable transition metal for catalysis is palladium. Renowned for its application in cross-couplings, palladium (II) complexes with heteroaromatic ligands are undeniably useful, and for this reason PyTri palladium (II) complexes were synthesized. Like platinum (II), palladium (II) complexes generally have a four-coordinate, square-planar geometry. The palladium source $PdCl_2$ was thoroughly unreactive for complexation (potential reduction to palladium black), so the starting material palladium dichloride bis-acetonitrile ($PdCl_2MeCN_2$) was selected. With a slight excess of metal, the mono-complex R-PyTri($PdCl_2$) is synthesized in near-quantitative yields at room temperature (**Scheme 5.5**).

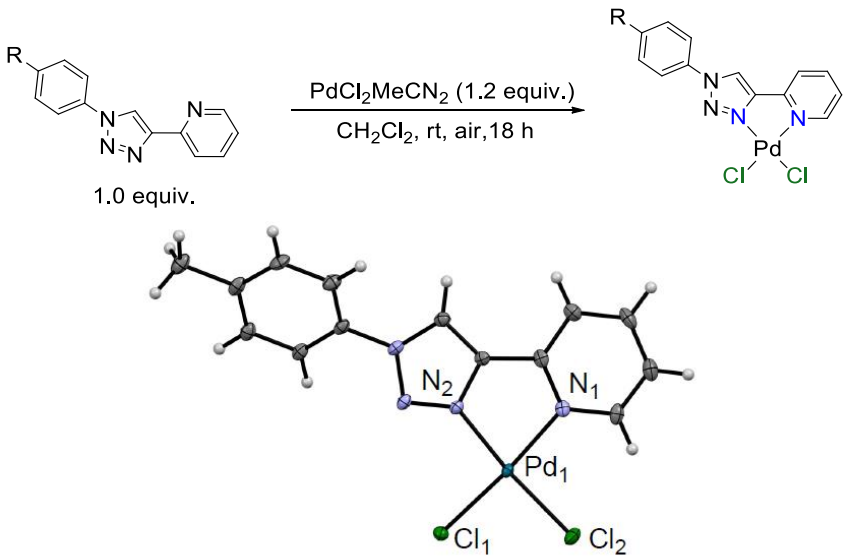

Scheme 5.5 Mono-PyTri palladium complexes synthesized, and X-ray crystal structure confirms a 1 ligand to 1 metal ratio

^{1}H NMR spectra was collected for the series of mono-PyTri complexes and, as predicted, downfield shifting was observed for all the resonances (**Figure 5.2**). What was surprising was that even though the pyridine “flips” to bind to the

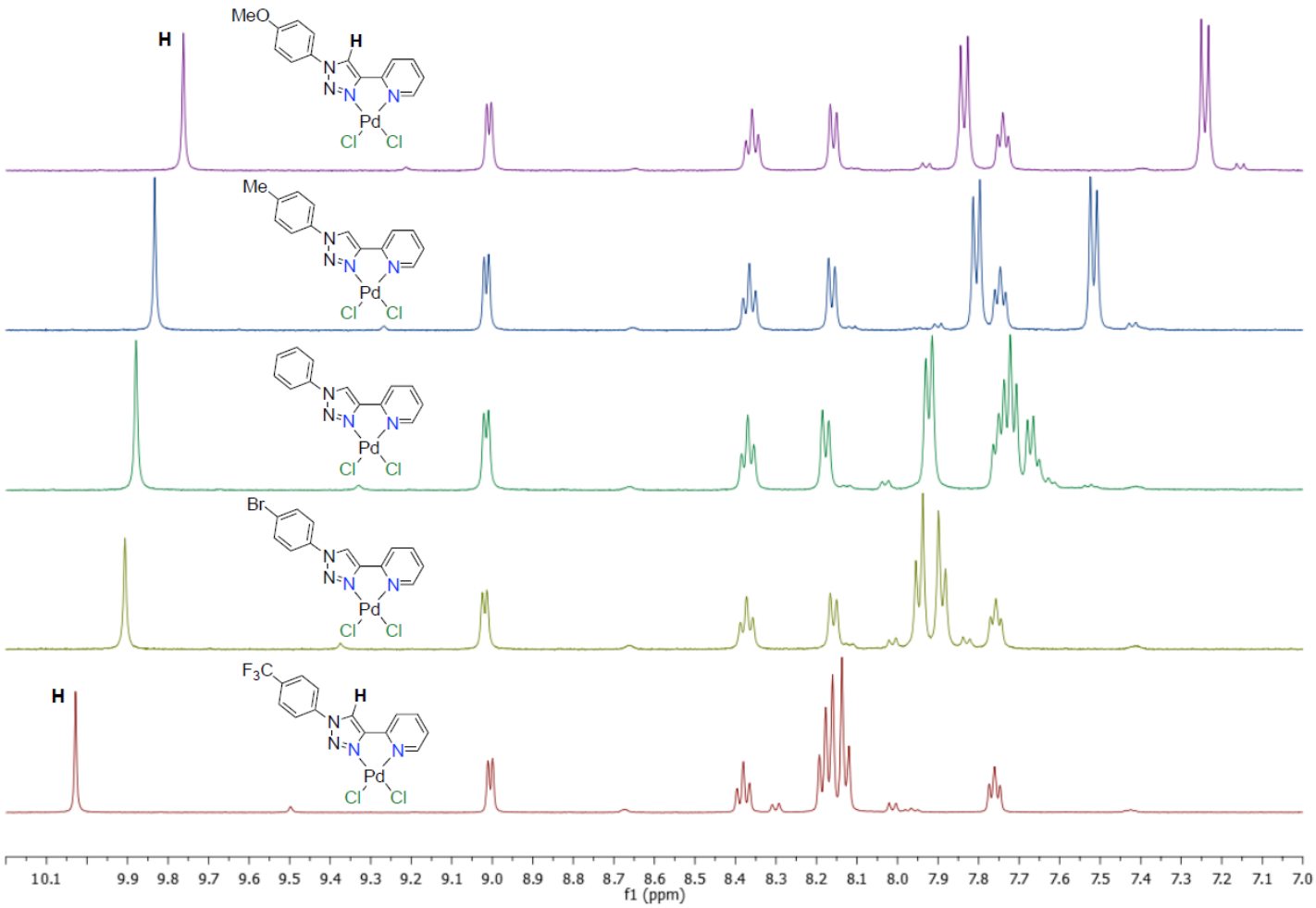

Figure 5.2 ^{1}H NMR comparison of electronically different R-PyTri($PdCl_2$) complexes

metal center, the most downfield resonance remains the triazole backbone proton.

It was proposed that, like the platinum (II) PyTri complexes, a bis-PyTri palladium (II) complex could be formed using a 2:1 ligand:metal ratio and using the starting material tetrakis(acetonitrile) palladium(II) tetrafluoroborate ($Pd(MeCN)_4(BF4)_2$) (**Scheme 5.6**). The bis complexes were synthesized in high yield and characterized fully, as with the other complexes.

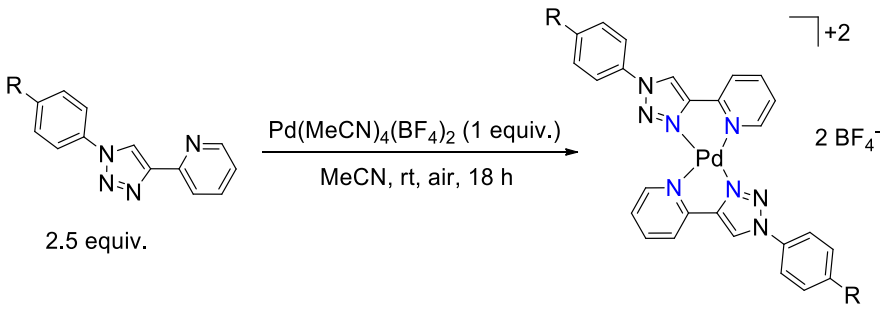

Scheme 5.6 Synthesis of Bis-PyTri palladium (II) complexes

As palladium (II) complexes are ubiquitous in cross-coupling reactions, the viability of the mono R-PyTri($PdCl_2$) complexes was tested in a variety of Suzuki-Miyaura cross couplings using aryl halides and aryl boronic acids. As most catalysts for this reaction contain ligands based on electron rich phosphines[54-58] or N-heterocyclic carbenes,[59-65] it is inherently valuable to create efficient catalysts with tunable ligands to determine how electron density of the ligand affects turnover. It was determined that PyTri($PdCl_2$) complexes are quite good at catalyzing Suzuki-Miyaura cross-coupling reactions, having over 10,000 catalytic turnovers with high functional group tolerance and selectivity (**Scheme 5.7**).

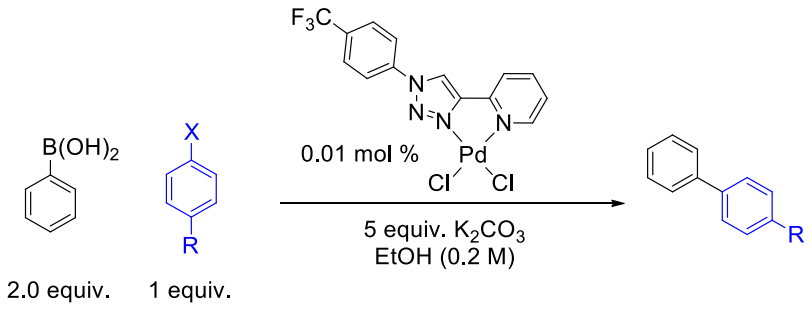

Scheme 5.7 R-PyTri($PdCl_2$) complexes are efficient catalysts for Suzuki cross coupling reactions

In parallel to the synthesis of novel palladium and platinum complexes which employ PyTri ligands, an effort was being made to form complexes using metals which have less precedent. Due to the success of the gold (III) PyQuin complexes, a series of gold (III) PyTri complex was sought to be synthesized to determine their stability, geometry, and how they function as catalysts for organic transformations.

5.3 Synthesis of Pyridyl Triazole (PyTri) Gold (III) Chloride Complexes

While it may seem like the synthesis of gold (III) PyTri complexes should be facile due to the development of the PyQuin($AuCl_3$) complexes, there are a few important distinctions between the ligands. First, pyridylquinoline-based ligands conform to unorthodox geometries due to proton-X (where, in this case, X is a halide ligand on the metal center) repulsion; pyridyltriazole ligands, on the other hand, have the aniline fragment attached through a sigma bond to the nitrogen, not a fused ring. For this reason, the geometry around the gold center should be its preferred four coordinate, square planar configuration (**Scheme**

5.8). The second important difference is that, when in a square planar geometry, the gold (III) center can have either two PyTri ligands and three non-coordinating anions or one PyTri ligand, two halides, and one non-coordinating anion. Regardless of which metal:ligand ratio forms, the result is going to be a cationic complex.

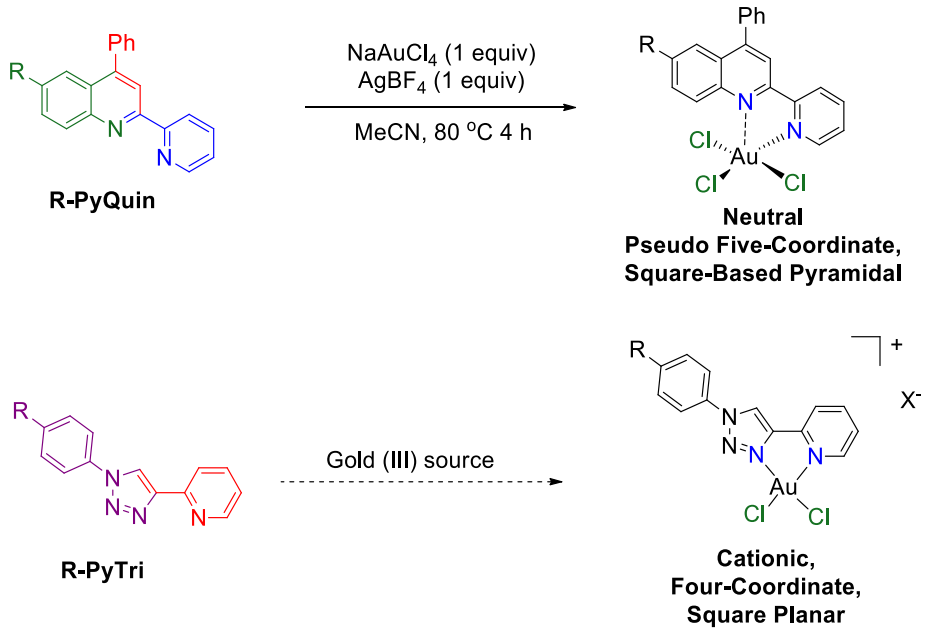

Scheme 5.8 PyQuin gold (III) complex serves as precedent for R-PyTri$(AuCl_2)^+$ complex

Using the synthesis of the gold (III) PyQuin complexes as a foundation, initial conditions were to use $NaAuCl_4$ as a gold (III) source, $AgBF_4$ as a halide abstracting agent, and PyTri ligand all in a 1:1:1 equivalence and run in acetonitrile. It was quickly determined that, should one PyTri ligand bind to the gold center and form a cationic complex, the necessary stoichiometry of $AgBF_4$ had to be increased to 2 equivalents from 1, as two chlorides must be abstracted

from the $NaAuCl_4$ salt. The first difference that was noticed was the solubility of the PyTri ligand versus the PyQuin ligand in acetonitrile: the methyl and methoxy PyTri were fairly soluble in acetonitrile, however the unsubstituted (R = H), Br, and CF_3 PyTri required refluxing temperature to dissolve. This was initially seen as problematic, as without homogeneity and full dissolution of ligand it would be unable to bind to the metal. Fortunately, it was observed that if the sodium tetrachloroaurate and ligand were stirred at slightly elevated temperature together in acetonitrile, all solids went into solution fully. This was not only convenient, but it also gave more evidence for the pathway these complexations take. The first step is a ligand-gold association, what has been referred to as a pre-complex, which as a pair is more soluble than ligand alone. It is this pre-complex which undergoes halide abstraction to form a discrete complex (**Scheme 5.9)**.

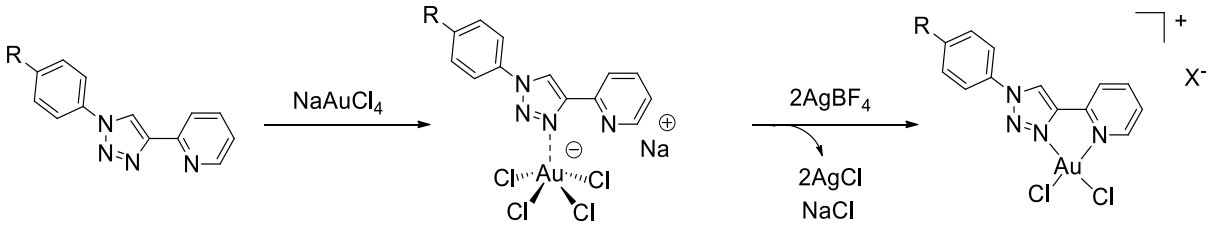

Scheme 5.9 Complexation mechanism with PyTri ligand involves salt pair intermediate

One of the advantages of this process is the facile nature of its isolation. Ligand, gold, and the silver halide abstraction agent all go into solution at elevated temperature. Upon abstraction of chlorides which, in turn forms complex, a fluffy white precipitate of AgCl forms. Removal of this solid leaves behind an orange-

yellow supernatant which, upon concentration, yields spectroscopically pure PyTri$(AuCl_2)^+$ complex (**Scheme 5.10**).

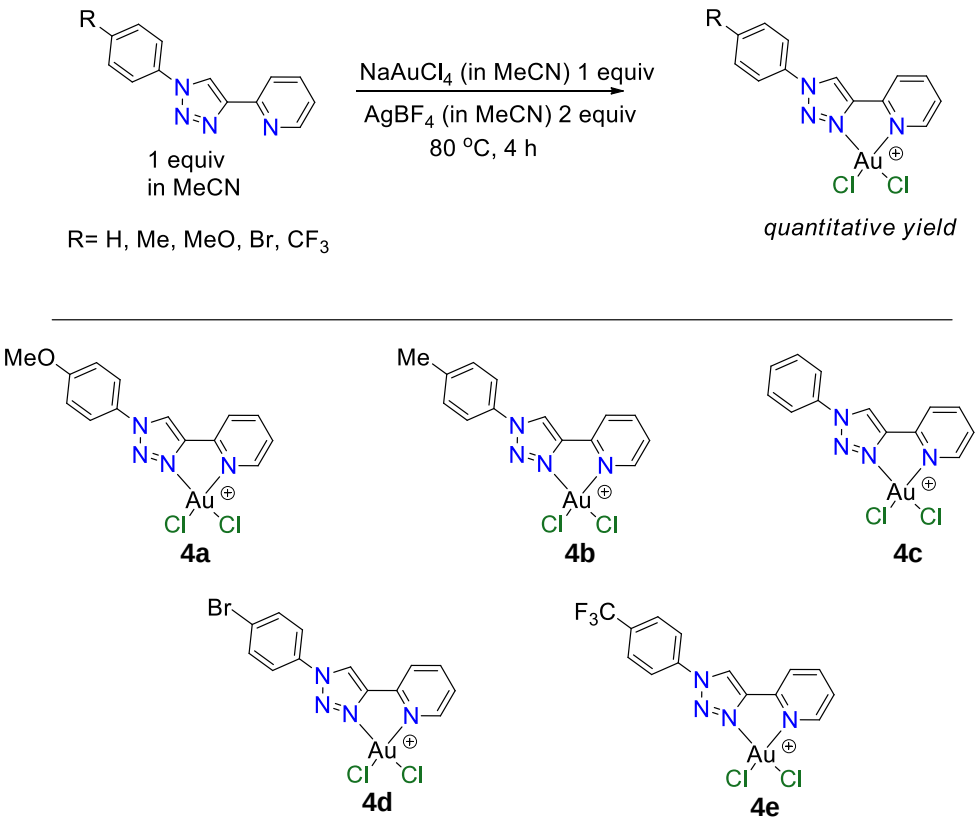

Scheme 5.10 Synthesis for series of cationic R-PyTri$(AuCl_2)^+$ complexes

Once the series of complexes was successfully synthesized and isolated (R = MeO-, Me-, H-, Br-, & CF_3-), ^{1}H NMR was used to observe the effect that the ligand substituent has on the complex's chemical shifts (**Figure 5.3**) and a number of unexpected things were seen.

The first trend noticed is that the cationic gold (III) PyTri complexes follow a similar pattern to the other complexes: as the "R-" substituent on the PyTri

ligand is changed from more electron donating (MeO-, Me-) to neutral (H-), to electron withdrawing (Br-, CF_3-) the chemical shift of the complex's resonances moved downfield. While this can be seen by peak picking the individual signals of a complex and comparing them to the other complexes, the fact remains that at first glance the spectra seem to hardly differ from one another. The difference between the triazole proton of the most electron rich complex, MeO-PyTri$(AuCl_2)^+$, and the most electron poor complex, CF_3-PyTri$(AuCl_2)^+$, is only 0.285 ppm. While this may seem small, in comparison the difference between the analogous palladium (II) complexes is 0.240 ppm. It also turns out that the binding of the ligand to metal doesn't change the magnitude of how much the substituent affects the chemical shift of triazole proton. Unbound, the difference

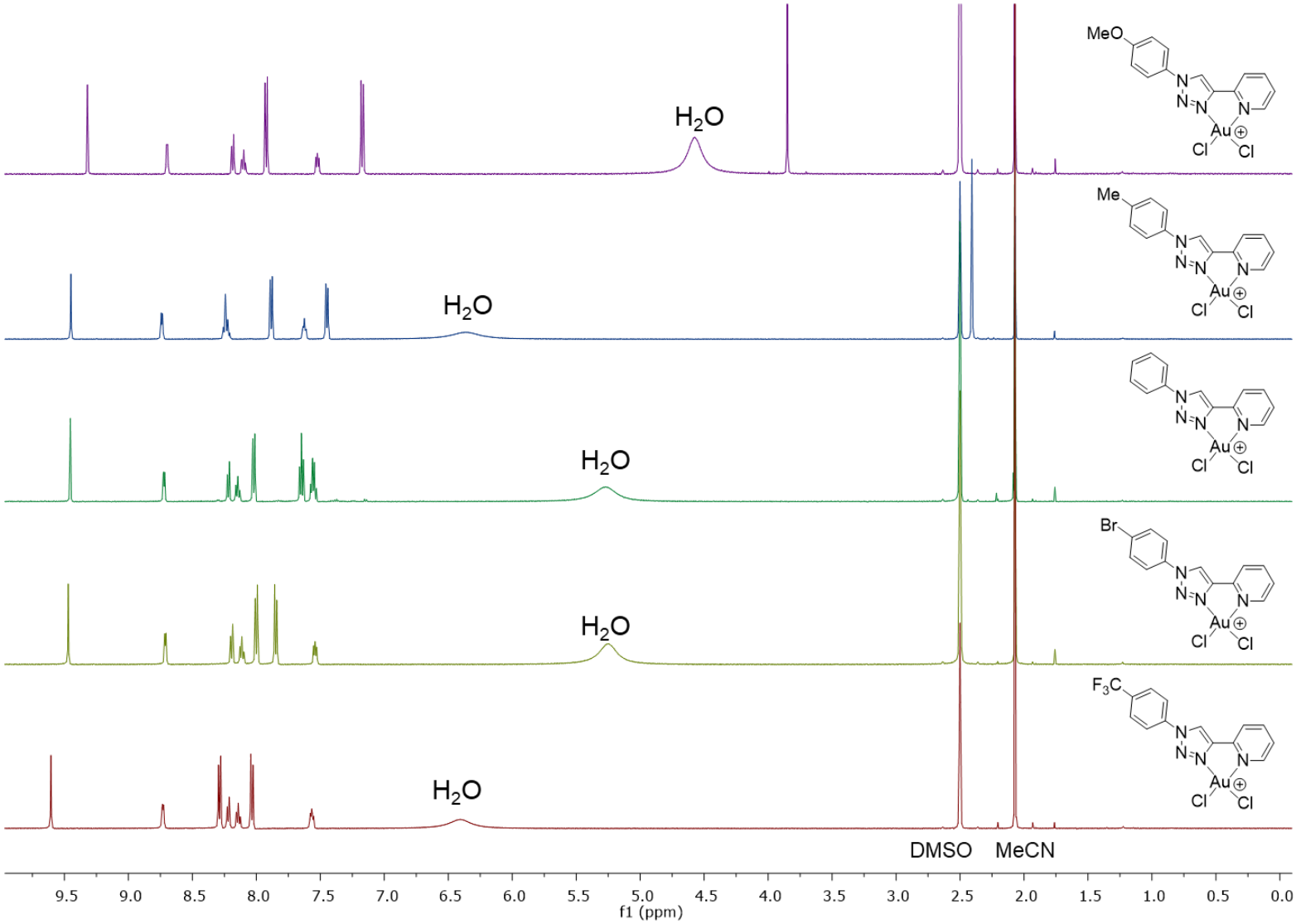

Figure 5.3 ^{1}H NMR comparison of electronically different R-PyTri($AuCl_2$)$^{+}$ complexes

between CF_3-PyTri and MeO-PyTri is 0.235 ppm, indicating that the electronic effect of the substituent is not dampened by complex formation.

Another noticeable trait that the spectra in **Figure 5.3** have is the presence of a broad resonance that appears to show up with no particular trend. Due to the issue of solubilizing these gold (III) complexes, the ^{1}H NMR spectra was taken in deuterated dimethylsulfoxide (DMSO). In DMSO-d6, the two solvent reference peaks are at 2.50 ppm (for the methyl groups on dimethylsulfoxide) and 3.33 ppm for water impurities. Due to DMSO being quite hydroscopic, water can even be seen in brand-new bottles and even freshly cracked ampules. As is evident by the shown spectra, these broad resonances (which can only be attributed to water) show up in quite the range, from 4.5-6.5 ppm. As gold (III) complexes have almost no precedent in solution-phase studies and the presence of a downfield-shifted water resonance, this was a new phenomenon being observed. The only literature precedent that was able to be found for this sort of occurrence was in 2000, where Ross & Lowe observed the downfield displacement of the NMR signal of water in deuterated dimethylsulfoxide upon the addition of deuterated trifluoroacetic acid.[66] As the solution of DMSO-d6 was made more acidic, the water peak was both shifted downfield and broadened significantly. In the case of the PyTri$(AuCl_2)^+$ complexes, there is no added acid, however due to the cationic nature of the complex, the ionic strength of the DMSO-d6 solution is increased. It was proposed that cationic gold (III) complexes can cause a similar effect to the water peak in DMSO, however this

needed to be observed with another complex to verify. So, another cationic gold complex was synthesized, PyQuin$(AuCl_2)^+BF_4^-$, and instead of taking the ^1H NMR in $CDCl_3$ as had previously been done with the PyQuin gold (III) complexes, it was taken in DMSO. As predicted, the water peak is not seen at its standard chemical shift of 3.33, but instead it is broadened and quite downfield shifted at 6.75 ppm (**Figure 5.4)**.

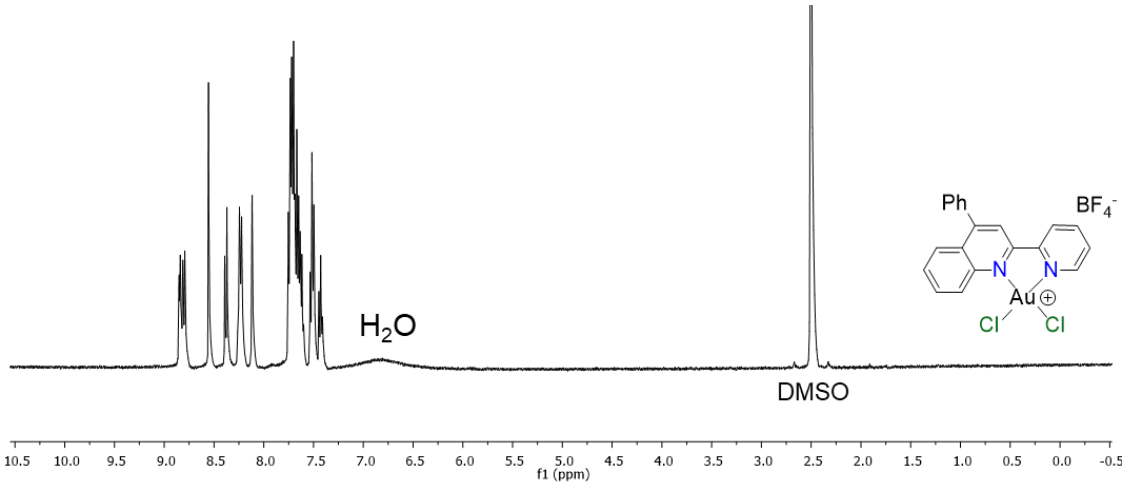

Figure 5.4 ^1H NMR spectrum of cationic PyQuin$(AuCl_2)^+BF_4^-$ shows downfield shifted water peak when taken in deuterated DMSO

With the series of R-PyTri$(AuCl_2)^+$ synthesized and their corresponding ^1H NMR spectra ratified, the next part of characterizing these novel complexes was attaining an x-ray crystal structure. As there is incredibly limited precedent for gold complexes in general and absolutely no instance of using pyridyltriazole ligands being bound to gold, a crystal structure is vital for confirming the proposed structure, oxidation state, and geometry.

Finding a recrystallization solvent for the PyTri$(AuCl_2)^+$ complexes was surprisingly taxing: due to the complex's low solubility in common organic solvents, strongly polar solvents are required for full solubility. Unfortunately, once dissolved the complex does not precipitate out of solution in solvents like DMSO, so less-common solvents were tested. The Crowley group has reported the syntheses of PyTri metal complexes and, in order to get x-ray quality crystals, nitromethane was utilized. In nitromethane ($MeNO_2$), the PyTri gold (III) complexes showed very low solubility even when boiling, however the $MeNO_2$ went from clear and colorless to a faint yellow color, suggesting small amounts of complex were being solubilized. After capping and letting sit in an NMR tube for over a month without agitation, x-ray quality crystals developed and were isolated. With the assistance of Prof. Arnold Rheingold at the University of California San Diego x-ray diffraction data was obtained, and the proposed structure was verified (**Figure 5.5**).

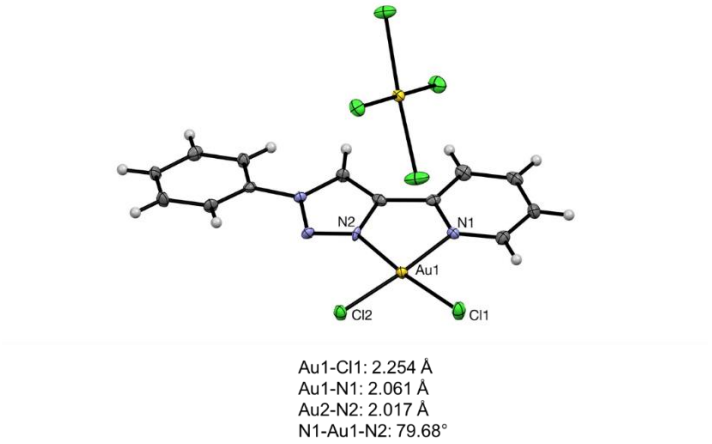

Figure 5.5 X-ray crystal structure confirms PyTri$(AuCl_2)^+AuCl_4^-$ complex

The x-ray crystal data confirmed that the isolated gold (III) complexes consist of one PyTri ligand, one gold atom, and two chlorine atoms to form a square-planar, four-coordinate system. Additionally, the presence of a non-coordinating anion confirms that the gold remained in the +3 oxidation state and was not reduced by the nitrogen ligand. What was surprising about the crystal structure was that even though the synthesis uses one equivalent of PyTri ligand, one equivalent of $NaAuCl_4$, and *two* equivalents of $AgBF_4$, the non-coordinating anion in the crystal structure is $AuCl_4^-$ as opposed to the expected BF_4^-. Stoichiometry alone shows that there are twice as many BF_4^- anions in solution as $AuCl_4^-$, so the preference for a tetrachloroaurate anion is unusual. In addition to it being improbable, the implication of having a gold complex with a gold anion is that this reaction is wasteful with an expensive reagent. It was then quite fortunate to find precedent that this is not an uncommon phenomenon when gold (III) complexes form ordered crystals. In terms of Hard Soft Acid Base (HSAB) theory, large diffuse (soft) ions prefer to pair together over small and compact (hard) ions. It has been observed before that cationic gold (III) complexes preferentially form crystals with gold (III) anions and, despite efforts to perform anion exchange, the non-coordinating anion remains $AuCl_4^-$.[67] Due to the fact that there is precedent for this unexpected ion pair, and that the crystal formation took over a month, the crystal structure was deemed sufficient.

Looking at the x-ray data, the cationic gold (III) PyTri complex bears many similarities to the palladium and platinum analogues. The bidentate PyTri ligand

has a bite angle of 79.68° in the Ph-PyTri($AuCl_2$)$^+$$AuCl_4^-$ complex, which is comparable to a 2,2´-bipyridine complex. Bond lengths are similar to previously synthesized complexes (aside from the PyQuin($AuCl_3$) complex as there is no need for a long-distance electrostatic interaction), with the triazole-gold bond (2.017 Å) being shorter than the gold-pyridine bond (2.061 Å). It was proposed that the triazole nitrogen was a stronger chelate than the pyridine and this comparison in bond length confirms the hypothesis. It is important to note that this is a divergence from the PyQuin gold (III) complexes, where the pyridine had a significantly shorter bond length to gold than the quinoline-gold bond (2.04 Å to 2.63 Å, respectively). The difference in nitrogen chelation strength is somewhat moot in this situation, however when complexes are made with metals that choose one over the other due to their desire for a linear geometry, this becomes very important (and will be discussed in later chapters).

The fact that the PyTri($AuCl_2$)$^+$ complexes display short Au-N bond lengths was promising, as the endgame for these novel gold (III) compounds was to explore their use in catalysis. Their stability in solution (as seen by ^{1}H NMR) and facile synthesis are both important qualities in developing a new catalyst. As described in depth earlier in this document, there are many different types of chemical transformations that have shown to be assisted by a gold (III) catalyst.[68] The important distinction is that the precedent uses either gold (III) salts (such as $NaAuCl_4$ or $HAuCl_4$) or they synthesize a single catalyst which is difficult to modify post-complexation. Our method boasts the ability to synthesize the series

of complexes which can not only be tested for catalytic activity for a chemical reaction but can also be compared to each other to determine whether a more electron-rich or electron-deficient catalyst is preferable. This data is key for determining exactly *how* the gold (III) catalysts act when facilitating transformations, thus increasing the scientific community's understanding of these unexplored metal complexes.

5.4 PyTri($AuCl_2$)$^+$-Catalyzed Hydroamination Yields Novel 1,4-Dihydroquinoline

Discussed in the introduction of this document, there inherent value in developing ways to access small, nitrogen-containing molecules. Specifically, methods towards nitrogen heterocycles are especially valuable as they boast stability in physiological environments without sacrificing therapeutic activity.[69] These "privileged scaffolds" can be ways to predict viability as a drug target, with the general principle asserting that similar chemical constructs should have similar biological effects.[70] One method that the Larsen group has explored in depth is the tandem hydroamination-alkynylation reaction to yield tetrasubstituted propargylamines (**Scheme 5.11**).[71]

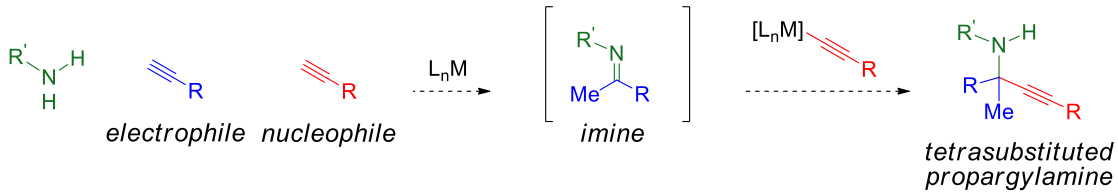

Scheme 5.11 In-lab precedent of metal-catalyzed tandem hydroamination/alkynylation

It was observed that while this reaction can be catalyzed using a wide array of metal halides and triflates, a 10 mol % loading of copper (II) triflate was found to be optimal. Because of the large amount of in-lab precedent that this reaction had, it was selected to be a good test reaction to see if the gold (III) PyTri complexes had catalytic activity. As shown in the above figure, the first step of this process is a hydroamination, where an amine nucleophile adds its N-H bond across an electrophilic alkyne, forming an imine intermediate. A second equivalent of alkyne is converted to a metal acetylide and, acting as a nucleophile, attacks the imine yielding the tetrasubstituted propargylamine product. Due to their extensive precedent in the Larsen group, the alkyne/amine pair of phenylacetylene and aniline were selected.

Using the published conditions of 10 mol % catalyst loading, 1 equivalent of aniline, 2 equivalents of phenylacetylene, and a reaction temperature of 110 °C, an initial test was run using Ph-PyTri$(AuCl_2)^+$. It was incredibly surprising that according to the gas chromatogram, not only did no propargylamine form, but there was no trace of the imine intermediate. It was proposed that, since anilines are fairly poor nucleophiles, the reaction just may need longer to reach imine and product. After 3 days, it was observed that some imine had formed as well as a heavier (by GC) product (**Scheme 5.12**). This sample was analyzed by mass spectrometry, which found a parent M^+ peak of 298.1590, a mass which corresponds to one aniline and two phenylacetylene moieties.

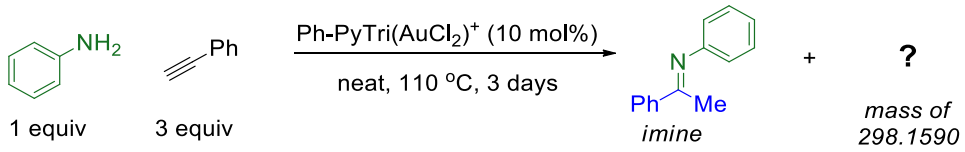

Scheme 5.12 Initial reaction of $PyTri(AuCl_2)^+$-catalyzed hydroamination gives imine and significant amount of product with mass of one aniline and two alkyne molecules

This crude mixture was purified using column chromatography and, using the initial GC chromatogram to verify, the product with the heavier mass was isolated cleanly. Expecting this product to simply be the propargylamine, ^{1}H NMR was used to verify the proposed structure; this was quickly determined to be invalid due to the presence of what appeared to be either a benzyl-type sp^3 proton or a proton on an sp^2 carbon (**Figure 5.7,** H_b). Eventually, it was determined that instead of the initial propargylamine product (**Figure 5.6-Xa)**, the formed product was a 1,4-dihydroquinoline (**Figure 5.6-Xb**), a heterocycle with almost no literature precedent.

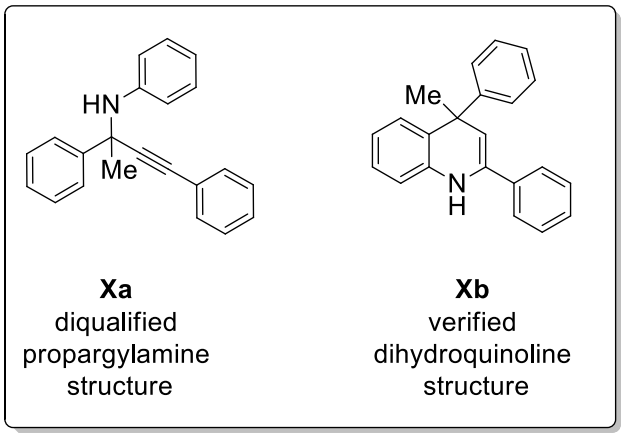

Figure 5.6 Expected product from reaction shown in **Scheme 5.11** is propargylamine **Xa**, however, NMR spectra of isolated product show that product is actually 1,4-dihydroquinoline **Xb**.

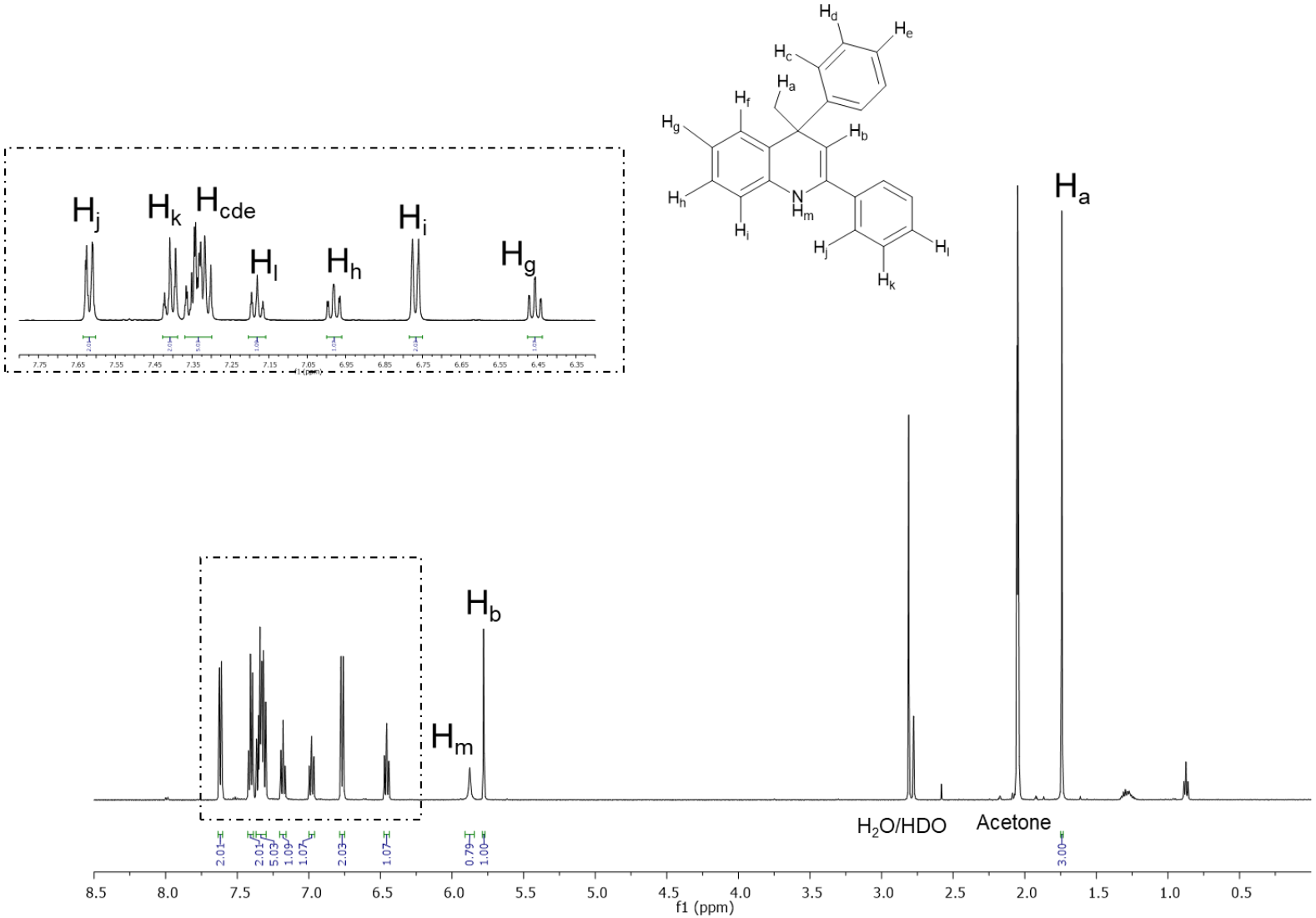

Figure 5.7 ^{1}H NMR of unprecedented 1,4-dihydroquinoline product

Recent reports have shown that 1,4-dihydroquinolines and other partially-saturated quinolines are effective anti-cancer, anti-hypercholesterolemia, and P-glycoprotein inhibitors.[72-74] In addition unique activity that their heteroaromatic analogues may not possess, there lies value in the possibility for further functionalization of these products, for example oxidative additions to the enamine p-system.[75] As the product is quite valuable, developing this method was given priority.

With the proton spectrum fully labeled, a ^{13}C NMR was necessary for fully characterization. When the carbon NMR spectrum was compared to the structure, however, there was an absence of one resonance. The dihydroquinoline product should possess 18 unique carbon signals, however the NMR spectrum only showed 17. As this type of compound has almost no literature precedent, the characterization needed to absolutely verify the proposed structure. Using the two-dimensional NMR experiment heteronuclear single quantum coherence spectroscopy (HSQC), the ^{1}H and ^{13}C NMR spectra were compared to determine which proton resonances correlate to which carbon resonances. Accidental degeneracy of carbon resonances can be clearly seen in the 6.9-8.0 ppm range on the ^{1}H spectrum and 125-130 ppm range on the ^{13}C spectrum (**Figure 5.8**).

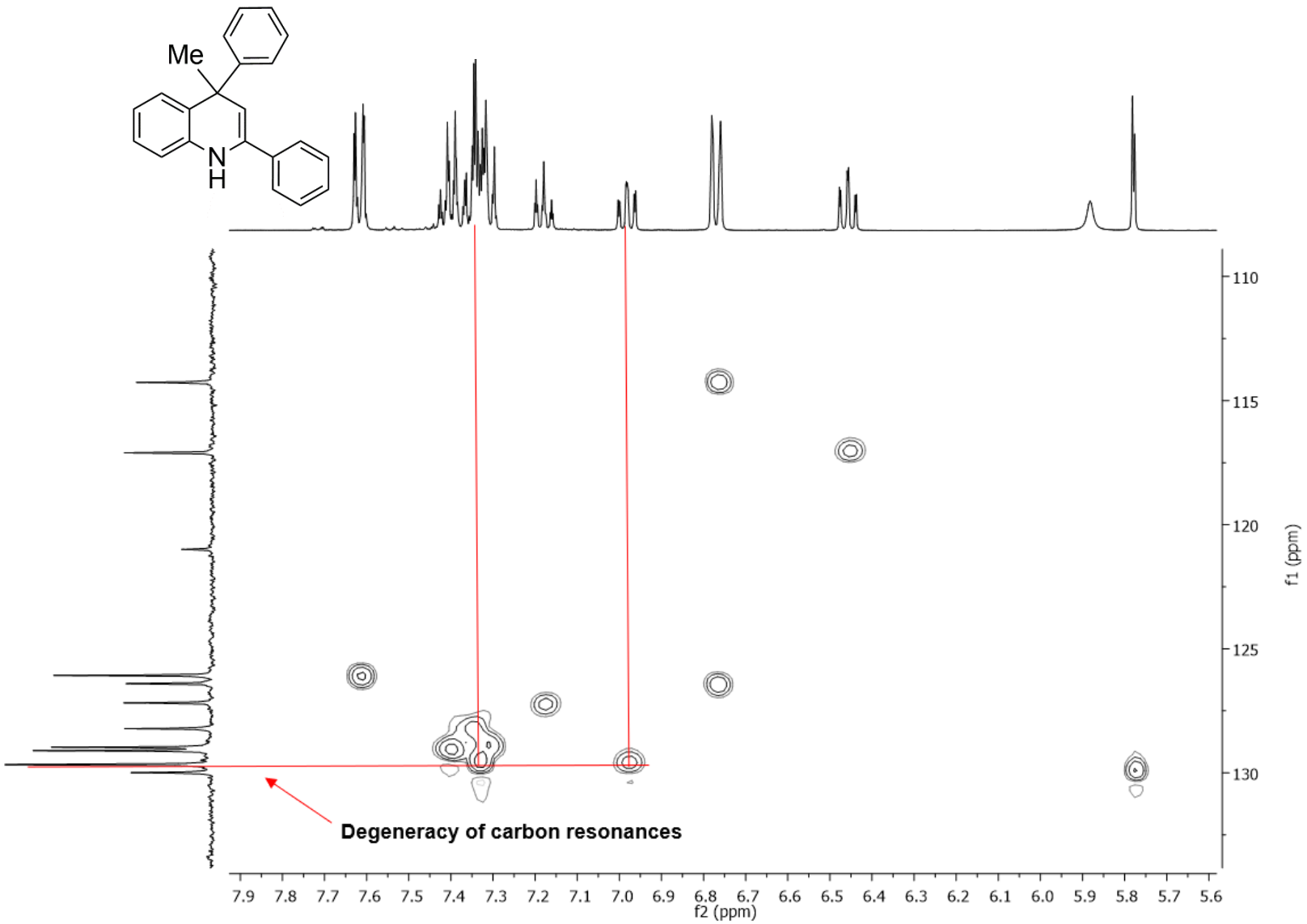

Figure 5.8 HSQC spectrum for the 1,4-dihydroquinoline product indicating degeneracy of carbon resonances

This degeneracy supports the 18 unique carbon resonances that should be present and, with this last piece of data, the structure was confirmed.

As was the initial goal of this reaction, the effect of changing the R- group on the R-PyTri($AuCl_2$)$^+$ catalyst and how it affects the dihydroquinoline synthesis was investigated. Using the standard reaction of aniline and phenylacetylene, the series of PyTri($AuCl_2$)$^+$ complexes were tested to see how the R-substituents changed conversion to product. As this reaction can require up to 3 days, the 1 mmol reaction was set up with 3 equivalents of phenylacetylene to ensure that, over the course of the reaction, alkyne was not being lost due to it boiling off. Conversion to product was determined through integrating the peak on the gas chromatogram and comparing it to that of an internal dodecane standard that was spiked into the reaction mixture. These GC yields (displayed in **Table 5.1** are uncorrected, as a burn ratio was not constructed since these products can be isolated cleanly using column chromatography.

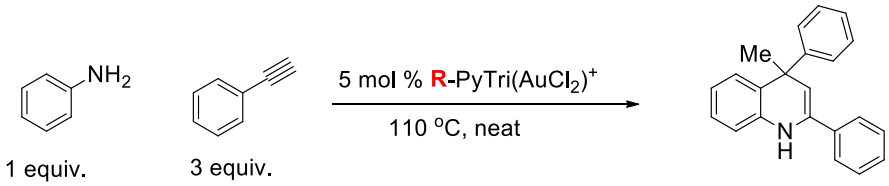

Catalyst	% Yield (24 h)	% Yield (48 h)	% Yield (72 h)
MeO-PyTri($AuCl_2$)$^+$ R = MeO	15	20	23
Me-PyTri($AuCl_2$)$^+$ R = Me	19	29	50
PyTri($AuCl_2$)$^+$ R = H	22	45	50
Br-PyTri($AuCl_2$)$^+$ R = Br	19	26	30
CF_3-PyTri($AuCl_2$)$^+$ R = CF_3	16	21	22

Table 5.1 Uncorrected GC yields for 1,4-dihydroquinoline synthesis for PyTri($AuCl_2$)$^+$ series

After a reaction time of 1 day, there is virtually no difference in conversion to product by changing the catalyst (with the unsubstituted PyTri($AuCl_2$)$^+$ complex giving slightly better yield). This isn't entirely surprising, as the initial conditions showed no product until at least 48 hours of reaction time. At 2 days, the small trend hinted at after 24 hours was confirmed: the PyTri($AuCl_2$)$^+$ complex with no electron-donating or electron-withdrawing substituent was giving the highest conversion to product. After 72 hours, the Me-PyTri($AuCl_2$)$^+$ had equivalent product conversion to the unsubstituted complex, however it had significantly more side products.

It was predicted that either a more electron-rich or electron-poor complex would change the yield and, from there, conclusions could be made regarding the gold (III) catalyst's role in the reaction; the fact that the complex with *neither* an EDG or EWG on its ligand gave the best conversion was somewhat puzzling. It suggested that the reaction's mechanism goes through two energy barriers, one where the electrophile requires activation and the other where a nucleophile needs activation. The mechanism shown in **Scheme 5.13** is a proposed pathway of how a 1,4-dihydroquinoline is reached.

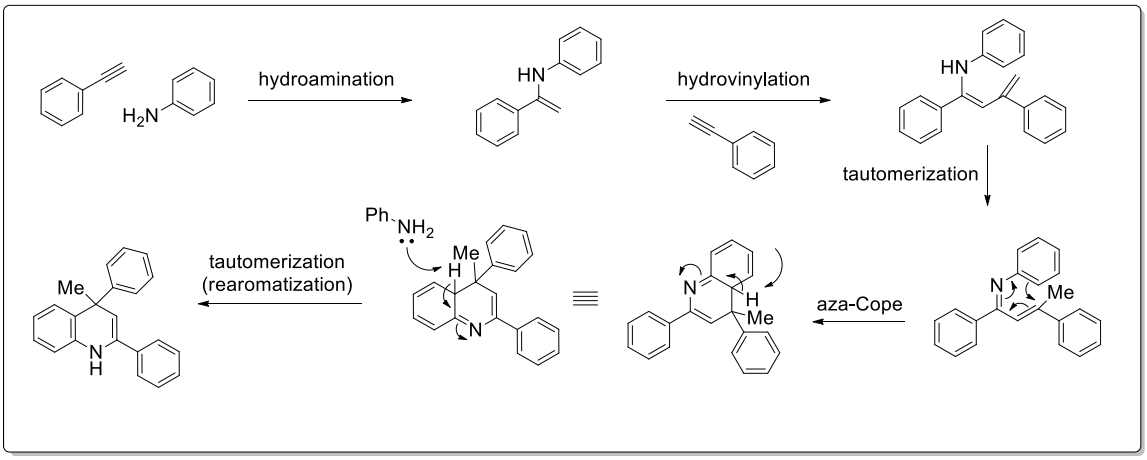

Scheme 5.13 Proposed mechanism for 1,4-dihydroquinoline formation

As expected, the first step of this reaction is the hydroamination of phenylacetylene by the aniline nucleophile. The formed imine intermediate can tautomerize between imine and enamine which, under $Cu(OTf)_2$ conditions, is attacked by a copper acetylide as the imine. With the $PyTri(AuCl_2)^+$ catalyst,

however, the enamine acts as a nucleophile and hydrovinylates a second equivalent of phenylacetylene. This intermediate undergoes enamine-imine tautomerization, forming a triene which undergoes an aza-Cope [3,3]-sigmatropic rearrangement. The tetrahydroquinoline product of this cyclization is oxidized and rearomatized, forming the 1,4-dihydroquinoline. While this is just a proposed mechanism, certain postulations which support the mechanism needed to be investigated in order to make the mechanism more valid.

The reason that hydroamination/alkynylation can be catalyzed with a variety of different metal catalysts is that they all are able to coordinate to the alkyne, activate it for deprotonation, and form a metal acetylide to act as a nucleophile as opposed to the alkyne's initial role as an electrophile. This leads to the assumption that gold (III), unlike the rest of the metal catalysts which catalyze the formation of propargylamine, is unable to form metal acetylides and functions solely as a Lewis acid. As further evidence of this, the reaction between phenylacetylene and aniline was run with 10 mol % of 20 different catalysts (Brønsted acids, Lewis acids, metal triflates, etc.) and the only catalyst that facilitated the formation of 1,4-dihydroquinoline was the R-PyTri$(AuCl_2)^+$.

To determine if 1,4-dihydroquinoline forms because of gold (III), the PyTri ligand, or the PyTri$(AuCl_2)^+$ complex as a whole, controls were run using different gold sources. It was observed that even with other gold (III) and gold (I) metal complexes, there is no conversion to 1,4-dihydroquinoline. One very interesting observation was that upon adding phenylacetylene to weighed-out gold (I)

chloride, a significant amount of gas evolved from the solution. This gas, assumed to be HCl, is released upon the formation of the phenylacetylene-gold metal acetylide. When the same process is tested with gold (III) chloride, no gas is seen and by ^{1}H NMR, the alkyne proton is unaffected. This strongly suggests that gold (III) is at least less likely to form an acetylide which, based on the proposed mechanism, can explain why the second step is a hydrovinylation with the enamine as opposed to alkynylation on the imine.

Coordination of the PyTri$(AuCl_2)^+$ complex to the alkyne activates the alkyne for nucleophilic attack without converting it to a nucleophile. This activation results in 1,4-dihydroquinoline formation but also explains the appearance of an unorthodox side product. As the reaction progresses over the course of 3 days, both aniline and alkyne are consumed (as their respective GC peaks reduce to nothing); however, the conversion to product never goes beyond 50% and the initial imine is consumed as it forms. Other than starting materials and the 1,4-dihydroquinoline product, there is one product that consistently forms. After isolation and characterization (^{1}H & ^{13}C NMR and mass spectrometry), the side product was found to be 1,3,5-triphenylbenzene. Since the product forms from an alleged aza-Cope rearrangement, it is not illogical to believe three equivalents of alkyne could cyclize through the assistance of the gold (III) catalyst. This supports the theory that the gold complex is present in both the hydrovinylation and aza-Cope steps of the proposed mechanism. With the product from this reaction isolated and characterized, an effort was made to

see how robust this synthesis could be in terms of changing the aniline and alkyne starting material which, ideally, would offer a modular route to these novel heterocycles.

5.5 Derivatization of PyTri($AuCl_2$)$^+$ Catalysis and Gold Nanoparticle Limitations

Using the series of PyTri($AuCl_2$)$^+$ complexes, it was determined what sort of gold complex will facilitate the synthesis of 1,4-dihydroquinoline products the most efficiently. Unfortunately, the yield was unable to surpass an uncorrected GC conversion of ~50%. The conversion to product was somewhat attributed to the cyclization of phenylacetylene to a 1,3,5-triphenylbenzene product, however this did not give an explanation as to why the aniline appears to be fully consumed. If the lack of product formation was due to alkyne alone, the aniline concentration would stay constant as it has no alkyne to react with. If the aniline was participating in the hydrovinylation and sitting at the imine/enamine intermediate, that species would also be visible on the gas chromatogram. Using the precedent set by the PyQuin($AuCl_3$) complexes when exposed to aniline nucleophiles, the PyTri($AuCl_2$)$^+$ complexes were investigated in terms of ability to undergo ligand exchange.

In order to have multiple ways to determine if ligand exchange occurs, it was decided that the F-PyTri($AuCl_2$)$^+$ complex would be ideal. The fluorine handle allows ^{19}F NMR in addition to the traditional characterization methods of ^{1}H NMR and UV-Vis. Dissolving F-PyTri($AuCl_2$)$^+$ in DMSO gives a pale yellow

solution (ligand is colorless in solution), however upon addition of 10 mol% CF_3-aniline, the solution turns deep purple as it did with the R-PyQuin($AuCl_3$) complexes (**Figure 5.9**). A similar experiment was conducted using a 10 mol % addition of t-butanol (as opposed to the aniline) and the solution remained clear and colorless. UV-Vis spectra were collected for the two solutions of F-PyTri$(AuCl_2)^+$ complex with an added nucleophile as well as a control solution of F-PyTri$(AuCl_2)^+$ complex in DMSO.

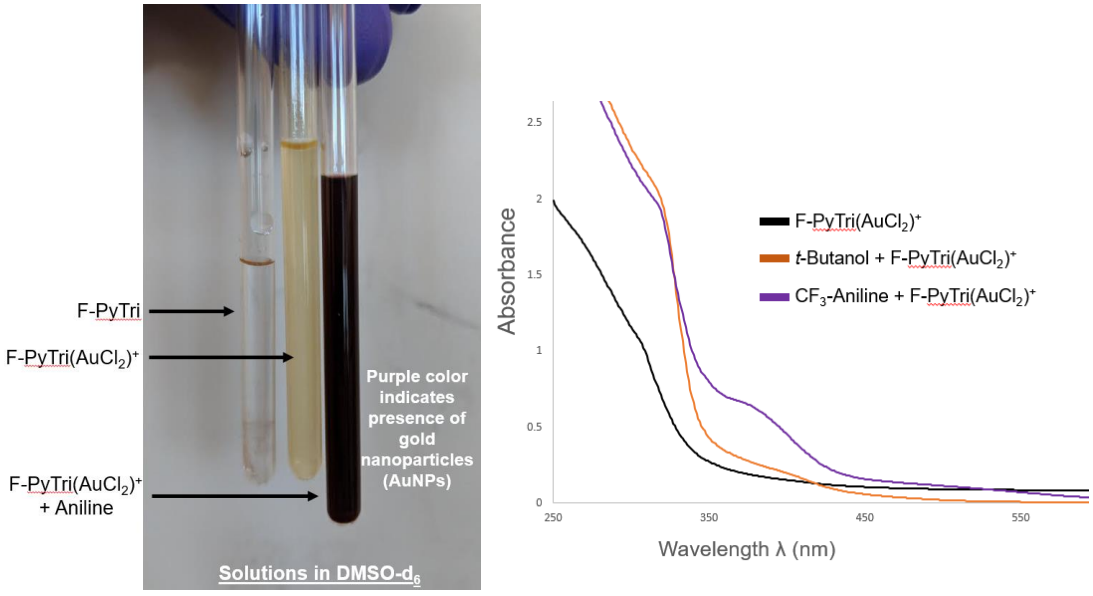

Figure 5.9 Addition of CF_3-aniline to PyTri gold (III) complex solution results in gold nanoparticle formation; addition of alcoholic nucleophile *t*-butanol does not result in same dramatic effect

The overlaid spectra clearly show that addition of t-butanol increases the absorbance of the control spectrum as a whole. The addition of CF_3-aniline to the F-PyTri$(AuCl_2)^+$, on the other hand, shows an increase in absorbance at 400 nm,

which is within the range that gold nanoparticles are known to have strong absorbances.

Based on these findings and those with the PyQuin gold (III) ligand exchange studies, it appears that anilines are effective reducing agents for gold (III) species, resulting in the formation of colloidal gold. Generally, gold nanoparticles are synthesized using gold salts (not gold complexes) and are reduced/stabilized using amines or alcohols.[76] The Blanchard group recently screened the potency of reducing agents used for gold nanoparticle formation and surprisingly, they found that anilines specifically were quite *ineffective* at forming gold nanoparticles, which is the complete opposite of what the Larsen lab has observed with our gold (III) complexes.[77] The reason for this is that, upon exposure to gold nanoparticles, anilines participate in competitive polymerization reactions rather than reducing the metal.[78] Aniline polymerization occurs via the two-electron loss of the amine, resulting in a nitrenium cation; this cation is attacked by the aniline benzene ring in an electrophilic aromatic substitution, which propagates until eventual termination. This process, namely the residual electrons that are released in the nitrenium cation initiation step, has been found to be catalyzed quite efficiently with colloidal gold. The gold nanoparticles were observed by both UV-Vis (a strong absorbance between 400-700 nm) as well as the yellow solution turning vibrantly purple.

This relationship between gold (III), anilines, and gold nanoparticles explains the difficulty these novel gold complexes have had in catalyzing

reactions to full conversion. For example, in the reaction where a PyTri($AuCl_2$)$^+$ converts phenylacetylene and aniline to a 1,4-dihydroquinoline, there are many other processes occurring: the aniline starting material is reducing gold (III) catalyst to gold nanoparticles which, in turn, is causing polymerization of the aniline; additionally, the phenylacetylene starting material is undergoing cyclization/trimerization which is, in theory, being catalyzed by either the gold nanoparticles or gold (III) catalyst (neither of which has any precedent). The fact that both gold nanoparticles and the polymerized aniline are going to be undetectable by GC explains why the reactions appeared to have full consumption of starting material yet such low yields. Knowing that the reaction between an aniline and a phenylacetylene is going to have many factors working against it and that the yield may not be optimal, an effort was made to diversity the product using the modular nature of this reaction.

Since it was determined that changing the PyTri($AuCl_2$)$^+$ catalyst has a moderate (but not extreme) effect on the conversion of starting material to 1,4-dihydroquinoline product, the next step in this process was to vary the starting materials. As discussed in earlier chapters, the benefit of a modular synthesis with an aniline starting material is that anilines are commercially available with a variety of different substituents as well as being quite inexpensive. There are also commercially available phenylacetylenes, however there are significantly fewer variants, with those variants being somewhat pricey. However, as this reaction is only a single step and can give an undocumented product in moderate yields,

two additional para-substituted phenylacetylenes (MeO- and CF_3-) were purchased to see how they fared in this reaction. Additionally, four para-substituted anilines (MeO-, Me-, Br-, and CF_3-) were screened to observe how this affected conversion to 1,4-dihydroquinoline (**Scheme 5.14**).

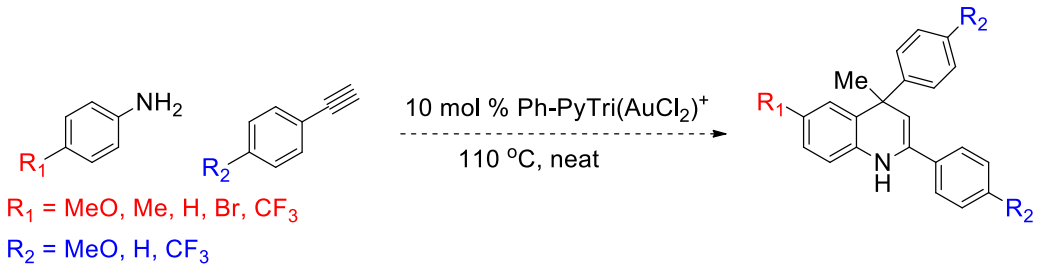

Scheme 5.14 Modular nature of 1,4-dihydroquinoline synthesis allows for installation of multiple substituents based on aniline and alkyne starting materials

Based on the proposed mechanism shown earlier in this chapter, adding donating or withdrawing groups on the two starting materials could have significant effects on the success of this reaction. Unfortunately, when phenylacetylene is replaced with either 4-methoxy-phenylacetylene or 4-trifluoromethy-phenylacetylene there is zero conversion to product over 3 days. It is interesting, however, that in the CF_3-phenylacetylene reaction there was a significant amount of imine formed (as seen by GC). Since the CF_3-substituted aryl alkyne would be more electrophilic, the initial hydroamination step should be significantly easier than with the unsubstituted phenylacetylene. The second step, the hydrovinylation, requires the enamine to act as a nucleophile and it is

possible that the CF_3-benzene moiety hinders this step. The 4-MeO-phenylacetylene shows neither imine nor product, which suggests the donating methoxy group makes the alkyne too electron-rich to undergo the initial hydroamination step.

Varying aniline yielded much different results. Switching from aniline to p-toluidine (R_1 = Me) gave the corresponding 1,4-dihydroquinoline product in low conversion. This product was isolated cleanly and both the ^1H and ^{13}C NMR spectra confirms the structure. Moving to a more electron-rich aniline, p-anisidine where R_1 = MeO, the conversion appeared to be very good by GC. Upon isolation, however, the product had a significantly different ^1H NMR than both the previously isolated 1,4-dihydroquinolines. The most obvious difference was this product's high degree of symmetry: with only 10 unique proton resonances and 17 unique carbons, this product clearly has a very different structure despite it having a mass equal to that of the predicted 1,4-dihydroquinoline. Eventually, the structure was elucidated and it was determined that instead of a 1,4-dihydroquinoline, the product being formed was a 1,4-dihydropyridine (**Figure 5.10**). These types of products have significantly more precedent than the dihydroquinolines as they are common intermediates in Hantzsch pyridine synthesis reactions.[80]

These heterocycles are quite valuable not only for the therapeutic value they have (seen in hugely successful drugs such as amlodipine), but also the ease of which they can be functionalized.[81] Due to the formation of a completely

different product, a mechanism as to why the 1,4-dihydropyridine forms instead of a 1,4-dihydroquinoline needed to be proposed. The working mechanism for how a 1,4-dihydropyridine is accessed is shown in **Scheme 5.15**; the key difference between the mechanism which gives 1,4-dihydroquinolines is the tautomerized hydrovinylation product cyclizes with a third equivalent of alkyne (an aza-Diels-Alder) instead of performing an intra-molecular aza-Cope.

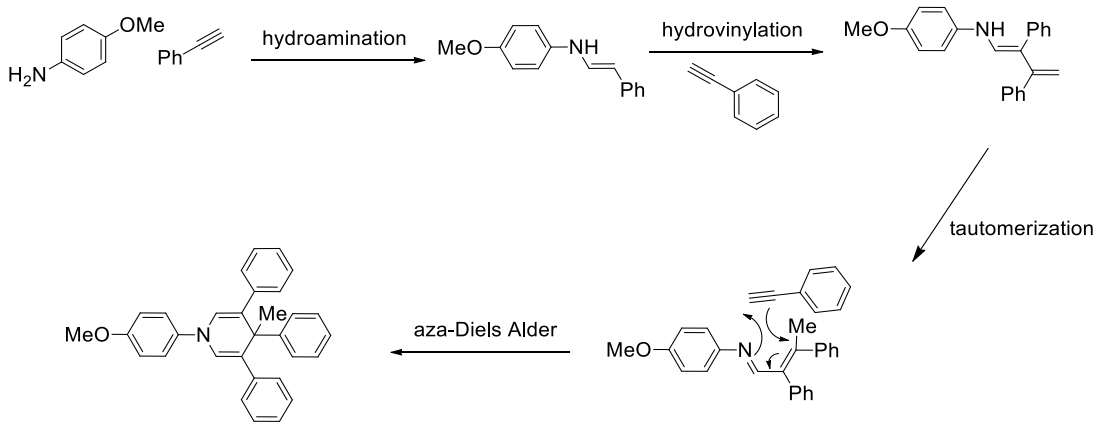

Scheme 5.15 Proposed mechanism for the formation of a 1,4-dihydropyridine involves an intermolecular aza-Diels Alder instead of the previously proposed intramolecular cyclization

The reason for this change in mechanism has yet to be determined absolutely, however this suggests that with a less electron-rich aza-diene, the intermolecular cyclization has too high of an energy barrier (which is why the intramolecular cyclization occurs). Regardless, the fact that these products are accessed not only through gold (III) catalysis, but that only the gold (III) catalysts are able to facilitate these transformations illustrate the value in developing novel gold (III) complexes.

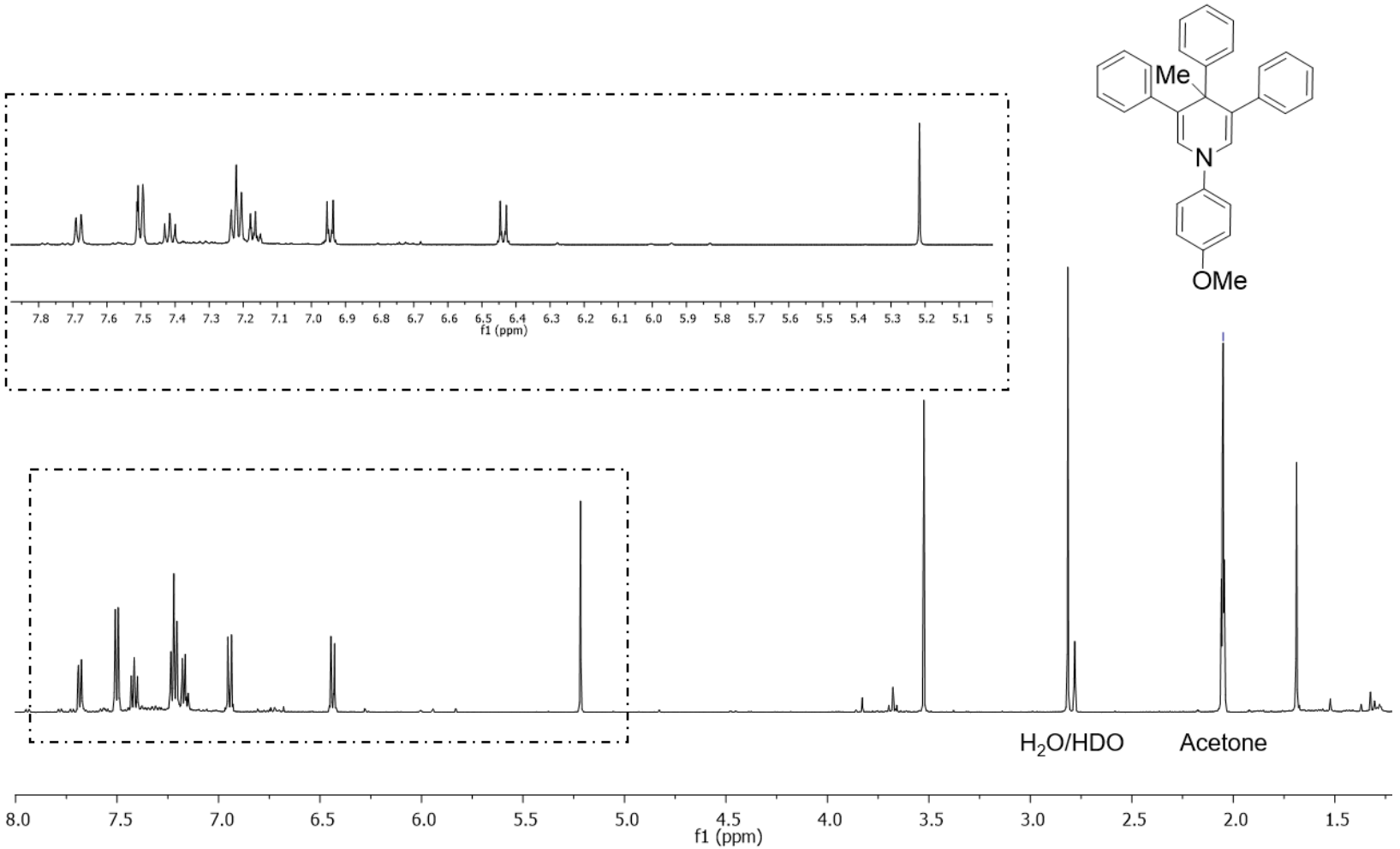

Figure 5.10 ^{1}H NMR of product from *p*-anisidine and phenylacetylene reaction is found to be 1,4-dihydropyridine instead of expected 1,4-dihydroquinoline

As insightful as these investigations into gold (III) complexes and their application as catalysts were, it is quite evident that there is much more that needs to be explored. The fact that these novel gold (III) catalysts showed unique reactivity that no other metal catalyst was able to achieve underscores how valuable they are. It is still not determined how exactly the PyTri ligand functions in terms of catalysis, but control reactions show that it is necessary for conversion to product. In comparison to the PyQuin ligand, the PyTri ligands were more stabilizing to the gold (III) without sacrificing its reactivity. This was attributed to the true four-coordinate square-planar geometry and the fact that the complex was overall cationic due to both nitrogen chelates on the PyTri ligand being L-type. Since the gold (III) complex with a more stabilizing ligand fared better, it was proposed that an even stronger complex may be less susceptible to reduction while still facilitating chemical transformations. For this reason, mixed X-type/L-type bidentate ligands and their corresponding gold complexes were investigated.

5.6 References:

1) Colombano, G.; Travelli, C.; Galli, U.; Caldarelli, A.; Chini, M. G.; Canonico, P. L.; Sorba, G.; Bifulco, G.; Tron, G. C.; Genazzi, A. A. *J. Med. Chem*. **2010**, *52*, 616.

2) Dziedzic, P.; Cisneros, J. A.; Robertson, M. J.; Hare, A. A.; Danford, N. E.; Baxter, R. H. G.; Jorgensen, W. L. *J. Am. Chem. Soc*. **2015**, *137*, 2996.

3) Khan, J. A.; Forouhar, F.; Tao, X.; Tong, L. *Expert Opin. Ther. Targets*. **2007**, *11*, 695.

4) Peterson, E. J.; Menon, V. R.; Gatti, L.; Kipping, R.; Dewasinghe, D.; Perego, P.; Povirk, L. F.; Farrel, N. P. *Mol. Pharm*. **2015**, *12*, 287.

5) Renfrew, A. K.; Bryce, N. S.; Hambley, T*. Chem. Eur. J.* **2015**, *21*, 15224.

6) Millett, A. J.; Habtemariam, A.; Romero-Canelon, I.; Clarkson, G. J.; Sadler, P J*. Organometallics.* **2015**, *34*, 2683.

7) Nardon, C.; Chiara, F.; Brustolin, L.; Gambalunga, A.; Ciscato, F.; Rasola, A.; Trevisan, A.; Fregona, D. *Chemistry Open.* **2015**, *4*, 183.

8) Liu, F.; Suryadi, J.; Bierbach, U. *Chem. Res. Toxicol*. **2015**, *28*, 2170.

9) Donnelly, P. S. *Dalton Trans*. **2011**, *40*, 999.

10) Hartinger, C. G.; Dyson, P. J. *Chem. Soc. Rev*. **2009**, *38*, 391.

11) Hannon, M. *J. Pure Appl. Chem*. **2007**, *79*, 2243.

12) Che, C. M.; Siu, F. M. *Curr. Opin. Chem. Biol*. **2010**, *14*, 255.

13) Sun, R. W. Y.; Che, C. M. Coord. *Chem. Rev*. **2009**, *253*, 1682.

14) Sun, R. W. Y.; Ma, D. L.; Wong, E. L. M.; Che, C. M. *Dalton Trans*. **2007**, 4884.

15) Mewis, R. E.; Archibald, S. J. Coord. *Chem. Rev*. **2010**, *254*, 1686.

16) Metzler-Nolte, N. *Top. Organomet. Chem*. **2010**, *32*, 195.

17) Ducani, C.; Leczkowska, A.; Hodges, N. J.; Hannon, M. J. *Angew. Chem.Int. Ed*. **2010**, *49*, 8942.

18) Sanchez-Cano, C.; Hannon, M. J. *Dalton Trans*. **2009**, 10702.

19) Rach, S. F.; Kuehn, F. E. *Chem. Rev*. **2009**, *109*, 2061.

20) Diez-Gonzalez, S.; Marion, N.; Nolan, S. P. *Chem. Rev*. **2009**, *109*, 3612.

21) Daugulis, O.; Do, H. Q.; Shabashov, D. *Acc. Chem. Res*. **2009**, *42*, 1074.

22) Gruetzmacher, H. *Angew. Chem., Int. Ed*. **2008**, *47*, 1814.

23) Correa, A.; Garcia Mancheno, O.; Bolm, C. *Chem. Soc. Rev*. **2008**, *37*, 1108.

24) Kempe, R. *Chem. Eur. J*. **2007**, *13*, 2764.

25) Sandee, A. J.; Reek, J. N. H. *Dalton Trans*. **2006**, 3385.

26) Wilkinson, M. J.; van Leeuwen, P. W. N. M.; Reek, J. N. H. *Org. Biomol.Chem*. **2005**, *3*, 2371.

27) Hein, J. E.; Fokin, V. V. *Chem. Soc. Rev*. **2010**, *39*, 1302.

28) Meldal, M.; Tornoe, C. W. *Chem. Rev*. **2008**, *108*, 2952.

29) Wu, P.; Fokin, V. V. *Aldrichim. Acta* **2007**, *40*, 7.

30) Bolje, A.; Kosmrij, J. *Org. Lett.* **2013**, *15*, 5084.

31) Nakamura, T.; Terashima, T.; Ogata, K.; Fukuzawa, S. I. *Org. Lett*. **2011**, *13*, 620.

32) Poulain, A.; Canseco-Gonzalez, D.; Hynes-Roche, R.; Muller-Bunz, H.; Schuster, O.; Stoeckli-Evans, H.; Neels, A.; Albrecht, M. *Organometallics* **2011**, *30*, 1021.

33) Nakamura, T.; Ogata, K.; Fukuzawa, S. I. *Chem. Lett*. **2010**, *39*, 920.

34) Partyka, D. V.; Gao, L.; Teets, T. S.; Updegraff, J. B.; Deligonul, N.; Gray, T. G. *Organometallics* **2009**, *28*, 6171.

35) Partyka, D. V.; Updegraff, J. B., III; Zeller, M.; Hunter, A. D.; Gray, T. G. *Organometallics* **2007**, *26*, 183.

36) Mathew, P.; Neels, A.; Albrecht, M. *J. Am. Chem. Soc*. **2008**, *130*, 13534.

37) Manbeck, G. F.; Brennessel, W. W.; Eisenberg, R. *Inorg. Chem*. **2011**, *50*, 3431.

38) Fleischel, O.; Wu, N.; Petitjean, A. *Chem. Commun*. **2010**, *46*, 8454.

39) Manbeck, G. F.; Brennessel, W. W.; Evans, C. M.; Eisenberg, R. *Inorg.Chem*. **2010**, *49*, 2834.

40) Chevry, A.; Teyssot, M. L.; Maisonial, A.; Lemoine, P.; Viossat, B.; Traikia, M.; Aitken, D. J.; Alves, G.; Morel, L.; Nauton, L.; Gautier, A. *Eur. J. Inorg. Chem*. **2010**, 3513.

41) Crowley, J. D.; Bandeen, P. H.; Hanton, L. R. *Polyhedron* **2010**, *29*, 70.

42) Crowley, J. D.; Bandeen, P. H. *Dalton Trans.* **2010**, *39*, 612.

43) Kumar, S. V.; Scottwell, S. O.; Waugh, E.; McAdam, C. J.; Hanton, L. R.; Brooks, H. J. L.; Crowley, J. D. *Inorg. Chem.* **2016**, *55*, 9767.

44) Kim, T. Y.; Elliot, A. B. S.; Shaffer, K. J.; McAdam, C. J.; Gordon, K. C.; Crowley, J. D. *Polyhedron* **2013**, *52*, 1391.

45) Zakharchenko, B. V.; Khomenko, D. M.; Doroschuk, R. O.; Lampeka, R. D. *Fr.-Ukr. J. Chem.* **2015**, *3*, 1.

46) Jindabot, S.; Teerachanan, K.; Thonkam, P.; Kiatisevi, S.; Khamnaen, T. Phiriyawirut, P.; Charoenchaidet, S.; Sooksimuang, T.; Kongsaeree, P.; Sangtrirutnugul, P. *J. Organomet. Chem.* **2014**, *750*, 35.

47) Lo, W. K. C.; Huff, G. S.; Cubanski, J. R.; Kennedy, A. D. W.; McAdam, C. J.; McMorran, D. A.; Gordon, K. C.; Crowley, J. D. *Inorg. Chem.* **2015**, *54*, 1572.

48) Schweinfurth, D.; Pattacini, R.; Strobel, S.; Sarkar, B. *Dalton Trans.* **2009**, 9291.

49) Schweinfurth, D.; Strobel, S.; Sarkar, B. *Inorganica Chim. Acta* **2011**, *374*, 253.

50) Pages, B. J.; Sakoff, J.; Gilbert, J.; Zhang, Y.; Li, F.; Preston, D.; Crowley, J. D.; Aldrich-Wright, J. R. *J. Inorg. Biochem.* **2016**, *165*, 92.

51) Felici, M.; Contreras-Carballada, P.; Vida, Y.; Smits, J. M. M.; Nolte, R. J. M.; De Cola, L.; Williams, R. M.; Feiters, M. C. *Chem. Eur. J*. **2009**, *15*, 13124.

52) Rudakov, E. S.; Shul'pin, G. B. Stable *J. Organomet. Chem.* **2015**, *793*, 4.

53) Abu-Surrah, A.; Kettunen, M. *Curr. Med. Chem.* **2006**, *13* (11), 1337.

54) Billingsley, K. L.; Anderson, K. W.; Buchwald, S. L.; *Angew. Chem. Int. Ed*. **2006**, *45*, 3484.

55) Fleckenstein, C.A.; Plenio, H. *Chem. Eur. J*. **2007**, *13*, 2701.

56) Fleckenstein, C.A.; Plenio, H. *J. Org. Chem*. **2008**, *73*, 3236.

57) Hoshi, T.; Nakazawa, T.; Saitoh, I.; Mori, A.; Suzuki, T.; Sakai, J.; Hagiwara, H. *Org. Lett*. **2008**, *10*, 2063.

58) Martin, R.; Buchwald, S. L. *Acc. Chem. Res*. **2008**, *41*, 1461.

59) Altenhoff, G.; Goddard, R.; Lehmann, C. W.; Glorius, F. *Angew. Chem. Int. Ed*. **2003**, *42*, 3690.

60) Diebolt, O.; Braunstein, P.; Nolan, S. P.; Cazin, C. S. J. *Chem. Commun*. **2008**, 3190.

61) Kantchev, E. A. B.; O'Brien, C. J.; Organ, M. G. *Angew. Chem. Int. Ed*. **2007**, *46*, 2768.

62) Marion, N.; Navarro, O.; Mei, J.; Stevens, E. D.; Scott, N. M.; Nolan, S. P. *J. Am. Chem. Soc.* **2006**, *128*, 4101.

63) Micksch, M.; Strassner, T. *Eur. J. Inorg. Chem*. **2012**, 5872.

64) O'Brien, C. J.; Kantchev, E. A. B.; Valente, C.; Hadei, N.; Chass, G. A.; Lough, A.; Hopkinson, A. C.; Organ, M. G. *Chem. Eur. J*. **2006**, *12*, 4743.

65) Organ, M. G.; Calimsiz, S.; Sayah, M.; Hoi, K. H.; Lough, A. J. *Angew. Chem. Int. Ed*. **2009**, *48*, 2383.

66) Ross, S. A.; Lowe, G. *Tetrahedron Lett.* **2000**, *41*, 3225.

67) Cinellu, M. A.; Maiore, L.; Minghetti, G.; Cocco, F.; Stoccoro, S.; Zucca, A.; Manassero, M.; Manassero, C. *Organometallics* **2009**, *28* (24), 7015.

68) Hashmi, A. S. K. *Chem. Rev*. **2007**, *107*, 3180.

69) Musiol, R. *Expert Opin. Drug Discov.* **2017**, *12* (6), 583.

70) Johnson, M.A.; Maggiora, G.M. Eds “Concepts and Applications of Molecular Similarity” Wiley, New York, **1990**.

71) Palchak, Z. L.; Lussier, D. J.; Pierce, C. J.; Yoo, H.; Larsen, C. H. *Adv. Synth. Catal.* **2015**, *357*, 539.

72) V. Sridharan, P. A. Suryavanshi and J. C. Menendez, *Chem. Rev*., **2011**, *111*, 7157.

73) J. A. Sikorski, *J. Med. Chem*.,**2006**, *49*, 1.

74) Hemmer, M.; Kraqczyk, S.; Simon, I.; Hilgeroth, A. *Bioorg. Med. Chem. Lett*. **2015,** *25,* 3005.

75) (a) Rudler, H.; Denise, B.; Xu, Y.; Parlier, A.; Vaissermann, *J. Eur. J. Org. Chem.* **2005**, *17*, 3724. (b) Ng, F. W.; Lin, H.; Danishefsky, S. J. *J. Am. Chem. Soc*. **2002**, *124*, 9812. (c) Schmidt, A.; Michalik, D.; Rotzoll, S.; Ullah, E.; Fischer, C.; Reinke, H.; Goerls, H.; Langer, P. *Org. Biomol. Chem*. **2008**, *6,* 2804. (d) Dounay, A. B.; Hatanaka, K.; Kodanko,J. J.; Oestreich, M.; Overman, L. E.; Pfeifer, L. A.; Weiss, M. M*. J. Am. Chem. Soc*. **2003**, *125*, 6261.

76) (a) Selvakannan, P. R.; Mandal, S.; Phadtare, S.; Gole, A.; Pasricha, R.; Adyanthaya, S. D.; Sastry, M. *J. Colloid Interface Sci*. **2004**, *269*, 97. (b) Bhargava, S. K.; Booth, J. M.; Agrawal, S.; Coloe, P.; Kar, G. *Langmuir* **2005**, *21*, 5949. (c) Aslam, M.; Fu, L.; Su, M.; Vijayamohanan, K.; Dravid, V. P. *J. Mater. Chem.* **2004**, *14*, 1795. (d) Iwamoto, M.; Kuroda, K.; Zaporojtchenko, V.; Hayashi, S.; Faupel, F*. Eur. Phys. J. D: Atomic, Mol., Opt. Phys*. **2003**, *24*, 365. (e) Leff, D. V.; Brandt, L.; Heath, J. R. *Langmuir* **1996**, *12*, 4723 (f) Subramaniam, C.; Tom, R. T.; Pradeep, T. *J. Nanopart. Res*. **2005**, *7,* 209.

77) Newman, J. D. S.; Blanchard, G. J. *Langmuir* **2006**, *22*, 5882.

78) Shan, J.; Han, L.; Bai, F.; Cao, S. *Polym. Adv. Technol*. **2003**, *14*, 330.

79) Mallick, K.; Witcomb, M. J.; Dinsmore, A.; Scurrell, M. S. *Macromol. Rapid Commun.* **2005**, *26*, 232.

80) (a) A. Kumar, R. A. Maurya, *Synlett*, **2008**, 883. (b) G. V. M. Sharma, K. L. Reddy, P. S. Lakshmi, P. R. Krishna, *Synthesis*, **2006**, 55. (c) A. Debache, R. Boulcina, A. Belfaitah, S. Rhouati, B. Carboni, *Synlett*, **2008**, 509. (d) R. Gupta, R. Gupta, S. Paul, A. Loupy, *Synthesis*, **2007**, 2835.

81) *World Health Organization*. "WHO Model List of Essential Medicines" **2015**.

5.7 Supporting Information

General Reagent Information

All reactions were set up on the benchtop in oven-dried glassware or dried scintillation vials. Flash column chromatography was performed using silica purchased from Silicycle. Solvents for chromatography were purchased from Fisher Chemicals and used as obtained. HPLC grade Tetrahydrofuran and Acetonitrile was purchased from Fisher Chemicals and dried via passage through activated alumina in a commercial solvent purification system (Pure Process Technologies, Inc.). NMR solvents were purchased from Acros Organics or Cambridge Isotope Laboratories and used as obtained. Anilines were purchased from Oakwood Chemicals, Chem-Impex International, and Acros Organics and distilled before use. 2-ethynylpyridinewas purchased from Ark Pharm Inc. and distilled before use. Sodium azide was purchased from Fisher Chemicals and used as obtained. Sodium nitrite was purchased from Wards Science and used as obtained. Sodium tetrafluoroborate was purchased from Strem Chemicals and used as obtained. Copper(I) iodide was purchased from Sigma Aldrich, stored in a glove box under Nitrogen and used as obtained. Sodium tetrachloroaurate dihydrate was purchased from Alfa Aesar and stored in a glove box under nitrogen and used as obtained.

General analytical information

^{1}H and ^{13}C NMR spectra were measured on a Varian Inova 500 (500 MHz) spectrometer using acetone-d_6 or $CDCl_3$ as solvents and tetramethylsilane as an internal standard. The following abbreviations are used singularly or in combination to indicate the multiplicity of signals: s - singlet, d - doublet, t - triplet, q - quartet, qn - quintet, sx - sextet, sp - septet, m - multiplet and br - broad. NMR spectra were acquired at 300 K. Gas chromatography (GC) was carried out on an Agilent Technologies 6850 Network GC System, and dodecane was used as the internal standard. ATR-IR spectra were taken on a Bruker:ALPHA FTIR Spectrometer. Attenuated total reflection infrared (ATR-IR) was used and the spectra was analyzed using the OPUS software with selected absorption maxima reported in wavenumbers (cm^{-1}). Mass spectrometric data was collected on a HP 5989A GC/MS quadrupole instrument. Exact masses were recorded on a Waters GCT Premier TOF instrument using direct injection of samples in methanol/acetonitrile into the electrospray source.

General Procedure for the Production of Pyridyl Triazoles (PyTri)

To a 20 mL scintillation vial equipped with a magnetic stir bar and PTFE coated screw cap was added copper(II) sulfate pentahydrate ($CuSO_4 \cdot 5\ H_2O$) and the vial was purged with argon for 5 min. Ethanol (EtOH) was added followed by DIH_2O in a ratio 2/3 EtOH and 1/3 DI-H_2O. Sodium ascorbate (Na•Asc) was added and the solution turns a dark brown color. Phenyl azide bearing the

desired substitution was added dropwise followed by dropwise addition of 2-ethynyl pyridine. The reaction was allowed to run at ambient temperature for 18h. Upon completion the reaction was diluted with H_2O and the product was extracted with ethyl acetate (EtOAc). The organic extracts were combined, washed with brine, and dried over sodium sulfate. Column chromatography was performed on silica using EtOAc/Hexanes as an eluent. The desired pyridyl triazoles were obtained as solids.

2-(1-(4-methoxyphenyl)-1H-1,2,3-triazol-4-yl)pyridine (MeOPyTri) (3a): $CuSO_4 \cdot 5\ H_2O$ (50 mg, 0.2 mmol) was added to a scintillation vial and purged with argon for 5 min. EtOH (14 mL) and DI-H_2O (7 mL) were added followed by Na•Asc (198 mg, 1 mmol). 1-azido-4-methoxybenzene (745 mg, 5 mmol) was added dropwise, followed by dropwise addition of 2-ethynylpyridine (222 µL, 2.2 mmol). The reaction was run at ambient temperature for 18 h to afford the title compound as a white solid in 97% yield (536 mg, 2.1 mmol) after a gradient column chromatography on silica gel (20% EtOAc/Hexanes up to 50% EtOAc/Hexanes). ATR-IR: 3142, 3004, 2924, 2841, 1591, 1514, 1258, 1023, 17 6824, 777, 716, 515 cm^{-1}. ^1H NMR (500 MHz, acetone-d_6) δ 8.85 (s, 1H), 8.62 (d,J = 4 Hz, 1H), 8.18 (d, J = 8 Hz, 1H), 7.92 (d, J = 8.5 Hz, 2H), 7.90 (t, J = 6 Hz,1H), 7.34 (t, J = 6 Hz, 1H), 7.17 (d, J = 9 Hz, 2H), 3.90 (s, 3H). ^{13}C NMR (125 MHz, acetone-d_6) δ 160.9, 151.4, 150.6, 149.6, 137.7, 131.5, 123.8, 122.8, 121.4, 120.5, 115.7, 56.0. HRMS calculated requires $[M+H]^+$: 253.1084. Found *m/z*: 253.0975.

2-(1-(4-methylphenyl)-1H-1,2,3-triazol-4-yl)pyridine (MePyTri) (3b):

$CuSO_4$ • 5 H_2O (50 mg, 0.2 mmol) was added to a scintillation vial and purged with argon for 5 min. EtOH (14 mL) and DI-H_2O (7 mL) were added followed by Na•Asc (198 mg, 1 mmol). 1-azido-4-methylbenzene (665 mg, 5 mmol) was added dropwise, followed by dropwise addition of 2-ethynylpyridine (222 µL, 2.2 mmol). The reaction was run at ambient temperature for 18 h to afford the title compound as a white solid in 98% yield (509 mg, 2.2 mmol) after column chromatography on silica gel (30% EtOAc/Hexanes). ATR-IR: 3118, 2999, 2921, 1591, 1517, 1400, 1232, 1035, 814, 792, 533, 471 cm^{-1}. ^1H NMR (500 MHz, acetone-d_6) δ 8.91 (s, 1H), 8.62 (d, J = 4 Hz, 1H), 8.19 (d, J = 8 Hz, 1H), 7.90 (m, 3H), 7.44 (d, J = 8 Hz, 2H), 7.35 (t, J = 6 Hz, 1H), 2.34 (s, 3H). ^{13}C NMR (125 MHz, acetone-d_6) δ 151.3, 150.6, 149.7, 139.7, 137.7, 135.9, 131.1, 123.8, 121.3, 121.1, 120.6, 21.0. HRMS calculated requires $[M+H]^+$: 237.1135. Found *m/z*: 237.1055.

2-(1-phenyl)-1H-1,2,3-triazol-4-yl)pyridine (PyTri) (3c):

$CuSO_4$ • 5 H_2O (175 mg, 0.5 mmol) was added to a scintillation vial and purged with argon for 5 min. EtOH (40 mL) and DI-H_2O (20 mL) were added followed by Na•Asc (693 mg, 3.5 mmol). 1-azido-benzene (1.55 g, 13 mmol) was added dropwise, followed by dropwise addition of 2-ethynylpyridine (707 µL, 7 mmol).

The reaction was run at ambient temperature for 18 h to afford the title compound as an orange solid in 90% yield (1.4 g, 6.3 mmol) after column chromatography on silica gel (30% EtOAc/Hexanes). ATR-IR: 3118, 3051, 1592, 1502, 1403, 1236, 1035, 756, 684, 533 cm^{-1}. ^{1}H NMR (500 MHz, acetone-d_6) δ 8.97 (s, 1H), 8.63 (d, J = 4.5 Hz, 1H), 8.20 (d, J = 7.5 Hz, 1H), 8.04 (d, J = 8 Hz, 2H), 7.92 (t, J = 7.5, 1H), 7.66 (t, J = 7 Hz, 2H), 7.54 (t, J = 7 Hz, 1H), 7.36 (t, J = 6.5 Hz, 1H). ^{13}C NMR (125 MHz, acetone-d_6) δ 151.2, 150.6, 149.8, 138.1, 137.7, 130.7, 129.6, 123.9, 121.4, 121.2, 120.6. HRMS calculated requires $[M+H]^+$: 223.0978. Found *m/z*: 223.0895.

2-(1-(4-bromophenyl)-1H-1,2,3-triazol-4-yl)pyridine (BrPyTri) (3d):

$CuSO_4$ • 5 H_2O (50 mg, 0.2 mmol) was added to a scintillation vial and purged with argon for 5 min. EtOH (14 mL) and DI-H_2O (7 mL) were added followed by Na•Asc (198 mg, 1 mmol). 1-azido-4-bromobenzene (990 mg, 5 mmol) was added dropwise, followed by dropwise addition of 2-ethynylpyridine (202 µL, 2.0 mmol). The reaction was run at ambient temperature for 18 h to afford the title compound as an off-white solid in 63% yield (377 mg, 1.3 mmol) after column chromatography on silica gel (30% EtOAc/Hexanes). ATR-IR: 3128, 3097, 3054, 2919, 1600, 1495, 1396, 1235, 1009, 817, 779, 494 cm^{-1}. ^{1}H NMR (500 MHz, acetone-d_6) δ 9.01 (s, 1H), 8.64 (d, J = 4 Hz, 1H), 8.18 (d, J = 8 Hz, 1H), 8.02 (d, J = 9 Hz, 2H), 7.92 (t, J = 8 Hz, 1H), 7.83 (d, J = 8.5 Hz, 2H), 7.36 (t, J = 5.5 Hz,

1H). ^{13}C NMR (125 MHz, acetone-d_6) δ 151.0, 150.6, 150.0, 137.8, 137.3, 133.8, 124.0, 123.0, 122.6, 121.5, 120.6. HRMS calculated requires $[M+H]^+$: 301.0083. Found *m/z*: 300.9958.

2-(1-(4-(trifluoromethyl)phenyl)-1H-1,2,3-triazol-4-yl)pyridine (CF_3PyTri) (3e): $CuSO_4$ • 5 H_2O (200 mg, 0.8 mmol) was added to a scintillation vial and purged with argon for 5 min. EtOH (40 mL) and DI-H_2O (20 mL) were added followed by Na•Asc (792 mg, 4 mmol). 1-azido-4-(trifluoromethyl)benzene (2.84 g, 15 mmol) was added dropwise, followed by dropwise addition of 2-ethynylpyridine (808 µL, 8 mmol). The reaction was run at ambient temperature for 18 h to afford the title compound as a white solid in 73% yield (1.69 g, 5.8 mmol) after column chromatography on silica gel (30% EtOAc/Hexanes). ATR-IR: 3121, 3092, 3060, 1570, 1409, 1322, 1159, 1105, 1066, 846, 785, 596, 496 cm^{-1}. ^{1}H NMR (500 MHz, acetone-d_6) δ 9.13 (s, 1H), 8.65 (d, J = 4.5 Hz, 1H), 8.32 (d, J = 8.5 Hz, 2H), 8.20 (d, J = 8 Hz, 1H), 8.01 (d, J = 8.5 Hz, 2H), 7.93 (td, J = 1.5 Hz, J = 8 Hz, 1H), 7.37 (td, J = 1.5 Hz, J = 4.5 Hz, 1H). ^{13}C NMR (125 MHz, acetone-d_6) δ 150.8, 150.7, 150.1, 140.8, 137.8, 130.7, 128.0, 126.0, 124.1, 123.8, 121.6, 120.7. HRMS calculated requires $[M+H]^+$: 291.0852. Found *m/z*: 291.0768.

General procedure for the production of $(PyTri)_2Pt(BF4)_2$ complexes: To an 8 mL scintillation vial equipped with a magnetic stir bar and Teflon-seal screw cap was added $PtCl_2$. MeCN was added as solvent followed by the PyTri

ligand bearing the desired substitution dissolved in minimal MeCN. The reaction was heated to 65 °C and allowed to run for 30 min. The reaction was removed from heat and $AgBF_4$, dissolved in minimal MeCN was added dropwise. The reaction was placed back on the heating block at 65 °C and allowed to proceed for 18 h. During this time, precipitation of the bis-complex occurred. This solid was collected using a centrifuge and washed 3 times with cold MeCN to remove impurities. The bis-complex was obtained as a tan solid and was recrystallized out of boiling MeCN.

Synthesis of $(CF_3$-PyTri$)_2Pt(BF_4)_2$:

$PtCl_2$ (26 mg, 0.1 mmol) was added to an 8 mL scintillation vial equipped with a magnetic stir bar and Teflon-seal screw cap. MeCN (5 mL) was added as solvent. CF_3-PyTri ligand (72 mg, 0.25 mmol) was dissolved in minimal MeCN and added dropwise. The reaction was placed on a heating block at 65 °C and allowed to stir for 30 min. The reaction was removed from heat and $AgBF_4$ (38 mg, 0.2 mmol) dissolved in minimal MeCN was added dropwise. The reaction was placed back on the heating block and stirred for 18 h at 65 °C during which time the desired complex precipitated out of solution. The title compound was obtained as a tan solid in 92% yield (87 mg, 0.092 mmol). ATR-IR: 3111, 1608, 1326, 1061, 846, 781, 518, 452 cm^{-1}. ^1H NMR (500 MHz, DMSO-d_6) δ 10.36 (s, 1H), 9.94 (d, J = 6 Hz, 1H), 8.72 (td, J = 1 Hz, J = 7 Hz, 1H), 8.51 (m, 3H), 8.26

(d, J = 8.5 Hz, 2H), 8.13 (td, J = 1 Hz, J = 6.5 Hz, 2H). ^{13}C NMR (125 MHz, DMSO-d_6) δ 152.5, 150.1, 147.6, 144.0, 138.4, 128.1, 127.8, 126.6, 124.9, 123.1, 122.6, 118.1.

General procedure for the production of PyTriPtCl$_2$ complexes:

To an 8 mL scintillation vial equipped with a magnetic stir bar and Teflon-seal screw cap was added $PtCl_2(DMSO)_2$. MeCN was added as solvent followed by the PyTri ligand bearing the desired substitution dissolved in minimal MeCN. The reaction was stirred at ambient temperature for 18 h. Once completed, the reaction solution was passed through a plug of Celite and concentrated until a saturated solution was obtained. Upon standing, the PyTriPtCl$_2$ complex precipitated as a microcrystalline powder. Recrystallization of these complexes occurred in $MeNO_2$.

Synthesis of PyTriPtCl$_2$:

$PtCl_2(DMSO)_2$ (46 mg, 0.11 mmol) was added to an 8 mL scintillation vial equipped with a magnetic stir bar and Teflon-seal screw cap. MeCN (5 mL) was added as solvent. PyTri ligand (22 mg, 0.1 mmol) was dissolved in minimal MeCN and added dropwise. The reaction was stirred at ambient temperature for 18 h. During this time the desired complex precipitated out of solution. The title compound was obtained as a tan solid in 90% yield (44 mg, 0.09 mmol). ATR-IR: 3147, 3057, 1628, 1594, 1500, 1464, 1285, 1074, 768, 695, 497, 431 cm^{-1}. ^{1}H NMR (500 MHz, DMSO-d_6) δ 9.91 (s, 1H), 9.35 (d, J = 6.5 Hz, 1H), 8.41 (td, J =

1.5 Hz, J = 6.5 Hz, 1H), 8.19 (d, J = 8 Hz, 1H), 7.93 (d, J = 7.5 Hz, 2H), 7.76 (td, J = 1 Hz, J = 4.5 Hz, 1H), 7.72 (t, J = 8 Hz, 2H), 7.67 (tt, J = 2 Hz, J = 7 Hz, 1H). ^{13}C NMR (125 MHz, DMSO-d_6) δ 149.0, 148.9, 148.6, 141.0, 136.1, 130.6, 130.3, 126.2, 124.9, 122.2, 121.1. Elemental analysis for PyTriPtCl_2 ($C_{13}H_{10}Cl_2N_4Pt$): *Calculated* – C: 31.98, H: 2.06, N: 11.48. *Found* – C: 31.57, H: 1.98, N: 11.26.

General procedure for the production of PyTriPdCl_2 complexes:

To an 8 mL scintillation vial equipped with a magnetic stir bar and Teflon-seal screw cap was added $PdCl_2(MeCN)_2$. DCM was added as solvent followed by the PyTri ligand bearing the desired substitution dissolved in minimal DCM. The reaction was stirred at ambient temperature for 18 h during which, precipitation of the complex occurred. The solid was collected via a centrifuge and washed 5 times with DCM to remove impurities. Recrystallization of these complexes occurred in DMF or $MeNO_2$.

Synthesis of Me-PyTriPdCl_2:

$PdCl_2(MeCN)_2$ (39 mg, 0.15 mmol) was added to an 8 mL scintillation vial equipped with a magnetic stir bar and Teflon-seal screw cap. DCM (5 mL) was added as solvent. MePyTri ligand (23 mg, 0.1 mmol) was dissolved in minimal DCM and added dropwise. The reaction was stirred at ambient temperature for 18 h. During this time the desired complex precipitated out of solution. The solid

was collected in a centrifuge tube and washed 5 times with DCM. The title compound was obtained as an orange solid in 83% yield (34 mg, 0.083 mmol). ATR-IR: 3095, 1623, 1514, 1462, 1283, 813, 774, 499, 419 cm^{-1}. ^{1}H NMR (500 MHz, DMSO-d_6) δ 9.83 (s, 1H), 9.01 (d, J = 5.5 Hz, 1H), 8.37 (t, J = 7.5 Hz, 1H), 8.16 (d, J = 7.5 Hz, 1H), 7.80 (d, J = 8 Hz, 2H), 7.75 (t, J= 6.5 Hz, 1H), 7.51 (d, J = 8 Hz, 2H), 2.43 (s, 3H). ^{13}C NMR (125 MHz, DMSO-d_6) δ 149.6, 148.2, 148.1, 141.6, 140.6, 133.6, 130.6, 125.8, 124.1, 122.0, 120.9 20.7.

General Procedure for the Production of PyTriAuCl$_2$ Complexes:

To a 20 mL scintillation vial equipped with a magnetic stir bar and Teflon-seal screw cap was added $NaAuCl_4$. MeCN was added as solvent followed by the PyTri ligand bearing the desired substitution dissolved in minimal MeCN. The reaction was placed on a heating block at 80 °C and allowed to stir for 1 hour. The reaction was then taken off the heat and silver tetrafluoroborate dissolved in minimal MeCN was added and returned to the heat. Precipitation of AgCl occurs as the reaction heats and stirs over 4 hours. The reaction was filtered through a Celite pipette plug into a vial and the filtrate was concentrated to give the product as a yellow solid. Recrystallization of these complexes occurred in MeCN or toluene.

Synthesis of MeO-PyTriAuCl$_2^+$

$NaAuCl_4 \cdot 2H_2O$ (99 mg, 0.25 mmol) was added to a 20 mL scintillation vial equipped with a magnetic stir bar and Teflon-seal screw cap. MeCN (5 mL) was

added as solvent. MeO-PyTri ligand (63 mg, 0.25 mmol) was dissolved in minimal MeCN and added. The reaction was placed on a heating block at 80 °C and allowed to stir for 1 hour. After one hour, silver tetrafluoroborate (97 mg, 0.5 mmol) dissolved in minimal MeCN was added. After 4 hours the reaction mixture was filtered through Celite and the filtrate concentrated to give the compound as a yellow solid in quantitative yield. ATR-IR: 3226, 3141, 3082, 3030, 1567, 1455, 1440,1373, 1331,458, 422 cm^{-1}. ^1H NMR (500 MHz, DMSO-d_6): 9.32 (s, 1H), 8.70 (d, J = 7.5 Hz, 1H), 8.18 (d, J = 7.5 Hz, 1H), 8.10 (t, J = 5.5 Hz, 1H), 7.93 (d, J = 7.5 Hz, 2H), 7.52 (t, J = 5.5 Hz, 1H), 7.17 (d, J = 7.5 Hz, 2H), 3.85 (s, 1H).

Synthesis of Me-PyTriAuCl$_2^+$

$NaAuCl_4 \cdot 2H_2O$ (99 mg, 0.25 mmol) was added to a 20 mL scintillation vial equipped with a magnetic stir bar and Teflon-seal screw cap. MeCN (5 mL) was added as solvent. Me-PyTri ligand (59 mg, 0.25 mmol) was dissolved in minimal MeCN and added. The reaction was placed on a heating block at 80 °C and allowed to stir for 1 hour. After one hour, silver tetrafluoroborate (97 mg, 0.5 mmol) dissolved in minimal MeCN was added. After 4 hours the reaction mixture was filtered through Celite and the filtrate concentrated to give the compound as a yellow solid in quantitative yield. ATR-IR: 3260, 3242, 3100, 3028, 1577, 1452, 1455,1368, 1328,460, 435 cm^{-1}. ^1H NMR (500 MHz, DMSO-d_6): 9.45 (s, 1H), 8.73 (d, J = 7.5 Hz, 1H), 8.24 (t, J = 5.5 Hz, 2H), 7.88 (d, J = 7.5 Hz, 2H), 7.62 (t, J = 5.5 Hz, 1H), 7.48 (d, J = 7.5 Hz, 2H), 2.41 (s, 3H).

Synthesis of PyTriAuCl$_2^+$

$NaAuCl_4 \cdot 2H_2O$ (99 mg, 0.25 mmol) was added to a 20 mL scintillation vial equipped with a magnetic stir bar and Teflon-seal screw cap. MeCN (5 mL) was added as solvent. PyTri ligand (55 mg, 0.25 mmol) was dissolved in minimal MeCN and added. The reaction was placed on a heating block at 80 °C and allowed to stir for 1 hour. After one hour, silver tetrafluoroborate (97 mg, 0.5 mmol) dissolved in minimal MeCN was added. After 4 hours the reaction mixture was filtered through Celite and the filtrate concentrated to give the compound as a yellow solid in quantitative yield. ATR-IR: 3250, 3262, 3122, 3024, 1587, 1466, 1457,1378, 1333,462, 440 cm^{-1}. ^{1}H NMR (500 MHz, DMSO-d_6): 9.49 (s, 1H), 8.73 (d, J = 7.5 Hz, 1H), 8.21 (d, J = 7.5 Hz, 1H), 8.14 (t, J = 5.5 Hz, 1H), 8.03 (d, J = 7.5 Hz, 2H), 7.65 (t, J = 5.5 Hz, 2H), 7.56 (m, J = 7.5 Hz, 2H)

Synthesis of Br-PyTriAuCl$_2^+$

$NaAuCl_4 \cdot 2H_2O$ (99 mg, 0.25 mmol) was added to an 20 mL scintillation vial equipped with a magnetic stir bar and Teflon-seal screw cap. MeCN (5 mL) was added as solvent. Br-PyTri ligand (75 mg, 0.25 mmol) was dissolved in minimal MeCN and added. The reaction was placed on a heating block at 80 °C and allowed to stir for 1 hour. After one hour, silver tetrafluoroborate (97 mg, 0.5 mmol) dissolved in minimal MeCN was added. After 4 hours the reaction mixture was filtered through Celite and the filtrate concentrated to give the compound as a yellow solid in quantitative yield. ATR-IR: 3253, 3244, 3128, 3044, 1597, 1462,

1456,1378, 1328,457, 429 cm^{-1}. ^1H NMR (500 MHz, DMSO-d_6): 9.47 (s, 1H), 8.71 (d, J = 7.5 Hz, 1H), 8.18 (d, J = 7.5 Hz, 1H), 8.11 (t, J = 5.5 Hz, 1H), 7.99 (d, J = 7.5 Hz, 2H), 7.86 (t, J = 5.5 Hz, 2H), 7.54 (t, J = 5.5 Hz, 1H)

Synthesis of CF_3-PyTriAuCl_2^+

$NaAuCl_4 \cdot 2H_2O$ (99 mg, 0.25 mmol) was added to an 20 mL scintillation vial equipped with a magnetic stir bar and Teflon-seal screw cap. MeCN (5 mL) was added as solvent. CF_3-PyTri ligand (73 mg, 0.25 mmol) was dissolved in minimal MeCN and added. The reaction was placed on a heating block at 80 °C and allowed to stir for 1 hour. After one hour, silver tetrafluoroborate (97 mg, 0.5 mmol) dissolved in minimal MeCN was added. After 4 hours the reaction mixture was filtered through Celite and the filtrate concentrated to give the compound as a yellow solid in quantitative yield. ATR-IR: 3260, 3234, 3130, 3042, 1600, 1455, 1441,1369, 1340,460, 411 cm^{-1}. ^1H NMR (500 MHz, DMSO-d_6): 9.61 (s, 1H), 8.73 (d, J = 5.5 Hz, 1H), 8.30 (d, J = 5.5 Hz, 2H), 8.22 (d, J = 5.5 Hz, 1H), 8.14 (t, J = 7.5 Hz, 1H), 8.04 (d, J = 7.5 Hz, 2H), 7.57 (t, J = 5.5 Hz, 1H)

Synthesis of 4-methyl-3,4-diphenyl-1,4-dihydroquinoline:

To an 8 ml vial, PyTriAuCl_2BF_4 (0.1 mmol, 49 mg) is added and purged with argon. Aniline (1 mmol, 90 µL) and phenylacetylene (3 mmol, 300 µL) are added and the placed on a heating block set to 110 °C. The reaction was allowed to heat and stir for 3 days, at which point it is removed from heat and cooled to

room temperature. Methylene chloride is added to solubilize the crude mixture and loaded onto a silica column. The product is separated from the crude mixture with column chromatography (1% Et_2O:Hexanes) and isolated in a 30% yield (90 mg) as an off-white solid. ATR-IR: 3367 (*broad*), 3150, 3122, 3017, 2850, 2795, 1661,1559, 1240 cm^{-1}. ^1H NMR (500 MHz, Acetone-d_6): 7.63 (d, J = 6 Hz, 2H), 7.42 (t, J = 6 Hz, 2H), 7.34 (m, 5H), 7.18 (t, J = 6 Hz, 1H), 7.00 (t, J = 6 Hz, 1H), 6.78 (d, J = 7.5 Hz, 2H), 6.47 (t, J = 6 Hz, 1H), 5.89 (s, broad, 1H), 5.79 (s, 1H), 1.76 (s, 3h). ^{13}C NMR (500 MHz, Acetone-d_6): δ 157.26, 151.93, 143.36, 138.74, 137.97, 130.75, 128.49, 128.34, 127.68, 127.47, 126.26, 125.57, 114.79, 113.05, 54.36, 39.62.

Synthesis of 1-(4-anisole)-4-methyl-3,4,5-triphenyl-1,4-dihydropyridine:

To an 8 ml vial, $PyTriAuCl_2BF_4$ (0.1 mmol, 49 mg) is added and purged with argon. *P*-anisidine (1 mmol, 123 mg) and phenylacetylene (3 mmol, 300 µL) are added and the placed on a heating block set to 110 °C. The reaction was allowed to heat and stir for 3 days, at which point it is removed from heat and cooled to room temperature. Methylene chloride is added to solubilize the crude mixture and loaded onto a silica column. The product is separated from the crude mixture with column chromatography (1% Et_2O:Hexanes) and isolated in an 18% yield (77 mg) as a tan solid. ATR-IR: 3020, 3002, 2976, 2950, 1876, 1840,1599, 980, 576 cm^{-1}. ^1H NMR (500 MHz, Acetone-d_6): 7.92 (s, 1H), 7.87 (d, J = 5.5 Hz, 2H), 7.69 (d, J = 5.5 Hz, 2H), 7.53 (m, 6H), 7.43 (t, J = 4 Hz, 4H), 7.22 (t, 4 Hz, 5H),

7.18 (d, J = 5.5 Hz, 2H), 7.01 (d, J = 7.5 Hz, 2H), 6.91 (t, J = 7.5 Hz, 2H), 6.81 (t, J = 5.5 Hz, 1H), 5.29 (s, 1H), 1.71 (s, 3H). ^{13}C NMR (500 MHz, Acetone-d_6): δ 149.73, 144.59, 139.71, 135.85, 129.09, 128.77, 128.21, 128.07, 127.32, 126.28, 125.51, 125.18, 120.10, 116.20, 113.37, 56.50.

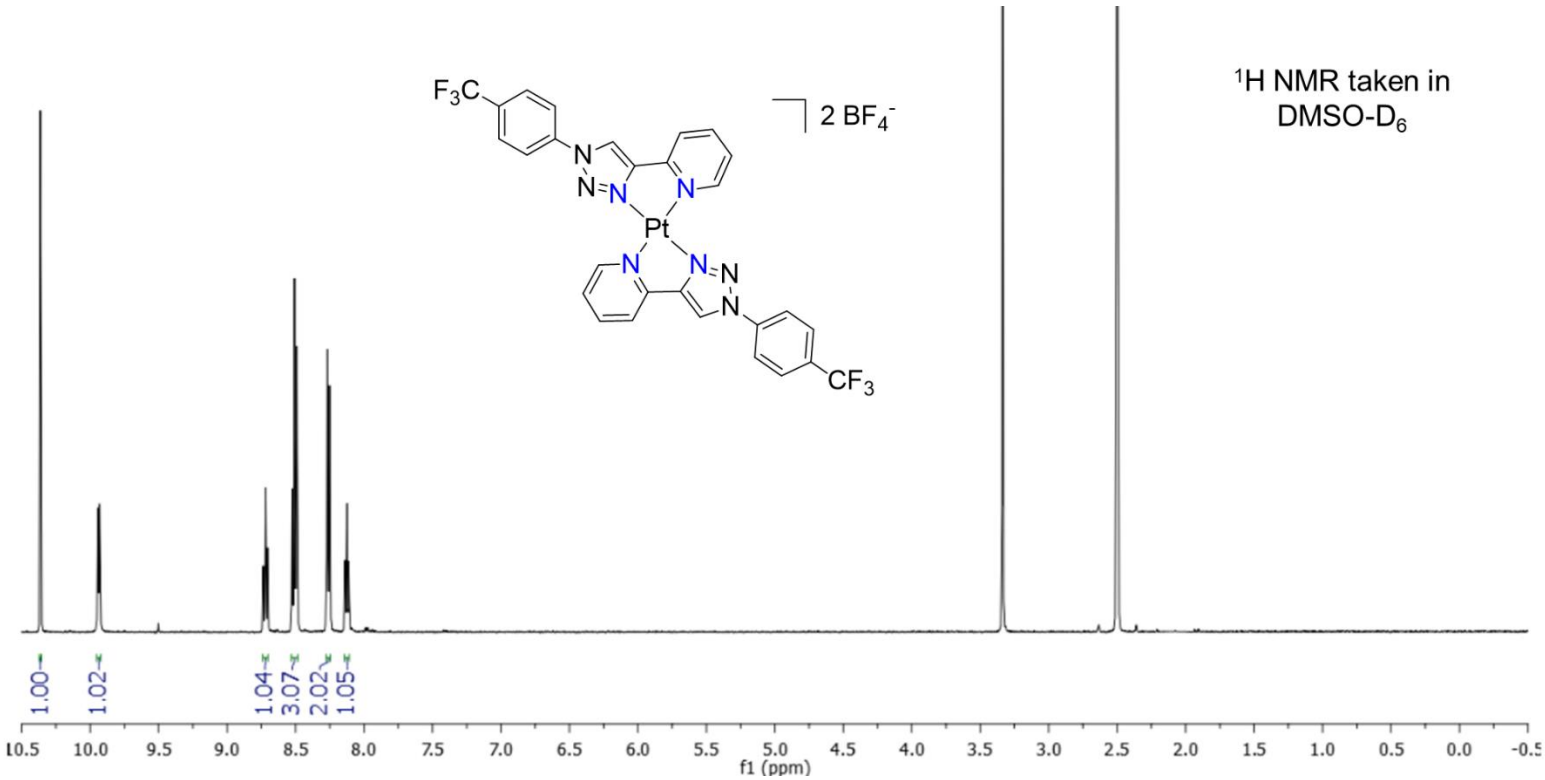
F3C
2 BF4-
Pt
CF3
1H NMR taken in
DMSO-D6
1.00
1.02
1.04
3.07
2.02
1.05
f1 (ppm)

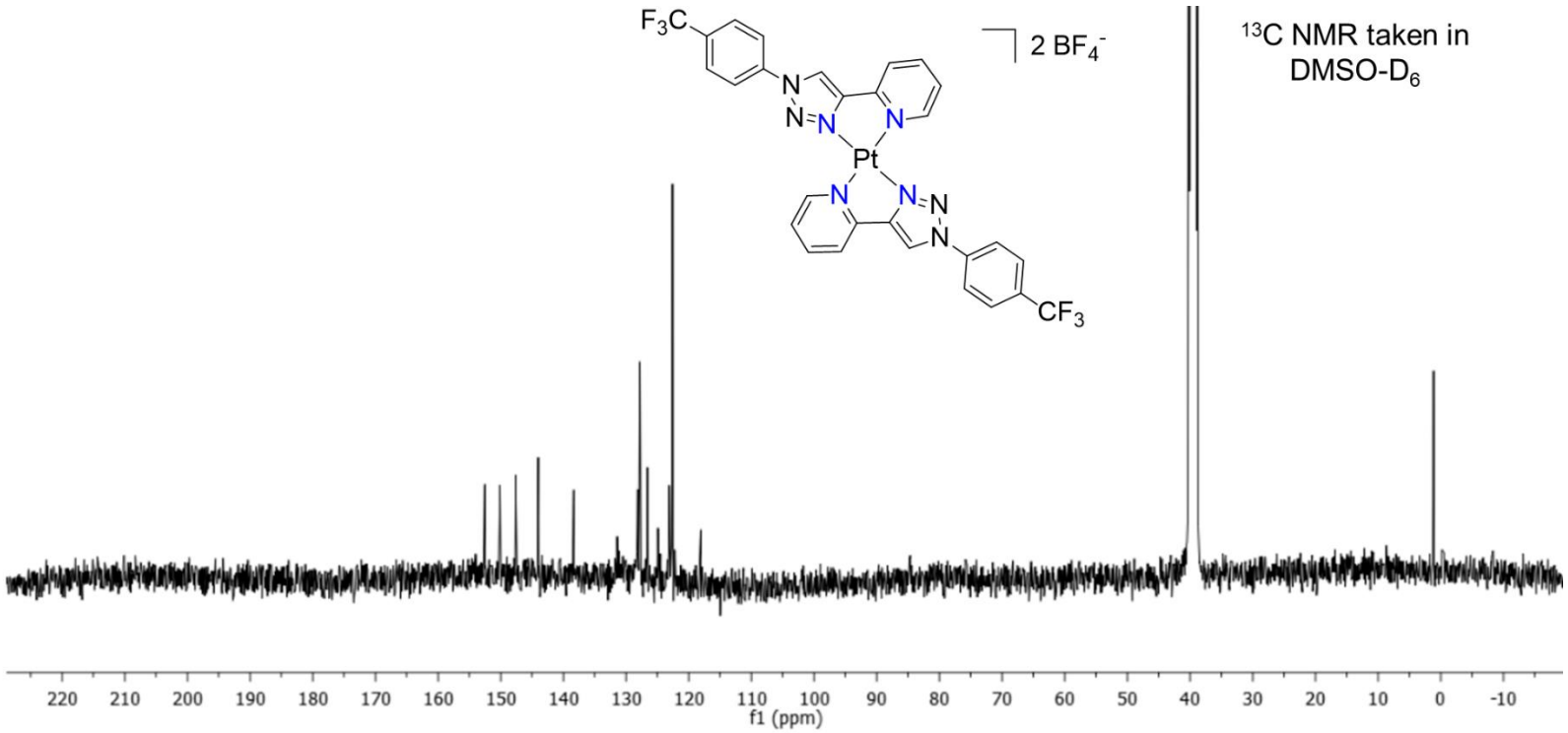
F3C
2 BF4-
13C NMR taken in
DMSO-D6
N
N
N
Pt
N
N
N
N
CF3
220 210 200 190 180 170 160 150 140 130 120 110 100 90 80 70 60 50 40 30 20 10 0 -10
f1 (ppm)

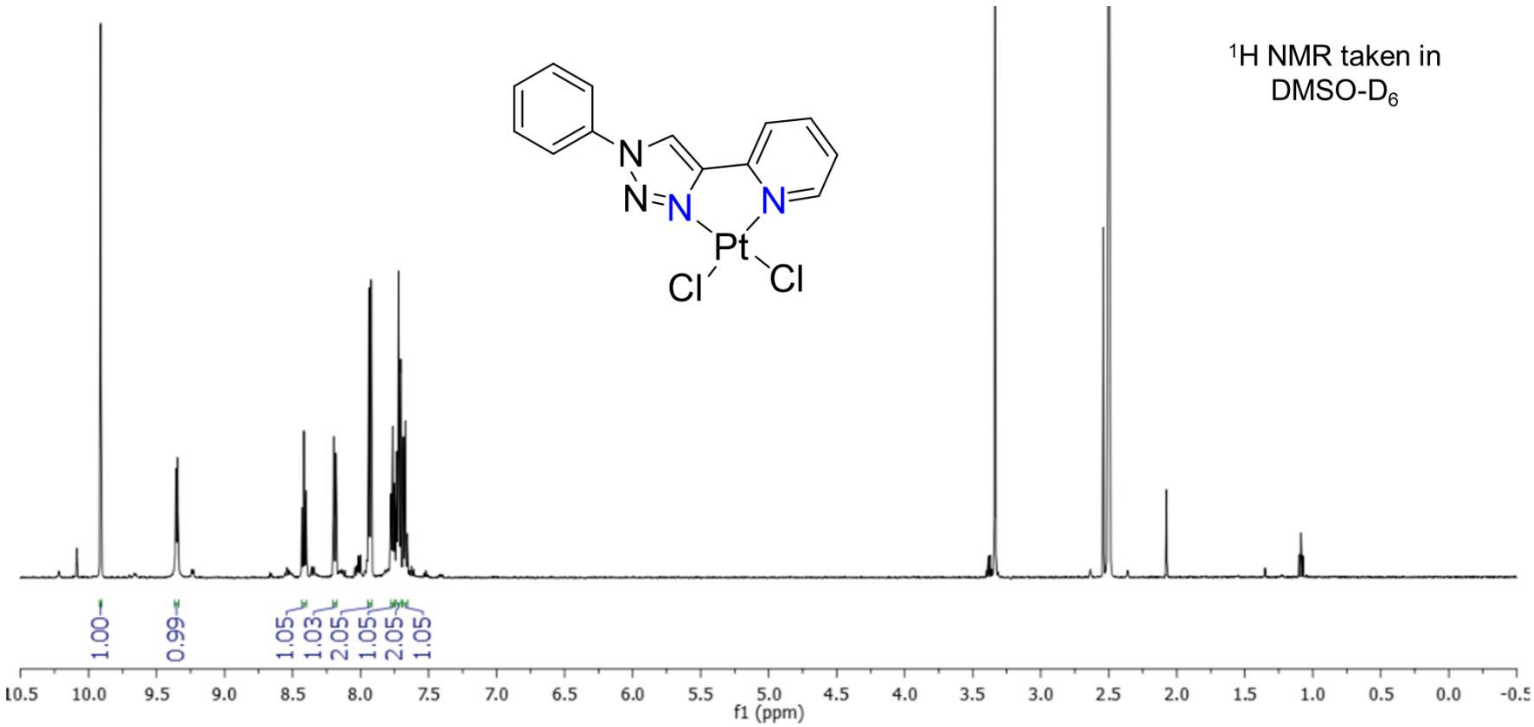
^{1}H NMR taken in
DMSO-D$_6$
N
N
N
N
Pt
Cl
Cl
1.00
0.99
1.05
1.03
2.05
1.05
2.05
1.05
10.5
10.0
9.5
9.0
8.5
8.0
7.5
7.0
6.5
6.0
5.5
5.0
4.5
4.0
3.5
3.0
2.5
2.0
1.5
1.0
0.5
0.0
-0.5
f1 (ppm)

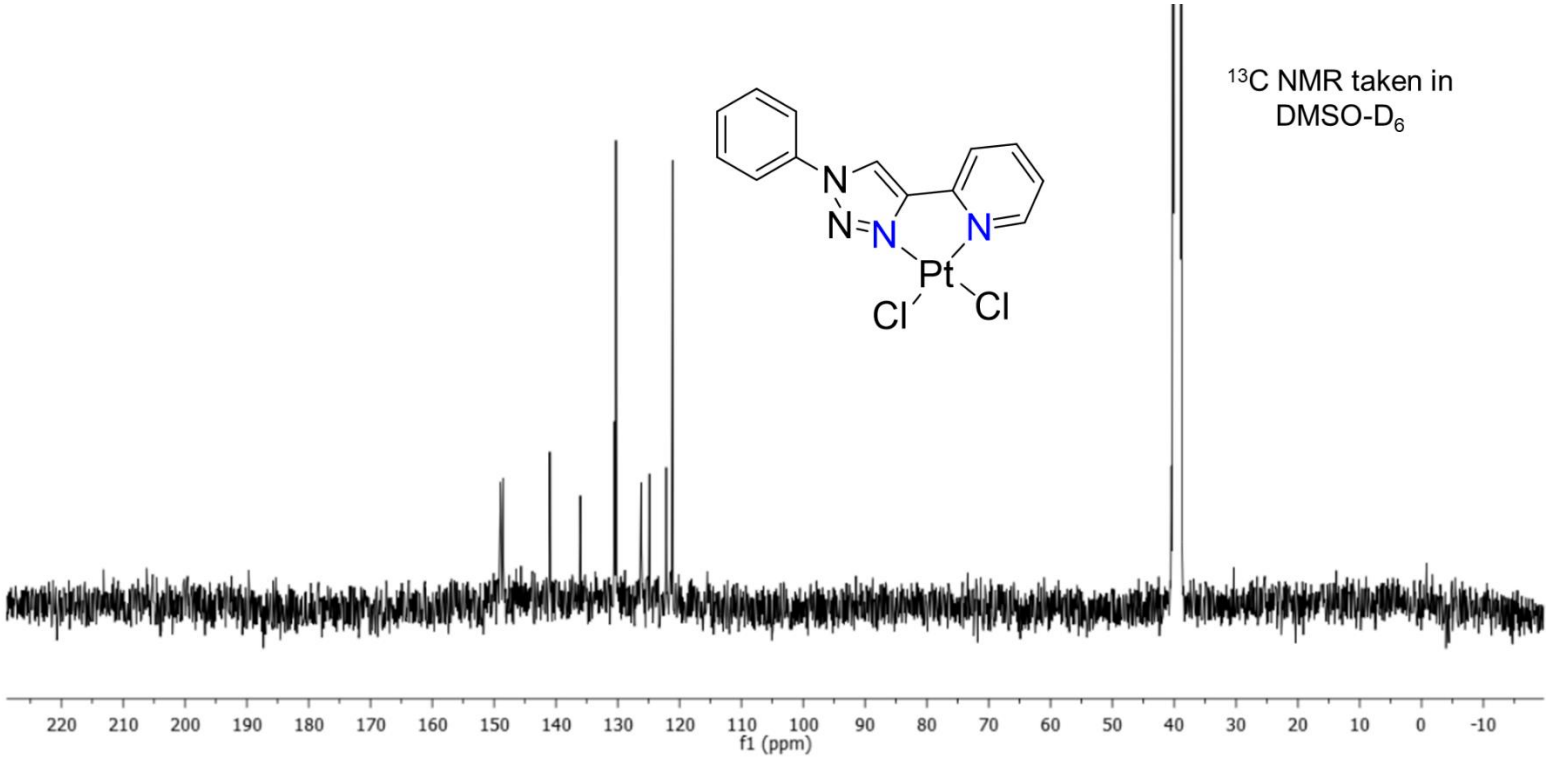
^{13}C NMR taken in
DMSO-D$_6$
N
N
N
N
Pt
Cl
Cl
220 210 200 190 180 170 160 150 140 130 120 110 100 90 80 70 60 50 40 30 20 10 0 -10
f1 (ppm)

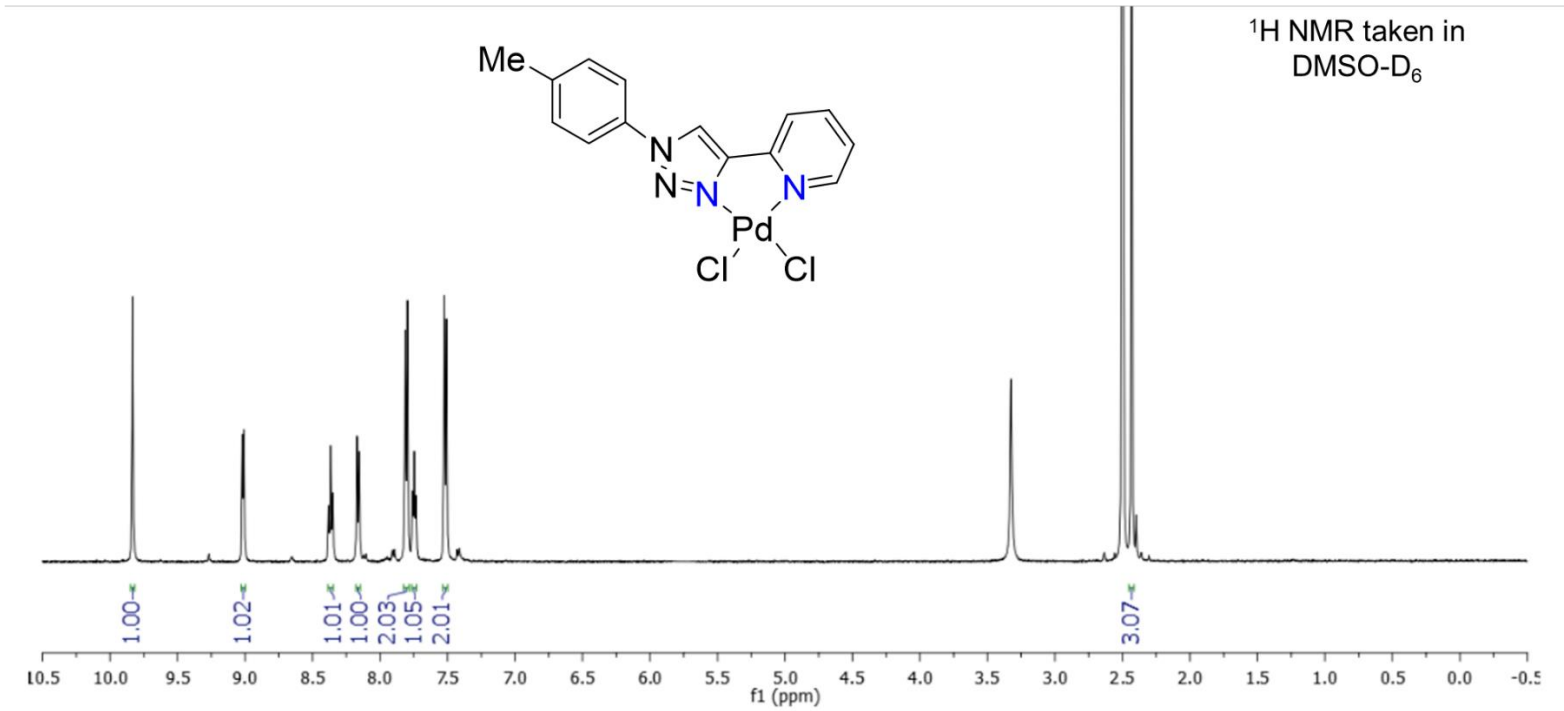
Me
N
N
N
N
Pd
Cl
Cl
^{1}H NMR taken in
DMSO-D$_6$
1.00
1.02
1.01
1.00
2.03
1.05
2.01
3.07
10.5
10.0
9.5
9.0
8.5
8.0
7.5
7.0
6.5
6.0
5.5
5.0
4.5
4.0
3.5
3.0
2.5
2.0
1.5
1.0
0.5
0.0
f1 (ppm)

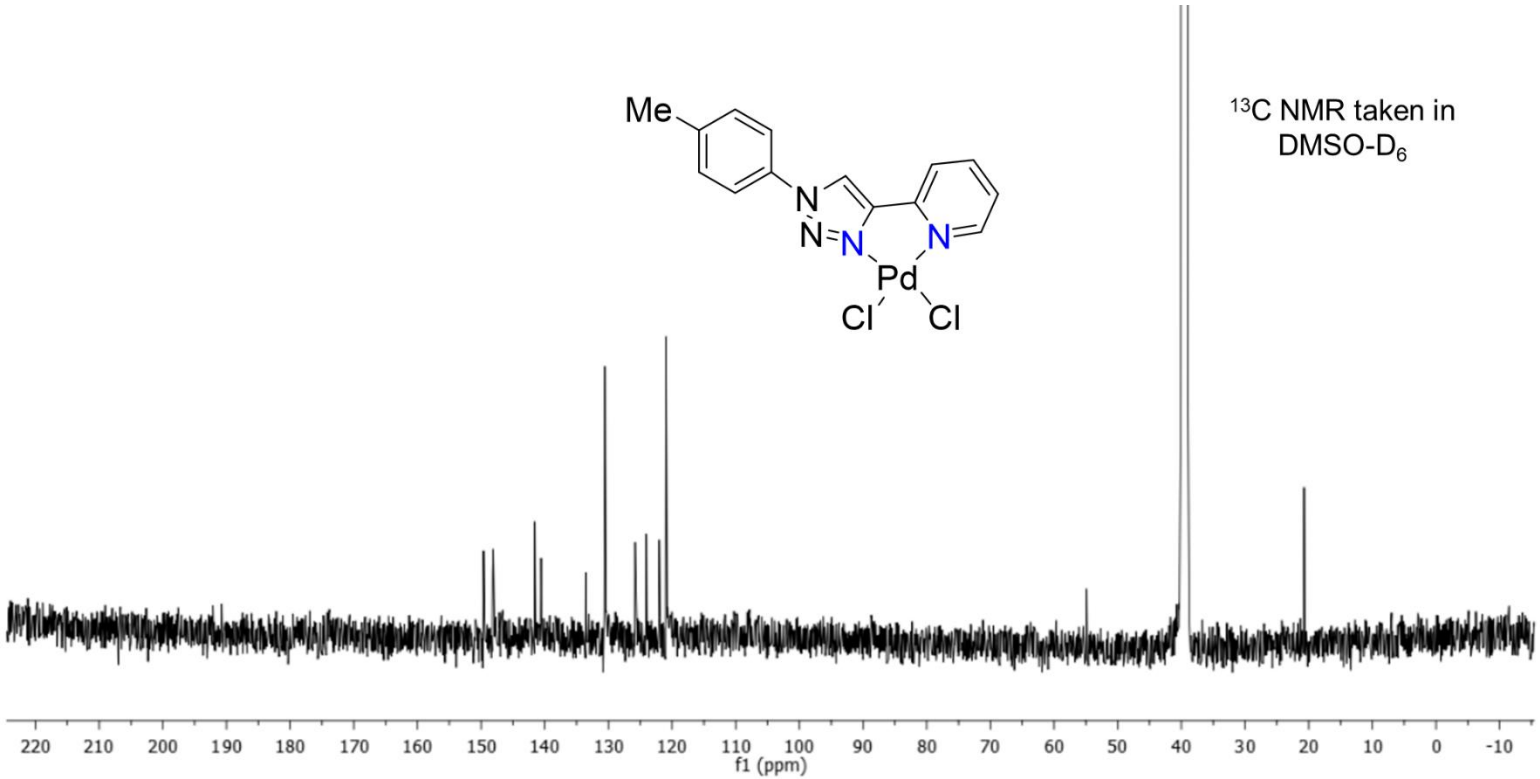
Me
N
N
N
N
Pd
Cl
Cl
^{13}C NMR taken in
DMSO-D$_6$
220 210 200 190 180 170 160 150 140 130 120 110 100 90 80 70 60 50 40 30 20 10 0 -10
f1 (ppm)

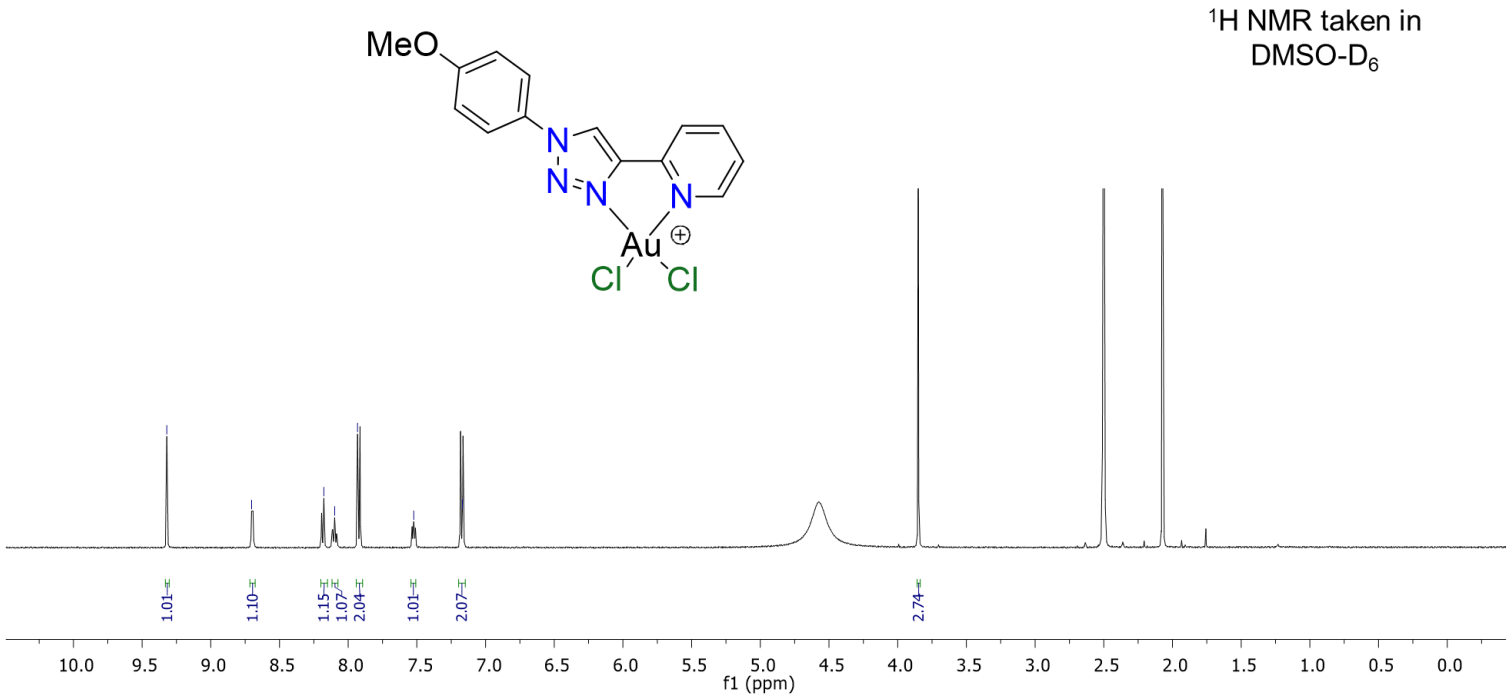
MeO
N
N
N
N
Au
Cl
Cl
^{1}H NMR taken in
DMSO-D$_6$
1.01
1.10
1.15
1.07
2.04
1.01
2.07
2.74
10.0
9.5
9.0
8.5
8.0
7.5
7.0
6.5
6.0
5.5
5.0
4.5
4.0
3.5
3.0
2.5
2.0
1.5
1.0
0.5
0.0
f1 (ppm)

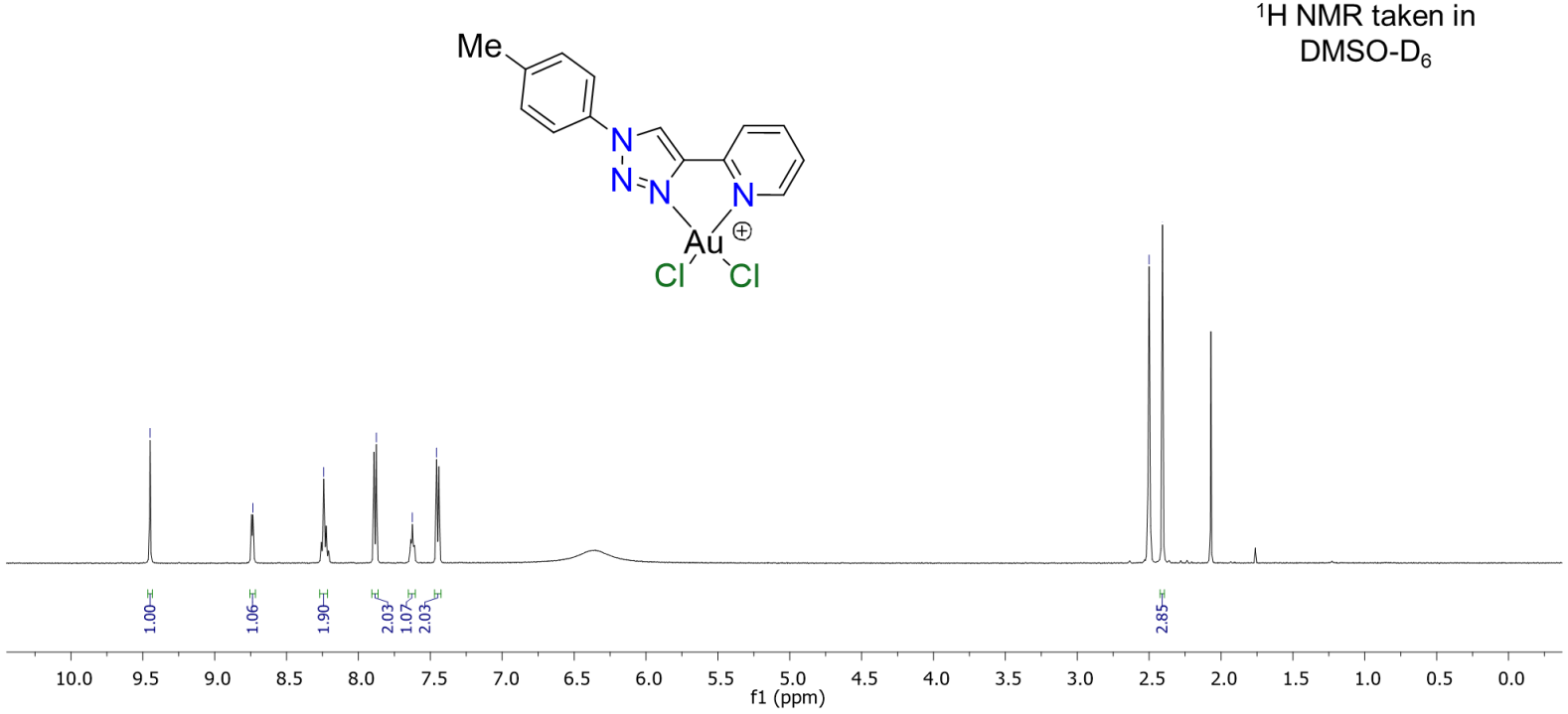
Me
N
N
N
N
Au
Cl
Cl
1H NMR taken in
DMSO-D6
1.00
1.06
1.90
2.03
1.07
2.03
2.85
10.0
9.5
9.0
8.5
8.0
7.5
7.0
6.5
6.0
5.5
5.0
4.5
4.0
3.5
3.0
2.5
2.0
1.5
1.0
0.5
0.0
f1 (ppm)

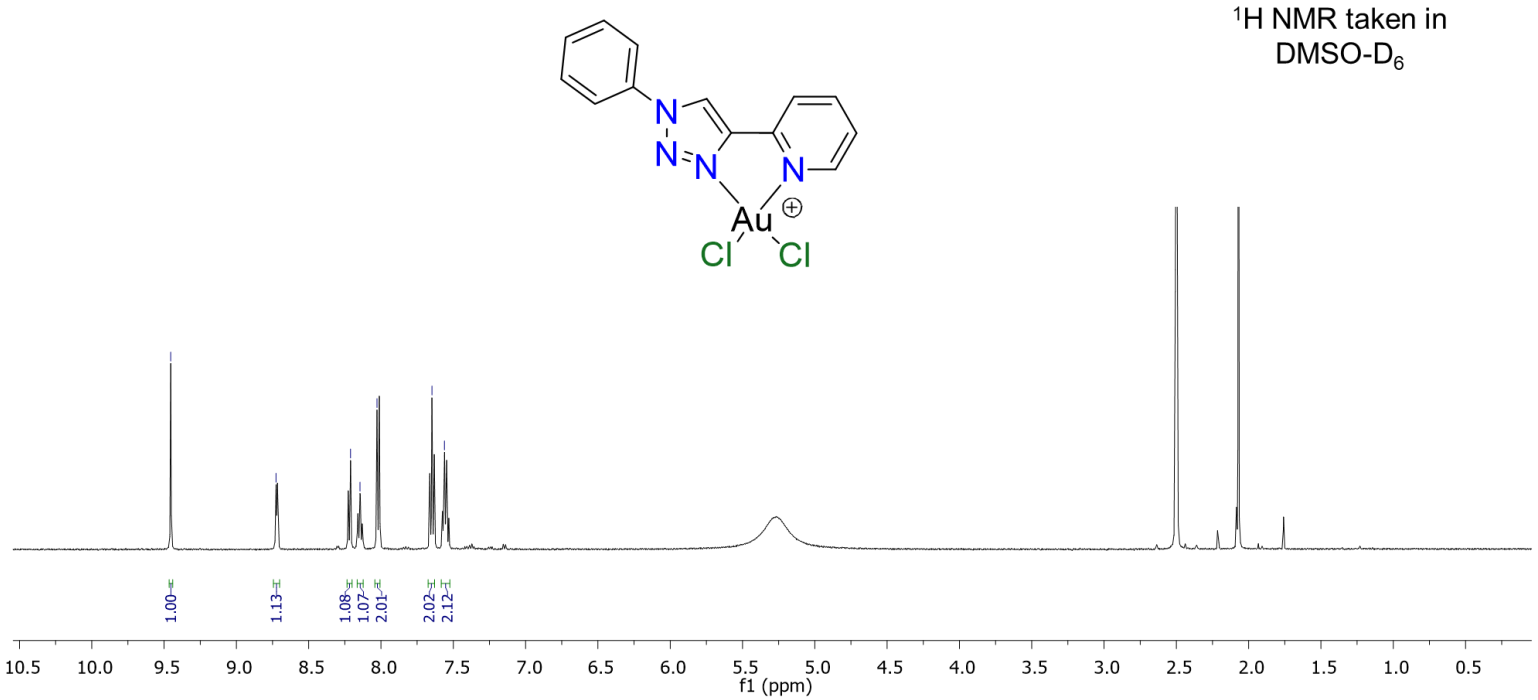
^{1}H NMR taken in
DMSO-D$_6$
N
N
N
N
Au
Cl
Cl
1.00
1.13
1.08
1.07
2.01
2.02
2.12
10.5 10.0 9.5 9.0 8.5 8.0 7.5 7.0 6.5 6.0 5.5 5.0 4.5 4.0 3.5 3.0 2.5 2.0 1.5 1.0 0.5
f1 (ppm)

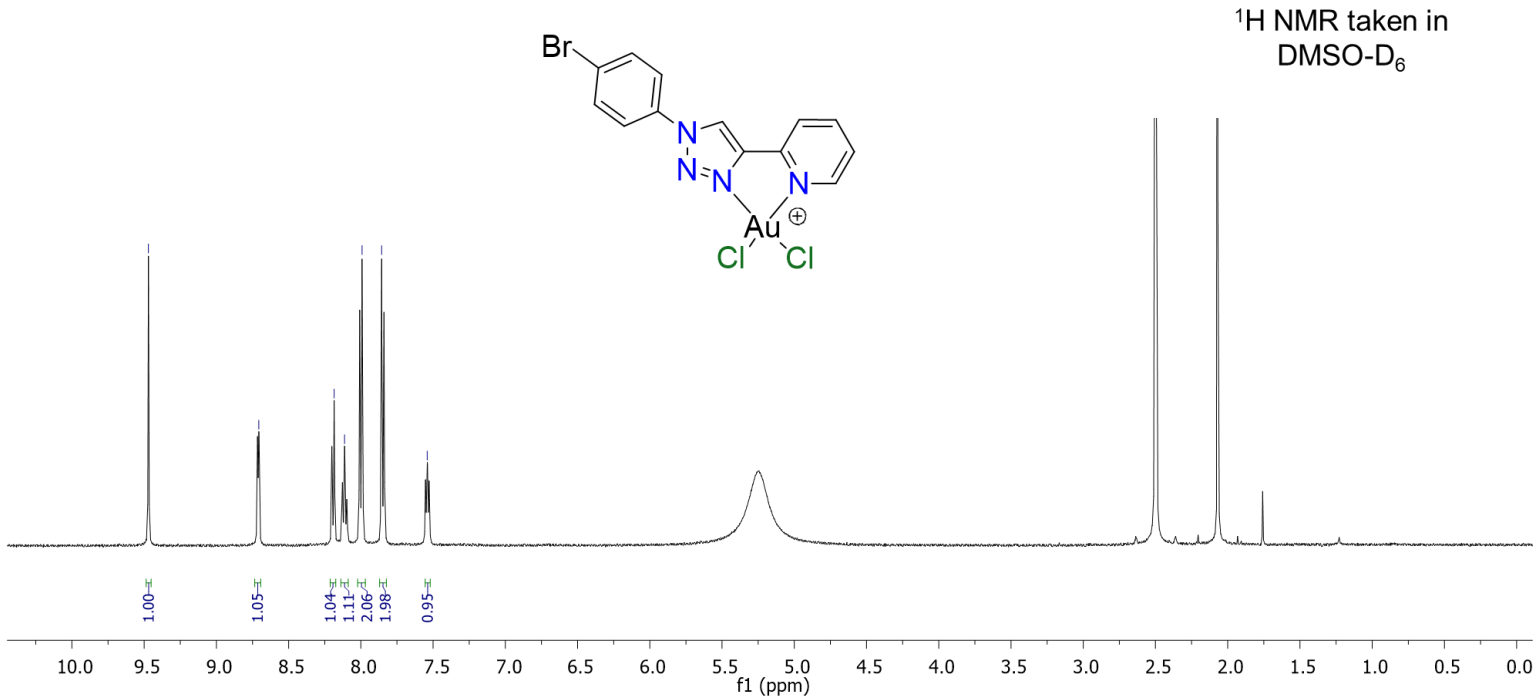
Br
N
N
N
N
Au
Cl
Cl
^{1}H NMR taken in
DMSO-D$_6$
1.00
1.05
1.04
1.11
2.06
1.98
0.95
10.0
9.5
9.0
8.5
8.0
7.5
7.0
6.5
6.0
5.5
5.0
4.5
4.0
3.5
3.0
2.5
2.0
1.5
1.0
0.5
0.0
f1 (ppm)

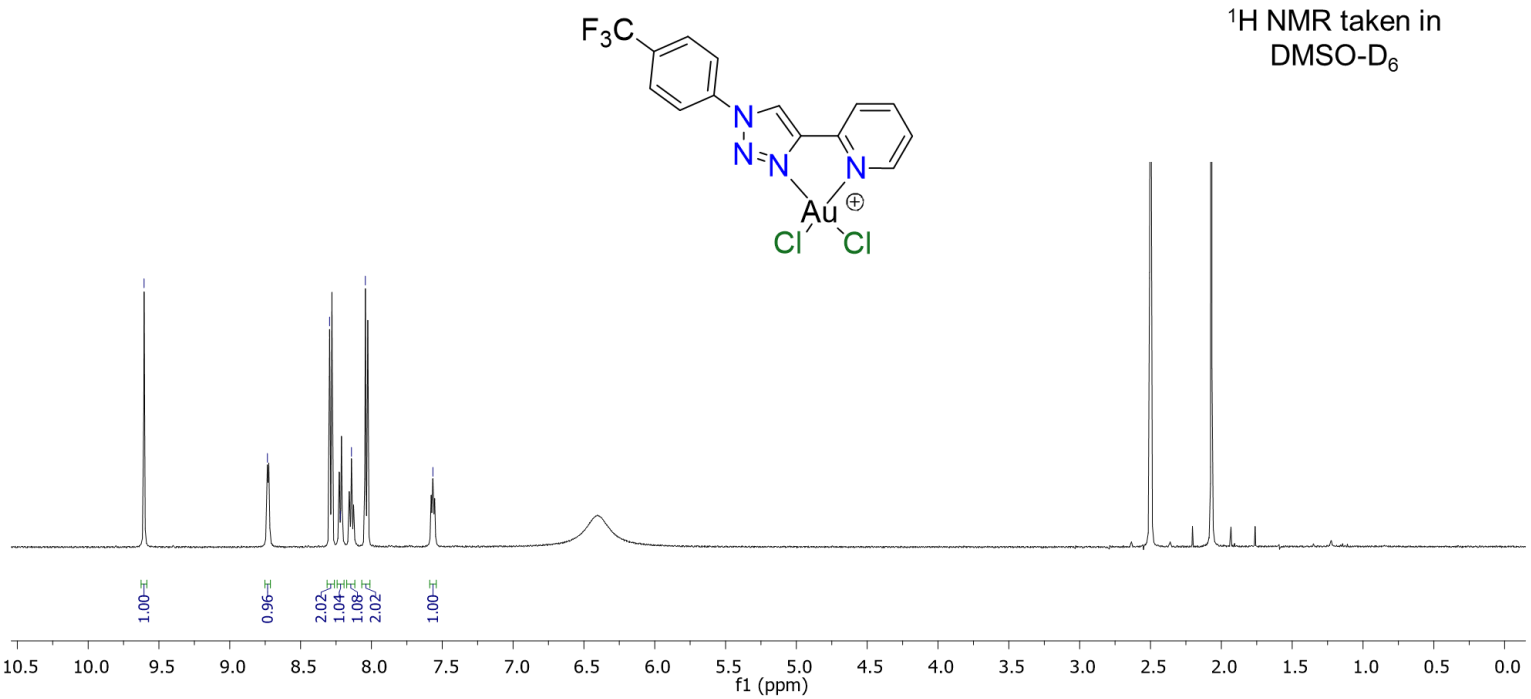
^{1}H NMR taken in
DMSO-D$_6$
F$_3$C
N
N
N
N
Au
Cl
Cl
1.00
0.96
2.02
1.04
1.08
2.02
1.00
10.5 10.0 9.5 9.0 8.5 8.0 7.5 7.0 6.5 6.0 5.5 5.0 4.5 4.0 3.5 3.0 2.5 2.0 1.5 1.0 0.5 0.0
f1 (ppm)

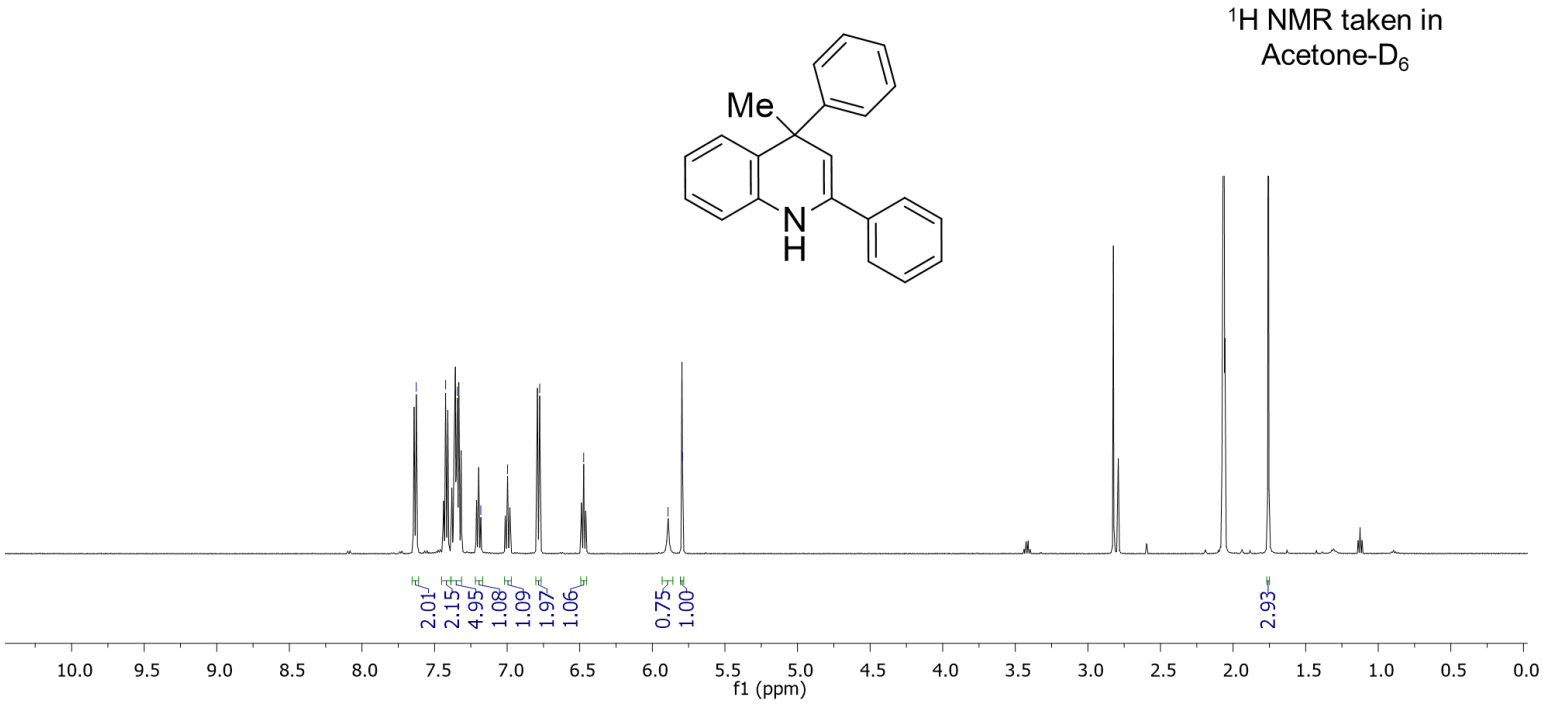
^{1}H NMR taken in
Acetone-D$_6$
Me
N
H
2.01
2.15
4.95
1.08
1.09
1.97
1.06
0.75
1.00
2.93
10.0
9.5
9.0
8.5
8.0
7.5
7.0
6.5
6.0
5.5
5.0
4.5
4.0
3.5
3.0
2.5
2.0
1.5
1.0
0.5
0.0
f1 (ppm)

^{13}C NMR taken in Acetone-D_6

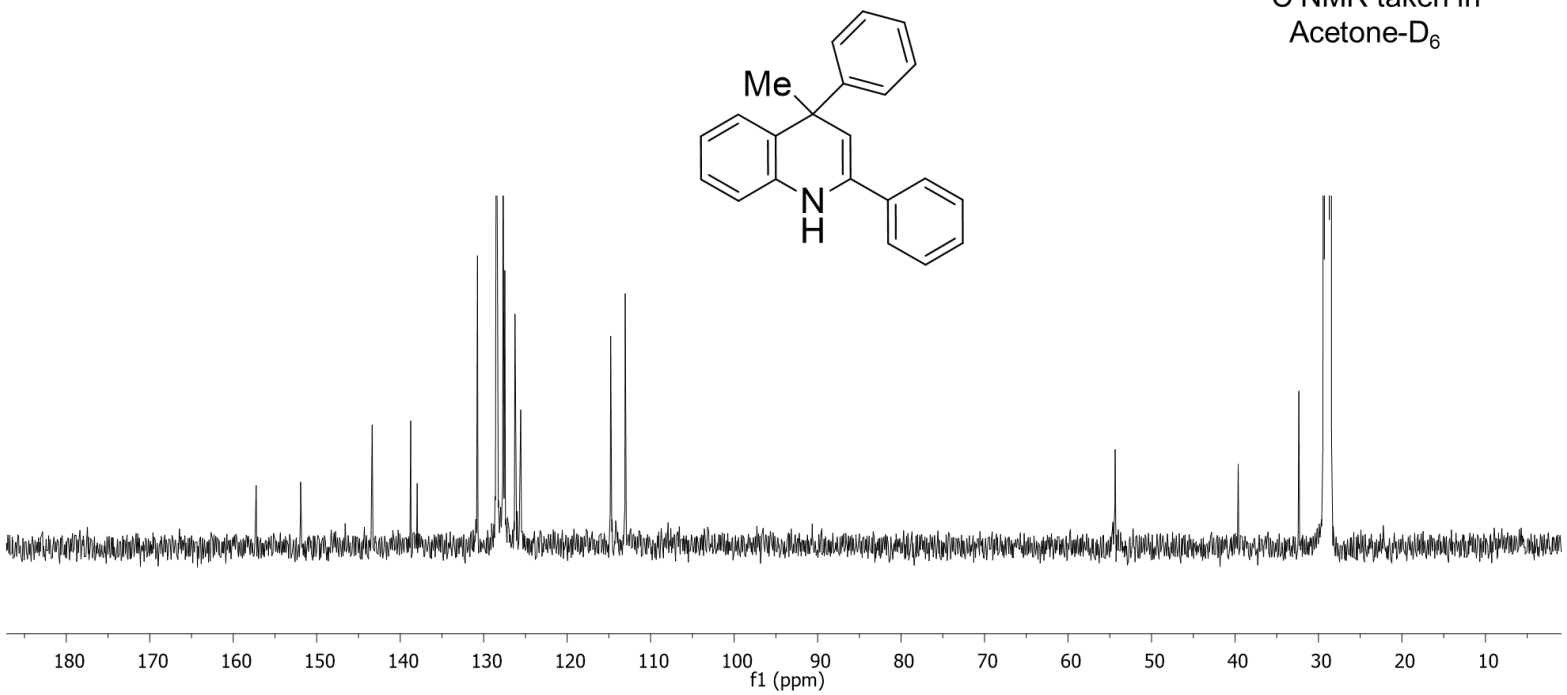

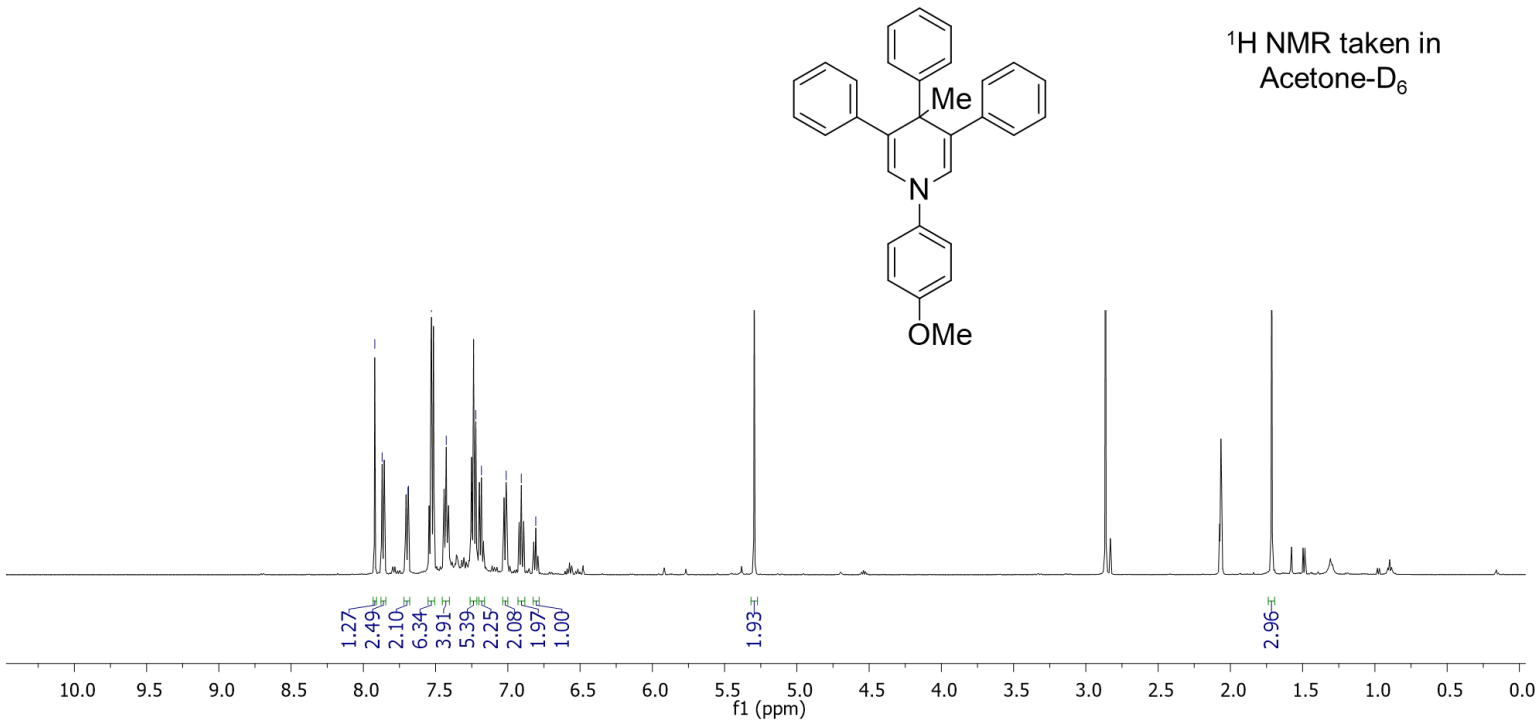
Me
N
OMe
^{1}H NMR taken in
Acetone-D$_6$
1.27
2.49
2.10
6.34
3.91
5.39
2.25
2.08
1.97
1.00
1.93
2.96
10.0
9.5
9.0
8.5
8.0
7.5
7.0
6.5
6.0
5.5
5.0
4.5
4.0
3.5
3.0
2.5
2.0
1.5
1.0
0.5
0.0
f1 (ppm)

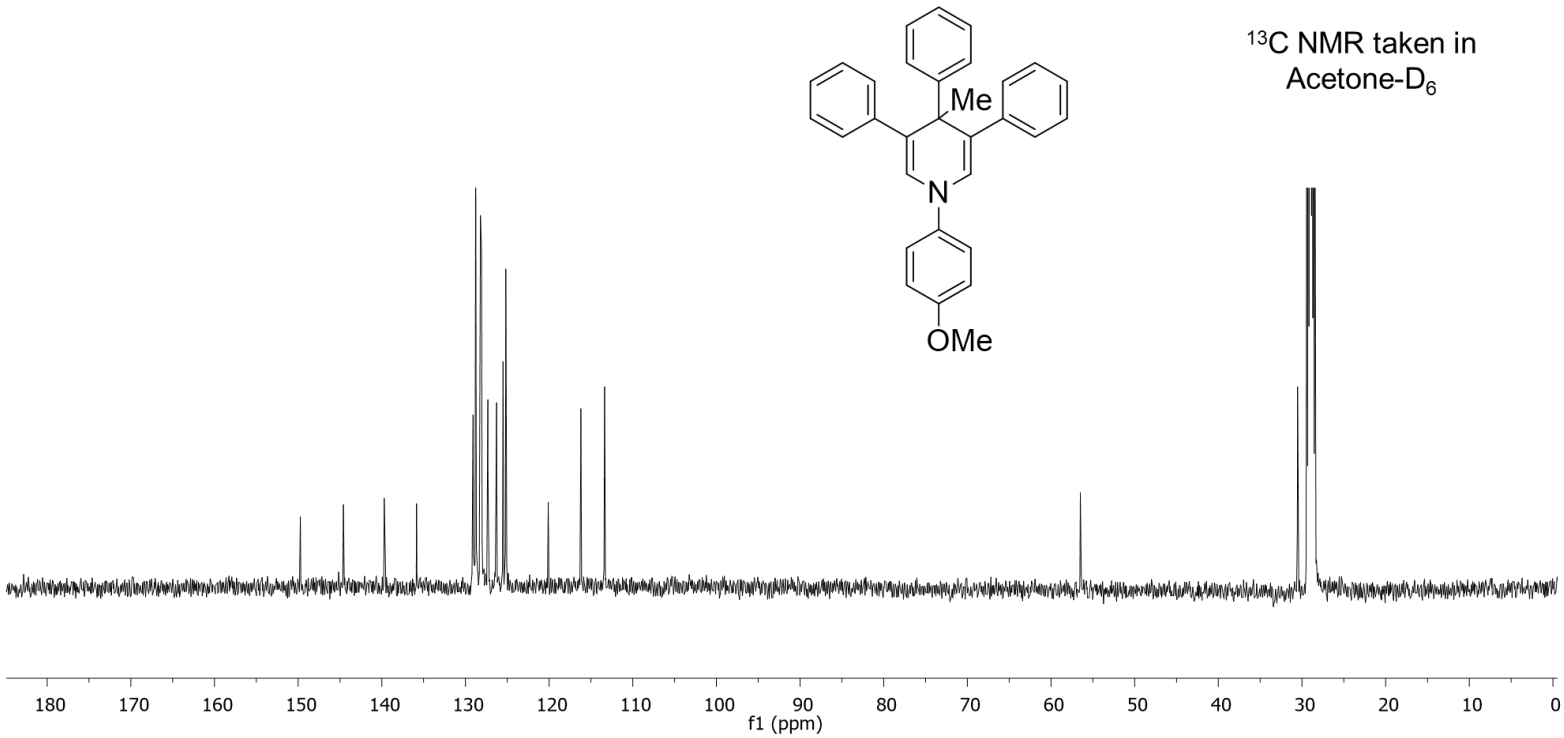
Me
N
OMe
^{13}C NMR taken in
Acetone-D$_6$
180
170
160
150
140
130
120
110
100
90
80
70
60
50
40
30
20
10
0
f1 (ppm)

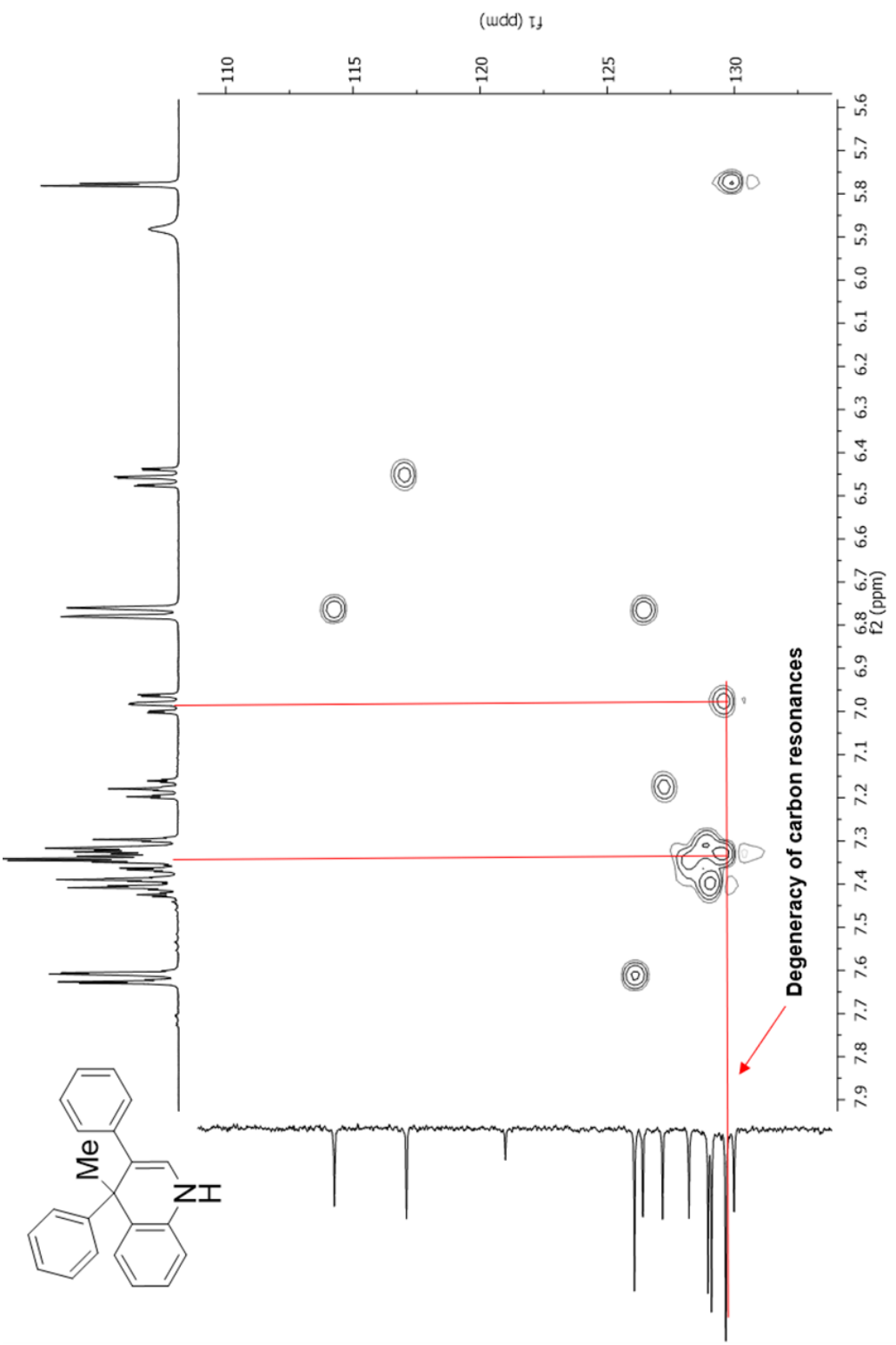
Me
NH
Degeneracy of carbon resonances
f1 (ppm)
f2 (ppm)

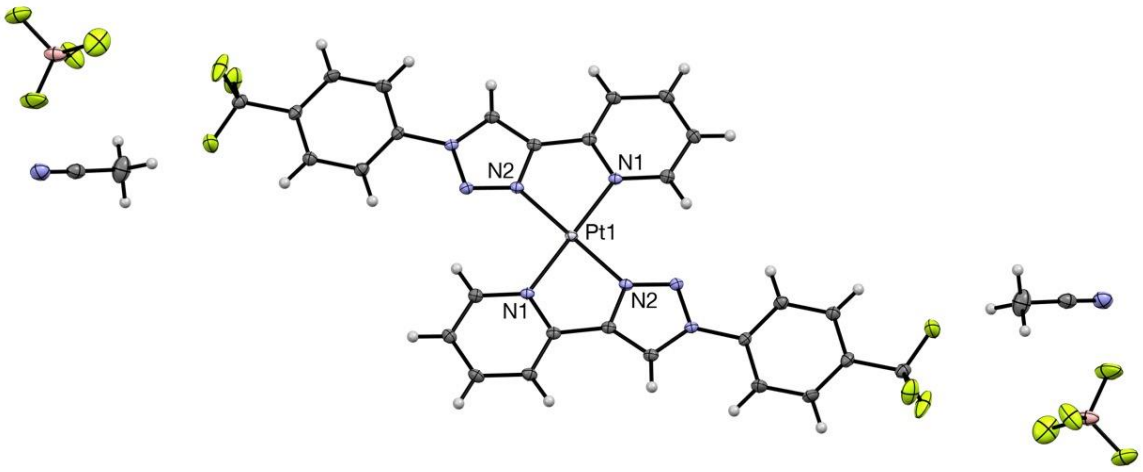

Crystal data and structure refinement for larsen26_0m_a.

Identification code	ZLP-3-7
Empirical formula	C32 H24 B2 F14 N10 Pt
Formula weight	1031.32
Temperature	100.0 K
Wavelength	0.71073 Å
Crystal system	Triclinic
Space group	P-1
Unit cell dimensions	a = 7.2410(3) Å □= 81.682(2)°.
	b = 11.1823(5) Å □= 89.9830(10)°.
	c = 11.4006(5) Å □ = 74.1850(10)°.
Volume	878.09(7) Å3
Z, Z'	1, 0.5
Density (calculated)	1.950 Mg/m3
Absorption coefficient	4.113 mm-1
F(000)	500
Crystal size	0.26 x 0.24 x 0.22 mm3
Theta range for data collection	1.807 to 28.286°.
Index ranges	-9<=h<=9, -14<=k<=14, -15<=l<=14
Reflections collected	15454
Independent reflections	4368 [R(int) = 0.0334]
Completeness to theta = 25.242°	100.0 %
Absorption correction	Semi-empirical from equivalents
Max. and min. transmission	0.5633 and 0.4870
Refinement method	Full-matrix least-squares on F2
Data / restraints / parameters	4368 / 0 / 269
Goodness-of-fit on F2	1.053
Final R indices [I>2sigma(I)]	R1 = 0.0169, wR2 = 0.0410
R indices (all data)	R1 = 0.0169, wR2 = 0.0410
Extinction coefficient	n/a

Largest diff. peak and hole 0.762 and -0.400 e.Å-3

Atomic coordinates (x 104) and equivalent isotropic displacement parameters (Å2x 103)
for larsen26_0m_a. U(eq) is defined as one third of the trace of the orthogonalized Uij tensor.

	x	y	z	U(eq)
Pt(1)	10000	10000	5000	10(1)
F(2)	-488(2)	5837(1)	3452(1)	31(1)
F(4)	13697(2)	6156(1)	8226(1)	36(1)
F(6)	13015(2)	8258(1)	8228(1)	36(1)
F(1)	1253(2)	5642(2)	1942(1)	33(1)
F(3)	1862(2)	4199(1)	3462(2)	37(1)
F(5)	11803(3)	7052(2)	9627(1)	50(1)
N(1)	9192(2)	10259(2)	6687(1)	11(1)
N(3)	7288(2)	8445(2)	4506(1)	12(1)
F(7)	10707(2)	7384(2)	7702(2)	44(1)
C(2)	9283(3)	10997(2)	8546(2)	15(1)
N(4)	5918(2)	8076(2)	5128(1)	11(1)
C(10)	2420(3)	6267(2)	4832(2)	19(1)
C(11)	2615(3)	6088(2)	3655(2)	14(1)
C(12)	3960(3)	6514(2)	2968(2)	15(1)
N(2)	7981(2)	9080(1)	5194(1)	11(1)
C(1)	9957(3)	10854(2)	7421(2)	14(1)
N(5)	3176(3)	1851(2)	-959(2)	25(1)
C(4)	7008(3)	9886(2)	8200(2)	14(1)
C(3)	7787(3)	10516(2)	8941(2)	15(1)
C(00L)	1330(3)	5442(2)	3120(2)	16(1)
C(9)	3534(3)	6899(2)	5333(2)	18(1)
C(13)	5077(3)	7162(2)	3460(2)	14(1)
C(5)	7738(3)	9772(2)	7089(2)	12(1)
C(8)	4834(3)	7355(2)	4631(2)	12(1)
C(15)	2881(3)	2683(2)	-454(2)	20(1)
C(7)	5734(3)	8471(2)	6204(2)	13(1)
C(6)	7079(3)	9120(2)	6241(2)	12(1)
C(14)	2489(4)	3737(2)	214(3)	34(1)
B(1)	12282(4)	7209(2)	8462(2)	24(1)

Bond lengths [Å] and angles [°] for larsen26_0m_a.

Pt(1)-N(1)	2.0475(15)
Pt(1)-N(1)#1	2.0475(15)
Pt(1)-N(2)	2.0000(16)
Pt(1)-N(2)#1	2.0000(16)
F(2)-C(00L)	1.342(2)
F(4)-B(1)	1.393(3)
F(6)-B(1)	1.407(3)
F(1)-C(00L)	1.328(2)
F(3)-C(00L)	1.336(2)
F(5)-B(1)	1.372(3)
N(1)-C(1)	1.346(2)
N(1)-C(5)	1.363(2)
N(3)-N(4)	1.340(2)
N(3)-N(2)	1.313(2)
F(7)-B(1)	1.385(3)
C(2)-C(1)	1.387(3)
C(2)-C(3)	1.383(3)
N(4)-C(8)	1.438(2)
N(4)-C(7)	1.357(2)
C(10)-C(11)	1.386(3)
C(10)-C(9)	1.380(3)
C(11)-C(12)	1.391(3)
C(11)-C(00L)	1.501(3)
C(12)-C(13)	1.390(3)
N(2)-C(6)	1.362(2)
N(5)-C(15)	1.135(3)
C(4)-C(3)	1.385(3)
C(4)-C(5)	1.382(3)
C(9)-C(8)	1.389(3)
C(13)-C(8)	1.386(3)
C(5)-C(6)	1.444(3)
C(15)-C(14)	1.458(3)
C(7)-C(6)	1.367(3)

N(1)-Pt(1)-N(1)#1	180.00(2)
N(2)-Pt(1)-N(1)	79.41(6)
N(2)#1-Pt(1)-N(1)#1	79.41(6)
N(2)#1-Pt(1)-N(1)	100.59(6)
N(2)-Pt(1)-N(1)#1	100.59(6)
N(2)-Pt(1)-N(2)#1	180.0
C(1)-N(1)-Pt(1)	126.41(13)
C(1)-N(1)-C(5)	117.90(16)
C(5)-N(1)-Pt(1)	115.69(12)

N(2)-N(3)-N(4)	105.03(14)
C(3)-C(2)-C(1)	119.87(18)
N(3)-N(4)-C(8)	120.11(15)
N(3)-N(4)-C(7)	112.21(15)
C(7)-N(4)-C(8)	127.69(16)
C(9)-C(10)-C(11)	120.29(19)
C(10)-C(11)-C(12)	120.83(18)
C(10)-C(11)-C(00L)	119.09(18)
C(12)-C(11)-C(00L)	120.07(18)
C(13)-C(12)-C(11)	119.34(18)
N(3)-N(2)-Pt(1)	133.50(12)
N(3)-N(2)-C(6)	111.25(15)
C(6)-N(2)-Pt(1)	115.24(12)
N(1)-C(1)-C(2)	121.90(18)
C(5)-C(4)-C(3)	118.90(18)
C(2)-C(3)-C(4)	118.71(17)
F(2)-C(00L)-C(11)	111.69(17)
F(1)-C(00L)-F(2)	106.17(17)
F(1)-C(00L)-F(3)	107.32(17)
F(1)-C(00L)-C(11)	113.17(17)
F(3)-C(00L)-F(2)	105.53(17)
F(3)-C(00L)-C(11)	112.46(16)
C(10)-C(9)-C(8)	118.53(18)
C(8)-C(13)-C(12)	118.99(18)
N(1)-C(5)-C(4)	122.71(18)
N(1)-C(5)-C(6)	112.90(16)
C(4)-C(5)-C(6)	124.39(18)
C(9)-C(8)-N(4)	118.73(17)
C(13)-C(8)-N(4)	119.27(17)
C(13)-C(8)-C(9)	121.98(18)
N(5)-C(15)-C(14)	179.0(2)
N(4)-C(7)-C(6)	104.53(16)
N(2)-C(6)-C(5)	116.67(16)
N(2)-C(6)-C(7)	106.98(16)
C(7)-C(6)-C(5)	136.33(17)
F(4)-B(1)-F(6)	108.1(2)
F(5)-B(1)-F(4)	110.3(2)
F(5)-B(1)-F(6)	109.6(2)
F(5)-B(1)-F(7)	111.4(2)
F(7)-B(1)-F(4)	108.3(2)
F(7)-B(1)-F(6)	109.0(2)

Symmetry transformations used to generate equivalent atoms:
#1 -x+2,-y+2,-z+1

Anisotropic displacement parameters (Å2x 103) for larsen26_0m_a. The anisotropic
displacement factor exponent takes the form: -2□2[h2 a*2U11 + ... + 2 h k a* b* U12]

	U11	U22	U33	U23	U13	U12
Pt(1)	10(1)	10(1)	9(1)	-2(1)	2(1)	-3(1)
F(2)	14(1)	38(1)	44(1)	-17(1)	3(1)	-10(1)
F(4)	34(1)	35(1)	28(1)	-11(1)	-4(1)	12(1)
F(6)	37(1)	33(1)	38(1)	1(1)	17(1)	-14(1)
F(1)	41(1)	53(1)	18(1)	-7(1)	0(1)	-32(1)
F(3)	36(1)	12(1)	61(1)	2(1)	-23(1)	-8(1)
F(5)	91(1)	37(1)	30(1)	-13(1)	37(1)	-29(1)
N(1)	11(1)	11(1)	11(1)	-1(1)	2(1)	-2(1)
N(3)	12(1)	12(1)	12(1)	-1(1)	1(1)	-4(1)
F(7)	25(1)	38(1)	62(1)	-2(1)	-6(1)	0(1)
C(2)	16(1)	15(1)	13(1)	-3(1)	1(1)	-3(1)
N(4)	10(1)	11(1)	12(1)	-1(1)	2(1)	-3(1)
C(10)	19(1)	22(1)	17(1)	1(1)	4(1)	-12(1)
C(11)	13(1)	12(1)	18(1)	-1(1)	-1(1)	-4(1)
C(12)	16(1)	17(1)	14(1)	-3(1)	2(1)	-6(1)
N(2)	11(1)	11(1)	11(1)	-1(1)	2(1)	-2(1)
C(1)	13(1)	14(1)	14(1)	-2(1)	1(1)	-3(1)
N(5)	22(1)	32(1)	23(1)	-4(1)	6(1)	-10(1)
C(4)	13(1)	16(1)	13(1)	-1(1)	2(1)	-3(1)
C(3)	16(1)	18(1)	11(1)	-3(1)	3(1)	-2(1)
C(00L)		15(1)	16(1)	19(1)	0(1)	-1(1) -5(1)
C(9)	21(1)	23(1)	13(1)	-2(1)	4(1)	-10(1)
C(13)	13(1)	15(1)	15(1)	-2(1)	3(1)	-4(1)
C(5)	11(1)	11(1)	12(1)	0(1)	0(1)	-1(1)
C(8)	11(1)	10(1)	14(1)	-1(1)	0(1)	-3(1)
C(15)	14(1)	26(1)	19(1)	2(1)	1(1)	-6(1)
C(7)	14(1)	12(1)	12(1)	-1(1)	2(1)	-3(1)
C(6)	11(1)	10(1)	12(1)	0(1)	2(1)	-1(1)
C(14)	26(1)	30(1)	49(2)	-16(1)	0(1)	-6(1)
B(1)	26(1)	21(1)	21(1)	-1(1)	11(1)	-2(1)

Hydrogen coordinates (x 104) and isotropic displacement parameters (Å2x 10 3)

for larsen26_0m_a.

	x	y	z	U(eq)	
H(2)	9848	11424	9044	18	
H(10)	1516	5953	5295	23	
H(12)	4114	6364	2169	18	
H(1)	10989	11186	7161	16	
H(4)	5988	9538	8450	17	
H(3)	7304	10615	9706	18	
H(9)	3414	7020	6140	22	
H(13)	5992	7469	3001	17	
H(7)	4866	8329	6798	16	
H(14A)		2199	4528	-339	51
H(14B)		3618	3670	719	51
H(14C)		1387	3723	709	51

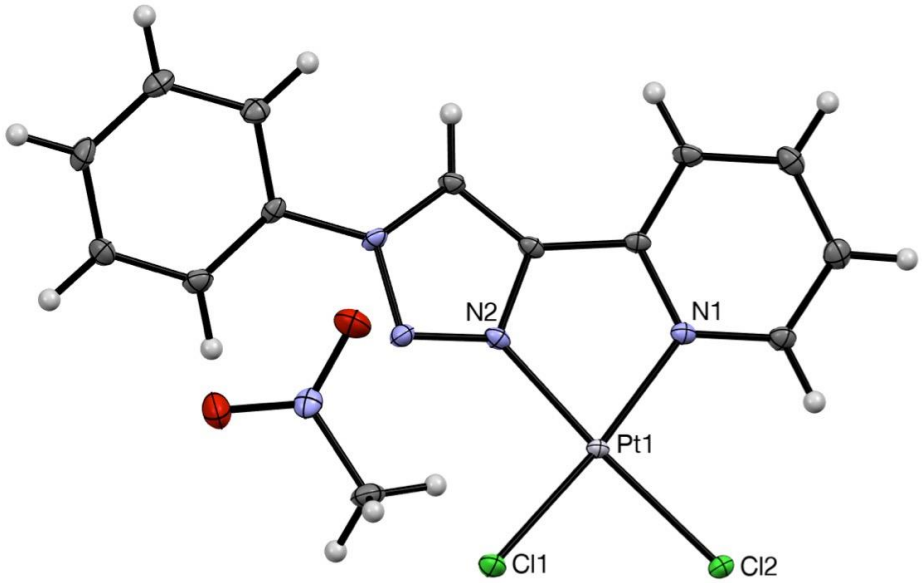

Crystal data and structure refinement for larsen27_0m_a.

Identification code	ZLP-3-11
Empirical formula	C14 H13 Cl2 N5 O2 Pt
Formula weight	549.28
Temperature	100.0 K
Wavelength	0.71073 Å
Crystal system	Triclinic
Space group	P-1
Unit cell dimensions	a = 8.5992(5) Å □= 108.356(2)°.
	b = 9.9079(6) Å □= 109.596(2)°.
	c = 11.2482(7) Å □ = 99.715(2)°.
Volume	815.56(9) Å3
Z	2
Density (calculated)	2.237 Mg/m3
Absorption coefficient	8.948 mm-1
F(000)	520
Crystal size	0.26 x 0.24 x 0.2 mm3
Theta range for data collection	2.097 to 28.380°.
Index ranges	-11<=h<=11, -13<=k<=11, -14<=l<=15
Reflections collected	12634
Independent reflections	4066 [R(int) = 0.0442]
Completeness to theta = 25.242°	100.0 %
Absorption correction	Semi-empirical from equivalents
Max. and min. transmission	0.4920 and 0.3611

Refinement method Full-matrix least-squares on F2
Data / restraints / parameters 4066 / 0 / 212
Goodness-of-fit on F2 1.026
Final R indices [I>2sigma(I)] R1 = 0.0269, wR2 = 0.0615
R indices (all data) R1 = 0.0290, wR2 = 0.0624
Extinction coefficient n/a
Largest diff. peak and hole 1.827 and -1.412 e.Å-3

Atomic coordinates (x 104) and equivalent isotropic displacement parameters (Å2x 103)
for larsen27_0m_a. U(eq) is defined as one third of the trace of the orthogonalized Uij tensor.

	x	y	z	U(eq)
Pt(1)	3158(1)	8452(1)	6002(1)	9(1)
Cl(2)	2478(1)	9050(1)	7861(1)	14(1)
Cl(1)	269(1)	7582(1)	4555(1)	16(1)
O(2)	4269(3)	4499(3)	3387(3)	24(1)
N(2)	3961(4)	7945(3)	4498(3)	10(1)
O(1)	1896(4)	2904(3)	1707(3)	26(1)
N(1)	5771(4)	9291(3)	7126(3)	10(1)
N(3)	3128(4)	7259(3)	3152(3)	12(1)
N(4)	4396(4)	7239(3)	2698(3)	11(1)
N(5)	2716(4)	3826(3)	2898(3)	15(1)
C(5)	6744(4)	9182(4)	6381(4)	10(1)
C(7)	5990(4)	7907(4)	3741(4)	12(1)
C(12)	1840(5)	4958(4)	-1029(4)	16(1)
C(1)	6578(5)	10043(4)	8503(4)	13(1)
C(6)	5708(4)	8372(4)	4905(4)	10(1)
C(10)	4529(5)	6535(4)	-688(4)	16(1)
C(3)	9338(5)	10639(4)	8412(4)	16(1)
C(8)	3901(5)	6585(4)	1238(4)	11(1)
C(4)	8527(5)	9831(4)	6994(4)	13(1)
C(2)	8343(5)	10739(4)	9164(4)	16(1)
C(13)	2314(5)	5510(4)	377(4)	14(1)
C(9)	5034(5)	7104(4)	724(4)	14(1)
C(11)	2937(5)	5467(4)	-1554(4)	16(1)
C(14)	1775(5)	4153(4)	3788(4)	19(1)

Bond lengths [Å] and angles [°] for larsen27_0m_a.

Pt(1)-Cl(2)	2.2854(9)
Pt(1)-Cl(1)	2.2900(9)
Pt(1)-N(2)	1.989(3)
Pt(1)-N(1)	2.035(3)
O(2)-N(5)	1.227(4)
N(2)-N(3)	1.314(4)
N(2)-C(6)	1.359(4)
O(1)-N(5)	1.227(4)
N(1)-C(5)	1.363(4)
N(1)-C(1)	1.347(5)
N(3)-N(4)	1.351(4)
N(4)-C(7)	1.349(4)
N(4)-C(8)	1.437(4)
N(5)-C(14)	1.480(5)
C(5)-C(6)	1.456(5)
C(5)-C(4)	1.385(5)
C(7)-H(7)	0.9500
C(7)-C(6)	1.363(5)
C(12)-H(12)	0.9500
C(12)-C(13)	1.384(5)
C(12)-C(11)	1.376(5)
C(1)-H(1)	0.9500
C(1)-C(2)	1.378(5)
C(10)-H(10)	0.9500
C(10)-C(9)	1.385(5)
C(10)-C(11)	1.382(5)
C(3)-H(3)	0.9500
C(3)-C(4)	1.390(5)
C(3)-C(2)	1.385(5)
C(8)-C(13)	1.381(5)
C(8)-C(9)	1.394(5)
C(4)-H(4)	0.9500
C(2)-H(2)	0.9500
C(13)-H(13)	0.9500
C(9)-H(9)	0.9500
C(11)-H(11)	0.9500
C(14)-H(14A)	0.9800
C(14)-H(14B)	0.9800
C(14)-H(14C)	0.9800

Cl(2)-Pt(1)-Cl(1)	90.06(3)
N(2)-Pt(1)-Cl(2)	174.82(8)
N(2)-Pt(1)-Cl(1)	94.90(9)

N(2)-Pt(1)-N(1)	79.84(12)
N(1)-Pt(1)-Cl(2)	95.30(9)
N(1)-Pt(1)-Cl(1)	173.67(8)
N(3)-N(2)-Pt(1)	132.6(2)
N(3)-N(2)-C(6)	111.7(3)
C(6)-N(2)-Pt(1)	115.7(2)
C(5)-N(1)-Pt(1)	115.5(2)
C(1)-N(1)-Pt(1)	125.5(2)
C(1)-N(1)-C(5)	118.7(3)
N(2)-N(3)-N(4)	104.3(3)
N(3)-N(4)-C(8)	118.2(3)
C(7)-N(4)-N(3)	112.1(3)
C(7)-N(4)-C(8)	129.7(3)
O(2)-N(5)-C(14)	118.3(3)
O(1)-N(5)-O(2)	123.6(3)
O(1)-N(5)-C(14)	118.1(3)
N(1)-C(5)-C(6)	113.0(3)
N(1)-C(5)-C(4)	122.1(3)
C(4)-C(5)-C(6)	124.8(3)
N(4)-C(7)-H(7)	127.4
N(4)-C(7)-C(6)	105.1(3)
C(6)-C(7)-H(7)	127.4
C(13)-C(12)-H(12)	119.8
C(11)-C(12)-H(12)	119.8
C(11)-C(12)-C(13)	120.4(4)
N(1)-C(1)-H(1)	119.2
N(1)-C(1)-C(2)	121.7(3)
C(2)-C(1)-H(1)	119.2
N(2)-C(6)-C(5)	115.8(3)
N(2)-C(6)-C(7)	106.7(3)
C(7)-C(6)-C(5)	137.5(3)
C(9)-C(10)-H(10)	120.0
C(11)-C(10)-H(10)	120.0
C(11)-C(10)-C(9)	120.0(4)
C(4)-C(3)-H(3)	120.5
C(2)-C(3)-H(3)	120.5
C(2)-C(3)-C(4)	118.9(3)
C(13)-C(8)-N(4)	120.1(3)
C(13)-C(8)-C(9)	121.6(3)
C(9)-C(8)-N(4)	118.2(3)
C(5)-C(4)-C(3)	118.6(3)
C(5)-C(4)-H(4)	120.7
C(3)-C(4)-H(4)	120.7
C(1)-C(2)-C(3)	119.9(4)

C(1)-C(2)-H(2)	120.0
C(3)-C(2)-H(2)	120.0
C(12)-C(13)-H(13)	120.6
C(8)-C(13)-C(12)	118.7(3)
C(8)-C(13)-H(13)	120.6
C(10)-C(9)-C(8)	118.6(4)
C(10)-C(9)-H(9)	120.7
C(8)-C(9)-H(9)	120.7
C(12)-C(11)-C(10)	120.7(4)
C(12)-C(11)-H(11)	119.7
C(10)-C(11)-H(11)	119.7
N(5)-C(14)-H(14A)	109.5
N(5)-C(14)-H(14B)	109.5
N(5)-C(14)-H(14C)	109.5
H(14A)-C(14)-H(14B)	109.5
H(14A)-C(14)-H(14C)	109.5
H(14B)-C(14)-H(14C)	109.5

Symmetry transformations used to generate equivalent atoms:

Anisotropic displacement parameters (Å2x 103) for larsen27_0m_a. The anisotropic
displacement factor exponent takes the form: -2□2[h2 a*2U11 + ... + 2 h k a* b* U12]

	U11	U22	U33	U23	U13	U12
Pt(1)	6(1)	11(1)	9(1)	3(1)	4(1)	3(1)
Cl(2)	11(1)	18(1)	11(1)	3(1)	6(1)	3(1)
Cl(1)	8(1)	23(1)	13(1)	4(1)	4(1)	4(1)
O(2)	14(1)	28(2)	25(2)	8(1)	7(1)	3(1)
N(2)	7(1)	11(1)	13(1)	5(1)	3(1)	4(1)
O(1)	24(2)	24(2)	17(2)	2(1)	5(1)	-2(1)
N(1)	9(1)	11(1)	12(2)	5(1)	5(1)	3(1)
N(3)	11(1)	16(2)	10(2)	5(1)	6(1)	5(1)
N(4)	10(1)	15(2)	11(2)	6(1)	7(1)	7(1)
N(5)	19(2)	13(2)	14(2)	7(1)	7(1)	5(1)
C(5)	8(2)	12(2)	13(2)	6(1)	5(1)	5(1)
C(7)	8(2)	15(2)	13(2)	6(2)	4(1)	4(1)
C(12)	10(2)	20(2)	13(2)	5(2)	2(2)	4(1)
C(1)	10(2)	16(2)	14(2)	6(2)	5(2)	6(1)

C(6)	7(1)	11(1)	13(1)	5(1)	3(1)	4(1)
C(10)	19(2)	19(2)	16(2)	9(2)	11(2)	7(2)
C(3)	11(2)	17(2)	16(2)	6(2)	2(2)	4(1)
C(8)	12(2)	15(2)	9(2)	5(1)	5(1)	8(1)
C(4)	7(2)	19(2)	15(2)	9(2)	4(2)	5(1)
C(2)	15(2)	14(2)	16(2)	4(2)	6(2)	7(1)
C(13)	12(2)	19(2)	16(2)	8(2)	8(2)	7(1)
C(9)	16(2)	13(2)	16(2)	7(2)	8(2)	4(1)
C(11)	20(2)	21(2)	9(2)	5(2)	6(2)	9(2)
C(14)	17(2)	21(2)	24(2)	8(2)	14(2)	6(2)

Hydrogen coordinates (x 104) and isotropic displacement parameters (Å2x 10 3)
for larsen27_0m_a.

	x	y	z	U(eq)
H(7)	7075	8028	3677	14
H(12)	750	4222	-1636	19
H(1)	5913	10094	9033	15
H(10)	5276	6879	-1061	19
H(3)	10556	11114	8859	19
H(4)	9182	9725	6457	16
H(2)	8876	11288	10134	19
H(13)	1564	5156	744	17
H(9)	6130	7831	1330	17
H(11)	2596	5080	-2521	20
H(14A)		2603	4589	4757	29
H(14B)		936	3226	3599	29
H(14C)		1162	4862	3596	29

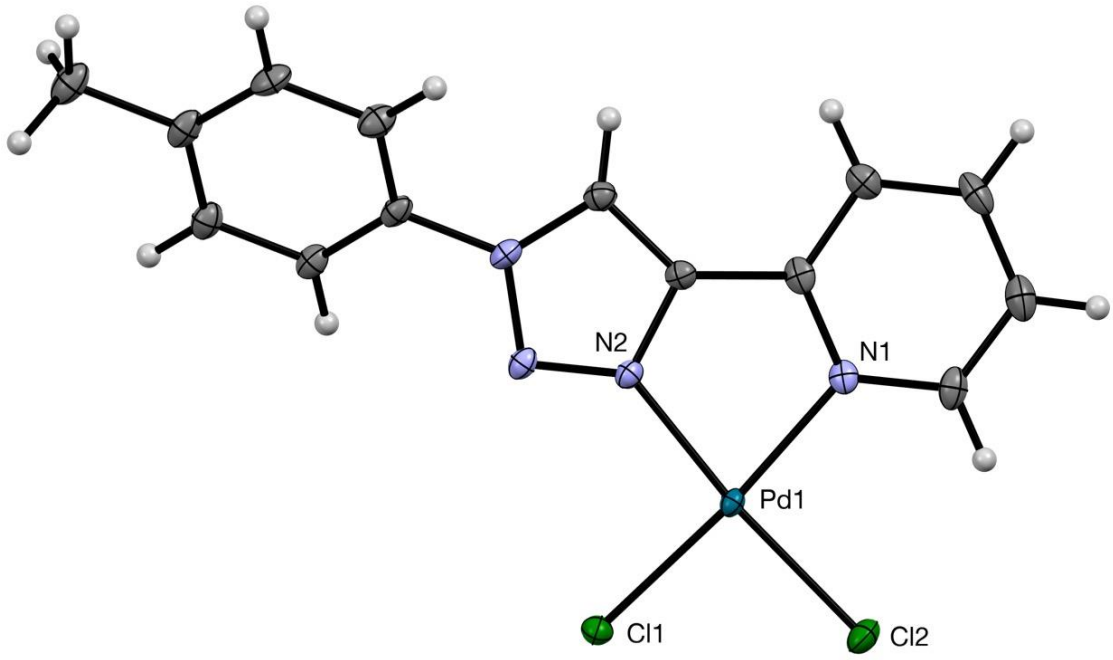

Crystal data and structure refinement for larsenxx_0m_a.

Identification code	larsenxx_0m_a
Empirical formula	C14 H12 Cl2 N4 O0.25 Pd
Formula weight	417.58
Temperature	100.0 K
Wavelength	0.71073 Å
Crystal system	Monoclinic
Space group	P 21/c
Unit cell dimensions	a = 11.0752(4) Å □= 90°.
	b = 7.1960(3) Å □= 94.668(2)°.
	c = 18.7616(7) Å □ = 90°.
Volume	1490.29(10) Å3
Z	4
Density (calculated)	1.861 Mg/m3
Absorption coefficient	1.603 mm-1
F(000)	824
Crystal size	0.3 x 0.28 x 0.24 mm3
Theta range for data collection	1.845 to 28.277°.
Index ranges	-14<=h<=14, -9<=k<=5, -25<=l<=25

Reflections collected	17077
Independent reflections	3697 [R(int) = 0.0674]
Completeness to theta = 25.242°	99.9 %
Absorption correction	Semi-empirical from equivalents
Max. and min. transmission	0.2541 and 0.2102
Refinement method	Full-matrix least-squares on F2
Data / restraints / parameters	3697 / 0 / 191
Goodness-of-fit on F2	1.103
Final R indices [I>2sigma(I)]	R1 = 0.0451, wR2 = 0.1166
R indices (all data)	R1 = 0.0487, wR2 = 0.1194
Extinction coefficient	n/a
Largest diff. peak and hole	2.671 and -0.758 e.Å-3

Atomic coordinates (x 104) and equivalent isotropic displacement parameters (Å2x 103)
for larsenxx_0m_a. U(eq) is defined as one third of the trace of the orthogonalized Uij tensor.

	x	y	z	U(eq)
Pd(1)	5970(1)	3108(1)	5195(1)	11(1)
Cl(1)	6572(1)	4033(1)	6328(1)	15(1)
Cl(2)	7857(1)	3718(1)	4833(1)	19(1)
N(1)	5272(3)	2246(4)	4201(2)	13(1)
N(2)	4289(3)	2394(4)	5426(2)	12(1)
N(3)	3702(3)	2436(4)	6004(2)	14(1)
N(4)	2596(3)	1740(4)	5795(2)	14(1)
C(1)	5839(3)	2336(6)	3594(2)	18(1)
C(2)	5273(4)	1765(6)	2947(2)	22(1)
C(3)	4104(4)	1067(6)	2918(2)	21(1)
C(4)	3512(3)	987(5)	3539(2)	17(1)
C(5)	4121(3)	1610(5)	4172(2)	14(1)
C(6)	3589(3)	1686(5)	4855(2)	13(1)
C(7)	2481(3)	1260(5)	5097(2)	15(1)
C(8)	1676(3)	1650(5)	6293(2)	15(1)
C(9)	480(3)	2036(5)	6048(2)	19(1)
C(10)	-408(3)	1955(5)	6530(2)	20(1)
C(11)	-116(3)	1531(5)	7249(2)	18(1)
C(12)	1097(3)	1188(5)	7483(2)	18(1)
C(13)	1992(3)	1229(5)	7008(2)	16(1)
C(14)	-1089(4)	1452(6)	7771(2)	23(1)

Bond lengths [Å] and angles [°] for larsenxx_0m_a.

Pd(1)-Cl(1)	2.2744(8)
Pd(1)-Cl(2)	2.2921(8)
Pd(1)-N(1)	2.055(3)
Pd(1)-N(2)	2.012(3)
N(1)-C(1)	1.347(5)
N(1)-C(5)	1.352(5)
N(2)-N(3)	1.310(4)
N(2)-C(6)	1.368(4)
N(3)-N(4)	1.351(4)
N(4)-C(7)	1.351(5)
N(4)-C(8)	1.438(5)
C(1)-H(1)	0.9500
C(1)-C(2)	1.383(6)
C(2)-H(2)	0.9500
C(2)-C(3)	1.385(6)
C(3)-H(3)	0.9500
C(3)-C(4)	1.383(5)
C(4)-H(4)	0.9500
C(4)-C(5)	1.392(5)
C(5)-C(6)	1.454(5)
C(6)-C(7)	1.376(5)
C(7)-H(7)	0.9500
C(8)-C(9)	1.395(5)
C(8)-C(13)	1.392(5)
C(9)-H(9)	0.9500
C(9)-C(10)	1.390(6)
C(10)-H(10)	0.9500
C(10)-C(11)	1.395(6)
C(11)-C(12)	1.401(5)
C(11)-C(14)	1.514(5)
C(12)-H(12)	0.9500
C(12)-C(13)	1.386(5)
C(13)-H(13)	0.9500
C(14)-H(14A)	0.9800
C(14)-H(14B)	0.9800
C(14)-H(14C)	0.9800

Cl(1)-Pd(1)-Cl(2)	90.88(3)
N(1)-Pd(1)-Cl(1)	174.85(9)
N(1)-Pd(1)-Cl(2)	94.25(9)

N(2)-Pd(1)-Cl(1)	94.57(9)
N(2)-Pd(1)-Cl(2)	174.10(9)
N(2)-Pd(1)-N(1)	80.33(12)
C(1)-N(1)-Pd(1)	125.9(3)
C(1)-N(1)-C(5)	119.0(3)
C(5)-N(1)-Pd(1)	115.0(2)
N(3)-N(2)-Pd(1)	134.6(2)
N(3)-N(2)-C(6)	111.6(3)
C(6)-N(2)-Pd(1)	113.7(2)
N(2)-N(3)-N(4)	104.5(3)
N(3)-N(4)-C(8)	120.1(3)
C(7)-N(4)-N(3)	112.8(3)
C(7)-N(4)-C(8)	127.0(3)
N(1)-C(1)-H(1)	119.4
N(1)-C(1)-C(2)	121.3(4)
C(2)-C(1)-H(1)	119.4
C(1)-C(2)-H(2)	120.1
C(1)-C(2)-C(3)	119.8(4)
C(3)-C(2)-H(2)	120.1
C(2)-C(3)-H(3)	120.4
C(2)-C(3)-C(4)	119.2(3)
C(4)-C(3)-H(3)	120.4
C(3)-C(4)-H(4)	120.8
C(3)-C(4)-C(5)	118.4(4)
C(5)-C(4)-H(4)	120.8
N(1)-C(5)-C(4)	122.2(3)
N(1)-C(5)-C(6)	113.6(3)
C(4)-C(5)-C(6)	124.2(3)
N(2)-C(6)-C(5)	117.3(3)
N(2)-C(6)-C(7)	106.8(3)
C(7)-C(6)-C(5)	135.9(3)
N(4)-C(7)-C(6)	104.3(3)
N(4)-C(7)-H(7)	127.9
C(6)-C(7)-H(7)	127.9
C(9)-C(8)-N(4)	118.8(3)
C(9)-C(8)-C(13)	121.2(3)
C(13)-C(8)-N(4)	120.0(3)
C(8)-C(9)-H(9)	120.7
C(8)-C(9)-C(10)	118.7(4)
C(10)-C(9)-H(9)	120.7
C(9)-C(10)-H(10)	119.4
C(9)-C(10)-C(11)	121.2(4)
C(11)-C(10)-H(10)	119.4
C(10)-C(11)-C(12)	118.8(3)

C(10)-C(11)-C(14)	120.8(3)
C(12)-C(11)-C(14)	120.4(3)
C(11)-C(12)-H(12)	119.6
C(13)-C(12)-C(11)	120.9(3)
C(13)-C(12)-H(12)	119.6
C(8)-C(13)-H(13)	120.4
C(12)-C(13)-C(8)	119.2(3)
C(12)-C(13)-H(13)	120.4
C(11)-C(14)-H(14A)	109.5
C(11)-C(14)-H(14B)	109.5
C(11)-C(14)-H(14C)	109.5
H(14A)-C(14)-H(14B)	109.5
H(14A)-C(14)-H(14C)	109.5
H(14B)-C(14)-H(14C)	109.5

Symmetry transformations used to generate equivalent atoms:

displacement parameters (Å2x 103) for larsenxx_0m_a. The anisotropic displacement factor exponent takes the form: -2□2[h2 a*2U11 + ... + 2 h k a* b* U12]

	U11	U22	U33	U23	U13	U12
Pd(1)	10(1)	11(1)	12(1)	2(1)	2(1)	1(1)
Cl(1)	14(1)	18(1)	14(1)	0(1)	0(1)	0(1)
Cl(2)	12(1)	24(1)	21(1)	4(1)	4(1)	0(1)
N(1)	14(1)	12(2)	13(1)	2(1)	1(1)	5(1)
N(2)	12(1)	12(2)	13(1)	1(1)	2(1)	0(1)
N(3)	13(1)	12(1)	17(1)	2(1)	4(1)	1(1)
N(4)	10(1)	14(2)	18(2)	1(1)	3(1)	-1(1)
C(1)	22(2)	16(2)	17(2)	5(2)	7(1)	6(1)
C(2)	28(2)	23(2)	15(2)	1(1)	5(2)	8(2)
C(3)	29(2)	20(2)	12(2)	-3(1)	-3(1)	8(2)
C(4)	21(2)	14(2)	16(2)	0(1)	-1(1)	2(1)
C(5)	18(2)	10(2)	15(2)	0(1)	2(1)	6(1)
C(6)	13(2)	10(2)	16(2)	-1(1)	1(1)	1(1)
C(7)	14(2)	14(2)	18(2)	-1(1)	1(1)	-1(1)
C(8)	13(2)	11(2)	21(2)	-1(1)	6(1)	-1(1)
C(9)	15(2)	19(2)	24(2)	4(1)	1(1)	1(1)
C(10)	11(2)	21(2)	29(2)	2(2)	2(1)	1(1)
C(11)	18(2)	12(2)	26(2)	2(2)	8(1)	1(1)

C(12)	19(2)	14(2)	20(2)	2(1)	6(1)	0(1)
C(13)	14(2)	12(2)	21(2)	1(1)	5(1)	2(1)
C(14)	19(2)	17(2)	33(2)	4(2)	10(2)	3(2)

Hydrogen coordinates (x 104) and isotropic displacement parameters (Å2x 10 3)
for larsenxx_0m_a.

	x	y	z	U(eq)
H(1)	6644	2800	3610	22
H(2)	5684	1852	2523	26
H(3)	3714	648	2478	25
H(4)	2710	519	3533	21
H(7)	1793	747	4832	18
H(9)	275	2348	5561	23
H(10)	-1228	2193	6367	24
H(12)	1309	924	7973	21
H(13)	2811	972	7169	19
H(14A)	-1188	166	7928	34
H(14B)	-1856	1902	7536	34
H(14C)	-853	2237	8186	34

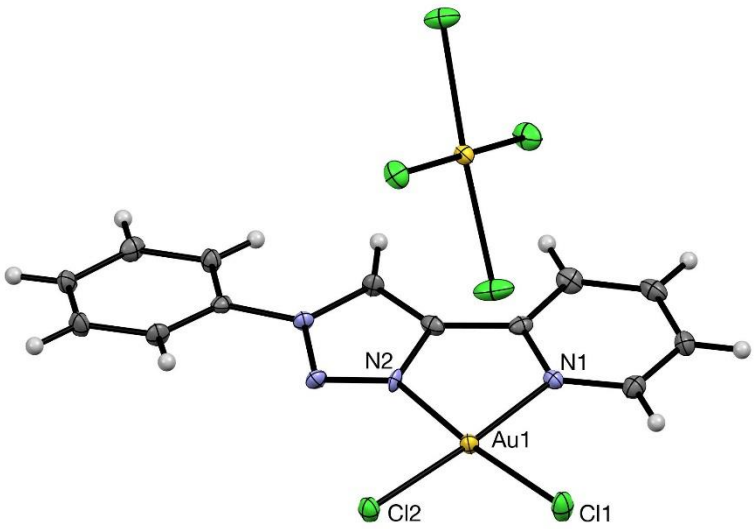

Crystal data and structure refinement for larsen09_0m_a.

Identification code	ZLP-2-174
Empirical formula	C13 H10 Au2 Cl6 N4
Formula weight	828.88
Temperature	100 K
Wavelength	0.71073 Å
Crystal system	Triclinic
Space group	P-1
Unit cell dimensions	a = 8.2608(4) Å □= 73.756(2)°.
	b = 9.8841(5) Å □= 89.018(2)°.
	c = 12.3256(6) Å □ = 79.336(2)°.
Volume	948.89(8) Å3
Z	2
Density (calculated)	2.901 Mg/m3
Absorption coefficient	16.293 mm-1
F(000)	752
Crystal size	0.3 x 0.24 x 0.16 mm3
Theta range for data collection	2.371 to 27.876°.
Index ranges	-10<=h<=9, -12<=k<=12, -14<=l<=16
Reflections collected	10948
Independent reflections	4427 [R(int) = 0.0265]
Completeness to theta = 25.242°	98.8 %
Absorption correction	Semi-empirical from equivalents
Max. and min. transmission	0.2622 and 0.1441

Refinement method Full-matrix least-squares on F2
Data / restraints / parameters 4427 / 0 / 226
Goodness-of-fit on F2 1.023
Final R indices [I>2sigma(I)] R1 = 0.0196, wR2 = 0.0389
R indices (all data) R1 = 0.0257, wR2 = 0.0405
Extinction coefficient n/a
Largest diff. peak and hole 0.781 and -1.041 e.Å-3

Atomic coordinates (x 104) and equivalent isotropic displacement parameters (Å2x 103)
for larsen09_0m_a. U(eq) is defined as one third of the trace of the orthogonalized Uij tensor.

	x	y	z	U(eq)
Au(1)	4454(1)	231(1)	8117(1)	11(1)
Au(2)	4265(1)	3731(1)	4171(1)	12(1)
Cl(2)	6669(1)	536(1)	9013(1)	16(1)
Cl(4)	6918(1)	4112(1)	4063(1)	18(1)
Cl(1)	5897(1)	-1834(1)	7887(1)	20(1)
Cl(6)	1601(1)	3386(1)	4334(1)	22(1)
Cl(5)	3505(1)	5697(1)	2659(1)	22(1)
Cl(3)	5087(1)	1678(1)	5593(1)	28(1)
N(2)	2988(4)	2066(3)	8211(3)	11(1)
N(1)	2335(4)	112(3)	7318(3)	12(1)
N(3)	3230(4)	3068(3)	8663(3)	12(1)
N(4)	1855(4)	4051(3)	8372(3)	12(1)
C(3)	-650(5)	165(4)	6338(3)	18(1)
C(9)	68(5)	6117(4)	8744(3)	14(1)
C(8)	1637(4)	5316(4)	8774(3)	12(1)
C(4)	-413(5)	1328(4)	6704(3)	16(1)
C(11)	1193(5)	7600(4)	9669(3)	16(1)
C(5)	1090(5)	1284(4)	7188(3)	12(1)
C(6)	1509(4)	2375(4)	7656(3)	13(1)
C(7)	756(4)	3685(4)	7746(3)	13(1)
C(2)	636(5)	-985(4)	6453(3)	16(1)
C(13)	2993(5)	5650(4)	9203(3)	15(1)
C(1)	2118(5)	-987(4)	6935(3)	16(1)
C(10)	-147(5)	7281(4)	9191(3)	16(1)
C(12)	2756(5)	6797(4)	9671(3)	17(1)

Bond lengths [Å] and angles [°] for larsen09_0m_a.

Au(1)-Cl(2)	2.2621(9)
Au(1)-Cl(1)	2.2540(9)
Au(1)-N(2)	2.017(3)
Au(1)-N(1)	2.061(3)
Au(2)-Cl(4)	2.2872(9)
Au(2)-Cl(6)	2.2858(9)
Au(2)-Cl(5)	2.2815(10)
Au(2)-Cl(3)	2.2786(11)
N(2)-N(3)	1.310(4)
N(2)-C(6)	1.352(5)
N(1)-C(5)	1.373(5)
N(1)-C(1)	1.340(5)
N(3)-N(4)	1.331(4)
N(4)-C(8)	1.450(4)
N(4)-C(7)	1.360(4)
C(3)-H(3)	0.9500
C(3)-C(4)	1.393(5)
C(3)-C(2)	1.381(5)
C(9)-H(9)	0.9500
C(9)-C(8)	1.383(5)
C(9)-C(10)	1.390(5)
C(8)-C(13)	1.378(5)
C(4)-H(4)	0.9500
C(4)-C(5)	1.374(5)
C(11)-H(11)	0.9500
C(11)-C(10)	1.388(5)
C(11)-C(12)	1.384(5)
C(5)-C(6)	1.453(5)
C(6)-C(7)	1.362(5)
C(7)-H(7)	0.9500
C(2)-H(2)	0.9500
C(2)-C(1)	1.370(5)
C(13)-H(13)	0.9500
C(13)-C(12)	1.393(5)
C(1)-H(1)	0.9500
C(10)-H(10)	0.9500
C(12)-H(12)	0.9500

Cl(1)-Au(1)-Cl(2)	90.13(3)
N(2)-Au(1)-Cl(2)	95.59(9)
N(2)-Au(1)-Cl(1)	174.15(9)
N(2)-Au(1)-N(1)	79.68(12)

N(1)-Au(1)-Cl(2)	175.28(9)
N(1)-Au(1)-Cl(1)	94.59(9)
Cl(6)-Au(2)-Cl(4)	177.87(3)
Cl(5)-Au(2)-Cl(4)	89.88(4)
Cl(5)-Au(2)-Cl(6)	90.57(4)
Cl(3)-Au(2)-Cl(4)	89.57(4)
Cl(3)-Au(2)-Cl(6)	90.13(4)
Cl(3)-Au(2)-Cl(5)	175.98(4)
N(3)-N(2)-Au(1)	132.0(3)
N(3)-N(2)-C(6)	112.9(3)
C(6)-N(2)-Au(1)	115.0(2)
C(5)-N(1)-Au(1)	114.6(2)
C(1)-N(1)-Au(1)	125.2(3)
C(1)-N(1)-C(5)	120.2(3)
N(2)-N(3)-N(4)	103.4(3)
N(3)-N(4)-C(8)	119.4(3)
N(3)-N(4)-C(7)	113.3(3)
C(7)-N(4)-C(8)	127.2(3)
C(4)-C(3)-H(3)	120.4
C(2)-C(3)-H(3)	120.4
C(2)-C(3)-C(4)	119.2(4)
C(8)-C(9)-H(9)	120.8
C(8)-C(9)-C(10)	118.5(3)
C(10)-C(9)-H(9)	120.8
C(9)-C(8)-N(4)	118.8(3)
C(13)-C(8)-N(4)	118.7(3)
C(13)-C(8)-C(9)	122.5(3)
C(3)-C(4)-H(4)	120.6
C(5)-C(4)-C(3)	118.8(4)
C(5)-C(4)-H(4)	120.6
C(10)-C(11)-H(11)	119.7
C(12)-C(11)-H(11)	119.7
C(12)-C(11)-C(10)	120.5(3)
N(1)-C(5)-C(4)	120.8(3)
N(1)-C(5)-C(6)	113.6(3)
C(4)-C(5)-C(6)	125.5(4)
N(2)-C(6)-C(5)	116.8(3)
N(2)-C(6)-C(7)	106.4(3)
C(7)-C(6)-C(5)	136.8(4)
N(4)-C(7)-H(7)	128.0
C(6)-C(7)-N(4)	104.0(3)
C(6)-C(7)-H(7)	128.0
C(3)-C(2)-H(2)	119.9
C(1)-C(2)-C(3)	120.3(4)

C(1)-C(2)-H(2)	119.9
C(8)-C(13)-H(13)	120.8
C(8)-C(13)-C(12)	118.4(3)
C(12)-C(13)-H(13)	120.8
N(1)-C(1)-C(2)	120.6(4)
N(1)-C(1)-H(1)	119.7
C(2)-C(1)-H(1)	119.7
C(9)-C(10)-H(10)	120.0
C(11)-C(10)-C(9)	119.9(4)
C(11)-C(10)-H(10)	120.0
C(11)-C(12)-C(13)	120.1(4)
C(11)-C(12)-H(12)	120.0
C(13)-C(12)-H(12)	120.0

Symmetry transformations used to generate equivalent atoms:

Anisotropic displacement parameters (Å2x 103) for larsen09_0m_a. The anisotropic
displacement factor exponent takes the form: -2□2[h2 a*2U11 + ... + 2 h k a* b* U12]

	U11	U22	U33	U23	U13	U12
Au(1)	10(1)	11(1)	13(1)	-5(1)	-2(1)	0(1)
Au(2)	12(1)	13(1)	10(1)	-3(1)	0(1)	-3(1)
Cl(2)	13(1)	16(1)	20(1)	-8(1)	-4(1)	-1(1)
Cl(4)	13(1)	23(1)	20(1)	-7(1)	2(1)	-5(1)
Cl(1)	16(1)	17(1)	30(1)	-14(1)	-5(1)	2(1)
Cl(6)	15(1)	27(1)	22(1)	-3(1)	-1(1)	-10(1)
Cl(5)	16(1)	21(1)	21(1)	6(1)	0(1)	0(1)
Cl(3)	23(1)	25(1)	25(1)	9(1)	0(1)	-1(1)
N(2)	13(2)	7(2)	14(2)	-7(1)	2(1)	-1(1)
N(1)	12(2)	13(2)	12(2)	-4(1)	-2(1)	-2(1)
N(3)	13(2)	9(2)	14(2)	-3(1)	-2(1)	2(1)
N(4)	10(2)	10(2)	14(2)	-4(1)	-2(1)	1(1)
C(3)	15(2)	24(2)	14(2)	-4(2)	-2(2)	-4(2)
C(9)	12(2)	15(2)	18(2)	-6(2)	-2(2)	-3(2)
C(8)	15(2)	10(2)	9(2)	-2(2)	1(2)	-1(2)
C(4)	12(2)	21(2)	16(2)	-6(2)	4(2)	-2(2)
C(11)	19(2)	14(2)	15(2)	-8(2)	-3(2)	1(2)
C(5)	13(2)	12(2)	11(2)	-1(2)	3(2)	-1(2)

C(6)	10(2)	17(2)	11(2)	-2(2)	0(2)	-4(2)
C(7)	7(2)	13(2)	18(2)	-5(2)	-1(2)	0(2)
C(2)	20(2)	16(2)	15(2)	-7(2)	-2(2)	-3(2)
C(13)	11(2)	13(2)	19(2)	-6(2)	-2(2)	3(2)
C(1)	17(2)	14(2)	17(2)	-5(2)	1(2)	-2(2)
C(10)	16(2)	15(2)	17(2)	-6(2)	4(2)	1(2)
C(12)	14(2)	17(2)	21(2)	-9(2)	-6(2)	-1(2)

Hydrogen coordinates (x 104) and isotropic displacement parameters (Å2x 10 3)
for larsen09_0m_a.

	x	y	z	U(eq)
H(3)	-1684	162	6013	22
H(9)	-842	5878	8426	17
H(4)	-1274	2137	6621	19
H(11)	1036	8375	9998	19
H(7)	-294	4219	7443	15
H(2)	492	-1777	6196	19
H(13)	4065	5109	9180	18
H(1)	3001	-1775	7000	19
H(10)	-1209	7857	9169	20
H(12)	3667	7030	9993	20

Chapter 6: Novel Gold Complexes with Mixed X/L-Type Pyridyl Pyrazole Ligands

6.1 Introduction

When describing organic molecules functioning as ligands for metal complexes, they are generally referred to as either X-type or L-type. Anionic X-type ligands form discrete bonds with metal centers and change the oxidation state of the metal by +1; L-type ligands are electrostatic dative interactions which coordinate to the metal due to its electrophilic nature and does not change the metal's oxidation state. There has been a surge of interest in synthesizing multi-dentate ligands which employ both X-type and L-type ligands.[1] Not only are mixed ligand complex of transition metals found in biological systems,[2] but mixed ligands have shown greater therapeutic activity than their strictly L-type analogues.[3] Commonly, these metal complexes are formed with amino acids as ligands, however the ability to design heterocyclic mixed ligands would bring the ability to tune to the ligand and corresponding complex. Looking at the collection of nitrogen heterocycles, there are only a few aromatic species which contain a nitrogen that can act as an X-type donor. Pyrazoles and their derivatives are heterocycles which contain two adjacent nitrogen atoms, one of which being an N-H. Pyrazoles have a history of possessing biological and pharmaceutical activity including being present in the multi-billion dollar generating drug

Celebrex.[4] In addition to being sought for their bioactive properties, pyrazoles also have precedent as ligands in metal complexes.[5]

Their rich history in coordination chemistry lies in both the nucleophilicity of the sp^2 hybridized nitrogen as well as the acidity of the N-H to function as a chelate when there is substitution on the pyrazole ring.[6] For a bidentate heterocyclic ligand, however, a pyridine is bound to the 3 position which acts as an L-type donor and allows the pyrazole N-H to act as an X-type donor. These ligands, referred to as pyridyl-pyrazoles or PyPyrs, have been used to form metal complexes with a wide array of metals including Fe,[7] Co,[8-9] Cu,[8,10-12] Ag,[12] Ir,[13-14] Rh,[14] Os,[14] Mo,[15] Pd,[16-17] Pt,[16] and Ru.[14,18] Accessing pyridyl pyrazoles can be done in a number of ways, however the most attractive way from a synthesis standpoint is through generating an *in situ* aryl diazomethane followed by a 1,3-cyclization with 2-ethynylpyridine. An optimized method for this synthesis has been developed by the Larsen group, allowing for the installation of substituents on the aryl backbone simply by changing the starting aldehyde (**Scheme 6.1**).

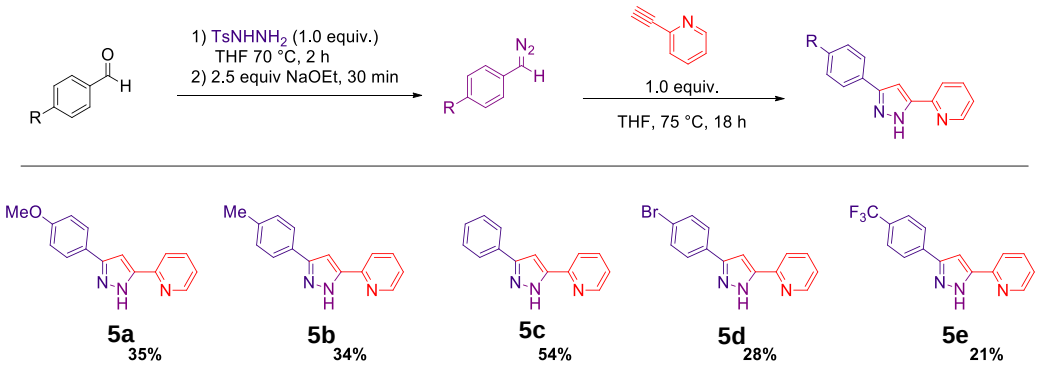

Scheme 6.1 Modular synthesis of mixed X/L-type PyPyr ligands

While this process is somewhat low yielding, the R-PyPyr ligands can be accessed in a single step without column chromatography as the product is isolated through recrystallization. Unlike previously synthesized ligands where the resting state in solution is with the pyridine pointed away from the nitrogen on the respective heterocycle it is bound to, the PyPyr ligand's N-H bond disrupts this trend. Initially, acquiring ^{1}H NMR for these ligands was incredibly difficult. Due to hydrogen-bonding between the pyridine nitrogen and the N-H of the pyrazole, the molecule prefers to sit where the N-H is shared, however it does not rest as a discrete structure in this conformation. As the sigma bond which connects the pyridine and pyrazole rotates, the ^{1}H resonances broaden in the NMR spectrum, leading to a difficult to analyze spectrum in $CDCl_3$. Switching solvents to deuterated trifluoroacetic results in protonation and resolution of the ^{1}H NMR spectrum.

Although there is much literature and in-lab precedent for the formation of metal complexes with L-type bidentate ligands, mixed X/L ligands pose some unique complications. For the PyPyr ligand to have one neutral and one anionic nitrogen, the N-H has to be deprotonated at some point. Initially, this was believed to be a necessary step prior to introduction of the metal source (**Scheme 6.2**).

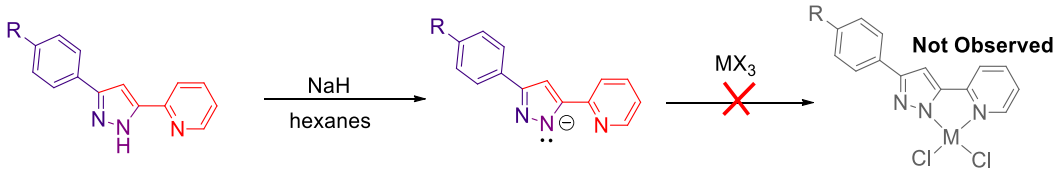

Scheme 6.2 Deprotonation of PyPyr ligand prior to metal introduction unsuccessful

However, deprotonating the pyrazole prior to exposing the ligand to a metal source resulted in no discrete complex formation. After finding precedent from the Crowley group (who has made metal complexes with similar types of pyrazole pyridine ligands), the N-H deprotonation occurs after the initial metal binding (**Scheme 6.3**).

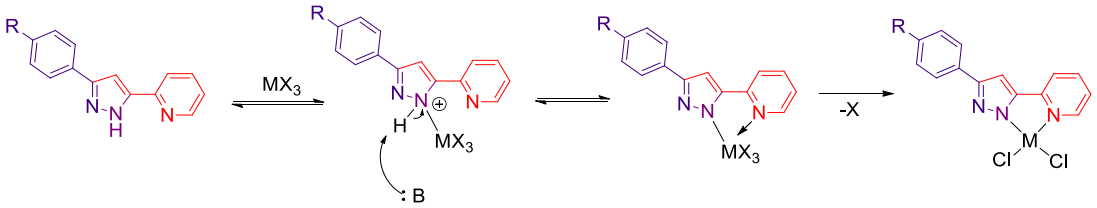

Scheme 6.3 Direct complexation successful due to initial pyrazole N-H binding to metal

The bound metal acidifies the N-H which is deprotonated by some basic species (likely a pyrazole pyridine molecule) which results in the X-type nitrogen-metal bond formation. The pyridine's lone pair of electrons are then attracted to the electrophilic metal center, coordinates to it, and loss of one of the initial X-type ligands (likely a halide) gives the PyPyr metal complex.

When determining the viability of a metal complex that employs X-type ligands, both the preferred geometry and the oxidation state of the metal are important to consider. Certain metals, specifically group 10 metals in a +2-

oxidation state such as palladium (II), nickel (II), and platinum (II), have been used to make PyPyr-metal complexes. However, since these complexes have a +2-oxidation state and the PyPyr ligand has both X-type and L-type chelates, it is observed that one of two things can happen: either a bis-PyPyr metal complex forms (**Scheme 6.4 - Path A)** giving an overall neutral complex or the PyPyr ligand isomerizes (turning both nitrogen chelates into L-type) and forms a mono-PyPyr metal complex (**Scheme 6.4 - Path B**).

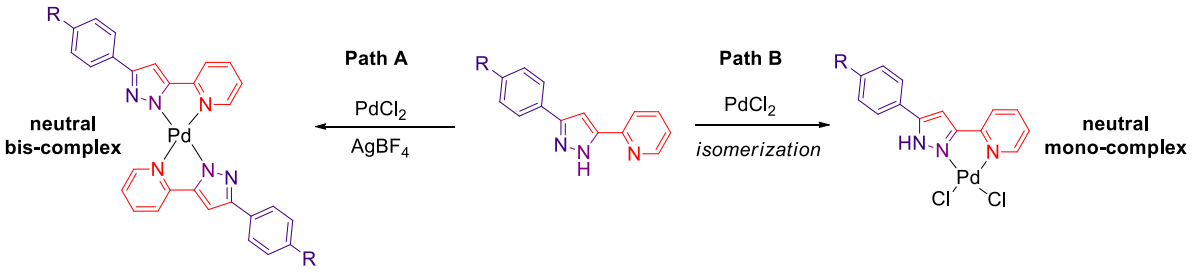

Scheme 6.4 PyPyr ligands allow for both mono- and bis-complexes, with the mono-complexes likely resulting in isomerization of the ligand

This phenomenon is not explicitly mentioned by the Pons group, however the X-ray crystal data of their PyPyr($PdCl_2$) complex clearly shows an isomerized ligand. The fact that the ligand isomerizes is actually quite reasonable, as the complex would be overall net anionic if the mixed X/L pyrazole pyridine bound as intended, which would be a significantly less stable complex.

While there is precedent for four-coordinate, square-planaer PyPyr metal complexes which employ metals with a +2-oxidation state, there are no examples of analogous complexes that use metals in a +3-oxidation state. The major

difference in switching to a higher oxidation state metal is that for the mono-complexes, there is no drive for the ligand to isomerize. With two X-type halide ligands and one non-isomerized PyPyr ligand, the overall charge of the complex would be neutral and ideally quite stable. The X-type PyPyr chelate should hold the metal much tighter, thus lowering the possibility of reduction and ligand dissociation. Additionally, for the bis-PyPyr complexes, the overall net charge with two PyPyr ligands on a +3-metal center would be cationic, a significantly more preferable charge than the potential anionic complexes formed from a non-isomerized ligand on a +2-metal center. With these in mind, the clear direction is to use the tunable PyPyr ligands to form gold (III) metal complexes.

6.2 Synthesis of R-PyPyr Gold (III) Chloride Complexes

Using the PyQuin($AuCl_3$), PyQuin$(AuCl_2)^+$, and PyTri$(AuCl_2)^+$ complexes as a model, an effort was made to synthesize a PyPyr gold (III) complex. Due to the fact that a gold (III) complex would require three X-type ligands to be net neural, the expected structure would be a square-planar, four-coordinate R-PyPyr($AuCl_2$) complex. As mentioned previously, attempts to deprotonate the ligand as an initial step was deemed unnecessary, so the complexation was designed the same as with previous complexes: gold salt ($NaAuCl_4$) and ligand (PyPyr) are stirred together for 1 hour at elevated temperature followed by addition of necessary equivalents of the halide abstracting reagent silver tetrafluoroborate ($AgBF_4$) while heating and stirring until precipitation of silver chloride (AgCl) (**Scheme 6.5**).

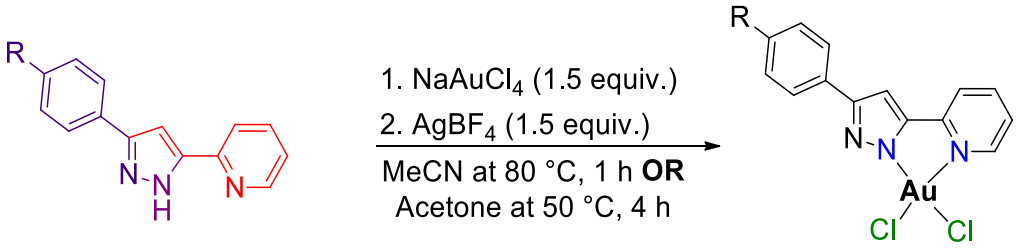

Scheme 6.5 Adapting the PyQuin and PyTri gold (III) complex synthesis is successful for forming mono-PyPyr($AuCl_2$) complex

In a similar manner to the PyTri ligands, the PyPyr ligands had varying degrees of solubility in common organic solvents. For complexation to occur in high yields, the reaction must be run at elevated temperatures, ideally 80 °C, however both the Br-PyPyr and CF_3-PyPyr ligands were completely insoluble in hot acetonitrile. For this reason, the Br-PyPyr($AuCl_2$) and CF_3-PyPyr($AuCl_2$) syntheses were run in acetone and could only be run at 50 °C to limit the solvent boiling off. Fortunately, the complexations were successful in acetone however they did require significantly longer reaction times than the complexations run in acetonitrile (4 hours and 1 hour, respectively). Generally, the complexations give quantitative conversion to gold complex with 1 equivalent of ligand, 1 equivalent of gold salt, and the necessary equivalents of silver tetrafluoroborate (in this case, 1 equivalent). For the PyPyr($AuCl_2$) complexes, however, an extra half equivalent of both the gold and silver was required to get full consumption of the ligand. Since these complexes are isolated via a plug filtration and concentration of a hot supernatant, full ligand consumption is absolutely necessary.

With a working method developed for the R-PyPyr($AuCl_2$) complexes, a series was made using the analogous series of PyPyr ligands (**Scheme 6.6**).

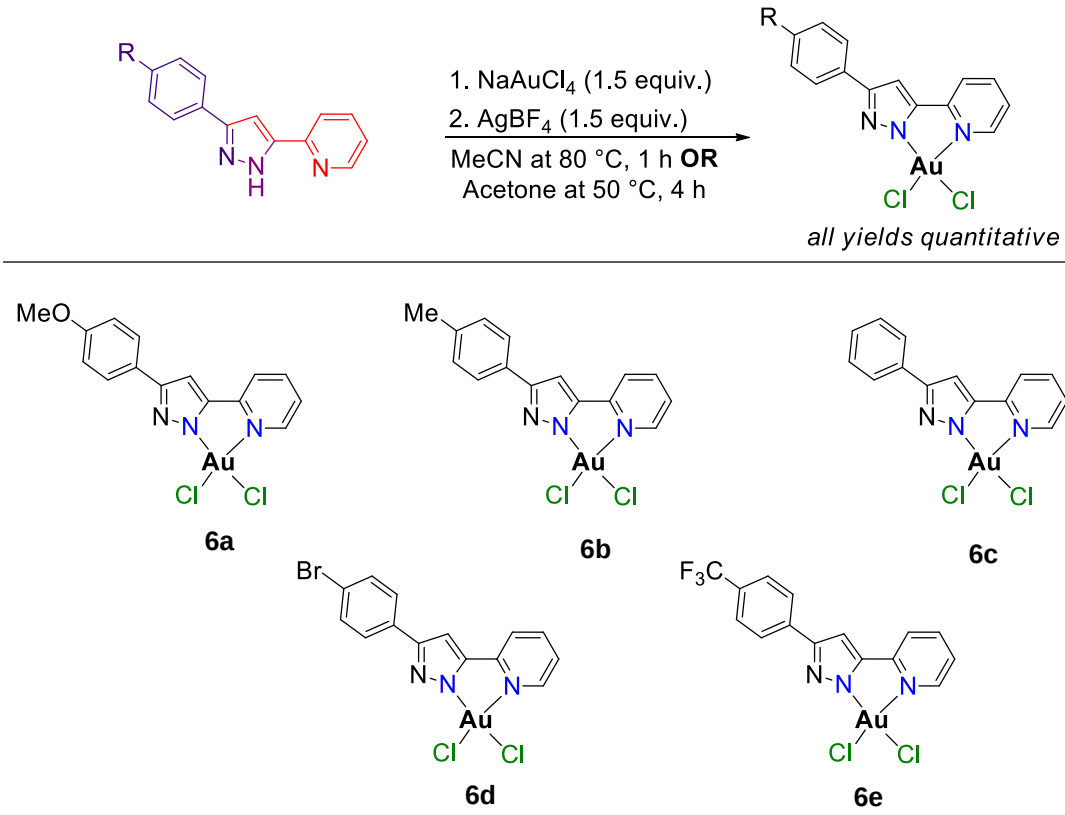

Scheme 6.6 Series of R-PyPyr($AuCl_2$) complexes synthesized in quantitative yields

The series of complexes were isolated, fully characterized, and compared to one another. When the library of PyPyr ligands was completed, ^{1}H NMR spectroscopy was used to see the effect of the ligand substituent. As seen before with the PyQuin and PyTri ligands, the chemical shift of the resonances responds to the electron-donating/electron-withdrawing nature of the R-group. To ensure that the effect carries through to the gold (III) complexes, the ^{1}H NMR spectra for the complexes were stacked to illustrate this effect (**Figure 6.1**). As with the other

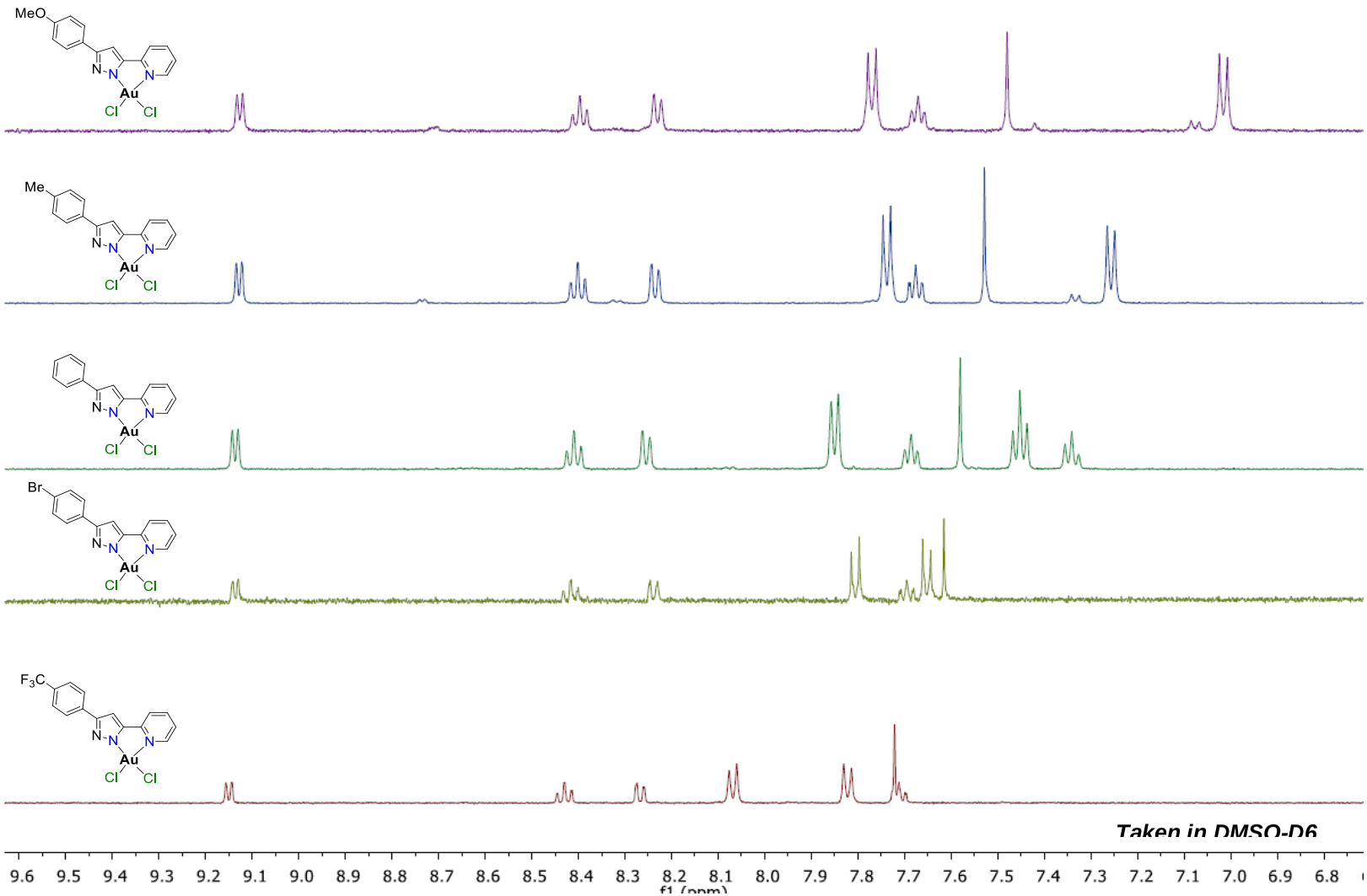

Figure 6.1 ^{1}H NMR comparison of electronically different R-PyPyr($AuCl_2$) complexes

complexes that have been synthesized using novel Larsen lab heteroaromatic ligands, there are certain resonances that can be used to track the electronic nature of the complex quite effectively. In the case of the R-PyPyr($AuCl_2$) complexes, the key resonance to follow is the singlet belonging to the proton on the pyrazole backbone. This chemical shift of this proton is effected solely by the donating/withdrawing effect of the R-group. As clearly shown in the ^1H NMR stack, the effect is quite evident, with the singlet moving downfield going from the electron-donating methoxy (MeO) to the electron withdrawing trifluoromethyl (CF_3) substituent.

One change that would be quite beneficial to observe would be the change between an unbound R-PyPyr ligand and its corresponding gold (III) complex. Unfortunately, this is near-impossible to observe due to the pyrazole's N-H and pyridine nitrogen hydrogen bonding which distorts the spectrum. As stated earlier, the spectrum resolves significantly when taken in deuterated trifluoromethylacetic acid, and the comparison between the two solvents is shown in **Figure 6.2**.

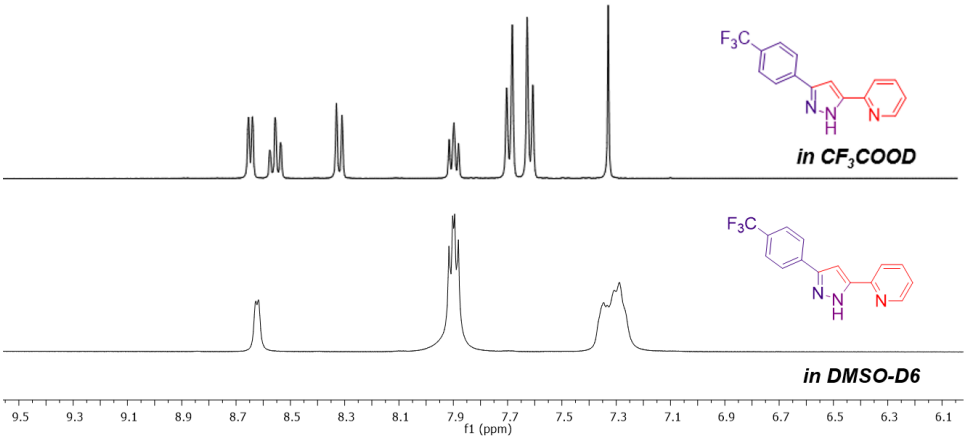

Figure 6.2 Comparison of the resolution of ^{1}H NMR spectra for the CF_3-PyPyr ligand in deuterated DMSO and in deuterated trifluoroacetic acid

The coalescence of the resonances is resolved upon deuteration from the acetic acid NMR solvent which mimics the dipole minimization of the PyQuin and PyTri ligands. Interestingly, the only resonances that are not broadened in the DMSO PyPyr spectrum are the ones belonging to the aryl ring due to their distance from the nitrogen atoms. If the peak order of the ligand taken in deuterated trifluoroacetic acid is compared to the peak order of the complex in DMSO, the same sort of “pyridine flip” is observed. The most upfield resonance, the singlet attributed to the pyrazole C-H, moves downfield significantly upon binding due to the electrophilic metal withdrawing and delocalizing the electrons in the heterocycle.

Even with mass spectrometry confirming the chemical formula and both ^{1}H & ^{13}C NMR spectra, to confirm the proposed structure of these novel gold (III) complexes an x-ray quality crystal needed to be obtained. Somewhat

unsurprisingly, the solubility of the PyPyr($AuCl_2$) complexes was quite low in common organic solvents, even hot nitromethane which had worked for previously synthesized gold (III) complexes. In order to form sufficient crystals to obtain crystallographic data, a more in-depth process for crystal growth was required. The PyPyr($AuCl_2$) complex was stirred in refluxing dichloromethane for 30 minutes until the solution above the complex was pale yellow. This solution was cooled (any formed precipitate was filtered off) and pipetted into an NMR tube until halfway full. Hexanes was then *carefully* pipetted on top of the methylene chloride solution of complex. The slow diffusion of the clear hexanes layer into the yellow methylene chloride/PyPyr($AuCl_2$) complex layer was allowed over the course of 3 weeks unperturbed. As the polarity of the methylene chloride slowly lowers, this allows very slow crystal growth which resulted in small, cubic yellow-orange crystals to form. These crystals were collected and analyzed at the University of San Diego X-Ray Crystallography lab of Prof. Arnold Rheingold and the results are shown in **Figure 6.3**.

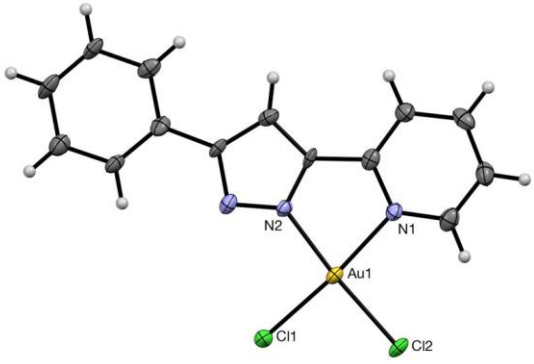

Figure 6.3 X-ray crystal structure for PyPyr($AuCl_2$) complex verifies no isomerization occurs

As proposed, the complex is an overall neutral, four-coordinate, square-planar gold (III) complex with the PyPyr ligand chelating in a mixed X/L-type bidentate fashion. Based on the bond angle formed between the pyridine nitrogen, gold (III) atom, and pyrazole nitrogen, the bite-angle even for a mixed X/L bidentate ligand is still comparable to a traditional 2,2´-bipyridine bite angle. What is most evident through the crystallographic data is the difference in binding strength of the pyrazole X-type nitrogen and the pyridine L-type nitrogen. It was proposed that by using an X-type ligand anchor in conjunction with an L-type ligand, the overall system would be more stable and less susceptible to reduction. As shown by the bond lengths, the pyrazole nitrogen-gold bond is significantly shorter (0.074 Å) than the pyridine nitrogen-gold bond. This verifies that the anionic nitrogen holds the gold more tightly and, in theory, gives a more stable complex.

As mentioned earlier, when the synthesis of the R-PyPyr($AuCl_2$) complexes were run using 1 equivalent of PyPyr ligand and 1 equivalent of gold salt, it was observed that not only was there not full consumption of PyPyr ligand, but also there was an impurity observed in the ^1H NMR that looked a lot like the complex, just shifted downfield significantly. This product was suspected to be a gold (III) complex consisting of two PyPyr ligands to one gold center. To force this as the major product, the stoichiometry of the reaction was modified to a 2.5:1 ratio of ligand to sodium tetrachloroaurate. Since the ligand (as seen with the mono PyPyr($AuCl_2$) complex) is acting as a mixed X/L ligand, the gold salt

only requires abstraction of one halide, since the complex is overall cationic with one non-coordinating anionic ligand (**Scheme 6.7**).

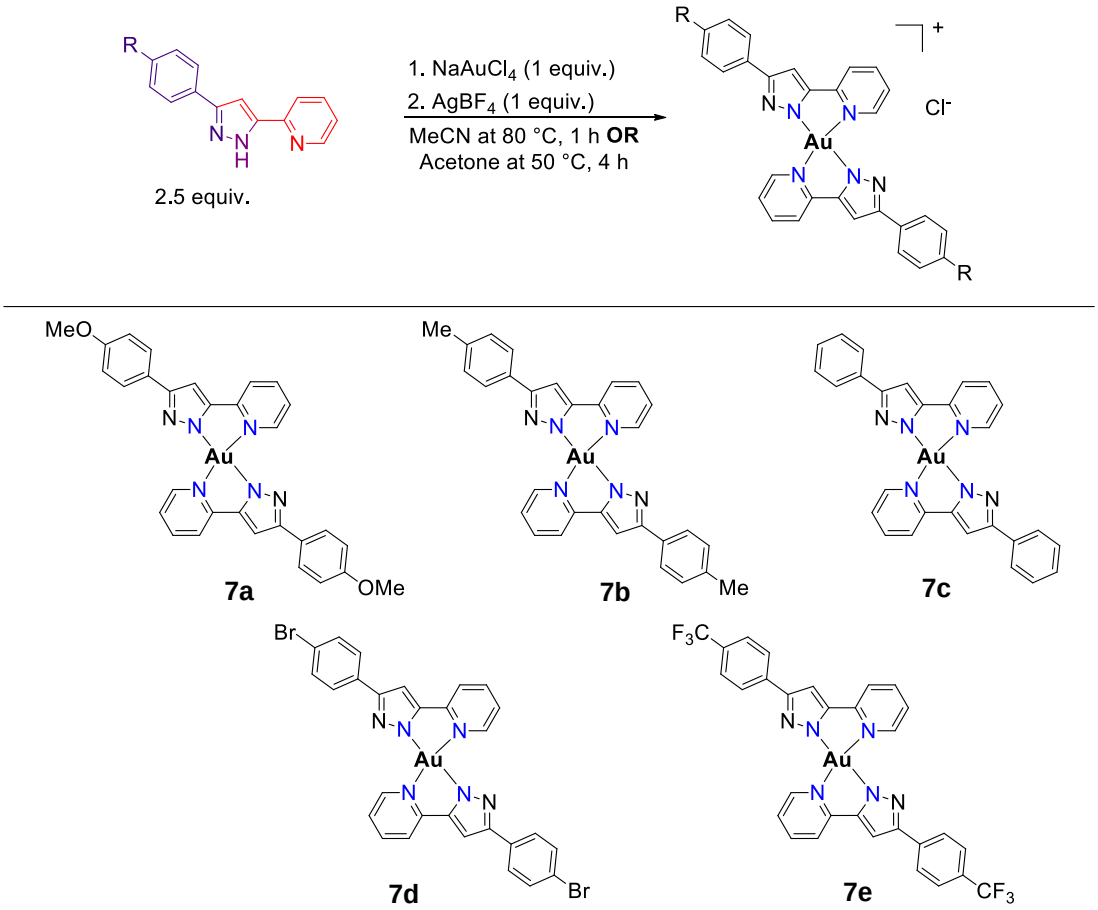

Scheme 6.7 Synthesis of cationic bis-PyPyr gold (III) complexes

Unlike the other gold (III) complexation reactions, the product of this reaction is quite large and insoluble in the reaction solvent, resulting in its precipitation upon forming. The issue that arises with this is that upon halide abstraction by the single equivalent of $AgBF_4$, one equivalent of silver chloride forms and precipitates alongside the product. This is not so much problematic as it is

inconvenient, as the $(PyPyr_2)Au^+$ complex can be isolated away from silver chloride through recrystallization.

When comparing the ^1H NMR spectra of the bis $(PyPyr)_2Au^+$ complex to the mono $PyPyr(AuCl_2)$ complex, the pattern of resonances is almost identical except for the chemical shift (**Figure 6.4**). The downfield shifting is quite dramatic: for example, the most downfield doublet in the mono complex is 9.15 ppm but in the bis complex the further downfield resonance is 10.65. A shift the magnitude of 1.5 ppm is quite extreme, which is what initially planted the seed of a potential bis-PyPyr complex. The cationic nature of the gold (III) center clearly has a great impact on the electronics of the complex, which is quite interesting as the cationic $PyQuin(AuCl_2)^+$ is not as downfield shifted as the neutral $PyQuin(AuCl_3)$. This could possibly be attributed to the fact that in the $(PyPyr)_2Au^+$ complex, all of the ligands are heteroaromatic (with two of the chelates being X-type) so there is a significant amount of electron delocalization. Regardless of the chemical shift range, the effect of the PyPyr R-group is still observed, as the pyrazole singlet can be observed shifting downfield as the substituent goes from electron donating (MeO-) to electron withdrawing (CF_3-). Unfortunately, the bis PyPyr gold (III) complexes were incredibly difficult to grow crystals with and for this reason, no X-ray crystallographic data was able to be obtained for them. With ^1H and ^{13}C NMR and mass spectrometry finding the correct masses, the proposed structure is confirmed.

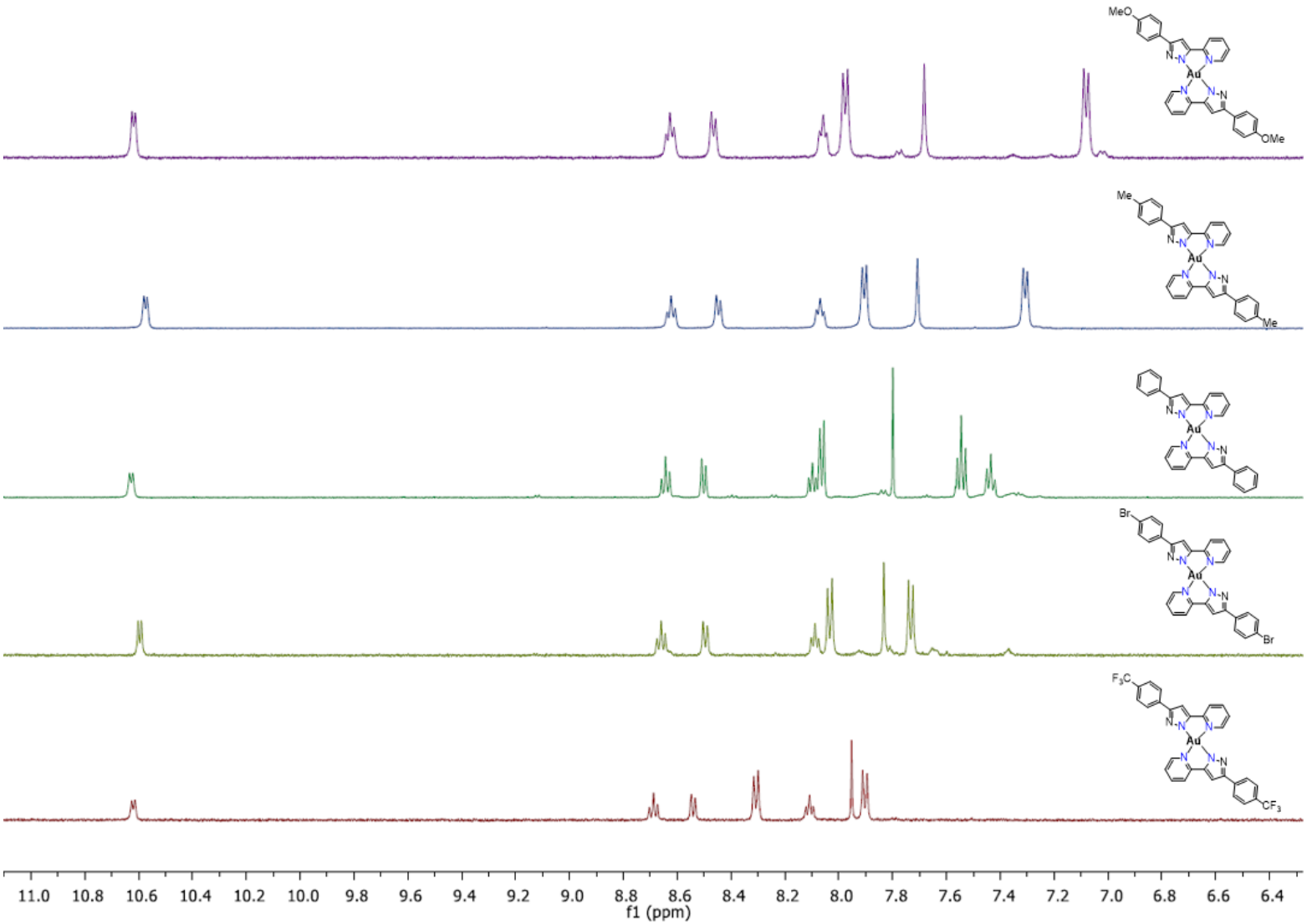

Figure 6.4 ^{1}H NMR comparison of electronically different bis $(PyPyr)_2Au^+$ complexes

Due to the significant downfield shifting that occurs between the mono- and bis-PyPyr gold (III) complexes, comparing their ^{1}H NMR spectra is quite illustrative (**Figure 6.5**).

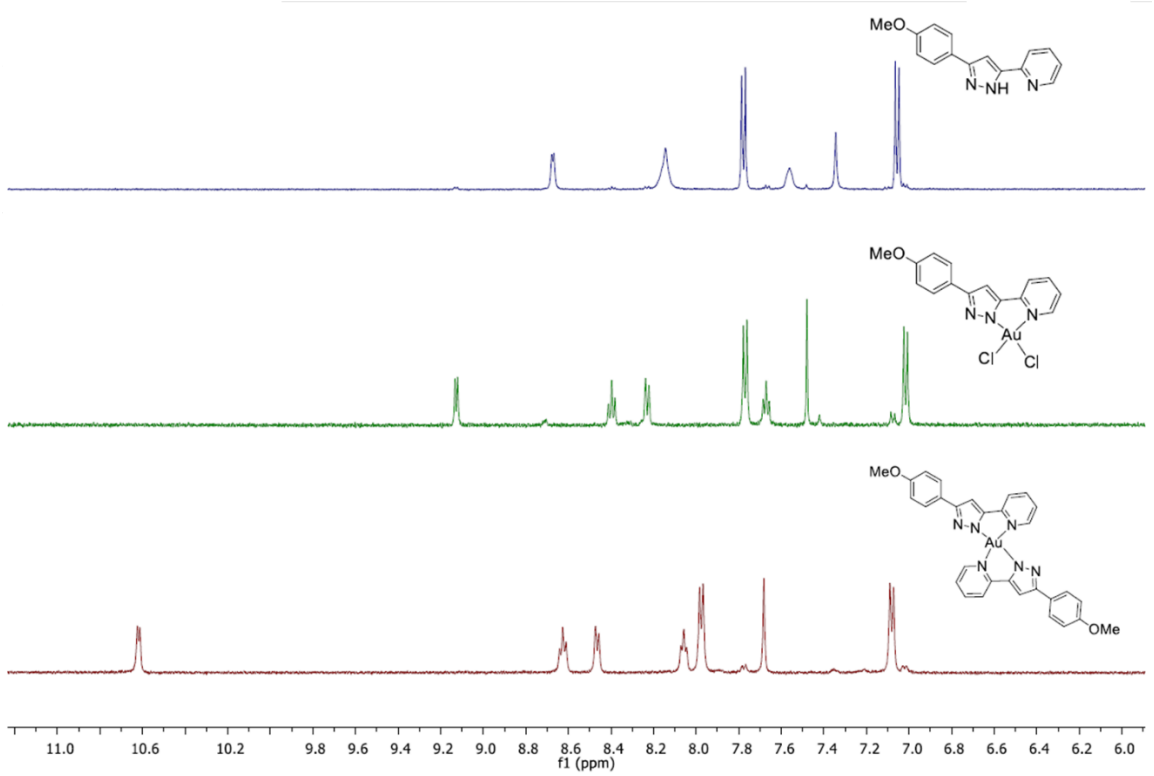

Figure 6.5 ^{1}H NMR comparison of MeO-PyPyr ligand, mono-PyPyr gold (III) complex, and bis-PyPyr gold (III) complex illustrating the significant downfield shifting of resonances

As noted earlier, the MeO-PyPyr has some broadened peaks due to hydrogen-bonding, however the general chemical shifts for each set of resonances can still be observed changing going from unbound ligand to the mono MeO-PyPyr($AuCl_2$) complex to the bis $(MeO\text{-}PyPyr)_2Au^+$ complex. It is evident that the two complexes are quite different from one another and, should they be explored as potential catalysts, the results could be very insightful in terms of gold (III)

chemistry as a whole. Since the PyPyr ligands have shown to be quite adept at forming both interesting and discrete metal complexes, an effort was made to see how they function when bound to other isoelectronic metals to form novel complexes.

6.3 Synthesis of R-PyPyr Platinum (II) Chloride Complexes

Developing methods for the synthesis of metal complexes which can be used both in a therapeutic and catalytic applications is of incredibly high value. Arguably the most famous and effective metal-based therapeutic, cisplatin has shown to be an incredibly potent anti-cancer drug (as described in detail earlier in this document). While synthesizing novel gold (III) complexes, there was always the potential to use the heteroaromatic ligands synthesized in the Larsen group to form platinum (II) complexes that are similar to cisplatin. Because all of the ligands described herein have been bidentate nitrogen ligands, the move to synthesizing of cisplatin analogues is actually quite facile. As with any metal complex, there is some finessing required in terms of metal source, inclusion of halide abstracting agent, solvent etc. however, the fact that both the mono PyTri($PtCl_2$) and bis $(PyTri)_2PtCl_2$ complexes were synthesized with little trouble was quite encouraging.

The main difference in using the mixed X/L-type PyPyr ligand is, of course, the oxidation state of the platinum metal. Since platinum (II) forms the common four-coordinate, square-planar geometry, it is expected that the complex would consist of one PyPyr ligand and two halide X-type ligands. If the

PyPyr ligand functioned as intended, with the pyrazole N-H acting as an anionic X-type chelate and the pyridine nitrogen acting as a neutral L-type chelate, the resulting complex would be overall anionic. Because of this, the likely scenario is that upon binding to the platinum (II) center, the ligand will undergo isomerization to make both nitrogen's L-type with the pyrazole N-H now at the 5 position (**Scheme 6.8**).

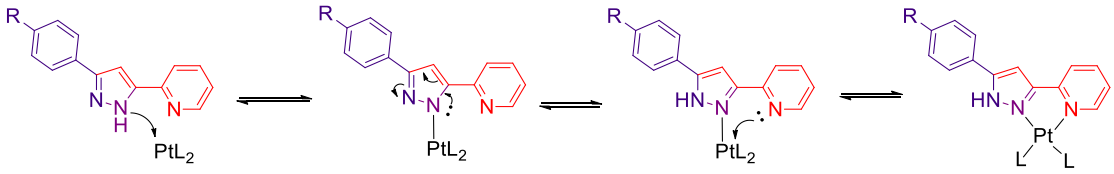

Scheme 6.8 Upon binding to the platinum metal center, isomerization of the ligand occurs which results in both nitrogen chelates being L-type and forming a net neutral complex

This PyPyr($PtCl_2$) complex would be overall neutral and therefore more stable, however the desired purpose of having a mixed X/L-type bidentate ligand becomes somewhat moot.

To determine if isomerization occurs with platinum (II), a method for synthesizing the PyPyr($PtCl_2$) complex series needed to be developed. There is a good amount of precedent of platinum complexes, especially those employing bidentate nitrogen ligands, and even some within the Larsen group itself. Similar to the gold complexation reactions, there are many different platinum (II) sources that have been successful, the main three being platinum dichloride ($PtCl_2$), potassium tetrachloroplatinate (K_2PtCl_4), and dichloro-bis(dimethylsulfoxide) platinum ($Pt(DMSO)_2Cl_2$). In past reactions, it has been observed that the most

successful complexations occur when using a metal source with all coordination sites occupied and labile ligands. $PtCl_2$ is analogous to $AuCl_3$ and $PdCl_2$, both of which were quite unsuccessful in forming complexes with any of the Larsen ligands. K_2PtCl_4 is somewhat analogous to $NaAuCl_4$, the gold salt that has been instrumental in forming gold (III) complexes, however it also requires stoichiometric silver tetrafluoroborate ($AgBF_4$) to abstract chlorides and free up coordination sites. $Pt(DMSO)_2Cl_2$ was successful for the PyTri platinum (II) complexes and is analogous to the palladium source $Pd(MeCN)_2Cl_2$ which was used for all palladium complexes synthesized in the Larsen group. For these reasons, dichloro-bis(dimethylsulfoxide) platinum was chosen as a starting point for the PyPyr platinum (II) complexes.

When metal salts have solvent ligands such as acetonitrile on $Pd(MeCN)_2Cl_2$ or dimethylsulfoxide on $Pt(DMSO)_2Cl_2$, ideally the reaction is run in that same solvent. However, if this reaction were to be run in DMSO, the product would be very difficult to isolate due to everything being solubilized in a hard to remove solvent. For this reason, the reaction was run in acetonitrile, another labile ligand that is easily displaced should it bind to the platinum center. It was found that at room temperature, stirring R-PyPyr ligand and the platinum source $Pt(DMSO)_2Cl_2$ in acetonitrile yields a yellow precipitate, determined to be the R-PyPyr($PtCl_2$) complex (**Scheme 6.9**).

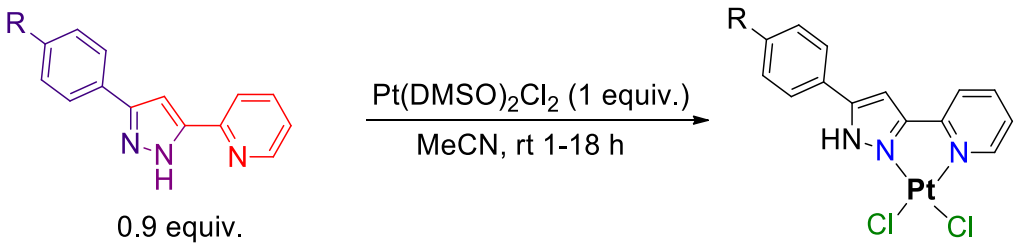

Scheme 6.9 Using the platinum (II) source $Pt(DMSO)_2Cl_2$, the mono complex R-PyPyr($PtCl_2$) is synthesized directly at room temperature

Due to the ligand not being fully used up when run in a 1:1 ligand to metal ratio, the ligand is undercut by 10% to ensure complete consumption. Interestingly, the precipitate forms significantly faster when an electron-rich ligand is used (20 minutes for MeO-PyPyr) than when an electron-poor ligand is used (18 hours for CF_3-PyPyr).

The platinum (II) PyPyr complexes that are isolated from this reaction share many qualities with the PyTri palladium (II) complexes, one of which being the “fluffiness” of the solid when they precipitate out of solution. Filtering the solid away from the supernatant was incredibly difficult, as the solid would clog the filter paper and was very difficult to scrape off when isolated. For this reason, the solid was isolated from the crude supernatant through centrifuging, removing the supernatant, and washing the solid with acetone. The acetone/complex suspension was then centrifuged again, supernatant removed, and washed. This process was repeated until the acetone no longer picked up any color from the solid and also showed nothing by TLC. With the series of these PyPyr platinum

(II) complexes synthesized, they needed to be characterized to confirm the suspected structure.

Based on the mass spectrometry data alone, it was believed that the solid was at least a mono-PyPyr platinum (II) complex and not a bis-PyPyr complex. This conclusion was drawn due to the mass of the different R-group complexes changing by the mass of only *one* R-group, not two. For instance, the M^+ of the H-PyPyr platinum complex differs from the Me-PyPyr platinum complex by 14 amu, not 28 (which would indicate a mono, not bis complex). Additionally, the ^1H NMR are downfield shifted but not to the extreme amount that was seen for the $(PyPyr)_2Au^+$ complex. While the ^1H NMR do appear to suggest complexation, the initial spectra obtained were quite concerning. With one PyPyr ligand on the platinum center, there should be 8 resonances on the ^1H NMR; however, when the spectrum was acquired in DMSO-D_6 (the normal NMR solvent for these metal complexes) 13 individual resonances are seen not including any overlapping resonances. Even if the phenyl ring was somehow made non-symmetric, the maximum individual protons possible would be 10; if there were two PyPyr ligands present and there was no symmetry, there should be 16. It was suspected that maybe, since DMSO can complex to platinum (II) as it is present in the platinum source, some sort of PyPyr platinum (II) DMSO adduct is forming in solution. For this reason, the exact same complex was dissolved in deuterated nitromethane and, as shown in the comparison in **Figure 6.6**, there is only one complex present.

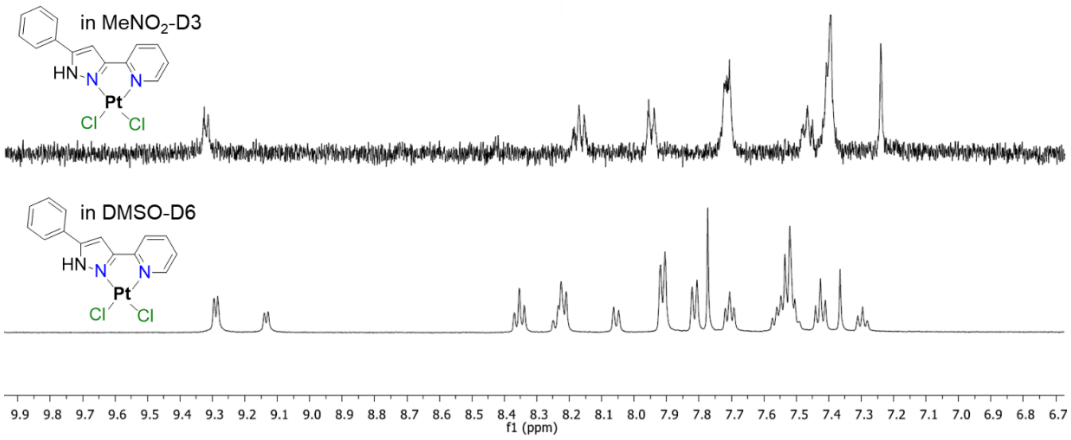

Figure 6.6 PyPyr($PtCl_2$) complex appears to form observable adduct with DMSO solvent by ^1H NMR; this is not observed when spectrum is acquired in deuterated $MeNO_2$

Both the DMSO and $MeNO_2$ solutions of PyPyr($PtCl_2$) are completely clear and it is not believed that the nitromethane is only dissolving one compound selectively. When the series of complexes are taken in deuterated nitromethane, the expected downfield shifting can be observed (**Figure 6.7**) as the R-group on the PyPyr ligand moves from electron-donating (MeO-) to neutral (H-) to electron withdrawing (CF_3-). The series of complexes were made in moderate yields (**Scheme 6.10**) and characterized, however x-ray quality crystals were unable to be obtained. Based on the data collected, the proposed structure of a neutral, four-coordinate square-planar platinum (II) complex with two chloride ligands and one isomerized PyPyr ligand is believed to be correct. In addition to making the mono PyPyr platinum complexes, it was hoped that the analogous bis PyPyr complexes could be synthesized as well, as they were successfully formed with both gold (III) and palladium (II). Despite trying a myriad of conditions (high excess of ligand,

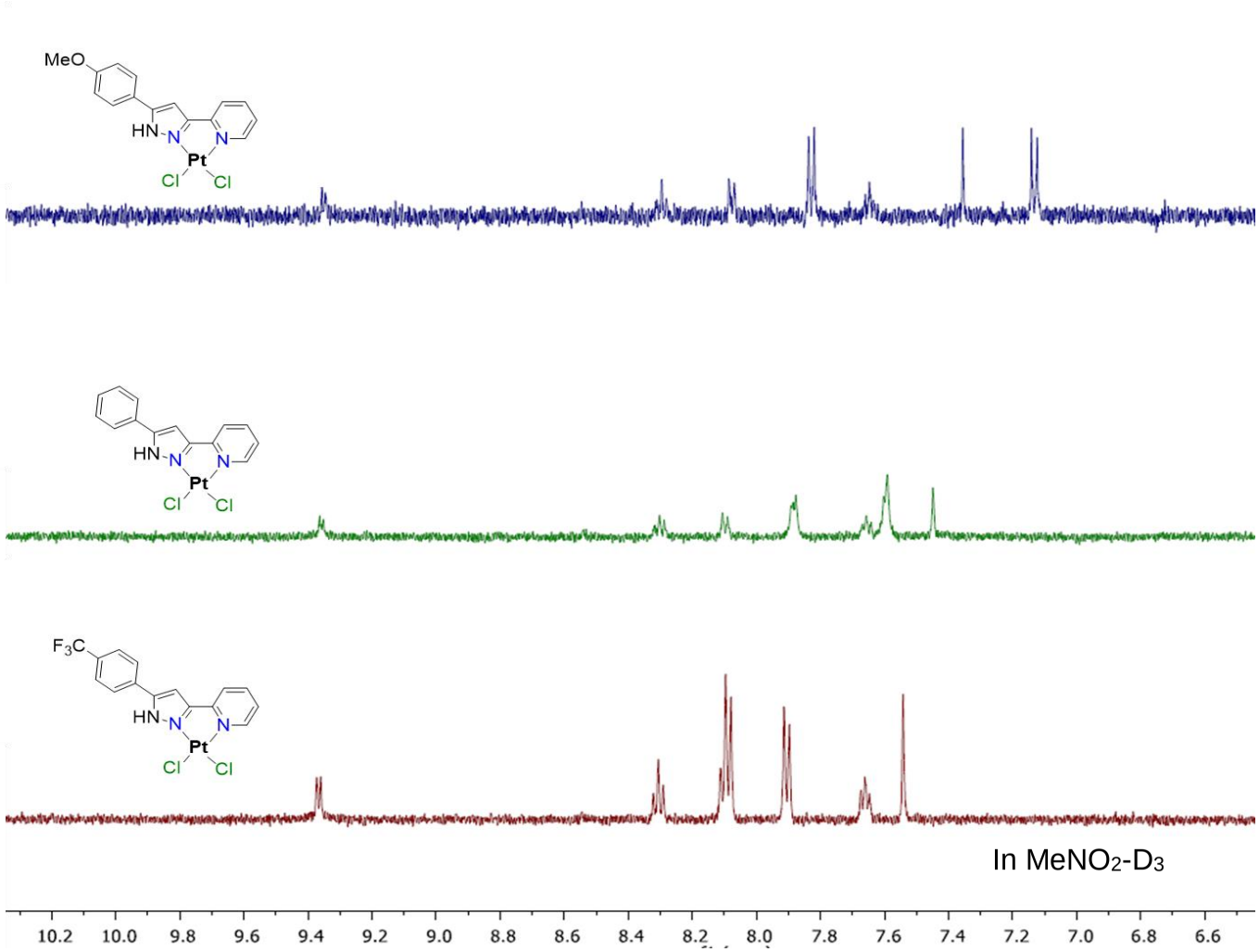

Figure 6.7 ^{1}H NMR comparison of electronically different R-PyPyr($PtCl_2$) complexes

addition of silver tetrafluoroborate, pre-abstracting halides on platinum salt prior to ligand addition, high temperature, and utilizing the different platinum salts K_2PtCl_4 and $PtCl_2$) there was no evidence that a bis-PyPyr platinum (II) complex ever forms.

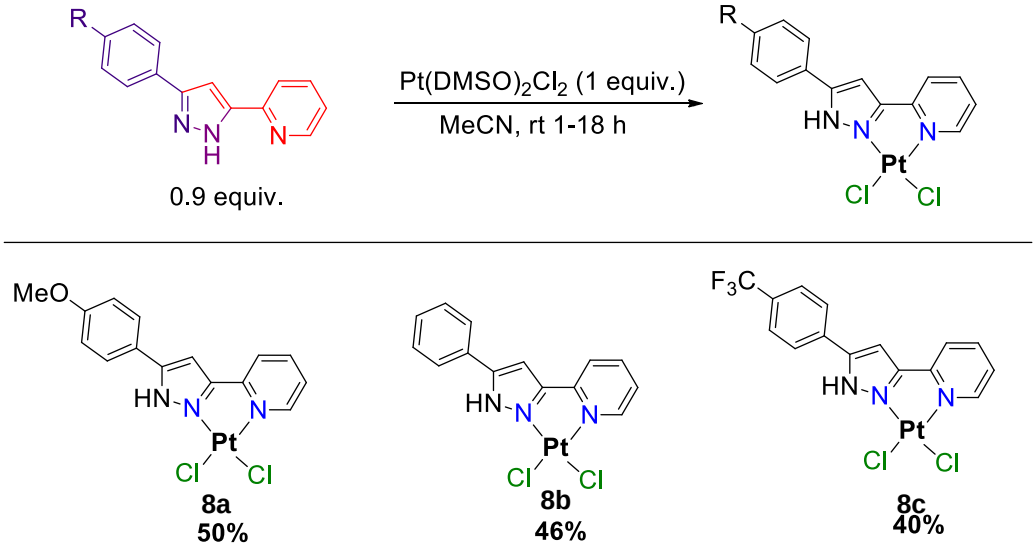

Scheme 6.10 With excess of platinum (II), mono-PyPyr($PtCl_2$) complexes are synthesized in moderate yields

It is proposed that perhaps the platinum (II) cation is too soft (based on Hard Soft Acid Base Theory) to form a dicationic complex with two non-coordinating chlorides, which are relatively hard anions. Regardless, the fact that the R-PyPyr($PtCl_2$) series was able to be synthesized cleanly and efficiently from these novel ligands is significant, as it opens the possibility for testing their bioactivity in comparison to the ubiquitous cisplatin.

6.4 Synthesis of R-PyPyr Copper (II) Chloride Complexes

Although a metal that has had a significant impact on the research conducted in the Larsen lab, copper complexes using our heteroaromatic ligands had yet to be explored. The first copper (II) complex synthesized with a Larsen ligand was, as mentioned near the beginning of this document, not desired.[19] Adapting the three-component chemistry that is used to aryl- and alkylquinolines,[20] using copper (II) triflate to catalyze the 2-(2′-pyridyl)quinoline (PyQuin) synthesis resulted in product-binding inhibition which led to the adaptation of using triflic acid (**Scheme 6.11**).

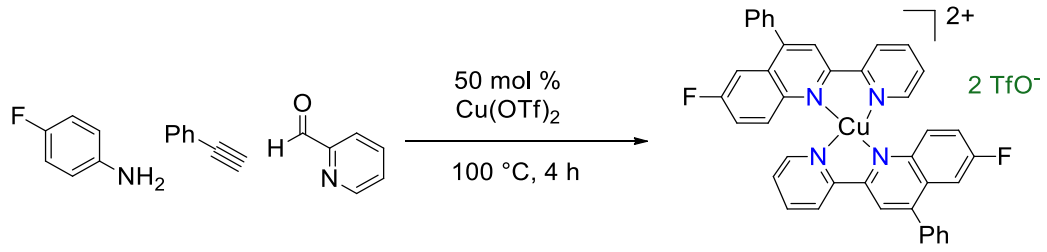

Scheme 6.11 Using copper catalyst for PyQuin synthesis yields undesirable copper (II) complex, resulting in product binding inhibition

This complex was confirmed by high-resolution mass spectrometry after increasing catalyst loading to 50 mol % to encourage its formation.

It was observed that the PyQuin ligand, when in the presence of copper (II), will form the bis-PyQuin dicationic copper (II) complex shown. Given that the PyQuin ligands were consistently observed to be the least stable, at least in gold (III) complexes, making copper complexes with other heteroaromatic ligands could potentially be quite facile. Copper (II) is also isoelectronic to gold (III),

palladium (II), and platinum (II), so within the Larsen group itself there is much precedence with the expected copper complexes. The PyPyr ligands had given inconsistent results when bound to metal centers thus far: with palladium and platinum (II), the ligands isomerize to pyrazole-pyridine chelates where both nitrogen atoms are L-type; with the gold (III) complexes, the PyPyr ligands do not isomerize and form mixed X/L-type chelates with the metal center. For this reason, it was decided that copper (II) would be a good middle-ground transition metal to try complexing with the PyPyr ligands, as it is in the same group as gold, but significantly harder (in terms of Hard Soft Acid Base Theory).

In an effort to use analogous reaction conditions as the other complexes, 2.5 equivalents of PyPyr ligand were stirred with the copper (II) source $CuCl_2$ in acetonitrile (**Scheme 6.12**). The expected complexes were either to be a neutral $(PyPyr)_2Cu$ where the ligand does not isomerize or a dicationic $(PyPyr)_2Cu$ complex with the isomerized PyPyr ligands.

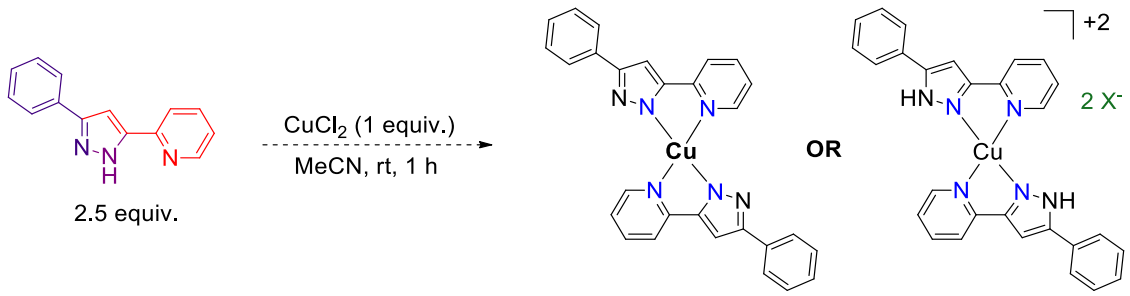

Scheme 6.12 Two possible structures for a PyPyr copper (II) complex, one where the PyPyr ligand functions as a mixed X/L ligand and the other where it isomerizes.

It is important to note that copper (II) in solution is a vibrant aqua blue, and in general a copper species that is blue is believed to be copper in a +2-oxidation

state. Upon addition of ligand to the blue acetonitrile-copper chloride solution, the reaction mixture has a dramatic event occur: first, the solution goes from aqua blue to emerald green. Copper (II) solutions are consistently blue, however a green copper solution is almost always indicative of copper (I). The color change suggests that in addition to binding, the PyPyr ligand reduces the copper (II) to copper (I), which also suggests that ligand isomerization occurs. After letting react for an hour, the solution was concentrated and a vibrantly green solid was collected. Normally, this solid would be characterized using NMR, however copper (II) is paramagnetic. The unpaired electrons in the crystal-field splitting diagram of this copper complex have their own magnetic moment which interferes with the magnet of the NMR, thus rendering the spectrum unintelligible. For this reason, x-ray crystallography is the only option to determine if the ligand bound to the copper and what geometry the copper complex adopts. The green solid was dissolved in minimal hot acetonitrile and this solution was allowed to sit unperturbed for one week in order to form crystals. This was successful, and the crystals of the copper PyPyr complexes were a stunning emerald green and quite cubic in shape (**Figure 6.8**).

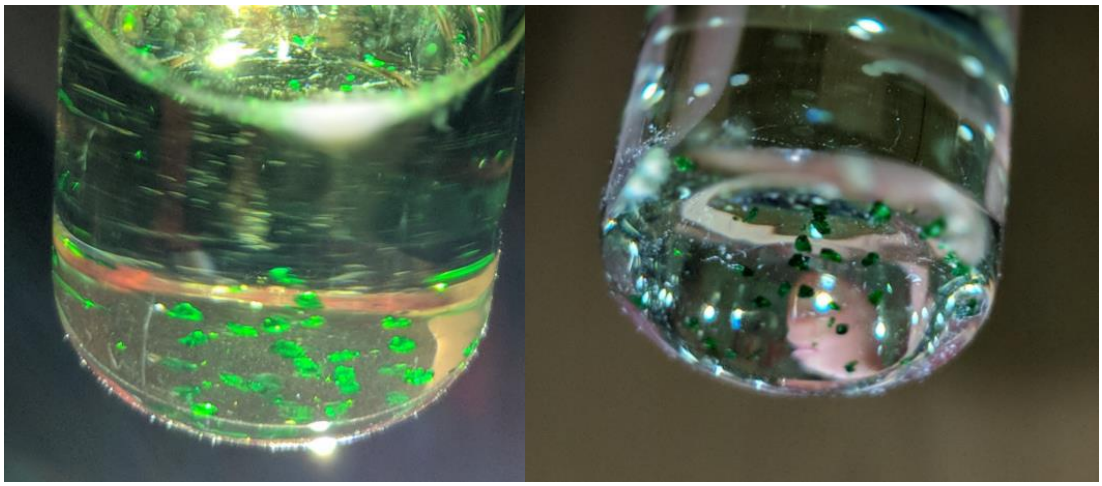

Figure 6.8 PyPyr copper complex is intensely green and crystallizes in small cubic solids

When the XRD was completed on the copper complexes by Prof. Arnold Rheingold at the University of California San Diego crystallography lab, the results were incredibly surprising. The structure given by the x-ray data of the complex was neither of the proposed structures (**Figure 6.9)**: the copper (II) appears to be unreduced, with two isomerized PyPyr ligands, one coordinated chloride ligand, and one non-coordinating chloride anion (**Scheme 6.13**).

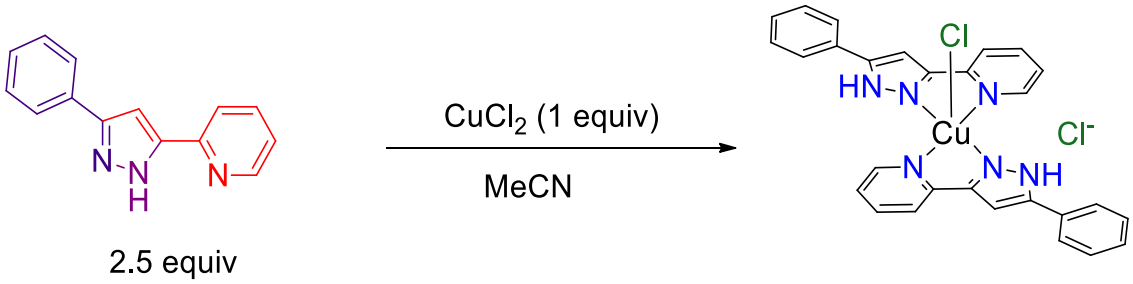

Scheme 6.13 Complexation with PyPyr ligand and copper (II) chloride yields the isomerized $(PyPyr)_2CuCl^+ Cl^-$ complex

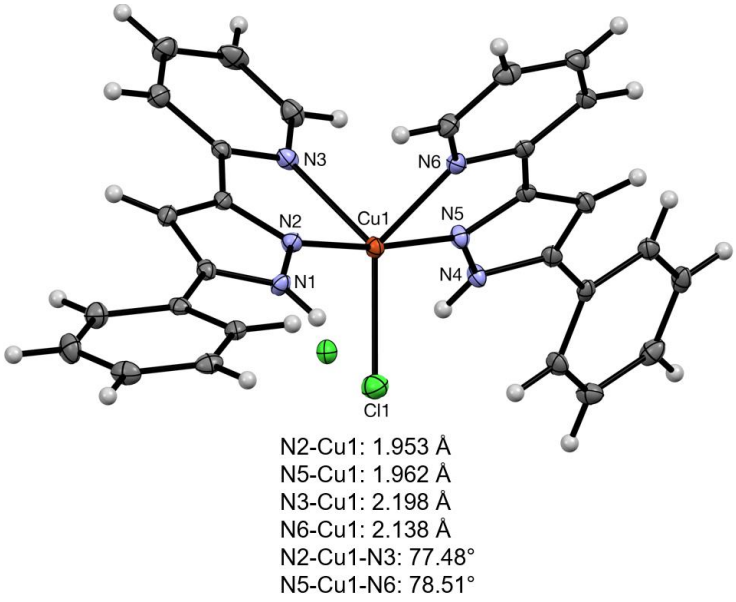

Figure 6.9 X-ray crystal structure of isolated copper complex displays unprecedented geometry with two L/L PyPyr ligands and one coordinated chloride ligand.

In comparison to previous complexes with PyPyr and PyTri ligands, the bond lengths are quite similar: the copper-pyrazole and copper-pyridine lengths are close to the observed bond lengths for both gold (III) and palladium (II), however the bite angle formed between the bidentate ligand and the metal center is quite small (>80°, normal bipyridine bite angle). The difference between the pyrazole nitrogen and pyridine nitrogen tracks with what has been previously observed – that the pyrazole is a stronger chelate, even when isomerized, than the pyridine. Even though the isolated complex is completely different than what was expected, this 5-coordinate complex has no literature precedent and an incredibly unique, almost butterfly-like geometry. The fact that two heteroaromatic ligands, the PyQuin and PyPyr, can form such dramatically different complexes with the same metal illustrates how much there still is to

discover. A sector of chemistry that still needs significant development is the comparison of bioactive ligands and their corresponding metal complexes to determine how the metal affects the ligand's therapeutic potential. Whether synthesized for their bioactivity, catalytic potential, or simply just to see what happens, metal complexes with tunable organic ligands have significant value in countless chemical applications.

6.5 References

1) Shivankar, V. S.; Gavali, L. V.; Yadav, S. P.; Thakkar, N. V. *ISOR J. Appl. Chem.* **2013**, *3 (6),* 31.

2) Varnagy, K.; Sovago, I. *Inorganica Chimica Acta*, **1988,** *151,* 117.

3) Shivankar, V.S.; Thakkar, N. V. *Acta Poloniae Pharmaceutica* **2004**, *61* 127.

4) (a) Qiao, J. X.; Cheng, X. H.; Smallheer, J. M.; Galemmo, R. A.; Drummond, S.; Pinto, D.; Cheney, D. L.; He, K.; Wong, P. C.; Luettgen, J. M.; Knabb, R. M.; Wexler, R. R.; Lam, P. *Bioorg. Med. Chem. Lett.* **2007**, *17*, 1432. (b) Singh, P.; Paul, K.; Holzer, W. *Bioorg. Med. Chem*. **2006**, *14*, 5061. (c) Ache, H. *J. Angew. Chem. Int. Ed.* **1989**, *28*, 1.

5) (a) Zhu, L. B.; Cheng, L.; Zhang, Y. X.; Xie, R. G.; You, J. S. *J. Org. Chem.* **2007**, *72*, 2737. (b) Kufelnicki, A.; Wozniczka, M.; Checinska, L.; Miernicka, M.; Budzisz, E. *Polyhedron* **2007**, *26*, 2589. (c) Ovejero, P.; Mayoral, M. J.; Cano, M.; Lagunas, M. C. *J. Organomet. Chem*. **2007**, *692*, 1690. (d) Burling, S.; Field, L. D.; Messerle, B. A.; Rumble, S. L. *Organometallics* **2007**, *26*, 4335. (e) Kealey, S.; Long, N. J.; Miller, P. W.; White, A.; Hitchcock, P. B.; Gee, A. *Dalton Trans.* **2007**, 2823. (f) Kawatsura, M.; Aburatani, S.; Uenishi, J. *Tetrahedron* **2007**, *63*, 4172. (g) Attanasi, O. A.; Berretta, S.; Crescentini, L. D.; Favi, G.; Filippone, P.; Giorgi,G ; Lillini, S.; Mantellini, F. *Tetrahedron Lett*. **2007**, *48*, 2449. (h) Cottineau, B.; Chenault, J. *Synlett* **2002**, 769.

6) (a) Trofimenko, S. *Chem. Rev*. **1972**, *72*, 497. (b) Trofimenko, S. *Prog. Inorg. Chem*. **1986**, *34*, 115. (c) Trofimenko, S. *Chem. Rev.* **1993**, *93*, 943. (d) La Monica, G.; Ardizzoia, G.A. *Prog. Inorg. Chem*. **1997**, *46*, 151. (e) Mukherjee, R. *Coord. Chem. Rev*. **2000**, *203*, 151. (f) Vos, J. G.; Groeneveld, W. C. *Inorg. Chim. Acta* **1978**, *26*, 71. (g) Catalan, J.; Abboud, J. L. M.; Elguero, J. *Adv. Heterocycl. Chem.* **1987**, *41*, 187.

7) Nfor, E. N.; Asobo, P. F.; Nenwa, J.; Nfor, O. N.; Njapba, J. N.; Njong, R. N.; Offiong, O. E. *Int. J. Inorg. Chem.* **2013**, 987574.

8) Pons, J.; Chadghan, A.; Alvarex-Larena, A.; Piniella, J. F.; Ros, J. *Inorg. Chim. Acta* **2001**, *324*, 342.

9) Chadghan, A.; Pons, J.; Caubet, A.; Casabo, J.; Ros, J.; Alvarex-Larena, A.; Piniella, J. F. *Polyhedron* **2000**, *19*, 855.

10) Pons, J.; Chadghan, A.; Casabo, J.; Alvarex-Larena, A.; Piniella, J. F. Ros, J. *Polyhedron* **2001**, *20*, 2531.

11) Pons, J.; Lopez, X.; Casabo, J.; Teixidor, F.; Caubet, A.; Ruis, J.; Miravitlles, C. *Inorg. Chim. Acta* **1992**, *195*, 61.

12) Munakata, M.; Wu, L. P.; Yamamoto, M.; Kuroda-Sowa, T.; Maekawa, M.; Kawata, S.; Kitagawa, S. *J. Chem. Soc. Dalton. Trans.* **1995**, *1*, 4099.

13) Ho, M.; Cheng, Y.; Wu, L.; Chou, P.; Lee, G.; Hsu, F.; Chi, Y. *Polyhedron* **2007**, *26*, 4886.

14) Gupta, G.; Zheng, C.; Wang, P.; Rao, K. M. *Z. Anorg. Allg. Chem.* **2010**, *636*, 758.

15) Thiel, W. R.; Eppinger, J. *Chem. Eur. J.* **1997**, *3*, 696.

16) Pons, J.; Chadghan, A.; Casabo, J.; Alvarex-Larena, A.; Piniella, J. F.; Ros, J. *Inorg. Chem. Commun.* **2000**, *3*, 296.

17) (a) Perez, J. A.; Pons, J.; Solans, X.; Font-Bardia, M.; Ros, J. *Inorg. Chim. Acta* **2005**, *358*, 617. (b) Montoya, V.; Pons, J.; Garcia-Anton, J.; Solans, X.; Font-Bardia, M.; Ros, J. *Organometallics* **2007**, *26*, 3183. (c) Montoya, V.; Pons, J.; Branchadell, V.; Garcia-Anton, J.; Solans, X.; Font-Bardia, M.; Ros, J. O*rganometallics* **2008**, *27*, 1084.

18) (a) Benet-Buchholz, J.; Comba, P.; Llobet, A.; Roeser, S.; Vadivelu, P.; Wiesner, S. *Dalton Trans*. **2010**, *39*, 3315. (b) Roeser, S.; Maji, S.; Benet-Buchholz, J.; Pons, J.; Llobet, A. *Eur. J. Inorg.Chem.* **2013**, *2*, 232. (c) Kashiwame, Y.; Watanabe, M.; Araki, K.; Kuwata, S.; Ikariya, T. *Bull. Chem.Soc. Jpn.* **2011**, *84*, 251. (d) Muller, K.; Sun, Y.; Heimermann, A.; Menges, F.; Niedner-Schatteburg, G.; van Wullen, C.; Thiel, W. R. *Chem. Eur. J.* **2013**, *19*, 7825.

19) Laguna, E. M.; Olsen, P. M.; Sterling, M. D.; Eichler, J. F.; Rheingold, A. L.; Larsen, C. H. *Inorg. Chem.* **2014**, *53* (23), 12231.

20) Meyet, C. E.; Pierce, C. J.; Larsen, C. H. *Org. Lett.* **2012**, *14* (4), 964.

6.6 Supporting Information

General Reagent Information

All reactions were set up on the benchtop in oven-dried glassware or dried scintillation vials. HPLC grade Acetonitrile (MeCN), Dichloromethane (DCM), and Tetrahydrofuran (THF) was purchased from Fisher Chemicals and dried via passage through activated alumina in a commercial solvent purification system (Pure Process Technologies, Inc.). All other organic solvents were obtained from Fisher Chemicals or Acros Organics and dried over either sodium sulfate or molecular sieves (4Å). NMR solvents were purchased from Acros Organics or Cambridge Isotope Laboratories and used as obtained. The palladium precursors were stored in a glove box under nitrogen. Bis(acetonitrile)dichloropalladium(II) (PdCl2(MeCN)2) was purchased from Chem Impex Int'l Inc and was used as obtained. Sodium tetrachloroaurate dihydrate was purchased from Alfa Aesar and stored in a glove box under nitrogen and used as received. Platinum bis(dimethylsulfoxide)dichloride was purchased from Chem Impex Int'l Inc and stored in a glove box under nitrogen and used as received.

General analytical information

^{1}H and ^{13}C NMR spectra were measured on a Varian Inova 500 (500 MHz) or a Bruker Avance NEO 400 (400 MHz) spectrometer using CF_3COOD or DMSO-*d*6 as solvents and tetramethylsilane as an internal standard. The following abbreviations are used singularly or in combination to indicate the multiplicity of signals: s - singlet, d - doublet, t - triplet, q - quartet, qn - quintet, sx - sextet, sp -

septet, m - multiplet and br - broad. NMR spectra were acquired at 300 K. Gas chromatography (GC) was carried out on an Agilent Technologies 6850 Network GC System, and dodecane was used as the internal standard. ATR-IR spectra were taken on a Bruker:ALPHA FTIR Spectrometer. Attenuated total reflection infrared (ATR-IR) was used and the spectra was analyzed using the OPUS software with selected absorption maxima reported in wavenumbers (cm-1). X-ray diffraction data was obtained using a suitable crystal on a 'Bruker APEX-II CCD' diffractometer. The crystal was kept at 100.0 K during data collection. Using Olex2, the structure was solved with the ShelXT structure solution program using Intrinsic Phasing and refined with the XL refinement package using Least Squares minimization.

General Procedure for the Production of Pyridine Pyrazole (PyPyr) Ligands

To an oven dried 250 mL round bottom flask equipped with a magnetic stir bar and reflux condenser was added tosyl hydrazine followed by THF. The solution was stirred at ambient temperature until the hydrazine dissolves. Benzaldehyde bearing the desired substitution was added drop wise and the reaction was heated to 70 °C and stirred for 2 h. The reaction was then cooled to ambient temperature and 2.5 equivalents of sodium ethoxide (NaOEt) were added. The solution was stirred for 30 min during which the generation of the diazo intermediate occurred. The solution was then diluted with additional THF and 2-ethynylpyridine was added dropwise. The reaction was heated to reflux for 18 h.

Upon completion, the reaction was quenched with DI-H_2O and the product was extracted with diethyl ether. After the organic extracts are combined and dried over sodium sulfate the solvent was removed to yield a crude oil. This oil was taken up in MeCN and the solution was placed in a beaker located in the freezer. The desired substituted PyPyr ligand crystalized out of solution over the course of 48 h. Subsequent recrystallizations in MeCN yield pure PyPyr ligand as white / off-white crystalline solids.

2-(3-(4-methoxyphenyl)-1H-pyrazol-5-yl)pyridine (5a):

To an oven dried 250 mL round bottom flask equipped with a magnetic stir bar and reflux condenser was added tosyl hydrazine (930 mg, 5 mmol) followed by THF (60 mL). After all solids are dissolved, *p*-anisaldehyde (607 µL, 5 mmol) was added dropwise. The solution was heated to 70 °C and stirred for 2 h. The reaction was then cooled to ambient temperature and NaOEt (850 mg, 12.5 mmol) was added). After 30 min of stirring the solution was diluted with additional THF (40 mL), and 2-ethynylpyridine (507 µL, 5 mmol) was added dropwise. The reaction was then heated to reflux and stirred for 18 h. Upon completion the reaction was quenched with DI-H_2O (100 mL) and extracted with diethyl ether. After drying the organic extract was concentrated to yield an orange oil that was taken up in MeCN and the solution was left standing in the freezer for 48 h. After additional recrystallizations in MeCN the title compound was obtained as a white solid in 35% yield (443 mg, 1.75 mmol). ATR-IR: 3257, 2959, 2837, 1313, 1247,

1153, 1031, 776, 526, 479 cm^{-1}. ^{1}H NMR (400 MHz, CF_3COOD) δ 8.71 (d, J = 5.5 Hz, 1H), 8.59 (t, J = 8.5 Hz, 1H), 8.37 (d, J = 8 Hz, 1H), 7.96 (t, J = 7 Hz, 1H), 7.59 (d, J = 8.5 Hz, 2H), 7.32 (s, 1H), 7.00 (d, J = 8.5 Hz, 2H), 3.83 (s, 3H). ^{13}C NMR (100 MHz, CF_3COOD) δ 144.44, 143.94, 137.62, 137.30, 136.44, 123.48, 122.84, 121.51, 114.27, 110.82, 107.96, 99.60, 50.66. HRMS calculated requires $[M+H]^+$: 252.1131. Found *m/z*: 252.1236.

2-(3-(4-methylphenyl)-1H-pyrazol-5-yl)pyridine (5b):

To an oven dried 250 mL round bottom flask equipped with a magnetic stir bar and reflux condenser was added tosyl hydrazine (930 mg, 5 mmol) followed by THF (60 mL). After all solids are dissolved, *p*-tolualdehyde (589 µL, 5 mmol) was added dropwise. The solution was heated to 70 °C and stirred for 2 h. The reaction was then cooled to ambient temperature and NaOEt (850 mg, 12.5 mmol) was added). After 30 min of stirring the solution was diluted with additional THF (40 mL), and 2-ethynylpyridine (507 µL, 5 mmol) was added dropwise. The reaction was then heated to reflux and stirred for 18 h. Upon completion the reaction was quenched with DI-H_2O (100 mL) and extracted with diethyl ether. After drying the organic extract was concentrated to yield an orange oil that was taken up in MeCN and the solution was left standing in the freezer for 48 h. After additional recrystallizations in MeCN the title compound was obtained as a white solid in 34% yield (405 mg, 1.7 mmol). ATR-IR: 3029, 2916, 1596, 1563, 1452, 1152, 771, 493 cm^{-1}. ^{1}H NMR (400 MHz, CF_3COOD) δ 8.70 (d, J = 5.5 Hz, 1H),

8.58 (t, J = 7.5 Hz, 1H), 8.36 (d, J = 8 Hz, 1H), 7.95 (t, J = 7 Hz, 1H), 7.45 (d, J = 8.5 Hz, 2H), 7.33 (s, 1H), 7.17 (d, J = 8 Hz, 2H), 2.22 (s, 3H). ^{13}C NMR (100 MHz, CF_3COOD) δ 145.24, 143.94, 138.86, 137.35, 136.18, 125.66, 122.91, 121.59, 121.40, 117.19, 108.68, 99.81, 15.09. HRMS calculated requires $[M+H]^+$: 236.1182. Found *m/z*: 236.1467.

2-(3-phenyl-1H-pyrazol-5-yl)pyridine (5c):

To an oven dried 250 mL round bottom flask equipped with a magnetic stir bar and reflux condenser was added tosyl hydrazine (930 mg, 5 mmol) followed by THF (60 mL). After all solids are dissolved, benzaldehyde (508 µL, 5 mmol) was added dropwise. The solution was heated to 70 °C and stirred for 2 h. The reaction was then cooled to ambient temperature and NaOEt (850 mg, 12.5 mmol) was added). After 30 min of stirring the solution was diluted with additional THF (40 mL), and 2-ethynylpyridine (507 µL, 5 mmol) was added dropwise. The reaction was then heated to reflux and stirred for 18 h. Upon completion the reaction was quenched with DI-H_2O (100 mL) and extracted with diethyl ether. After drying the organic extract was concentrated to yield an orange oil that was taken up in MeCN and the solution was left standing in the freezer for 48 h. After additional recrystallizations in MeCN the title compound was obtained as a white solid in 54% yield (598 mg, 2.7 mmol). ATR-IR: 3235, 3059, 1596, 1468, 756, 657, 484, 419 cm^{-1}. ^{1}H NMR (400 MHz, CF_3COOD) δ 8.65 (d, J = 5.5 Hz, 1H), 8.55 (t, J = 6.8 Hz, 1H), 8.33 (d, J = 8 Hz, 1H), 7.91 (t, J = 6.8 Hz, 1H), 7.53 (m,

2H), 7.33 (m, 4H). ^{13}C NMR (100 MHz, CF_3COOD) δ 144.81, 143.87, 138.08, 137.10, 136.77, 126.90, 124.91, 122.59, 121.37, 121.29, 120.49, 99.80. HRMS calculated requires $[M+H]^+$: 222.1026. Found *m/z*: 222.1548.

2-(3-(4-bromophenyl)-1H-pyrazol-5-yl)pyridine (5d):

To an oven dried 250 mL round bottom flask equipped with a magnetic stir bar and reflux condenser was added tosyl hydrazine (930 mg, 5 mmol) followed by THF (60 mL). After all solids are dissolved, 4-bromobenzaldehyde (925 mg, 5 mmol) was added dropwise. The solution was heated to 70 °C and stirred for 2 h. The reaction was then cooled to ambient temperature and NaOEt (850 mg, 12.5 mmol) was added). After 30 min of stirring the solution was diluted with additional THF (40 mL), and 2-ethynylpyridine (507 µL, 5 mmol) was added dropwise. The reaction was then heated to reflux and stirred for 18 h. Upon completion the reaction was quenched with DI-H_2O (100 mL) and extracted with diethyl ether. After drying the organic extract was concentrated to yield an orange oil that was taken up in MeCN and the solution was left standing in the freezer for 48 h. After additional recrystallizations in MeCN the title compound was obtained as a white solid in 28% yield (415 mg, 1.4 mmol). ATR-IR: 3206, 1593, 1560, 1372, 1006, 954, 774, 511, 490, 468 cm^{-1}. ^{1}H NMR (400 MHz, CF_3COOD) δ 8.70 (d, J = 6 Hz, 1H), 8.60 (t, J = 8 Hz, 1H), 8.36 (d, J = 8 Hz, 1H), 7.95 (t, J = 7.2 Hz, 1H), 7.53 (d, J = 8.5 Hz, 2H), 7.46 (d, J = 8.5 Hz, 2H), 7.32 (s, 1H). ^{13}C NMR (100 MHz, CF_3COOD) δ143.86, 143.47, 138.85, 137.53, 136.93, 128.30, 122.71,

122.33, 121.22, 120.99, 119.95, 99.59. HRMS calculated requires $[M+H]^+$: 300.0131. Found *m/z*: 300.0230.

2-(3-(4-(trifluoromethyl)phenyl)-1H-pyrazol-5-yl)pyridine (5e):

To an oven dried 250 mL round bottom flask equipped with a magnetic stir bar and reflux condenser was added tosyl hydrazine (930 mg, 5 mmol) followed by THF (60 mL). After all solids are dissolved, 4-trifluoromethylbenzaldehyde (670 µL, 5 mmol) was added dropwise. The solution was heated to 70 °C and stirred for 2 h. The reaction was then cooled to ambient temperature and NaOEt (850 mg, 12.5 mmol) was added). After 30 min of stirring the solution was diluted with additional THF (40 mL), and 2-ethynylpyridine (507 µL, 5 mmol) was added dropwise. The reaction was then heated to reflux and stirred for 18 h. Upon completion the reaction was quenched with DI-H_2O (100 mL) and extracted with diethyl ether. After drying the organic extract was concentrated to yield an orange oil that was taken up in MeCN and the solution was left standing in the freezer for 48 h. After additional recrystallizations in MeCN the title compound was obtained as a white solid in 21% yield (297 mg, 1.05 mmol). ATR-IR: 3232, 1616, 1566, 1454, 1301, 1104, 776, 595, 474, 408 cm^{-1}. ^1H NMR (400 MHz, CF_3COOD) δ 8.62 (d, J = 6 Hz, 1H), 8.53 (t, J = 8 Hz, 1H), 8.29 (d, J = 8 Hz, 1H), 7.88 (t, J = 6.8 Hz, 1H), 7.67 (d, J = 8.5 Hz, 2H), 7.59 (d, J = 8.5 Hz, 2H), 7.31 (s, 1H). ^{13}C NMR (100 MHz, CF_3COOD) δ 143.80, 142.64, 139.27, 137.95, 136.70, 128.50,

124.75, 122.06, 121.70, 120.70, 120.37, 117.67, 99.89. HRMS calculated requires $[M+H]^+$: 290.0900. Found *m/z*: 290.1012.

General Procedure for the Production of Pyridine Pyrazole Palladium Dichloride Complexes:

In an oven dried 8 mL scintillation vial equipped with a magnetic stir bar was added palladium dichloride bisacetonitrile. The vial was purged with argon for 5 min. Dry dichloromethane (DCM) was added and the solution was stirred for 5 min to allow the initial palladium complex to dissolve. The pyridine pyrazole (PyPyr) ligand bearing the desired substitution was dissolved in minimal DCM and added to the reaction dropwise. The complexation was allowed to proceed at ambient temperature for 18 h. During this time precipitation of the PyPyr palladium dichloride complex occurred. This solid was isolated via centrifuge and washed 5 times with additional DCM. The complex was isolated as a solid and was recrystallized via slow evaporation in $MeNO_2$.

2-(3-phenyl-pyrazol-5-yl)pyridine palladium dichloride:

$PdCl_2(MeCN)_2$ (26 mg, 0.1 mmol) was added to an 8 mL scintillation vial and flushed with argon for 5 min. Dry DCM (5 mL) was added and the solution was stirred until all solids are dissolved. The solution takes on a dark orange color. PyPyr ligand (22 mg. 0.1 mmol) dissolved in DCM (~1 mL) was added dropwise. Complexation occurred at ambient temperature over 18 h. The title compound

was isolated as a yellow solid in 86% yield (34 mg, 0.086 mmol). ATR-IR: 3236, 3136, 1617, 1561, 1492, 1466, 1444, 812, 764, 487, 424 cm^{-1}. ^{1}H NMR (500 MHz, DMSO-d_6) δ 8.93 (d, J = 5.5 Hz, 1H), 8.31 (t, J = 8 Hz, 1H), 8.20 (d, J = 7.5 Hz, 1H), 7.90 (d, J = 7 Hz, 2H), 7.72 (s, 1H), 7.68 (t, J = 6.5 Hz, 1H), 7.52 (m, 3H). ^{13}C NMR (100 MHz, DMSO-d_6) δ 152.9, 151.2, 149.9, 147.5, 141.8, 130.5, 129.3, 127.8, 127.6, 125.9, 122.9, 103.6.

General Procedure for the Production of Mono-Pyridine Pyrazole Gold Dichloride Complexes:

In an oven dried 20 mL scintillation vial equipped with a magnetic stir bar was added sodium tetrachloroaurate (1.5 equiv). The vial was purged with argon for 5 min. Dry acetonitrile (5 ml) was added and the solution was stirred for 5 min to allow the gold salt to dissolve. The pyridine pyrazole (PyPyr) ligand (1 equiv.) bearing the desired substitution was dissolved in minimal acetonitrile (if MeO-PyPyr, Me-PyPyr, or Ph-PyPyr) or minimal acetone (if Br-PyPyr or CF_3-PyPyr) and added to the reaction dropwise. The vial was placed onto a heated block and refluxed for 1 hour. After 1 hour, silver tetrafluoroborate (1.5 equiv.) was added and the reaction was returned to the heat. During this time, silver chloride precipitates out of the solution indicating complexation has occurred (between 1 and 18 hours, depending on the PyPyr substituent). The reaction mixture was filtered through a Celite pipiette plug and the filtrate was concentrated down to yield the PyPyr($AuCl_2$) complex in quantitative yield.

Synthesis of MeO-PyPyr($AuCl_2$) (6a):

$NaAuCl_4 \cdot 2H_2O$ (60 mg, 0.15 mmol) was added to a 20 mL scintillation vial equipped with a magnetic stir bar and Teflon-seal screw cap. MeCN (5 mL) was added as solvent. MeO-PyPyr ligand (25 mg, 0.10 mmol) was dissolved in minimal MeCN and added. The reaction was placed on a heating block at 80 °C and allowed to stir for 1 hour. After one hour, silver tetrafluoroborate (29 mg, 0.15 mmol) dissolved in minimal MeCN was added. After 4 hours the reaction mixture was filtered through Celite and the filtrate concentrated to give the compound as a yellow solid in quantitative yield. ATR-IR: 3240, 3126, 1772, 1722, 1516, 1420, 1415, 1177, 802, 427 cm^{-1}. ^1H NMR (500 MHz, DMSO-d_6) δ 9.13 (d, J = 5.5 Hz, 1H), 8.40 (t, J = 5.5 Hz, 1H), 8.22 (d, J = 5.5 Hz, 1H), 7.78 (d, J = 7.5 Hz, 2H), 7.67 (t, J = 5.5 Hz, 1H), 7.48 (s, 1H), 7.01 (d, J = 7.5 Hz, 2H), 3.80 (s, 3H).

Synthesis of Me-PyPyr($AuCl_2$) (6b):

$NaAuCl_4 \cdot 2H_2O$ (60 mg, 0.15 mmol) was added to a 20 mL scintillation vial equipped with a magnetic stir bar and Teflon-seal screw cap. MeCN (5 mL) was added as solvent. Me-PyPyr ligand (23 mg, 0.10 mmol) was dissolved in minimal MeCN and added. The reaction was placed on a heating block at 80 °C and allowed to stir for 1 hour. After one hour, silver tetrafluoroborate (29 mg, 0.15 mmol) dissolved in minimal MeCN was added. After 4 hours the reaction mixture was filtered through Celite and the filtrate concentrated to give the compound as a yellow solid in quantitative yield. ATR-IR: 3222, 3206, 1789, 1760, 1546, 1433,

1423, 1208, 852, 466 cm^{-1}. ^1H NMR (500 MHz, DMSO-d_6) δ 9.12 (d, J = 5.5 Hz, 1H), 8.40 (t, J = 5.5 Hz, 1H), 8.24 (d, J = 5.5 Hz, 1H), 7.73 (d, J = 7.5 Hz, 2H), 7.68 (t, J = 5.5 Hz, 1H), 7.53 (s, 1H), 7.25 (d, J = 7.5 Hz, 2H), 2.34 (s, 3H).

Synthesis of PyPyr($AuCl_2$) (6c):

$NaAuCl_4 \cdot 2H_2O$ (60 mg, 0.15 mmol) was added to a 20 mL scintillation vial equipped with a magnetic stir bar and Teflon-seal screw cap. MeCN (5 mL) was added as solvent. PyPyr ligand (22 mg, 0.10 mmol) was dissolved in minimal MeCN and added. The reaction was placed on a heating block at 80 °C and allowed to stir for 1 hour. After one hour, silver tetrafluoroborate (29 mg, 0.15 mmol) dissolved in minimal MeCN was added. After 4 hours the reaction mixture was filtered through Celite and the filtrate concentrated to give the compound as a yellow solid in quantitative yield. ATR-IR: 3212, 3220, 1929, 1860, 1596, 1420, 1313, 1224, 879, 468 cm^{-1}. ^1H NMR (500 MHz, DMSO-d_6) δ 9.14 (d, J = 5.5 Hz, 1H), 8.40 (t, J = 5.5 Hz, 1H), 8.27 (d, J = 5.5 Hz, 1H), 7.84 (d, J = 7.5 Hz, 2H), 7.69 (t, J = 5.5 Hz, 1H), 7.58 (s, 1H), 7.45 (m, 2H), 7.34 (m, 1H).

Synthesis of Br-PyPyr($AuCl_2$) (6d):

$NaAuCl_4 \cdot 2H_2O$ (60 mg, 0.15 mmol) was added to a 20 mL scintillation vial equipped with a magnetic stir bar and Teflon-seal screw cap. MeCN (5 mL) was added as solvent. Br-PyPyr ligand (30 mg, 0.10 mmol) was dissolved in minimal acetone and added. The reaction was placed on a heating block at 80 °C and

allowed to stir for 1 hour. After one hour, silver tetrafluoroborate (29 mg, 0.15 mmol) dissolved in minimal MeCN was added. After 4 hours the reaction mixture was filtered through Celite and the filtrate concentrated to give the compound as a yellow solid in quantitative yield. ATR-IR: 3202, 3198, 2990, 1736, 1522, 1478, 1467, 1245, 890, 666 cm^{-1}. ^1H NMR (500 MHz, DMSO-d_6) δ 9.14 (d, J = 5.5 Hz, 1H), 8.42 (t, J = 5.5 Hz, 1H), 8.24 (d, J = 5.5 Hz, 1H), 7.81 (d, J = 7.5 Hz, 2H), 7.70 (t, J = 5.5 Hz, 1H), 7.65 (s, 1H), 7.62 (d, J = 7.5 Hz, 1H).

Synthesis of CF_3-PyPyr($AuCl_2$) (6e):

$NaAuCl_4 \cdot 2H_2O$ (60 mg, 0.15 mmol) was added to a 20 mL scintillation vial equipped with a magnetic stir bar and Teflon-seal screw cap. MeCN (5 mL) was added as solvent. CF_3-PyPyr ligand (29 mg, 0.10 mmol) was dissolved in minimal acetone and added. The reaction was placed on a heating block at 80 °C and allowed to stir for 1 hour. After one hour, silver tetrafluoroborate (29 mg, 0.15 mmol) dissolved in minimal MeCN was added. After 4 hours the reaction mixture was filtered through Celite and the filtrate concentrated to give the compound as a yellow solid in quantitative yield. ATR-IR: 3212, 3188, 2770, 1746, 1622, 1528, 1468, 1235 930, 686 cm^{-1}. ^1H NMR (500 MHz, DMSO-d_6) δ 9.15 (d, J = 5.5 Hz, 1H), 8.43 (t, J = 5.5 Hz, 1H), 8.27 (d, J = 5.5 Hz, 1H), 8.06 (d, J = 7.5 Hz, 2H), 7.81 (d, J = 7.5 Hz, 2H), 7.22 (m, 2H).

General procedure for the production of $(PyPyr)_2AuBF_4$ complexes:

To a 20 mL scintillation vial equipped with a magnetic stir bar and Teflon-seal screw cap was added sodium tetrachloroaurate dihydrate (1 equiv). MeCN was added as solvent followed by the PyPyr ligand (2.5 equiv.) dissolved in minimal MeCN. After stirring for 1 hour, silver tetrafluoroborate (1 equiv.) dissolved in minimal MeCN was added. The reaction was stirred at ambient temperature for 18 h during which, precipitation of silver chloride and the complex occurred. The complex was isolated away from the silver chloride by filtering the solids and boiling them in acetonitrile. The hot acetonitrile (with bis complex dissolved in it) was pipetted away from silver chloride and concentrated to afford the title complex in moderate yields.

Synthesis of $(MeO\text{-}PyPyr)_2AuBF_4$ (7a):

$NaAuCl_4 \cdot 2H_2O$ (40 mg, 0.1 mmol) was added to an 8 mL scintillation vial equipped with a magnetic stir bar and Teflon-seal screw cap. MeCN (5 mL) was added as solvent. MeO-PyPyr ligand (63 mg, 0.25 mmol) was dissolved in minimal MeCN and added dropwise. After stirring for 1 hour, silver tetrafluoroborate (20 mg, 0.1 mmol) dissolved in minimal MeCN was added. The reaction was stirred at ambient temperature for 18 h during which time the desired complex precipitated out of solution. The solid was collected and recrystallized in acetonitrile. The title compound was obtained as a yellow solid in 42% yield (30 mg). ATR-IR: 3244, 3124, 1771, 1720, 1522, 1410, 1408, 1178,

817, 450 cm^{-1}. ^1H NMR (500 MHz, DMSO-d_6) δ 10.61 (d, J = 2 Hz, 2H), 8.62 (t, J = 3 Hz, 2H), 8.47 (d, J = 5 Hz, 2H), 8.05 (t, J = 3 Hz, 2H), 7.98 (d, J = 5 Hz, 4H), 7.68 (s, 2H), 7.07 (d, J = 5 Hz, 4H), 3.83 (s, 6H).

Synthesis of (Me-PyPyr)$_2$AuBF$_4$ (7b):

$NaAuCl_4 \cdot 2H_2O$ (40 mg, 0.1 mmol) was added to an 8 mL scintillation vial equipped with a magnetic stir bar and Teflon-seal screw cap. MeCN (5 mL) was added as solvent. Me-PyPyr ligand (59 mg, 0.25 mmol) was dissolved in minimal MeCN and added dropwise. After stirring for 1 hour, silver tetrafluoroborate (20 mg, 0.1 mmol) dissolved in minimal MeCN was added. The reaction was stirred at ambient temperature for 18 h during which time the desired complex precipitated out of solution. The solid was collected and recrystallized in acetonitrile. The title compound was obtained as a yellow solid in 38% yield (25 mg). ATR-IR: 3232, 3216, 1792, 1722, 1568, 1456, 1410, 1200, 952, 492 cm^{-1}. ^1H NMR (500 MHz, DMSO-d_6): δ 10.58 (d, J = 2 Hz, 2H), 8.62 (t, J = 3 Hz, 2H), 8.45 (d, J = 5 Hz, 2H), 8.07 (t, J = 3 Hz, 2H), 7.90 (d, J = 5 Hz, 4H), 7.71 (s, 2H), 7.30 (d, J = 5 Hz, 4H), 3.17 (s, 6H).

Synthesis of (PyPyr)$_2$AuBF$_4$ (7c):

$NaAuCl_4 \cdot 2H_2O$ (40 mg, 0.1 mmol) was added to an 8 mL scintillation vial equipped with a magnetic stir bar and Teflon-seal screw cap. MeCN (5 mL) was

added as solvent. PyPyr ligand (55 mg, 0.25 mmol) was dissolved in minimal MeCN and added dropwise. After stirring for 1 hour, silver tetrafluoroborate (20 mg, 0.1 mmol) dissolved in minimal MeCN was added. The reaction was stirred at ambient temperature for 18 h during which time the desired complex precipitated out of solution. The solid was collected and recrystallized in acetonitrile. The title compound was obtained as a yellow solid in 20% yield (22 mg). ATR-IR: 3222, 3210, 1919, 1856, 1520, 1440, 1329, 1120, 820, 668 cm^{-1} ^1H NMR (500 MHz, DMSO-d_6): δ 10.63 (d, J = 2 Hz, 2H), 8.63 (t, J = 3 Hz, 2H), 8.51 (d, J = 5 Hz, 2H), 8.06 (t, J = 3 Hz, 4H), 7.80 (d, J = 5 Hz, 4H), 7.53 (s, 2H), 7.43 (d, J = 5 Hz, 4H).

Synthesis of (Br-PyPyr)$_2$AuBF$_4$ (7d):

$NaAuCl_4 \cdot 2H_2O$ (40 mg, 0.1 mmol) was added to an 8 mL scintillation vial equipped with a magnetic stir bar and Teflon-seal screw cap. MeCN (5 mL) was added as solvent. Br-PyPyr ligand (75 mg, 0.25 mmol) was dissolved in minimal MeCN and added dropwise. After stirring for 1 hour, silver tetrafluoroborate (20 mg, 0.1 mmol) dissolved in minimal MeCN was added. The reaction was stirred at ambient temperature for 18 h during which time the desired complex precipitated out of solution. The solid was collected and recrystallized in acetonitrile. The title compound was obtained as a yellow solid in 40% yield (48 mg). ATR-IR: 3212, 3108, 2997, 1686, 1510, 1457, 1400, 1395, 900, 886 cm^{-1}.^1H NMR (500 MHz, DMSO-d_6): δ 10.58 (d, J = 2 Hz, 2H), 8.67 (t, J = 3 Hz, 2H), 8.48

(d, J = 5 Hz, 2H), 8.08 (t, J = 3 Hz, 2H), 8.04 (d, J = 5 Hz, 4H), 7.84 (s, 2H), 7.72 (d, J = 5 Hz, 4H).

Synthesis of (CF_3-PyPyr)$_2$$AuBF_4$ (7e):

$NaAuCl_4 \cdot 2H_2O$ (40 mg, 0.1 mmol) was added to an 8 mL scintillation vial equipped with a magnetic stir bar and Teflon-seal screw cap. MeCN (5 mL) was added as solvent. CF_3-PyPyr ligand (72 mg, 0.25 mmol) was dissolved in minimal MeCN and added dropwise. After stirring for 1 hour, silver tetrafluoroborate (20 mg, 0.1 mmol) dissolved in minimal MeCN was added. The reaction was stirred at ambient temperature for 18 h during which time the desired complex precipitated out of solution. The solid was collected and recrystallized in acetonitrile. The title compound was obtained as a yellow solid in 35% yield (42 mg). ATR-IR: 3112, 3007, 2898, 1550, 1520, 1445, 1430, 1122, 880, 456 cm^{-1}.^{1}H NMR (500 MHz, DMSO-d_6): δ 10.61 (d, J = 2 Hz, 2H), 8.68 (t, J = 3 Hz, 2H), 8.53 (d, J = 5 Hz, 2H), 8.29 (t, J = 3 Hz, 2H), 8.10 (d, J = 5 Hz, 4H), 7.96 (s, 2H), 7.89 (d, J = 5 Hz, 4H).

General procedure for the production of PyPyrPtCl2 complexes:

To an 8 mL scintillation vial equipped with a magnetic stir bar and Teflon-seal screw cap was added $PtCl_2(DMSO)_2$. MeCN was added as solvent followed by the PyPyr ligand bearing the desired substitution dissolved in minimal MeCN. The reaction was stirred at ambient temperature for 18 h. Once completed, the

reaction solution was passed through a plug of Celite and concentrated until a saturated solution was obtained. Upon standing, the PyPyrPtCl$_2$ complex precipitated as a crystalline powder. Recrystallization of these complexes occurred in MeNO$_2$.

Synthesis of MeO-PyPyr(PtCl$_2$) (8a):

PtCl$_2$(DMSO)$_2$ (42 mg, 0.1 mmol) was added to an 8 mL scintillation vial equipped with a magnetic stir bar and Teflon-seal screw cap. MeCN (5 mL) was added as solvent. MeO-PyPyr ligand (22 mg, 0.09 mmol) was dissolved in minimal MeCN and added dropwise. The reaction was stirred at ambient temperature for 18 h. During this time the desired complex precipitated out of solution. The solid was brought up in minimal hot nitromethane and precipitated out as red crystals in 50% yield (23 mg). ATR-IR: 3118, 2935, 1736, 1513, 1463, 1239, 1014, 833, 775, 513, 423 cm^{-1}.^{1}H NMR (500 MHz, MeNO$_2$-*d*$_3$): 9.35 (d, J = 2 Hz, 1H), 8.30 (m, 1H), 8.06 (m, 1H), 7.85 (d, J = 6 Hz, 1H), 7.64 (m, 1H), 7.36 (s, 1H), 7.13 (d, J = 6 Hz, 1H), 3.92 (s, 3H).

Synthesis of PyPyr(PtCl$_2$) (8b):

PtCl$_2$(DMSO)$_2$ (42 mg, 0.1 mmol) was added to an 8 mL scintillation vial equipped with a magnetic stir bar and Teflon-seal screw cap. MeCN (5 mL) was added as solvent. PyPyr ligand (20 mg, 0.09 mmol) was dissolved in minimal MeCN and added dropwise. The reaction was stirred at ambient temperature for

18 h. During this time the desired complex precipitated out of solution. The solid was brought up in minimal hot nitromethane and precipitated out as red crystals in 46% yield (22 mg). ATR-IR: 3120, 2944, 1757, 1529, 1500, 1339, 1224, 935, 765, 520, 404 cm^{-1}.^{1}H NMR (500 MHz, $MeNO_2$-d_3): 9.35 (m, 1H), 8.30 (d, J = 3 Hz, 1H), 8.11 (m, 1H), 7.89 (m, 2H), 7.66 (m, 1H), 7.59 (m, 3H), 7.45 (s, 1H).

Synthesis of CF_3-PyPyr($PtCl_2$) (8c):

$PtCl_2(DMSO)_2$ (42 mg, 0.1 mmol) was added to an 8 mL scintillation vial equipped with a magnetic stir bar and Teflon-seal screw cap. MeCN (5 mL) was added as solvent. CF_3-PyPyr ligand (26 mg, 0.09 mmol) was dissolved in minimal MeCN and added dropwise. The reaction was stirred at ambient temperature for 18 h. During this time the desired complex precipitated out of solution. The solid was brought up in minimal hot nitromethane and precipitated out as red crystals in 40% yield (20 mg). ATR-IR: 3115, 2980, 2870, 1530, 1520, 1434, 1230, 1100, 990, 560, 405 cm^{-1}.^{1}H NMR (500 MHz, $MeNO_2$-d_3): 9.36 (d, J = 3 Hz, 1H), 8.30 (d, J = 3 Hz, 1H), 8.10 (m, 3H), 7.91 (m, 2H), 7.66 (m, 1H), 7.54 (s, 1H).

Synthesis of $(PyPyr)_2CuCl_2$:

Copper (II) chloride (13 mg, 0.1 mmol) was added to an 8 mL scintillation vial equipped with a magnetic stir bar and Teflon-seal screw cap. Acetonitrile (5 mL) was added as solvent. PyPyr ligand (55 mg, 0.25 mmol) was dissolved in minimal acetonitrile and added dropwise. The solution immediately turned green

and opaque and was left to stir for 2 hours, during which time a green precipitate formed. The solid was collected, dissolved in hot acetone, and allowed to recrystallize. The product was collected as vibrant, green, cubic crystals in 15% yield (10 mg). Due to paramagnetic nature of the title complex, NMR was unable to be collected, however x-ray crystallographic data was deemed sufficient.

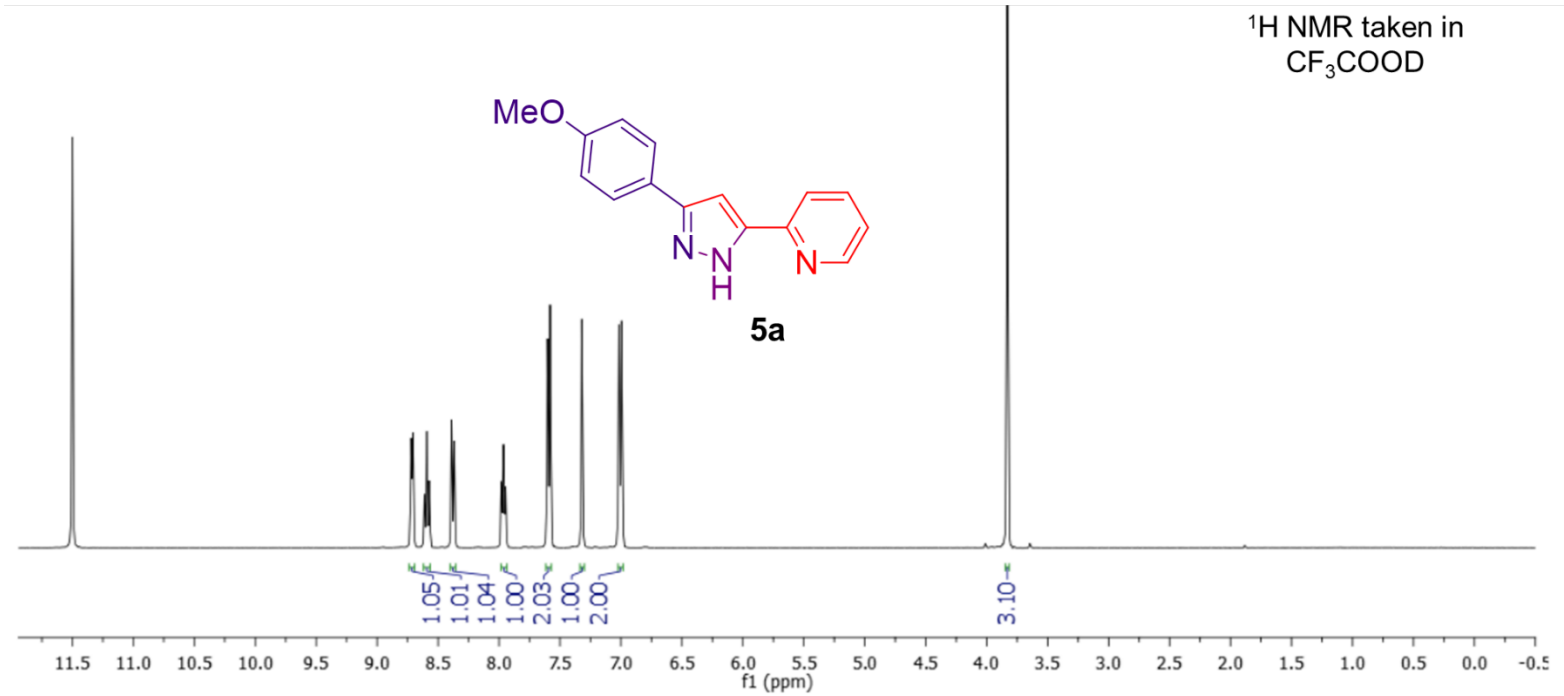
^{1}H NMR taken in
CF_3COOD
MeO
N
N
H
N
5a
1.05
1.01
1.04
1.00
2.03
1.00
2.00
3.10
11.5 11.0 10.5 10.0 9.5 9.0 8.5 8.0 7.5 7.0 6.5 6.0 5.5 5.0 4.5 4.0 3.5 3.0 2.5 2.0 1.5 1.0 0.5 0.0 -0.5
f1 (ppm)

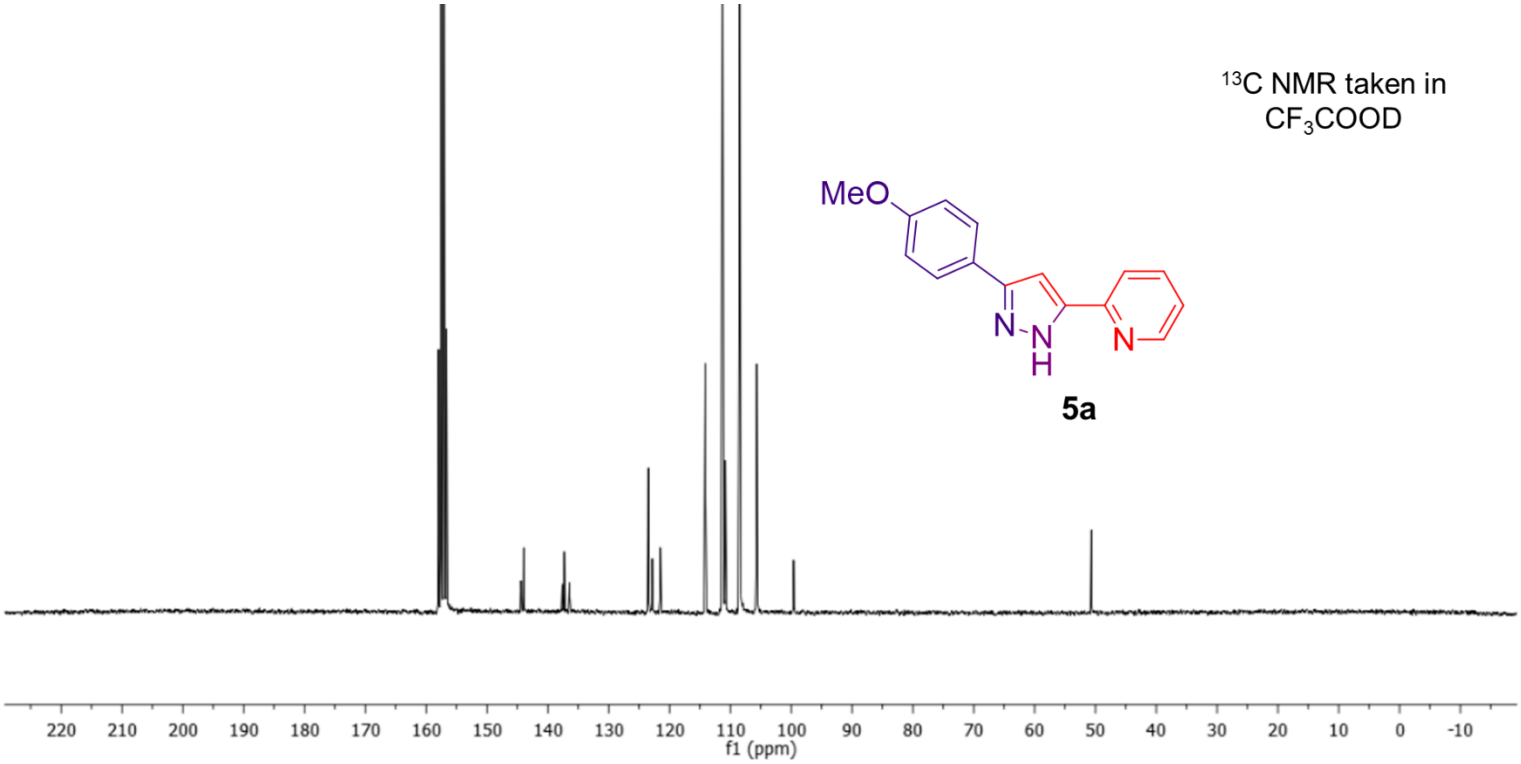
^{13}C NMR taken in
CF_3COOD
MeO
N
N
H
N
5a
220 210 200 190 180 170 160 150 140 130 120 110 100 90 80 70 60 50 40 30 20 10 0 -10
f1 (ppm)

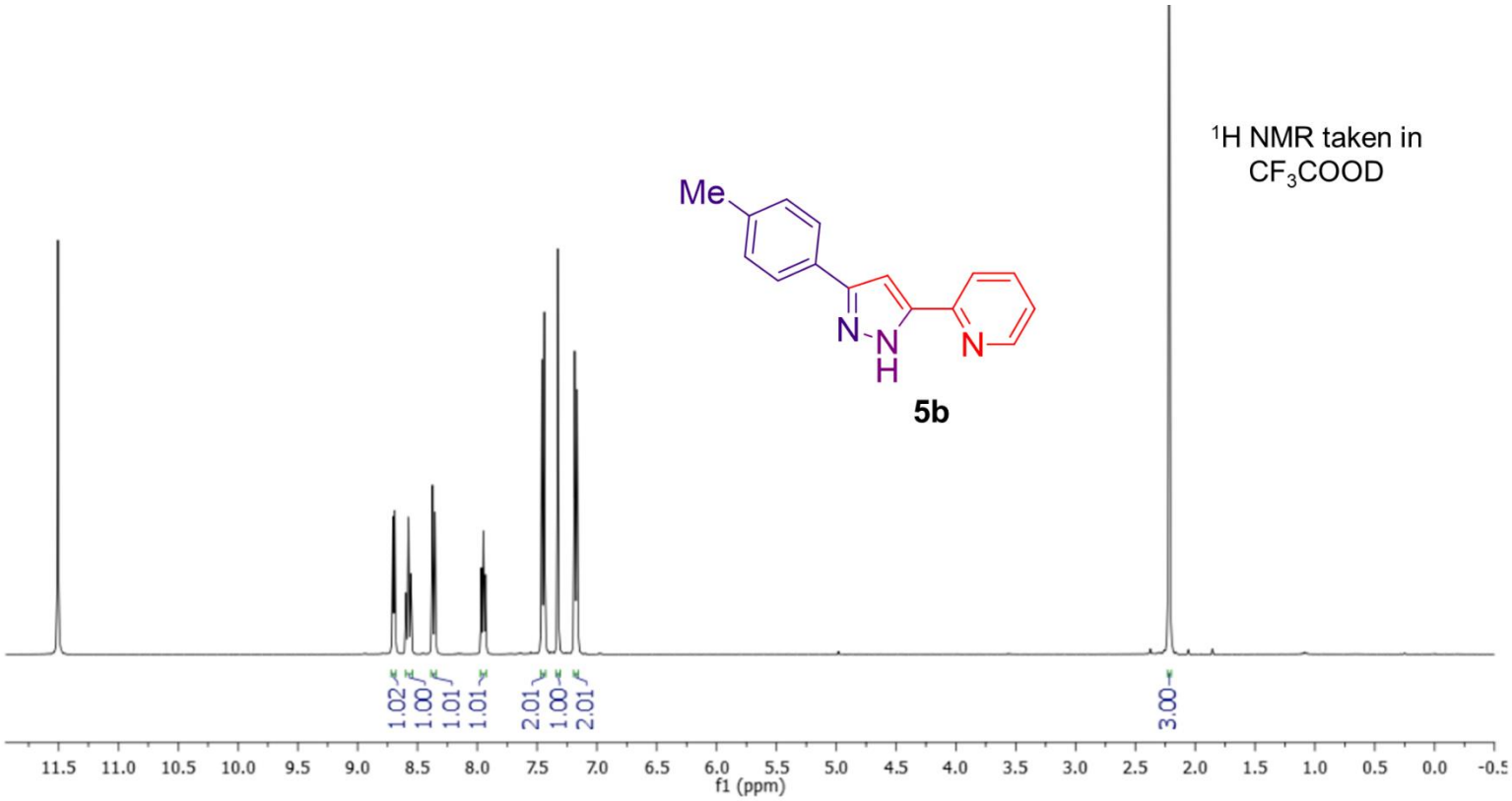
^{1}H NMR taken in
CF_3COOD
Me
N
N
H
N
5b
1.02
1.00
1.01
1.01
2.01
1.00
2.01
3.00
11.5 11.0 10.5 10.0 9.5 9.0 8.5 8.0 7.5 7.0 6.5 6.0 5.5 5.0 4.5 4.0 3.5 3.0 2.5 2.0 1.5 1.0 0.5 0.0 -0.5
f1 (ppm)

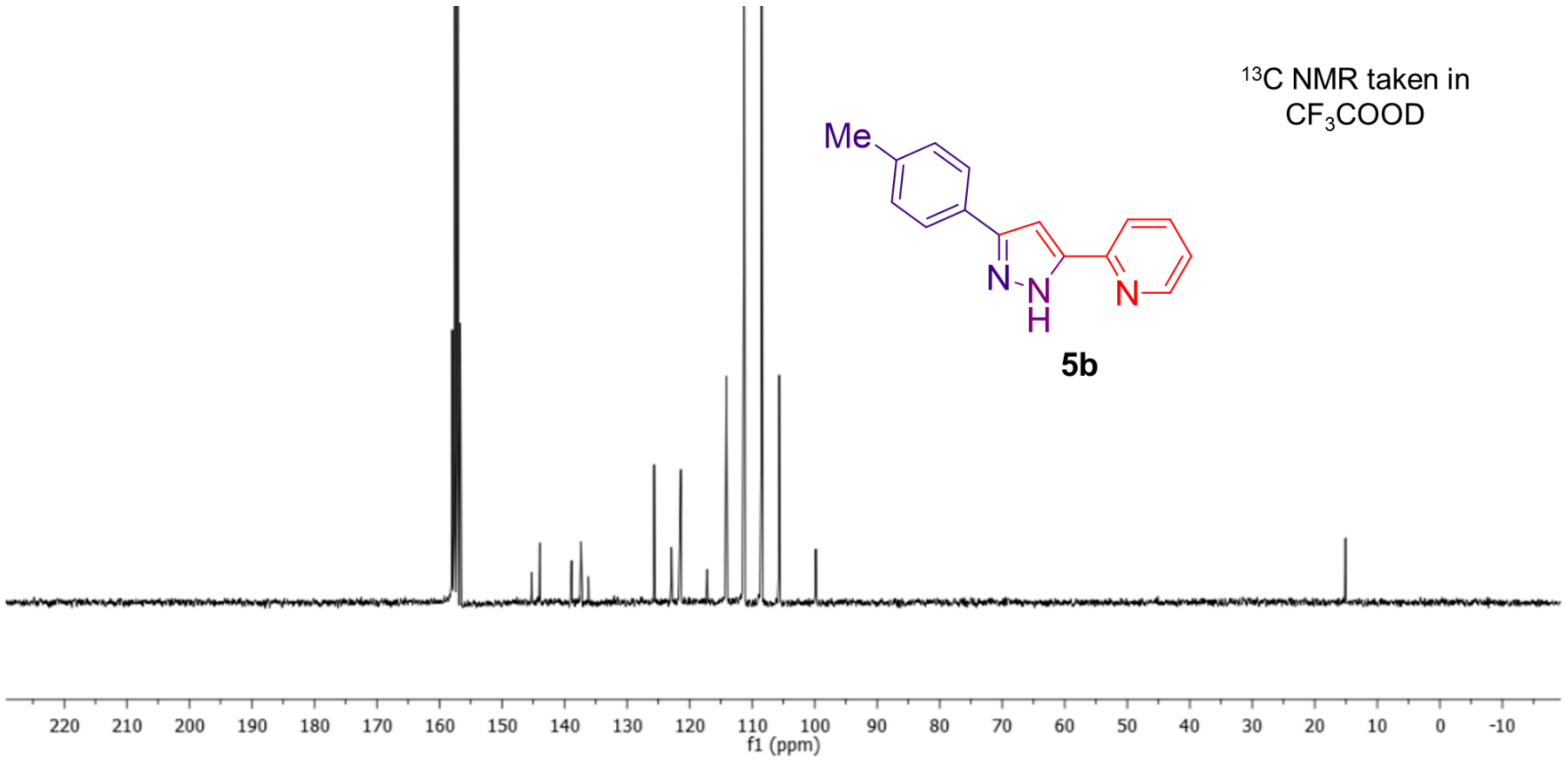
^{13}C NMR taken in
CF_3COOD
Me
N
N
H
N
5b
220 210 200 190 180 170 160 150 140 130 120 110 100 90 80 70 60 50 40 30 20 10 0 -10
f1 (ppm)

^{1}H NMR taken in
CF_3COOD

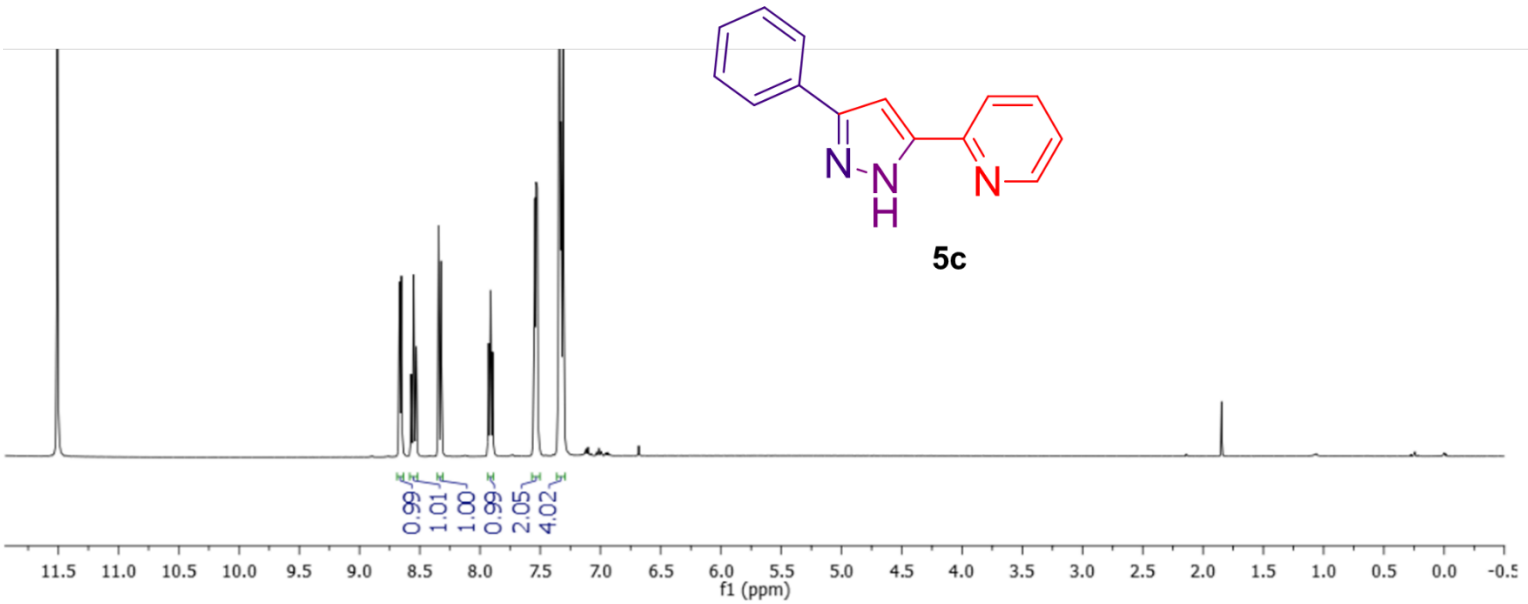

5c

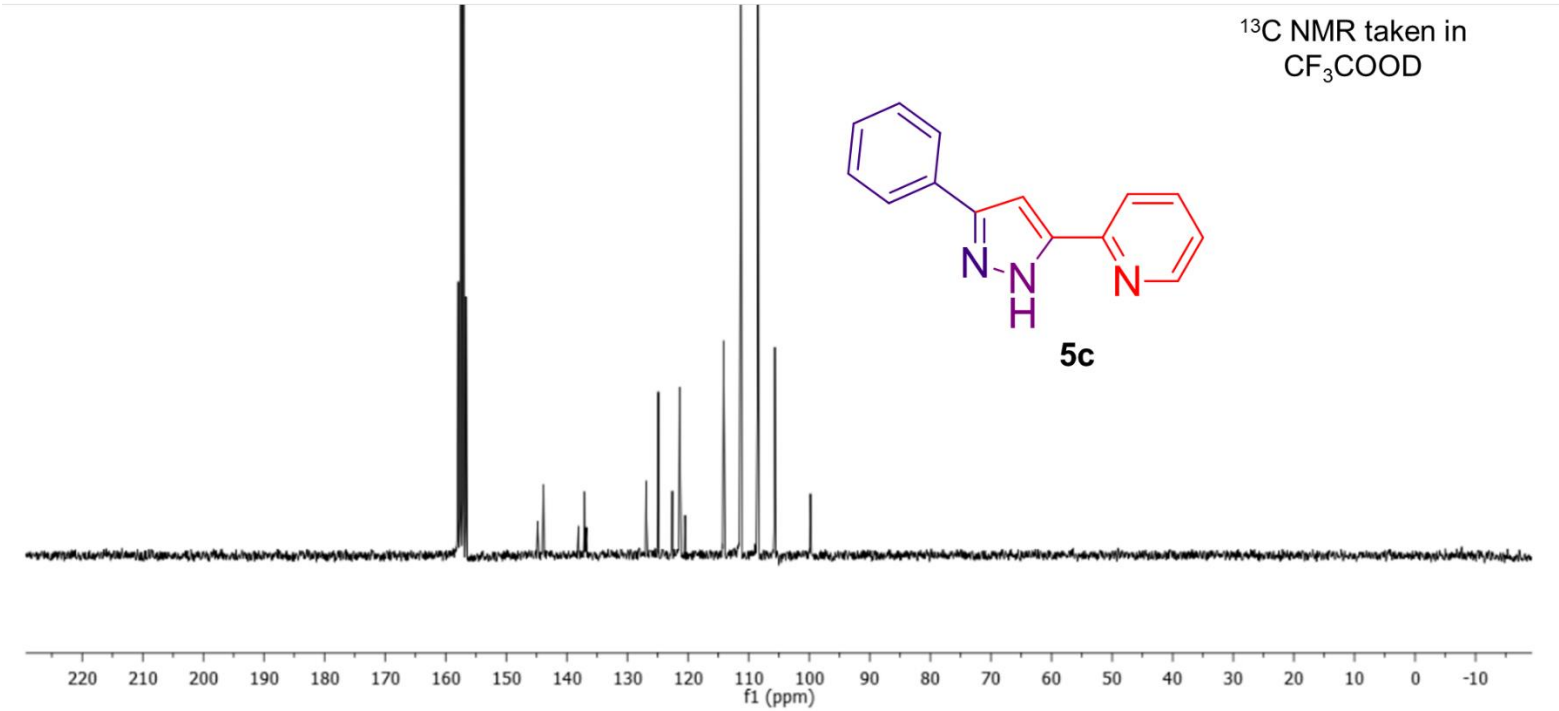
^{13}C NMR taken in
CF_3COOD
N
N
H
N
5c
220 210 200 190 180 170 160 150 140 130 120 110 100 90 80 70 60 50 40 30 20 10 0 -10
f1 (ppm)

^{1}H NMR taken in CF_3COOD

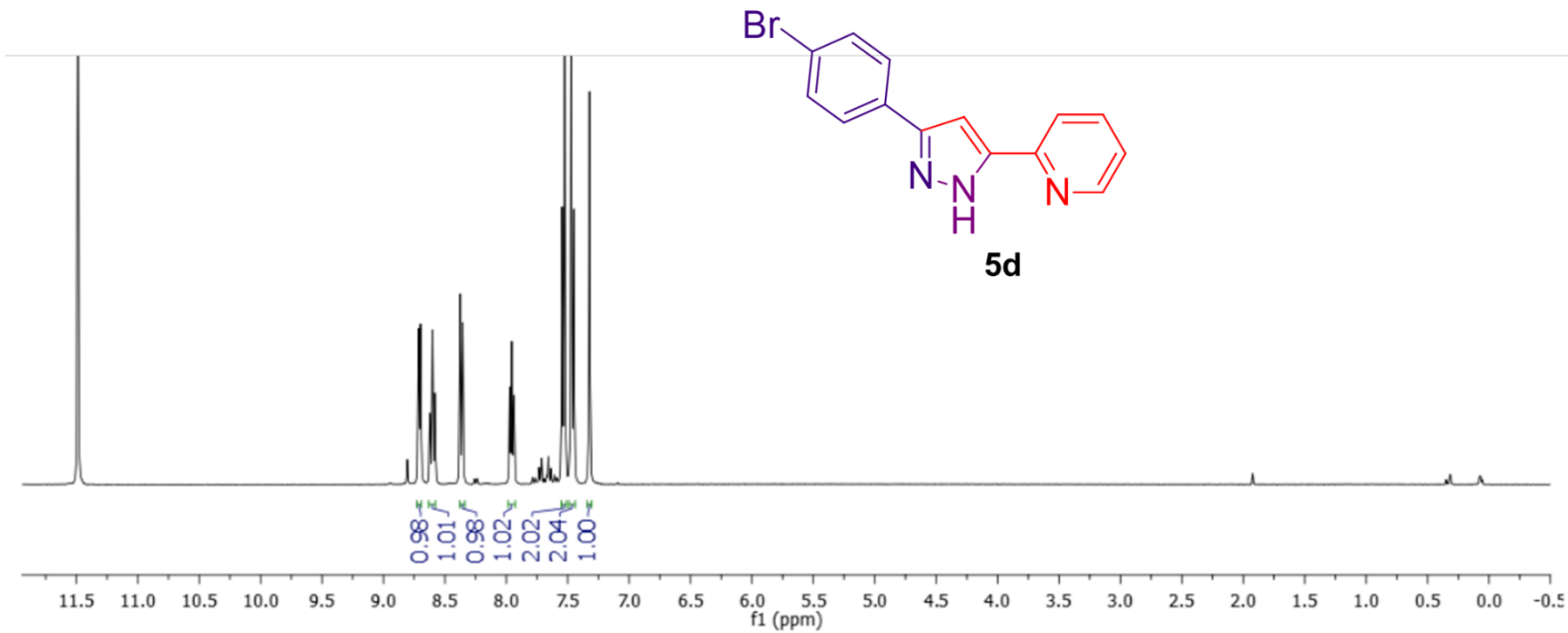

5d

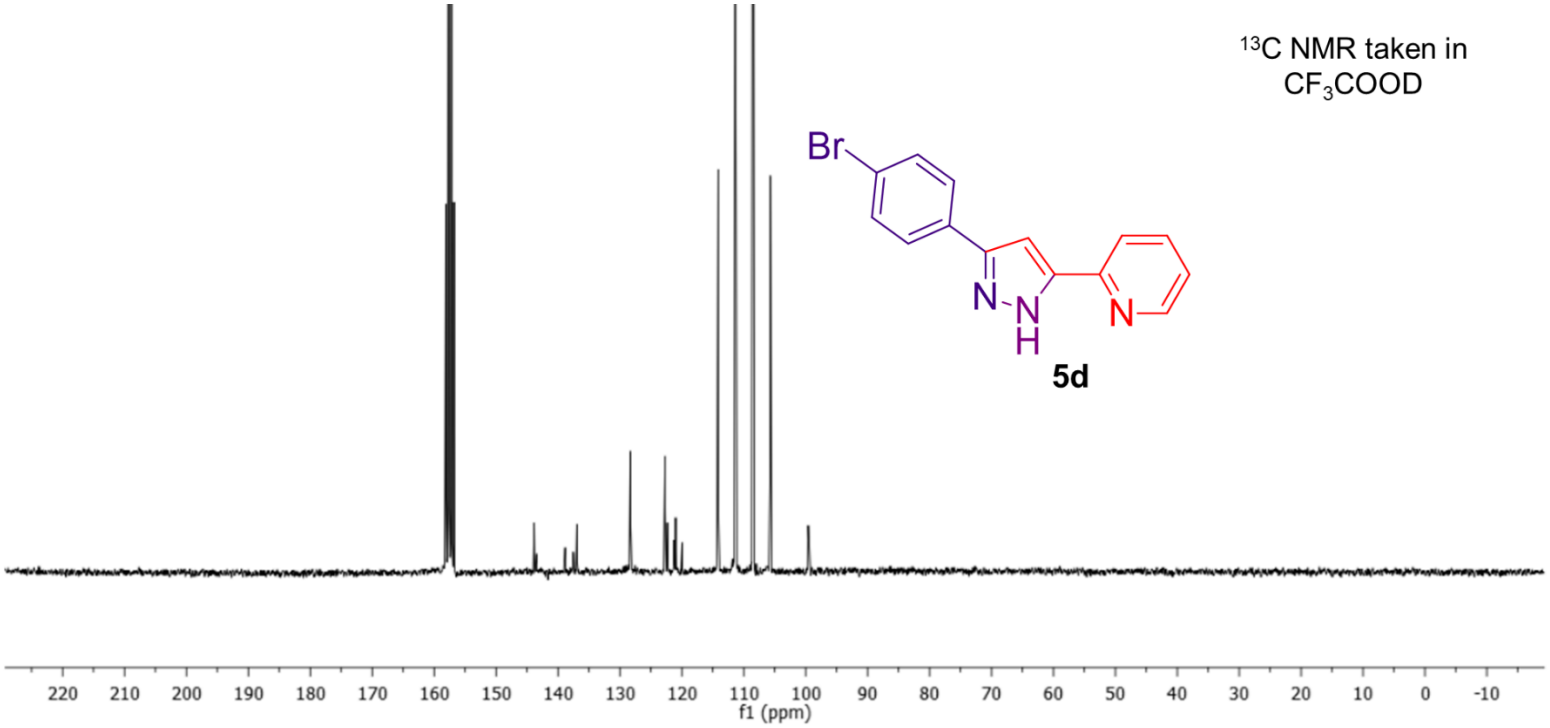
^{13}C NMR taken in
CF_3COOD
Br
N
N
H
N
5d
220 210 200 190 180 170 160 150 140 130 120 110 100 90 80 70 60 50 40 30 20 10 0 -10
f1 (ppm)

^{1}H NMR taken in CF_3COOD

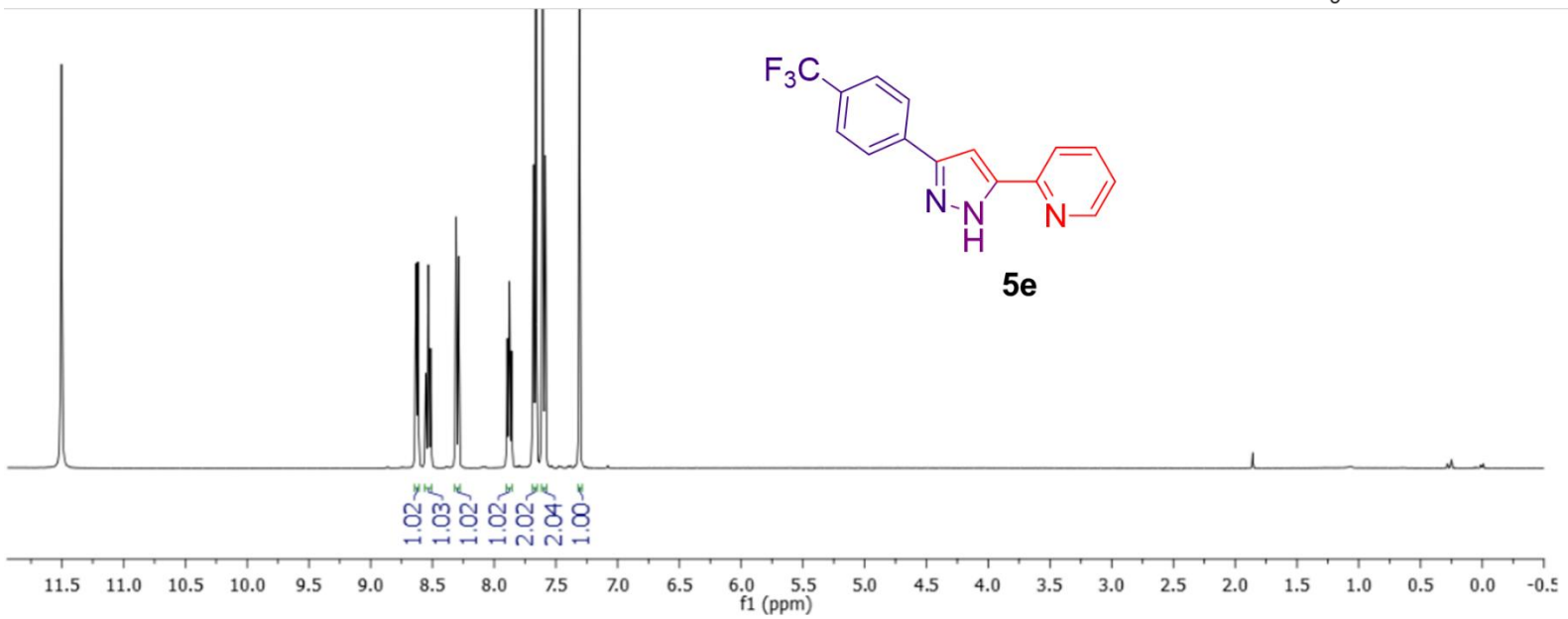

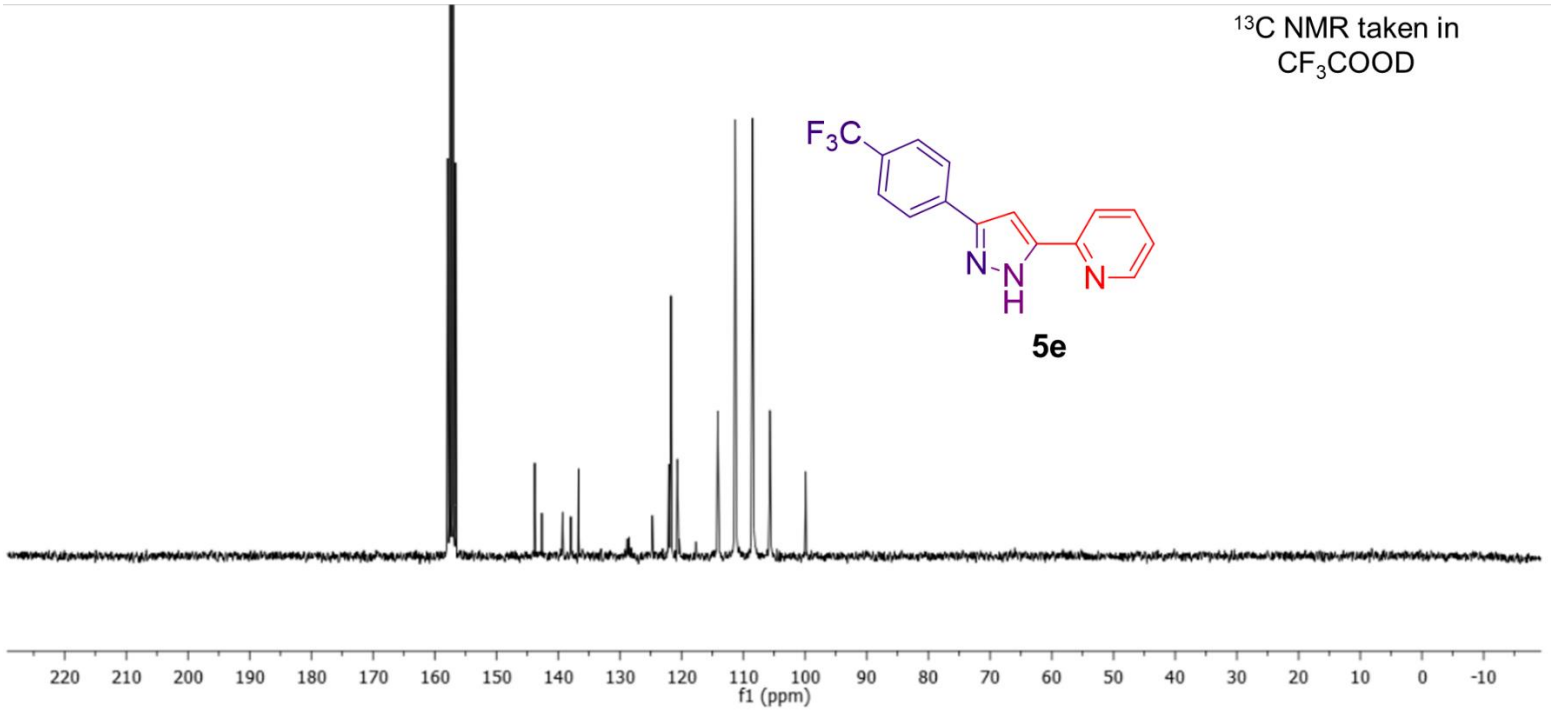
^{13}C NMR taken in
CF_3COOD
F_3C
N
N
H
N
5e
220 210 200 190 180 170 160 150 140 130 120 110 100 90 80 70 60 50 40 30 20 10 0 -10
f1 (ppm)

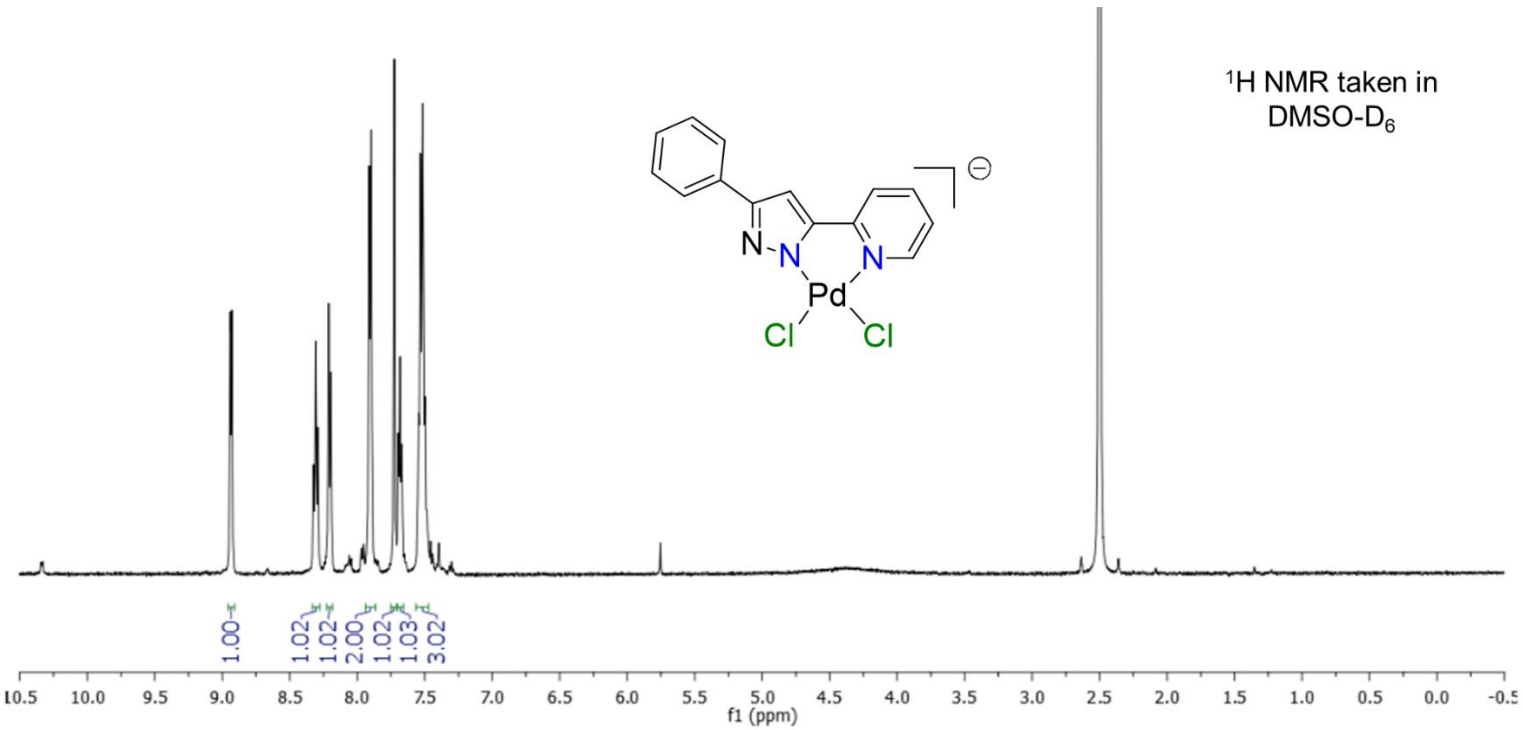
^{1}H NMR taken in
DMSO-D$_6$
N
N
N
Pd
Cl
Cl
⊖
1.00
1.02
1.02
2.00
1.02
1.03
3.02
10.5 10.0 9.5 9.0 8.5 8.0 7.5 7.0 6.5 6.0 5.5 5.0 4.5 4.0 3.5 3.0 2.5 2.0 1.5 1.0 0.5 0.0 -0.5
f1 (ppm)

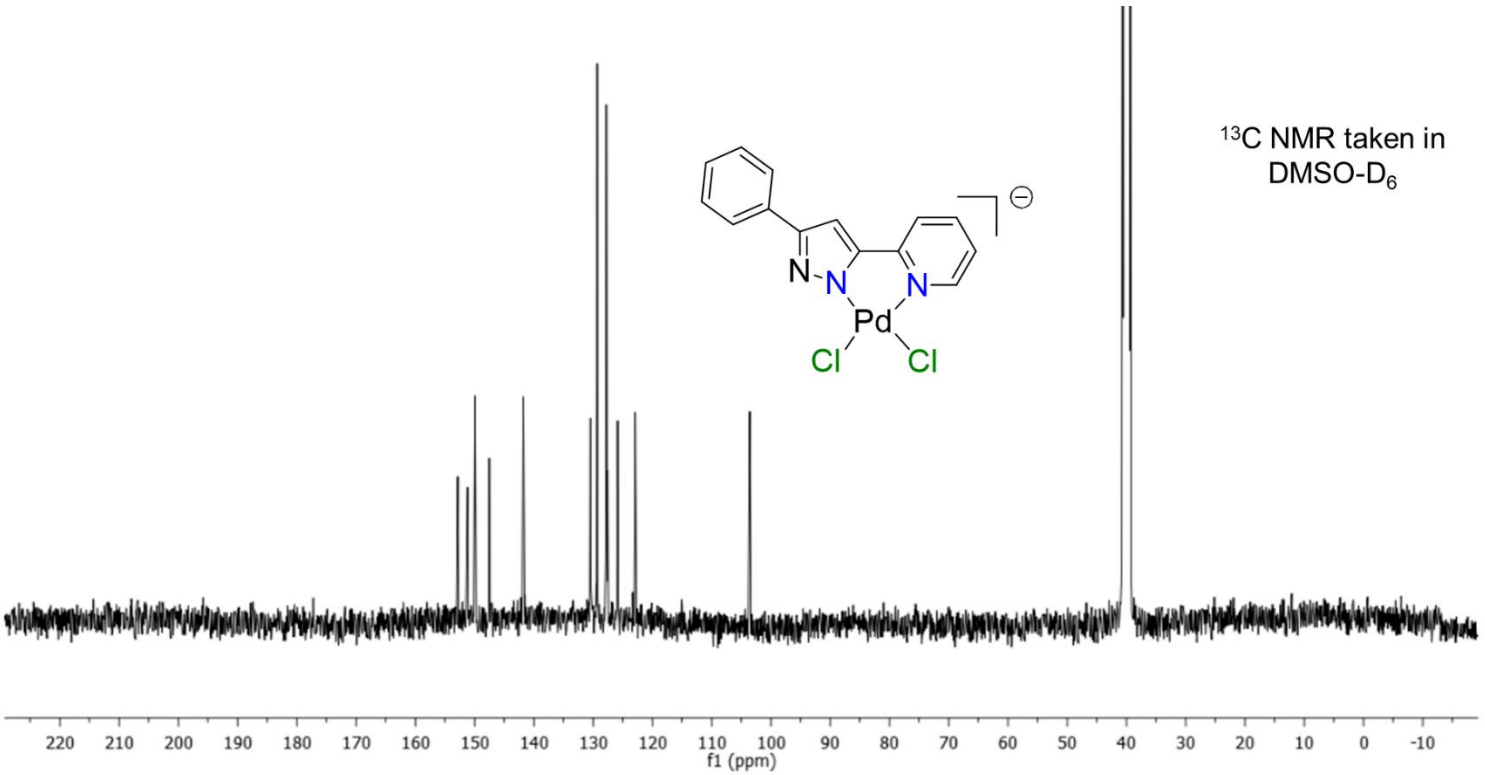
^{13}C NMR taken in
DMSO-D$_6$
N
N
N
Pd
Cl
Cl
⊖
220 210 200 190 180 170 160 150 140 130 120 110 100 90 80 70 60 50 40 30 20 10 0 -10
f1 (ppm)

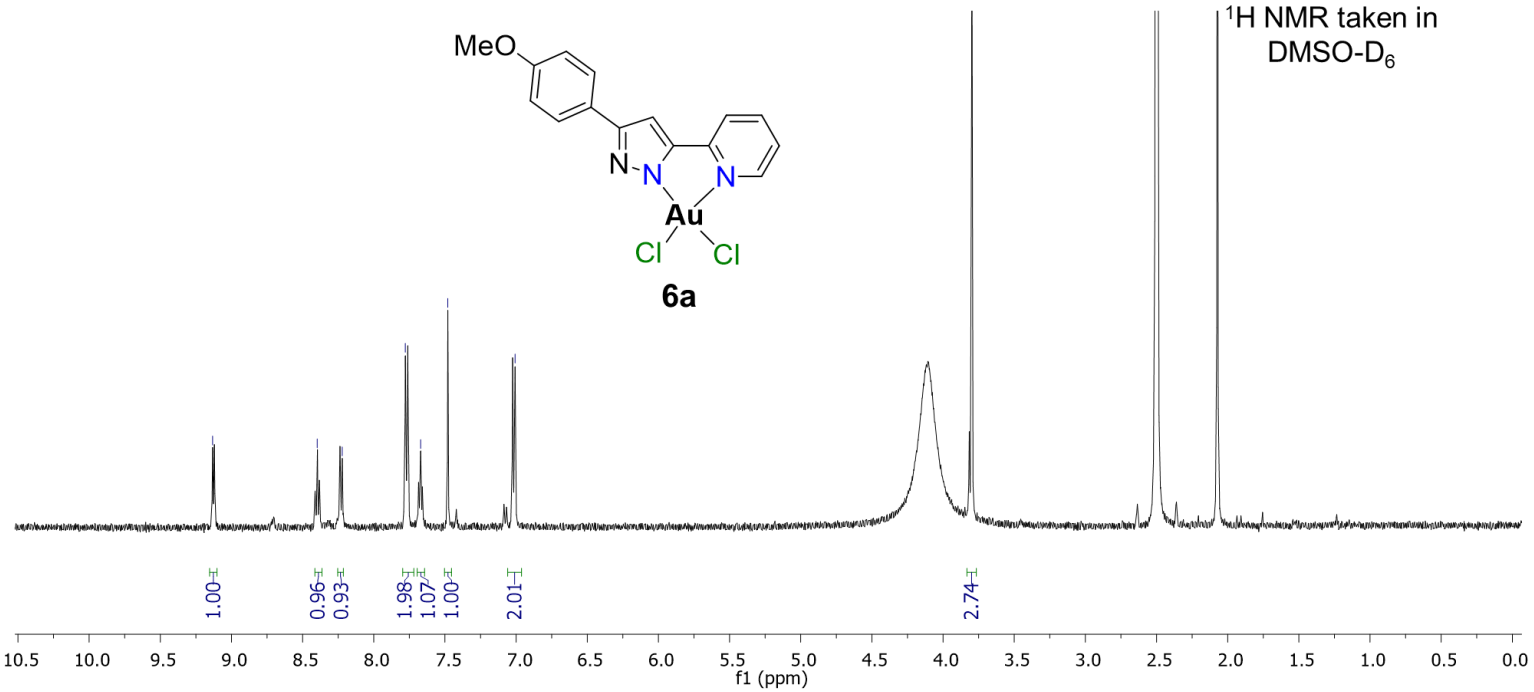
MeO
N
N
N
Au
Cl
Cl
6a
^{1}H NMR taken in
DMSO-D$_6$
1.00
0.96
0.93
1.98
1.07
1.00
2.01
2.74
10.5 10.0 9.5 9.0 8.5 8.0 7.5 7.0 6.5 6.0 5.5 5.0 4.5 4.0 3.5 3.0 2.5 2.0 1.5 1.0 0.5 0.0
f1 (ppm)

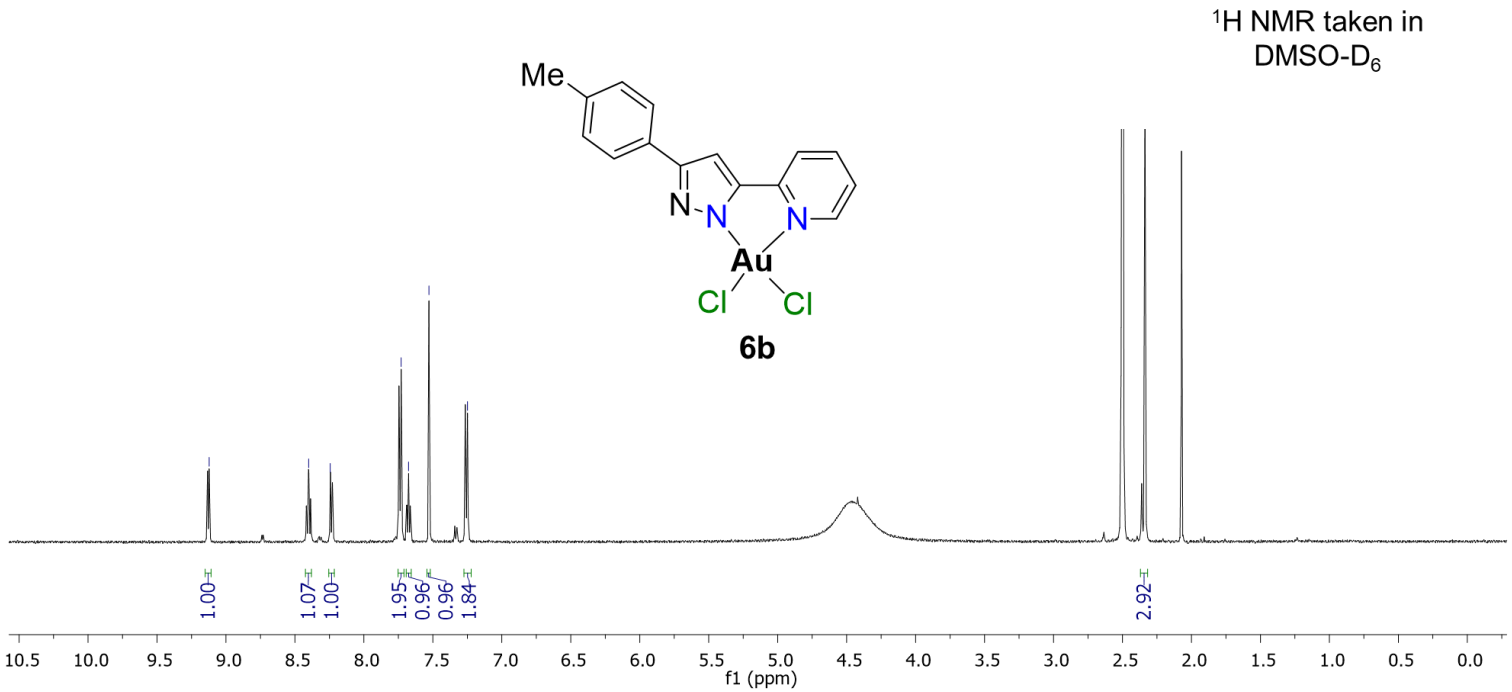
^{1}H NMR taken in
DMSO-D$_6$
Me
N
N
N
Au
Cl
Cl
6b
1.00
1.07
1.00
1.95
0.96
0.96
1.84
2.92
10.5 10.0 9.5 9.0 8.5 8.0 7.5 7.0 6.5 6.0 5.5 5.0 4.5 4.0 3.5 3.0 2.5 2.0 1.5 1.0 0.5 0.0
f1 (ppm)

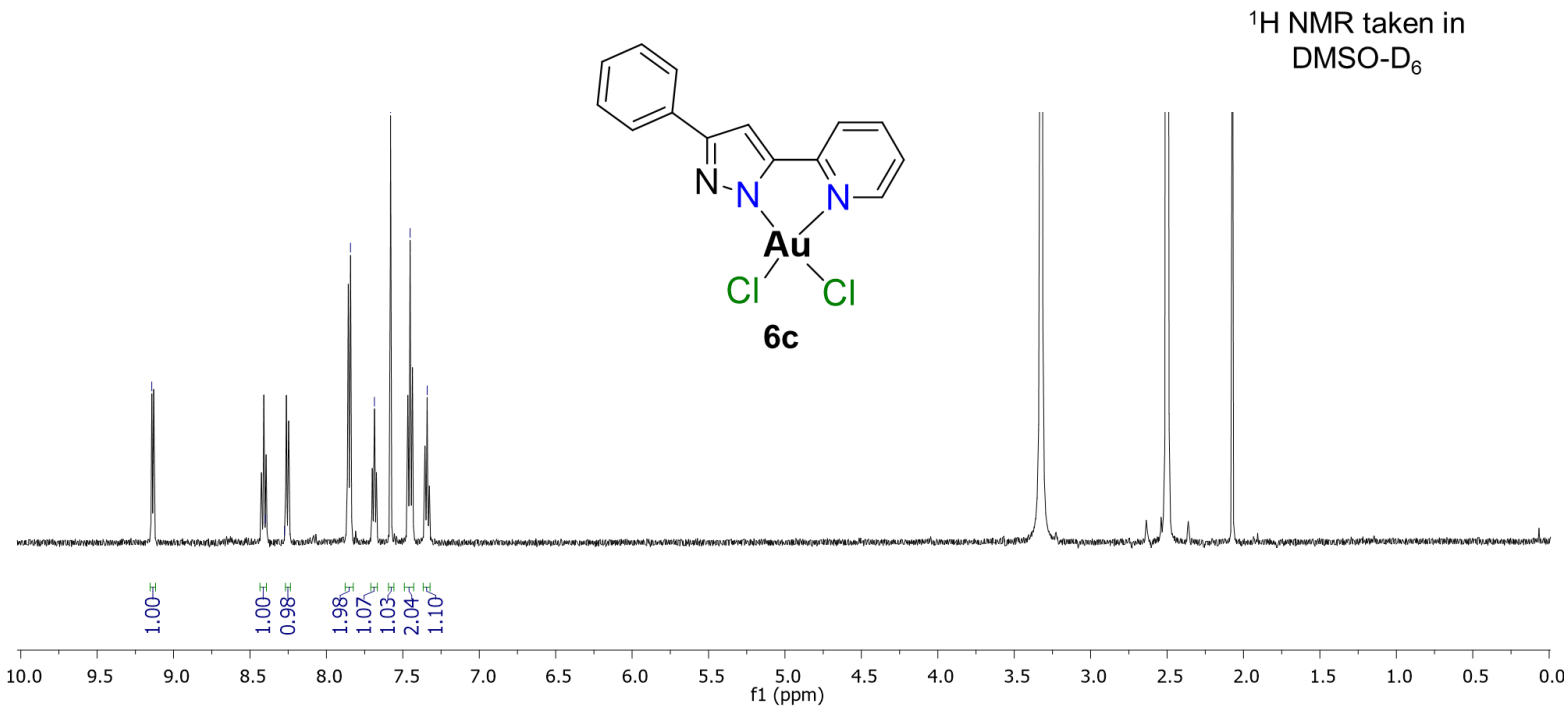
^{1}H NMR taken in
DMSO-D$_6$
N
N
N
Au
Cl
Cl
6c
1.00
1.00
0.98
1.98
1.07
1.03
2.04
1.10
10.0
9.5
9.0
8.5
8.0
7.5
7.0
6.5
6.0
5.5
5.0
4.5
4.0
3.5
3.0
2.5
2.0
1.5
1.0
0.5
0.0
f1 (ppm)

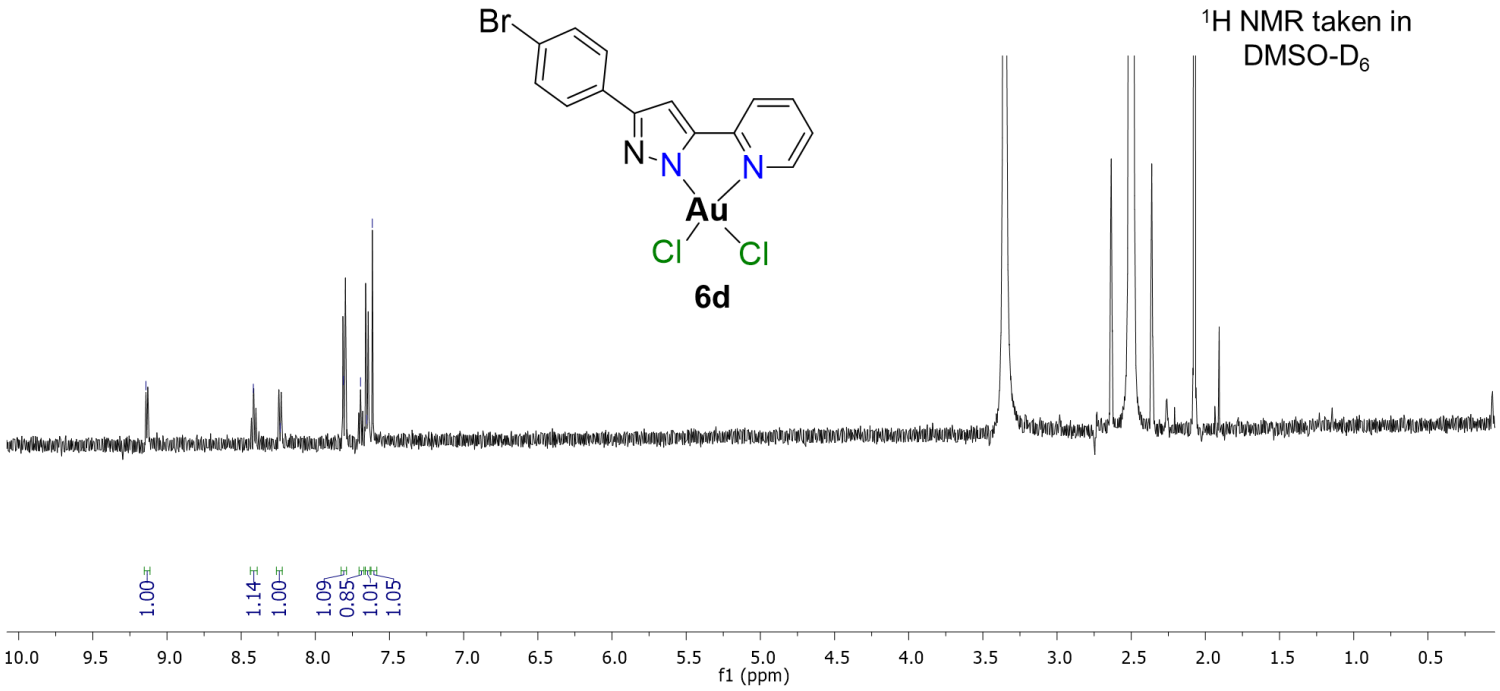
Br
N
N
N
Au
Cl
Cl
6d
^{1}H NMR taken in
DMSO-D$_6$
1.00
1.14
1.00
1.09
0.85
1.01
1.05
10.0
9.5
9.0
8.5
8.0
7.5
7.0
6.5
6.0
5.5
5.0
4.5
4.0
3.5
3.0
2.5
2.0
1.5
1.0
0.5
f1 (ppm)

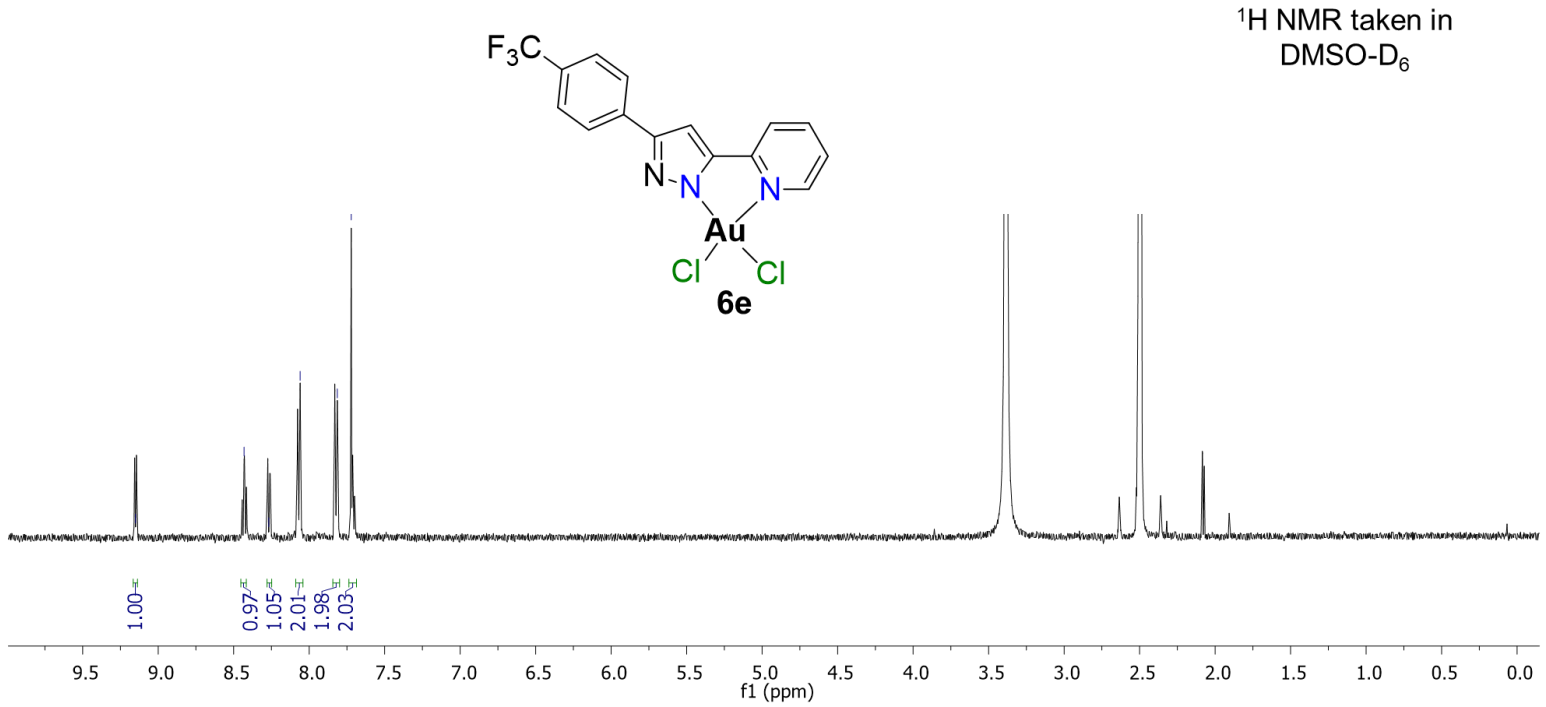
^{1}H NMR taken in
DMSO-D$_6$
F$_3$C
N
N
N
Au
Cl
Cl
6e
1.00
0.97
1.05
2.01
1.98
2.03
9.5
9.0
8.5
8.0
7.5
7.0
6.5
6.0
5.5
5.0
4.5
4.0
3.5
3.0
2.5
2.0
1.5
1.0
0.5
0.0
f1 (ppm)

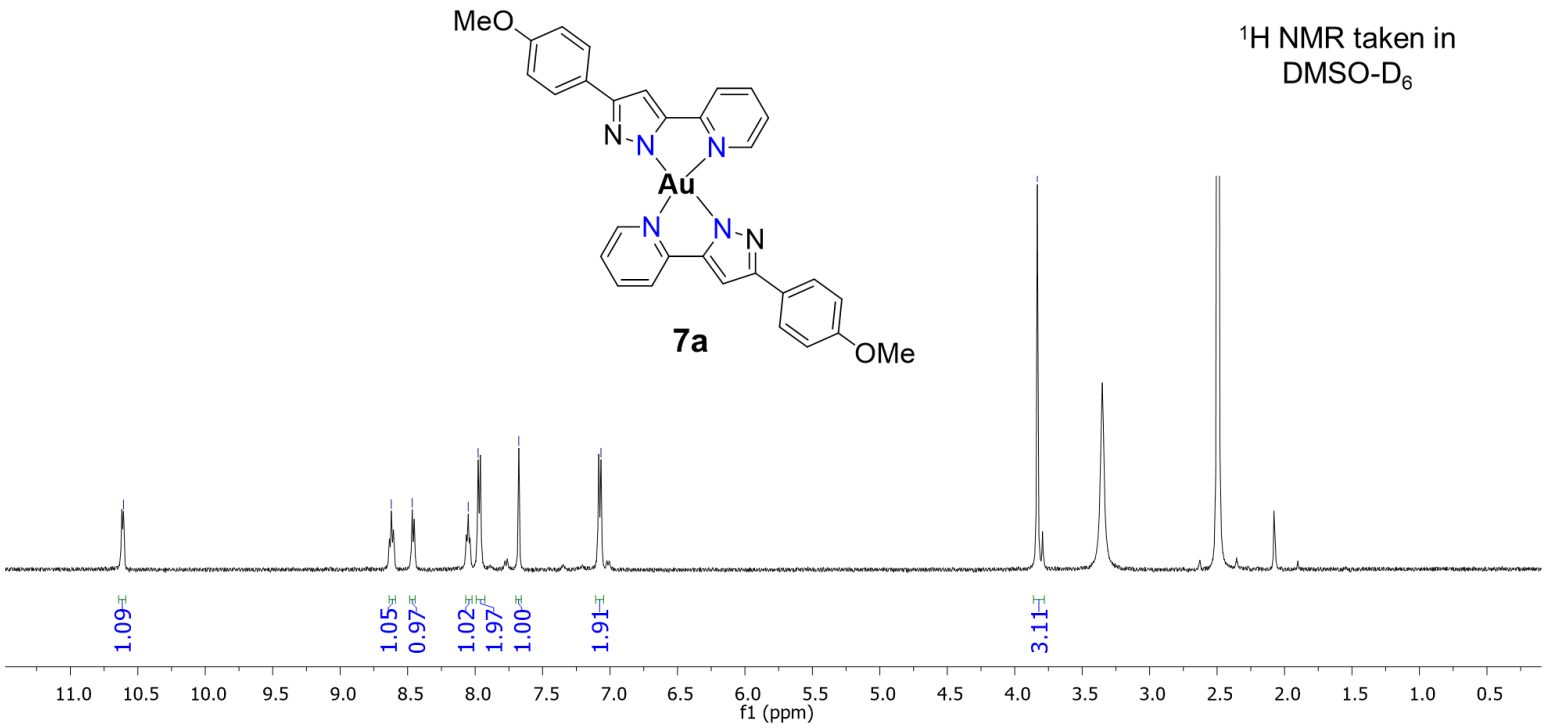
MeO
N
N
N
Au
N
N
N
OMe
7a
^{1}H NMR taken in
DMSO-D$_6$
1.09
1.05
0.97
1.02
1.97
1.00
1.91
3.11
11.0
10.5
10.0
9.5
9.0
8.5
8.0
7.5
7.0
6.5
6.0
5.5
5.0
4.5
4.0
3.5
3.0
2.5
2.0
1.5
1.0
0.5
f1 (ppm)

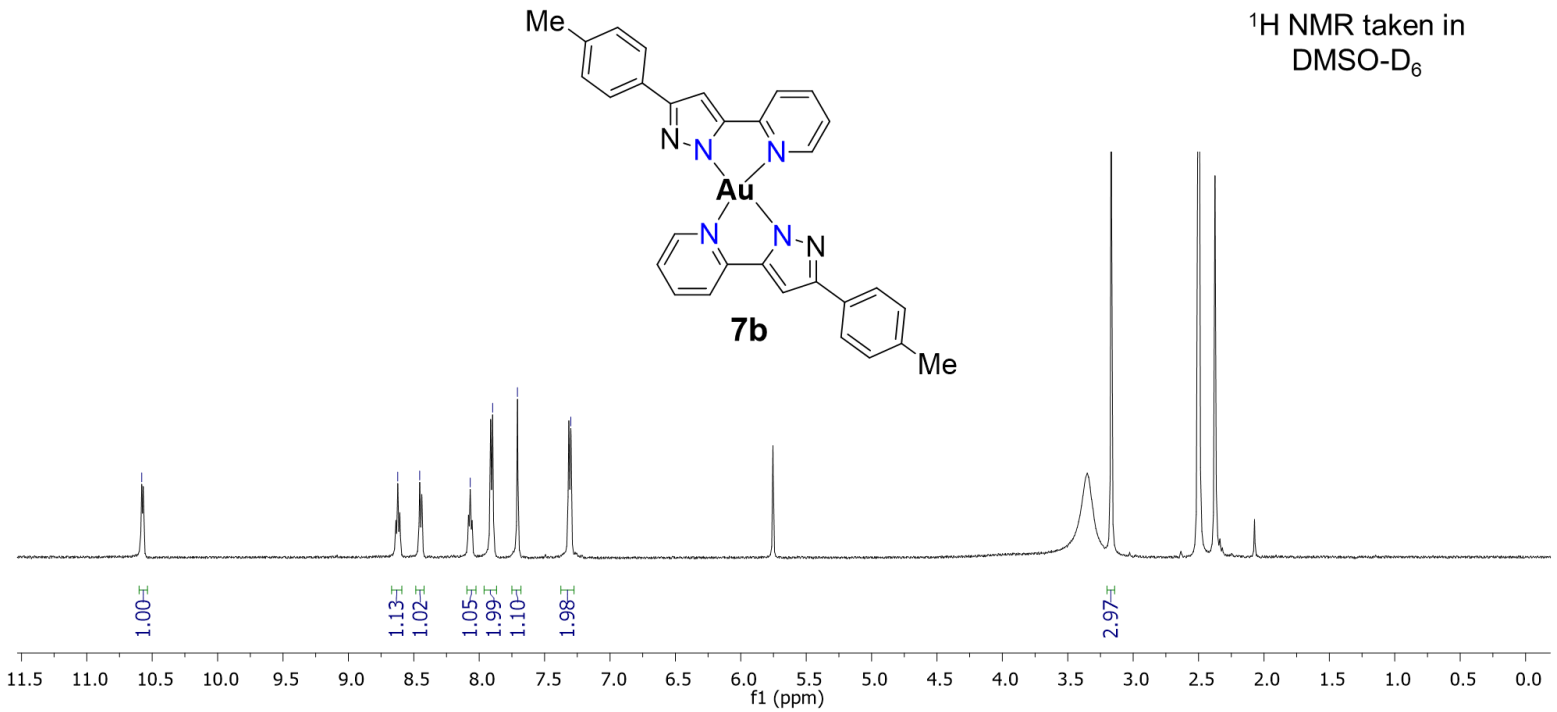
Me
N
N
N
Au
N
N
N
Me
7b
^{1}H NMR taken in
DMSO-D$_6$
1.00
1.13
1.02
1.05
1.99
1.10
1.98
2.97
11.5 11.0 10.5 10.0 9.5 9.0 8.5 8.0 7.5 7.0 6.5 6.0 5.5 5.0 4.5 4.0 3.5 3.0 2.5 2.0 1.5 1.0 0.5 0.0
f1 (ppm)

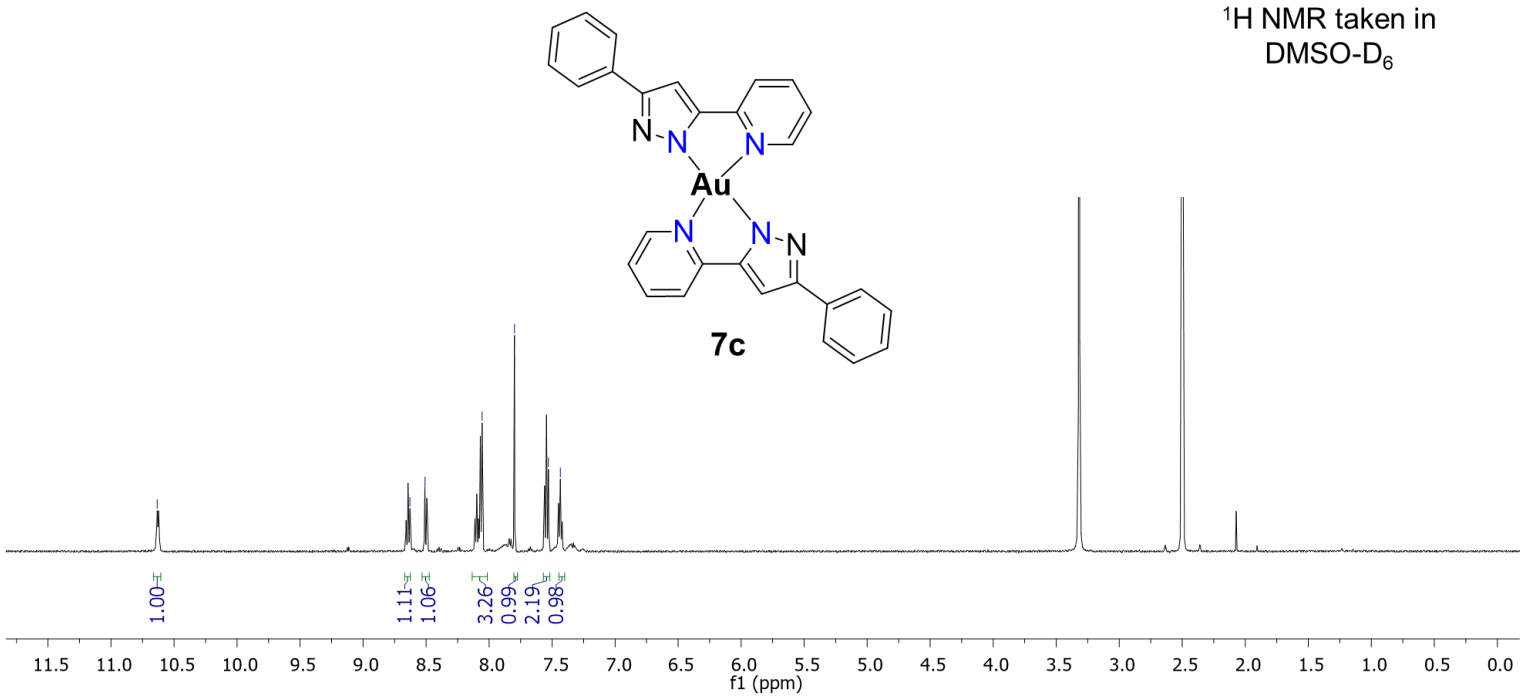
^{1}H NMR taken in
DMSO-D$_6$
Au
7c
1.00
1.11
1.06
3.26
0.99
2.19
0.98
11.5 11.0 10.5 10.0 9.5 9.0 8.5 8.0 7.5 7.0 6.5 6.0 5.5 5.0 4.5 4.0 3.5 3.0 2.5 2.0 1.5 1.0 0.5 0.0
f1 (ppm)

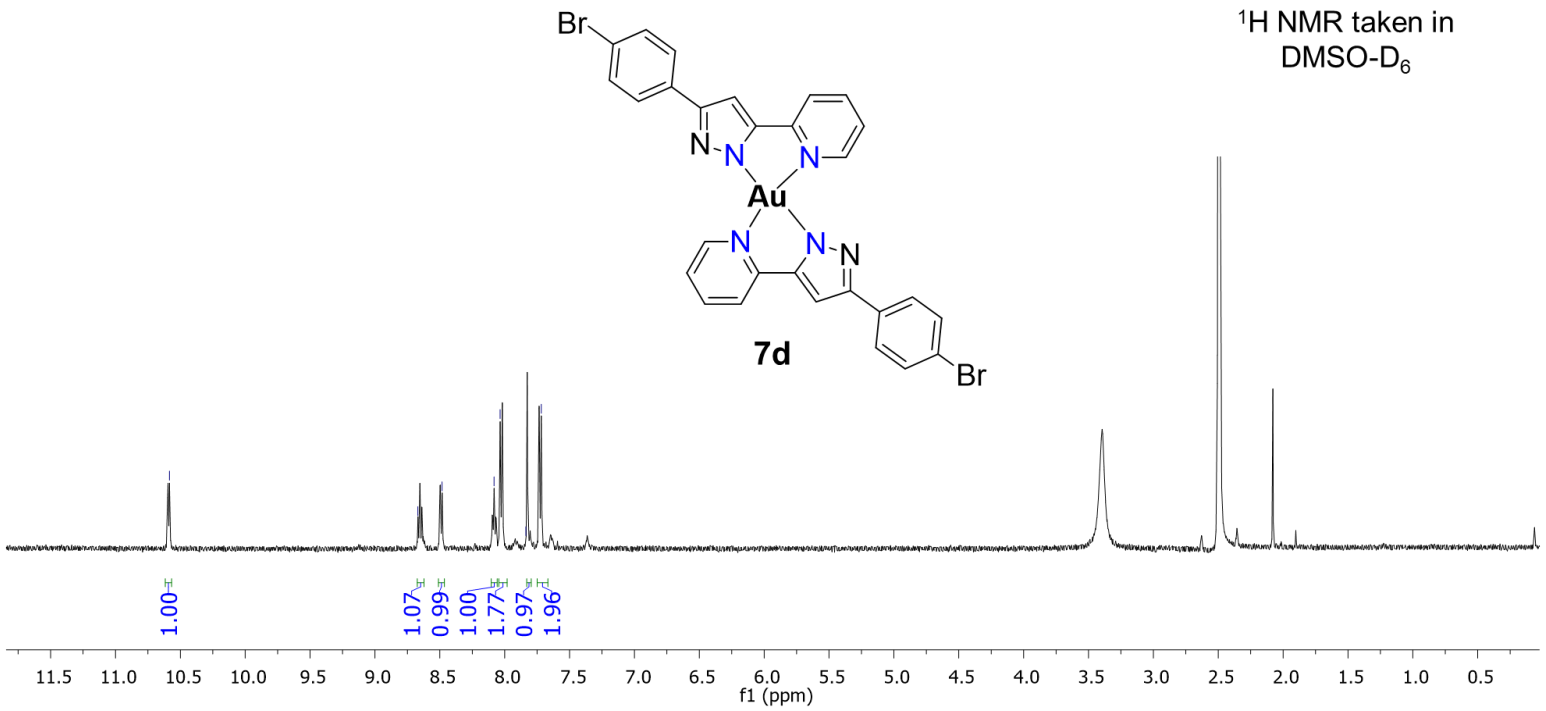
Br
N
N
N
Au
N
N
N
Br
7d
^{1}H NMR taken in
DMSO-D$_6$
1.00
1.07
0.99
1.00
1.77
0.97
1.96
11.5 11.0 10.5 10.0 9.5 9.0 8.5 8.0 7.5 7.0 6.5 6.0 5.5 5.0 4.5 4.0 3.5 3.0 2.5 2.0 1.5 1.0 0.5
f1 (ppm)

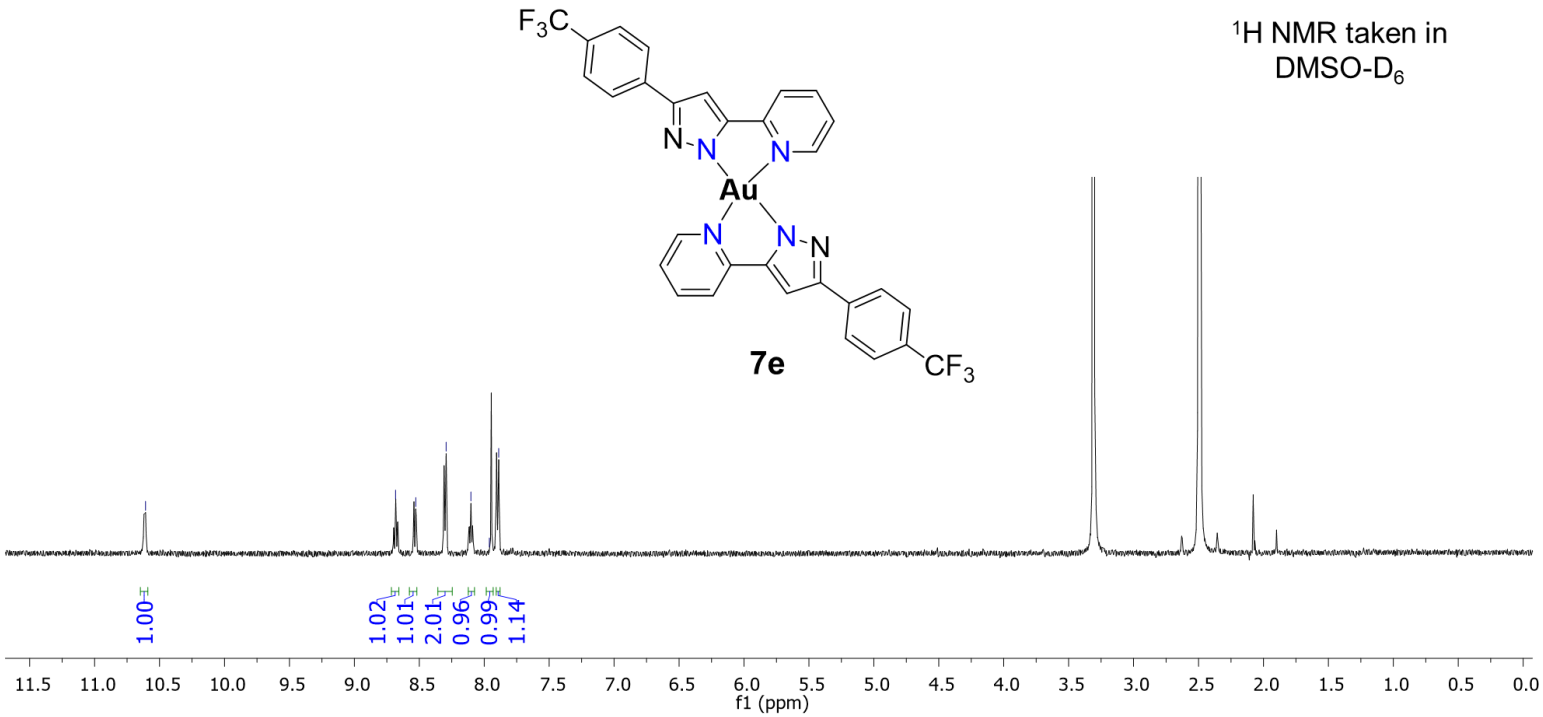
F3C
N
N
N
Au
N
N
N
CF3
7e
1H NMR taken in
DMSO-D6
1.00
1.02
1.01
2.01
0.96
0.99
1.14
11.5 11.0 10.5 10.0 9.5 9.0 8.5 8.0 7.5 7.0 6.5 6.0 5.5 5.0 4.5 4.0 3.5 3.0 2.5 2.0 1.5 1.0 0.5 0.0
f1 (ppm)

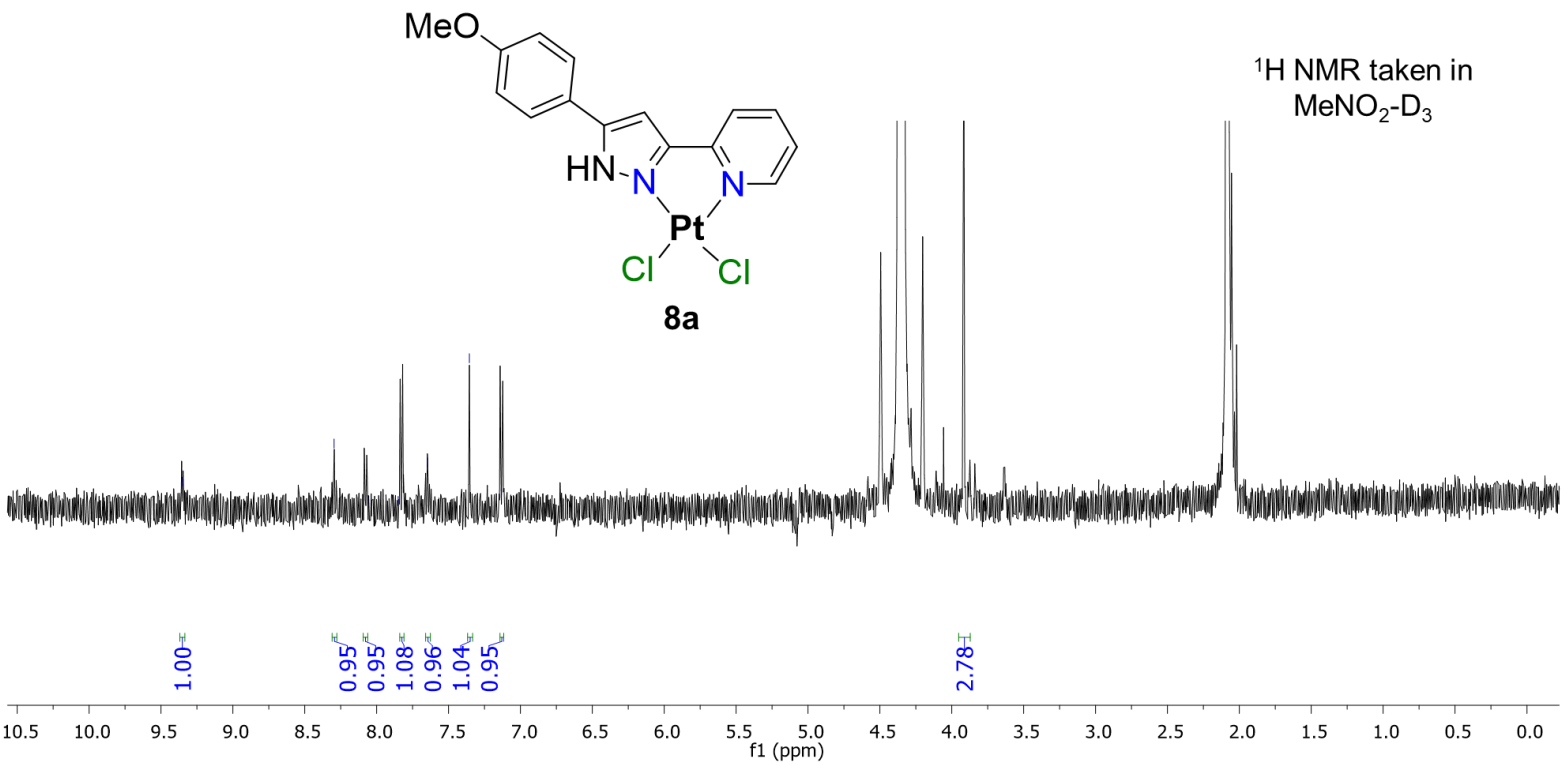
MeO
HN
N
N
Pt
Cl
Cl
8a
^{1}H NMR taken in
$MeNO_2$-D_3
1.00
0.95
0.95
1.08
0.96
1.04
0.95
2.78
10.5 10.0 9.5 9.0 8.5 8.0 7.5 7.0 6.5 6.0 5.5 5.0 4.5 4.0 3.5 3.0 2.5 2.0 1.5 1.0 0.5 0.0
f1 (ppm)

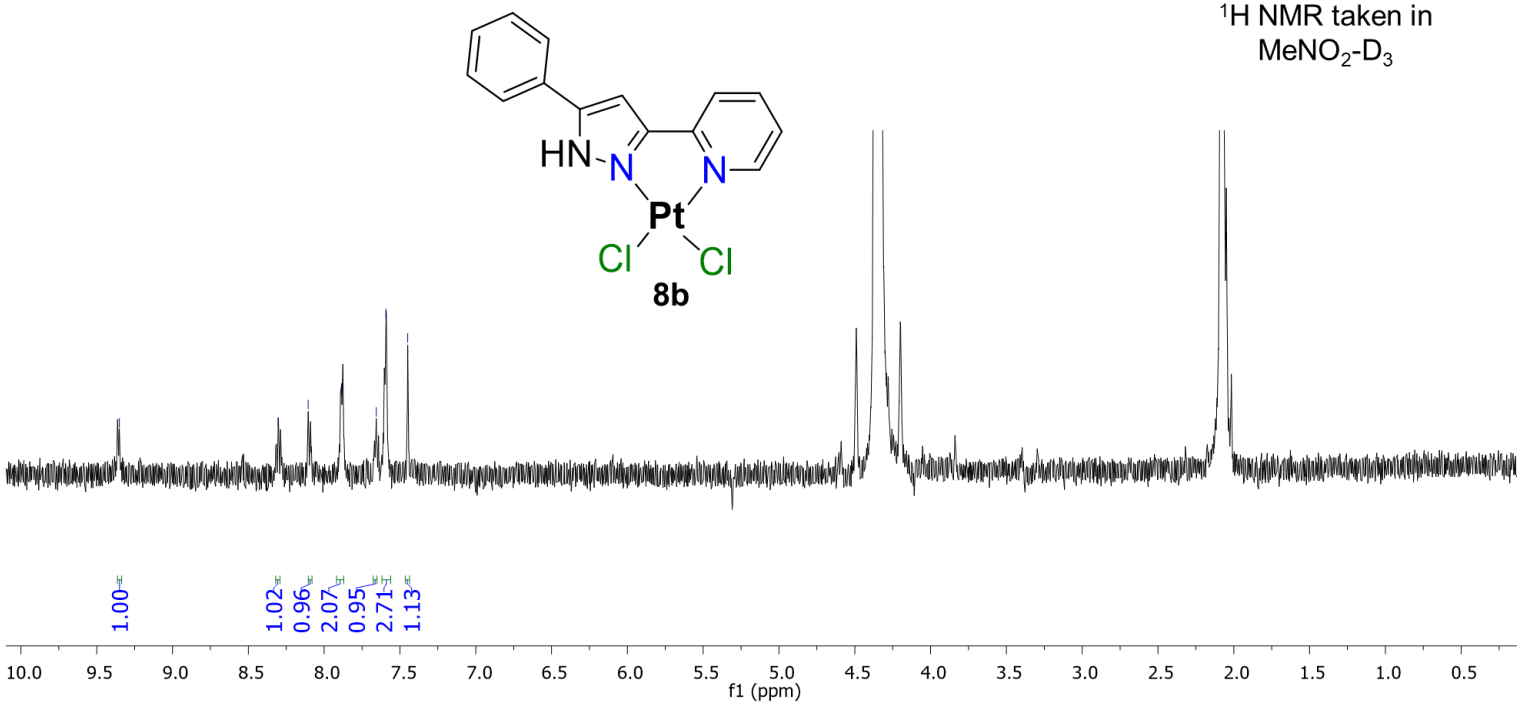
^{1}H NMR taken in
$MeNO_2$-D_3
HN
N
N
Pt
Cl
Cl
8b
1.00
1.02
0.96
2.07
0.95
2.71
1.13
10.0
9.5
9.0
8.5
8.0
7.5
7.0
6.5
6.0
5.5
5.0
4.5
4.0
3.5
3.0
2.5
2.0
1.5
1.0
0.5
f1 (ppm)

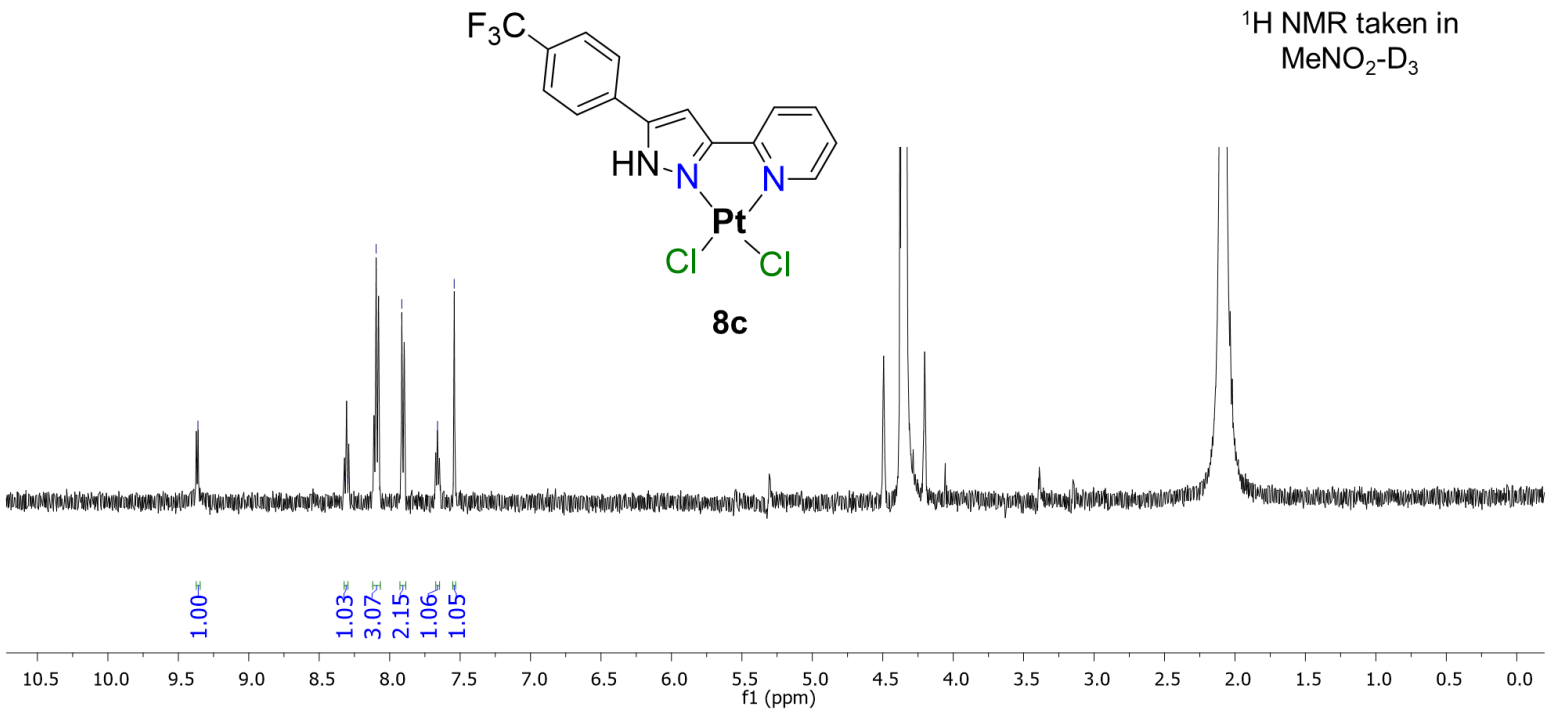
F3C
HN
N
N
Pt
Cl
Cl
8c
1H NMR taken in
MeNO2-D3
1.00
1.03
3.07
2.15
1.06
1.05
10.5 10.0 9.5 9.0 8.5 8.0 7.5 7.0 6.5 6.0 5.5 5.0 4.5 4.0 3.5 3.0 2.5 2.0 1.5 1.0 0.5 0.0
f1 (ppm)

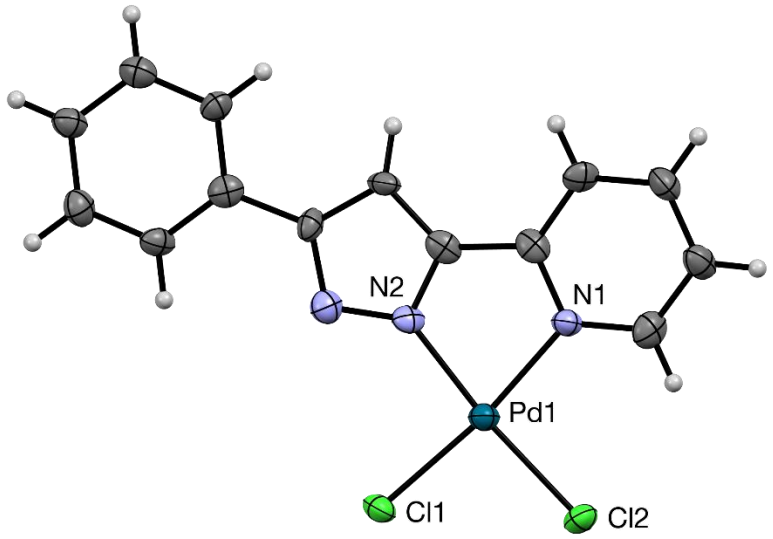

Crystal data and structure refinement for larsen22_0m_a.

Identification code	larsen22_0m_a	
Empirical formula	C14 H10 Cl2 N3 Pd	
Formula weight	397.55	
Temperature	100.0 K	
Wavelength	1.54178 Å	
Crystal system	Monoclinic	
Space group	P 21/c	
Unit cell dimensions	a = 8.448(2) Å	α= 90°.
	b = 21.242(5) Å	β= 117.669(15)°.
	c = 8.7304(17) Å	γ = 90°.
Volume	1387.5(6) $Å^3$	
Z	4	
Density (calculated)	1.903 Mg/m^3	
Absorption coefficient	14.260 mm^{-1}	
F(000)	780	
Crystal size	0.16 x 0.09 x 0.04 mm^3	
Theta range for data collection	4.162 to 58.964°.	
Index ranges	-9<=h<=8, -23<=k<=23, 0<=l<=9	
Reflections collected	6364	
Independent reflections	6364 [R(int) = 0.077]	
Completeness to theta = 58.964°	99.8 %	
Absorption correction	Semi-empirical from equivalents	
Max. and min. transmission	0.1665 and 0.0488	
Refinement method	Full-matrix least-squares on F^2	
Data / restraints / parameters	6364 / 0 / 170	
Goodness-of-fit on F^2	1.059	
Final R indices [I>2sigma(I)]	R1 = 0.0857, wR2 = 0.2151	
R indices (all data)	R1 = 0.1075, wR2 = 0.2305	
Extinction coefficient	n/a	

Largest diff. peak and hole 1.299 and -1.066 e.Å^{-3}

Atomic coordinates (x 10^4) and equivalent isotropic displacement parameters (Å^{2}x 10^3) for larsen22_0m_a. U(eq) is defined as one third of the trace of the orthogonalized U^{ij} tensor.

	x	y	z	U(eq)
Pd(1)	1543(2)	4168(1)	7482(2)	25(1)
Cl(1)	2931(5)	4746(2)	9970(5)	31(1)
Cl(2)	566(5)	3435(2)	8769(6)	32(1)
N(1)	242(17)	3776(7)	5060(19)	25(3)
N(2)	2311(17)	4752(7)	6134(19)	24(3)
N(3)	3373(18)	5264(8)	6480(20)	29(3)
C(1)	-790(20)	3254(9)	4610(30)	33(4)
C(2)	-1650(20)	3045(9)	2930(20)	33(4)
C(3)	-1420(20)	3371(10)	1660(20)	34(4)
C(4)	-360(20)	3896(9)	2120(20)	28(4)
C(5)	460(20)	4095(9)	3810(20)	28(4)
C(6)	1630(20)	4642(9)	4470(20)	26(4)
C(7)	2220(20)	5095(9)	3660(20)	27(4)
C(8)	3350(20)	5476(8)	5000(20)	25(4)
C(9)	4386(13)	6033(4)	4956(13)	27(4)
C(10)	4260(13)	6214(5)	3372(11)	28(4)
C(11)	5191(14)	6738(5)	3271(11)	34(4)
C(12)	6249(14)	7082(5)	4752(14)	31(4)
C(13)	6375(13)	6901(5)	6336(11)	33(4)
C(14)	5444(14)	6377(5)	6438(11)	29(4)

Bond lengths [Å] and angles [°] for larsen22_0m_a.

Pd(1)-Cl(1)	2.288(5)
Pd(1)-Cl(2)	2.286(4)
Pd(1)-N(1)	2.053(15)
Pd(1)-N(2)	2.014(14)
N(1)-C(1)	1.35(2)
N(1)-C(5)	1.37(2)
N(2)-N(3)	1.35(2)
N(2)-C(6)	1.31(2)
N(3)-C(8)	1.36(2)
C(1)-H(1)	0.9500
C(1)-C(2)	1.37(3)
C(2)-H(2)	0.9500
C(2)-C(3)	1.39(3)
C(3)-H(3)	0.9500
C(3)-C(4)	1.37(3)
C(4)-H(4)	0.9500
C(4)-C(5)	1.37(3)
C(5)-C(6)	1.46(3)
C(6)-C(7)	1.41(3)
C(7)-H(7)	0.9500
C(7)-C(8)	1.38(3)
C(8)-C(9)	1.482(18)
C(9)-C(10)	1.3900
C(9)-C(14)	1.3900
C(10)-H(10)	0.9500
C(10)-C(11)	1.3900
C(11)-H(11)	0.9500
C(11)-C(12)	1.3900
C(12)-H(12)	0.9500
C(12)-C(13)	1.3900
C(13)-H(13)	0.9500
C(13)-C(14)	1.3900

C(14)-H(14)	0.9500

Cl(2)-Pd(1)-Cl(1)	92.38(17)
N(1)-Pd(1)-Cl(1)	171.4(4)
N(1)-Pd(1)-Cl(2)	95.0(4)
N(2)-Pd(1)-Cl(1)	93.6(4)
N(2)-Pd(1)-Cl(2)	174.0(4)
N(2)-Pd(1)-N(1)	79.1(6)
C(1)-N(1)-Pd(1)	126.7(13)
C(1)-N(1)-C(5)	118.7(16)
C(5)-N(1)-Pd(1)	114.6(12)
N(3)-N(2)-Pd(1)	136.4(12)
C(6)-N(2)-Pd(1)	116.2(12)
C(6)-N(2)-N(3)	107.3(14)
N(2)-N(3)-C(8)	109.8(15)
N(1)-C(1)-H(1)	119.1
N(1)-C(1)-C(2)	121.8(18)
C(2)-C(1)-H(1)	119.1
C(1)-C(2)-H(2)	120.3
C(1)-C(2)-C(3)	119.3(18)
C(3)-C(2)-H(2)	120.3
C(2)-C(3)-H(3)	120.5
C(4)-C(3)-C(2)	119.0(18)
C(4)-C(3)-H(3)	120.5
C(3)-C(4)-H(4)	120.0
C(3)-C(4)-C(5)	120.0(17)
C(5)-C(4)-H(4)	120.0
N(1)-C(5)-C(4)	121.2(17)
N(1)-C(5)-C(6)	113.3(15)
C(4)-C(5)-C(6)	125.5(17)
N(2)-C(6)-C(5)	116.6(16)
N(2)-C(6)-C(7)	110.6(16)
C(7)-C(6)-C(5)	132.7(16)
C(6)-C(7)-H(7)	127.9

C(8)-C(7)-C(6)	104.3(15)
C(8)-C(7)-H(7)	127.9
N(3)-C(8)-C(7)	107.9(15)
N(3)-C(8)-C(9)	122.9(15)
C(7)-C(8)-C(9)	129.2(15)
C(10)-C(9)-C(8)	118.2(10)
C(10)-C(9)-C(14)	120.0
C(14)-C(9)-C(8)	121.7(10)
C(9)-C(10)-H(10)	120.0
C(9)-C(10)-C(11)	120.0
C(11)-C(10)-H(10)	120.0
C(10)-C(11)-H(11)	120.0
C(12)-C(11)-C(10)	120.0
C(12)-C(11)-H(11)	120.0
C(11)-C(12)-H(12)	120.0
C(13)-C(12)-C(11)	120.0
C(13)-C(12)-H(12)	120.0
C(12)-C(13)-H(13)	120.0
C(14)-C(13)-C(12)	120.0
C(14)-C(13)-H(13)	120.0
C(9)-C(14)-H(14)	120.0
C(13)-C(14)-C(9)	120.0
C(13)-C(14)-H(14)	120.0

Symmetry transformations used to generate equivalent atoms:

Anisotropic displacement parameters ($Å^2 x\ 10^3$) for larsen22_0m_a. The anisotropic displacement factor exponent takes the form: $-2\pi^2[\ h^2\ a^{*2}U^{11} + ...\ + 2\ h\ k\ a^*\ b^*\ U^{12}\ ]$

	U^{11}	U^{22}	U^{33}	U^{23}	U^{13}	U^{12}
Pd(1)	30(1)	24(1)	21(1)	1(1)	12(1)	2(1)
Cl(1)	36(2)	33(3)	19(2)	-4(2)	10(2)	-2(2)
Cl(2)	42(2)	27(3)	28(2)	7(2)	18(2)	-1(2)
N(1)	31(7)	23(9)	19(8)	1(6)	11(6)	2(6)
N(2)	32(7)	20(8)	23(9)	-1(7)	16(6)	6(6)
N(3)	34(7)	25(9)	32(9)	-2(7)	17(6)	2(6)
C(1)	41(9)	21(11)	42(13)	1(9)	24(9)	6(8)
C(2)	39(9)	25(11)	27(11)	-1(9)	8(8)	3(8)
C(3)	34(9)	35(12)	25(10)	-8(9)	8(8)	-4(8)
C(4)	35(8)	20(10)	28(11)	8(8)	14(8)	11(7)
C(5)	26(8)	27(11)	30(10)	-4(9)	14(7)	7(7)
C(6)	24(7)	25(10)	26(11)	-1(8)	9(7)	12(7)
C(7)	27(8)	37(11)	15(9)	2(8)	9(7)	-1(7)
C(8)	30(8)	17(10)	34(11)	-3(8)	20(8)	-2(7)
C(9)	27(8)	26(11)	31(10)	4(8)	15(7)	9(7)
C(10)	32(8)	24(11)	28(10)	5(8)	13(7)	0(7)
C(11)	34(9)	39(13)	27(10)	1(9)	12(8)	2(8)
C(12)	35(9)	30(11)	24(11)	2(8)	12(8)	4(8)
C(13)	36(9)	25(11)	36(12)	-5(9)	15(8)	0(8)
C(14)	43(9)	20(10)	23(10)	3(8)	15(8)	8(8)

Hydrogen coordinates (x 10^4) and isotropic displacement parameters ($Å^2$x 10^3) for larsen22_0m_a.

	x	y	z	U(eq)
H(1)	-925	3026	5475	39
H(2)	-2389	2682	2637	39
H(3)	-1997	3231	493	40
H(4)	-198	4123	1266	34
H(7)	1910	5129	2473	32
H(10)	3537	5979	2360	34
H(11)	5105	6861	2188	41
H(12)	6886	7440	4683	37
H(13)	7098	7136	7349	40
H(14)	5530	6254	7520	34

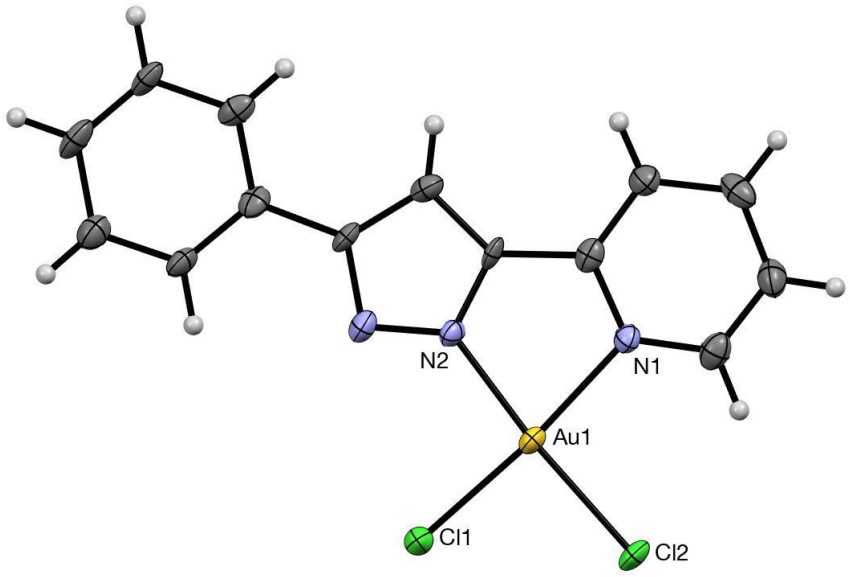

Crystal data and structure refinement for larsen21_a.

Identification code	MDS-1-291	
Empirical formula	C14 H10 Au Cl2 N3	
Formula weight	488.12	
Temperature	100.0 K	
Wavelength	1.54178 Å	
Crystal system	Triclinic	
Space group	P-1	
Unit cell dimensions	a = 8.8600(9) Å	α= 63.631(7)°.
	b = 13.5455(19) Å	β= 73.428(7)°.
	c = 13.6960(18) Å	γ = 80.778(7)°.
Volume	1410.4(3) $Å^3$	
Z	4	
Density (calculated)	2.299 Mg/m^3	
Absorption coefficient	23.018 mm^{-1}	
F(000)	912	
Crystal size	0.17 x 0.13 x 0.08 mm^3	
Theta range for data collection	3.645 to 68.429°.	
Index ranges	-10<=h<=10, -14<=k<=16, 0<=l<=16	
Reflections collected	8763	
Independent reflections	8763 [R(int) = 0.0332]	
Completeness to theta = 67.679°	99.7 %	
Absorption correction	Semi-empirical from equivalents	
Max. and min. transmission	0.323 and 0.111	
Refinement method	Full-matrix least-squares on F^2	
Data / restraints / parameters	8763 / 0 / 362	
Goodness-of-fit on F^2	1.040	
Final R indices [I>2sigma(I)]	R1 = 0.0426, wR2 = 0.1017	
R indices (all data)	R1 = 0.0501, wR2 = 0.1066	
Extinction coefficient	n/a	

Largest diff. peak and hole 2.506 and -1.161 e.Å^{-3}

Atomic coordinates (x 10^4) and equivalent isotropic displacement parameters (Å^{2}x 10^3) for larsen21_a. U(eq) is defined as one third of the trace of the orthogonalized U^{ij} tensor.

	x	y	z	U(eq)
Au(1')	3328(1)	4630(1)	2782(1)	19(1)
Au(1)	8562(1)	-248(1)	7956(1)	18(1)
Cl(2')	5456(3)	5203(2)	1278(2)	28(1)
Cl(2)	7280(3)	-1157(2)	9801(2)	28(1)
Cl(1)	10891(3)	-986(2)	8378(2)	30(1)
Cl(1')	4922(3)	4129(2)	3965(2)	33(1)
N(2)	9499(9)	580(7)	6322(7)	18(2)
N(2')	1366(10)	4130(7)	3997(7)	22(2)
N(3')	1124(11)	3592(7)	5107(7)	22(2)
N(1')	1689(10)	5171(7)	1823(7)	19(2)
N(3)	11002(10)	689(7)	5728(7)	22(2)
C(9)	12340(13)	1607(9)	3735(9)	22(2)
N(1)	6534(10)	461(7)	7406(7)	19(2)
C(6')	15(13)	4461(8)	3641(8)	21(2)
C(1')	2035(13)	5683(9)	697(9)	25(2)
C(8)	10911(12)	1304(8)	4654(8)	19(2)
C(6)	8469(12)	1091(8)	5684(8)	19(2)
C(8')	-471(11)	3581(8)	5491(8)	16(2)
C(3)	4039(13)	1495(10)	6450(10)	28(2)
C(14')	-210(14)	2507(9)	7471(9)	27(2)
C(11)	13670(13)	2559(9)	1766(9)	26(2)
C(5)	6822(12)	1045(8)	6274(9)	20(2)
C(7)	9324(13)	1580(9)	4585(9)	23(2)
C(4)	5582(13)	1562(9)	5777(9)	25(2)
C(11')	-3466(15)	2434(9)	8269(10)	30(3)
C(7')	-1206(12)	4105(9)	4599(9)	23(2)
C(5')	168(13)	5040(9)	2445(9)	24(2)

C(9')	-1167(13)	3009(8)	6713(8)	20(2)
C(14)	13816(13)	1185(9)	3962(9)	23(2)
C(1)	5092(13)	381(9)	8067(10)	26(2)
C(10)	12274(14)	2294(8)	2631(9)	24(2)
C(3')	-715(13)	5981(10)	751(9)	31(3)
C(13)	15198(14)	1443(10)	3121(9)	28(2)
C(12)	15122(14)	2144(9)	2005(9)	30(3)
C(2)	3828(13)	895(10)	7607(10)	29(2)
C(10')	-2796(13)	2972(9)	7117(9)	24(2)
C(4')	-1046(13)	5444(10)	1910(9)	28(2)
C(13')	-883(14)	1967(10)	8619(10)	31(3)
C(12')	-2496(15)	1924(9)	9011(9)	32(3)
C(2')	858(15)	6097(10)	147(9)	30(3)

Bond lengths [Å] and angles [°] for larsen21_a.

Au(1')-Cl(2')	2.287(2)
Au(1')-Cl(1')	2.259(3)
Au(1')-N(2')	1.994(9)
Au(1')-N(1')	2.065(8)
Au(1)-Cl(2)	2.289(2)
Au(1)-Cl(1)	2.258(3)
Au(1)-N(2)	1.991(8)
Au(1)-N(1)	2.072(8)
N(2)-N(3)	1.340(12)
N(2)-C(6)	1.338(14)
N(2')-N(3')	1.330(12)
N(2')-C(6')	1.355(14)
N(3')-C(8')	1.360(13)
N(1')-C(1')	1.342(13)
N(1')-C(5')	1.364(14)
N(3)-C(8)	1.350(13)
C(9)-C(8)	1.468(14)
C(9)-C(14)	1.403(15)
C(9)-C(10)	1.392(15)
N(1)-C(5)	1.358(13)
N(1)-C(1)	1.328(14)
C(6')-C(7')	1.385(15)
C(6')-C(5')	1.444(14)
C(1')-C(2')	1.363(16)
C(8)-C(7)	1.416(15)
C(6)-C(5)	1.449(14)
C(6)-C(7)	1.380(14)
C(8')-C(7')	1.399(15)
C(8')-C(9')	1.481(13)
C(3)-C(4)	1.404(16)
C(3)-C(2)	1.394(17)
C(14')-C(9')	1.397(15)

C(14')-C(13')	1.395(15)
C(11)-C(10)	1.411(15)
C(11)-C(12)	1.387(17)
C(5)-C(4)	1.385(15)
C(11')-C(10')	1.399(16)
C(11')-C(12')	1.391(18)
C(5')-C(4')	1.377(16)
C(9')-C(10')	1.391(15)
C(14)-C(13)	1.386(15)
C(1)-C(2)	1.378(16)
C(3')-C(4')	1.383(15)
C(3')-C(2')	1.396(17)
C(13)-C(12)	1.411(16)
C(13')-C(12')	1.376(17)

Cl(1')-Au(1')-Cl(2')	90.09(10)
N(2')-Au(1')-Cl(2')	174.7(3)
N(2')-Au(1')-Cl(1')	94.9(3)
N(2')-Au(1')-N(1')	80.3(3)
N(1')-Au(1')-Cl(2')	94.9(2)
N(1')-Au(1')-Cl(1')	173.1(3)
Cl(1)-Au(1)-Cl(2)	90.18(9)
N(2)-Au(1)-Cl(2)	175.2(2)
N(2)-Au(1)-Cl(1)	94.6(2)
N(2)-Au(1)-N(1)	80.0(3)
N(1)-Au(1)-Cl(2)	95.2(2)
N(1)-Au(1)-Cl(1)	174.3(2)
N(3)-N(2)-Au(1)	131.2(7)
C(6)-N(2)-Au(1)	115.7(6)
C(6)-N(2)-N(3)	113.1(8)
N(3')-N(2')-Au(1')	131.9(7)
N(3')-N(2')-C(6')	113.4(9)
C(6')-N(2')-Au(1')	114.6(7)
N(2')-N(3')-C(8')	104.5(8)

C(1')-N(1')-Au(1')	124.8(7)
C(1')-N(1')-C(5')	121.5(9)
C(5')-N(1')-Au(1')	113.5(7)
N(2)-N(3)-C(8)	104.5(8)
C(14)-C(9)-C(8)	119.6(9)
C(10)-C(9)-C(8)	121.8(10)
C(10)-C(9)-C(14)	118.6(10)
C(5)-N(1)-Au(1)	112.9(7)
C(1)-N(1)-Au(1)	125.0(7)
C(1)-N(1)-C(5)	122.1(9)
N(2')-C(6')-C(7')	106.2(9)
N(2')-C(6')-C(5')	117.1(10)
C(7')-C(6')-C(5')	136.7(10)
N(1')-C(1')-C(2')	120.2(10)
N(3)-C(8)-C(9)	121.0(9)
N(3)-C(8)-C(7)	111.0(9)
C(7)-C(8)-C(9)	128.0(9)
N(2)-C(6)-C(5)	116.2(9)
N(2)-C(6)-C(7)	107.5(9)
C(7)-C(6)-C(5)	136.3(10)
N(3')-C(8')-C(7')	110.8(8)
N(3')-C(8')-C(9')	119.2(9)
C(7')-C(8')-C(9')	129.9(9)
C(2)-C(3)-C(4)	117.6(10)
C(13')-C(14')-C(9')	120.3(11)
C(12)-C(11)-C(10)	120.5(10)
N(1)-C(5)-C(6)	115.0(9)
N(1)-C(5)-C(4)	119.7(9)
C(4)-C(5)-C(6)	125.3(10)
C(6)-C(7)-C(8)	104.0(9)
C(5)-C(4)-C(3)	119.8(10)
C(12')-C(11')-C(10')	119.7(11)
C(6')-C(7')-C(8')	105.1(9)
N(1')-C(5')-C(6')	114.0(9)

N(1')-C(5')-C(4')	119.5(10)
C(4')-C(5')-C(6')	126.5(10)
C(14')-C(9')-C(8')	120.9(10)
C(10')-C(9')-C(8')	119.9(10)
C(10')-C(9')-C(14')	119.2(10)
C(13)-C(14)-C(9)	121.8(10)
N(1)-C(1)-C(2)	119.9(10)
C(9)-C(10)-C(11)	120.2(11)
C(4')-C(3')-C(2')	118.8(10)
C(14)-C(13)-C(12)	119.3(11)
C(11)-C(12)-C(13)	119.6(10)
C(1)-C(2)-C(3)	120.8(11)
C(9')-C(10')-C(11')	120.3(11)
C(5')-C(4')-C(3')	119.9(11)
C(12')-C(13')-C(14')	120.2(12)
C(13')-C(12')-C(11')	120.3(11)
C(1')-C(2')-C(3')	120.1(10)

Symmetry transformations used to generate equivalent atoms:

Anisotropic displacement parameters ($Å^2 x\ 10^3$) for larsen21_a. The anisotropic displacement factor exponent takes the form: $-2\pi^2[\ h^2\ a^{*2}U^{11} + ...\ + 2\ h\ k\ a^*\ b^*\ U^{12}\ ]$

	U^{11}	U^{22}	U^{33}	U^{23}	U^{13}	U^{12}
Au(1')	19(1)	19(1)	15(1)	-4(1)	-1(1)	-4(1)
Au(1)	18(1)	19(1)	12(1)	-4(1)	0(1)	-4(1)
Cl(2')	20(1)	35(1)	21(1)	-7(1)	5(1)	-9(1)
Cl(2)	26(1)	34(1)	12(1)	-2(1)	3(1)	-6(1)
Cl(1)	19(1)	38(2)	19(1)	-1(1)	-3(1)	0(1)
Cl(1')	25(1)	40(2)	25(1)	-1(1)	-10(1)	-7(1)
N(2)	16(4)	20(4)	14(4)	-4(3)	-1(3)	-6(3)
N(2')	20(4)	21(5)	21(4)	-4(4)	-5(4)	-4(3)
N(3')	28(5)	17(4)	14(4)	-2(3)	-3(4)	-2(4)
N(1')	20(4)	17(4)	17(4)	-2(3)	-8(4)	-3(3)
N(3)	21(4)	24(5)	17(4)	-8(4)	2(4)	-4(4)
C(9)	24(5)	29(6)	18(5)	-13(4)	-3(4)	-7(4)
N(1)	17(4)	23(4)	17(4)	-10(4)	-2(3)	0(3)
C(6')	30(5)	16(5)	18(5)	-6(4)	-10(4)	-1(4)
C(1')	24(5)	29(6)	16(5)	-7(4)	3(4)	-10(4)
C(8)	22(5)	19(5)	10(4)	-5(4)	4(4)	-7(4)
C(6)	17(5)	18(5)	14(5)	-5(4)	7(4)	-8(4)
C(8')	19(5)	17(5)	10(4)	-7(4)	2(4)	-7(4)
C(3)	27(6)	31(6)	35(6)	-21(5)	-17(5)	9(5)
C(14')	30(6)	29(6)	17(5)	-9(5)	-2(5)	-3(5)
C(11)	32(6)	19(5)	15(5)	-4(4)	6(5)	-7(4)
C(5)	22(5)	18(5)	21(5)	-11(4)	0(4)	-4(4)
C(7)	29(6)	22(5)	14(5)	-4(4)	-3(4)	-3(4)
C(4)	23(5)	28(6)	22(5)	-11(5)	-5(4)	0(4)
C(11')	36(6)	20(6)	28(6)	-8(5)	9(5)	-17(5)
C(7')	18(5)	29(6)	25(5)	-15(5)	-1(4)	-5(4)
C(5')	27(5)	21(5)	22(5)	-11(4)	0(4)	-5(4)
C(9')	29(5)	14(5)	13(5)	-3(4)	0(4)	-6(4)
C(14)	25(5)	24(5)	14(5)	-4(4)	1(4)	-9(4)

C(1)	28(6)	22(5)	26(6)	-11(5)	1(5)	-5(4)
C(10)	35(6)	15(5)	19(5)	-7(4)	-2(5)	-4(4)
C(3')	27(6)	39(7)	24(6)	-4(5)	-13(5)	-4(5)
C(13)	28(6)	30(6)	23(5)	-9(5)	-1(5)	-7(5)
C(12)	37(6)	25(6)	19(5)	-6(5)	9(5)	-12(5)
C(2)	19(5)	41(7)	32(6)	-20(5)	-4(5)	-1(5)
C(10')	26(5)	26(6)	24(5)	-14(5)	2(5)	-12(4)
C(4')	24(6)	33(6)	26(6)	-9(5)	-8(5)	-4(5)
C(13')	35(6)	27(6)	23(6)	-10(5)	1(5)	2(5)
C(12')	43(7)	26(6)	18(5)	-9(5)	11(5)	-12(5)
C(2')	41(7)	28(6)	19(5)	-1(5)	-13(5)	-9(5)

Hydrogen coordinates (x 10^4) and isotropic displacement parameters ($Å^2$x 10^3)
for larsen21_a.

	x	y	z	U(eq)
H(1')	3104	5756	283	30
H(3)	3171	1846	6127	33
H(14')	904	2532	7204	32
H(11)	13615	3024	1014	31
H(7)	8936	2004	3932	28
H(4)	5774	1959	4985	30
H(11')	-4579	2417	8544	37
H(7')	-2305	4196	4640	28
H(14)	13870	710	4712	28
H(1)	4931	-30	8857	31
H(10)	11285	2586	2459	28
H(3')	-1542	6267	373	38
H(13)	16185	1151	3294	34
H(12)	16060	2332	1422	36
H(2)	2799	840	8085	35
H(10')	-3457	3313	6607	29
H(4')	-2109	5353	2336	34
H(13')	-227	1629	9132	37
H(12')	-2948	1545	9793	39
H(2')	1108	6466	-650	36

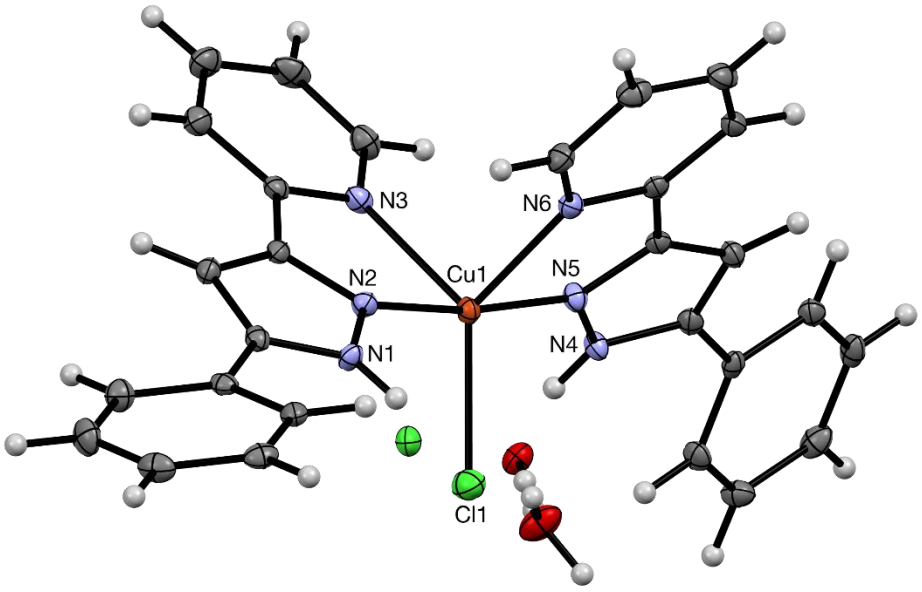

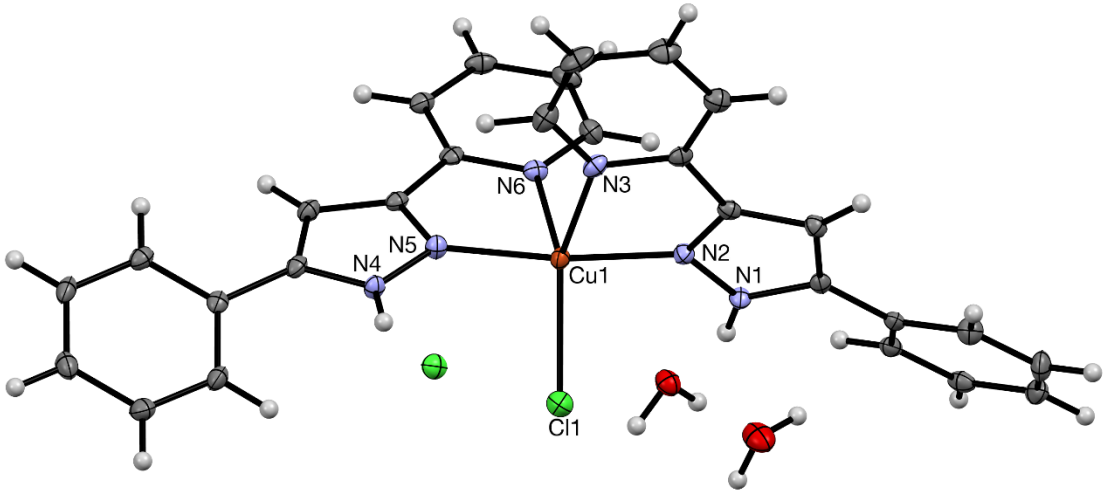

Crystal data and structure refinement for larsen23.

Identification code	MDS-2-17	
Empirical formula	C28 H26 Cl2 Cu N6 O2	
Formula weight	612.99	
Temperature	100.0 K	
Wavelength	0.71073 Å	
Crystal system	Triclinic	
Space group	P-1	
Unit cell dimensions	a = 9.3872(5) Å	α= 67.575(2)°.

	b = 12.4644(8) Å β= 82.689(2)°.
	c = 12.7697(8) Å γ = 81.228(2)°.
Volume	1361.08(14) $Å^3$
Z	2
Density (calculated)	1.496 Mg/m^3
Absorption coefficient	1.037 mm^{-1}
F(000)	630
Crystal size	0.29 x 0.25 x 0.22 mm^3
Theta range for data collection	1.779 to 25.743°.
Index ranges	-7<=h<=11, -14<=k<=15, -15<=l<=15
Reflections collected	9227
Independent reflections	4675 [R(int) = 0.0180]
Completeness to theta = 25.242°	89.9 %
Absorption correction	Semi-empirical from equivalents
Max. and min. transmission	0.322 and 0.265
Refinement method	Full-matrix least-squares on F^2
Data / restraints / parameters	4675 / 0 / 358
Goodness-of-fit on F^2	1.046
Final R indices [I>2sigma(I)]	R1 = 0.0282, wR2 = 0.0670
R indices (all data)	R1 = 0.0342, wR2 = 0.0702
Extinction coefficient	n/a
Largest diff. peak and hole	0.334 and -0.320 $e.Å^{-3}$

Atomic coordinates (x 10^4) and equivalent isotropic displacement parameters ($Å^2$x 10^3) for larsen23. U(eq) is defined as one third of the trace of the orthogonalized U^{ij} tensor.

	x	y	z	U(eq)
Cu(1)	2724(1)	2630(1)	4995(1)	12(1)
Cl(2)	4425(1)	3228(1)	1528(1)	16(1)
Cl(1)	4527(1)	3815(1)	4406(1)	21(1)
O(2)	3980(2)	3864(1)	7071(1)	17(1)
O(1)	4580(2)	4343(1)	8829(1)	26(1)
N(5)	1481(2)	3609(2)	3777(1)	13(1)
N(2)	3742(2)	1542(2)	6299(1)	12(1)
N(6)	705(2)	2793(2)	5937(1)	13(1)
N(4)	1711(2)	4210(2)	2654(1)	13(1)
N(1)	4490(2)	1696(2)	7052(1)	12(1)
N(3)	2581(2)	927(2)	4897(1)	14(1)
C(9)	4014(2)	408(2)	6448(2)	12(1)
C(10)	3305(2)	37(2)	5706(2)	12(1)
C(23)	128(2)	3980(2)	4071(2)	12(1)
C(20)	486(2)	5708(2)	1021(2)	12(1)
C(6)	6093(2)	597(2)	8596(2)	12(1)
C(24)	-345(2)	3498(2)	5283(2)	12(1)
C(7)	5225(2)	680(2)	7682(2)	12(1)
C(19)	-849(2)	6119(2)	552(2)	15(1)
C(22)	-520(2)	4806(2)	3122(2)	13(1)
C(28)	381(2)	2299(2)	7060(2)	16(1)
C(15)	1749(2)	6036(2)	337(2)	16(1)
C(25)	-1721(2)	3752(2)	5737(2)	14(1)
C(18)	-914(3)	6832(2)	-582(2)	17(1)
C(1)	5788(2)	1381(2)	9158(2)	14(1)
C(27)	-972(3)	2494(2)	7569(2)	19(1)
C(14)	1860(3)	668(2)	4202(2)	18(1)
C(13)	1832(3)	-466(2)	4272(2)	22(1)
C(8)	4944(2)	-172(2)	7308(2)	13(1)

C(26)	-2032(2)	3240(2)	6900(2)	17(1)
C(3)	7745(3)	391(2)	10345(2)	18(1)
C(21)	526(2)	4939(2)	2226(2)	13(1)
C(2)	6611(2)	1280(2)	10026(2)	16(1)
C(5)	7228(2)	-295(2)	8926(2)	17(1)
C(4)	8048(3)	-395(2)	9799(2)	20(1)
C(16)	1678(3)	6746(2)	-800(2)	18(1)
C(11)	3345(3)	-1120(2)	5821(2)	17(1)
C(17)	346(3)	7150(2)	-1260(2)	19(1)
C(12)	2600(3)	-1370(2)	5086(2)	20(1)

Bond lengths [Å] and angles [°] for larsen23.

Cu(1)-Cl(1)	2.2813(6)
Cu(1)-N(5)	1.9618(17)
Cu(1)-N(2)	1.9530(17)
Cu(1)-N(6)	2.1378(17)
Cu(1)-N(3)	2.1984(18)
O(2)-H(2A)	0.8702
O(2)-H(2B)	0.8699
O(1)-H(1B)	0.8700
O(1)-H(1C)	0.8701
N(5)-N(4)	1.347(2)
N(5)-C(23)	1.342(3)
N(2)-N(1)	1.344(2)
N(2)-C(9)	1.341(3)
N(6)-C(24)	1.352(3)
N(6)-C(28)	1.342(3)
N(4)-H(4)	0.8800
N(4)-C(21)	1.353(3)
N(1)-H(1)	0.8800
N(1)-C(7)	1.350(3)
N(3)-C(10)	1.355(3)
N(3)-C(14)	1.337(3)
C(9)-C(10)	1.465(3)
C(9)-C(8)	1.391(3)
C(10)-C(11)	1.388(3)
C(23)-C(24)	1.466(3)
C(23)-C(22)	1.394(3)
C(20)-C(19)	1.397(3)
C(20)-C(15)	1.396(3)
C(20)-C(21)	1.472(3)
C(6)-C(7)	1.470(3)
C(6)-C(1)	1.396(3)
C(6)-C(5)	1.395(3)

C(24)-C(25)	1.389(3)
C(7)-C(8)	1.389(3)
C(19)-H(19)	0.9500
C(19)-C(18)	1.384(3)
C(22)-H(22)	0.9500
C(22)-C(21)	1.386(3)
C(28)-H(28)	0.9500
C(28)-C(27)	1.382(3)
C(15)-H(15)	0.9500
C(15)-C(16)	1.386(3)
C(25)-H(25)	0.9500
C(25)-C(26)	1.387(3)
C(18)-H(18)	0.9500
C(18)-C(17)	1.388(3)
C(1)-H(1A)	0.9500
C(1)-C(2)	1.385(3)
C(27)-H(27)	0.9500
C(27)-C(26)	1.383(3)
C(14)-H(14)	0.9500
C(14)-C(13)	1.387(3)
C(13)-H(13)	0.9500
C(13)-C(12)	1.386(3)
C(8)-H(8)	0.9500
C(26)-H(26)	0.9500
C(3)-H(3)	0.9500
C(3)-C(2)	1.390(3)
C(3)-C(4)	1.383(3)
C(2)-H(2)	0.9500
C(5)-H(5)	0.9500
C(5)-C(4)	1.391(3)
C(4)-H(4A)	0.9500
C(16)-H(16)	0.9500
C(16)-C(17)	1.389(3)
C(11)-H(11)	0.9500

C(11)-C(12)	1.386(3)
C(17)-H(17)	0.9500
C(12)-H(12)	0.9500

N(5)-Cu(1)-Cl(1)	95.14(6)
N(5)-Cu(1)-N(6)	78.51(7)
N(5)-Cu(1)-N(3)	98.55(7)
N(2)-Cu(1)-Cl(1)	92.25(6)
N(2)-Cu(1)-N(5)	172.47(8)
N(2)-Cu(1)-N(6)	95.63(7)
N(2)-Cu(1)-N(3)	77.48(7)
N(6)-Cu(1)-Cl(1)	129.88(5)
N(6)-Cu(1)-N(3)	98.47(7)
N(3)-Cu(1)-Cl(1)	131.49(5)
H(2A)-O(2)-H(2B)	104.5
H(1B)-O(1)-H(1C)	104.5
N(4)-N(5)-Cu(1)	134.64(14)
C(23)-N(5)-Cu(1)	118.09(13)
C(23)-N(5)-N(4)	106.07(16)
N(1)-N(2)-Cu(1)	132.89(13)
C(9)-N(2)-Cu(1)	119.75(14)
C(9)-N(2)-N(1)	106.40(16)
C(24)-N(6)-Cu(1)	113.35(13)
C(28)-N(6)-Cu(1)	128.40(14)
C(28)-N(6)-C(24)	118.24(18)
N(5)-N(4)-H(4)	124.4
N(5)-N(4)-C(21)	111.30(17)
C(21)-N(4)-H(4)	124.4
N(2)-N(1)-H(1)	124.5
N(2)-N(1)-C(7)	111.01(16)
C(7)-N(1)-H(1)	124.5
C(10)-N(3)-Cu(1)	112.19(13)
C(14)-N(3)-Cu(1)	129.57(15)
C(14)-N(3)-C(10)	118.19(18)

N(2)-C(9)-C(10)	115.98(18)
N(2)-C(9)-C(8)	110.37(18)
C(8)-C(9)-C(10)	133.65(19)
N(3)-C(10)-C(9)	113.94(18)
N(3)-C(10)-C(11)	122.4(2)
C(11)-C(10)-C(9)	123.63(19)
N(5)-C(23)-C(24)	116.17(17)
N(5)-C(23)-C(22)	110.39(17)
C(22)-C(23)-C(24)	133.39(19)
C(19)-C(20)-C(21)	119.18(19)
C(15)-C(20)-C(19)	119.31(19)
C(15)-C(20)-C(21)	121.50(18)
C(1)-C(6)-C(7)	121.37(18)
C(5)-C(6)-C(7)	119.51(18)
C(5)-C(6)-C(1)	119.11(19)
N(6)-C(24)-C(23)	113.49(18)
N(6)-C(24)-C(25)	122.32(19)
C(25)-C(24)-C(23)	124.17(19)
N(1)-C(7)-C(6)	122.08(18)
N(1)-C(7)-C(8)	107.14(18)
C(8)-C(7)-C(6)	130.75(19)
C(20)-C(19)-H(19)	119.9
C(18)-C(19)-C(20)	120.3(2)
C(18)-C(19)-H(19)	119.9
C(23)-C(22)-H(22)	127.3
C(21)-C(22)-C(23)	105.30(19)
C(21)-C(22)-H(22)	127.3
N(6)-C(28)-H(28)	118.7
N(6)-C(28)-C(27)	122.7(2)
C(27)-C(28)-H(28)	118.7
C(20)-C(15)-H(15)	119.9
C(16)-C(15)-C(20)	120.2(2)
C(16)-C(15)-H(15)	119.9
C(24)-C(25)-H(25)	120.7

C(26)-C(25)-C(24)	118.6(2)
C(26)-C(25)-H(25)	120.7
C(19)-C(18)-H(18)	119.9
C(19)-C(18)-C(17)	120.2(2)
C(17)-C(18)-H(18)	119.9
C(6)-C(1)-H(1A)	119.8
C(2)-C(1)-C(6)	120.42(19)
C(2)-C(1)-H(1A)	119.8
C(28)-C(27)-H(27)	120.5
C(28)-C(27)-C(26)	118.9(2)
C(26)-C(27)-H(27)	120.5
N(3)-C(14)-H(14)	118.6
N(3)-C(14)-C(13)	122.9(2)
C(13)-C(14)-H(14)	118.6
C(14)-C(13)-H(13)	120.7
C(12)-C(13)-C(14)	118.6(2)
C(12)-C(13)-H(13)	120.7
C(9)-C(8)-H(8)	127.5
C(7)-C(8)-C(9)	105.08(18)
C(7)-C(8)-H(8)	127.5
C(25)-C(26)-H(26)	120.4
C(27)-C(26)-C(25)	119.3(2)
C(27)-C(26)-H(26)	120.4
C(2)-C(3)-H(3)	120.0
C(4)-C(3)-H(3)	120.0
C(4)-C(3)-C(2)	119.9(2)
N(4)-C(21)-C(20)	122.65(19)
N(4)-C(21)-C(22)	106.92(18)
C(22)-C(21)-C(20)	130.42(19)
C(1)-C(2)-C(3)	120.1(2)
C(1)-C(2)-H(2)	120.0
C(3)-C(2)-H(2)	120.0
C(6)-C(5)-H(5)	119.9
C(4)-C(5)-C(6)	120.2(2)

C(4)-C(5)-H(5)	119.9
C(3)-C(4)-C(5)	120.2(2)
C(3)-C(4)-H(4A)	119.9
C(5)-C(4)-H(4A)	119.9
C(15)-C(16)-H(16)	119.9
C(15)-C(16)-C(17)	120.1(2)
C(17)-C(16)-H(16)	119.9
C(10)-C(11)-H(11)	120.8
C(12)-C(11)-C(10)	118.5(2)
C(12)-C(11)-H(11)	120.8
C(18)-C(17)-C(16)	119.9(2)
C(18)-C(17)-H(17)	120.0
C(16)-C(17)-H(17)	120.0
C(13)-C(12)-C(11)	119.4(2)
C(13)-C(12)-H(12)	120.3
C(11)-C(12)-H(12)	120.3

Symmetry transformations used to generate equivalent atoms:

Anisotropic displacement parameters ($Å^2 x\ 10^3$) for larsen23. The anisotropic displacement factor exponent takes the form: $-2\pi^2[\ h^2\ a^{*2}U^{11} + ...\ + 2\ h\ k\ a^*\ b^*\ U^{12}\ ]$

	U^{11}	U^{22}	U^{33}	U^{23}	U^{13}	U^{12}
Cu(1)	11(1)	12(1)	12(1)	-4(1)	-3(1)	1(1)
Cl(2)	14(1)	13(1)	20(1)	-7(1)	0(1)	0(1)
Cl(1)	20(1)	18(1)	22(1)	-3(1)	-4(1)	-4(1)
O(2)	21(1)	14(1)	16(1)	-6(1)	-2(1)	-2(1)
O(1)	38(1)	21(1)	22(1)	-9(1)	-5(1)	-9(1)
N(5)	12(1)	14(1)	12(1)	-5(1)	-1(1)	0(1)
N(2)	12(1)	12(1)	13(1)	-4(1)	-3(1)	-1(1)
N(6)	12(1)	12(1)	15(1)	-7(1)	0(1)	-2(1)
N(4)	10(1)	15(1)	11(1)	-4(1)	0(1)	1(1)
N(1)	14(1)	10(1)	14(1)	-5(1)	-3(1)	-1(1)
N(3)	11(1)	18(1)	16(1)	-9(1)	-1(1)	-1(1)
C(9)	11(1)	11(1)	13(1)	-5(1)	2(1)	-2(1)
C(10)	9(1)	15(1)	15(1)	-7(1)	2(1)	-2(1)
C(23)	10(1)	11(1)	15(1)	-6(1)	-1(1)	-2(1)
C(20)	14(1)	9(1)	15(1)	-7(1)	-4(1)	0(1)
C(6)	11(1)	13(1)	10(1)	-1(1)	0(1)	-4(1)
C(24)	12(1)	11(1)	16(1)	-7(1)	-2(1)	-3(1)
C(7)	10(1)	13(1)	11(1)	-3(1)	1(1)	0(1)
C(19)	13(1)	15(1)	20(1)	-9(1)	-3(1)	-1(1)
C(22)	10(1)	14(1)	17(1)	-7(1)	-2(1)	0(1)
C(28)	18(1)	13(1)	15(1)	-3(1)	-1(1)	-2(1)
C(15)	12(1)	17(1)	19(1)	-7(1)	-6(1)	0(1)
C(25)	11(1)	13(1)	21(1)	-8(1)	-1(1)	-1(1)
C(18)	17(1)	13(1)	23(1)	-7(1)	-11(1)	2(1)
C(1)	12(1)	12(1)	16(1)	-3(1)	1(1)	-3(1)
C(27)	22(1)	18(1)	16(1)	-7(1)	3(1)	-6(1)
C(14)	15(1)	23(1)	19(1)	-10(1)	-3(1)	1(1)
C(13)	17(1)	31(1)	27(1)	-19(1)	-2(1)	-6(1)
C(8)	14(1)	11(1)	14(1)	-4(1)	0(1)	-1(1)

C(26)	14(1)	19(1)	22(1)	-12(1)	5(1)	-5(1)
C(3)	19(1)	23(1)	13(1)	-3(1)	-5(1)	-7(1)
C(21)	12(1)	13(1)	17(1)	-7(1)	-4(1)	-1(1)
C(2)	19(1)	17(1)	12(1)	-5(1)	3(1)	-7(1)
C(5)	18(1)	17(1)	17(1)	-7(1)	-2(1)	-1(1)
C(4)	18(1)	19(1)	18(1)	-3(1)	-7(1)	4(1)
C(16)	16(1)	19(1)	18(1)	-6(1)	-2(1)	-6(1)
C(11)	16(1)	16(1)	19(1)	-7(1)	1(1)	-2(1)
C(17)	26(1)	14(1)	16(1)	-3(1)	-7(1)	-2(1)
C(12)	21(1)	18(1)	27(1)	-13(1)	1(1)	-4(1)

Hydrogen coordinates (x 10^4) and isotropic displacement parameters ($Å^2$x 10^3) for larsen23.

	x	y	z	U(eq)
H(2A)	4331	4397	6465	26
H(2B)	4196	4028	7631	26
H(1B)	4438	4037	9565	39
H(1C)	4713	5063	8686	39
H(4)	2528	4137	2251	15
H(1)	4499	2369	7125	15
H(19)	-1715	5907	1014	18
H(22)	-1476	5195	3096	16
H(28)	1111	1796	7524	19
H(15)	2661	5771	651	19
H(25)	-2433	4267	5261	17
H(18)	-1824	7105	-898	20
H(1A)	5013	1988	8945	16
H(27)	-1170	2122	8366	22
H(14)	1344	1288	3637	22
H(13)	1298	-620	3771	26
H(8)	5308	-976	7580	16
H(26)	-2964	3398	7234	21
H(3)	8310	323	10938	22
H(2)	6400	1818	10403	19
H(5)	7442	-836	8553	20
H(4A)	8819	-1005	10021	24
H(16)	2541	6957	-1265	21
H(11)	3871	-1728	6390	20
H(17)	299	7642	-2037	22
H(12)	2617	-2153	5140	24